Cyprus University of Technology
Faculty of Engineering and Technology

Doctoral Dissertation

NUMERICAL STUDY ON THE SEISMIC RETROFITTING OF MASONRY-INFILLED RC FRAMES USING TEXTILE-REINFORCED MORTAR

Christiana A. Filippou

Limassol, March 2021

CYPRUS UNIVERSITY OF TECHNOLOGY

FACULTY OF ENGINEERING AND TECHNOLOGY

DEPARTMENT OF CIVIL ENGINEERING AND GEOMATICS

Doctoral Dissertation

NUMERICAL STUDY ON THE SEISMIC RETROFITTING OF MASONRY-INFILLED RC FRAMES USING TEXTILE-REINFORCED MORTAR

Christiana A. Filippou

Limassol, March 2021

Approval Form

Doctoral Dissertation

NUMERICAL STUDY ON THE SEISMIC RETROFITTING OF MASONRY-INFILLED RC FRAMES USING TEXTILE-REINFORCED MORTAR

Presented by

Christiana A. Filippou

Supervisor: Christis Z. Chrysostomou, Professor

Signature _____

Member of the committee: Diofantos G. Hadjimitsis, Professor

Signature _____

Member of the committee: Ioannis Ioannou, Professor

Signature _____

Cyprus University of Technology

Limassol, March 2021

Doctoral Dissertation

NUMERICAL STUDY ON THE SEISMIC RETROFITTING OF MASONRY-INFILLED RC FRAMES USING TEXTILE-REINFORCED MORTAR

Presented by

Christiana A. Filippou

Supervising Committee:

Supervisor: Christis Z. Chrysostomou, Professor

Member of the committee: Elia A. Tantele, Associate Professor

Member of the committee: Georgios Constantinides, Associate Professor

Cyprus University of Technology

Limassol, March 2021

Copyrights

The approval of the dissertation by the Department of Civil Engineering and Geomatics does not imply necessarily the approval by the Department of the views of the writer.

ACKNOWLEDGEMENTS

I would like to thank all people who have helped in this research. The research presented in this dissertation has been a long journey, during which I had the unique opportunity to meet and collaborate with a number of great individuals. These individuals had a great influence in my life as a researcher that made this journey a priceless and unforgettable experience.

First and foremost, I wish to express my deepest appreciation to my supervisor Professor Christis Z. Chrysostomou for the opportunity to pursue a PhD under his guidance and for his unparalleled assistance, inspiration, and encouragement for this research during these years. The impetus for this research came from his desire to understand the complex behavior of masonry-infilled frame structures, an interest that I have inherited over the last five years. This research was achieved by his expertise, and I have thoroughly enjoyed tackling challenging problems under his mentorship. Professor Christis Z. Chrysostomou did not only provide me with his exceptional guidance and help me develop critical thinking, but he also taught me how to be a researcher.

I would also like to express my sincere thanks to Dr. Nicholas Kyriakides (Associate Professor) for his interest, encouragement, and insight during the writing of the thesis. His experience, scientific knowledge and ideas have, without doubt, significantly influenced my research.

Additionally, I am pleased to acknowledge several others who contributed directly or indirectly to this research. I thank my research committee members, Dr. Elia A. Tantele (Associate Professor) and Dr. Georgios Constantinides (Associate Professor) for reviewing this work. I also thank my examination committee members Dr. Diofantos G. Hadjimitsis (Professor) and Dr. Ioannis Ioannou (Professor).

I also thank Dr. Rogiros Illampas for his friendship, support and useful questions and comments through the learning process for these years.

This work has been performed with the help of all my friends and I would like to thank them for their encouragement during these years. I would like to explicitly express my appreciation to Constantinos and Elena who have always been there for me, in both good and difficult times. Their continuous support, positivism, and belief in me have

given me the strength and energy to achieve my goals. I would like to thank my friends Gregoria, Maria, Iro, Thekla, Christina, and Iliana for their support throughout the years and for helping me to disconnect from this demanding job keeping me accompanied during the writing of the thesis.

Finally yet importantly, I would like to thank my family for their unconditional love and affection throughout my life. Thanks for everything they have done for me without whose support this work would never had been possible to achieve. My mother and my father have been throughout the years low-profile heroes who always made sure I had everything needed to focus on my studies. The sacrifices they have made are a priceless lesson for life. Special thanks to my brothers Marinos and Dr. Theodoros who have been at my side along these years. I wish to express my appreciation to my brother Theodoros for his encouragement and insight during the writing of the thesis.

ABSTRACT

Most of the existing reinforced concrete buildings with masonry infill walls around the world have been built before the development of new seismic regulations posing them more susceptible to collapse during an earthquake event. For this reason, the seismic retrofitting of existing infilled frame buildings is nowadays one major challenge of earthquake risk mitigation.

Over the past decade, the Textile Reinforced Mortar (TRM) composite material, encompassing a combination of inorganic matrix (lime- or cement-based) and non-corrosive multi-axial textile fabrics, has emerged as a promising novel alternative for seismic retrofitting of masonry-infilled RC frame buildings. Nevertheless, a deeper investigation in the research area of TRM is required considering the lack of design guidelines, the limited existing research regarding the use of TRM for retrofitting masonry-infilled RC frames, and the need to enhance the implementation of this composite material as a regular method for retrofitting existing buildings in practical engineering.

In this context, the present study focuses on investigating numerically the seismic retrofitting of masonry-infilled RC frames using TRM. Essential step towards this direction is the development of a simplified model able to predict the tensile behavior of TRM.

The study conducted herein has three main contributing parts. In the first part, a new simple and easy to-implement analytical model able predict the tensile behavior of TRM in terms of stress-strain is proposed. The proposed model, which extends an established model that applies for fiber-brittle matrix to TRM, using recommendations for reinforced concrete, proved accurate, since the analytical curves properly fit with those obtained from relevant available experimental studies. A parametric study is also performed to examine the sensitivity of the proposed model to a range of parameters. In the second part of this study, a detailed finite element model of the masonry-infilled RC frame, with and without TRM, considering the infill-frame interaction and the non-linear behavior of the constituent components of the structure, and using the proposed analytical model of TRM to define the tensile behavior of TRM, has been developed and validated using selected experimental study conducted in the past. Sensitivity

analyses are then performed to examine the behavior of integral and non-integral infilled frames subjected to in-plane cyclic loading, and to investigate the influence of the stiffness properties of the infill-frame interface on the in-plane cyclic response of retrofitted infilled frame model. The third part of the study focuses on investigating numerically the parameters that affect the in-plane behavior of masonry infilled-RC frames retrofitted with TRM under cyclic loading such as: the TRM reinforcement ratio and the type of mortar used for binding the textile reinforcement. Furthermore, the effect of the presence of different size of central opening on the lateral response of masonry-infilled RC frames subjected to cyclic loading is studied, and the use of TRM for retrofitting masonry-infilled RC frames with openings is also investigated by carrying out numerical experiments. As part of this study, a detailed review of the broader literature in the area of infilled frames and in the area of TRM as a composite material, and as a method for retrofitting masonry-infilled RC frames was undertaken.

As a result of this research work, it was concluded that the TRM can be considered as a suitable method for seismic retrofitting masonry-infilled RC frame buildings with and without openings. Moreover, the proposed analytical model of TRM can be useful to facilitate the implementation of numerical models of retrofitted structures using TRM, and further to develop design guidelines. The research work, presented in this thesis, is valuable as it contributes to expand the knowledge related to TRM, while promoting the prospective use of this novel material for retrofitting existing structures.

Keywords: Textile Reinforced Mortar (TRM); masonry-infilled RC frames; openings; cyclic loading; non-linear analysis; finite element modeling; analytical modeling.

TABLE OF CONTENTS

LIST OF TABLES

LIST OF FIGURES

CHAPTER 1

1. INTRODUCTION

1.1 Global context

Reinforced concrete buildings with masonry infill walls is the most usual construction typology globally dispersed for commercial, industrial, and family residential use. Most of them are located in high seismic regions such as; the Mediterranean Europe, the Middle East, New Zealand and South Asia. Observations from past earthquakes proved the vulnerability of these buildings due to the high degree of damage observed causing casualties and high economic losses. The vast majority of the existing masonry-infilled reinforced concrete (RC) frame buildings around the world have been built before the development of new seismic regulations, posing them more susceptible to collapse during an earthquake event. However, masonry infill walls are usually considered as non-structural elements in the analysis and design process, although in a seismic event, they carry in-plane and out-of-plane loads. Considering the common construction of masonry-infilled RC frames in several countries, it is of utmost importance to evaluate the seismic performance and to seismically retrofit such type of buildings.

The seismic retrofitting of masonry-infilled RC frame buildings is nowadays a challenging engineering problem. Over the years, different retrofitting approaches have been proposed and used so that these buildings can be enhanced to satisfy the modern seismic design codes. However, many of these approaches do not fit with the economic demands of the buildings' owners or technical knowledge of the workmanship due to the inherent complexity of various methods, and due to difficulties to implement with regards to the building configuration. Owing to the need for introducing innovative materials, recently, the Textile Reinforced Mortar (TRM) composite material has received attention, as a sustainable solution for retrofitting RC and masonry structures.

The TRM composite material, encompassing a combination of inorganic matrix (lime- or cement-based) and non-corrosive multi-axial textile fabrics, has emerged as a promising novel alternative for seismic retrofitting of masonry-infilled RC frame buildings. The variety of the types of fibers used for assembling the textile reinforcement and of the matrix used for binding the textile reinforcement, leads to a wide range of possible mechanical properties of the TRM composite material. The use of TRM for seismic retrofitting infilled frames is a relatively new concept, and therefore, a deeper investigation is required.

Being aware of the importance of masonry infill wall on the response of infilled frame buildings under earthquake loads, in the last few years, the new codes include some provisions regarding the influence of infill walls on the seismic response of infilled frames. Eurocode 8 (EC8-1) is the first seismic design code which introduced design principles for masonry-infilled RC frame buildings and detailed rules for the application of these principles. Guidelines for the seismic evaluation of masonry-infilled RC frames have been provided in reports published by the Federal Emergency Management Agency (FEMA) 273, 306 and 368, International Building Code (IBC 2018) and by the American Society of Civil Engineers (ASCE) 41-17. Furthermore, the new codes include essential guidance for retrofitting existing buildings due to the urgent need for improving their seismic performance. Guidelines for seismic retrofitting of structural or non-structural components of a building have been provided in reports published by Eurocode 8–part 3 (EC8-3), FEMA 308 and (ASCE) 41-17. The recent design guidelines reported by the American Concrete Institute (ACI) 549-13 includes a simplified approach regarding the application of TRM.

Considering the lack of design guidelines and the limited research regarding the use of the TRM for seismic retrofitting masonry-infilled RC frame buildings, and the need to enhance the implementation of this composite material as a regular method for retrofitting existing buildings in practical engineering, there is an urgent need to extend today’s knowledge regarding the effectiveness of using the TRM to reduce the seismic vulnerability of masonry-infilled RC frame buildings.

1.2 Research motivation and objectives

During the last decade, the TRM as a novel approach for retrofitting RC and masonry structures has received great attention in the scientific world. Although significant research has been conducted and reported for retrofitting columns, beams, and masonry walls using TRM, much less has been carried out for masonry-infilled RC frames. More specifically, experimental or numerical studies aiming to investigate the effectiveness of TRM to improve the lateral response of masonry-infilled RC frames, under either monotonic or cyclic loading, are still regarded very limited. Adding to this, none of either past experimental or numerical studies were geared towards the retrofitting of masonry-infilled frames with openings using TRM. Therefore, to enhance the implementation of TRM as a regular method for retrofitting existing buildings in practical engineering, a crucial step is to expand today's knowledge regarding the retrofitting of masonry-infilled RC frames with TRM, and to assess the effectiveness of using the TRM composite material for retrofitting infilled frames with openings, as well.

Despite the evolution of using the TRM as a sustainable and compatible solution for retrofitting RC and masonry structures, and the several experimental studies conducted so far towards the mechanical characterization of TRM composite material, a simplified model able to predict the mechanical behavior of this composite material has not yet been developed. Consequently, the implementation of numerical models of retrofitted structures using TRM is difficult to be achieved. Numerical tests are necessary in order to study in more depth this method by taking into account all the possible critical parameters able to affect the effectiveness of using the TRM for the seismic retrofitting of RC and masonry structures without performing experimental tests which are economically prohibitive and timely. It is important to mention that the existing codes do not cover design matter with a systematic approach regarding the application of TRM, and there are only some over-simplified approaches, such as the International Code Council (ICC-Evaluation Service 2013) and ACI 549. Therefore, a simple and easy to-implement model to define the stress-strain relationship of TRM under tensile loading is important to be developed in order to facilitate the implementation of

numerical models of retrofitted structures using TRM, and further to develop design guidelines for RC and masonry structures retrofitted with TRM.

Taking into consideration all the above, there is a global need to study in more depth the effectiveness of using the TRM composite material for the seismic retrofitting of existing buildings. In this context, the general motivation of this thesis is summarized as follows:

- To develop a simplified analytical model, able to predict the tensile behavior of TRM composite material in terms of stress-strain;
- To identify and assess the critical parameters that are able to influence the effectiveness of TRM for the seismic retrofitting of masonry-infilled RC frames;
- To assess the effectiveness of using the TRM for retrofitting of masonry-infilled RC frames with and without openings.

Based on the above points, the aim of this research reported herein is twofold: (1) create a simplified model able to predict the behavior of TRM under tensile loading, and (2) assess the effectiveness of using the TRM composite material for retrofitting masonry-infilled RC frames with and without openings. To achieve this aim, the following objectives need to be addressed:

Develop and assess a simple and easy-to-implement analytical model able to define the stress-strain relationship of TRM under tensile loading, without any required information from experimental tests, and examine the sensitivity of the proposed model to a range of parameters.

Develop a detailed finite element model of an experimentally tested 2/3 scaled three-story masonry-infilled RC frame with and without TRM considering the infill-frame interaction and the non-linear behavior of the constituent components of the structure, and using the proposed analytical model of TRM to define the tensile behavior of TRM.

Validate the developed numerical models by comparing the numerical results with those obtained from the selected experimental case-study conducted in the past, and examine the behavior of integral and non-integral infilled frames subjected to cyclic loading, and the influence of the stiffness properties of the infill-frame interface on the in-plane cyclic response of retrofitted infilled frames.

Investigate numerically the parameters that affect the in-plane behavior of masonry infilled-RC frames retrofitted with TRM under cyclic loading such as the TRM reinforcement ratio and the type of mortar used for binding the textile reinforcement.

Investigate numerically the effect of the presence of different size of central openings on the lateral response of masonry-infilled RC frames subjected to cyclic loading, and the use of TRM for the seismic retrofitting of masonry-infilled RC frames with openings.

This study aims to meet these objectives in order to bridge the literature gap regarding the retrofitting of masonry-infilled RC frame buildings using TRM.

1.3 Dissertation outline

This dissertation consists of three main thematic sections as follows: (a) the development and the assessment of a simple analytical model able to predict the tensile behavior of TRM in terms of stress-strain; (b) the development and the validation of a finite element (FE) numerical model of masonry-infilled RC frame with and without TRM; and (c) the parametric study, through numerical experiments, aiming to examine the critical parameters that influence the effectiveness of TRM for retrofitting masonry-

infilled RC frames, and to investigate the effectiveness of using the TRM for retrofitting masonry-infilled RC frames with openings. Following the above-mentioned thematic sections, this thesis is divided into eight chapters, as described below.

Chapter 1 begins with the background and motivations of this research and presents the objectives and the significance of the current study. Chapter 2 provides a review of previous research so that the research objectives of this thesis can be contextualized. This Chapter presents the failure mechanisms and the possible failure modes that may occur on masonry-infilled RC frames subjected to lateral loading. Furthermore, Chapter 2 gives an overview of the experimental investigations found in the literature regarding the lateral response of infilled frames. The modeling strategies proposed by researchers, so far, for representing masonry-infilled frames are also given in this Chapter. Chapter 2 concludes with a broad overview of the experimental and numerical studies conducted so far regarding the use of TRM for the retrofitting of masonry-infilled RC frames.

Chapter 3 provides sufficient background knowledge of TRM as a composite material, regarding its constituent materials and its mechanical characterization, and the numerical and analytical models that exist so far for representing this composite. Next, Chapter 3 presents a simple and easy to implement analytical model, able to define the stress-strain relationship of TRM under tensile loading. The proposed analytical model extends the Aveston-Cooper-Kelly (ACK) theory, which applies for fiber-brittle matrix to TRM, using the recommendations proposed by Eurocode 2 and *fib* Model Code 2010 for predicting the crack spacing and the fracture energy of the composite material, respectively. The assessment of the proposed model is discussed by comparing its results with those obtained by studies conducted in the past. Chapter 3 concludes with a parametric study regarding the parameters that can influence the tensile behavior of TRM according to the proposed model.

Chapter 4 comprises a detailed description of the development of the FE model of masonry-infilled RC frame with and without TRM. Firstly, the experimental case-study used for calibration purposes in the current study is presented. Then, the choice of the commercial software used for the purpose of this study is discussed. The assumptions considered for the development of the numerical models are also included in this

Chapter. A brief description of the type of elements and material models used for the development of the numerical models is given in this Chapter. Chapter 4 presents also the validation of each of the material models used in this study using relevant experimental tests. Finally, the constrains and loading scheme considered in the masonry-infilled RC frame model with and without TRM, and the type of analysis used in this numerical study, are described in Chapter 4.

Chapter 5 is composed of the validation of the numerical models, and of the discussion of the results obtained from the numerical analyses. The results obtained from the linear static, eigenvalue, and cyclic non-linear analysis of the bare frame model, and of the masonry-infilled RC frame model, with and without TRM, are presented and compared with the results obtained from the selected experimental case-study conducted in the past, at global and local level. After the validation of the masonry-infilled RC frame model with and without TRM, sensitivity analyses are performed to examine the behavior of integral and non-integral infilled frames subjected to cyclic loading, and to investigate the influence of the stiffness properties of the infill-frame interface on the in-plane cyclic response of retrofitted infilled frames.

Chapter 6 includes the parametric study through numerical experiments for examining the critical parameters that are able to influence the effectiveness of TRM for the seismic retrofitting of masonry-infilled RC frames. Numerical experiments are performed, using the validated numerical model, to investigate firstly the influence of the amount of external TRM reinforcement ratio, by means of using the different number of TRM layers and different geometry of textile reinforcement on each floor of the structure (changing the strengthening scheme), and secondly to examine the effect of using different types of cement-based matrix for binding the textile reinforcement on the in-plane lateral response of a three-story masonry-infilled RC frame retrofitted with TRM under cyclic loading.

Chapter 7 presents the effectiveness of using the TRM as a retrofitting method for masonry-infilled RC frame buildings with openings. Firstly, numerical experiments are performed to investigate the effect of the presence of different size of central opening on the lateral response of a three-story masonry-infilled RC frame under cyclic loading.

The results obtained from these numerical tests are discussed and compared with those obtained from the relevant studies available in the literature. Then, the effectiveness of using the TRM as a retrofitting technique for infilled frames with openings is investigated, by performing numerical experiments on the three-story masonry-infilled RC frame model with different size of central openings retrofitted with TRM under in-plane cyclic loading.

Chapter 8 presents an overview of the current study and summarizes the findings and conclusions obtained for each of the different tasks of this research. Recommendations for future research are also pointed out.

Appendices are included at the end of this dissertation to provide additional data and information that were generated in this study.

1.4 Significance of the research

The present study aims to investigate numerically the effectiveness of using the TRM to reduce the seismic vulnerability of masonry-infilled RC frame buildings. A vital step to achieve this aim is the development of a simplified model able, to predict the tensile behavior of TRM composite material. This study provides research innovation due to the following:

- The proposed simple analytical model of TRM, able to estimate the tensile behavior of TRM in terms of stress-stain, contributes to facilitate the implementation of numerical models of retrofitted structures using TRM, and opens the door to expand the application of the new composite material by the engineering community, and to develop design guidelines;
- The detailed FE numerical model of masonry-infilled RC frame with and without TRM developed in this study can be treated parametrically in order to perform numerical tests, which are necessary to study in more depth this method without performing experimental tests which are economically prohibitive and timely;
- The numerical investigation of the response of integral and non-integral infilled frames subjected to cyclic loading, and of the influence of infill-frame interface

properties on the in-plane cyclic response of retrofitted infilled frame model facilitates the clarification of the complex issue of the masonry infill-frame interaction;

- The numerical investigation of the effect of the TRM reinforcement ratio and of the type of mortar used for binding the textile reinforcement on the in-plane cyclic response of masonry-infilled RC frames retrofitted with TRM expands today's knowledge regarding the parameters able to influence the TRM's efficiency;
- The numerical investigation of the effect of central openings on the lateral response of masonry-infilled RC frames subjected to cyclic loading enhances today's knowledge regarding the lateral response of infilled frames with openings;
- The assessment of the effectiveness of TRM for the seismic retrofitting of masonry-infilled RC frames with openings contributes to expand the use of this composite material as a regular method for retrofitting existing buildings.

The findings from the current study make several contributions to the existing literature. Particularly, this thesis consists of an extended summary of the following papers:

- Filippou, C. A., Kyriakides, N. C. and Chrysostomou, C. Z. (2018): 'Finite element model of masonry-infilled RC frame',16th European conference on Earthquake engineering, June 2018 Thessaloniki, Greece
- Filippou, C. A., Kyriakides, N. C and Chrysostomou, C. Z. (2019): 'Numerical Modeling of Masonry-infilled RC Frame',The Open Construction and Building Technology Journal, doi: 10.2174/187483680191301
- Filippou, C.A, Chrysostomou, C.Z and Kyriakides, N. (2019): 'Numerical Modeling of Masonry-Infilled RC Frame Strengthened With TRM', 7th ECCOMAS Thematic Conference on Computational Methods in Structural Dynamics and Earthquake Engineering, June 2019, Crete, Greece
- Filippou, C. A., Kyriakides, N. C. and Chrysostomou, C. Z. (2020) 'Numerical Modeling and Simulation of the In-Plane Response of a Three-

Storey Masonry-Infilled RC Frame Retrofitted with TRM', Advances in Civil Engineering, 2020. doi: 10.1155/2020/6279049

- Filippou, C., Kyriakides, N. and Chrysostomou, C. Z. (2020) 'Effect of connection detail at interface of masonry- infilled RC frames retrofitted with TRM', 17th World Conference on Earthquake Engineering, 17WCEE September 2020,Sendai, Japan
- Filippou, C. A. and Chrysostomou, C. Z. (2020) 'Analytical model for textile reinforced mortar under monotonic loading', Construction and Building Materials Journal doi: 10.1016/j.conbuildmat.2020.120178
- Filippou, C. A., Kyriakides, N. Chrysostomou, C. Z. (2021): 'Strengthening of masonry-infilled RC frames with openings using TRM', under review in Bulletin of Earthquake Engineering journal, BEEE-D-19-00411R2
- Filippou, C. A., Furtado, A, Teresa, Kyriakides, N.C and Chrysostomou, C. Z. (2021) 'Seismic retrofitting of masonry-infilled RC frames using textile reinforced mortars (TRM): an experimental and numerical studies overview' under review in Journal of Earthquake Engineering.

CHAPTER 2

2. LITERATURE REVIEW

2.1 Introduction

Following the main scope of this thesis, a general review of the existing research in the area of masonry-infilled RC frames and in the area of TRM as a retrofitting method for masonry-infilled RC frames is definitely necessary in order to cover the literature background of the research objectives of this study, as described in previous section.

Firstly, a general review is presented regarding the failure mechanisms observed on masonry-infilled RC-frame buildings during an earthquake and the possible failure modes that may occur on infilled frames under lateral loading (section 2.2). The literature review is then extended to past experimental studies aiming to investigate the response of masonry-infilled frames under different loading conditions, and the effect of infill walls on the lateral response of RC frames (section 2.3). This is followed by a brief review of the modeling strategies available today for simulating infilled frame structures (section 2.4). An extensive overview of the published experimental and numerical studies regarding the retrofitting of masonry-infilled RC frames using TRM is also presented (section 2.5). Finally, a summary of the literature review is presented (section 2.6).

2.2 Failure mechanisms and failure modes of masonry-infilled RC frames

The seismic performance of masonry-infilled RC frame buildings is an intricate issue, which has attracted the attention of structural engineers since the 1950's due to the variety and complexity of observed failure mechanisms on this type of buildings during an earthquake. Despite the several decades of research regarding the assessment of the seismic performance of masonry-infilled RC frames, the exact role of masonry infill

wall in a RC building during an earthquake is not yet clearly understood, and it therefore remains a major issue in the structural engineers' community. For the purpose of this research, it is important to study the failure mechanisms and the possible failure modes of masonry-infilled RC-frame buildings under lateral loading in order to develop an accurate numerical model able to predict the response of masonry-infilled RC frames, with and without openings, under cyclic loading, and in order to evaluate appropriate retrofitting techniques for this type of structural system.

The seismic vulnerability of infilled frames was investigated by several researchers, and most of them tried to examine the contribution of infill walls on the response of RC frames under lateral loading. They concluded that the existence of masonry infill wall in RC frame contributes to an increase in the lateral capacity of the building and, at the same time, it may introduce brittle shear failure mechanisms associated with the infill-frame interaction. The irregular distribution of the infill wall in plan and elevation in RC frame buildings can be addressed as one of the main causes of the structural collapse observed during an earthquake (Romão et al. 2013), since different types of failure mechanisms occur on infilled frames due to large concentration of demand in a few members of the structure, such as: (a) *soft-story mechanism* (Syrmakezis and Asteris 2001), where the stiffness at lower floors is smaller than the stiffness at the stories above (Figs.2.1 a); b) *short-column mechanism* (Asteris et al. 2013), where the infill wall is shorter than the column height (Fig. 2.1 b); and c) *plan torsion effect* (Chiou et al. 1999), where the infills are located in plan in a building asymmetrically.

(a) (b)

Figure 2.1: Typical failure mechanisms of masonry-infilled RC frame buildings: (a) *soft-story mechanism* (Çağatay 2005) and (b) *short-column mechanism* (Pradhan et al. 2012).

A common example of the irregular distribution of the infill wall in elevation in RC frame, all over the world, is called *pilotis*, where there are infill walls in all the stories of a frame except for the base story, that is typically used as a commercial or parking area. Adding to the above-mentioned failure mechanisms, when the infill wall is restrained by a frame, it can develop significant out-of-plane resistance causing the *arching effect*, which is mainly dependent on the slenderness of the infill wall (Dawe and Seah 1989; Angel 1994; Shing and Mehrabi 2002; Da Porto et al. 2013).

It is important to mention that the infill wall is usually treated as a non-structural element and its interaction with the bounding frame is ignored in the seismic design of such structural systems. The presence of infill-walls in RC-frames usually considered in the design of buildings only through the application of additional loads distributed along the beams and columns of bounding frames. Although, the masonry infills are designed primarily to carry vertical loads within the structure, in a seismic event, however, they also carry in-plane shear or out-of-plane flexural loads resulting from the earthquake (Palieraki et al. 2018, Donà et al. 2017), the out-of-plane failures turning out to be more disastrous than the in-plane ones (Dawe and Seah 1989; Shing and Mehrabi 2002; Basha and Kaushik 2016b; Zuccaro et al. 2017; Palieraki et al. 2018).

For the purpose of this research, the in-plane failure of infilled frames is discussed in more detail, since the out-of-plane one is beyond the scope of this research. Past studies showed that at early stage of lateral loading, the infill wall separates from the surrounding frame (Fig. 2.2 a) and a diagonal compression diagonal path develops along the two opposite loaded corners of the infill wall (i.e., the infill wall acts as a diagonal strut, as will be mentioned in sections 2.3 and 2.4), and as the lateral load is increased, failure occurs eventually in either the frame or the infill wall. Most researchers, (Merhabi et al. 1996; Crisafulli 1997; Shing and Mehrabi 2002; El-Dakhakhni et al. 2003; Asteris et al. 2011) reported that, when an infilled frame is subjected to lateral loads, five distinct modes of failure (Fig. 2.2) are possible:

- *Frame failure mode* associates with a weak frame, or with weak joints in the frame, or with strong frame infilled with a strong infill wall, where plastic hinges in the beams and columns near the joints are developed, or failure of

beam-column joints occur, or failure at the column mid-height occur with horizontal sliding cracks at the mid-height of the infill wall. The last one introduces a *short-column mechanism*, as previously described.

- *Infill sliding shear failure mode*, associates with weak mortar joint of the infill bounded with strong frame, where horizontal sliding cracks develop through bed joints. This failure mode can result in the ductile behavior of infilled frames, provided that the brittle shear failure of the columns can be avoided.
- *Infill diagonal compression failure mode* associates with weak slender flexible infill walls, where crushing in the central region of a wall takes place. This failure mode is accompanied by out-of-plane deformation.
- *Corner crushing failure mode* associates with strong frame with weak infill, and it consists of crushing in a loaded corner area of the infill wall due to a biaxial compression state. A *corner crushing failure* is characterized by the compressive failure of the infill wall.
- *Infill diagonal cracking failure mode* take places when the frame is more flexible than the infill wall, or in a frame with weak joints where cracking develops along the compressed diagonal of the infill wall. More specifically, stair-step-type diagonal cracking along the mortar bed and head joints develop. The diagonal cracking failure mode often takes place with simultaneous initiation of *sliding shear failure mode*.

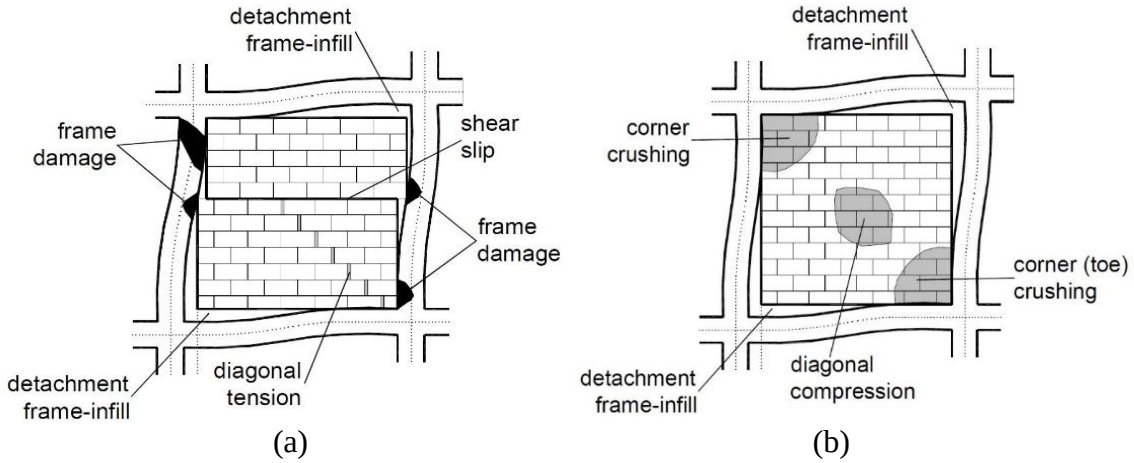

Figure 2.2: Failure modes of infilled frames (a) *Sliding shear*, *diagonal cracking* and *frame failure* mode and (b) *Conner crushing* and *diagonal compression* failure mode (Asteris et al. 2011).

It should be noted that these failure modes are only applicable to the case of infilled frames without openings. Several researchers, who studied the behavior of infilled frames with openings under lateral loading, concluded that the failure modes and crack patterns of infilled frames with openings are affected by the location and the size of the opening (Buonopane and White 1999; Chiou et al. 1999; Kakaletsis and Karayannis 2009; Asteris et al. 2011; Nila et al. 2018). They also reported, that when infilled frames have window or door openings, at early stage of lateral loading, detachment of the infill wall from the surrounding frame is observed (i.e., the infill acts as two or three diagonal struts), while *diagonal compression* (crushing of masonry segments between columns and openings), *diagonal cracking* and *sliding shear failure* mode are possible to occur, due to the development of diagonal and sliding cracks along the bed joints in the infill wall above and below the opening. As the lateral load is increased on infilled frames with openings, the cracking which occurs at the corner of the openings propagate towards the loaded corners of the infill wall leads to *corner crushing* and *frame failure* mode. The existence of an opening in an infill wall may create unfavorable effects, depending on its location and size, while the *short-column mechanism* is typical for some types of windows, since the infill walls are not continuous through the height of the frame (Asteris et al. 2011).

To conclude, the existence of infill walls in RC frames can introduce brittle shear failure mechanisms associated with the infill-frame interaction, such as *soft-story mechanism*, *short-column mechanism* and *plan torsion effects*, while five failure modes are possible to occur on infilled frames, with and without openings, under lateral loading. Many researchers have studied the behavior of infilled frames under lateral loading in order to identify the parameters influencing their behavior as will be discussed in the following section.

2.3 Experimental investigations of masonry-infilled RC frames

Over the years, several experimental and in-situ tests have been carried out aiming to evaluate the effect of infill walls on the response of frame buildings under lateral loading and to define the parameters that are able to influence the seismic performance of infilled frames. Following the objectives of the current research, some of the past

experimental studies which focused on the in-plane behavior of infilled frames, with and without openings, under monotonic and cyclic loading are reviewed in this part of the thesis, since some of these studies will be used to calibrate the material models used in this numerical study and to assess the masonry-infilled RC frame model with and without openings. The following general review is not intended to be an exhaustive summary of the literature, since this is not necessary for the purpose of this research.

The complex nature of the interaction between concrete or steel frames with masonry infill walls under lateral loads has been studied since the late 1950s'. Polyakov (1956) was the first who identified the structural importance of infill walls through large–scaled tests on masonry-infilled steel frames (test program carried out from 1948 to 1953). He reported that the lateral response of infilled steel frames is affected by several parameters such as: the type of masonry units, the type of mortar, the presence of openings and the type of loading (monotonic and cyclic). In the same period, Thomas (1953) and Wood (1958) demonstrated through their experimental campaigns that a relatively weak infill wall can contribute significantly to the stiffness and strength of a flexible RC frame. Later, Polyakov (1960) performed tests on a three-bay, three-story infilled steel frames and observed that the infill wall separated from the surrounding frame, so that a diagonal compression path developed along the two opposite corners of the infill wall. Polyakov was the first to suggest that the infilled frame works as a braced frame and that the masonry infill wall could be represented by a diagonal no-tension strut element (Fig. 2.10 in the following section). Furthermore, Holmes (1961) confirmed Polyakov's suggestion regarding the formation of a strut mechanism, while the aforementioned author proposed predictive equations for the width of the equivalent strut, as will be discussed in the next section. The experimental study conducted by Stafford Smith (1962) showed that the infill wall separated from the frame over three-quarters of the length of the frame members. Author also confirmed Polyakov's suggestion regarding the development of a diagonal compression path along the two opposite corners of the wall (Fig. 2.3 a). Later, Stafford Smith (1966, 1967) performed another set of tests on small-scale infilled steel frames with different dimensions of the columns and beams, and developed an analytical approach to predict the lateral stiffness and strength of infilled frames, based on an equivalent strut concept, using an

alternative method to the one of Polyakov (1960) for calculating the effective width of the diagonal strut. After Polyakov's suggestion regarding the strut mechanism, many researchers performed experimental studies to examine the behavior of infilled frames under lateral loading, and most of them developed analytical models (predictive equations) to estimate the width, the mechanical properties, the number, the configuration and constitutive laws (hysteretic models) of the equivalent struts. Some of them will be presented in the next section (Mallick, and Severn 1967; Mainstone 1971; Mainstone and Weeks 1970; Kadir 1974; Bertero and Brokken 1983).

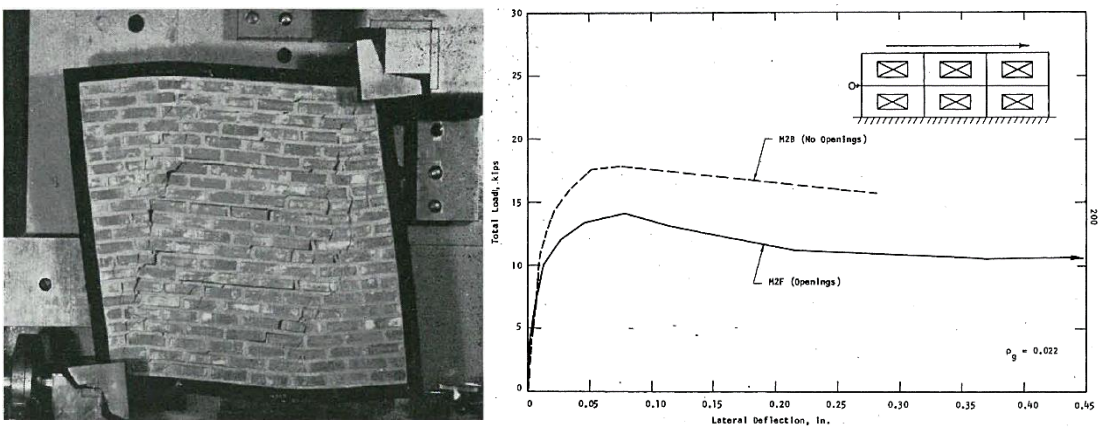

(a) (b)

Figure 2.3: (a) Formation of diagonal strut mechanism in infilled steel frames (Stafford-Smith 1966), and (b) Lateral load versus displacement for infilled frames with and without opening (Fiorato et al. 1970).

Fiorato et al. (1970) tested 1/8-scale masonry-infilled RC frames under monotonic lateral loading, in order to examine the influence of various parameters such as: the number of stories, the number of bays, the reinforcement detailing in RC frame, and the existence of openings in infill walls. The results showed that infill walls increase the stiffness and the strength of RC frames, while the presence of an opening in an infilled frame resulted in a more flexible system with lower lateral capacity, compared to the infilled frame without opening, as shown in Fig. 2.3 (b). The influence of openings and of their position on the in-plane behavior of masonry-infilled frames under lateral loading was also examined by Mallick and Garg (1971). These authors demonstrated that, if an opening is provided at either end of the loaded diagonal of a non-integral infilled frame its lateral strength and stiffness is reduced by about 70%-80%, while this reduction is about 60%-70% for an integral infilled frame. In addition, the results

showed that the loss of the strength and stiffness for both types of infilled frames due to a centrally located square opening having dimension one-fifth of the infill wall is about 25%-50%, compared to infilled frames without opening. They also concluded that the interaction between frame and infill wall is adversely affected as the opening position is moved towards the compression diagonal. Furthermore, Liauw (1972) reported that openings with a width of one-fifth that of the wall cause a reduction on the stiffness of an integral infilled frame by about 43%, and by about 62% in the case of a non-integral infilled frame. Moreover, both Mallick and Garg (1971) and Liauw (1972) showed that the reduction on the lateral capacity of the infilled frames due to openings is larger for a non-integral infilled frame, compared to an integral one. In the same concept, Dawe (1985) investigated the effect of the opening location on the behavior of masonry-infilled steel frames under lateral loading, and recommended that the best location for a window or door opening is at the center of the infill wall, because if the opening interrupts the compression diagonal it gives an opportunity for two diagonal struts to develop in the infill wall.

Liauw (1979) and Liauw and Kwan (1983,1984) studied experimentally and analytically the effect of shear connectors (using anchors) on the behavior of four-story infilled steel frames under cyclic loading. They concluded that the presence of connectors at the infill-frame interface increases the stiffness, strength and the ultimate load (40%-50%) of the infilled frame, while the slip and the gap-opening between infill wall and frame is increased when no connectors are provided leading, to a decrease in dissipated energy. In a subsequent paper, Liauw and Kwan (1992) concluded that the masonry infill walls contribute to an increase in the strength of RC frames, testing of a 1/3-scale infilled RC frame under seismic loading.

Bertero and Brokken (1983) found that the presence of an infill wall in RC frame increases its lateral stiffness, strength, and lateral resistance, testing of a 1/3-scale three-story, one-bay masonry-infilled RC frame, under quasi-static cyclic and monotonic loads (Fig. 2.4 a). Their results showed that the response of the infilled frame under lateral loading was influenced by the way the infill was fabricated, including the quality of the materials, and by the interface between the infill wall and the bounding frame. Furthermore, Zarnic and Tomazevic (1988) conducted cyclic tests on bare frames and

on masonry-infilled RC frames and found a significant increase about 80% on the lateral capacity of RC frames due to the existence of infill walls. They also demonstrated that, after the development of diagonal cracks on the infill wall, the infill does not contribute significantly to the increase of the lateral capacity of the frame. Based on the above observations, they concluded that, when an infilled frame is subjected to large lateral loading, the frame takes significant part of the lateral load, leading to shear failure of the column, and to a significant reduction of the stiffness of the structure, as shown in Fig. 2.4 (b).

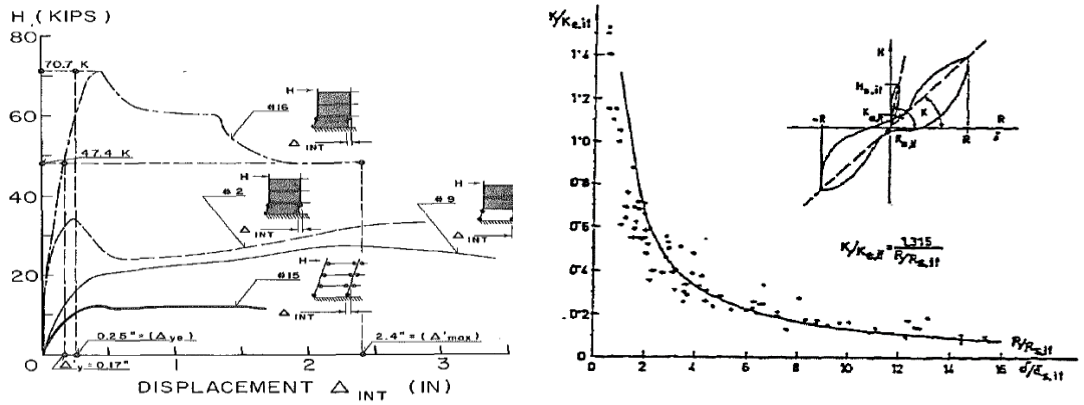

(a) (b)

Figure 2.4: (a) Lateral load versus inter-story drift ratio for four different infilled frames tested by Bertero and Brokken (1983), and (b) stiffness degradation of the infilled frame under cyclic loads (Zarnic and Tomazevic 1988).

Mehrabi et al. (1994) conducted monotonic tests on 1/2-scale infilled RC frames, aiming to investigate the influence of various parameters, such as: the relative strength and stiffness of the infill with respect to those of the bounding frame, the lateral load history, and the aspect ratio of the infill wall. In the same concept, Merhabi et al. (1996) carried out an experimental study on 12 half-scale, single story, one or two-bay bare and masonry (hollow or solid blocks) infilled RC frames, under monotonic and cyclic loading. The results showed that the lateral capacity of infilled frames is higher, compared to that of bare frames. In addition, the authors observed that specimens with strong frames and strong infill walls had larger load resistance and dissipated energy than those with weak frames and weak infill walls, as shown in Fig. 2.5. From the experimental results obtained from both studies, it is observed that if the infill wall is stiff with respect to the frame, and the columns are not ductile, a shear failure in the

frame may suddenly occur, while when the frame elements are flexible, the infill wall is expected to fail leading to a ductile behavior. Later, Shing and Mehrabi (2002) reported the possible failure modes which can be observed on infilled frames, as described in the previous section.

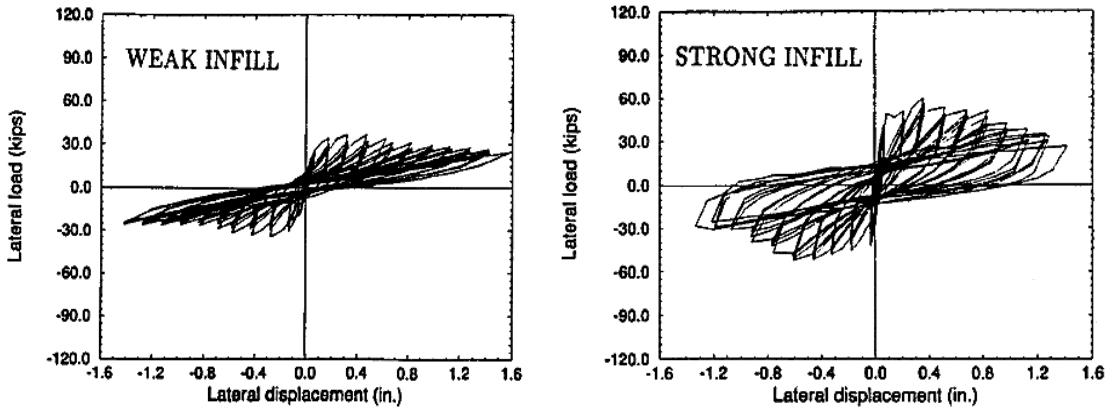

(a) (b)

Figure 2.5: Lateral load versus displacement for (a) weak frames and weak infill walls and (b) for strong frames and strong infill walls (Merhabi et al. 1996).

Mosalam et al. (1997) tested one and two-bay, and one and two-story masonry-infilled steel frames, under quasi-static and pseudo-dynamic loading, using different types of infill walls (mortar and bricks) and various geometrical configurations of the frame and the infill wall. The results from this study showed that the relative strength of concrete blocks with respect to mortar joints significantly influences the mode of failure of the infilled frame. In terms of the influence of the number of bays, the ultimate capacity of the two-bay structure was two times greater than that of the single-bay structure and its initial stiffness was 1.7 times higher. Also, the authors concluded that the presence of openings in infilled frames leads to more ductile behavior and reduces the stiffness of solid infilled frames by about 40%. Later, Hashemi and Mosalam (2006) performed a shake-table test on a 3/4-scale, one-bay masonry-infilled RC frames and concluded that the presence of an infill wall in RC frame contributes to increase its stiffness and damping coefficient by 3.8 and 2 times, respectively.

The lateral response of infilled RC frames was also examined by Chiou et al. (1999) where three specimens RC bare frame, partially filled frame with window opening and full infilled frame were subjected to in-plane monotonic loading. The results showed

that the mortar joints influence the failure mode of the infilled frame. The same observation is reported in Mosalam et al. (1997a, b). In the partially filled frame a *short-column mechanism* was observed, as shown in Fig. 2.6 (a). The full infilled frame showed higher stiffness and strength than the other two specimens. In the same period, pseudo-dynamic tests on a half-scale, two-story, two-bay infilled RC frames with window openings at the second story were performed by Buonopane and White (1999). From the experimental results, it was observed that *sliding shear* and *diagonal cracking failure mode* occurred on the infilled frame, accompanied by the shear failure of the columns, while different crack patterns and strut mechanisms was observed between the two stories of the specimens.

During the ’90s, a number of shake-table tests have been carried out on masonry-infilled steel or RC frames (Kwan and Xia 1995 and Lee and Woo 2002). Valiasis and Stylianidis (1989) and Benetti et al. (1998) concluded that the presence of the infill wall in RC frame increases its strength and stiffness, while this increase is more pronounced in the case of the integral infilled frame, compared to the non-integral one. This observation is also supported by Mallick and Garg (1971) and Liauw (1972). The results obtained from the pseudo-dynamic tests on infilled frames conducted by Negro and Verzeletti (1996) and Fardis and Panagiotakos (1997) showed that the infill walls have a great effect on the reduction of inter-story drifts of frames. Figure 2.6 (b) presents the results from the Negro and Verzeletti (1996) study in terms of dissipated energy of the soft-story infilled frame, uniform infilled frame, and of the bare frame.

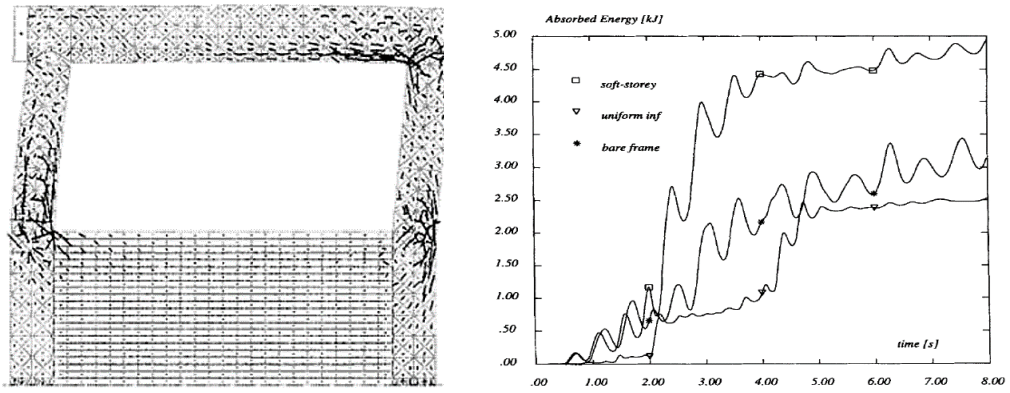

(a) (b)

Figure 2.6: (a) *Short-column mechanism* on RC frame partially filled with masonry wall (Chiou et al. 1999) and (b) Dissipated energy for three different infilled frames tested by frame Negro and Verzeletti (1996).

Murty and Jain (2000) performed cyclic tests on infilled RC frames and concluded that the stiffness and the strength of the infilled frame is 4.3 and 2 times greater, respectively, compared to that of the bare frame. In the same period, Manos et al. (2000) investigated the influence of masonry infills on the seismic response of multi-story RC frames by testing small-scale frames, with and without infill wall, under base-motion excitation. The results showed that the presence of the infill in RC frame increases its the fundamental frequency and the bare frame reached its maximum strength at drifts of 1%, while the infilled frame reached its maximum strength at 2% drift. Calvi and Bolognini (2001) tested a single bay, single story masonry-infilled RC frame under in-plane and out-of-plane loading to investigate the interaction between infill wall and bounding frame. The results showed that infill walls enhanced the lateral capacity and the dissipated energy of the bare frame by about 85%. Al-Chaar et al. (2002) indicated the increase in the ultimate and in the residual strength of frames, due to the presence of infill walls, by testing four 1/2-scale, single-story, non-ductile RC frames with and without infill walls, under monotonic static loading.

Kakaletsis and Karayannis (2008, 2009) examined the behavior of masonry-infilled RC frames with openings under in-plane cycling loading. It was pointed out that the presence of the central window and door opening significantly influences the behavior of masonry-infilled RC frames in terms of stiffness, dissipated energy and crack patterns (Fig. 2.7). The authors observed that, in the cases where the opening percentage was equal to 12.5% and 25%, leads to a decrease of the lateral strength of the infilled frame 19% and 32%, respectively. In addition, in the case of a large size opening in the infilled frame, the infill-frame separation occurred at early stage of lateral loading, before yielding occurred at the column reinforcement. The authors also concluded that the size and the location of the opening influence the lateral response of infilled frames, since larger openings lead to higher ultimate limit state and more ductile manner behavior of the structure, while moving the opening towards the center of the infilled frame resulted in further decrease in its lateral strength, stiffness and its ductility. In the same concept, Anil and Altin (2007) and Voon and Ingham (2008) conducted cyclic tests on infilled frames with openings (with different configurations and locations). Both studies showed that the strength, stiffness, and the dissipated energy of the infilled

frame is much larger than of the bare frame despite the presence of the opening. Furthermore, the test results obtained from both studies showed a reduction of the strength of the infilled frame, as the height of an opening increases.

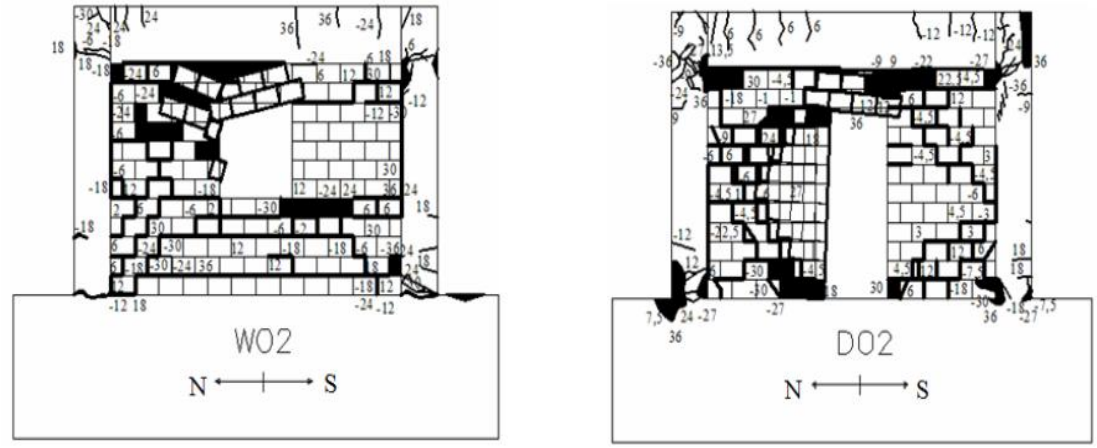

(a) (b)

Figure 2.7: Crack pattern in masonry-infilled RC frame with: (a) central window opening, and (b) central door opening (Kakaletsis and Karayannis 2009).

Pujol and Fick (2010) tested a full-scale, three-story RC frame, with and without infill walls, under cyclic loading and concluded that the infill wall can significantly increase the stiffness and the strength of the frame. The drift ratio of the infilled frame was equal to 1.5%. Later, Stylianidis (2012) performed in-plane cyclic tests on single-story, one-bay,1/3-scale masonry-infilled RC frames. The results showed that separation of the infill wall from the surrounding frame at the non-loaded corners of the infill wall occurred at relatively low displacements, at higher displacements *diagonal cracking* and *sliding shear failure* modes occurred. The author also concluded that the construction of a brick wall with a width equal to half the width of the adjacent columns, can double the strength of the system and triple the dissipated energy. In the same period, Stavridis (2012) carried out shake-table test on a 2/3-scale, three-story, two-bay, infilled RC frame. Minor cracks developed in the infill wall during the design-level, and as the base motion increased, the diagonal cracks in the masonry infill wall gradually propagated to the frame, leading to the development of significant diagonal shear cracks in the RC columns in the first story, causing a *soft-story mechanism*.

Decanini et al. (2012) identified the effect of openings on the in-plane behavior of infilled frames under lateral loading, by examining 143 numerical and experimental tests available in the literature. They concluded that the area and the location of openings significantly affect the stiffness and the strength of infilled frames. The authors found that openings located in the corner of the infilled frame may cause unfavorable effects, like *short-column* mechanism. The authors reported that, during early lateral loading, the cracks develop firstly at the corner of the opening, and as the lateral load increases, they propagate towards the compressed corners of the infilled frame. In addition, in this study, an extension of the equivalent strut model for solid infills to infills with opening was proposed, in order to predict the effective width of the strut of the infilled frame with opening (more details are provided in the following section). Following the same concept, Nwofor (2012) investigated numerically and experimentally the contribution of the openings (i.e.,different size of central opening) to the reduction of the shear strength of the infilled frame. The effect of different size of central opening on the in-plane behavior of infilled frames under lateral loading was also studied by Tasnimi and Mohebkhah (2011). The results showed that the presence of openings causes a reduction in the stiffness and lateral strength of the solid infilled frame, while infilled frames with openings are not always more ductile than those without openings (solid infilled).

Cavaleri and Di Trapani (2014) performed cyclic tests on single-story, single-bay masonry-infilled RC frames considering different kinds of masonry infills, and proposed an analytical model (single-strut model) to predict the strength and stiffness of masonry-infilled RC frames. Jiang et al. (2015) investigated experimentally the response of masonry-infilled RC frames under cyclic loading, using rigid and weak connection between the infill wall and RC frame. The results showed that the increase on the lateral capacity of the structure due to infill walls is significantly greater in the infilled frame with rigid connection, compared to the infilled frame with a weak connection, while the infilled frame with weak connection failed at a load in-between that of the bare frame and the infilled with rigid connection. In the same period, Akhoundi et al. (2015) conducted an experimental study on two reduced-scale masonry-infilled RC frames under in-plane and out-of-plane loading. For the in-plane behavior of

infilled frame, the authors observed that stair-step-type cracks developed, passing through the mortar joints, while for the out-of-plane one, two-way *arching mechanism* developed on the infilled frame.

Li et al. (2016) studied the lateral response of infilled frames through experimental tests on 1/3-scale, four-bay, two-story infilled RC frames, under in-plane cyclic loading, and proposed an analytical model to evaluate the seismic response of infilled frames. In the same period, Basha and Kaushik (2016) concluded that the infilled frames were significantly stiffer (7-10 times) and stronger (1.6-2.5 times) and dissipated more energy (1-2.3 times), than the corresponding bare frames, based on the results obtained from their tests on half-scale, single-story masonry-infilled RC frames under in-plane cyclic loading. These authors also concluded that, strong-frame and weak-infill configuration leading to the shear failure of the columns. The same observation is also reported in Zarnic and Tomazevic (1988), Mehrabi et al. (1994) Buonopane and White (1999a) and Stavridis (2012). The shear failure of the columns is primarily attributed to the weakening of the connection between column and infill wall, while, as the imposed load is increased, the effective contact length between column and infill wall decreases. Recently, Suzuki et al. (2017) tested five, 1/4-scaled infilled frames under in-plane cyclic loading and the number of spans (single or double), number of stories (single or double), and stacking pattern of the infill (horizontal or vertical) were selected as investigation parameters. The influence of these parameters on the formation of a diagonal path along the two opposite corners of the infill wall is presented in Fig. 2.8.

Dautaj et al. (2018) tested 2/3-scale, single-bay, single-story RC frames infilled with hollow and solid clay block masonry units under cyclic loading. The test results showed that the type of masonry unit influences the failure mode of the infilled frame. Particularly, in the frames infilled with hollow clay blocks, shear failure of the infill wall, beam-column joint failure, and formation of flexural hinges in part of the RC frame were observed, while in the frames infilled with solid clay bricks, shear failure of the column and of the infill wall observed.

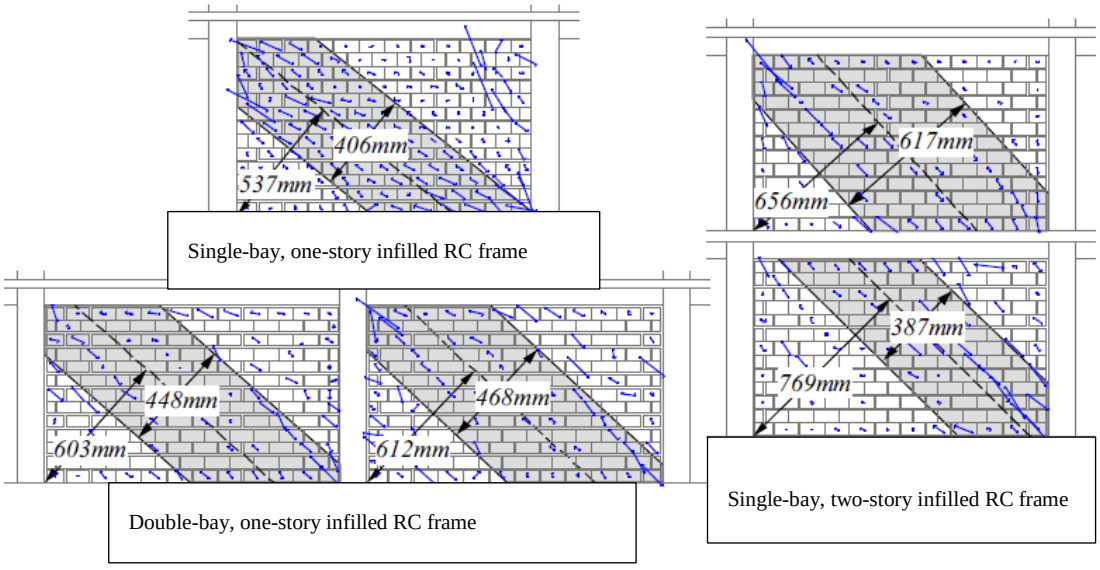

Figure 2.8: The width of the diagonal compression strut for different configurations of masonry-infilled RC frames (Suzuki et al. 2017).

Studies have been also conducted, aiming to examine the effect of the gap-opening between the infill wall and the frame on the behavior of masonry-infilled RC frames under lateral loading, are still very limited, while most of them are numerical studies. On the other hand, the effect of the gap-opening at the infill-frame interface on the lateral response of masonry-infilled steel frames is relatively better studied experimentally (Liauw and Kwan 1984). For example, Dawe and Seah (1989) conducted a series of experiments on infilled steel frames, and concluded that the gap-opening at the infill-beam interface significantly reduces the ultimate load carried by the infilled frame, while the gap-opening at the infill-column provided little reduction in the load carrying capacity of the infilled frame. Similar conclusions were reported by Kadir (1974), Yong (1984), Flanagan and Bennett (1999) and Nazief (2014). Recently, Teguh (2017) and Gao et al. (2018) performed cyclic tests on masonry-infilled RC frames, in order to investigate the effect of gap-opening between the frame and the infill wall on the lateral response of infilled frames. Gao et al. (2018) concluded that the cohesion of the sliding surfaces determines the lateral load capacity of infilled frames, since this parameter influences the sliding at the infill-frame interface. In addition, the aforementioned authors proposed different contact schemes at the infill-frame interface in the design of infilled frames to predict the real response of such structures.

Allen et al. (2016) conducted an experimental study, aiming to investigate the lateral response of infilled frames with openings. The results showed that the geometry of the infill wall and the loading ratio have a significant impact on the failure mode and on the lateral capacity of masonry-infilled frames with openings. Tekeli and Aydin (2017) performed cyclic test on masonry-infilled RC frames with openings, and the size and the location of the opening were selected as investigation parameters. The authors concluded that the drift ratio of infilled frame increases as the size of the opening increases, while the dissipated energy and the stiffness of the infilled frame are significantly reduced by increasing the size of the opening. Recently, Morandi et al. (2018) performed an experimental study on full-scale, single-story, single-bay RC frames with strong masonry infill walls, with and without openings, under in-plane cyclic load. They observed that diagonal shear cracks were developed in the columns due to the relatively high resistance of the strong infill wall compared to that of the frame. Furthermore, the lateral strength of the infilled frame decreased by about 45%, compared to that of solid infilled frame, due to the high corner-to-corner diagonal cracks developed on the infilled frame with openings. In the same concept, Ahani et al. (2019) evaluated experimentally and numerically the effect of different percentages of openings on the behavior of infilled frame under cyclic loading. The results showed that the increase of the percentage of the opening leads to a significant reduction in the lateral strength and stiffness of the infilled frame.

It is worth mentioning that over the years, several experimental studies have been also conducted to examine the out-of-plane behavior of infilled frames under lateral loading. Some of their conclusions are briefly presented in this paragraph, although the scope of this thesis does not include the out-of-plane behavior of infilled frames. Most of the researchers observed that as the infill wall is restrained by a bounding frame it can develop out-of-plane resistance, due to the formation of an *arching mechanism*, as mentioned in the previous section. They also concluded that the out-of-plane resistance of infilled frames depends on the slenderness ratio (height-to-thickness) and on the compressive strength of the infill wall. The out-of-plane strength of infilled frames reduces by increasing the slenderness of the infill wall. Some authors also reported that the aspect ratio of the infill wall also affects the out-of-plane behavior of infilled frames

(Dawe and Seah 1989; Angel 1994). Recently, experimental tests were conducted by Furtado et al. (2016) and Ricci et al. (2018), aiming to investigate the behavior of infilled RC frames under out-of plane loading, after previous in-plane damages. They concluded that significant reduction in the initial stiffness and in the maximum strength of the infilled frame was obtained in the specimen with previous in-plane damage, compared to that with no previous in-plane damage. Furthermore, Di Domenico et al. (2019) investigated the out-of-plane response of infilled frames, using different height-to-thickness slenderness ratios and boundary conditions. A systematic review of experimental studies regarding the out-of-plane behavior of masonry-infilled RC frames under lateral loading recently reported in Furtado et al. (2018).

To conclude, all the above-mentioned studies mainly differ in the number of stories and bays, in the scale of the tested specimens (full or reduced), in the load application scheme, in the boundary conditions, in the geometry of the infilled frame (with and without openings), in the material used for assembling the infilled frame, etc., and provide a large amount of information about the in-plane lateral response of infilled frames such as: failure modes, stiffness, lateral strength, stiffness degradation, dissipated energy, crack patterns etc. Most of the studies concluded that the presence of the infill wall in RC frame contributes to increase significantly its lateral capacity, and to change its failure mechanism, leading to brittle shear failures of the structure, as mentioned in the previous section. The behavior of masonry-infilled RC frames under lateral loading is complex, due to a high number of parameters that are involved in this type of structure. These parameters can be classified into five different categories, as follows: (1) the geometry and mechanical properties of the infill wall, (2) the geometry and mechanical properties of the surrounding frame, (3) the characteristics of the infill–frame interface, (4) the presence of the openings, and (5) the quality of the materials used and the workmanship. It is important to mention that extensive literature review regarding the experimental studies conducted in the area of the infilled frames can be found in Bruneau (1994), Pradhan et al. (2012), Surendran (2012), Ahmed et al. (2017), Lingeshwaran and Poluraju (2019) and Furtado and De Risi (2020).

2.4 Numerical investigation of masonry-infilled RC frames

Over the years, several strategies and computational methods have been proposed and adopted for the modeling of masonry-infilled RC frames. Nevertheless, the analytical and numerical modeling of masonry-infilled RC frames is a complex task, due to the combination of many materials involved in this type of structure, while a reliable constitute law for masonry infill wall (which is a non-linear anisotropic composite material that consists of brick units and jointing mortar) is not available yet. Following the objectives of this research, the modeling methods that exist so far for simulating masonry-infilled frames are introduced and briefly discussed in this part of the thesis, while the modeling approaches for TRM composite material will be presented in Chapter 3. In the literature, two modeling methods, typically adopted for infilled frames, exist on the level of detail by which the infill wall is modeled, i.e., the macro-modeling and micro-modeling (Lourenco 1996, Crisafulli 2000a). The micro-modeling can be considered in four levels, as presented in Fig. 2.9, and each level provides a different level of accuracy.

This part of the thesis provides sufficient background knowledge regarding the modeling of infilled frames through a brief description of both the macro-modeling (section 2.4.1), and micro-modeling (section 2.4.2) approaches. This is followed by the advantages and disadvantages of each approach (section 2.4.3).

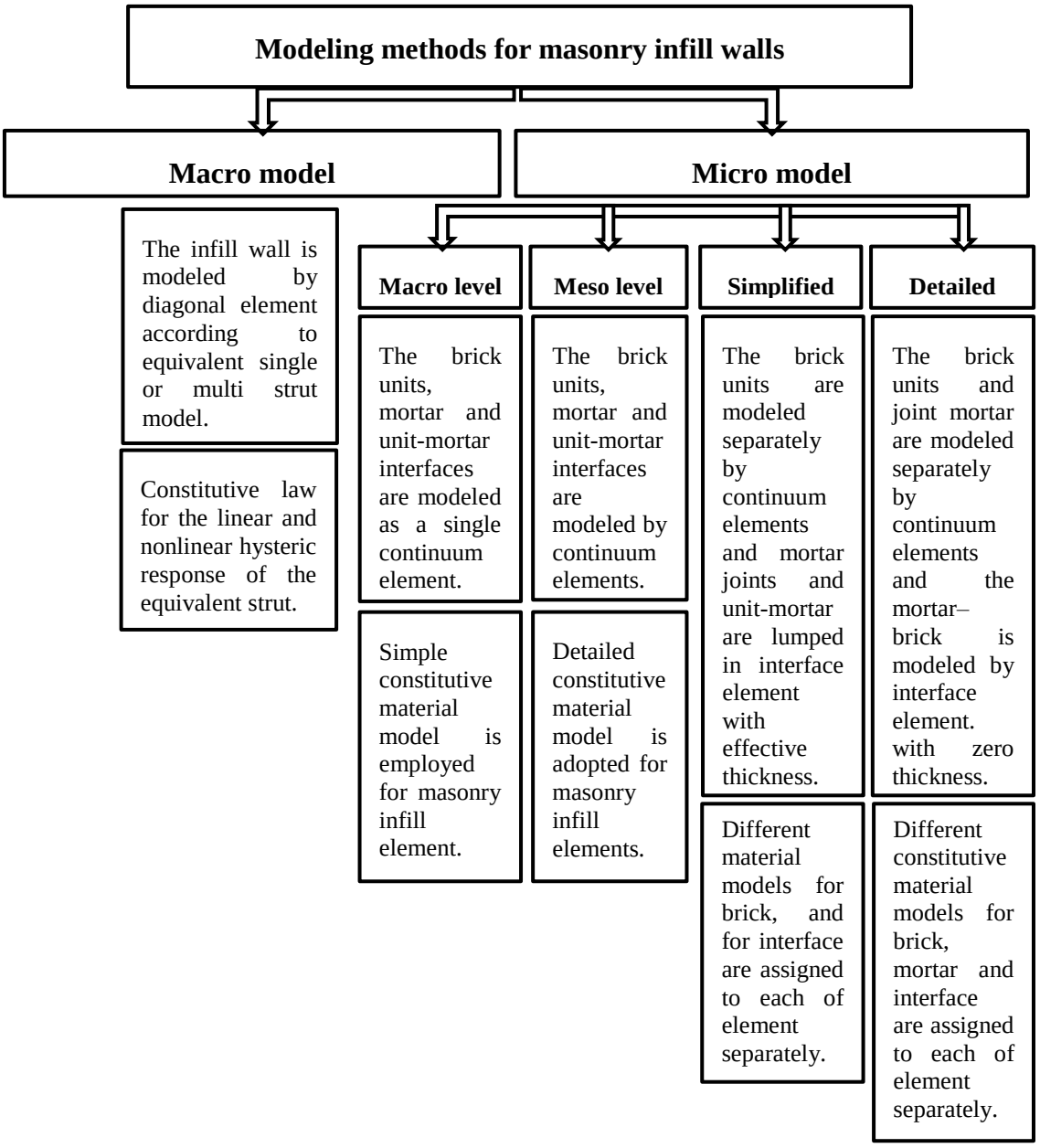

Figure 2.9: Modeling methods for masonry-infilled RC frames.

2.4.1 Macro-modeling

Macro-modeling is a simple and efficient approach for capturing the global response of masonry-infilled RC frames. According to this approach, the infill wall is considered as a diagonal no-tension strut element, while a reliable constitutive law is required for this element. The macro-modeling of infill walls, namely the equivalent strut model,

represents all the important properties of the infill wall, including its strength, stiffness, and deformation capacity.

As mentioned in section 2.3, Polyakov (1960) was the first who suggested that an infill wall subjected to lateral loads could be represented by a diagonal no-tension strut element (Fig. 2.10 a). After this observation, many researchers developed analytical models (predictive equations) to estimate the width, the mechanical properties, the number, the configuration and constitutive laws (hysteretic models) of the equivalent struts. Some of these analytical models are briefly referred to here. Holmes (1961) suggested that the width (w) of the diagonal strut is equal to 1/3 of the diagonal length of the infill (d). Following this approach, Stafford-Smith (1962;1967) developed predictive equations to calculate the effective width of the strut (the ratio w/d varied from 0.10 to 0.25), as a function of the contact length between the frame and infill wall, by taking into account the slip and the friction at the infill-frame interface. Later, Mainstone (1971) and (1974) used the same approach to that of Stafford-Smith (1962) to calculate the contract length between the infill wall and frame, and among others, proposed a predictive equation for calculating the effective width of the diagonal strut. The analytical model proposed by Mainstone (1971;1974) is a widely used approach and it is also recommended by FEMA 306 guidelines. According to this approach, the contact length between the infill wall and frame is expressed as a function of the non-dimensional parameter, λh, where λh represents the relative infill wall-to-frame stiffness, as follows:

$$\lambda h = h * \sqrt[4]{\frac{E_w t_w \sin\theta_{str}}{4 E_c I_c H_{cl}}} \tag{2.1}$$

where E_w is the modulus of elasticity of the infill wall, H_{cl} is the clear height of the infill, E_c is the modulus of elasticity of concrete, θ_{str} is the inclination of the diagonal strut to the horizontal, arctan (H_{cl}/L_{cl}), and I_c is the moment of inertia of the column section with respect to the axis perpendicular to the plane of the infill wall. For calculating the effective width of the diagonal strut as a function of λh, the author proposed the following:

$$\frac{w}{d} = 0.16 * \lambda h^{-0.3} \quad (2.2)$$

$$\frac{w}{d} = 0.175 * \lambda h^{-0.4} \quad (2.3)$$

where w is the width of the equivalent strut, and d is the length of the diagonal of the infill.

Over the years, several researchers proposed detailed equations for estimating the width of the equivalent strut based on the ratio of the elastic characteristics of the infill wall to that of the surrounding frame (Liauw and Kwan 1984, Klinger and Bertero 1978, Bazãn and Meli, 1980, Bertero and Brokken 1983, Dawe 1985, Paulay and Priestley 1992, Durrani and Luo 1994, Flanagan and Bennett 1999). Some of these models are widely used by other researchers (Crowley and Pinho 2006; Perera 2005; Sattar and Liel 2010; and Kareem and Güneyisi 2019). In the more recent past, an alternative method for estimating the width of the equivalent strut, based on a dynamic structural identification strategy, was presented by Papia et al. (2003). Later, Amato et al. (2008) introduced a new equation for calculating the stiffness of the equivalent strut by taking into account the vertical load transferred from the bounding frame to the infill wall. Furthermore, Cavaleri and Di Trapani (2014) proposed a model for calculating the width of the equivalent strut based on the strength and the stiffness of the infilled frame.

After several years of research, some researchers investigated that the single strut configuration is not adequate enough for simulating the infill wall, and the infill-frame interaction in a local sense (Thiruvengadam, 1985, Al-chaar, 2002, Buonopane and White, 1999, Crisafulli 1997, El-Dakhakhni et al. 2004, Saneinejad and Hobbs 1995). Therefore, to overcome this drawback, they proposed that the infill wall could be represented by diagonal multi-strut elements, where the number of struts and their configurations are dependent on the contact length between the infill wall and the frame. The multi-strut approach leads to different results of the lateral response of infilled frames in comparison to the single-strut approach (Syrmakezis 1986 and Zarnic and Tomazevic 1988). Chrysostomou (1991) and Chrysostomou et al. (2002) proposed a multi-strut model considering six compression-only inclined struts, as shown in Fig. 2.10 (b). Later, El-Dakhakhni (2001, 2002, 2004,) proposed a macro model with

multiple struts, one strut in diagonal and two struts off-diagonal, to estimate the stiffness and the ultimate load capacity of the infilled steel frame under lateral loading. Crisafulli (1997) investigated the influence of using different configurations of the struts on the response of infilled frames under lateral loading. Afterwards, Crisafulli and Carr (2007) developed a new multi-strut model that includes two parallel off-diagonal struts and a special shear spring, considering the diagonal tension failure and shear failure of the infill wall. According to this approach, the width of each equivalent strut was half of that of a single strut. Later, Burton and Deierlein (2013) developed a simple model by utilizing a pair of inelastic compression struts in each diagonal of the infill wall (dual-strut model). This dual-strut model can capture the strength and stiffness degradation of the infill wall, considering the shear failure of the column. Recently, Sattar and Liel (2016) proposed a multi-strut model including two diagonal compression struts in each direction of the infill wall. This model also focused on the modeling of RC frame elements in order to capture the interaction between the infill wall and the frame.

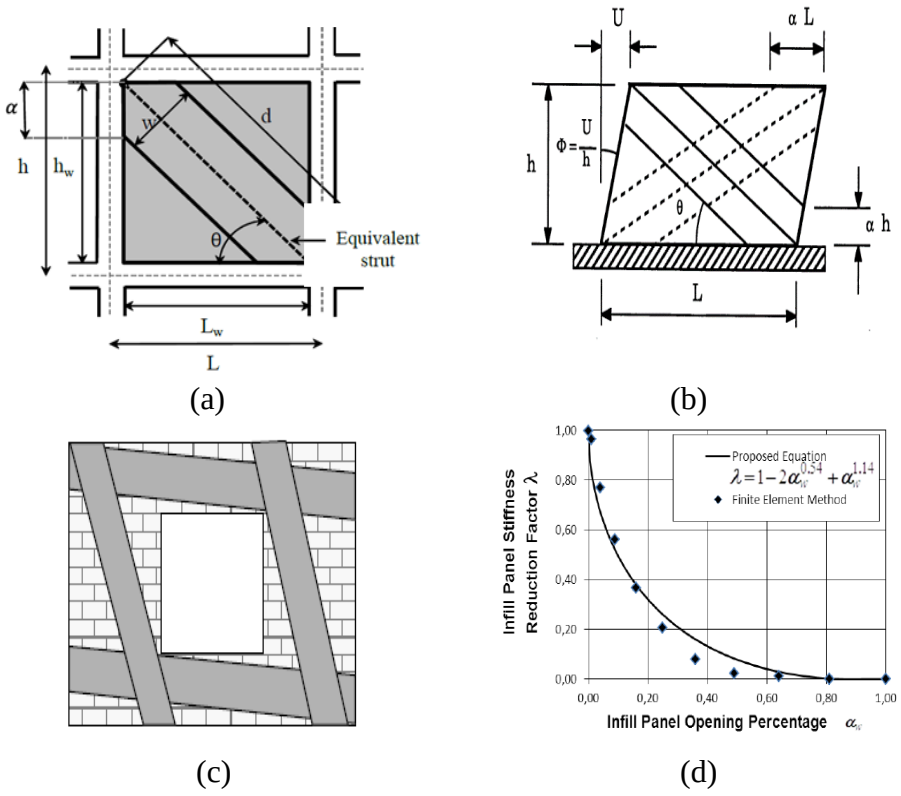

Figure 2.10: (a) Single-strut model, (b) Six-strut idealization of the infill wall (Chrysostomou 1991), (c) configuration of the struts for infill wall with opening (Al-chaar 2002), and (d) Stiffness reduction factor of the infill wall in relation to the opening percentage (Asteris 2003).

Furthermore, in order to represent the infill wall with openings, some researchers proposed the use of several diagonal struts around the opening (Liauw 1972, , Al-chaar 2002 and Tasnimi and Mohebkhah 2011), as shown in Fig. 2.10 (c), some others proposed the application of proper coefficients to modify the stiffness and strength of the equivalent strut of the solid infill wall (Achyutha et al.1986, Dawe 1985, Al-Chaar et al. 2003, Mondal and Jain, 2008, Decanini et al. 2014, Mohammadi and Nikfar 2013, Papia et al. 2003 and Rathi and Pajgade 2012). Most of the studies that exist so far focused on the second approach. Asteris (2003), and later Asteris et al. (2011), among others, proposed an equation for estimating the stiffness of the infill wall as a function of the effective width of the strut, whereas the maximum capacity of the infill wall was related to a predefined failure mode. In the same study, the authors proposed a reduction factor for the stiffness of the equivalent strut to estimate the stiffness of the infill wall when an opening is presented (Fig. 2.10 d). Later, Decanini et al. (2014) investigated the effect of openings on the lateral capacity of infilled frames, and they proposed a reduction factor for the strength and the stiffness of the infill wall considering the dimensions of the opening and the presence of reinforcing elements around the opening. Several empirical expressions have been proposed to quantify the expected level of the reduction of the strength and stiffness in partially masonry-infilled frames. Some recent proposals are reported in Akhoundi and Farhad (2016), Asteris et al. (2016), Su and Cai (2017) and in Humayun-Basha et al. (2020).

Over the years, several studies have been conducted in order to investigate force-displacement relationships and hysteretic models adapted for the equivalent strut element, in order to perform non-linear analysis on infill frames under cyclic or dynamic loading (Doudoumis and Mitsopoullou 1986, Andreaus 1988, Chrysostomou 1991, Moroni et al. 1996, Madan et al. 1997, Flores and Alcocer 1996, Combescure and Pegon 2000, Mojsilovic 2013). For example, Klingner and Bertero (1978) proposed a force-axial deformation relationship, where the compression strength envelope curve exhibits an exponential degradation beyond the peak strength. Cavaleri (2002) and Cavaleri and Di Trapani (2014) introduced some modification to the model developed by Klingner and Bertero (1978). Furthermore, Panagiotakos and Fardis (1996), Fardis (1996; 2000) proposed a constitutive law for the equivalent strut element as shown in

Fig. 2.11 (a). In addition, these authors proposed a hysteretic shear force-displacement relationship, as shown in Fig. 2.11 (b), which requires three empirical parameters to control the loading and unloading branches. Dolšek and Fajfar (2008) proposed an alternative constitutive law for the equivalent strut, which is theoretically similar to that of Panagiotakos and Fardis (1996). The only difference between the two models is the assumption of the zero-residual strength.

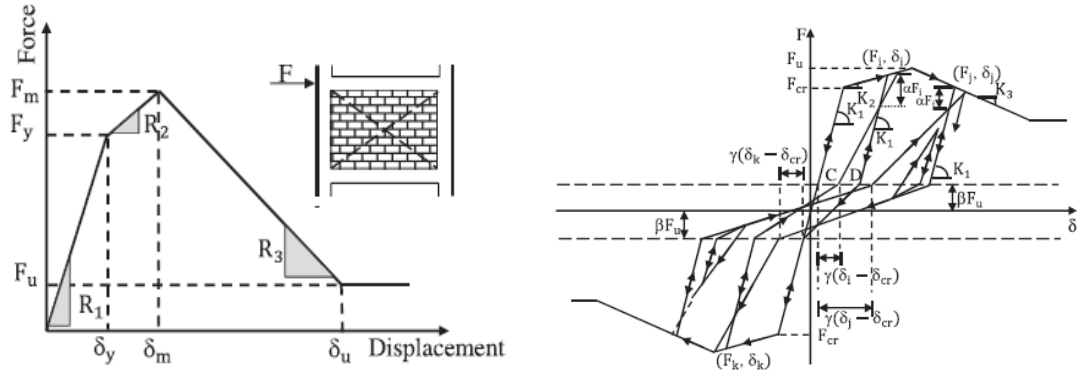

(a) (b)

Figure 2.11: (a) Force-displacement relationship (envelope curve), and (b) hysteretic cyclic law for the equivalent strut element proposed by Panagiotakos and Fardis (1996).

Chrysostomou (1991) and Chrysostomou et al. (2002) proposed a constitutive law for the equivalent strut elements, considering both the stiffness and strength degradation of the infill wall, as shown in Fig. 2.12. This approach takes into account most of the parameters that affect the behavior of infilled frame under lateral loading. Furthermore, this model needs a small number of parameters to be employed and allows the analysis of multi-story structures. Later, Liberatore and Decanini (2004) proposed a model assuming four branches skeleton curve of the lateral force-displacement relationship. These authors also proposed a simple hysteretic model, considering the degradation of the stiffness and of the strength of the infill wall. Later, Crisafulli and Carr (2007) proposed a hysteretic model considering different failure mechanisms on the infilled frame. The hysteretic response of the shear spring element, which is included in his model, is modeled following an elasto-plastic rule with variable shear strength. Furthermore, Varum and Costa (2010), proposed an analytical model for predicting the behavior of infill walls subjected to earthquake loads. Kadysiewski and Mosalam (2009)

proposed a model considering a simplified elasto-plastic behavior of the infill wall for both tension and compression (with different yield forces in the two loading directions and a small post-yield stiffness inserted to minimize convergence problems), and by taking into account the interaction between in-plane and out-of-plane load bearing capacities of infill wall. Later, Chrysostomou and Asteris (2012) proposed equations, as a simplified method for estimating the in-plane stiffness, strength, and deformation capacity of infills, considering different failure modes of infilled frames, while a parametric study was performed to compare the results of these equations against the experimental ones.

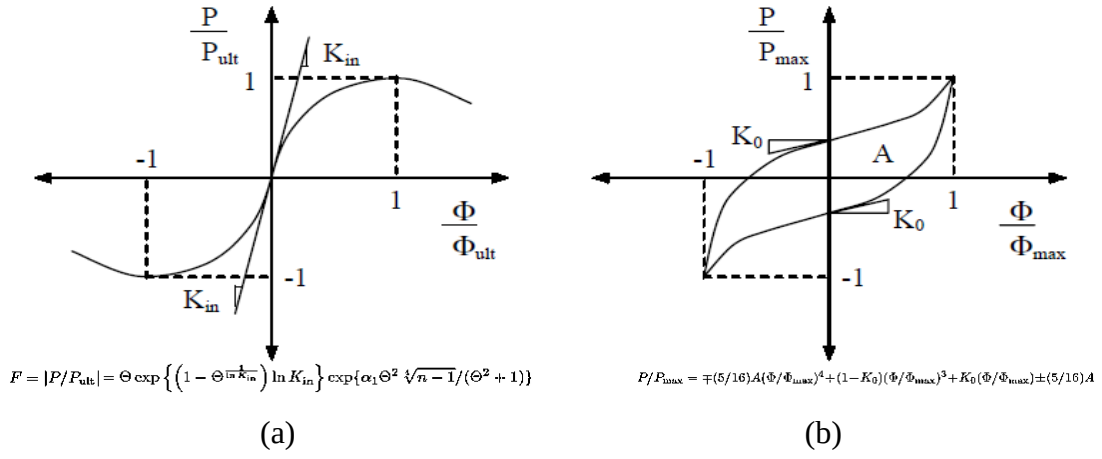

(a) (b)

Figure 2.12: (a) Strength envelope and (b) hysteretic loops for diagonal strut element proposed by Chrysostomou (1991).

To conclude, several studies have been conducted so far aiming to estimate the width, the mechanical properties, the number, the configuration of the equivalent strut element and to investigate a reliable constitutive law that may be adopted for this element. Furthermore, studies have been also conducted in order to estimate the strength and stiffness reduction in partially infilled masonry wall. Some of these studies are briefly presented in this part of the thesis, since the development of macro-model of infilled frames is beyond the scope of this research. More relevant studies regarding the macro-modeling approach were summarized in Asteris et al. (2011), Crisafulli (2000), Surendran and Kaushik (2012). Tarque at al. (2015), Trapani et al. (2016) and Mohammad et al. (2017).

2.4.2 Micro-modeling

A substantially different approach from the macro modeling one has been proposed by researchers which have adopted an “exact representation” of infills called micro-modeling approach. This approach is able to reproduce in a better, detailed and more accurate way the infill wall, and the infill-frame interaction. As shown in Fig. 2.9, the micro-modeling approach can be divided in four levels and each level provides different complexity and accuracy (Asteris and Tzamtzis 2003 and Lourenço, 2002). Figure 2.13 shows the required elements for the macro-, meso-, simplified- and detailed-model of infill wall, where for each element an appropriate constitutive material model must be adopted. It is important to mention that the modeling of masonry-infilled frames includes the infill-frame interface element. An appropriate model must be adopted for this element in order to reproduce adequately the frictional effect in contact regions and the detachment at the infill-frame interface. Overall, the development of a micro-model of an infilled frame is quite complex due to the large amount of information required for the material models adopted for each component of the structure and due to the high computational effort involved.

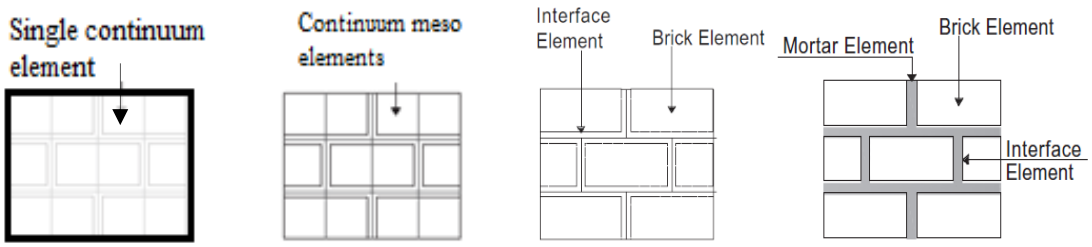

Figure 2.13: Micro-modeling approaches: (a) macro level, (b) meso level, (c) simplified micro-model, and (d) detailed micro-model (Asteris and Tzamtzis 2003) .

The first studies referring to micro-modeling of infilled frames were caried out by Mallick and Severn (1967) and Mallick and Grag (1971), where in these studies the developed infilled frame model was able to capture local effects, such as: the cracking and crushing of the infill wall, and the slip between the infill wall and the frame. The infill wall is modeled by shell elements, the frame was modeled by beam elements and the interaction between the infill wall and the frame was represented by an interface

element. Later, Liauw and Kwan (1984) developed an infilled frame model where the infill wall was modeled by continuum elements and a linear elastic brittle isotropic material model is adopted for these elements (the material model becomes anisotropic after cracking occurs on the infill wall). Dhanasekar and Page (1986) presented a micro-model of infilled frame capable of reproducing the local failures of the masonry infill wall. In this model, the masonry infill wall was modeled homogenously using continuum elements and the material properties of the infill wall (orthotropic failure model) were defined by the results obtained from biaxial tests on 186 half-scale square infill walls. In addition, one-dimensional (1D) joint element was used to model the separation at the infill-frame interface. El-Haddad (1991) developed an infilled frame model able to capture the cracking at the frame and the separation at the infill-frame interface. In this model, the frame members are divided into un-cracked beam elements, and cracked beam elements while the material model adopted for frame members takes into consideration the effects of axial, flexural and shear deformations due to cracking. The masonry infill wall is modeled as plane-stress four node quadrilateral element.

Lotfi and Shing (1991) proposed a homogenous smeared-crack material model as shown in Fig. 2.14 (a), able to capture accurately the flexural failure of the infill wall. Later, Lotfi and Shing (1994) developed a non-linear brick-mortar interface model to capture the normal stress, the shear stress and the dilatancy at the brick-mortar interface (dilatancy is defined as the vertical displacement of the bricks due to the shear forces occur at the brick-mortar interface). The authors assessed the combination of using their interface model with the smeared crack model to predict the shear capacity and dilatancy of the infill wall, by comparing the numerical results obtained from the numerical analysis with the available experimental data. Several researchers proposed plasticity-based continuous-interface models in order to capture the tension and the shear behavior of brick-mortar interface. For example, Mehrabi and Shing (1994; 1997) proposed a simplified constitutive model of mortar joint for describing the cracking and the sliding at the brick-mortar interface. This model includes the non-linear hardening behavior of the brick-mortar interface. The authors compared the numerical results with the results obtained from monotonic and cyclic tests on half-scale specimens of masonry-infilled RC frame, and they found a good agreement in terms of the lateral

capacity of the infill wall. Lourenco, (1995), Lourenço and Rots (1996), and Lourenço et al. (1997) also proposed an elasto-plastic constitutive model for brick-mortar interface. This model includes a straight tension cut-off, the Coulomb friction law, and an elliptical cap, as shown in Fig. 2.14 (b), considering the softening of the tensile strength, compressive strength and of the cohesion of the brick-mortar interface, and considering also the coupling between its tensile and shear failure. For the masonry bricks, the authors proposed an anisotropic continuum model that includes a Rankine type yield surface for tension and a Hill type yield surface for compression. The authors concluded that using their proposed material models for modeling infill walls, the peak-load and post-peak shear behavior of infill walls is predicted adequately, since the numerical results compare well with the experimental ones.

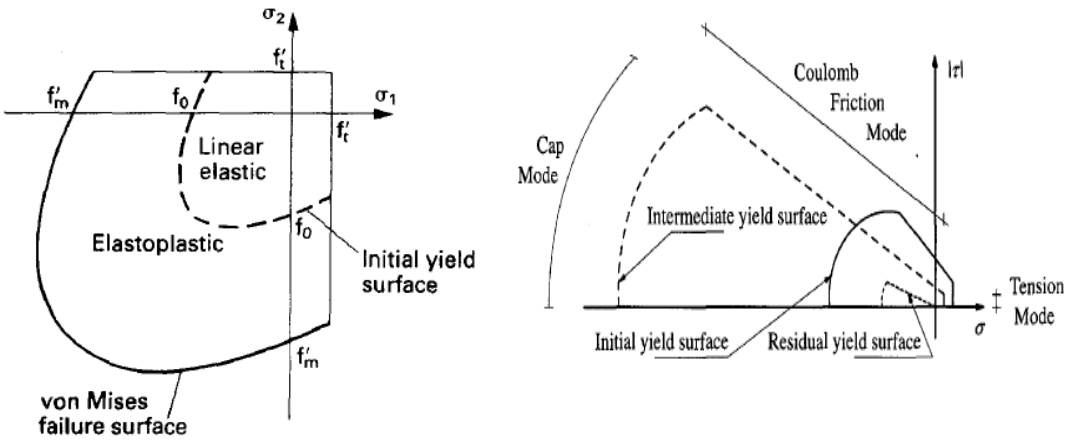

(a) (b)

Figure 2.14: (a) Smeared-crack material model of infill walls proposed by Lotfi and Shing (1991), and (b) interface model proposed by Lourenco (1995).

Mosalam et al. (1997) proposed different modeling strategies to simulate the infilled frames, with and without openings, using smeared-crack models for describing the non-linear behavior of the components of the structure. Chiou et al. (1998) developed an infilled frame model by discretizing the brick units and concrete members into blocks interconnected with contact springs, while a plasticity-based continuous interface model adopted for these springs, which is proposed by the authors for capturing the shear sliding in the joint. Gambarotta and Lagomarsino (1998) and Magenes (1998) proposed homogeneous material models for describing the complex behavior of masonry infill

walls, following the equivalent diagonal strut approach (section 2.4.2). These material models need only a few parameters (mainly strength parameters) in order to be used. Papa (1996) proposed an orthotropic material model for inifll walls, considering the texture of the brick and the mortar. Singh at al. (1998) developed a micro-model of an infilled frame, in which the masonry infill wall was modeled as a homogeneous element, and a continuum material model with linearly elastic behavior until failure, and Von Mises failure criterion with a tension cut off was adopted for this element in order to capture the crushing of the masonry infill wall. This model, however, cannot capture accurately the shear failure of the column and the sliding shear failure of the masonry infill wall. Later, Dawe et al. (2001) proposed a constitutive material model of infill walls, considering the crushing failure of the infill wall. Berto et al. (2002) developed a specific damage model for masonry infill wall, including its orthotropic brittle nature, by considering different elastic and inelastic properties along the two directions of the infill wall.

Asteris (2003) proposed a new criterion for infill-frame separation, by describing the evolution of the natural response of infilled frames subjected to seismic lateral loads as a boundary condition problem. According to this method, the infill wall elements linked to the elements of the surrounding frame at two corner points, points A and B as shown in Fig. 2.15. Then, the nodal displacements computed, and it was checked whether the elements of the infill wall overlap the elements of the surrounding frame. Different contact lengths between the infill wall and the surrounding frame were observed, based on the derived deformed mesh (Fig. 2.15). Following this method, the authors investigated the influence of the different size of openings on the lateral response of masonry-infilled frames and proposed a stiffness reduction factor (section 2.4.2).

Oliveira and Lourenço, (2004) also proposed a cyclic non-linear constitutive material model for brick-mortar interface. Then, they developed a masonry wall model using 8-node continuum plane-stress elements to model the masonry units and using an interface element with effective thickness to model the brick-mortar interface. The comparison between the numerical and experimental results shows the ability of the masonry infill wall model to capture the lateral capacity of the infill wall under cyclic loading.

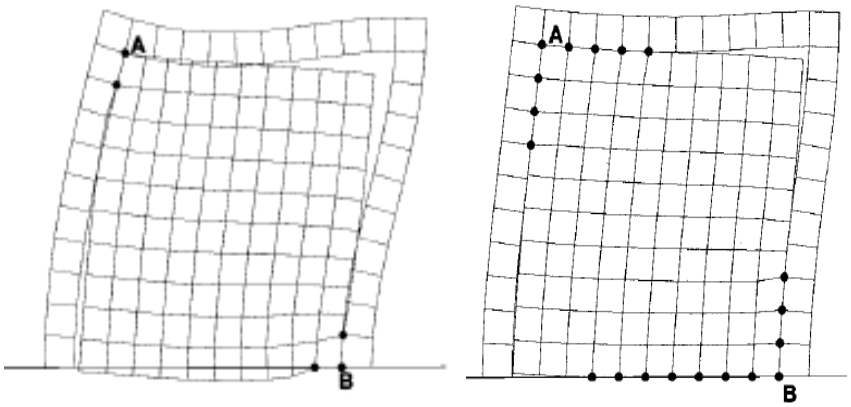

Figure 2.15: Deformed shape (mesh) of one-story, one-bay infilled frame using the method of contact points proposed by Asteris (2003).

Pasticier et al. (2007) developed an infilled frame model (using SAP2000 commercial software) and defined the possible location of plastic hinges that might developed along each element based on equivalent strut approach. It is important to mention that, several researchers proposed homogeneous material models for describing the non-linear brittle behavior of the infill wall follows the equivalent diagonal strut approach (Benedetti at al. 2008, Chen at al. 2008, Furtado et al. 2015, Mojsilović 2011, Decanini et al. 2004, Varum et al. 2010). Stavridis (2009) and Stavridis and Shing (2010) developed a complex FE model of masonry-infilled RC frame by combining the smeared approach (for masonry units) and discrete crack approach (for mortar joints). This model can capture the *diagonal cracking*, *sliding shear*, and *corner crushing* failure mode and the flexural and shear failure of the concrete columns (*frame failure mode*) as well. Following the same concept, Koutromanos et al. (2011) used a new cohesive crack interface model and an improved smeared crack model to capture the lateral response of infilled frames under cyclic loading. Recently, a detailed infilled frame model was developed by Petracca et al. (2017) including interface elements for mortar-joints, and continuum elements for brick units. In addition, in this study critical issues for the micro-modeling approach were analyzed carefully. Sarhosis and Lemos (2018) developed a masonry-infilled RC-frame micro-model using masonry units and mortar-joint elements, and these elements are bonded together by zero thickness interface element. The failures occurred on the infill wall model were compared well against the experimental ones.

The above-mentioned studies used interface elements with appropriate models in order to reproduce the infill-frame detachment. Recently, several numerical studies conducted in order to investigate the effect of the gap-opening at the infill-frame interface on the response of masonry-infilled RC frames under lateral loading (Kareem and Güneyisi 2019, Sonpal et al. 2019). The authors concluded that the calibration of several sensitive parameters of the interface model is required to obtain reliable results. Several authors proposed equations for quantifying the stiffness of the infill-frame interface and of the brick-mortar interface (Lourenço 1996, Cur 1994, Asteris et al. 2013; Ehgri and King 2018, Dolatshahi 2011, Lin et al. 2014). Such approaches are aiming to capture well the local interaction effects at the infill-frame interface. It is important to mention that in the numerical modeling of infilled frames, the definition of the infill-frame interface constitutes a quite sensitive question that was treated in different ways by the researchers.

In recent years, due to significant advances in FE methods, a number of commercial programs are available for a non-linear FE analysis of infilled frames, such as ABAQUS, ANSYS, DIANA, ATENA, LS-DYNA, LUSAS, MARC, VECTOR, MASA, OpenSees, ADINA etc. Each of these software tools has capabilities to model masonry-infilled frames in two or in three dimensions (2D or 3D) using several types of analysis (eigenvalue analysis, cyclic analysis, dynamic analysis, etc.). In addition, each of these software packages has an extensive library of elements and constitutive material models in order to capture the linear and the non-linear behavior of the concrete, reinforcement bar, brick, mortar joint and their interaction. Sanya (2006) reviewed and compared the capabilities of different software tools such as: ANSYS, ABAQUS, ADINA, and DIANA FEA for modeling the masonry infill walls. Over the years, several numerical studies have been conducted using different commercial FE software for simulating the complex behavior of masonry-infilled RC frames, but for the purpose of this study, those of using DIANA FEA software are briefly presented here. Al-chaar and Mehrabi (2008) used DIANA FEA software to develop an infilled frame model, where the masonry units and the concrete elements were represented with smeared-crack material model (Fig. 2.16 a). In addition, an interface element is used for the brick-mortar and infill-frame interface while a combined Coulomb friction, tension

cutoff, and compression cap model is adopted for this element. In this study, several material parameters required adjustment in order to represent the experimental results accurately. Other examples of using DIANA FEA software for modeling infilled frames can be found in Dolatshahi and Aref (2011), Al-Chaar and Mehrabi (2008), Kyriakides and Billington (2011), Siamak (2013) and Stavridis 2009). Recently, numerical models were also developed using the DIANA FEA software in order to simulate the behavior of masonry-infilled RC frames with openings subjected to lateral loading (Fig. 2.16 b) (Scheen 2016, Akhoundi et al. 2016, Scheen 2016, Allen et al. 2017, Ahani et al. 2019, Proença et al. 2019).

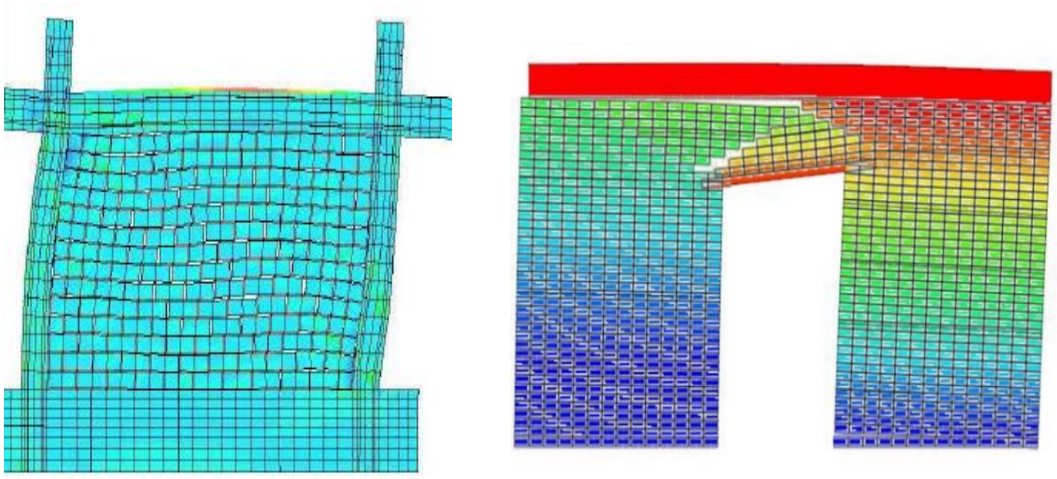

(a) (b)

Figure 2.16: (a) Infilled frame model using DIANA FEA (Al-chaar and Mehrabi 2008) and (b) infilled frame model with openings using DIANA FEA (Scheen 2016).

All the above-mentioned studies used different micro-modeling strategies with different level of complexity and accuracy to develop a masonry-infilled RC frame model. In addition, some researchers proposed constitutive material models for the infill wall, the bricks and for the brick-mortar interface. Although several micro-models of infilled frame have been developed and several constitutive material models for each component of this type of structure have been proposed, in this section some of them are briefly presented, since the development of a novel micro-model for masonry-infilled RC frames is beyond the scope of this research. More relevant studies regarding the micro-modeling approach are summarized in Lourenço (1996), Roca et al. (2010), Asteris et al. (2011), Crisafulli (2000), Surendran and Kaushik (2012), Tarque et al.

(2015), Trapani et al. (2016), Asteris et al. (2013), Furtado et al. (2015), Shadlou and Kashani (2019) and D'Altri et al. (2019).

2.4.3 Advantages and disadvantages of each modeling approach

The literature overview presented above underlines the strategies and computational methods which have been proposed or adopted so far for simulating the complex behavior of masonry-infilled RC frames. The discussed modeling approaches range from the simplest to the most complex, and they always have the common difficulty to be at the same time accurate and computationally affordable. The macro-modeling approach compared to the more detailed micro-modeling approach, shows significant practical advantages. Specifically, the diagonal equivalent single-strut or multi-strut models can provide a good approximation despite their simplicity, while special attention is needed for the constitutive law used for the equivalent-strut element. In practice-oriented analyses on large structural members or full structures where a detailed description of the interaction between adjacent elements may not be necessary, the macro-modeling approach is recommended. A drawback of the macro-modeling approach lays in its description of the damage as a smeared property spreading over the structure. On the other hand, the micro-modeling approach proved to be the most accurate approach for capturing the real physic of the problem such as the infill-frame interaction, the sliding of the brick units along the mortar joints, the cracking on infill walls and on RC members. Despite these advantages, the micro-modeling approach presents difficulties related to the non-linear behavior of the many materials involved in this type of structure, to the detail modeling of the infill wall (brick units, mortar joints, brick-mortar interface) and to the interaction between the infill wall and the frame. The parameters required for the material models involved in this type of a structure are not always available or not easy to determine, and this could present a big drawback for the FE analysis of masonry-infilled RC frames. Hence, using the micro-modeling approach the proper calibration of the masonry infill material model and of the interface model (brick-mortar interface and infill-frame interface) may be a really difficult task, since masonry infill wall is highly heterogeneous, and the definition of the properties of the brick-mortar and infill-frame interface needs the knowledge of several experimental

data. The computational cost of FE analysis of infilled frames is usually extremely high, because of the large number of elements and degrees of freedom involved. Therefore, the application of micro-modeling to complex structural systems requires high computational cost limiting the use of a detailed micro-modeling to simple case-studies. In nowadays micro-modeling approach is suitable mainly for research purposes.

To conclude, the analytical and numerical modeling of masonry-infilled RC frames is a complex task, using either the macro-modeling or micro-modeling approach, due to the large number of parameters that are able to influence the behavior of infilled frames as mentioned in section 2.3. Therefore, in order to simulate this type of structure appropriate experience is needed to handle all the parameters that may reduce the accuracy of the model and increase the computation cost.

2.5 Seismic retrofitting of masonry-infilled RC frames using TRM: an experimental and numerical studies overview

Several retrofitting techniques have been proposed and used over the years so that the existing buildings can be enhanced to satisfy current seismic design codes. Amongst them, the Textile Reinforced Mortar (TRM) composite material has received attention as a sustainable, and more compatible solution for retrofitting RC and masonry structures, than the widely used ones such as: concrete jacketing (Pinto, Varum, and Molina 2002), fiber reinforced polymers (FRP) (Hamilton 2005; Marcari et al. 2007), etc., due to its very small thickness and durability features. Simultaneously, the use of inorganic matrix (TRM) instead of epoxy resins, as FRPs, overcomes some of FRP drawbacks (high cost, incompatibility with substrate materials, inability to apply on wet surfaces, etc.). TRM is a composite material, which consists of finely grained inorganic-matrix (cement-or lime-based) and textile, made of fibers, which is used as reinforcement. The interest of using the TRM composite material for retrofitting masonry wall elements and masonry-infilled RC frames has been rising for almost a decade as shown in Fig. 2.17. This composite commonly referred to as Textile Reinforced Concrete (TRC) was initially meant to be integrated in new civil applications(precast material), Textile Reinforced Mortar (TRM) or as Fabric

Reinforced Cementitious Matrix (FRCM). From Fig. 2.17, it is observed that significant research has been conducted and reported for retrofitting masonry wall elements during the last five years, however, much less has been carried for retrofitting masonry-infilled RC frames.

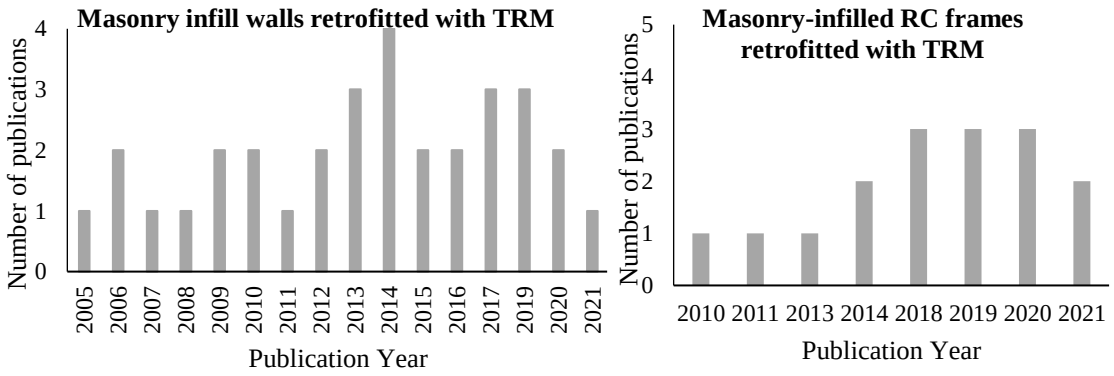

(a) (b)

Figure 2.17: Number of publications per year regarding (a) masonry walls retrofitted with TRM, (b) masonry-infilled RC frames retrofitted with TRM.

This part of the thesis provides a state-of-the-art review of the experimental (section 2.5.1) and numerical studies (section 2.5.2) conducted so far aiming to examine the effectiveness of using the TRM composite material for retrofitting infilled frames. In order to cover completely all aspects of this topic, a briefly description of the experimental and numerical studies conducted so far regarding the use of TRM for retrofitting masonry wall elements is also presented. This section concludes by presenting some variables able to influence TRM's efficiency for retrofitting infilled frames, and for masonry wall elements, as well (section 2.5.3).

2.5.1 Experimental investigation

In 2015, eight combined in-plane and out-of-plane monotonic tests on specimens composed of full-scale one-bay, one-storey RC frames filled with non-load-bearing clay masonry walls using three different strengthening solutions including the TRM (Table 2.1) were carried out by Da Porto et al. (2015). Based on their results, the authors concluded that the use of different strengthening solutions (including TRM) contributes

to reduce the failures that occurred on infilled frames leading to a significantly increase on deformation capacity, strength, dissipated energy, and on the secant stiffness of the infilled frames as presented in Table 2.1. Furthermore, the authors investigated that the use of anchorages (steel ties) to connect the TRM to the upper beam, does not significantly improve the in-plane and out-of-plane response of retrofitted infilled frames compared to the corresponding ones without anchorage (only TRM strengthening).

Table 2.1: Results for the in-plane test of retrofitted specimen Da Porto et al. (2015)

Retrofitting technique	**F_{max} (%)**	**Drift level at F_{max} (%)**	**Ratio of dissipated to input energy (%)**	**K_{max} (%)**
Plaster made of natural hydraulic lime and geo-polymer binder	-2%	37%	1%	-2%
Plaster made of natural hydraulic lime and geo-polymer binder	-4%	1%	13%	-3%
Plaster made of natural hydraulic lime and geo-polymer binder with basalt and steel fibers mesh anchored with steel ties	-2%	-36%	15%	5%
Lime-gypsum plaster	-27%	37%	9%	-35%
Lime-gypsum plaster with basalt and steel fibers mesh	-35%	1%	-8%	-44%
Natural hydraulic lime plaster	-29%	2%	3%	-44%
Natural hydraulic lime plaster with basalt and steel fibers mesh	-35%	-35%	1%	-39%

Koutas et al. (2014a) performed an experimental study to investigate the effectiveness of using TRM for retrofitting 2/3-scaled, three-story masonry-infilled RC frames subjected to in-plane cyclic loading. In the retrofitted specimen, anchors (custom-made from a commercial textile made of uncoated basalt fiber rovings) were placed along

with the slab-infill interfaces on both sides of the first and second story. Seven cycles of displacement loading were applied to the retrofitted specimen (top-drift ratio equal to 1.33%). The results showed that the TRM provides 56% increase in the infilled frame's lateral strength, while the deformation capacity at the ultimate strength state of the retrofitted infilled frame is increased by 52% compared to the corresponding one of the unretrofitted infilled frame. Also, the TRM-retrofitted specimen dissipated 22.5% more energy than the unretrofitted specimen ones, for the same loading history. Furthermore, the authors concluded that the presence of custom-fabricated textile-based anchors was proved particularly useful in delaying or even preventing the debonding of TRM. More details about this experimental case-study will be discussed in Chapter 4, since this study is used for calibration purposes in the current numerical study.

Akhoundi et al. (2018) studied the in-plane behavior of seven half-scale (scale factor equal to 0.54) masonry-infilled RC frames with and without glass-TRM under cyclic loading (Fig. 2.18 a). In this study, a similar application of the TRM retrofitting technique to that of Koutas et al. (2014a) was used. A particular type of connector (L-shape glass grid) was used in this study to create a better bond between the TRM and the infill wall as shown in Fig. 2.18 (b). Vertical load equal to 80kN per column corresponding to 20% of the column's axial force capacity, and six cycles of displacement loading were applied to the retrofitted specimen (drift ratio equal to 3.5%). Based on their results, the authors observed that by strengthening the masonry infills and connecting them to the RC frame by merely extending the retrofitting layers to the faces of the columns and the beam, resulting to an increase on the stiffness and ultimate strength of the infilled frame by about 40%. The dissipated energy of the retrofitted infilled frame is increased by about 39%-51% compared to that of the unretrofitted one. Figs. 2.18 (c) and (d) present the force versus displacement curve (hysteric curves) for unretrofitted and retrofitted specimens, respectively. Furthermore, the authors proposed that a different type of connectors should be used instead of those used in this study due to their brittle failure.

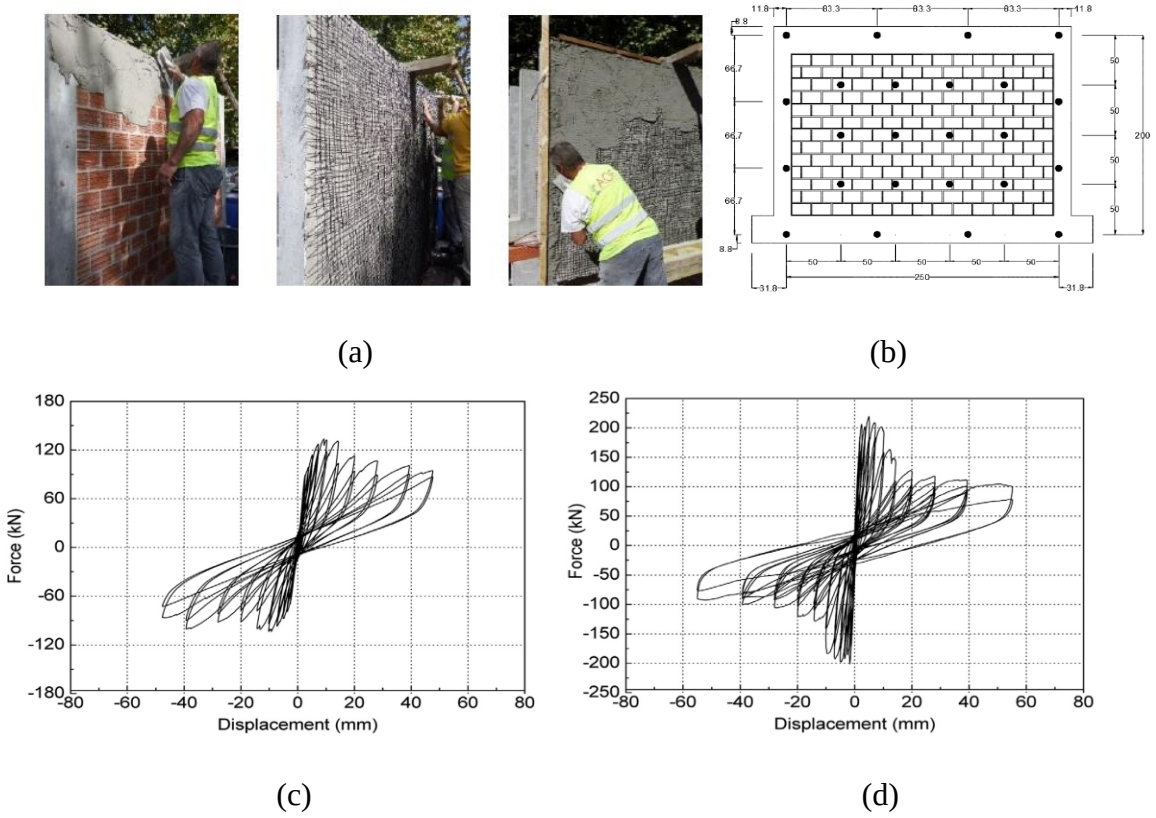

Figure 2.18: (a) TRM retrofitting technique installation procedure, (b) location and the number of the connectors used in the retrofitted specimens, (c) force versus displacement curve for unretrofitted and (d) for TRM retrofitted infilled frame (Akhoundi et al. 2018).

Ismail et al. (2018) conducted cyclic tests on nine 2/3-scaled infilled RC frames retrofitted with TRM. In this study three different TRM layouts were examined; the orthogonal full-surface application of TRM, the diagonal band of TRM by varying its width, and three different types of fiber material for assembling the textile reinforcement were used for TRM (i.e. basalt, carbon, and glass), as shown in Fig. 2.19. From the results, it was observed that all the retrofitted infilled frames exhibited almost the same failures without any rupture or deboning of the TRM. Furthermore, the infill-frame separation was observed in each specimen at the early loading stage. In the case of TRM diagonal bands, cracks perpendicular to the strips were observed on infill walls, while in the case of full-face TRM, only minor cracks appeared in the bottom beam-infill interface. In both cases, a few diagonal cracks were observed on the TRM surface. The authors concluded that using diagonal bands of TRM with width equal to 1/6 of the infill diagonal length is the most effective configuration for retrofitting the infilled

frames. Furthermore, the in-plane strength and load capacity of the basalt-TRM retrofitted specimen were higher than the corresponding ones of the carbon-TRM retrofitted specimen. The increase on the lateral capacity of the infilled frames due to basalt-TRM was 40%. The glass-TRM retrofitted infilled frame's lateral capacity was increased by 32% compared to that of the unretrofitted one.

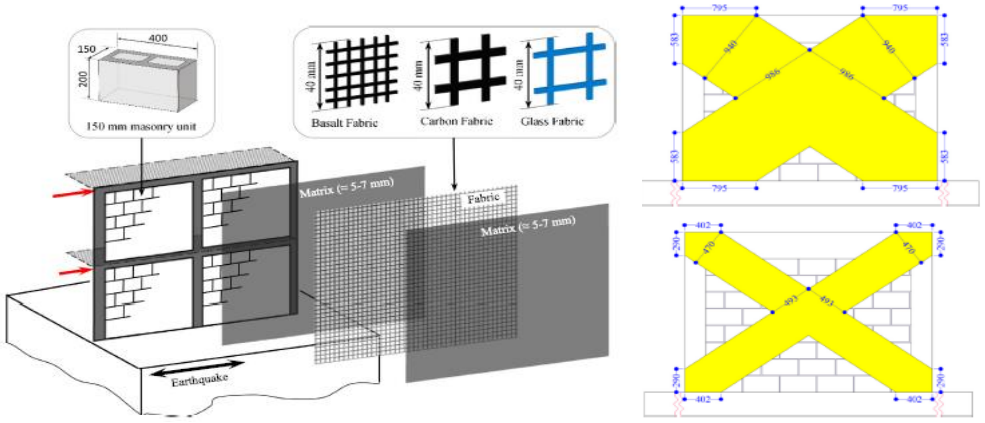

(a) (b)

Figure 2.19: Graphical illustration of the TRM application: (a) full-face TRM, and (b) two diagonal band of TRM with different widths (Ismail et al. 2018).

Sagar et al. (2019) conducted an experimental study on six single-story, single-bay half-scale masonry-infilled RC frames under bidirectional loading (application of slow cyclic drifts for in-plane loading and shake table–generated ground motion for out-of-plane loading) to evaluate the effectiveness of using a fabric-reinforced cementitious matrix for retrofitting infilled frames. The investigated parameters were the fabric application method, the presence of anchors, and the fabric's orientation. From the test results, the authors observed that the retrofitted infilled frame using direct application of fabric exhibited better performance (better bond characteristics between the composite and masonry infill) compared to that of using indirect application of the fabric. They also concluded that the mechanical anchors effectively limited the separation of the infill from the frame, resulting in an enhanced bidirectional resistance of the retrofitted infilled frame. The orthogonal orientation of the fabric (parallel to the bed joints) was more effective than the oblique direction one, since the retrofitted specimens with orthogonal orientation of the fabric provides a more ductile behavior than the ones of using oblique orientation of the fabric.

It is important to mention that over the years, tests on masonry wall elements retrofitted with TRM under either diagonal compression or in-plane lateral loading have been carried out. The research regarding the use of TRM for retrofitting masonry walls begins in the early 2000s, and it has been performed by Papanicolaou et al. (2006, 2007, 2011). These authors investigated the behavior of masonry wall elements retrofitted with TRM under diagonal compression loading (Figs. 2.20 a and b), and the response of masonry wall elements retrofitted with TRM and FRP under both in-plane, and out-of-plane loading (Figs. 2.20 c and d). The authors concluded that the TRM contributes to increase the shear strength and ductility of the masonry walls by about 6 and 13 times, respectively, by constraining the diagonal cracks that occurred on the walls (Figs. 2.20 a and b), since the shear stresses of the wall are transferred to TRM at local level, and this composite sustains these shear stresses due to its high compressive and tensile capacity. According to the authors, the shear capacity and failures of TRM-retrofitted walls depend on the bond conditions between the wall and the TRM. The authors concluded that the behavior of masonry walls retrofitted with TRM under in-plane lateral loading is affected by various parameters such as: the number of strengthening layers (one or two layers, applied on both sides), the type of grid (open mesh structures comprising of carbon, glass or basalt fibers and polypropylene or polyester), the type of mortars used for assembling the textile reinforcement, and by the compressive stress level applied to retrofitted masonry wall elements undergoing in-plane loading. The authors reported that the walls receiving double TRM-layer their strength increases by about 10%-30% compared to that of the walls with single TRM-layer. Also they concluded that even in the weakest TRM configurations (‘low-tech’ textiles combined with low-strength mortars), the strength and deformability of the retrofitted walls increase by 400% and 130%, respectively, compared to the corresponding ones of the unretrofitted wall. Additionally, they found out that adding more TRM-layers, beyond 1.5% reinforcement ratio is not efficient. The failure of the TRM-retrofitted infill walls under in-plane loading includes the complete crushing of the masonry wall, and the local buckling of the textile reinforcement as presented in Fig. 2.20 (d).

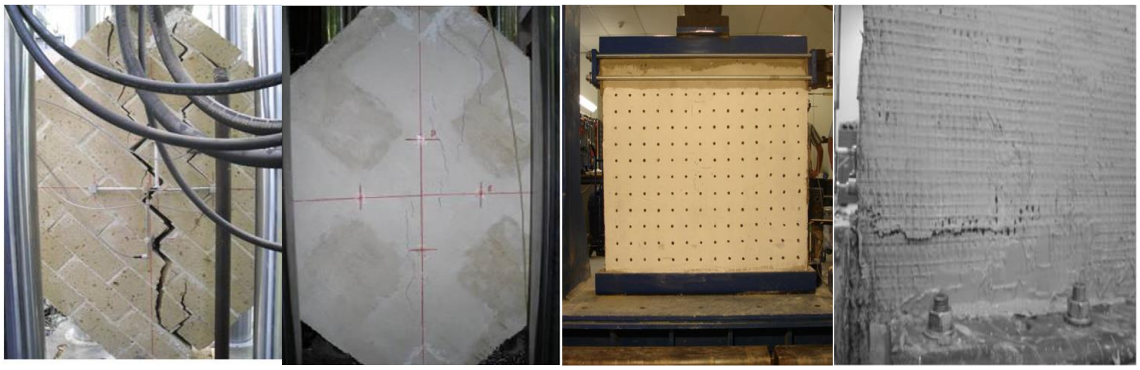

(a) (b) (c) (d)

Figure 2.20: (a) Crack pattern in the masonry wall under diagonal loading without TRM and (b) with TRM, (c) test set-up for in-plane loading, and (d) failures on the retrofitted infill wall under in-plane loading (Papanicolaou et al. 2006, 2007, 2011).

Following the concept of Papanicolaou et al. (2006, 2007, 2011), Parisi et al. (2013) and Prota et al. (2006) conducted diagonal compression tests on masonry wall elements retrofitted with cement-based matrix (compressive strength varies from 16MPa to 24 MPa, and flexural strength equal to 5.5MPa) coated with alkali resistance glass-textile. Both studies reported that using this composite material with different configuration, one or two layers of composite on one or two sides of the wall, the strength and the ductility of masonry wall elements increase, while this composite does not influence the initial stiffness of masonry wall elements. Specifically, Prota et al. (2006) concluded that the shear strength of the retrofitted wall is increased by about 1.7 and 2 times for one and two layers of TRM, respectively, compared to that of the unretrofitted wall. The authors also concluded that the bond between the masonry wall and the strengthening material plays a critical role in providing adequate load-carrying capacity of the retrofitted walls.

Another experimental study aiming to examine the behavior of retrofitted masonry walls under compression loading was conducted by Babaeidarabad et al. (2014) considering one- to four-layers of carbon fabric-reinforced cementitious matrix (FRCM). The cementitious matrix had a compressive strength of 19.5 MPa, and the modulus of elasticity of the carbon textile was 80 GPa. The authors investigated that the shear capacity of the retrofitted wall is 1.95 and 2.36 times higher for one and four

layers, respectively, compared to that of the unretrofitted wall. Also they reported that the FRCM contributes to increase the strength and ductility of the masonry wall by constraining the diagonal shear cracks that occurred on the wall. The authors also concluded that the shear capacity and the failures of FRCM-retrofitted masonry wall elements are affected by the level of the reinforcement ratio, as also reported Papanicolaou et al. (2006, 2007, 2011).

Bernat et al. (2013) performed experimental test to examine the response of masonry wall elements retrofitted with TRM under in-plane compressive eccentric load which was uniformly distributed on the wall's width. In this study various parameters were investigated such as: the type of mortar (three different mortar compressive strengths equal to 42.2 MPa, and 14.5 MPa and 34.5 MPa for Portland-lime- and pozzolana-based mortar, respectively), the type of fiber (glass, or carbon grids), and the possible benefit of using anchors between the masonry wall and the TRM (rectangular pieces of glass, or carbon grid were rolled to pass through a hole in the wall). The authors concluded that the connectors are necessary to enhanced the bond strength between the wall and the TRM, and consequently to increase the vertical load-bearing capacity of retrofitted walls as shown in Table 2.2. Furthermore, the vertical load-bearing capacity (Nmax) of the TRM-retrofitted masonry wall elements is increased by about 100% compared to that of the unretrofitted ones. Also, the authors concluded that the retrofitted wall's stiffness and vertical load-bearing capacity are highly depended on the type of mortar used for binding the textile reinforcement and on the of fiber's material used for assembling the textile as shown in Table 2.2.

Table 2.2: Increase in load-bearing capacity of masonry walls due to TRM (Bernat et al. 2013).

Fibre grid	**Mortar**	**Connectors**	**N_{max}(kN)**	**Load-bearing capacity increment (%)**
1Glass	Portland-based	0	299.7	87
2Glass	Portland-based	0	390.3	143
1Glass	Lime-based	0	285.6	78
2Glass	Lime-based	0	414	158
1Carbon	Pozzolana-based	6	313.5	96
1Carbon	Pozzolana-based	9	330.2	106

Augenti et al. (2010) performed in-plane cyclic tests on full-scale unreinforced masonry (URM) wall with a door opening retrofitted with inorganic matrix-grid composites (which consisted of hydraulic lime and sand, and a glass fiber textile) (Fig. 2.21 a). The tensile strength of the matrix and glass grid was 6 MPa and 1276 MPa, respectively. Cyclic displacement loading was applied at the top of the beam up to a near-collapse state (drift ratio 3%). The authors concluded that this retrofitting method contributes to increase significantly the lateral capacity and dissipated energy of masonry walls with openings by restoring the load-bearing capacity to the one of an as-built wall without opening, and by delaying the strength degradation of the wall due to presence of the opening. The results obtained from this study in terms of force versus displacement are presented in Figs. 2.21 (b) and (c) for the unretrofitted and retrofitted specimen, respectively.

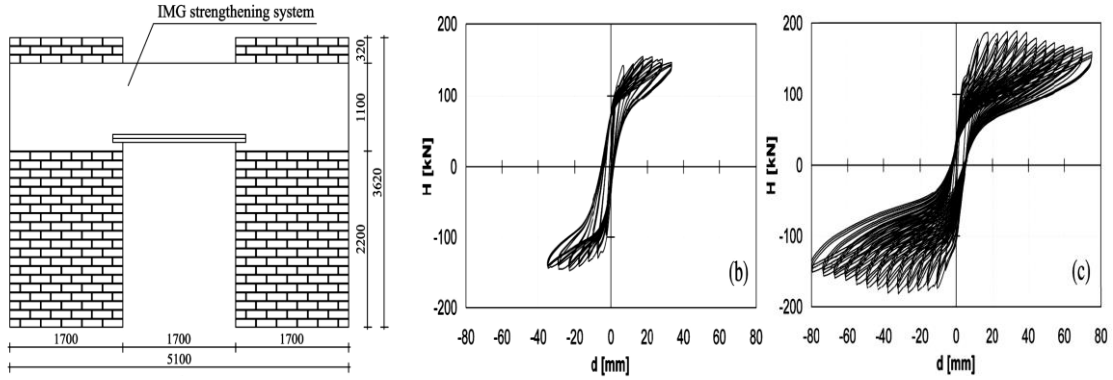

(a) (b) (c)

Figure 2.21: (a) Strengthening scheme of the masonry wall with door opening, (b) Experimental force-displacement curve of the unretrofitted infill wall, and (c) of the retrofitted infill wall (Augenti et al. 2010).

Table 2.3 summarizes all the studies mentioned above including the authors' major observations and the results derived from each study to present a global picture of the research regarding the effectiveness of using TRM composite material for retrofitting infilled frames subjected to in-plane lateral loading, and its evolution, as well, for the benefit of the reader.

Table 2.3: Summary of testing campaigns of infilled frames retrofitted with TRM under in-plane loading.

Author	Type of test	Major observations and results
Da Porto et al. (2015)	In-plane and out-of-plane monotonic loading.	the damages of infilled frames are reduced, the crack pattern changes, higher in-plane deformation capacity and dissipated energy. The use of anchorages does not significantly change the in-plane behavior of retrofitted infilled RC frame.
Koutas et al. (2014a)	In-plane cyclic loading (1.35% drift ratio)	56% increase in the lateral strength of infilled frame, 52% higher deformation capacity and 22.5% dissipated energy. The presence of custom-fabricated textile-based anchors was proved particularly effective in delaying or even preventing the debonding of TRM.
Akhoundi et al. (2018)	In-plane cyclic loading (3% drift ratio)	Increase in lateral stiffness and ultimate strength by about 40% and increase in dissipated energy by about 39%-51%) one of infilled frames. Using connectors creates better bond between TRM and infill wall.
Ismail et al. (2018)	In-plane monotonic loading	The diagonal bands of TRM with width equal to $1/6^{th}$ of the infill diagonal length is the most effective configuration of retrofitting infilled frames. Increase in strength and load capacity of retrofitted infilled frames using Basalt-TRM instead of carbon-TRM.
Sagar et al. (2019)	In-plane loading and shake table–for out-of-plane loading.	Direct application of fabric is better that the indirect one. Mechanical anchors were useful by limiting the separation of infills from the frame, resulting in an enhanced lateral capacity. Orthogonal orientation of the fabric parallel to bed joints was more effective than oblique orientation (more ductile behavior of retrofitted infilled frames)

2.5.2 Numerical investigation

Whereas a significant number of experimental studies have been carried out aiming to examine the response of masonry-infilled RC frames with TRM under in-plane lateral loading, much less has been conducted for simulating the complex behavior of this type of structure using either simple approaches (macro-modeling) or more detailed approaches (micro-modeling). In the literature, there are only three studies in which the complex behavior of masonry-infilled RC frames is modeled following a simple modeling approach, macro-modeling, and these studies are deeply analyzed in the following paragraphs. None of the past studies were geared towards the numerical modeling of masonry-infilled frames with TRM following the micro-modeling approach. Therefore, in order to cover completely all the aspects regarding the numerical modeling of infilled frames with TRM, the numerical studies conducted so far in which the masonry walls with TRM are modeled following either micro-modeling or macro-modeling approach are also presented in the following paragraphs.

Koutas et al. (2014b) developed a simple macro-model of infilled frame with TRM to predict the behaviour of the TRM-retrofitted three-story masonry-infilled RC frame subjected to in-plane cyclic loading that was studied experimentally by the authors as presented in section 2.5.1. In this model, a single-strut (compression) and a single-tie (tension) elements are used to represent the infill wall and the TRM, respectively. Fardis and Panagiotakos (1997) model is adopted for the single-strut element for simulating the non-linear cyclic behavior of the infill wall. The RC members were modelled by linear elastic beam-column elements and rotational spring elements are used at the beams and columns to simulate the plastic hinges. To define the tensile behavior of the single-tie (tension) element, the so-called effective strain of TRM was required. The authors concluded that this macro-model can adequately represent the masonry-infilled RC frame's experimental response with and without TRM, while the best agreement between experimental and numerical results in terms of the maximum base-shear was achieved considering that the effective strain for one layer of glass-TRM is equal to 0.8%. The authors also concluded that this macro-model of retrofitted infilled frame is sensitive to the value of effective strain of TRM used, leading the effective strain of TRM as a key parameter for the tie-model.

Pohoryles and Bournas (2020a) proposed a macro-model of infilled frames with TRM following the same approach as Koutas et al. (2014b) but using an additional tensile tie-model aiming to take into account in more detail the contribution of TRM. This model was calibrated using experimental data gathered from the literature. The authors concluded that the definition of the effective strain of TRM was crucial for developing an accurate tensile tie-model. For this reason, in this study an empirical equation for estimating the effective strain of the TRM is proposed and presented a good correlation with experimental data, although that the experimental data were limited. Later, Pohoryles and Bournas (2020b) modified their proposed model where the new one comprising a tie-model which takes into account the tensile strength of the composites material, while the increase of the compressive strut width due to the improving connection of the infill to the frame causing by this composite material is included in the model. Also in this study empirical equations for tie and strut strength was

developed, while the strut model was calibrated in terms of experimentally obtained stiffness.

During the last ten years, several numerical studies have been also conducted aiming to develop an accurate micro-model of masonry wall with TRM using different commercial FE software (MIDAS-FEA, ABAQUS, and DIANA FEA). For example, Parisi et al. (2011) developed finite element (FE) micro-model of masonry wall with TRM, in the DIANA FEA software to represent the experimental study conducted by Augenti et al. (2010), as described in the previous section (section 2.5.1). In this numerical study, the brick units and the mortar joints (and unit-mortar interface) were separately modeled using isotropic continuum elements (shell elements, eight-node quadrilateral plane-stress element). The strengthening system was modelled as grid reinforcement (tension elements) embedded in the mortar continuum elements. A smeared crack model was used for the brick units and for mortar joint elements, using the Rankine yield criterion for tension, and the Von-mises criterion for compression. The results obtained from the pushover analysis of the numerical model are compared well with those obtained from the experiment as shown in Fig. 2.22 (a). An analytical model was also developed in this study to predict the lateral strength of masonry walls with openings, with and without retrofitting, considering different failure modes of the infill wall.

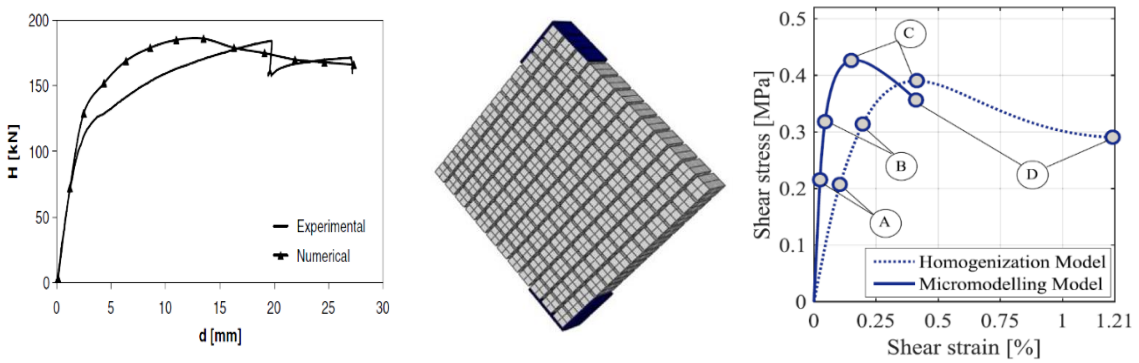

(a) (b) (c)

Figure 2.22: (a) Comparison between numerical and experimental results in terms of force versus displacement (Parisi et al. 2011), (b) 3D micro-model of FRCM-retrofitted masonry wall and (c) comparison between micro and macro modeling approach in terms of shear stress versus strain (Bertolesi et al. 2016).

Bertolesi et al. (2016) developed a three dimensional (3D) micro-model in ABAQUS to analyze the behavior of masonry wall elements retrofitted with TRM under diagonal compression loading (Fig. 2.22 b). Eight-node quadrilateral elements were used for brick units and mortar joints, while the Concrete Damage Plasticity model accompanied by multi-directional Drucker-Prager, and Mohr-Coulomb strength criterion was adopted for these elements. The strengthening material was modeled as truss reinforcement (tension elasto-brittle criterion for fibers) embedded into a cementitious-matrix mesh (3D eight-node element), assuming perfected bond between them. An analytical model of the masonry wall with TRM was also proposed considering the bond between the strengthening material and the masonry wall, while this model was unable to capture the shear failure that occurred on the TRM-retrofitted infill wall. Both models fit satisfactorily well the experimental data as shown in Fig. 2.22 (c).

A two-dimensional (2D) micro-model of masonry wall with TRM was developed by Basili et al. (2016) using MIDAS-FEA software to simulate the behavior of masonry walls retrofitted with basalt-TRM under diagonal compression loading that was studied experimentally by Prota et al. (2006). The masonry wall was modeled by isotropic continuum elements, while a smeared crack model with different non-linear softening functions for the tensile and compressive behavior of the wall was adopted for these elements. The basalt-textile and the mortar were modeled separately by continuum elements, using tension elastic-brittle material model for textile reinforcement. In this numerical model, the TRM was perfectly bonded to the masonry wall. After the calibration of the numerical model, a sensitivity analysis was performed, and the results showed that the response of unretrofitted masonry wall under diagonal compression loading is mostly influenced by the tensile properties of the masonry wall (strength and fracture energy), while the retrofitted masonry wall model is sensitive to the Young's modulus and to the compressive fracture energy of the mortar used for TRM. The authors also concluded that the number of layers of basalt-TRM influences the stiffness and the shear stress of retrofitted masonry walls subjected to diagonal compression loads.

Wang et al. (2017) developed a numerical model of masonry wall element with TRM in DIANA FEA software aiming to examine the effectiveness of using the TRM for

retrofitting masonry wall elements. The model's accuracy was validated by comparing the numerical results to experimental data taken from the literature. Eight-node shell elements were used for the mortar and masonry wall (Fig. 2.23 a), while the TRM was modeled by embedded reinforcement in the mortar elements (perfect bond between mortar and textile). In this numerical model, perfect bond between masonry wall and TRM was considered. The Total Strain Rotating Crack model was adopted for mortar elements, while for wall elements a softening anisotropic elasto-plastic continuum model was used (Hill type criterion for compression and Rankine type yield criterion for tension). After the calibration of the numerical model, pushover analysis was performed on selected case-studies, where the influence of different TRM strengthening schemes and materials on the lateral response of two-story masonry wall with large central door opening was investigated (Fig. 2.23 b). The numerical results showed that the masonry wall element with steel-TRM has higher load-bearing capacity and ductility than the corresponding ones of the masonry wall with basalt- and glass-TRM as shown in Fig. 2.23 (c).

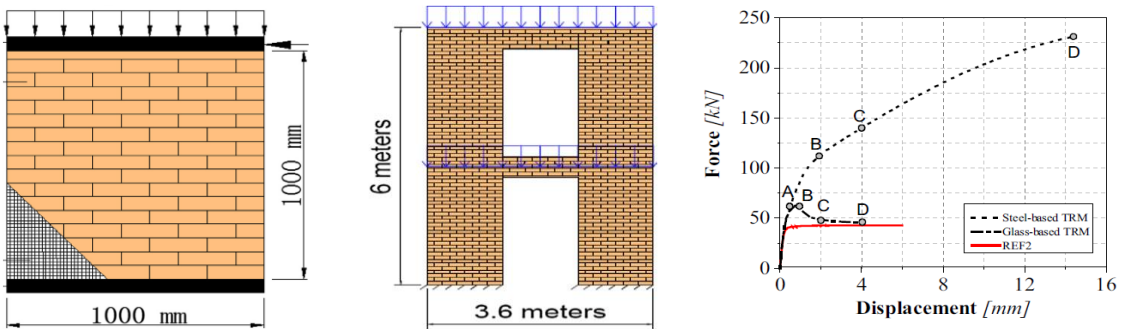

(a) (b) (c)

Figure 2.23: (a) Geometry of the TRM-retrofitted masonry wall element, (b) geometry of the selected case-study, and (c) force versus displacement curve of masonry wall with steel- and glass-TRM and without TRM (Wang et al. 2017).

It is important to mention that over the years studies have also been conducted aiming to propose analytical equations for predicting the strength, stiffness, deformation capacity of masonry wall elements retrofitted with TRM. For example, Bernat et al. (2013) proposed an analytical model to predict the axial force-bending moment interaction curve for masonry walls with TRM when subjected to out-of-plane loading considering

two failure modes; tensile failure of TRM, and compressive failure of masonry wall, while perfect bond was assumed between textile and mortar, and between TRM and masonry wall. Furthermore, Kouris et al. (2019) proposed design guidelines for strengthening masonry walls using TRM considering the compressive and flexural failure of the masonry wall, and the tensile failure of the TRM (rupture and debonding of TRM). The in-plane and out-of-plane capacity of strengthened masonry wall elements was estimated through cross-section analysis considering the above failure modes. In these equations the ultimate stress and strain of TRM is required in order to take into account the failure of TRM (tensile rupture of TRM, or debonding of TRM where the cohesive failure occurs either in the wall or in the mortar). Finally, in this study an equation for estimating the required thickness of TRM to avoid the overturning of masonry wall was proposed. The analytical design method proposed by Kouris et al. (2019) was verified against experimental results.

To conclude, the studies conducted so far for simulating the complex behavior of infilled frames with TRM are very limited, and therefore more numerical studies must be carried out aiming to simulate the behavior of masonry-infilled RC frames retrofitted with TRM subjected to in-plane lateral loads using either simple approaches (macro-modeling) or more detailed approaches (micro-modeling) while well calibrated micro-models may be used to fine-tune macro-models.

2.5.3 Main parameters influencing the effectiveness of TRM retrofitting technique

It is crucial to summarize the parameters that can influence the effectiveness of using the TRM composite material for retrofitting masonry-infilled RC frames. To achieve this the main finding obtained from the above mentioned studies, where the effectiveness of using the TRM for retrofitting either masonry-infilled frames or masonry wall elements is investigated, are summarized to classify the critical parameters that affect the efficiency of this retrofitting solution.

Reviewing the literature as presented in previous sections (sections 2.5.1 and 2.5.2) it can be concluded that the response of TRM-retrofitted infilled frames subjected to lateral loads, and the response of masonry wall elements with TRM subjected either to diagonal compression loading or in-plane loading depend on the following parameters:

(1) the bond conditions between the wall and TRM, (2) the compressive and tensile capacity of TRM, and by (3) the adhesion properties of the textile-matrix interface. These parameters depend mainly on the type of the inorganic-matrix used for binding the textile reinforcement and by the mechanical and geometric characteristics of the textile reinforcement (geometry, layout, number of textile, reinforcement ratio etc.) because these factors determine the type of failure of the TRM such as: rupture of the TRM or slippage of the textile from the mortar, and the debonding of TRM from the substrate.

Regarding the type of inorganic-matrix used for assembling the textile reinforcement, Triantafillou (2011) and Koutas et al. (2014a) reported that the chemical bond (shear bond strength and adhesion properties) between the textile and the mortar, and between the TRM and substrate is the key parameter influencing the effectiveness of using TRM for retrofitting concrete and masonry elements. They also recommended that special type of inorganic-matrix must be used for assembling the textile reinforcement instead of using conventional mortars. Therefore, the matrix composition must be such as to achieve full penetration with the textile and full bonding to the substrate. The minimum requirements for the mechanical properties of the inorganic matrix used for retrofitting structures are defined in the European Standard EN 1504-3 (four classes of repair mortar). Besides the type of inorganic matrix, the textile mesh's geometry and layout are also important factors influencing the effectiveness of this technique. As derived from previous sections, the strength and stiffness of TRM-retrofitted masonry wall elements and of TRM-retrofitted infilled frames are usually higher if the mesh spacing of the textile allows the mortar to pass and be correctly bonded to the substrate. Nevertheless, more studies must be conducted to investigate the influence of the type of the mortar and of the geometry of the textile on the response of infilled frames under lateral loading.

As previously mentioned the effectiveness of TRM is depends highly on the textile reinforcement ratio. It is important to note that the textile reinforcement ratio depends on the number of textile layers and on the geometry of the textile (the fiber in each threat and spacing between the threats in the textile). Most of the existing studies found out that the load-carrying capacity, the strength and deformation capacity of TRM-

retrofitted masonry wall elements are increased by increasing the reinforcement ratio while this increase is not proportional to the increase of the reinforcement ratio due to a different failure mechanism that may develop between the layers. The above observation that was observed for masonry wall elements with TRM applies also to infilled frames with TRM. Regarding the effect of the reinforcement ratio on the response of masonry wall elements with TRM under either diagonal compression loading or lateral loading, Papanicolaou et al. (2006, 2007, 2011), concluded that for walls receiving a double TRM-layer their strength increases by about 10%-30% compared to that of the walls with single TRM-layer, while Prota et al. (2006) concluded that the shear strength of the retrofitted wall is increased by about 1.7 and 2 times for one and two layers of TRM, respectively, compared to that of the unretrofitted wall. Considering the lack of experimental or numerical studies regarding the influence of the reinforcement ratio on the effectiveness of using TRM for retrofitting infilled frames, further relevant studies must be carried out.

Besides the above-mentioned parameters, the fiber's material used for assembling the textile (glass, steel, carbon, ballast) also influences the effectiveness of this retrofitting method since by changing the fiber's material, the tensile capacity of the TRM is also changed (as will be discussed in Chapter 3). For example, previous studies showed that using glass-TRM on masonry wall elements resulted in higher load capacity, than the one of using basalt-TRM, despite its lower tensile strength compared to basalt-TRM. Furthermore, Ismail et al. (2018) concluded that the in-plane strength and load capacity of the basalt-TRM retrofitted infilled frames was higher than the corresponding ones of the carbon-TRM retrofitted specimen, while the increase on the lateral capacity of the infilled frames due to basalt-TRM was 40%. More studies must be carried out aiming to examine the influence of the fiber's material used for assembling the textile on the response of infilled frames retrofitted with TRM under in-plane loading.

Finally, the type of the connectors used to anchor the TRM to the infill wall (which prevent the delamination of TRM) and the type of anchors used to provide anchorage of the TRM to the bounding RC frame elements, are the most important parameters regarding the TRM strengthening method when used on masonry-infilled RC frames, since they contribute to prevent the TRM debonding, and consequently the brittle

failures that may occur on infilled frames such as the shear failure of the columns. Therefore, more research is necessary to investigate this innovating technique by taking into account all the possible failures that may occur on infilled frames with TRM in order to improve the bond condition between the TRM and the masonry-infilled RC frame, and consequently the in-plane behavior of infilled frames retrofitted with TRM.

2.6 Summary and conclusions

This Chapter provides the necessary background knowledge regarding the lateral behavior of masonry-infilled RC-frame buildings and the major existing modeling approaches for simulating this type of structure. Following the objectives of the current study, the experimental and numerical studies conducted so far aiming to investigate the effectiveness of using the TRM composite material for retrofitting masonry-infilled RC frames are deeply analysed to provide full insight concerning the TRM retrofitting technique. The following paragraphs summarize the content of each of the different tasks presented in previous sections, and present also the conclusions obtained from this literature review.

The high vulnerability of masonry-infilled frame buildings when subjected to in-plane and out-of-plane loadings was investigated by several researchers so far. Most of them concluded that the existence of infill walls in RC frames can introduce brittle shear failure mechanisms associated with the infill-frame interaction such as *soft-story mechanism, short column mechanism* and *plan torsion effects*, although in many cases infill walls have a positive contribution to the lateral resistance of frames. Five failure modes are possible to occur on infilled frames with and without openings under lateral loading as follows: *Frame failure, Infill sliding shear failure, Infill diagonal compression failure, Corner crushing,* and *Infill diagonal cracking* failure mode. The failure modes and crack patterns of infilled frames with openings are influenced by the location and by the size of the opening (*diagonal compression* and *diagonal cracking failure modes*). The most important failure mode observed in infilled frames under lateral loads is the *frame failure mode* since weak frames or weak joints mostly appear in existing buildings since most of them were constructed without any seismic design provisions.

Many researchers reported that the presence of infill walls in RC frames contributes to a significant increase of the lateral strength, stiffness, dissipated energy of the bare frames but at the same time it introduces brittle shear failure mechanisms as previously mentioned. The behavior of masonry-infilled RC frames subjected to lateral loading is complex due to a high number of parameters that are involved in this type of structure such as: the infill wall geometry and mechanical properties, the geometry and mechanical properties of the surrounding frame, the characteristics of the infill–frame interface, the infill-frame relative stiffness and strength, the presence of openings, the quality of the materials used and the workmanship etc.

Despite of the popularity of masonry-infilled RC-frame buildings and their long existence, it is still difficult to assess their behavior under earthquake loading, as well as extremely hard to predict the lateral response of such type of buildings due to the large number of parameters involved. Two modeling strategies are typically adopted for infilled frames, based on the level of detail by which the infill wall is modeled, namely: macro-modeling and micro-modeling, where the micro-modeling can be considered in four levels and each level provides different level of accuracy. The macro-modeling approach compared to the micro-modeling, shows significant practical advantages. On the other hand, the micro-modeling approach proved to be the most accurate approach to capture the real behavior of infilled frames since more complex issues are considered in this approach such as; the infill-frame interaction, the sliding of the brick units along mortar joints, the cracking propagation on infills and on RC elements.

The TRM composite material has received attention as a sustainable and more compatible solution for retrofitting RC and masonry structures, due to its very small thickness and durability features. Over the years significant research has been conducted and reported for retrofitting masonry wall elements, however, much less has been carried out for retrofitting masonry-infilled RC frames. The effectiveness of using the TRM composite material for seismic retrofitting masonry-infilled RC frames depends on: (1) the bond conditions between the wall and TRM, (2) the compressive and tensile capacity of TRM, and (3) by the adhesion properties of the textile-matrix interface. These parameters depend mainly on the type of the inorganic-matrix used for binding the textile reinforcement and on the mechanical and geometric characteristics of the

textile reinforcement (geometry, layout, number of textiles, reinforcement ratio etc.). The type of connectors used to anchor the TRM to the infill wall and the type of anchors used to provide anchorage of the TRM to the bounding RC frame elements, are the most important parameters regarding the TRM strengthening method when used on masonry-infilled RC frames.

This literature review that was presented in previous sections allows the following conclusions to be drawn:

- Very few studies were performed on infill walls within RC frames retrofitted with TRM; therefore, experimental or numerical tests would be very important in order to characterize the seismic behavior of infilled frames retrofitted with TRM;
- There is a need to facilitate the implementation of the numerical models of retrofitted structures using TRM, since the numerical tests of masonry-infilled RC frames retrofitted with TRM following either the macro- or micro- modeling approach are necessary in order to study in more depth this method by taking into account all the possible critical parameters able to affect its efficiency without performing experimental tests which are economically prohibitive;
- None of either past experimental or numerical studies were geared towards the use of TRM for retrofitting masonry-infilled RC frames with openings;
- No specific guidelines exist for infill walls within RC frames retrofitted with TRM, leading to the inapplicability of this method in real structures;
- More experimental and numerical studies are necessary to investigate the parameters influencing the effectiveness of TRM for retrofitting masonry-infilled RC-frames in order to develop future guidelines in which the design and detailing using this strengthening solution is achieved. It would be important to formulate simplified methodologies by which a designer may assess the benefits of using TRM to reduce the seismic vulnerability of masonry infills (local level) and of entire buildings (global level).

The above conclusions motivate the aims of this thesis.

CHAPTER 3

3. ANALYTICAL MODEL OF TEXTILE REINFORCED MORTAR: MONOTONIC LOADING

3.1 Introduction

The interest for TRM as a retrofitting method for RC and masonry structures has been rising for almost a decade. Nevertheless, the application of the TRM as a method of retrofitting masonry-infilled RC frames is a relatively new concept (section 2.5, Fig. 2.17 b), and therefore more relevant studies must be performed. One way to achieve this is to investigate numerically the effectiveness of using the TRM as a method for retrofitting masonry-infilled RC frames, which is one of the objectives of this study. In order to facilitate the implementation of numerical models on retrofitted structures using TRM, and further to develop design guidelines, it is important to develop simplified models able to predict the behavior of this composite material. Towards this direction, in this part of the thesis, a simple and easy-to-implement tri-linear analytical model is proposed to define the stress-strain relationship of TRM under tensile loading.

Over the years, research, has been also conducted regarding the effectiveness of using the TRM composite material for retrofitting RC members, such as: beams, columns and slabs (Papanicolaou et al. 2009, Ortlepp et al. 2009, Di Ludovico et al. 2010a,b, García et al. 2010,Triantafillou 2011, Mechtcherine 2013, Colajanni et al. 2014, Gil et al. 2014), and for retrofitting masonry walls and masonry-infilled frames (section 2.5). Nevertheless, reliable simplified models are important to facilitate the use of TRM for the seismic retrofitting of existing buildings in practical engineering. In this context, relevant design approaches or analytical models have been proposed so far for the application of TRM on RC elements, masonry walls and masonry-infilled frames, as briefly presented in section 2.5 (Wiberg 2003, Bruckner et al. 2006, Ombres 2011,

Bernat et al. 2013, Babaeidarabad et al. 2014, Tetta et al. 2018, Kouris et al. 2019). According to these approaches, the contribution of TRM, where the TRM usually works under tensile loads, is accounted for by introducing an additional term to the equations usually employed for unstrengthened members following the guidelines (ACI) 549-13. These approaches do not take into account the complexity of the bond stress transfer between the TRM external strengthening layer and RC elements or masonry walls. It is important to mention that the existing codes do not cover the design matter with a systematic approach regarding the application of TRM, and there are only some over-simplified approaches, such as International Code Council (ICC-Evaluation Service 2013) and (ACI) 549-13 guidelines. More specifically, ACI 549-13 guidelines provide equations for an idealized bilinear constitutive law of TRM-confined concrete members (flexural strength) with the effective tensile strain in the composite material limited to a value of 0.12%. Note that a value of 0.4% corresponds to the design limit for retrofitting masonry walls in ACI 549, while for out-of-plane loads this design value is equal to 0.12%.

Despite the evolution of using the TRM as a sustainable and compatible solution for retrofitting RC and masonry structures and the several experimental studies conducted so far towards the mechanical characterization of TRM composite material, a simplified model able to predict the mechanical behavior of this composite material has not yet been developed. In the literature, there are numerical and analytical models that simulate the behavior of TRM, which show an excellent correlation with the experimental data (Holler et al. 2004, Richter and Zastrau 2006, Graf et al. 2007, Larrinaga et al. 2013, Rampini et al. 2019). Nevertheless, most of these models are complicated to implement, require the use of specific software, and experimental data in order to be applied. The interest of the research community regarding the study of the textile reinforced inorganic-matrix composite, experimentally or numerically, is presented in Fig. 3.1. In the studies included in Fig. 3.1, this composite material is referred with several terms, such as Textile Reinforced Concrete composite materials (TRC), Textile Reinforced Mortar (TRM), and Fabric Reinforced Cementitious Matrix (FRCM). In this thesis, the acronyms TRM, as well as FRCM, will be used as synonyms referring to composites that employ matrices.

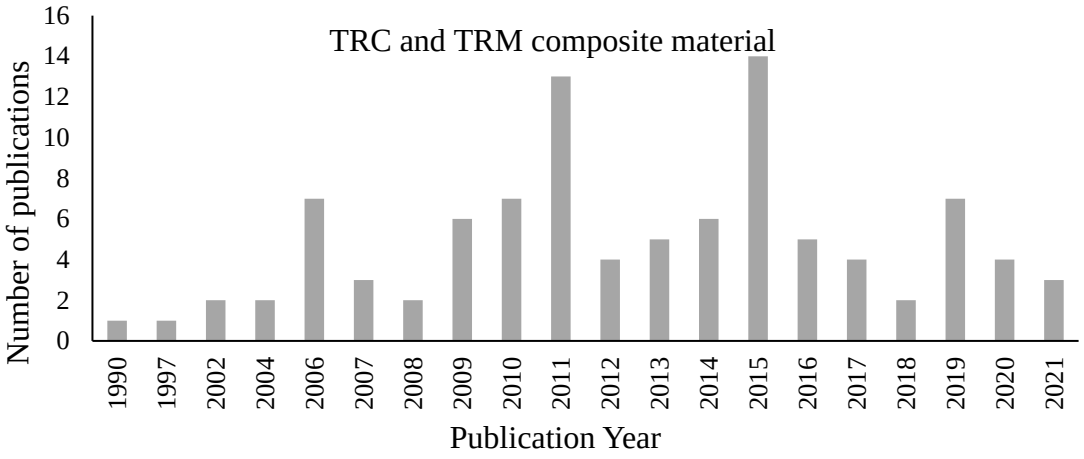

Figure 3.1: Number of publications per year regarding the mechanical characterization of TRM and TRC composite materials.

Considering the above limitations, there is an urgent need to develop a simple and easy to-implement model to define the tensile behavior of TRM in terms of stress-strain, in order to facilitate the implementation of numerical or analytical models of retrofitted structures using TRM, and further to develop design guidelines for RC and masonry structures retrofitted with TRM. Therefore, in this part of the thesis a simple analytical model is proposed for predicting the tensile behavior of TRM in terms of stress-strain. Firstly, a brief description of the TRM composite material regarding its constituent materials and its mechanical behavior is presented, while a short description regarding the numerical and analytical models that exist so far for representing the tensile behavior of TRM is also presented (section 3.2). Following that, the proposed analytical model of TRM is presented (section 3.3), which extends the Aveston–Cooper–Kelly (ACK) theory, which applies for fiber-brittle matrix, to TRM, using the recommendations proposed by Eurocode 2 (section 3.3.2) and *fib* Model Code 2010 (section 3.3.3) for predicting the crack spacing and the fracture energy of the composite material, respectively. Then, the analytical model of TRM is verified by comparing its results with those obtained by experimental and analytical studies conducted in the past (section 3.4). After the assessment of the proposed model, a parametric study is performed to examine the parameters that can influence the tensile behavior of TRM according to the proposed model (section 3.5). The summary and the main conclusions regarding the proposed model are presented at the end of this Chapter (section 3.6).

3.2 TRM composite material

A general review of research in the area of TRM composite material is definitely necessary in order to cover the literature background of the research objectives of the present study, as described in the previous sections. Therefore, in this section, a brief description of the TRM composite material regarding its constituent materials and its mechanical behavior (tensile behavior) is presented, as well as the parameters that can influence the tensile behavior of TRM. This is followed by a short description regarding the numerical and analytical models that exist so far for representing the composite materials consisting of inorganic-matrix reinforced with fibers or textiles, with more emphasis on the analytical modeling of TRM for capturing its tensile behavior (stress-strain relationship). This part of the literature review mainly focuses on the tensile behavior of TRM, since the bending behavior of this composite and the bond mechanism at the textile-matrix interface (bond stress-slip relations) are beyond the scope of this research.

3.2.1 Definition of TRM

TRM is a composite material consisting of finely grained cement- or lime-based matrix and textile, made of fibers, which is used as reinforcement (Fig. 3.2). The textile comprises of yarns (roving) that cross each other at constant angles and it is assembled as a fabric (woven, braided, knitted and stitched) (Mobasher 2011). Yarn is made up of several hundred, up to thousands, individual parallel-alignment filaments (fibers). Two different bond zones exist inside a yarn; the sleeve, and the core zone (Hegger and Voss 2008a). In the sleeve zone (25% of the cross-sectional area of the yarn), the filaments contact the matrix and adhesion bond dominates (Häußler-Combe and Hartig 2007 and Banholzer et al. 2006). In contrast, the central–core filaments of a yarn (75 % of the area of the yarn) do not have immediate connection to the matrix, but they contact the adjacent filaments or those that remain partially unconnected, as the inorganic matrix with high viscosity cannot reach narrow spaces (Hartig et al. 2008 and Peled et al. 2008). The failure of about 10% up to 20% of the filaments of a yarn is sufficient for the failure of the whole yarn to occur, based on enhanced fiber bundle models (Shams et al.

2014). Fibers which have been used and explored in TRM include but are not limited to: alkali-resistant glass (AR-glass) fibers with linear elastic elongation up to 2% and modulus of elasticity between 70 GPa-80 GPa, carbon fibers with modulus of elasticity between 200 GPa and 250 GPa and elastic elongation between 0.7% and 1.5 %, basalt fibers with modulus of elasticity between 70 GPa and 95 GPa and tensile strength of about 2000 MPa, and aramid fibers with modulus of elasticity between 60 GPa and 130 GPa and rupture strain up to 2%. It is import to mention that, recently the research community focusing on using natural fibers for assembling the textile reinforcement. The inorganic matrix in TRM differs from that typically used in conventional mortars. Highly flowable mortar is needed to adequately penetrate the textile reinforcement in order to provide sufficient bond strength and load transfer at the textile-matrix interface. The mix composition of the inorganic matrix used in TRM usually includes: water–to-binder ratio ranging from 0.18-0.50, pozzolanic additives, such asfly ash and silica fume, polymers and short fibers (steel, glass, carbon and synthetics) (Brockmann 2007, Mobasher et al. 2004, Garmendia et al. 2011). The mechanical properties of the mortar used for binding the textile reinforcement cover a wide range of values, such as: compressive strength ranging from 10 MPa to 70 MPa, tensile strength equal to 2-8 MPa, Young's modulus equal to 8–40 MPa, and fracture energy ranging between 30-150 Nm (Butler et al. 2006, Hinzen and Brameshuber 2006, Silva et al. 2011, Brameshuber 2014). The minimum requirements for the mechanical properties of the inorganic matrix used for retrofitting structures are defined in the European Standard EN 1504-3 (four classes of repair mortar).

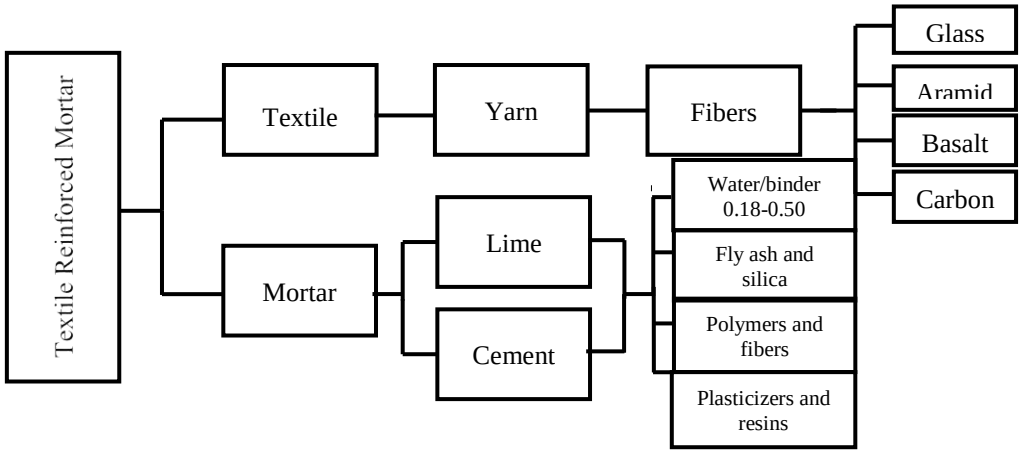

Figure 3.2: Schematic representation of constituent materials of TRM.

3.2.2 Mechanical behavior of TRM

Several experimental and numerical studies have been carried out in order to investigate the mechanical behavior of the composite material consisting of cement or lime-based matrix, reinforced with textile, through tension or bending tests. In both test setups, the composite material (TRC, TRM or FRCM) shows very similar behavior to conventional reinforced concrete. Although these composites may consist of a variety of textiles and matrices, an idealized tri-linear stress-strain relationship may be considered to describe their behavior under tensile load, as shown in Fig. 3.3 : State I (the uncracked matrix), State II (the crack formation), and State III (the crack stabilization and failure) (Jesse et al. 2005, 2008; Molter 2005; Hegger et al. 2006a; Mobasher 2011). State I corresponds to the elastic state of the uncracked TRM, where the load is mainly supported by the mortar. Consequently, the stiffness of the TRM at State I is approximately equal to the modulus of elasticity of the mortar, since the contribution of the textile to the stiffness of the composite is negligible at this State. The first crack takes place once the tensile strength of the inorganic matrix is reached, where the load is transferred through the micro-cracks to the textile reinforcement (Yao et al. 2016). After this pre-cracking state, State II begins with multi-cracking formations until the tensile strength of the mortar is reached once again. The number and the width of the cracks are influenced by the textile reinforcement ratio, the bond strength between the textile and the matrix, and the tensile failure strain of the mortar. In this State, the strain is increased due to the multi-cracking formation on the composite, while the stress remains constant. During this State, the composite presents non-linear behavior due to the debonding that occurs on the textile–matrix interface, which causes the ‘‘softening’’ of the stiffness of the composite material. Once the cracking is completed, the stiffness of the composite rises again while mobilizing the reinforcement’s stiffness in State III. The stress-strain relation of the composite in State III is mainly influenced by the properties of the textile reinforcement. Therefore, during this State the deformation increases without the appearance of any further cracks and the fabric is strained upwards.

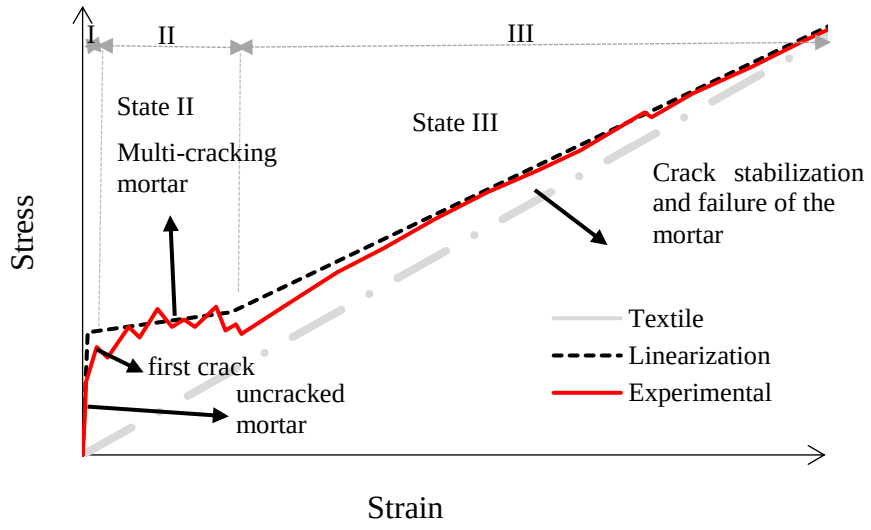

Figure 3.3: Typical stress-strain curve of TRM composite under tensile loading (in red) and linearization of the response of TRM (in dotted black) with indication of cracking states.

Table 3.1 summarizes some of the published studies regarding the mechanical characterization of TRM through tension tests. The major observations and the typical values (average values or minimum and maximum values) of the tensile stress-strain curve of this composite material found by the authors are included in the table, for the benefit of the reader. From Table 3.1 it can be concluded that the behavior of TRM composite material under tensile loading depends upon its constituent materials (the layout and the geometry of the textile and yarn, the type of the fiber's material, the reinforcement ratio, the composition of matrix, etc.), (Mesticou et al. 2017) and consequently by their positive or negative interaction when combined as a composite (Caggegi et al. 2017).

Reviewing the literature, the following conclusions are obtained regarding the parameters that can influence the tensile behavior of the TRM. Firstly, the fabrication of the textile influences the tensile behavior of TRM, mainly in States II and III, and secondly in the first cracking state (Peled and Bentur 2003; Mobasher 2005; Hegger and Voss 2008a; Contamine et al. 2011; El Messiry et al. 2014). Peled and Bentur (2003) concluded that woven and weft knit fabrics can improve the performance of the composite material at large deformations (State III), compared to other type of fabrics. On the other hand, Hegger and Voss (2008a) concluded that a composite material with

tricot textile showed greater tensile strength when first cracking occurs than the other textile structures. The mesh opening or the loop size of the textile (i.e., distance between the yarns) is another parameter that affects the tensile behavior of the composite material mainly at high (State III) and low (State I) strain levels, since the composite material with the larger loop size of textile exhibited better bond strength between the textile and the matrix than the smaller one, which led to increasing the stress and strain capacity of the composite at State I. But, in terms of ductility, the composite material with smaller loop size has higher ultimate strain (State III) than the one with larger (Peled et al. 2008a, b; Colombo et al. 2013; Portal 2013). Furthermore, the geometry of the yarn (i.e., the density, the diameter and the fineness) influences the bond conditions between the textile and the matrix, and consequently the tensile behavior of TRM in State II, since in the case where the roving or filament diameter is small, the penetration of the textile to matrix is low, and consequently relatively low friction between the inner filaments exists (Hegger and Voss 2008). On the other hand, the bond strength between core filaments increases in the case where the roving is impregnated with an epoxy resin, a concept which leads to improving the tensile performance of the composite material (Hegger et al. 2006). Apart from the above-mentioned parameters, the material of the fibers used for assembling the textile reinforcement (glass, steel, carbon, basalt), also influences the tensile behavior of TRM. The composite material with carbon textile has a higher ultimate tensile stress (by about 2 times), and a smaller bond strength than the textile of AR-glass (Ortlepp 2007; Hegger and Voss 2008). Adding to this, using textile with high modulus of elasticity enhances the bond strength, but the load transferred into the matrix decreases (Peled and Bentur 2003; Mobasher et al. 2006). Table 3.1 shows typical values of the tensile stress-strain curve of this composite material using different types of fibers for assembling the textile mesh, as obtained from several experimental studies. Besides the fiber's material, the textile reinforcement ratio also affects the tensile behavior of inorganic matrix composite materials (Jesse 2003; Peled and Bentur 2003; Hegger et al. 2006; Hegger and Voss 2008; Colombo et al. 2013; Rambo et al. 2015). The reinforcement ratio influences the multi-cracking formation of the composite material, since the number of cracks increases as the number of textile increases, while the distance between the cracks and the width of the cracks

are decreased (Larrinaga et al. 2013, 2014,Yao et al. 2016). Lastly, the type of matrix used for binding the textile reinforcement influences the tensile behavior of the composite at States I and II. The matrix composition must be such as to achieve full penetration with the textile, in order to enhance the bond strength between the matrix and the textile (Mobasher et al. 2004, Butler et al. 2010). Therefore, special attention should be given to the matrix composition, in order to achieve appropriate workability, curing time, fire resistance, flow ability, low values of creep and shrinkage, viscosity (rheology), compressive and tensile strength, Young's modulus and durability (Brockmann 2007). In order to achieve this, sand with small grain size, high binder contents (by addition of different pozzolanic additives), high performance plasticizers, short fibers, polymers and resins, must be used in the matrix. Experimental studies showed that, the addition of short fibers (steel, glass, carbon and synthetics) in the inorganic matrix improves the strength, crack development, load–deformation capacity, ductility, water absorption and the plastic shrinkage of TRM (Hinzen and Brameshuber 2006, Butler et al. 2006, Silva et al. 2011, Pereira et al. 2012, Brameshuber 2014). The parameters that can affect the tensile behavior of a composite material consisting of cement or lime-based matrix and textile are summarized in detail in the studies conducted by Brameshuber (2006), Peled et al. (2008a), Hegger et al. (2006), Moller (2001) and Colombo et al. (2013).

Table 3.1: Summary of the published studies related to the mechanical characterization of TRM through tension tests.

Experiment	Type of test – Number of layers – Parameters under investigation.	Type of textile	Type of mortar	Stress State I (MPa)	Stress State III (MPa)	Strain State I (%)	Strain State II (%)	Strain State III (%)	Main observation
Larrinaga et al. (2013)	31 specimens under tensile load (deformation rate 0.5mm/min). Four series (one to four textile layers) with seven specimens each.	Basalt textile E_f =67 GPa e_f = 1.8%	Cement-based mortar E_m= 8 -10GPa σ_{mu}= 2 -3MPa	10-12	8-14	0.02-0.04	0.40-0.15	1.9-2.1	Increasing the reinforcement ratio resulted in more brittle failure. The number of cracks increase with the number of textiles, while the distance between the cracks reduced.
Rampini et al. (2019)	25 specimens under tensile displacement loading (rate 0.02mm/s). The structure of the textile and the effect of short fibers were examined.	Seven type AR-Glass textiles E_f = 70-90 GPa σ_{fu} = 1-2 GPa.	Two types cement-based matrix F_{ctm}=5-14MPa	1.5-3.3	10-18	0.01-0.03	0.3-0.6	1.5-2	The coating and textile weaving influence the global capacity of the composites. Addition of short fibers provides an increase on the mechanical capacity of the composite. The heavy-duty textile controls better the slippage at the textile-matrix interface than other textiles.
Barhum and Mechtcherine (2012)	Tension tests (rate 0.5mm/min) on specimens with either 2 or 4 layers of Glass-textile with 0.5 % and 1% short fibers (AR-glass and carbon).	Glass textile σ_{fu} = 1.2 GPa E_f = 65 GPa	Finely grained concrete with and without short fibers σ_{mu} = 1.7-2.2 MPa	1.9-5	7-10	0.02-0.03	0.18-0.23	1.1-1.4	The first-crack stress of the composite increases by two to three times with the addition of 1.0% short fibers (control the micro-cracks). The short fibers (glass or carbon) improved the bond between the yarn and the surrounding matrix. The water-to-binder ratio influenced the bond strength at the textile-matrix interface.

Experiment	Type of test – Number of layers – Parameters under investigation.	Type of textile	Type of mortar	Stress State I (MPa)	Stress State III (MPa)	Strain State I (%)	Strain State II (%)	Strain State III (%)	Main observation
Häußler-Combe et al. (2004)	Uniaxial, deformation-controlled tension tests with rate 0.015mm/s. The textile reinforcement ratio ranging from 1.4% to 2%.	Glass textile σ_{fu} = 2 GPa E_f = 80 GPa	Cement-based matrix F_{ctm} = 7 MPa E_m = 30 GPa	6.8	15	0.024	0.23	1.5	The textile reinforcement does not reach its capability with respect to the stiffness and stress of the composite at State III due to the failure of the outer fibers of the yarn. The textile with low fineness leads to a smaller effective stress and strain at State II.
Hegger et al. (2006)	Tension tests (deformation rate 1mm/min) on specimens with reinforcement ratio 1.1% to 3.3% with fiber orientation 45º and 90°.	Glass textile σ_{fu} = 2 GPa E_f = 60-62 GPa.	Cement-based matrix with plasticizer and fly ash. E_m = 34 GPa, σ_{mu}= 4.4 MPa	4.2	10	0.02	0.19-0.24	1.2	Reduction factor equal to 0.5 on the tensile strength of the yarn to define the tensile strength of the composite at State III. The effectiveness of the textile decreases to about 50% for an angle of 45◦. The maximum crack width and crack spacing for two layers specimen was equal to 0.12 mm and 25 mm, respectively.
De Santis et al. (2017)	Tensile tests on Steel Reinforced Grout (SRG) systems. Ten laboratories Italy, Poland and Portugal were involved for a total of 150 tests.	Three Steel textiles E_f =130-186GPa e_{fu} = 1.2 -2.2%	Four types mortar F_{ctm}=2-10MPa E_m= 5-22 GPa	2.5-3.1	12-18	0.02-0.04	0.1-0.42	1.1-1.8	Improving the textile-mortar interlocking enhanced the strength and stiffness of the composite in States I and II. The stress value, at State III is reduced by 65 % of the steel initial strength. Average crack spacing: 24 mm, for lime-based and geopolymer mortar, and, 30 mm for lime-pozzolan based mortar, depending on the textile-to-matrix bond/interlocking.

Experiment	Type of test – Number of layers – Parameters under investigation.	Type of textile	Type of mortar	Stress State I (MPa)	Stress State III (MPa)	Strain State I (%)	Strain State II (%)	Strain State III (%)	Main observation
Felice et al. (2014)	Tensile and bond tests on basalt (B), carbon (C) and steel (S) textiles specimens (laboratories: Italy, Portugal, and Spain).	Basalt (B) Carbon (C) Steel (S) textiles	Three mortar types: lime, fiber and cement-based polymer mortar.	B: 3 C:5 S: 4	B: 13 C: 18 S: 14	B: 0.01 C: 0.009 S: 0.02	B: 0.34 C: 0.12 S: 0.4	B: 2 C: 0.75 S: 1.2	The failure tensile strength of the composite is lower than that of textile one. The mechanical properties of the mortar affect the initial non-cracked composite. Improving the bond conditions of the textile-matrix eliminates the slipping of the textile and reduces the cracks.
Bertolesi et al. (2014)	11 tensile tests (speed 0.5 mm/min) on cementitious mortar with PBO (polyparaphenylene benzobisoxazole) fiber grid.	PBO fiber material used for the textile E_f = 216 GPa σ_{fu} = 3.5 GPa	Cement based mortar with polymers E_m =4-6 GPa σ_{mu} = 2 MPa	2-3.6	10-14	0.04-0.13	0.24-0.81	1.27-2	Large variability in stress and strain at States I and II, and in modulus of elasticity in State III, due to irregularities of the cross section or wrapping and placement of the reinforcement in specimen. Also, cracks may appear outside the gauge length of the extensometer.
Antino and Papanicolaou (2017)	Tensile tests (rate 0.1mm/min) on specimens with carbon (C), glass(G), and basalt(B), steel (S) textile. The effect of fiber coating was studied.	Basalt(B), carbon (C), glass (G), and Steel (S) textile	Three types of mortar Lime, cement, with pozzolanic fibers F_{ctm}= 5-7MPa	B: 1.6 C:5 G: 2.3 S: 2	B: 6 C: 15 G: 7 S: 5	B: 0.03 C: 0.01 G: 0.02 S: 0.04	B: 0.32 C: 0.12 G: 0.5 S: 0.4	B: 1.2 C: 0.8 G: 2 S: 1.2	The failure tensile strength of the composite is lower than that of the textile one due to the rupture of fibers. Failure modes: rupture of the fibers at a major crack and slipping of the textile from the matrix at States II and III. The stress-transfer mechanism of inner fiber was improved by fully impregnate the fibers with resin (coating).

Experiment	Type of test – Number of layers – Parameters under investigation.	Type of textile	Type of mortar	Stress State I (MPa)	Stress State III (MPa)	Strain State I (%)	Strain State II (%)	Strain State III (%)	Main observation
Carozzi and Poggi (2015)	50 tensile tests on Carbon (C), Glass (G) and polyparaphenylene benzobisoxazole (PBO) specimen (rate 0.5mm/min).	Carbon (C), Glass (G) and PBO textiles	Three types of cement-based mortar σ_{mu}= 2 -5MPa	C:2.16 G: 2 PBO: 2	C: 14 G: 5 PBO:12	C: 0.02 G: 0.04 PBO:0.02	C: 0.18 G: 0.4 PBO: 0.24	C: 0.7 G: 1.2 PBO: 1.2	Crack spacing: 19-25 mm for PBO, 50 mm for glass, and 26-30 mm for carbon specimen. The geometry of the textile influenced the crack propagation and their width.

E_f is the modulus of elasticity of the textile, e_f is the failure strain of the textile, σ_{fu} is the failure strength of the textile, E_m, is the modulus of elasticity of the matrix, σ_{mu} is the tensile strength of the matrix and F_{ctm} is the tensile strength of the matrix obtained from bending test.

3.2.3 Modeling of TRM

Several numerical and analytical models have already been developed and used for the assessment of composite materials consisting of inorganic-matrix reinforced with fibers or textiles. Nevertheless, the modeling of textile reinforced inorganic-matrix composites is a complex task due to the high degree of heterogeneity of both the textile reinforcement and the matrix. The complex behavior of textile reinforced inorganic-matrix composites can be simulated either numerically or analytically, in both cases, two modeling strategies can be adopted, based on the level of detail by which textile reinforcement is modeled, namely: macro-modeling and micro-modeling, as shown in Fig. 3.4 (Hegger et al. 2006). The micro-modeling can be divided in four levels, as presented in Fig. 3.4, and each level provides a different level of accuracy (Chudoba et al. 2006). For both the macro- and micro-modeling approach, the inorganic-matrix is considered homogeneous and no distinction is made between its constituent materials.

Over the years, several detailed numerical models have been developed for the assessment of inorganic matrix with textile reinforcement composites, however, much less studies have been carried out aiming to develop analytical models for defining the mechanical characterization (tensile and bending behavior, and bond-slip relationship for textile-matrix interface) of the textile reinforced inorganic matrix composites. The following parts present some of these past studies, in order to provide sufficient background knowledge for the purpose of the current research. A short description of the past studies regarding the numerical modeling of the textile reinforced inorganic-matrix composite is particularly presented (section 3.2.4.1) to enhance the literature review previously presented in Chapter 2 concerning the modeling of masonry walls and masonry-infilled RC frames retrofitted with TRM. Furthermore, following the main scope of this part of the thesis (section 3.1), the analytical models (mainly macro-models) that exist so far for capturing the tensile behavior (stress-strain relationship) of composite materials consisting of inorganic-matrix reinforced with fibers or textiles are also presented (section 3.2.4.2). It is of utmost importance to present the available analytical models for predicting the tensile behavior of this kind of composite, since the proposed model is based on one of the established analytical models. Complex analytical models which include the bond-slip relationships of the textile-matrix interface are not presented in the following parts, because the prediction of the tensile

behavior of TRM composite material considering the bond conditions between the textile and the matrix in detail (micro-modeling based on Fig. 3.4) is beyond the scope of this research.

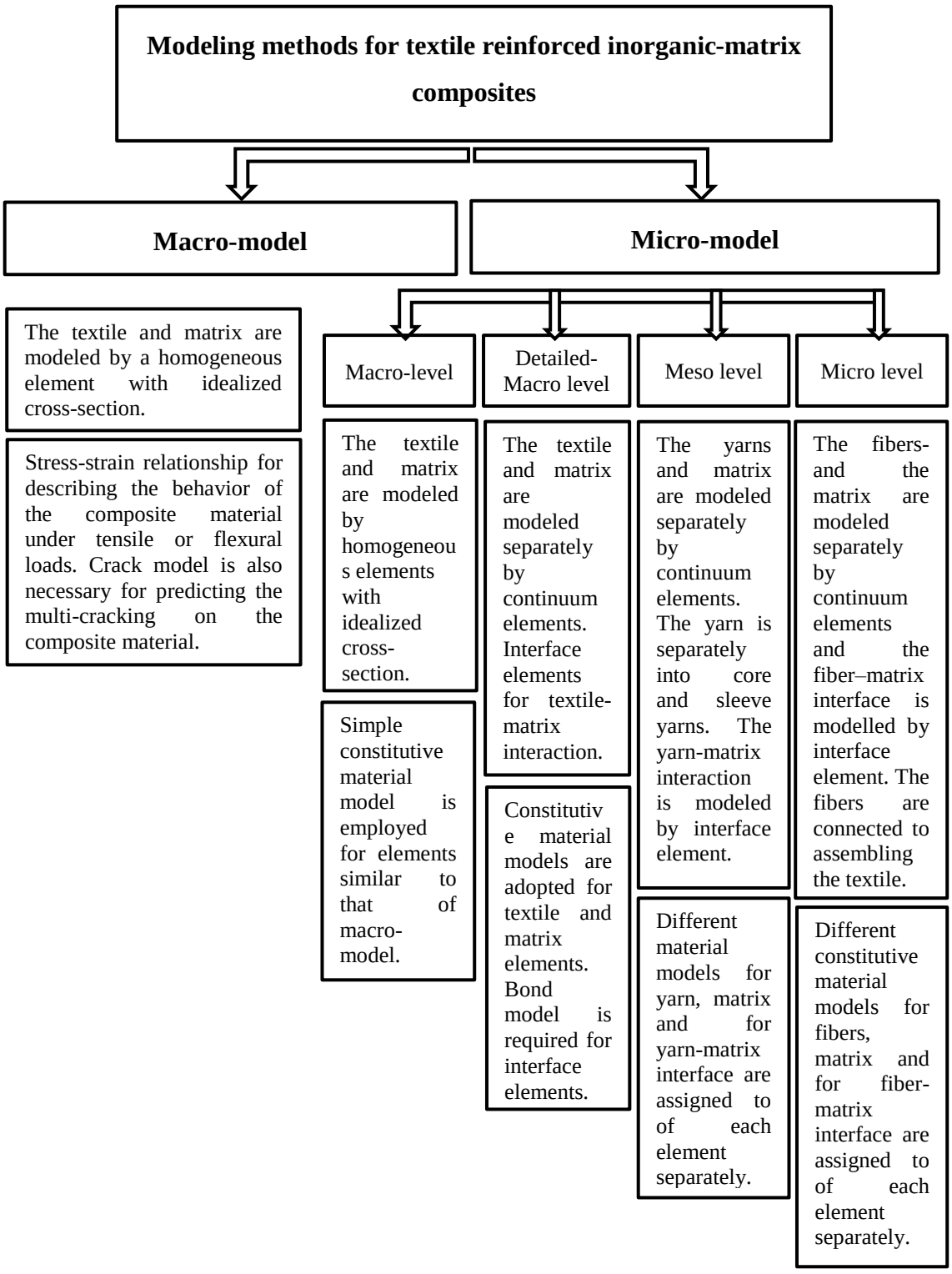

Figure 3.4: Modeling strategies for TRM.

3.2.3.1 Numerical modeling

Application of modern FE analysis methods is the prerequisite for the target–oriented development of new composite material, since by capturing its complex behavior it is possible to analyze and explain important phenomena. In recent years, several detailed numerical models have been developed for predicting the behavior of textile reinforced inorganic-matrix composites under tensile, flexural and pull-out loading, in order to analyze and explain the most important phenomena of its structural behavior, such as; connection between the fibers, the bond between the yarn and the matrix, crack evolution in the brittle composite, and debonding between the textile and the matrix.

Reviewing the literature it seems that the detailed numerical modeling (macro, meso and micro level Fig. 3.4) of this kind of composite material has received great attention in the scientific world, in the early 2000s (Häußler-Combe et al. 2004; Chudoba et al. 2006; Richter and Zastrau 2006; Graf et al. 2007). Hegger et al. (2006) examined the behavior of textile reinforced inorganic-matrix composite considering three different level of modeling, as presented in Fig. 3.4, i.e., detailed macro-modeling, meso-and micro-modeling. In this study, the impregnation of the textile to the matrix and the fiber orientation was not taken into account. Larrinaga et al. (2014) developed a 3D detailed micro-model of TRM, where eight-node elements were used for the mortar and a material model of concrete was adopted for these elements in order to capture the non-linear behavior of the mortar (Fig. 3.4). The basalt-roving was modeled by discrete bar elements, while when the ultimate strain of the basalt-fiber was reached, the roving collapsed in a brittle way. In addition, a bond-slip model for the mortar-to-basalt textile interface was assumed in this model. This numerical model represents accurately the multi-cracking formation of the composite, while the inclusion of bond-slip curves into the FE code proved not to be necessary for capturing the global tensile response of the TRM. Hartig and Häußler-Combe (2010) developed a detailed model of TRM consisting of a number of connected bars representing the matrix and the textile reinforcement, as shown in Fig. 3.5 (a). The bond between the matrix and the reinforcement was modeled by spring elements between adjacent nodes of different bars and bond-slip relations were adopted for these elements. In this model, linear elastic material behavior was assumed for each bar with a limited tensile strength. In case of a particular bar reached its tensile strength during the loading process, the failure was modeled by separating the corresponding bars. Following the same modeling approach,

Hartig and Häußler-Combe (2010) performed fiber and yarn pull-out numerical test, and they concluded that it is essential to take into account the reduction of the contact area between the fibers and the matrix due to the pull-out of the fibers from the matrix, which reduces the forces transferable over the interface. Furthermore, they concluded that in case of yarn pull-out tests, the stochastic properties of the fibers have to be taken into account to represent the failure behavior of the yarn appropriately. Moreover, Hatrig et al. (2004), considering the above modeling scheme (Fig. 3.5 a), developed a model able to predict the tensile behavior of textile reinforced inorganic-matrix under cyclic loading (in terms of stress-strain). The shape of the stress-strain curve in the computed cycles agreed in principle with the experimental one, although the unloading path reached a lower strain level. Bertolesi et al. (2014) developed a FE model of TRM consisting of four-noded plane-stress elements for mortar and two-noded truss elements for yarns. Three different material models were used for the mortar, and a typically elasto-plastic model was adopted for the yarns. The authors concluded that material models used for the mortar can affect significantly the tensile behavior of the composite in tension.

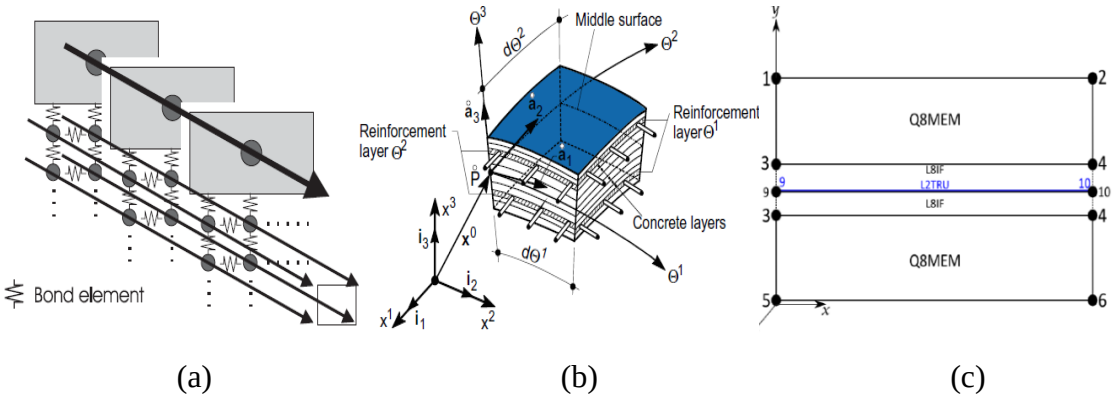

(a) (b) (c)

Figure 3.5: (a) FE model of textile reinforced matrix composite developed by Hartig and Häußler-Combe (2010), (b) Multi-layer textile-reinforced concrete model developed by Holler et al. (2004), (c) Connectivity of plane-stress element and truss-bar element with line-interface element (Williams et al. 2013).

Holler et al. (2004) developed a numerical model for simulating the behavior of textile reinforced inorganic-matrix composite under tensile loading, taking into account the bond characteristics between the textile and the matrix. The composite was modeled by continuum layers of uniaxial layers of reinforcement and of inorganic-matrix, as shown in Fig. 3.5 (b). A non-linear elastic-plastic damage model with material softening behavior was used for the inorganic-matrix. The material behavior of the fibers/yarns

was idealized as linear-elastic. Bond-interface element was considered for the textile-mortar interface (Fig. 3.5 b), while its bond-slip relationship was obtained from the past experimental test. The results obtained from the numerical model and from the experiment showed a good agreement. The authors concluded that the bond-slip relationship and the interaction between the fibers in the yarns are necessary in order to simulate different combinations of textile reinforcement and cementitious matrix. A 2D macro-scale FE model of textile reinforced inorganic-matrix was developed in DIANA FEA by Williams et al. (2013), as shown in Fig. 3.5 (c). This model includes 2D plane-stress elements for inorganic matrix, 1D bar element for textile reinforcement and 2D line interface element for textile-matrix interface. A bond-slip relationship obtained from the experimental pull-out test was used for capturing the behavior of the textile-matrix interface. The interface elements were connected to the 2D plane-stress elements by linking their closest adjacent nodes (Fig. 3.5 c). The authors concluded that the contact perimeter of yarns with matrix influences the bond at the textile-matrix interface, while as a contact perimeter increases, full interaction between the textile and the matrix was achieved.

It is important to mention that numerical studies have also been conducted, using different commercial FE software, to model the masonry walls and masonry-infilled RC frames retrofitted with TRM, as presented in the previous Chapter (section 2.5.3). In most of these studies, the TRM composite material was modeled as a grid reinforcement (tension elements) embedded in mortar continuum elements, assuming perfected bond between them (detailed macro level, based on Fig. 3.4), or it was modeled by continuum elements, hence the textile reinforcement and the mortar layer were lumped in a homogenized layer with thickness proportional to the number of layers (simplified macro level, based on Fig. 3.4).

All numerical models described in this section used different strategies with different level of complexity and accuracy to represent the textile reinforced inorganic-matrix composites. Despite the fact that several models have been proposed by researchers who adopted an “exact representation” of the composite, called meso- and micro-scale strategies, in this section some of them are briefly presented, since the development of a detailed micro-model for TRM is beyond the scope of this research. As will be presented in the next Chapter (section 4.5), the TRM composite material in this study is modeled by continuum elements, following the macro-level approach (Fig. 3.4).

3.2.3.2 Analytical modeling-ACK theory

A first attempt to predict the non-linear behavior of composite materials consisting of inorganic-matrix reinforced with fibers under tensile loads, in terms of stress-strain, as it is presented in section 3.2.3, was made by Aveston and co-workers, leading to the well-known ACK theory (Aveston and Cooper 1971a, b; Aveston and Kelly 1973, 1980). The ACK theory is an energy balanced approach that was developed from fracture mechanics. The ACK theory assumes that, when a crack occurs, debonding takes place over a certain distance, and the interaction between fiber and matrix becomes frictional, with constant surface shear stress. According to the ACK theory, the tensile behavior of the fiber brittle matrix composite can be described by a tri-linear stress–strain curve divided into three zones, as shown in Fig. 3.6. The ACK model allows the prediction of the stress and strain at the three zones during the tensile loading of the brittle matrix composite with continuous fibers aligned in the direction of the applied load.

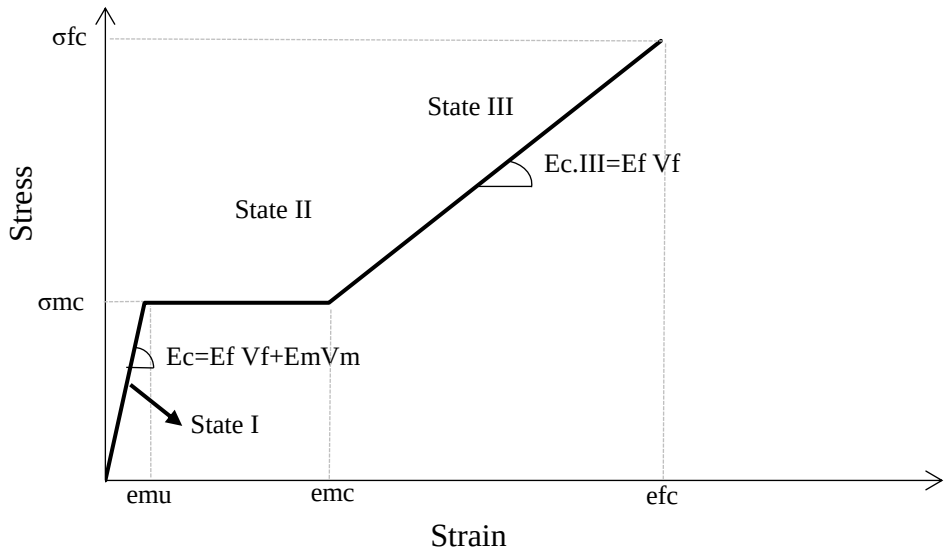

Figure 3.6: Stress-strain curve of fiber-brittle matrix composite under tensile load according to ACK model (indication of the salient points and stiffness at each State).

According to the ACK theory, the predicted strain capacity e_{mu} of the matrix with fibers at the first cracking on the composite is computed as:

$$e_{mu} = \left(\frac{12\,\tau\,\gamma_m\,E_f\,V_f^{\,2}}{E_c\,V_m\,r\,E_m^{\,2}} \right)^{1/3} \tag{3.1}$$

where τ is the shear strength of the matrix, γ_m is the fracture toughness of the matrix, r is the fiber radius, and E_c is the stiffness of the composite at State I, which obeys the law of mixture, as shown in Eq. (3.2), considering linear elastic behavior:

$$E_c = E_f V_f + E_m V_m \quad (3.2)$$

where E_f is the Young's modulus of the fibers and E_m is the one for the matrix, while V_f and V_m are the volume fractions of the fiber and matrix, respectively. Equation (3.1) is derived from the force balance between the load transferred from the fiber to the matrix in a certain distance (mean spacing between two parallel cracks) and the shear stress acting at the fiber-matrix interface, taking into account the fracture energy of the matrix when the first crack occurs. This is attributed to the fact that the ACK theory assumes that, when the first crack appears in the matrix, the load carried by the matrix is transferred into the fibers to bridge the crack, and then the load is linearly transferred from the fibers at the crack back into the matrix, while pure constant friction shear strength between the fiber and the matrix exists. The constant shear bond strength at the fiber-matrix interface, according to the above assumptions, is defined as:

$$\tau = \frac{r V_m \sigma_{mu}}{V_f 2x} \quad (3.3)$$

where σ_{mu} is the tensile strength of the matrix and x is the spacing between micro cracks.

The equivalent composite multi-cracking stress σ_{mc} of the corresponding strain capacity e_{mu} of the matrix with fibers at the first cracking is computed as follows:

$$\sigma_{mc} = E_c e_{mu} \quad (3.4)$$

As the loading increases, multi-cracking formation on the composite occurs where the strain in the composite is equal to the sum of the average strain supported by fibers $e_{mu} \frac{E_m V_m}{E_f V_f}$, which varies between 0.5-0.75, and the failure strain of the matrix. Based on the above, the composite strain e_{mc} when the multicracking is completed, at the breaking strain of the matrix, is calculated by Eq. (3.5):

$$e_{mc} = \left(1 + 0.667 \frac{E_m V_m}{E_f V_f}\right) e_{mu} \quad (3.5)$$

After the end of multi-cracking on the composite, the fibers alone support any further increase in load, while they are extending and slipping through the matrix, until their failure strain e_{fu} is reached. Therefore, the composite strain at the end of State III, is given by the fiber failure strain less a term, which represents the restriction of the extension of the fiber due to transfer of the load back into the matrix in-between two

cracks. This term is equal to the average strain supported by fibers $e_{mu}\frac{E_m\ V_m}{E_f\ V_f}$ in the multi-cracking region, as previously mentioned, where in State III this strain is ranging from 0.25 to 0.5, based on ACK theory. The composite strain at the end of State III e_{fc} can be determined by Eq. (3.6):

$$e_{fc} = \left(e_{fu} - 0.341\frac{E_m\ V_m}{E_f\ V_f}e_{mu}\right) \tag{3.6}$$

Considering the above, when the cracking is completed, only the fibers contribute to the stiffness of the composite, as presented below (Eq. 3.7):

$$E_{CIII} = E_f\ V_f \tag{3.7}$$

This well-known theory was the first satisfactory explanation of the multiple cracking that occurs on fiber-brittle matrix composites under tensile loading, and for this reason several studies used the ACK theory for predicting the tensile behavior of textile reinforced inorganic-matrix composites. Most of the researchers concluded that the ACK model gives a satisfactory prediction of the real tensile behavior of textile reinforced inorganic matrix, while the discrepancy between the results obtained from experiment and the ACK model is mainly in State II, multi-cracking zone, where in the real case the formation of the crack at State II is not occurring at constant stress, but continuously from a strain below the cracking strain of the matrix up to a significantly higher stress and strain (Peled and Bentur 1999; Brameshuber 2006; Cuypers and Wastiels 2006; Blom et al. 2008; Larrinaga et al. 2013, 2014). Nevertheless, according to several authors (Bentur and Mindess 1990; Zok and Barbara 1992; Pryce 1993; Ohno and Hannat 1994; Ahn and Curtin 1997; Curtin, et al. 1998; Curtin 1999, Brameshuber 2006), the main limitation of the ACK model is due to the stochastic nature of the cracks that occurs on composites (the matrix failure strength is introduced through probability distribution), which is not included in the ACK model.

Considering the limitation of the ACK theory, Curtin, et al. (1998,1999) used a Weibull distribution function (Weibull 1952) to describe the stochastic distribution of the matrix strength in order to predict the tensile behavior of ceramic-fibers reinforced inorganic-matrix composites. The stochastic cracking model defines the final crack spacing at certain composite stress, by dividing the final crack spacing with the percentage of the cracks that occur on the matrix, according to the stochastic distribution of the matrix strength. Later, Cuypers and Wastiels (2006) modified the stochastic cracking model

proposed by Curtin et al. (1998,1999), which applies to fiber reinforced matrix composites, and extended it to textile reinforced cementitious composites. Cuypers and Wastiels (2006) performed experimental tests on a glass-textile-reinforced cementitious-matrix composite under tensile loading, in order to investigate its stress-strain curve and to define the required parameters for the ACK model and for the stochastic cracking model. The authors proposed also a coefficient for modifying the relationship between shear strength and crack spacing (Eq. 3.3). In addition, the Weibull parameters are determined by the best fit of the experimental and predicted stress-strain curve of the textile cement-based matrix composite under tensile loading. Furthermore, Mobasher et al. (2006) proposed an analytical model, based on the ACK theory, for simulating the tensile behavior of textile-reinforced cement-based matrix composites. In this study, an empirically based damage evolution law (exponentially decaying function) was proposed for calculating the average crack spacing as a function of applied strain. This function was obtained from the experimental test conducted by the authors (glass-textile with cement-based matrix under tensile loading). In addition, on this model a stiffness degradation factor was used to simulate the decrease in the stiffness of the cracked matrix as the strain increases. Besides the use of the ACK model to determine the strain of the composite at State I, in that study, the tensile stress–strain curve in the post peak region was assumed to be an exponentially decaying function of the maximum stress, where the exponent coefficient was obtained by the experimental results. Later, Larrinaga et al. (2013) proposed a cracking model for predicting the tensile behavior of TRM based on the assumption that the behavior of reinforced concrete is similar with that of TRM under tensile loading. This model was developed according to the crack control expression included in Eurocode 2 for reinforced concrete, in order to predict the cracking (crack width) occurs in the composite material. All the information necessary to run this model is extracted from the data compiled in the experimental campaign conducted by the authors. Furthermore, a reduction factor was proposed equal to 0.65 in order to take into account the reduction of the failure strain occur in the basalt textile. The obtained results from this model were directly compared to the experimental data with good accuracy, although a discrepancy between the experimental and numerical results was observed regarding the ultimate strain (State III) of the composite. Recently, Rampini et al. (2019) used the ACK theory and the cracking model proposed by Cuypers and Wastiels (2006) in order to predict the tensile behavior of glass-textile

reinforced cementitious composites. The authors performed tensile tests on different types of glass-textile reinforced cementitious composites, and used the results obtained from these tests to define the required parameters for the above well-established simplified approaches. The authors concluded that, using the application of the stochastic cracking model, into ACK model, it is possible to predict the experimental TRM tensile stress-strain curves with a good accuracy, although discrepancy between the experimental and numerical results was observed regarding the cracking tensile stress (State I) and the ultimate strain (State III) of the composite.

Besides the development of analytical models for predicting the stress-strain relationship of textile reinforced cementitious composites, Jesse (2006), Brameshuber (2006), Hegger and Voss (2008b) and Ortlepp (2011) proposed equations to predict the tensile and flexural load-bearing capacity of textile reinforced cementitious composites, considering reduction coefficients obtained from their experimental campaigns. Several authors concluded that the above approaches are able to predict satisfactorily the ultimate capacity of elements made of textile reinforced cementitious matrix under bending or tensile loads, as well as under shear loads (Chudoba et al. 2006; Soranakom and Mobasher 2009; Portal 2013).

Reviewing the literature regarding the analytical models for predicting the tensile behavior of TRM, it can be pointed out that there is a need to develop a simple and easy to-implement analytical model able to define the tensile behavior of TRM under tensile loading in terms of stress-strain, without requiring the use of a specific software and experiments in order to be applied.

3.3 Proposed analytical model

The proposed tri-linear analytical model that defines the stress-strain relationship of TRM under tensile loading is presented in this part of the thesis. The non-linear approach is based on the well-established ACK theory, as presented in the previous section (section 3.2.3.2). The ACK theory, which applies to brittle-matrix composite with unidirectional fibers, is being extended to that of textile-reinforced-matrix composite, using equations for determining some of its parameters that in the original proposal had to be determined by tests, in order to develop a simple and easy to-implement model to define the stress-strain relationship for describing the tensile

behavior of TRM for every-day practice. In order to achieve this, the established assumptions for a reinforced concrete are employed in the modeling of the TRM composite material, since the behavior of reinforced concrete element under tensile loading is similar to that of TRM. In this context, the crack control expression, which is included in Eurocode 2 and the fracture energy expression, which is included in *fib* Model Code 2010, are used to facilitate the use of the ACK theory, without requiring testing. More details regarding the above methodologies considered in this study will be presented in sub-sections 3.3.1 and 3.3.2. These are followed by presenting in detail the development of the proposed analytical model (section 3.3.3).

3.3.1 Fracture energy

The fracture energy (G_f), as it is defined by *fib* Model Code 2010, is the amount of energy required to create a tensile crack of one unit of area. The fracture energy characterizes the resistance of quasi-brittle material subjected to tensile loads. The quasi-brittle materials (concrete or cement based matrix) have the ability to release energy due to the progressive crack propagation occurring on these materials, that breaks the continuity of flaws (Bažant et al. 1984, Bazant and Oh 1983, Gettu et al. 1990). In order to determine the crack propagation in quasi-brittle materials, cohesive models have been proposed. The cohesive or fictitious crack model describes the non-linear behavior of quasi-brittle material, in which non-linearity is introduced using a tension softening function. Based on a cohesive crack model, the well-known method to estimate the fracture energy of quasi-brittle material is to calculate the area under the post-peak stress versus crack opening displacement (σ-COD) curve, as shown in Fig. 3.7, in which the tensile strength (f_{ct}) of the material and the shape of the σ-COD curve (tension softening) are required (Bažant and Kazemi 1990, Bažant 2001,Bažant and Yu 2011). The required parameters for the cohesive crack model (σ-COD curve) can be determined using the results from uniaxial tensile test or from bending test. The shape of the tension softening function of the σ-COD curve can be assumed linear, bilinear, multi-linear, or even an exponentially decaying curve, with the bilinear tension softening function being the most common, as shown in Fig. 3.7.

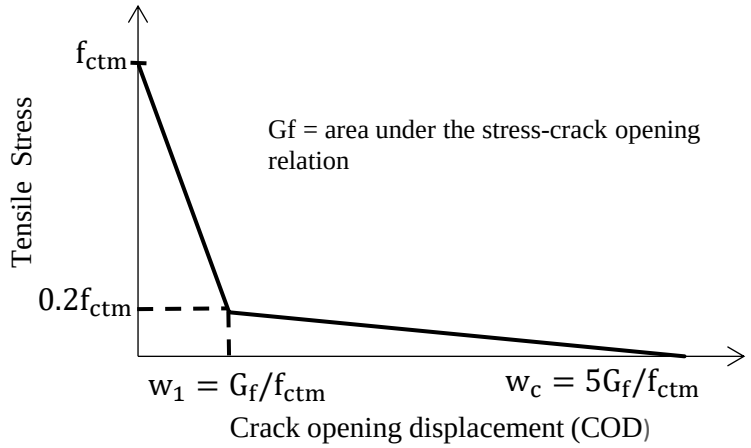

Figure 3.7: Tensile stress versus crack opening of concrete (*fib* Model Code 2010).

In the literature, several analytical models (cohesive crack models) have been proposed in order to define the tension softening behavior of quasi-brittle materials, and consequently to predict the fracture energy of this material using empirical mathematical expressions that correlate the fracture energy with the tensile strength of quasi-brittle material (Bažant and Yu 2011, Ramachandra Murthy et al. 2013, Lee and Lopez 2014). Amongst them, *fib* Model Code 2010 proposed an approximation for estimating the fracture energy G_f, expressed in N/m, of lightweight aggregate concrete, as follows:

$$G_f = 16\, n_1\ f_{ctm} \tag{3.8}$$

where f_{ctm} is the mean value of tensile strength of concrete and n_1 is calculated by Eq. (3.9), according to the *fib* Model Code 2010:

$$n_1 = \left(0.4 + 0.6\ \frac{\rho}{2200}\right) \tag{3.9}$$

where ρ is the density of the lightweight aggregate concrete in Kg/m³.

Therefore, the simple mathematical expressions proposed by *fib* Model Code 2010 (Eq. 3.8) which is able to describe the resistance of concrete subjected to tensile load, is used for estimating the fracture energy of the TRM under tensile loading, since the composite material has similar tensile behavior with that of concrete, before multi-cracking occurs in the composite (State I). More details regarding the adoption of Eq. (3.8) proposed by *fib* Model Code 2010 to modify the ACK model will be presented in section 3.3.3.

3.3.1 Crack spacing

Although the crack spacing and the width of the cracks of TRM under tensile loading have been examined in the experimental studies conducted in the past (Table 3.1), these studies are few, and therefore an established model that predicts the crack propagation on this composite is still lacking. On the other hand, several experimental studies have been carried out in order to investigate the crack propagation of the fiber-reinforced inorganic-matrix composites through tensile or bending tests (Peled et al. 2006, Kamal et al. 2008, Silva et al. 2009). The researchers concluded that the space between the cracks, and the crack width influence the tensile capacity of the fiber-reinforced composite materials. Furthermore, the post-cracking tensile stress of fiber–brittle matrix composite depended on matrix strength, fiber-matrix bond strength, fiber reinforcement ratio etc (Kamal et al. 2008, Silva et al. 2009, Soranakom and Mobasher 2010, Mobasher 2011). Although the fiber-reinforced matrix-composite does not have the same tensile behavior as the TRM, the same observations with the above were obtained from the experimental tests conducted on TRM under tensile loading (section 3.2.2). Furthermore, several researchers proposed cracking models to predict the width, the location, and the crack spacing of the fiber-reinforced composite-material in order to establish design tools for fiber-reinforced concrete structural elements, in which the tensile behavior of fiber composite is considerable (Hannant et al. 1978; Pryce and Smith 1992; Li et al. 1993; Carpinteri et al. 2006; Fantilli et al. 2009). For example, Krenchel (1975) proposed a mathematical expression to predict the mean crack spacing of the polypropylene fiber composite, in which the constant values were derived from his experimental tests. Krenchel (1975) concluded that the crack spacing, X', (which is the same as, x, in Eq. 3.3) is linearly related to the specific surface area (sfs) of the fibers as follows:

$$X' = \frac{\text{CONSTANT}}{\text{sfs}} \tag{3.10}$$

where the value of the constant is equal to 2.5 for the polypropylene fiber (Li et al. 1993) and sfs is computed as:

$$\text{sfs} = \frac{P_f}{A_f} V_f \tag{3.11}$$

where V_f is the volume fraction of the fiber, P_f is the perimeter of the fibers and A_f is the cross-sectional area of the fiber. Therefore, the final average crack spacing (X′) according to the Krenchel theory can be rewritten in the following form:

$$X' = 1.25\ \frac{r}{V_f} \tag{3.12}$$

where r is the radius of the fiber.

The above equation applies only to one type of fiber and, therefore additional information from experimental test is required in order to be applied to other types.

The knowledge of the cracking processes on textile reinforced matrix composites is of a crucial importance in estimating the tensile behavior of TRM. Therefore, a predictive equation to calculate the crack spacing of textile reinforced inorganic-matrix composite is required in order to extend the ACK theory to the TRM composite. Consequently, in order to apply the ACK model for TRM without requiring experimental tests, the recommendation from Eurocode 2 for calculating the crack spacing of steel reinforced concrete elements can be used for estimating the crack spacing of fiber-textile-brittle matrix materials, since the behavior of steel reinforced concrete is very similar to that of fiber or textile reinforced inorganic-matrix composite. According to Eurocode 2, the maximum final crack spacing, S_{rm}, for reinforced concrete linear elements is calculated as follows:

$$S_{rm} = K_1\ K_2\ K_4\ \frac{\varphi}{\rho_r} \tag{3.13}$$

where K_1 is the coefficient that takes account of the bond properties of the bonded reinforcement: K_1 is equal to 0.8 for high bond bars and 1.6 for bars with an effectively plain surface, K_2 is the coefficient that takes account of the distribution of strain: K_2 is equal to 0.5 for bending and 1 for pure tension, K_4 is equal to 0.425, φ is the bar diameter and ρ_r is the reinforcement ratio in tension.

The easy mathematical expression proposed by Eurocode 2 is used in this study for estimating the cracking spacing of TRM since the assumptions considered in ACK theory are similar to those of Eurocode 2 regarding the bond characteristic between the reinforcement (fiber or steel) and matrix (mortar or concrete). More details regarding the use of Eq. (3.13) for estimating the crack spacing (x) in Eq. (3.3) will be presented in the next section.

3.3.2 Development of the proposed model

As previously mentioned, a new simple-analytical approach of TRM is proposed by extending the ACK theory, which applies to fiber-brittle matrix, to textile-brittle matrix, namely TRM, and using appropriate equations for determining the fracture energy and the crack spacing of the TRM. Following this concept, it is necessary to adapt the parameters of the ACK model for fiber-brittle matrix to ones for the TRM, as follows:

- the γ_m, which is the fracture toughness of the matrix (Eq. 3.1), is replaced by the fracture energy of cement- or lime-based mortar G_f .
- As the materials are different, their representation of nomenclature also changes, as follows: V_f and V_m represent the volume fraction of textile and mortar, respectively, E_f and E_m represent the Young's modulus of the textile and mortar, respectively, r is the radius of the yarn, σ_{mu} is the tensile strength of the mortar, τ is the shear strength of the mortar, x is the crack spacing of TRM, e_{mu} is the strain capacity of TRM at State I and e_{fu} is the ultimate tensile strain of the textile.

The proposed model predicts the tensile strain capacity of the TRM at State I (e_{mu}) using the appropriate equations for estimating the fracture energy and crack spacing of TRM. To do so, the crack spacing and the fracture energy of TRM, which are required parameters to define the elastic strain capacity e_{mu} of the TRM composite according to the ACK theory (Eq. 3.1), are estimated according to the crack control expression that is included in Eurocode 2 (Eq. 3.13) and the fracture energy expression that is included in *fib* Model Code 2010 (Eq. 3.8), in order to revise the ACK theory, as described below.

The fracture energy of the TRM composite material can be estimated according to Eq. (3.8), which is included in the *fib* Model Code 2010, as previously presented (section 3.3.1), in which the tensile strength and the fracture energy of the concrete are related properties. As the materials are different, their nomenclature also changes, f_{ctm} is replaced by the mortar tensile strength σ_{mu} and ρ is replaced by the density of the mortar ρ_m. After these changes, Eq. (3.8) becomes:

$$G_f = 16\, n_1 \quad \sigma_{mu} \tag{3.14}$$

where n_1 is the reduction factor calculated as:

$$n_1 = \left(0.4 + 0.6\,\frac{\rho_m}{2200}\right) \tag{3.15}$$

From the methodologies available in the literature, this can be considered as the most simple and representative, since the composite material has similar tensile behavior with that of concrete before multi-cracking occurs. More specifically, the contribution of the textile reinforcement to the composite is negligible at State I, and therefore the fracture energy of the composite at this state is mainly due to the softening behavior of the cement- or lime-based matrix. Complementary to this, the equation referring to lightweight concrete seems to be more suitable for TRM, since the matrix composition used, in a sense, approaches that of lightweight concrete. In order to strengthen this point of view, a comparison with experimental data is given in Table 3.2. Table 3.2 presents the tensile strength and the fracture energy as obtained by a series of uniaxial deformation-controlled tension tests on TRM, conducted by Barhum and Mechtcherine (2012). The aforementioned study is the only one in the literature that measures directly the fracture energy of TRM so far. The results of the proposed approach (using Eq. 3.14) are compared and, as it can be observed from Table 3.2, provide reasonable agreement with the experimental ones. Therefore, it can be concluded that Eq. (3.14) can be considered a good approximation for estimating the fracture energy of the TRM composite material. Different formulations could be used instead, but they add complexity and require testing. The advantage of the proposed relation relies to its simplicity and minimal requirements.

Table 3.2: Comparison between experimental and analytical model results (using Eq. 3.14) regarding the fracture energy of cement-based composite with and without fibers.

	Matrix without fibers	**Matrix with 0.5% Carbon fibers**	**Matrix with 1 % Carbon fibers**	**Matrix with 0.5% Glass fibers**	**Matrix with 1 % Glass fibers**
Tensile strength (MPa)	1.75	2.43	2.46	1.82	1.98
Density of the matrix (Kg/ m³)	1945	1815	1815	1815	1815
Fracture energy as calculated by experimental test (Nm/m)	30- 40	30-40	32-42	20-30	30-40
Fracture energy according to Eq. (14) (Nm/m)	26.00	34.80	35.20	26.10	28.30

The mean crack spacing, x, of the TRM composite material is calculated according to Eq. (3.13), as described before (section 3.3.2). The easy mathematical expression proposed by Eurocode 2 is used for estimating the cracking spacing of TRM, because the assumptions considered in ACK theory are similar to those in Eurocode 2, where in both cases the bond strength between the reinforcement (fiber or steel) and the matrix (mortar or concrete) is considered constant during the tensile loading (Löfgren 2007). As mentioned in section 3.2.2, before cracking occurs in the fiber composite, the ACK theory assumes that a force balance exists between the load transferred from the fiber to the matrix over a certain distance, and the shear stress acting on the fiber-matrix interface. This assumption is also considered in Eurocode 2 for reinforced concrete elements, and therefore Eq. (3.13) can be transferred to textile-reinforced inorganic-matrix composite without modification, because the bond characteristics are included in the calculation of the transfer length or of the area of the textile. In this study, high bond conditions between the textile and the matrix are considered (Bartos 1981; Krüger et al. 2002; Xu et al. 2004; Lorenz and Ortlepp 2012), therefore the coefficient K_1 of Eq. (3.13), which takes into account the bond properties of the bonded reinforcement, takes the value of 0.8 as Eurocode 2 proposes for high-bonded reinforcement bars. In addition, the coefficient K_2 of Eq. (3.13) takes the value of 1, since the proposed approach defines the stress-strain relationship of TRM under tensile load. Therefore, after these assumptions are set, Eq. (3.13) can be written in the following form in order to calculate the crack spacing of TRM:

$$x = 0.68 \frac{r_{yarn}}{V_f} \tag{3.16}$$

where r_{yarn} is the radius of yarn. Eq. (3.16) is used for predicting the crack spacing of the TRM and it can be considered as a good approximation, as will be discussed in section 3.4. In addition, Eq. (3.16) has a very similar form to the one of the Krenchel theory (Eq. 3.12), which applies for fiber-reinforced inorganic-matrix.

After these concepts are set, it is possible to define the proposed tri-linear stress-strain relationship of TRM, following the ACK theory. The linear-elastic State I of the TRM is determined by calculating the strain capacity e_{mu} as follows:

$$e_{mu} = \left(\frac{1.41\ 10^{-4}\ n_1\ {\sigma_{mu}}^2\ E_f\ {V_f}^2}{E_c\ r_{yarn}\ {E_m}^2} \right)^{\frac{1}{3}} \tag{3.17}$$

where E_c is the composite stiffness in Stage I derived from the law of mixtures, as ACK theory proposes. The units of the coefficient $1.41\,10^{-4}$ in Eq. (3.17) are m^{-1}. The corresponding stress σ_{mc} at State I is estimated by Eq. (3.4), using the strain capacity e_{mu} according to Eq. (3.17). In addition, the TRM composite strain at the end of States II and III is calculated by Eqs. (3.5) and (3.6), as ACK theory proposes, using the elastic strain e_{mu} of the TRM composite as it is estimated in the proposed model (Eq. 3.17). The stress at State III can be calculated as:

$$\sigma_{fc} = E_{CIII}\, e_{fc} \tag{3.18}$$

where E_{CIII} is obtained from Eq. (3.7) as presented in section 3.2.3.2 and e_{fc} is the tensile strain of the textile (Eq. 3.6).

All the information necessary to apply the proposed model has been presented. This tri-linear analytical model that defines the stress-strain relationship of TRM under tensile load is simple and easy to-implement, since only the mechanical properties and geometric characteristics of the cement-based matrix and of the textile reinforcement are necessary, without any required information from experimental tests.

3.4 Assessment of the proposed approach

In this part of the thesis, the assessment of the proposed analytical model of TRM is presented using experimental and analytical studies conducted in the past. Table 3.3 summarizes the required data in order to apply the proposed tri-linear model in each case-study selected for the purpose of this study (with the notation Case N, where the N denotes the number of the case-study). The required data are: the volume fraction of the textile V_f, the tensile Young's modulus of the textile and mortar, E_f and E_m, respectively, the ultimate tensile strain capacity of the textile, e_{fu}, and of the mortar,σ_{mu}, and the radius of the yarn r_{yarn}. Most of the experimental and analytical studies used for the assessment of the proposed model are briefly described in Table 3.1 (section 3.2.2), and in section 3.2.3.2 of this Chapter. Although several experimental studies have been conducted regarding the mechanical characterization of textile reinforced matrix composite, only the ones that provide the necessary data to apply the model are used. It should be mentioned that in the fifth and eighth case-studies, although some of the required data were missing, these data were estimated from back

calculations. A detailed example for applying the proposed model is presented in Appendix I at the end of the thesis.

Table 3.3: Data from experimental case-studies.

	Textile-reinforcement				Cement-based mortar			
Case study	**E_f (GPa)**	**e_{fu} (%)**	**V_f (%)**	**A_{yarn} (mm^2)**	**E_m (GPa)**	**σ_{mu} (MPa)**	**V_m (%)**	**ρ_m (Kg/m^3)**
Case 1 (Larrinaga et al. 2013)	67	1.82	0.70	0.89	8.25	2.8	99.3	1950
	67	1.82	1.2	0.89	8.25	2.8	98.8	1950
Case 2 (Rampini et al. 2019)	70	2.8	0.56	0.89	42.90	6.30	99.4	1850
Case 3 (Barhum and Mechtcherine 2012)	64	1.50	1.12	0.48	18.95	2.16	98.88	2000
Case 4 (Barhum and Mechtcherine 2012)	64	1.50	2.11	0.48	18.95	2.16	97.89	2000
Case5 (Richter and Zastrau 2006)	76	1.70	1.40	0.12	30	7.00	98.60	1800
Case 6 (Häußler-Combe et al. 2004)	80	2.50	1.63	0.11	30	5.71	98.37	2000
Case 7 (Koutas et al. 2014)	73	2.5	1.30	0.95	30	2.16	98.83	2250
Case 8 (Hegger et al. 2006a)	61.25	1.60	2.20	0.85	34	4.00	97.80	2000
Case 9 (Carozzi and Poggi 2015)	203	1	0.45	0.42	7	2.5	99.55	1800
Case 10 (Bertolesi et al. 2014)	215	1.5	0.4	0.22	5	1.75	99.6	2000
Case 11 (De Santis et al. 2017)	186.5	1.7	0.6	0.53	11.42	1.8	99.4	1800
	186.5	1.7	0.6	0.53	22.4	3	99.4	1800
Case 12 (D'Antino and Papanicolaou 2017)	107	1.9	0.33	0.8	6	2.5	99.7	1950
Case 13 (De Felice et al. 2014)	67	1.9	1.2	0.58	15	2.5	98.8	1850

Figures 3.8 and 3.9 show the comparison of the results obtained from the proposed model (red line) with those obtained from the experimental test (blue line) and from the analytical model (green line) of the studies conducted by Larrinaga et al. (2013) and Rampini et al. (2019), respectively, in terms of stress-strain, (cases 1and 2). In these figures the blue lines represent the minimum and the maximum stress-strain curves

obtained from the experimental tests. Based on Figs. 3.8 and 3.9, it can be concluded that the proposed analytical model is able to represent the tensile behavior of the textile-reinforced matrix composite with good accuracy. The numerical model proposed by Rampini et al. (2019), as shown in Fig. 3.9, proved to be less effective to capture the tensile behavior of the composite, especially in States I and II, because this model probably reproduces results for a specific reinforcement ratio. From Figs. 3.8 and 3.9 it is also observed that the results obtained from the proposed model are similar to those of Larrinaga et al. (2013) and Rampini et al. (2019) models, concerning the response of the composite material at State III. The more accurate results for this State are those obtained from the model proposed by Larrinaga et al. (2013). Furthermore, from Fig. 3.8 it is observed that the proposed model presents much better results, compared to those obtained from the cracking model proposed by Larrinaga et al. (2013) regarding the strain at the end of the multi-cracking region (elastic strain e_{mu}).

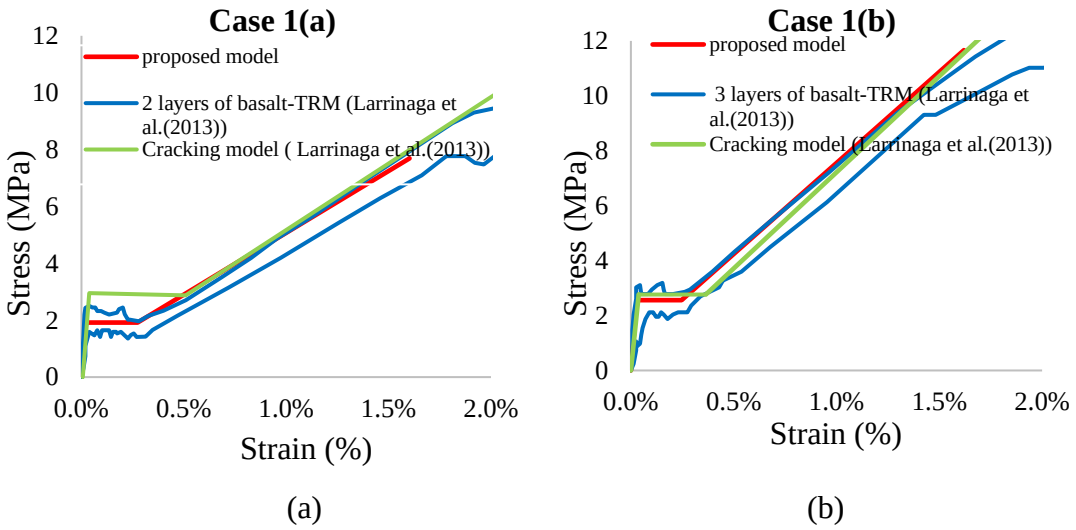

Figure 3.8: Comparison between the results obtained from the proposed model with those obtained from the experimental test (minimum and maximum) and analytical model provided by Larrinaga et al. (2013) for (a) two and (b) three layers of basalt-TRM.

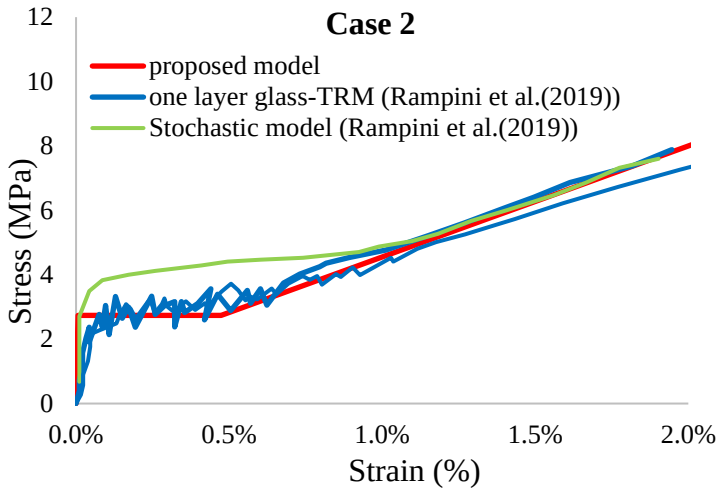

Figure 3.9: Comparison between the results obtained from the proposed model with those obtained from the experimental test and analytical model provided by Rampini et al. (2019) for one layer glass-TRM.

The comparison between the experimental (blue line) and proposed model (red line) results concerning the tensile behavior of TRM in terms of stress-strain is presented in Figs. 3.10 and 3.11 for case-studies 3-10. Also, Fig. 3.12 shows the comparison between the experimental (blue line) and proposed model (red line) results regarding the tensile behavior of a steel reinforced composite, considering two different types of mortar. Furthermore, Fig. 3.13 presents the tensile behavior of one and three layers of basalt textile reinforced matrix composite, as obtained from the experimental studies conducted by D'Antino and Papanicolaou (2017) and De Felice et al. (2014), respectively, and as obtained from the proposed model.

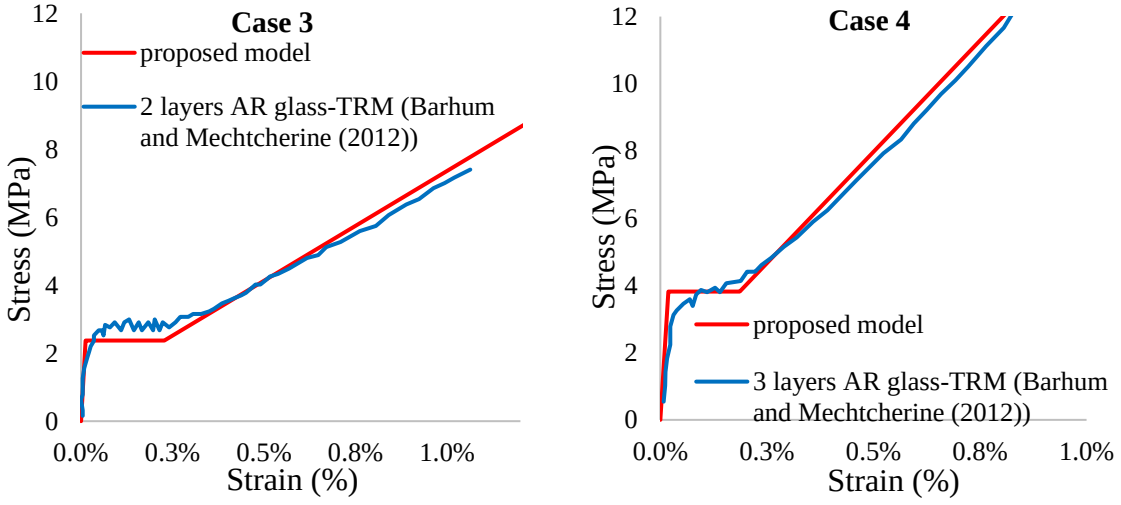

(a) (b)

Figure 3.10: Comparison between the proposed model and the experimental results for: (a) two and (b) four layers of (AR) Glass textile cement-based matrix composites (Barhum and Mechtcherine 2012).

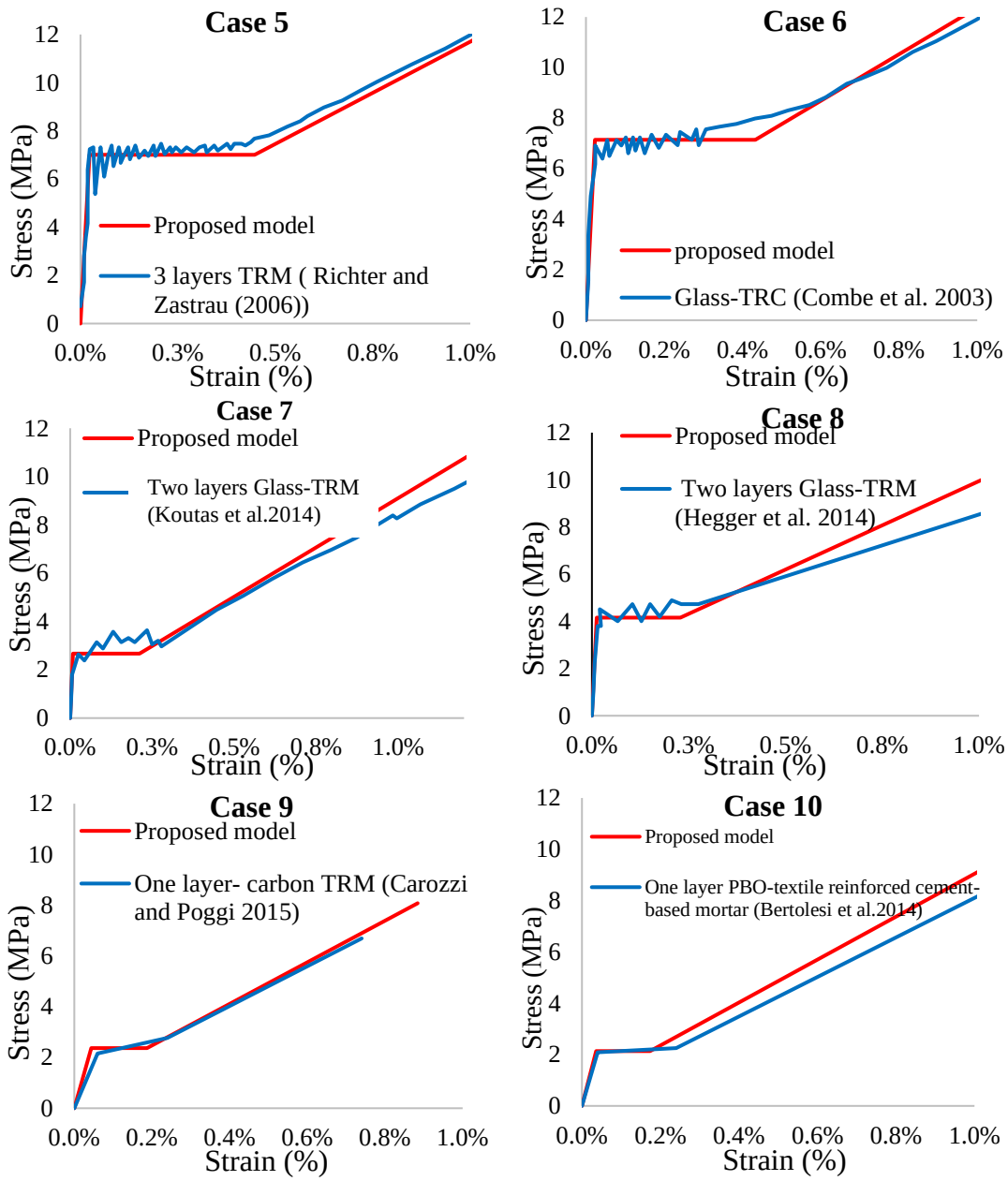

Figure 3.11: Comparison between the proposed model and the experimental results regarding the tensile behavior of textile composite material for Case-studies 5-10.

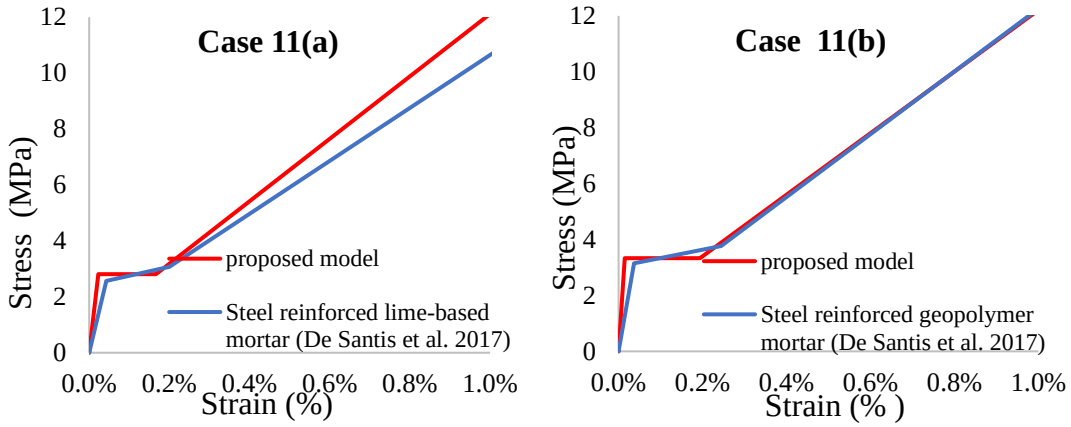

(a) (b)

Figure 3.12: Comparison between the proposed model and the experimental results regarding the tensile behavior of steel-textile composite material considering (a) lime-based mortar and (b) geopolymer mortar (De Santis et al. 2017).

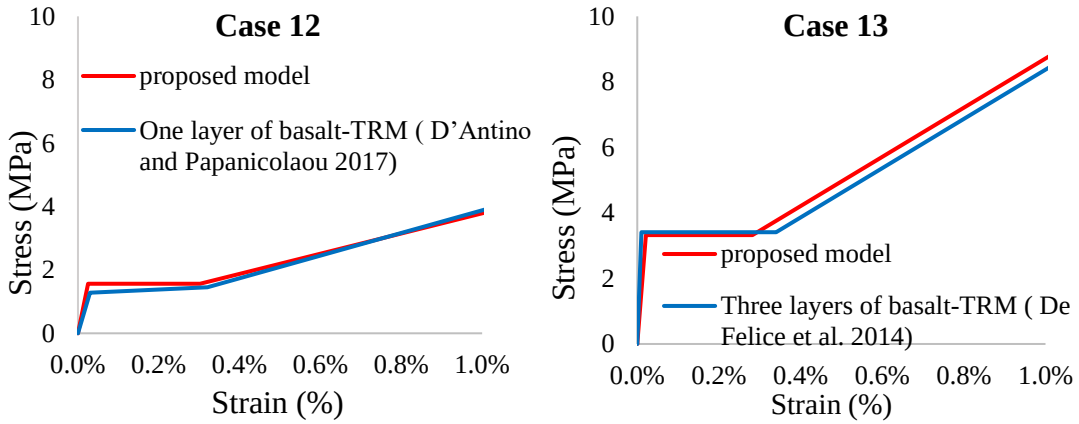

(a) (b)

Figure 3.13: Comparison between the proposed model and the experimental results for: (a) one layer of basalt composite (D'Antino and Papanicolaou 2017) and for (b) three layers of basalt textile with cement-based matrix (De Felice et al. 2014).

From the aforementioned comparisons (Fig. 3.8 to Fig. 3.13), it was possible to notice that the analytical curves seem to properly fit the experimental ones in almost all of the case-studies. The proposed model presents optimum results for the elastic un-cracked stress and strain and for the multi-cracking strain of the composite, since there are no significant differences between the analytical and the experimental data. It is important to mention that the comparison between experimental and analytical results in each case was obtained by considering the average values of several tests conducted during each experimental case-study. Remarkable deviation occurred in each testing and this is

reflected in the increase of the coefficient of variation obtained (20%-50%). Based on the above, it can be considered that the proposed model is accurate, since the discrepancy between experimental and analytical results is less than 30% in almost all of the case-studies. For example, from Fig. 3.10, it is observed that the proposed model overestimates the stress at State I by about 10% compared to the real one (Case 4), while the strain at State II is underestimated by about 20%. Furthermore, in Case 8 the proposed model overestimates the strain at first cracking, State I, by about 20%, compared to the real one. This is mainly attributed to the cracking spacing which is calculated according to Eq. (3.16), and it is equal to 18 mm, 30% lower compared to the real one, which is equal to 25 mm as shown in Table 3.1 (section 3.2.2). The same may be observed in Case 9, where the proposed approach underestimates the crack spacing by about 23%, leading to an overestimate of the stress and strain of the composite at State I by about 15%. Although the discrepancy between experimental and analytical data is relatively small, relevant experimental tests may be performed in order to modify Eq. (3.16) that defines the crack spacing of the composite to reduce this discrepancy. It is important to mention that by comparing Cases 3 to 8 it seems that the mechanical characterization of the composite material is almost the same, since in these studies almost the same glass-fiber material was used for assembling the textile reinforcement. In the Cases 1, 2, 12 and 13, basalt fiber is used, while in the other cases carbon, steel and PBO fiber was used. The typical values for the fibers used for assembling the textile reinforcement are given in section 3.2.1.

Although there are no significant discrepancies between the experimental and analytical data, the behavior of the composite material at State III is still not satisfactorily predicted, as shown in Figs. 3.11, 3.12 (a) and 3.13 (b). There is agreement on the first phase of this State, but as the strain increases it seems that the proposed model overestimates the slope at State III, leading to an overestimate on the stress of the TRM for a given strain at this State. This discrepancy is caused because the proposed model does not take into account the loss of stiffness observed in the composite by the end of the State III during the experiment (Table 3.1). Specifically, in a real case, a reduction of the reinforcement ratio during the test occurs, because part of the textile reinforcement fails due to a possible rupture of the fibers inside a roving before the composite enters in State III. The proposed model does not cover this behavior, due to the linearity hypothesis of the model for evaluating the effective amount of textile

reinforcement at State III by multiplying the volume fraction of the textile by the stiffness of the textile. Therefore, the linear expression that defines State III of the composite should be changed (i.e., a proper reduction coefficient must be set) in order to take into account, the strength degradation of the textile. Towards this direction, Ohno and Hannant (1994) proposed a reduction factor ranging from 0.6 to 0.9 and concluded that this factor depends on the number of fibers inside the yarn and the cross section of the yarn. In addition, Larrinaga et al. (2013) proposed that the tensile strain capacity of the basalt textile, e_{fu}, can be estimated using a reduction factor equal to 0.65 on the strain capacity of the basalt fibers, e_f. Relevant experiments must be carried out in order to find a proper coefficient to take into account the possible strength degradation of the textile under tensile loading.

To conclude, the proposed model proved accurate for predicting the stress-strain relationship of TRM under tensile loading, since the analytical curves almost coincide with the experimental ones in all experimental studies that have been taken into consideration in the present study. The discrepancy between the experimental and analytical data is less than 30% and this degree of approximation may be considered acceptable.

3.5 Parametric study

After the assessment of the proposed model, a parametric study is necessary in order to examine the sensitivity of the proposed model to a range of parameters, and to gather today's knowledge regarding the parameters that can influence the tensile behavior of TRM. In this part of the thesis, a parametric study is performed aiming to investigate the influence of the material of the fiber used for assembling the textile (section 3.5.1), the textile reinforcement ratio (section 3.5.2), the cross-sectional area of the yarn (roving) (section 3.5.3), and the influence of the mechanical properties of the cement- or lime-based matrix (section 3.5.4) on the tensile behavior of TRM in terms of stress-strain, as obtained from the proposed model. Table 3.4 presents the variable parameters (maximum and minimum values) which are considered in each case of this parametric study. It is important to note that in this parametric study, one or two parameters of the model are varied in each case, without taking into account the relationships between the various parameters. For instance, this study does not take into account the fact that the failure tensile strength of the matrix is related to its elastic modulus.

Table 3.4: Summary of the variable parameters considered in each case of the parametric study (maximum and minimum values).

Case study	Type of parameter	Minimum value	Maximum value
Influence of fiber's material used for assembling the textile	Four materials of fibers: Basalt, Carbon, Glass and Aramid	Basalt: E_f=70 GPa, $*\ \sigma_{fu}$=1.7 GPa Carbon: E_f=215 GPa, σ_{fu}= 2.1 GPa Glass: E_f= 70 GPa, σ_{fu}= 1.4 GPa Aramid: E_f=115 GPa, σ_{fu}= 2.3 GPa	Basalt: E_f=96 GPa, σ_{fu}=2.4 GPa Carbon: E_f=235 GPa, σ_{fu}= 2.3 GPa Glass: E_f= 80 GPa, σ_{fu}= 1.6 GPa Aramid: E_f=130 GPa, σ_{fu}= 2.6 GPa
	Modulus of elasticity (E_f) and the failure tensile strength (σ_{fu}) of the textile reinforcement	E_f=60 GPa σ_{fu}= 1.4 GPa	E_f=120 GPa σ_{fu}= 2.4 GPa
Influence of the reinforcement ratio	Reinforcement ratio (V_f)	1%	3%
Influence of the cross-sectional area of the yarn	Yarn cross-sectional area (A_{yarn})	0.07 mm²	0.95 mm²
Influence of the cement-based matrix	Modulus of elasticity (E_m)	8 GPa	35 GPa
	Tensile strength (σ_{mu})	1.5 MPa	8 MPa

*σ_{fu} is the ultimate tensile stress of the textile.

3.5.1 Fiber's material used for assembling the textile reinforcement

In this section, the influence of the fiber's material used for assembling the textile on the tensile behavior of TRM in terms of stress-strain, as obtained from the proposed model is investigated, considering : (1) four different types of fiber's material, and (2) different modulus of elasticity and failure tensile strength of the textile reinforcement as presented in Table 3.4. In both cases, the reinforcement ratio V_f is equal to 1.5% and the tensile strength of the matrix, σ_{mu}, is equal to 3 MPa. The influence of the fiber's material (Carbon, Aramid, AR-Glass, and Basalt) used for assembling the textile on the tensile stress-strain curve of TRM is presented in Fig. 3.14.

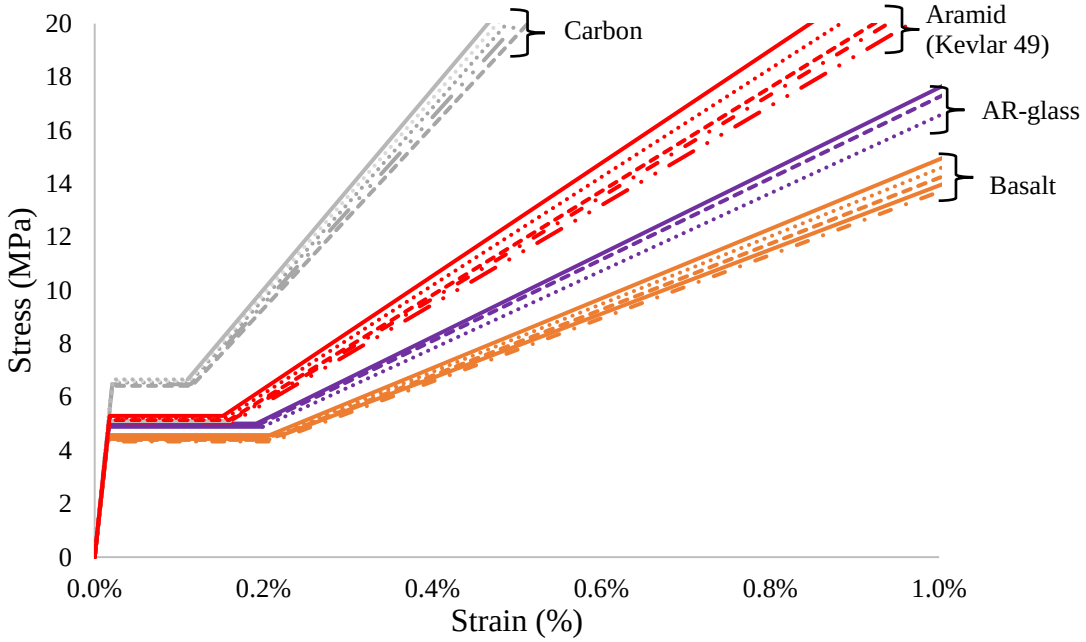

Figure 3.14: Tensile behavior of textile reinforced matrix composite considering Carbon, Aramid, AR-Glass, and Basalt fibers in the textile reinforcement as obtained from the proposed model in terms of stress-strain.

It is observed from Fig. 3.14 that there is no influence of the fiber's material on the stiffness and the strain of the non-cracked composite (State I), but, the carbon-fiber specimen has higher tensile stress at State I (by about 30%), compared to the other specimens, since its failure tensile stress is about two times greater than the

corresponding one of the other fibers, as mentioned in section 3.2.1 and as presented in Table 3.5. From Fig. 3.14, it is also observed that the fiber's material influences the multi-cracking formation of the composite material (strain capacity at State II), where the fiber with lower modulus of elasticity exhibited higher strain at the end of State II. Particularly, the strain of the basalt-fiber specimen at the end of State II is about two times greater, compared to that of the carbon-fiber specimen, while the modulus of elasticity of the carbon fibers was about three times greater of that of basalt fibers. This is an interesting observation, which is also supported by experimental tests performed by Brameshuber (2006), Carozzi and Poggi (2015), D'Antino and Papanicolaou (2017) and Ismail et al. (2018). Finally, there are many differences in the third phase, due to the different elastic moduli and tensile strengths of the fibers. Particularly, the ultimate stress of carbon and aramid textile reinforced inorganic-matrix composites (State III) is higher, compared to that of glass and basalt specimens, due to their relative low mechanical properties.

The aforementioned observations regarding the effect of the fiber's material used for assembling the textile on the tensile behavior of TRM are also supported by Fig. 3.14 which shows the influence of the modulus of elasticity and the failure strength of the textile reinforcement on the tensile behavior of the composite material. It is observed from Fig. 3.15 that the modulus of elasticity and the ultimate strength of the textile reinforcement affect the tensile behavior of the textile reinforced inorganic-matrix composites, mainly at State II and State III, as previously mentioned. Specifically, the specimen with double modulus of elasticity and tensile failure strength (red line) of the textile reinforcement exhibited almost two times smaller strain at the end of state II (green line).

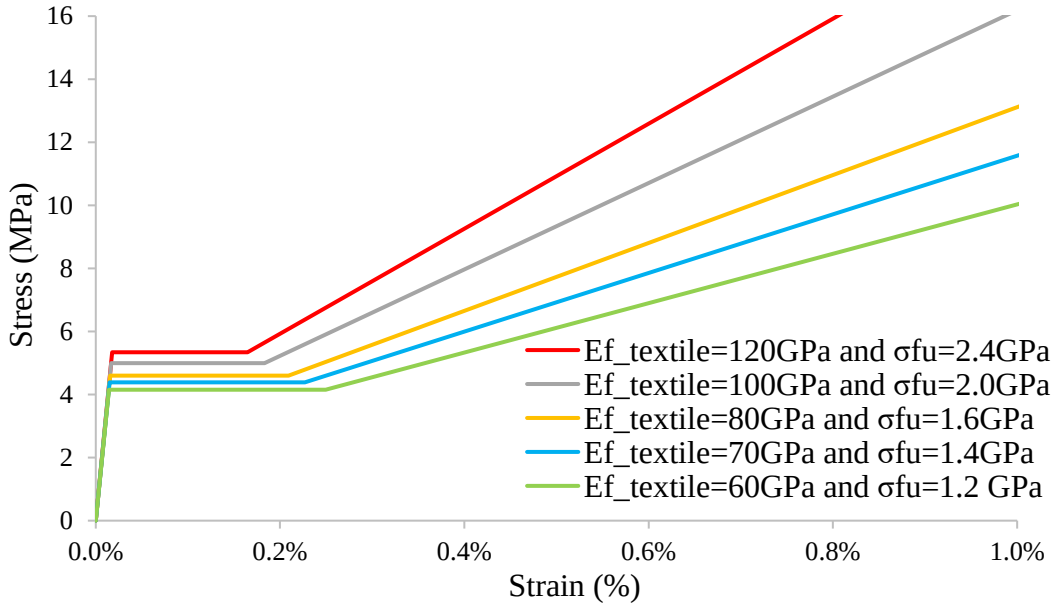

Figure 3.15: Tensile behavior of textile reinforced matrix composite considering different modulus of elasticity and ultimate tensile strength of textile reinforcement as obtained from the proposed model in terms of stress-strain.

Hence, the mechanical properties of the fibers used for assembling the textile reinforcement (elastic modulus and failure tensile strength) have significant influence on the tensile behavior of textile reinforced inorganic-matrix composites. In addition, the strain at the end of State II is almost inversely-proportional to the elastic modulus of the fiber used for assembling the textile reinforcement. Furthermore, it can be pointed out that, using high strength carbon fibers does not provide any benefit over lower-cost glass- or basalt-based textiles regarding the tensile behavior of the composite, except for the non-cracked composite state (State I), in which the tensile strength is higher when high strength carbon fibers are used.

3.5.2 Reinforcement ratio of the composite material

In this section, the influence of the reinforcement ratio V_f, ranging from 1% to 3%, by means of considering different spacing between the yarns in the textile (mesh opening ranges from 4-20 mm) on the tensile stress-strain curve of TRM, as obtained from the

proposed model, is investigated. In this parametric study, the modulus of elasticity and the tensile strength of the textile is equal to 90 GPa and 1500 MPa (Basalt or Glass fibers), respectively, and the tensile strength σ_{mu} and modulus of elasticity E_m of the matrix is equal to 3 MPa and 25 GPa, respectively. It is important to note that the reinforcement ratio is depended on the number of textile layers, the geometry of the textile (spacing between the yarns) and on the number of fibers in the yarn (Prota et al. 2006, Triantafillou 2011, Parisi et al. 2013, Bernat et al. 2013). In this parametric study, it is decided to vary the reinforcement ratio by changing the spacing between the yarns of the textile, for ease of calculations, while the volume fraction of the mortar V_m is changing accordingly (99%-97%). The same results with this parametric study will be obtained by either varying the textile geometry (loop size of the mesh) or the numbers of textile layers, since the proposed model does not depend on the way that the reinforcement ratio will be changed (this model does not take into account in detail the bond condition existing between the textile and the matrix in the real case).

The influence of the reinforcement ratio V_f on the tensile behavior of TRM is given in Fig. 3.16. From Fig. 3.16, it is observed that, by increasing the reinforcement ratio the tensile stress of the textile reinforced matrix composite before cracking occurred increases (stress at State I), but, there is no influence of the reinforcement ratio on the stiffness and the strain of the non-cracked composite (State I). Furthermore, from Fig. 3.16 it is observed that, by increasing the reinforcement ratio, the strain at the end of the multi-cracking formation of the composite material (strain capacity at State II) increases, but not proportionally. For example, in the case where the reinforcement ratio is equal to 1% and 3%, the stress at State I is equal to 2.20 MPa and 4.15 MPa, respectively, and the strain at State II is equal to 0.11% and 0.23%, respectively. This is attributed to the distance between the cracks, which decreases as the reinforcement ratio increases, as presented in Table 3.5 (cracking spacing of the composite material, as calculated by Eq. 3.16, considering different reinforcement ratio). This observation is also supported by the experimental tests performed by Larrinaga et al. (2013, 2014b). Finally, by increasing the textile reinforcement ratio the stiffness at State III increases,

as expected, since in this State only the fibers contribute to the stiffness of the composite. The same observations to the above, regarding the influence of the reinforcement ratio on the tensile behavior of the textile reinforced matrix composite, were reported in several past experimental studies (Jesse 2003; Peled and Bentur 2003; Hegger et al. 2006; Hegger and Voss 2008; Larrinaga et al. 2013; Colombo et al. 2013; Felice et al. 2014; Ombres 2014; Rambo et al. 2015; Raoof et al. 2016).

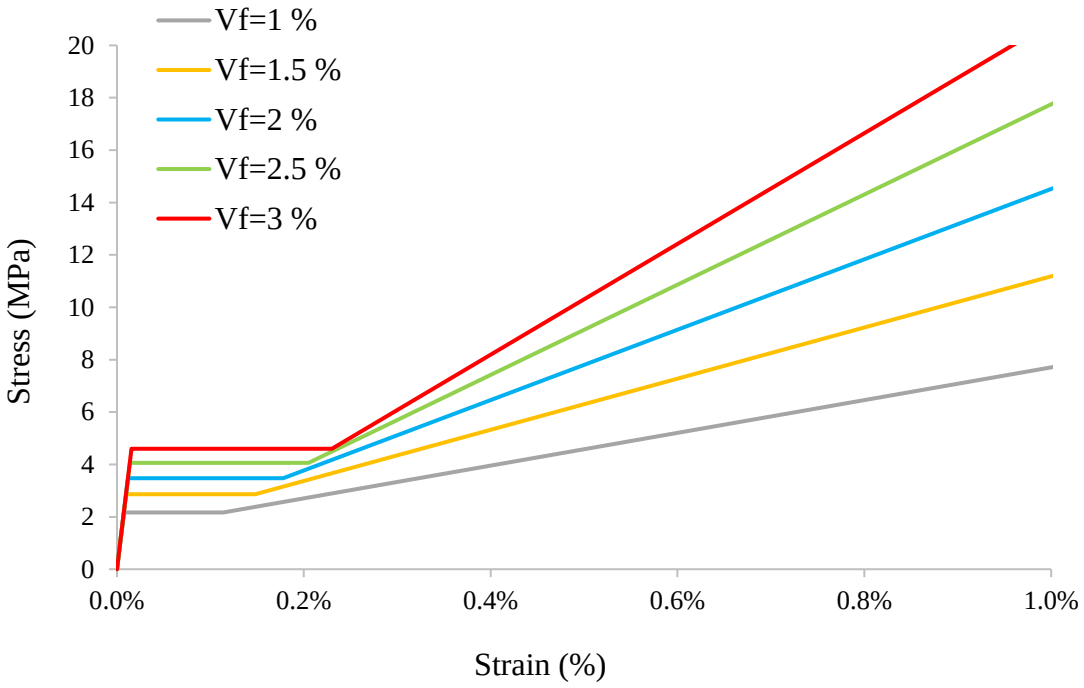

Figure 3.16: Tensile behavior of textile reinforced matrix composite with different reinforcement ratio (1%-3%) as obtained from the proposed model in terms of stress-strain.

Table 3.5: Crack spacing on the textile reinforced matrix composites with different reinforcement ratio according to the proposed model (Eq. 3.16).

Reinforcement ratio (V_f) %	1	1.5	2	2.5	3
Crack spacing (x) mm	54.20	36.25	27.1	21.70	18.00

The tensile behavior of the textile reinforced inorganic-matrix composites is strongly influenced by the level of textile reinforcement introduced in the inorganic matrix (Fig. 3.16), with the distance between the cracks playing an important role (Table 3.5). The results obtained from this parametric study they should be considered as an indication, since the proposed model does not taken into account that the geometry of the textile and the number of textile layers are able to control the bond strength between the textile reinforcement and the mortar (adhesion properties), and consequently the tensile capacity of the TRM (Mobasher et al. 2004; Hegger and Voss 2008; Peled et al. 2008, b; Butler et al. 2010;Colombo et al. 2013; Portal 2013). Therefore, from this study it is pointed out that, decreasing the spacing between the yarns, leads to an increases in the tensile capacity of the composite (States I and II), and this can be considered as an indication, since many researchers reported that when the spacing between the yarn in the textile is relatively small, the penetration of the textile to the matrix is low (low friction between the inner fibers, and between the textile and mortar), and this leads to a low tensile capacity of the composite before and after the cracking occurs (State I and II) (Hegger and Voss 2008; Peled et al. 2008a, b; Colombo et al. 2013; Portal 2013). Furthermore, increasing the reinforcement ratio may not provide a significant increase in the tensile capacity of the TRM due to brittle failure that may occur on the composite, due to different mechanisms may develop between the textile layers. Therefore, the geometry of the textile and the number of textiles must be such as to allow the mortar to pass and correctly bonded to the textile reinforcement. Consequently, relevant experimental tests may be performed on this composite by varying the reinforcement ratio (number of textile layers, spacing between the yarns and number of fibers in the yarn) in order to modify the Eq. (3.16) that defines crack spacing of the composite in such a way to take into account the effect of the reinforcement ratio on the tensile behavior of TRM.

3.5.3 Cross-sectional area of the yarn

In this section, the effect of the cross-sectional area of the yarn A_{yarn}, ranging from 0.1mm² to 0.8 mm², by means of considering different radius of the yarn (r_{yarn} =0.15-0.55mm), on the tensile stress-strain curve of TRM as obtained from the proposed model is investigated. In this parametric study, the modulus of elasticity and the tensile strength of the textile is equal to 90 GPa and 1500 MPa (Basalt or Glass fibers), respectively, and the tensile strength σ_{mu}, and modulus of elasticity E_m of matrix is equal to 3MPa and 25GPa, respectively. In addition, in this parametric study where the effect of the cross-sectional area of the yarn (roving) is examining the reinforcement ratio V_f remains constant equal to 1%.

The cross-sectional area of the yarn (the radius of the yarn) affects the tensile behavior of the textile reinforced matrix composite as shown in Fig. 3.17, since by increasing the cross-sectional area of the yarn, the stress of the composite material before cracking occurred (State I) decreases, and the strain capacity of the composite at the end of multi-cracking formation on the composite (State II) also decreases. This is also confirmed by the tests on composites reinforced with AR-glass textile with different yarn diameter conducted by Moller (2001) and by other studies (Hegger et al. 2006; Peled et al. 2008). According to the proposed model by increasing the radius of the yarn of the textile by about four times (the cross-section area by about 14 times) the strain capacity of the composite at State II is decreased by 37% (comparison between purple and red line in Fig. 3.17). Furthermore, the stiffness of the textile-reinforced matrix composite at State I and at State III is not affected significantly by the cross-sectional area of the yarn.

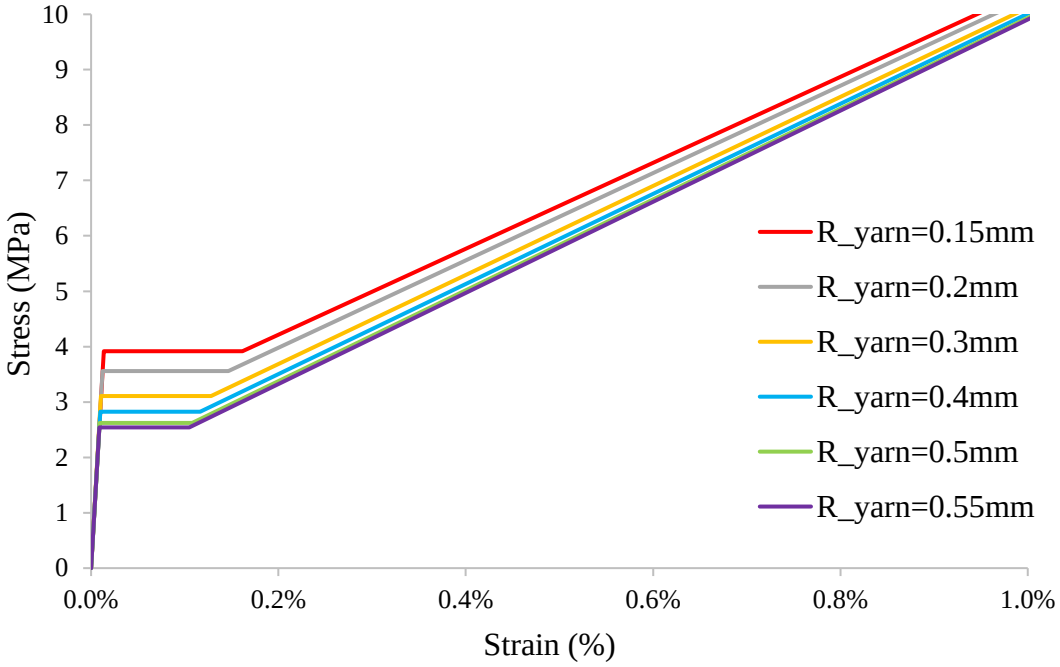

Figure 3.17: Tensile behavior of textile reinforced matrix composite considering different radius of the yarn in the textile as obtained from the proposed model in terms of stress-strain.

From Fig. 3.17 it is observed that the yarn geometry influences the tensile behavior of the textile-reinforced matrix composite before cracking occurs and at the end of multi-cracking formation of the composite. As previously mentioned (section 3.5.2), the results obtained from this study can be considered as indication since the proposed model does not take into account in detail the bond condition existing between the textile and matrix in the real case. For instance by decreasing the radius of the yarn, the tensile capacity of the TRM may not increases significantly as resulted from this model because in the case where the radius of the yarn is relatively small the penetration of the textile to matrix is low (low friction between the inner filaments exists) leading to a low tensile capacity of the composite (Hegger and Voss 2008). Therefore, relevant experimental tests are needed in order to modify the Eq. (3.17) that defines the composite strain at State I to take into account the bond conditions between the textile reinforcement and the matrix in the case where the geometry of the yarn is varied.

3.5.4 Inorganic-matrix used for binding the textile reinforcement

Besides the influence of the geometry and the mechanical properties of the textile on the tensile behavior of the TRM, the effect of the type of matrix used for binding the textile reinforcement is investigated, as well. In order to achieve this, the two main parameters of the model, namely the modulus of elasticity E_m, and the tensile strength of mortar σ_{mu}, are varied separately as indicated in Table 3.4. Specifically, in the case where the effect of the tensile strength of the matrix is examining the modulus of elasticity of the matrix remains constant equal to 20 GPa while in the case where the modulus of elasticity of the matrix is examining the tensile strength of the matrix is equal to 3MPa. In both cases, the modulus of elasticity and the tensile strength of the textile is equal to 90 GPa and 1500 MPa (Basalt or Glass fibers), and the reinforcement ratio V_f is equal to 1%.

The influence of the tensile strength and the modulus of elasticity of the matrix on the tensile behavior of textile reinforced matrix composite is presented in Fig. 3.18. From Fig. 3.18 it is observed that the effect of the tensile strength of the matrix on the tensile behavior of the composite is more pronounced compared to that of the modulus of elasticity of the matrix, although both parameters influence the level of the stress and strain of the composite before and after cracking occurs in the composite (State I and State II). More specifically, as the tensile strength of the matrix increases the tensile stress and strain at State I and the strain level of the multiple cracking plateau of the stress-strain curve increases (at State II). This increase is not proportional to that of the tensile strength of the matrix, since by increasing the tensile strength of the mortar almost seven times the cracking stress and strain of the composite at the State I and the strain at the end of the State II increase by about three times (comparison between red and orange line in Fig. 3.18 a). The same observations to the above were reported in the experimental studies conducted by Mobasher et al. (2004) and Butler et al. (2010). From Fig. 3.18 (b) it is also observed that the modulus of elasticity of the matrix affects mainly the tensile deformation of the uncracked textile reinforced matrix composite

(strain at State I) since by increasing the modulus of elasticity of the matrix, the strain at State I decreases. After the cracking is completed on the composite no significant influence of the modulus of elasticity and of the tensile strength of the matrix to the tensile behavior of the composite has been investigated (State III).

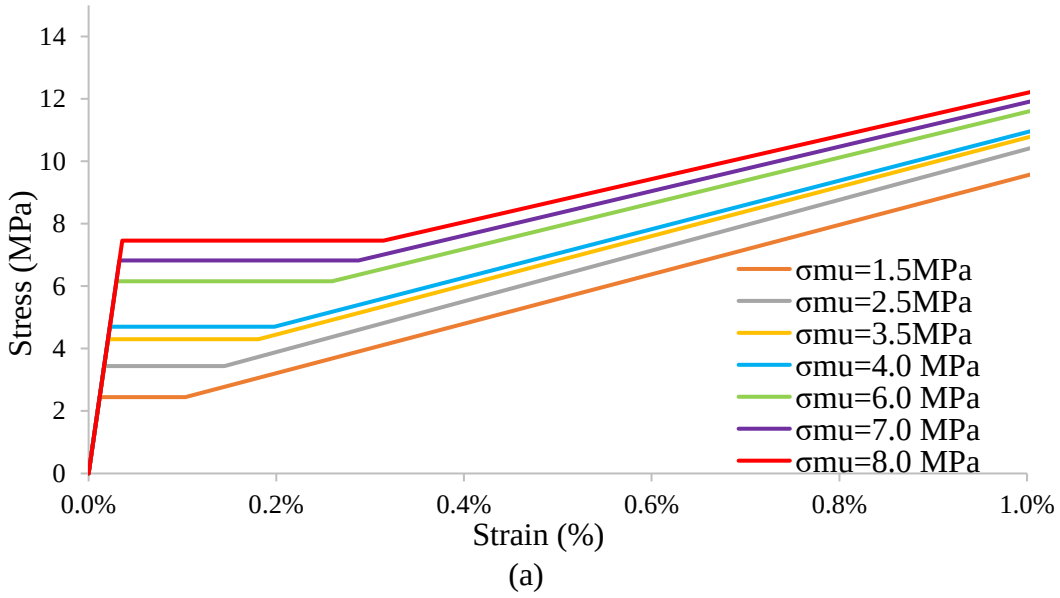

(a)

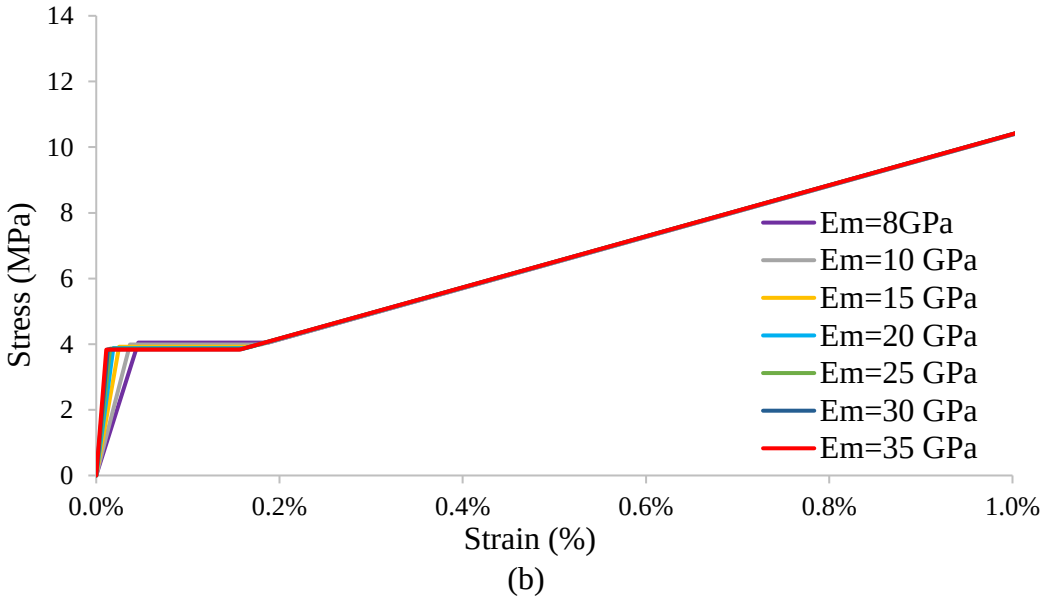

(b)

Figure 3.18: Tensile behavior of textile reinforced matrix composite in terms of stress-strain as obtained from the proposed model considering (a) different tensile strength of the matrix and (b) different modulus of elasticity of the matrix.

Considering the aforementioned, the potential way in order to increase the post cracking stress and strain of the composite (State I) and the strain at the end of the multi-cracking formation (State II) of the composite, is to increase the tensile strength of the matrix but in the same time keeping the modulus of elasticity in low level. It is important to note that the matrix composition used for binding the textile is able to determine whether the failure of the composite will occur under tensile loading such as: slippage of the textile from the matrix and debonding of the textile. Therefore, the type of the matrix can control the bond strength (adhesion properties) between textile reinforcement and mortar, and consequently the tensile capacity of the TRM (Mobasher et al. 2004; Hegger and Voss 2008; Peled et al. 2008a, b; Butler et al. 2010; Colombo et al. 2013; Portal 2013). The proposed model does not cover the effect of the type of matrix on the bond strength between the textile and matrix, consequently more relevant studies are needed.

3.6 Summary and conclusions

This part of the thesis aims to extend today's knowledge of TRM as a composite material, which is widely used in the recent years for seismic retrofitting RC and masonry structures. In order to achieve this, a brief literature review of the research that exist so far in the area of TRM composite material is presented and a simple and easy to-implement analytical model is proposed able to predict the tensile behavior of TRM in terms of stress-strain. This model is validated against the data resulted from past studies, and then a parametric study is performed to examine the sensitivity of the proposed model to a range of parameters.

Reviewing the literature, it is observed that several experimental studies have been conducted so far towards the mechanical characterization of TRM composite or similar composite (TRC). The TRM composite material shows complex behavior in tension derived from the heterogeneity of its constituent materials (inorganic matrix and textile made of fibers). The non-linear behavior of TRM under tensile loading in terms of stress-strain is divided into three states: State I the uncracked matrix, State II the crack

formation, and State III the crack stabilization and failure. The behavior of TRM composite material under tensile loading depends upon the mechanical properties and geometric characteristic of the mortar and textile and their positive or negative interaction when combined as a composite. The complex behavior of textile reinforced inorganic-matrix composites can be simulated either numerically or analytically, where in both cases two modeling strategies can be adopted, based on the level of detail by which the textile reinforcement is modeled, namely: macro-modeling and micro-modeling. Over the years, several detailed numerical models have been developed for the assessment of textile reinforced inorganic-matrix composites, however, much less studies have been carried out aiming to develop a fundamental model that governs the mechanical characterization of this type of composites. Nevertheless, most of these models are complicated to implement, require the use of specific software, and experimental data in order to be applied.

Considering the above, a simple and easy to-implement model able to define the tensile behavior of TRM in terms of stress-strain is developed in this study. The proposed non-linear approach is based on the well-established Aveston–Cooper–Kelly (ACK) theory, which applies to fiber-brittle matrix, extending it to textile-cement-based matrix (TRM). To do so, the model utilizes recommendations proposed by Eurocode 2 and by *fib* Model Code 2010 for estimating the crack spacing and the fracture energy of the composite material, respectively. Specifically, the proposed analytical model correlates the mechanical properties and geometric characteristics of the textile reinforcement and that of the inorganic matrix to define the stress-strain relationship of TRM under tensile loading, without any required information from experimental tests.

The proposed model proved accurate for predicting the tensile behavior of TRM in terms of stress-strain since the analytical curves almost coincide with the experimental ones in all experimental studies that have been taken into consideration in the present study. The cases analyzed in this work are constituted of different inorganic-matrix (lime- or cement-based matrices with a low or high content of polymers, fibers etc) and different fiber’s material for assembling the textile while the textiles are characterized

by different geometry, mass density and yarn treatment. Consequently, different systems were examined for the assessment of the proposed model. Furthermore, by comparing the experimental and analytical results it is observed that the discrepancy between them is less than 30% in almost all of case studies but this degree of approximation of the proposed model is considered acceptable since remarkable deviation occurred in each testing of this composite (coefficient of variation equal to 20%-50%). It is important to note that the proposed approach includes empirical components derived from Eurocode 2 and from *fib* Model Code 2010 (section 3.3), and consequently, its accuracy could be affected by different parameters such as: specimens' geometry, test set-up, textile coating, and presence of fibers in the cement based matrix.

A parametric study was also performed in order to examine the sensitivity of the proposed model to a range of parameters including the fiber's material used for assembling the textile, the reinforcement ratio, the cross-sectional area of the yarn and the mechanical properties of the cement-based matrix. From the parametric study the following conclusions are obtained:

- The fiber's material used for assembling the textile influences the strain of the composite at State II and the tensile capacity of the composite at State III, due to the different elastic moduli and tensile strengths of the fibers. The fiber with lower modulus of elasticity exhibited higher strain at the end of State II.
- Using high strength carbon fibers does not provide any benefit over lower-cost glass or basalt based textiles regarding the tensile behavior of the composite, except for the non-cracked composite state (State I), in which the tensile stress of the composite at this State is higher when high strength carbon fibers are used.
- The basalt-TRM shows similar behavior to glass-TRM at a much lower cost than carbon- or aramid-TRM, which makes them very appropriate for low-cost interventions
- By increasing the reinforcement ratio of the composite material, the tensile

stress at State I and the strain at State II increases but not proportionally due to different brittle failures that may occur between the textile layers, and due to the low penetration of the textile to matrix may exist. In addition, there is no influence of the reinforcement ratio on the stiffness and the strain at State I.

- The distance between the cracks decreases as the reinforcement ratio increases.
- By increasing the textile reinforcement ratio, the stiffness at State III increases, as expected, since in this State only the fibers contribute to the stiffness of the composite.
- By increasing the cross-sectional area of the yarn, the stress of the composite material at State I and the strain at State II decreases, therefore, by using a textile with a relatively small distance between the yarns or a textile with a relatively high density yarns the stress and strain of the composite before cracking occurs and at the end of multi-cracking (State I and State II) increase, considering that full penetration of the textile to matrix is achieved. The stiffness of the textile-reinforced matrix composite at State I and at State III is not affected significantly by the cross-sectional area of the yarn.
- By increasing the tensile strength of the matrix, the tensile capacity at State I and the strain level at State II increases.
- By increasing the modulus of elasticity of the matrix, the strain of the composite at State I and II decreases.
- The matrix composition and the geometric characteristics of the textile reinforcement must be such that to achieve full penetration of the textile to the matrix in order to enhance the bond strength (adhesion properties) at the textile-matrix interface, and further to avoid or event prevent the debonding or the slipping of the textile.

It is important to mention that this model provides the strength envelope of the tensile behavior of TRM. The cyclic behavior, that is described with the hysteresis loops, or

loading unloading curves are not considered in this model. Whenever relevant experimental studies become available regarding the cyclic behavior of TRM (Hatrig et al. 2004; Jesse 2004; Konrad et al. 2006; Carozzi and Poggi 2015), a hysteretic model for TRM may be developed. Furthermore, special attention must be paid when using this model for predicting the behavior of RC and masonry structures retrofitted with TRM. The bond between the concrete or other surfaces (masonry) with TRM must be taken into account in the modeling of RC and masonry structure with TRM through interface models in order to capture the debonding at substrate-TRM interface and the slipping of the TRM for the substrate.

Following the objectives of this study, as presented in Chapter 1, and considering that the degree of approximation of the proposed model is acceptable, this approach is used to develop the numerical model of masonry-infilled RC frame retrofitted with TRM (Chapter 4). The proposed analytical model of TRM is used for predicting the tensile behavior of TRM whenever the experimental data is not available as will be descripted in Chapter 4. Furthermore, the proposed analytical model is used for predicting the tensile behavior of TRM considering different textile reinforcement ratio, different textile geometry and different type of the mortar for binding the textile reinforcement in order to perform numerical experiments to assess the critical parameters which can influence the effectiveness of TRM for retrofitting masonry-infilled RC frames as will be presented in Chapter 6.

CHAPTER 4

4. DEVELOPMENT OF A NUMERICAL MODEL OF MASONRY INFILLED RC FRAME WITH AND WITHOUT TRM

4.1 Introduction

Following one of the objectives of this research which is to extend today's knowledge regarding the effectiveness of using the TRM composite material for seismic retrofitting masonry-infilled RC frames by performing numerical experiments it is a need to develop an accurate numerical model of masonry-infilled RC frames with and without TRM. Towards this direction, a two-dimensional (2D) FE model of 2/3 scale, three-story masonry-infilled RC frame with and without TRM is developed which are both experimentally tested under cyclic loading in the study carried out by Koutas et al. (2014).

In the present study, the numerical models were developed following a simple micro-modeling approach considering the geometry and materials' nonlinearity of the real case, and considering the inherent uncertainties associated with the mechanical properties of the materials involved in this type of structure (masonry infill wall, concrete, TRM), and with the properties of the infill-frame interface. The use of a simple micro-modeling approach, is considered the most viable solution to model the masonry-infilled RC frame with and without TRM, in opposition to a more sophisticated and detailed micro-modeling approach (micro-modeling strategies as shown in Figs. 2.9 and 3.4 or 3D finite elements) for the purpose of the study, where the numerical models are not intended to capture the response of the masonry infill wall and that of TRM in a very detailed way but to describe their structural response in a simple,

sufficient and accurate manner. For this reason, meso-modeling is used (section 2.4, Fig. 2.9) to simulate the infill wall, and macro-level approach (section 3.2, Fig. 3.4) is used for the TRM composite material.

In this part of the thesis, a detailed description regarding the development of the FE masonry-infilled RC frame model with and without TRM is presented. Firstly, a brief overview of the published experimental case-study used for calibration purposes in the current research is presented (section 4.2). Then the choice of the commercial software used for this study is clarified (section 4.3). This is followed by the assumptions considered for the development of the numerical models (section 4.4). Then, a brief description of the type of elements and material models which are selected from the extensive library offered by the commercial software tool is given (sections 4.5 and 4.6). In addition, the required parameters for the selected material models as input for a meaningful analysis, as well as, the validation of the each of the material models used in this study against available experimental data is also presented (section 4.6). After that, the constrains and loading scheme considered in the infilled frame model with and without TRM, and the type of analyses used in this numerical study are described (section 4.7 and 4.8, respectively). Finally, the modeling scheme followed in this study is summarized at the end of this Chapter (section 4.9).

4.2 Review of the experimental case-study

In this part of the thesis, a detailed description of the experimental case-study used for calibration purposes in this numerical study is presented. The selected experimental study has been carried out by Koutas et al. 2014 at the University of Patras (Greece) for his Ph.D. This study aimed to investigate the effectiveness of TRM for retrofitting 2/3 scale, three-story non-seismically designed masonry-infilled RC frames under in-plane cyclic loading. Two masonry-infilled frames were built and tested, with and without TRM (reference and retrofitted specimen). The scope of the non-seismically design of the infilled frame was to represent the existing non-ductile buildings built in southern

Europe in the 1960s. Full details about the experimental case-study can be found in Koutas et al. (2014a, b).

The geometry of the masonry-infilled RC frame is given in Figs. 4.1 (a) and (b). The scaled specimens had a total height of 6.0 m (2.0 m per story) and bay length of 2.73 m. The columns were of rectangular cross-section and the beams were T-section (Fig. 4.1 c). The longitudinal ribbed reinforcement had 12mm diameter (lap-spliced only at the base of the first story) and mean yield stress equal to 550 MPa (class of B500C), while smooth steel stirrups with mean value of yield stress equal to 270 MPa (class of S220) were used as transverse reinforcement for all concrete members. The thickness of the concrete cover was 10mm. For the construction of the RC frame, C16/20 class of concrete was used (classification based on Eurocode 2), with the mean compressive strength and modulus of elasticity equal to 27.2 MPa and 20-25 GPa, respectively.

The dimension of the infill wall was 2.27x1.67x0.17m as shown in Fig. 4.1 (a) leading to length-to-height aspect ratio equal to 1.36. The infill wall was constructed from perforated, fired clay bricks (185x85x55mm) with perforation running parallel to the unit's length (x-direction). The infill wall was composed of two independent wythes separated by a gap equal to 60mm. Lime mortar was used between the bricks, while the thickness of the bed and head mortar joint was equal to 10mm. The infilled frame was supported rigidly by the foundation RC beam plate (0.4 x 0.9 x 4.0 m) at the bottom of the frame. Compression and diagonal tests on infill walls with dimensions of 500x500mm and thickness of 55 mm were performed in order to determine the compressive and the shear strength of the infill wall, as well as, its elastic and shear modulus. The cement: lime: sand proportion in the mortar used to bind the bricks was 1∶1∶5. The average compressive and flexural strength of the mortar was 12.95 MPa and 2.6 MPa, respectively. The mean value of the compressive strength of the infill wall was 5.1 MPa and the modulus of elasticity perpendicular to the bed joints was 3.37 GPa. The value of diagonal cracking stress (shear strength) of the infill wall ranges from 0.30MPa to 0.8 MPa and the mean shear modulus was equal to 1.38 GPa.

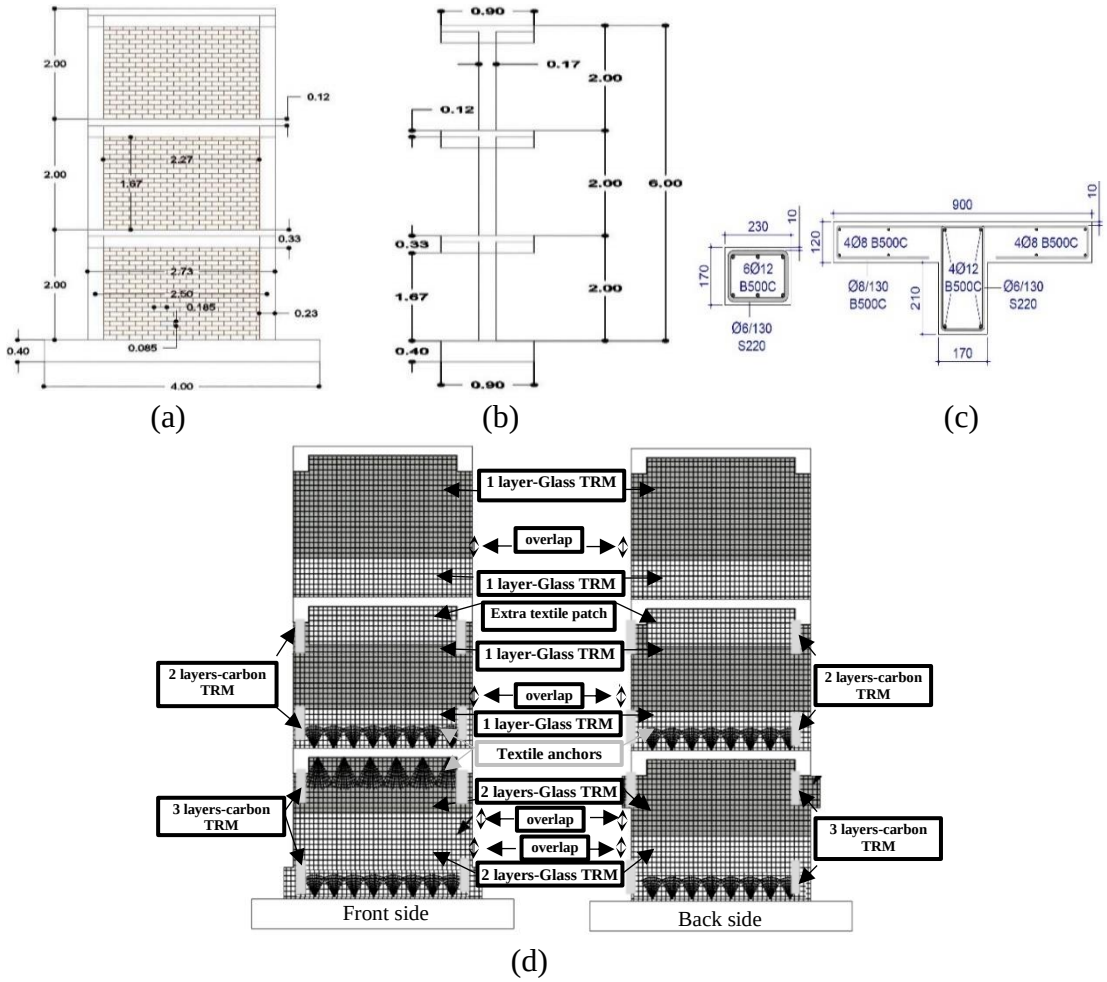

Figure 4.1: (a) Masonry-infilled RC frame in front view, and (b) in side view (all dimension in m), (c) sections of the rectangular RC columns and T-shaped RC beams and details of their reinforcement (all dimension in mm), and (d) strengthening scheme for the retrofitted infilled frame (Koutas et al. 2014).

The selection of the TRM retrofitting scheme was dictated according to the response of the unretrofitted specimen, especially from the failures that occurred on it. The strengthening scheme is presented in Fig. 4.1 (d) and includes the following:

- Strengthening the ends of columns at the first and second stories with three (9mm thickens) and two (6mm thickens) layers of carbon-TRM, respectively, fully wrapped around the column to form a closed jacket over a height of 420 mm. The column is strengthened to prevent its shear failure that occurred in the control specimen.

- Strengthening the two-sided of the infill walls with glass-TRM (externally bonded on the faces of the infill walls) by completely covering vertically the story clear height, and horizontally the area between the extremities of the bounding columns (due to its limited width the textile was applied with an overlap of about 300 mm along the entire length of each bay, near the bottom part of each story). The first story received two layers of TRM (thickness 12.5 mm) whereas the second and third stories received one layer of TRM (thickness 7.5 mm).
- In total, 11 and 8 textile-based anchors per side were placed at equal spaces along the infill-beam interfaces, at the first and second story, respectively, where the straight part of the anchor was inserted into predrilled holes filled with injected epoxy resin and the fanned parts is bonded by hand pressure on the top of the first TRM layer. The insertion of textile-based anchors is able to provide composite action of the jacket at the slab-infill interfaces of the first and second story, on both sides of the infill panels.

A general view of the test setup is presented in Fig. 4.2 (a). As shown in this figure the strong foundation beam was fixed to the laboratory floor through prestressing rods. A vertical load of 80 kN per story is considered to represent the axial permanent load in the columns through a set of four prestressing rods per story. Both specimens (infilled frame with and without TRM) were subjected to a sequence of quasi-static cycles of a predefined force pattern. More specifically, a history of imposed cycles of displacements was applied at the top-floor (Figs. 4.2 b and c), while at the same time an inverted triangular distribution of forces, to all three levels were keeping until the failure occurred (displacement loading was applied at the top-floor while force loading was applied at the second and first floor of the specimens). Seven and five cycles of displacement loading were applied to the masonry-infilled RC frame with and without TRM, respectively, as shown in Figs. 4.2 (c) and (b), respectively.

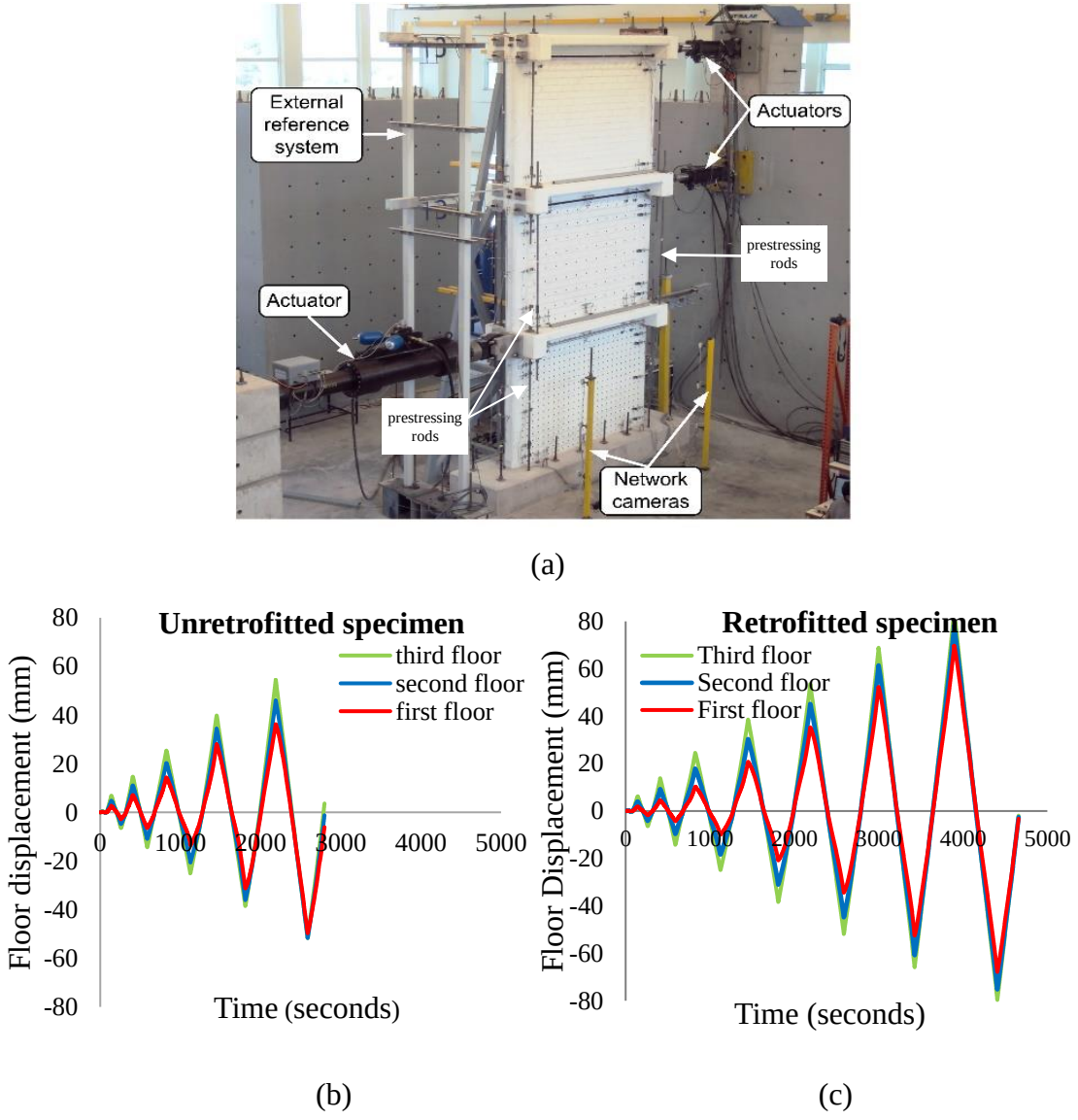

Figure 4.2: (a) Test setup, and (b) history of the imposed cyclic displacements for all stories for the unretrofitted and (c) for the retrofitted specimen (Koutas et al. 2014).

Free vibration tests were conducted in the masonry-infilled RC frame with and without TRM to identify the experimental fundamental period of the structure in each phase of the construction as shown in Table 4.1. In order to perform the free vibration tests, the specimens subjected to a static displacement loading at the top of the structure while the gravity loading of 80 kN per story was not considered for this test.

Table 4.1: Results of free vibration test.

Dynamic characteristic	Bare frame	Masonry-infilled RC frame	TRM- Masonry-infilled RC frame
Fundamental period (Seconds)	0.24	0.06	0.047

At early stage of the cyclic loading in the unretrofitted specimen, step-type cracks were formed running parallel to the diagonal of the infill wall at the first story. Upon increase the horizontal loading, the previously opened step-type cracks reopened, became wider, and propagated in the body of the infill wall as shown in Fig. 4.3 (a). Furthermore, horizontal sliding-type cracks were formed, one at top of the infill and the other slightly lower than mid-height that joined the tips of the step-type cracks of the previous cycle, and shear cracks were developed at the top of the columns at the first story. For the unretroffitted specimen, the maximum base-shear force was attained during the third cycle of loading equal to ±250 MPa (positive and negative direction) as shown in Fig. 4.3 (b).

During the first cycle of loading in the retrofitted specimen (positive and negative direction of loading), diagonal cracks appeared on the external face of the TRM jacket at the corners of the infill wall at the first story. As the lateral loading increases, diagonal and horizontal cracks were developed on the external face of TRM at the central region of the infill wall and close to the corners of the infill wall at the first floor of the structure as shown in Fig. 4.3 (c). Also, shear cracks were developed at the ends of the columns at the first floor. For the retrofitted infilled frame, the maximum base-shear is about ± 400 MPa during the fourth cycle of loading for both directions of loading as shown in Fig. 4.3 (d). During the subsequent cycles of loading, debonding of TRM from the beam surface on the back-side of the first story and local crushing of the infill wall near the two upper ends of the columns of the first story were occurred. Furthermore, debonding of TRM from the beam surface occurred on the front side of

the first story during the sixth cycle of loading due to fracture of the anchors at the top of the first floor.

Moreover, the infill-frame separation occurred at the early stages of cyclic loading in the retrofitted and unretrofitted specimen. The maximum gap-opening was 2.0 mm for the first story (column-infill wall interface), 1.5mm for the second story (bottom slab-infill wall interface), and 0.7mm for the third story (bottom slab-infill wall interface).

Masonry-infilled RC frame

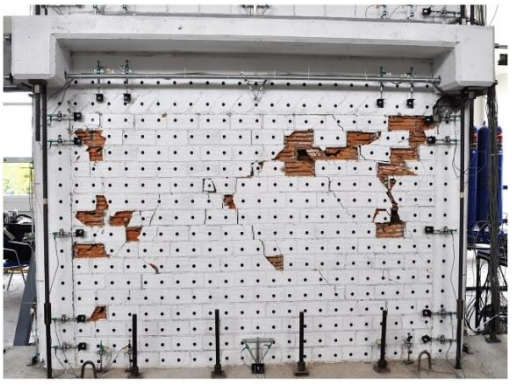

(a)

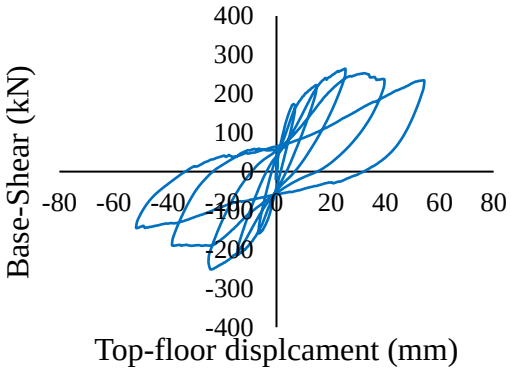

(b)

Masonry-infilled RC frame retrofitted with TRM

(c)

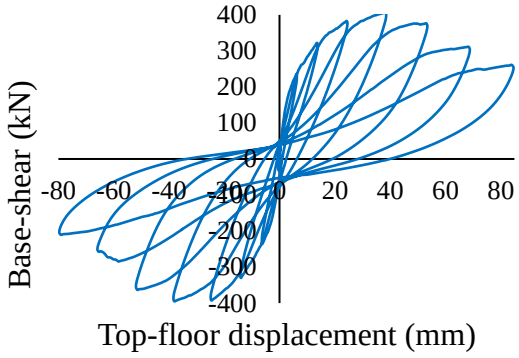

(d)

Figure 4.3: (a) Crack pattern on the infilled frame at the first floor at the end of the test, and (b) base-shear versus top-floor displacement for the unretrofitted specimen, (c) crack pattern in the retrofitted infilled frame at the first floor at the end of the test, and (d) base-shear versus top-floor displacement for the retrofitted specimen (Koutas et al. 2014).

The authors concluded that the TRM strengthening technique provides an increase in the lateral strength, deformation capacity and in the dissipated energy of infilled frames. Also, it was observed that the infill-frame separation was not avoided after applying the textile layers, and the response of the infill-frame system was far from monolithic. Furthermore, the authors concluded that the presence of custom-fabricated textile-based anchors was proved particularly effective in delaying or even preventing the debonding of TRM.

The above experimental case-study is used for calibration purposes in this numerical study, therefore, more details regarding the response of unretrofitted and TRM-retrofitted infilled frames under cyclic loading (base-shear versus top-floor displacement, failures occurred, gap-opening, etc.) will be presented in Chapter 5 where the results obtained from the non-linear cyclic analysis of the infilled frame with and without TRM are compared with the experimental ones.

4.3 Selection of software tool

A commercial software program must be selected in order to develop a numerical model to represent the behavior of masonry-infilled RC frame with and without TRM under several loading conditions, especially under cyclic loading. As mentioned in Chapter 2, section 2.4.3, several commercial programs are available for the non-linear FE analysis of infilled frames, such as ABAQUS, ANSYS, DIANA, ATENA, LS-DYNA, LUSAS, MARC, VECTOR, MASA, OpenSees, ADINA. Each of these software tools has capabilities to model the masonry-infilled RC frames in two or in three dimensions (2D or 3D) using several types of analyses (eigenvalue analysis, cyclic analysis, dynamic analysis, etc.). The computational cost of FE analysis of this type of structure is usually extremely high, due to the large number of parameters and degrees of freedom involved (section 2.4.3), and therefore, the selection of an appropriate commercial software program is important.

Reviewing the literature, it seems that many researchers used the DIANA (DIsplacment ANAlyzer) Finite Element Analysis (FEA) tool to perform numerical studies for examining the behavior of masonry-infilled RC frames under monotonic or cyclic loading (Dolatshahi and Aref, 2011; Al-Chaar et al. 2008; Kyriakides and Billington, 2011; Siamak, 2013 and Stavridis, 2009). Furthermore, numerical studies also carried out using DIANA FEA for simulating masonry walls retrofitted with TRM as described in Chapter 2, section 2.5.2 (Parisi et al. 2011; Bertolesi et al. 2016; Basili et al. 2016; Mininno et al. 2017 and Wang et al. 2017). Considering the aforementioned, and reviewing the study conducted by Sanya (2006) in which a comparison of the capabilities of different software tools is presented, it can be concluded that DIANA FEA is widely used for modeling masonry structures, and especially for modeling masonry-infilled RC frames.

Hence, it was decided to use the DIANA FEA commercial FE software tool for the purpose of the current study. DIANA FEA (Version 10.2) has an extensive library of elements and material models (linear and non-linear behavior) which can be used to model the concrete, reinforcement, infill wall and the TRM composite. Also, DIANA FEA is selected due to its user-friendly input and output formats, and integrated graphics capabilities. This software tool can be considered viable for this numerical study having in mind that the numerical model that will be developed should be as simple as possible without compromising its accuracy in order to be able to easily extend it to other applications of interest for further research by performing numerical tests.

4.4 Assumptions for the model definition

The assumptions considered for the development of a FE numerical model to represent the 2/3-scaled, three-story masonry-infilled RC frame with and without TRM that experimentally tested in the past (section 4.2) are presented in this part of the thesis.

Firstly, a 2D simplification is considered in this numerical study although that the complex behavior of masonry-infilled RC frames under lateral loading is a three-dimensional (3D) problem, especially in the case of out-of-plane loading. Despite the recent advances in computing resources, 3D numerical models are still not frequently used due to calculation time and complexity, and the two-dimensional (2D) simplification is therefore often used for its reduced calculation time and relative simplicity. For the purpose of this study it is not necessary to develop a 3D model because the torsional effects of the structure that being solve are negligible since the stiffness of the structure is distributed uniformly in the plan. Adding to this, only the in-plane response of the masonry-infilled RC frame structure will be studied since no bending outside of the plane of the structure was observed in the experiment. Based on the above mentioned, the 2D simplification is considered a viable solution to model the masonry-infilled RC frame with and without TRM where the stresses are calculated perpendicular to the direction of the load and the stresses perpendicular to the face of the members are zero.

Secondly, assumptions regarding the geometry of the real case specimens are necessary in order to develop a 2D model of the masonry-infilled RC frame with and without TRM similar as possible to that of the real case. In this concept, the masonry infill wall which is composed of two independent wythes separated by a gap equal to 60mm is assumed to be as a one masonry infill wall in the model with the same thickness as the two wythes. Furthermore, the beams which were of T- sections in the real case (Fig. 4.1 c) are modeled as rectangular beams while the weight of the rest of the beam section is imposed as a dead load at the top of each column as is going to be discussed in section 4.7. The cross-sectional area of the steel reinforcement (longitudinal ribbed reinforcement and steel stirrups) has a double area in the model compared to that used in the experiment in order to have in the model the total cross-sectional area of the steel reinforcement used in the experimental case-study. In the same concept, the TRM composite which was externally bonded in the two sides of columns and of masonry

infills in the experiment is modeled as one layer with thickness equal to the total thickness of the TRM used in the real case.

Furthermore, it is important to mention that the textile-based anchors which were placed along the infill-beam interfaces, at the first and second story in the real case, as shown in Fig. 4.1 (d), are not modeled. Therefore, the debonding of TRM from the infilled frame, which mainly provides the activation of these anchors, cannot be represented by this numerical model. Nevertheless, the bond condition provided by the existence of anchors is taken into account in the numerical model as will be described in the next section. Furthermore, the strong foundation beam is not modeled for simplicity reasons since no significant damage (rocking effect) was observed in the foundation beam during the experiment. Consequently, the fixed condition between the foundation beam and the infilled frame is considered in the numerical model by preventing any translation in the x- and y-direction at the bottom of the infilled frame.

Finally, the cyclic loading process followed in this numerical study is different from that of the experimental case-study. The masonry-infilled RC frame with and without TRM was subjected to a sequence of quasi-static cycles of a predefined force pattern as it is described in section 4.2. Specifically, displacement loading was applied at the top-floor while force loading was applied at the second and first floor where the reaction of the applied forces gives the history of the displacements at the second and first floor as shown in Figs. 4.2 (b) and (c). In order to simulate this loading scheme, displacement control analysis is used by applying only displacement loading at the three stories of the masonry-infilled RC frame. Hence, the cyclic loading process followed in this numerical study is different from that of experimental study since it is not possible to combine displacement and force analysis together. Adding to this, the displacement cyclic loading is discretized in loading steps in this numerical study instead of time steps used in the experiment (Fig. 4.2 b and c). The cyclic loading can be discretized either via regular load steps or time steps in this study since there is no time-dependent material behavior (e.g. material data varying in time) and no dynamic effects observed in the real case. Therefore, for simplicity reasons, and in order to reduce the

computational cost of the analysis, the displacement cyclic loading is discretized in load steps using automatic incrementation procedure in which both the number of steps and the corresponding size of each step are automatically computed by DIANA FEA. More details regarding the cyclic loading process followed in this study is going to be presented in section 4.9.

Following the purpose of this study, some assumptions are necessary regarding the geometry, material's nonlinearity and the loading process of the real case in order to develop a masonry-infilled RC frame model with and without TRM using DIANA FEA without high computational cost and without compromising its accuracy.

4.5 Modeling scheme

The modeling scheme used in this study in order to represent the three-story masonry-infilled RC frame with and without TRM that was studied experimentally in the past is presented here. Particularly, the type and the geometry of the elements, as well as the connection between them, considered on the infilled frame model with and without TRM are briefly presented in the following paragraphs. It is important to mention that the modeling scheme that is followed in this study is based on the assumptions described in the previous section.

For the purpose of this study, simple micro-modeling approach is used to model the masonry-infilled RC frame with and without TRM, as mentioned in section 4.1. The masonry infill wall, beam, column and the TRM composite are modeled separately by continuum elements, the steel reinforcements are modeled as bar elements, and the interaction between masonry infill wall and RC frame is modeled by interface element. Particularly, meso-modeling is used (Fig. 2.9) to simulate the masonry infill wall (the brick units, mortar and unit-mortar interfaces are modeled by continuum elements), and macro-level approach (Fig. 3.4) is used for the TRM composite where the textile reinforcement and mortar layer are lumped in a homogenized layer.

As mentioned in previous section, a 2D simplification is considered to model the masonry-infilled RC frame with and without TRM where the stresses are calculated

perpendicular to the direction of the load and the stresses perpendicular to the face of the members are zero (plane-stress elements). Therefore, the 2D numerical models are developed with a virtual thickness since the stresses in the out-of plane direction are negligible when the unretrofitted and retrofitted specimen subjected to in-plane cyclic loading in the experimental study. In this context, the concrete members, the masonry infill wall and the TRM composite are modeled separately by plane-stress elements. The coordinates of the nodes of these elements are in the x-y plane, and the thickness of the element is small in relation to the dimensions of the element in x-y plane. The plane-stress element can be loaded with distributed load on one or more edges or over the entire face of the element. DIANA FEA offers a number of plane-stress elements (T6MEM, Q8MEM, CT12M etc.) where in this study the CQ16M quadrilateral isoperimetric plane-stress element is used. This type of plane-stress element has eight nodes with two degrees of freedom; translation in x- and y-direction as shown in Fig. 4.4 and it is based on quadratic interpolation and 2x2 Gauss integration scheme. For the CQ16M plane-stress elements used for each component of the masonry-infilled RC frame model with and without TRM, representative material models are selected, as it will be described in the next section, to establish the relation between the generalized stress and strain vectors of each element.

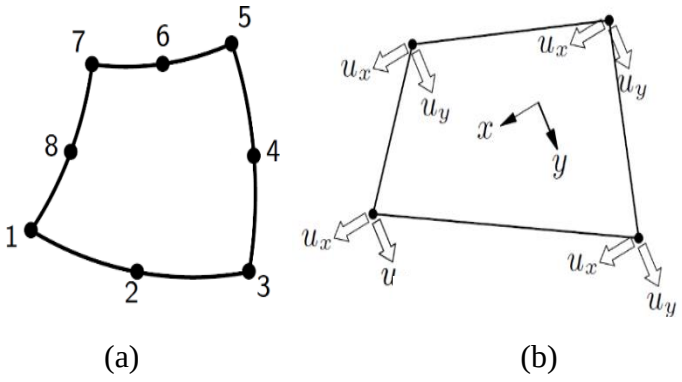

Figure 4.4: (a) CQ16M plane-stress element (number of nodes), and (b) degrees of freedom in plane-stress element; translation in x-and y-direction.

The longitudinal and the transverse (smooth steel stirrups) steel reinforcements used for concrete members (columns and beams) in the experimental case-study are also taken into account in the numerical model of infilled frame with and without TRM. Particularly, the steel reinforcement is considered embedded in the plane-stress elements used for concrete members, so-called mother elements. The relative slip between the reinforcement and the mother element is not considered in this study (perfect bond is assumed between steel reinforcement and concrete). Furthermore, the embedded reinforcement does not contribute to the weight of the mother element and neither diminishes its stiffness since DIANA FEA ignores the space occupied by the embedded reinforcement. DIANA FEA offers three types of reinforcement elements namely: bar, grid, and matrix. In this study, the steel reinforcement is modeled with two-noded bar element, and it is connected to the eight-noded concrete element (CQ16M) at the two external nodes. Therefore, a plane-stress element embeds a particle of a bar section that intersects one or two element edges as shown in Fig. 4.5. The location and the cross-sectional area of the reinforcement of each of the two-noded bar reinforcement element in the numerical model is similar as possible to that of the experimental specimens (according to the assumptions presented in previous section) as shown in Figs. 4.7 (a) and (b).

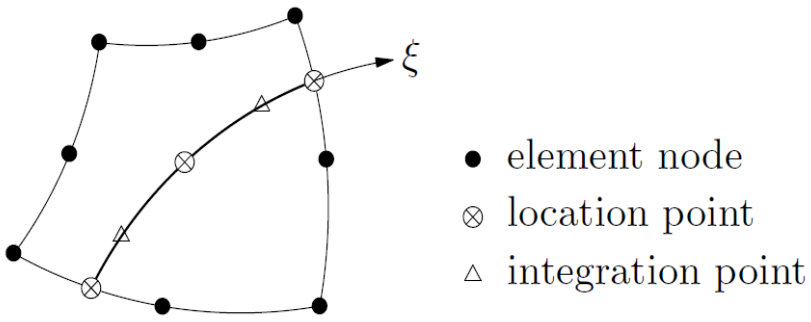

Figure 4.5: Two-noded reinforcement bar embedded in plane-stress element.

The representation of the bond conditions at the infill-frame interface is very important in order to capture the realistic response of the masonry-infilled RC frame under lateral loading as will be described in the next Chapter (section 5.5). In this context, the

interface between the masonry infill wall and RC frame is modeled by interface element offered by DIANA FEA since this interface element allows the geometrical discontinuity occurs between two adjacent members, such as the separation and the sliding. Specifically, the infill-frame interface element describes the interaction between masonry infill wall and frame in terms of a relation between the normal and shear tractions, and a relation between the normal and shear relative displacements across the interface. In this study, 2D line interface element is used between the plane-stress elements of the concrete members and those of the masonry infill wall. Specifically, three-point line interface element (CL12I) is used, as presented in Fig. 4.6. This curved line interface element has six nodes with two degrees of freedom in each node, where the variables are oriented in the x-y axes. The CL12I element is be able to fit with the CQ16M element used for concrete members, infill wall and TRM composite as shown in Fig. 4.6 (c) where DIANA FEA by default applies a three-point integration scheme for this element. The CL12I interface element, which is located at the perimeter of the infill wall at each story of the infilled frame model, has thickness equal to that of the infill wall (according to the assumptions presented in previous section) as shown in Fig. 4.8 (a). For the interface element used along the x-and y-direction at the infill-frame interface an appropriate model is adopted as will be presented in next section. It is important to note that the interaction between foundation beam with the infilled frame is included in the numerical model, although that the strong foundation RC-beam plate that used to support the infilled frame in the experimental case-study (Figs. 4.1 a and d) is not modeled for simplicity reasons (section 4.4). In order to represent this interaction, the last row of elements at the bottom of masonry-infill RC frame model with and without TRM are modeled as CQ16M plane-stress concrete elements (instead of infill wall elements) and a three-point line interface element (CL12I) is used between the last row of concrete elements and the infill wall elements as shown in Fig. 4.8 (a).

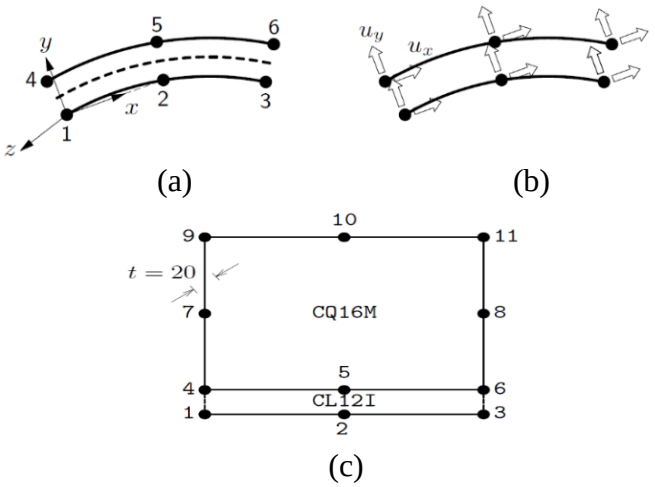

Figure 4.6: (a) Topology and (b) degree of freedom of the interface element, and (c) connection of CL12I interface element with CQ16M plane-stress element.

Figures 4.7 and 4.8 show the geometry and the mesh of the bare frame model and of the masonry-infilled RC frame model with and without TRM where the shape of elements is kept rectangular with nearly equal size. These figures show that the geometry of the numerical models is as close as possible to that of the real case, except the masonry infill wall in the first floor. The masonry infill wall at the base of the structure (first floor) has smaller height than the real case because one row of elements at the base of the infill wall is selected to represent the foundation beam, as previously mentioned (Fig. 4.7 c). Furthermore, the two independent wythes of the masonry infill wall separated by a gap equal to 60mm are modeled as a one homogenized layer by continuum elements with the same thickness as the two equals to 110 mm. For simplicity reasons and to finalize the mesh, the TRM composite layer is modeled separately at the external face of the columns, infill walls and of the beams although in the experiment a continuous TRM layer is externally bonded in the infilled frame (Fig. 4.1 d). Furthermore, the TRM composite is modeled as a homogenized layer by continuum elements with thickness equal to the total thickness of the TRM layers used in the real case (one to three layers of TRM in each side of the members). The height of glass- and carbon-TRM elements at the external face of the beams and columns, respectively, is adjusted to fit the mesh size of columns and beams as shown in Fig. 4.8.

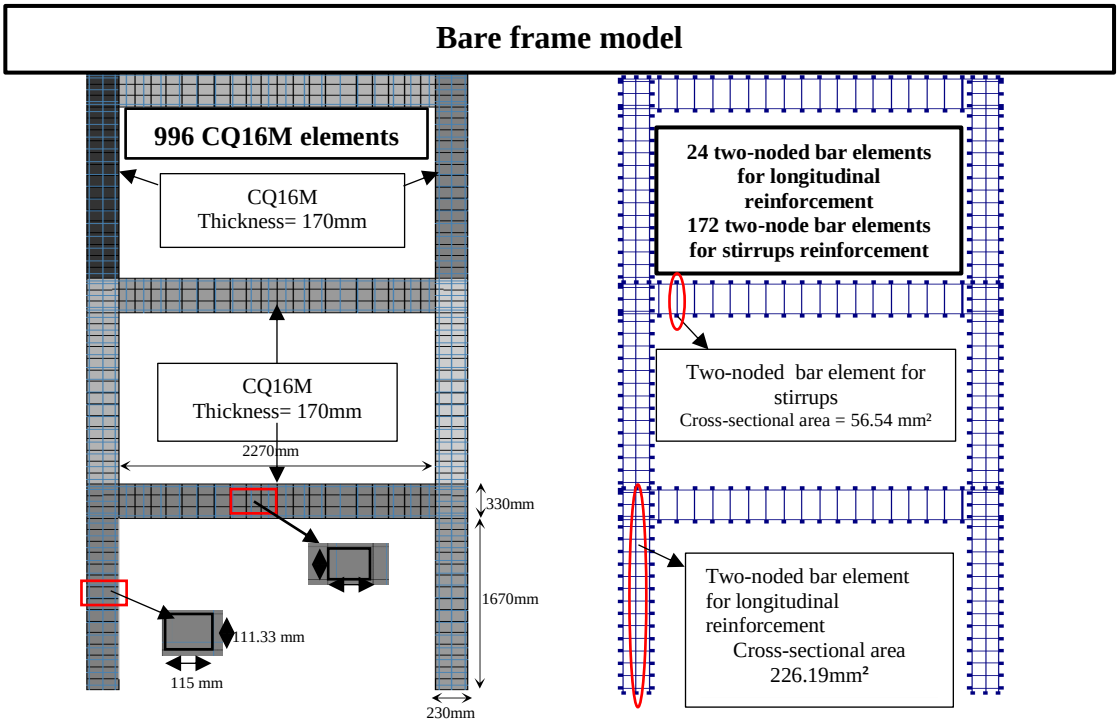

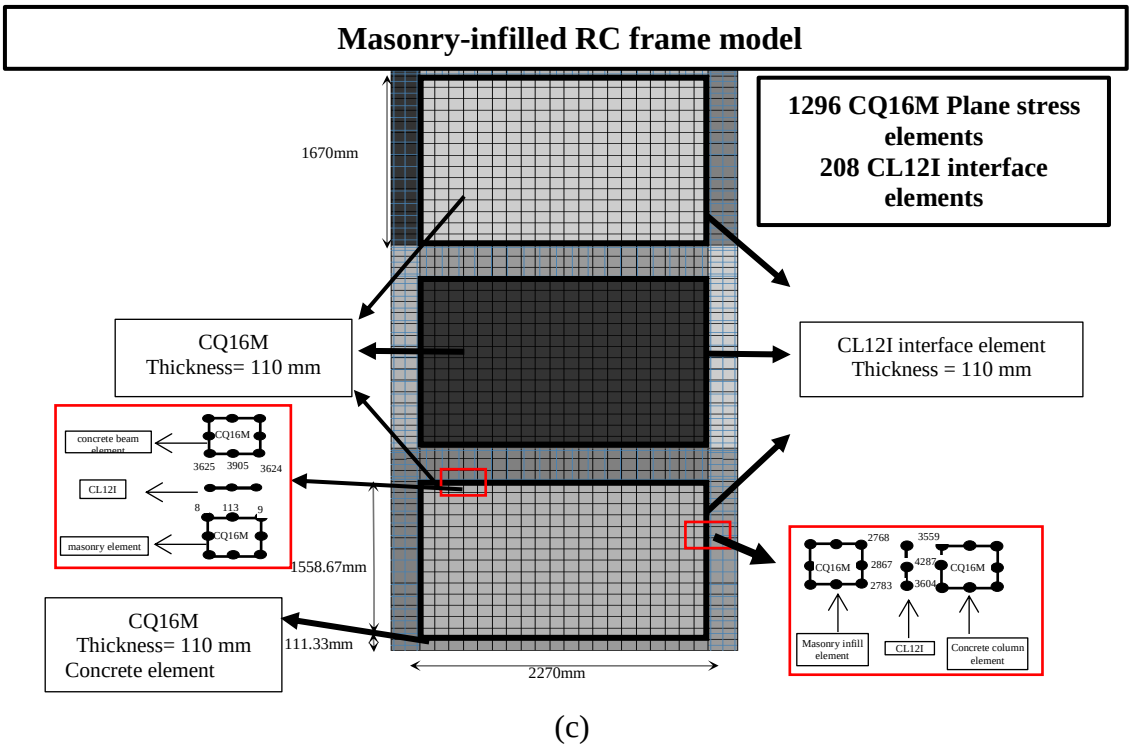

Figure 4.7: Geometry and mesh details of the (a) bare frame, (b) steel reinforcements in frame model, and (c) of the masonry-infilled RC frame model without TRM.

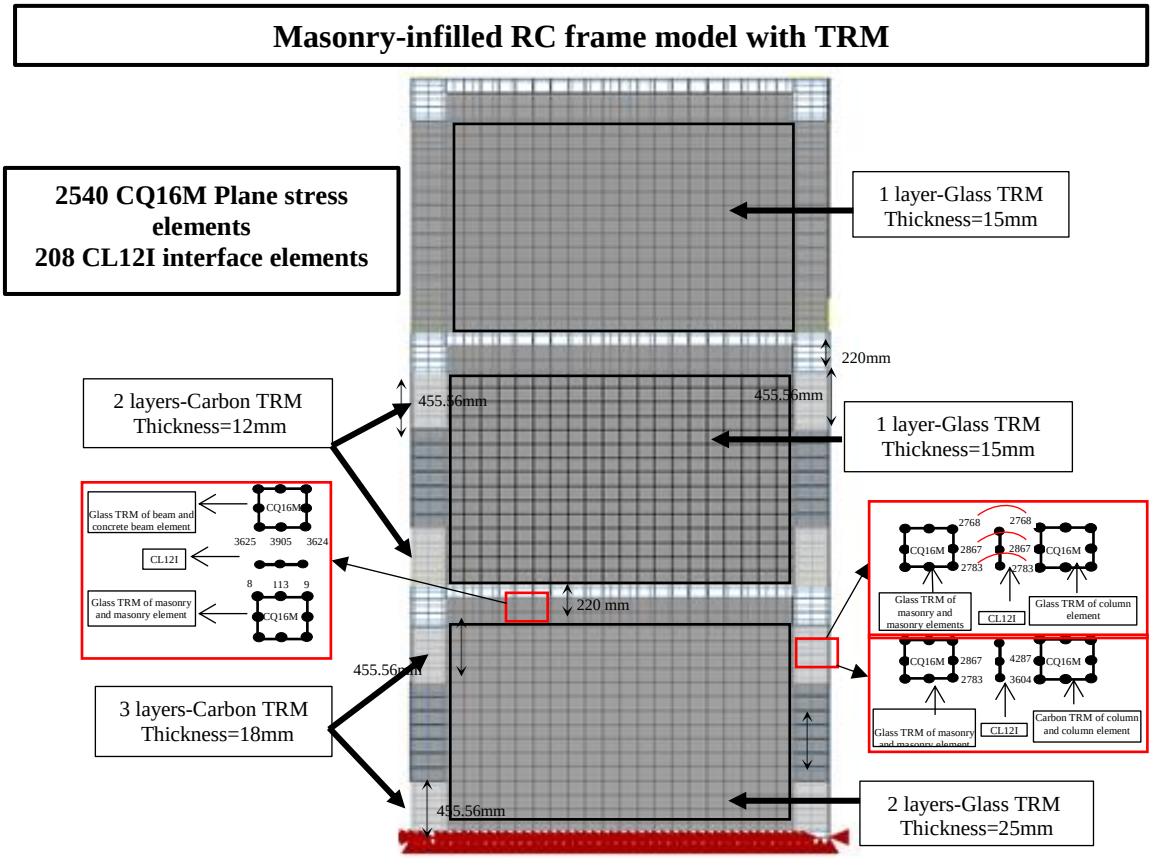

Figure 4.8: Geometry and mesh details of the masonry-infilled RC frame model with TRM.

It is important to mention that the following connectivity alternatives are considered in the masonry-infilled RC frame model with TRM (connectivity of the nodes of the plane-stress elements of beams, columns, masonry infill and of TRM, and the nodes of the three-point line interface element) in order to represent: (a) the continuity of TRM layer between the masonry infill wall and the bounding RC frame, (b) the bond conditions provided by the presence of textile anchors, and (c) the debonding and the rupture of TRM. Firstly, in this numerical model the glass- and carbon-TRM elements are fully bonded to masonry infill wall elements and to concrete elements, respectively, since in the experimental test no debonding of the TRM surface from the infill wall and from RC frame members was observed. In order to represent the continuity of TRM layer along the infill-frame interface, the glass-TRM elements at the external face of the infill wall are fully bonded to the glass-TRM elements at the external face of the beams

and columns. The bond condition provided by the existence of anchors at the top and bottom sides of the first and the second-floor beams (Fig. 4.1 d), is also accounted for in the numerical model. Specifically, in the case where the anchors at the top and bottom sides of the first and the second floors did not fail during the experiment, therefore, composite action of the TRM at the beam-infill interface can be considered, this is modeled assuming full bond connection between the TRM elements at the external face of the infill wall and the elements of the beam (full bond). In the case where the anchors failed (no composite action is provided of the TRM at the beam-infill interface), this connection is modeled with no bond between the TRM continuum layer at the external face of the infill wall and the elements of the beam (no bond). This applies only at the top beam of the first floor. Figure 4.8 shows in detail the connectivity of the nodes of the plane-stress elements in order to take into account the continuity of TRM layers, the existence of textile anchors and the rupture of TRM.

For the CQ16M plane-stress elements used for the concrete members, masonry infill wall, and TRM, and for two-noded bar element used for the steel reinforcement, and as well as for the three-point line interface element (CL12I) used for the infill-frame interface, representative models are selected to define the relation between the generalized stress and strain vectors of each element of the model as it will be described in the next section.

4.6 Material models

The finite element discretization scheme discussed in a previous section requires suitable material models to represent the non-linear behavior of RC members, masonry infill wall and of TRM. An appropriate model is also required for infill-frame interface elements in order to capture the interaction between the masonry infill wall and RC frame. In this part of the thesis, a brief description of the material models which are selected from the extensive library offered by DIANA FEA is presented.

In this study, the smeared crack approach is considered for the masonry-infilled RC frame model with and without TRM where the cracks develop throughout each element

of the model. More specifically, the discontinuity of the displacement field caused by the crack is spread across the element by changing the constitutive equation (material model) adopted for the element without defining a discrete element for the crack (discrete approach where the element mesh is changing). The smeared crack approach was first introduced by Rashid (1968) and Červenka and Gerstle (1970,1971) in which the cracks are smeared over a distinct area. On the other hand, in the discrete crack approach, that was first introduced by Saouma and Ingraffea (1981), the discontinuity of the displacement field resulting from the failure process (cracking) is introduced directly into the numerical model with an adaptive re-meshing technique in order to simulate the crack configuration. The discrete approach is directly based on the principles of fracture mechanics (Bazant and Oh 1983; Bazant 1984; Bažant and Kazemi 1990; Shah 1990; Planas et al. 2002; Murthy et al. 2009; Bažant and Yu 2011). This method is theoretically more suitable to capture the failure localization compare to the smeared crack approach, but it is usually more demanding because more specialized software is required due to the fact that the crack is modeled directly through an interface element that separates two elements in order to represent the displacement discontinuity. Although, in the smeared crack approach the continuity of the displacement field is not compatible with the real discontinuity, it is computationally more convenient to employ a smeared crack concept that does not required re-meshing. The smeared crack concept itself already offers a variety of possibilities regarding the direction of the crack, ranging from fixed single to fixed multi-directional and rotating. In the case where fixed crack model is considered the direction of the crack is fixed after the first crack occurs. On the other hand, when rotating crack model is used the direction of the crack changes by calculating the stress-strain relation for each integration point in the direction of the principal strains which determines the direction of the crack. Therefore, the crack rotation is an effective strategy keeping the principal tensile stresses under control. In the present work the rotating smeared crack approach is used.

The smeared crack models are defined through the combination of three factors as follows: (a) the failure criterion (constant or linear), (b) the cut transfer through the crack (total, constant or variable), and (c) the material softening behavior (brittle, linear, multi-linear or non-linear). Particularly, the smeared crack approach combines the failure surfaces in tension and compression to identify the crack opening and to define the crack orientation taking into account the material softening behavior (reduced material properties). According to the smeared crack approach, the crack occurs if the principal tensile stress is greater than the maximum tensile strength of the material which is defined by the failure surface selected. It is important to mention that the tension softening behavior of a brittle material depends on the energy required to create a tensile crack where this energy (fracture energy) characterizes the resistance of quasi-brittle materials subjected to tensile loads. Therefore, the fracture energy of a brittle material is necessary to estimate its tension softening behavior where the critical nominal stress decreases by increasing the loading before a strength limit of the material is reached.

Following the smeared crack approach, four material models are considered in this numerical study to reproduce the non-linear behavior of: (1) Concrete (section 4.6.1), (2) Steel reinforcement (section 4.6.2), (3) Masonry infill wall (section 4.6.3), and that of (4) TRM composite material (section 4.6.1). Furthermore, an appropriate model is adopted for the infill-frame interface elements in order to capture the gap-opening and the sliding between the masonry infill wall and RC frame (section 4.6.4). In this study, most of the required parameters to adapt the selected models in DIANA FEA are taken from the experimental case-study presented in section 4.2 and other parameters are taken from the literature as will be described in the following sub-sections. The numerical results were compared to the experimental results and some parameters of the models were adjusted to enhance the accuracy of the simulation results

4.6.1 Total Strain Crack model

The Total Strain Crack Model is one type of smeared crack models available in DIANA FEA and it is used in this study for describing the non-linear behavior of concrete and TRM composite material. The Total Strain Crack Model is introduced by Vecchio and Collins (1986) for describing the behavior of a brittle material in terms of stress-strain where the material is considered isotropic before crack occurs. This smeared crack model requires three factors in order to be defined: (1) the basic mechanical properties of the material (Young's modulus, Poisson's ratio, etc.), (2) the definition of the cracking orientation, and the (3) definition of the behavior of the material in tension, shear, and compression. In this section, the cracking orientation that is selected for the purpose of this study, and the selected material models able to describe the behavior of the concrete and TRM in tension and compression are discussed. The mechanical properties of the concrete and TRM, which are required in order to adapt the selected models in DIANA FEA will be presented in the next sub-sections (sections 4.6.1.1 and 4.6.1.2).

In this study, the crack orientation is selected to be rotating where the crack direction is calculated normal to the principal stress and rotates during the analysis with the principal strain axes always remains perpendicular to the direction of principal strain. Regarding the definition of the behavior of the concrete and TRM in tension and compression, DIANA FEA offers several material models able to describe the tensile and compressive behavior of a brittle quasi-brittle material in terms of stress-strain. The tension and compression softening models available in DIANA FEA are presented in Fig. 4.9 and in Fig. 4.10, respectively. Nevertheless, few of these models are available for in-plane actions including the cyclic non-linear behavior of the brittle materials which is necessary for the aims of this work.

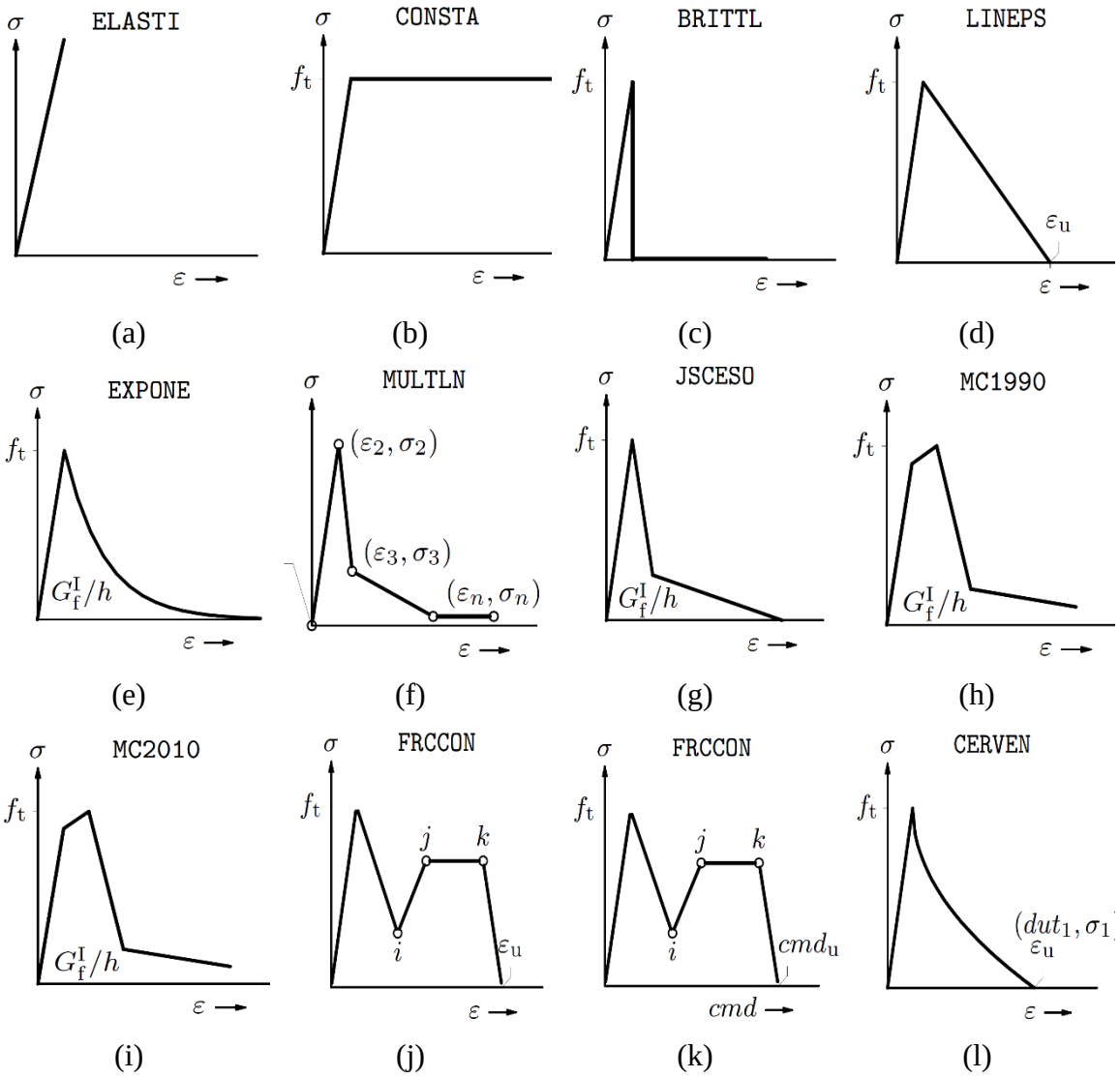

Figure 4.9: Tension softening curves for Total Strain Crack model (a) Linear, (b) Ideal, (c) Brittle, (d) linear, ultimate strain based, (e) exponential, (f) multi-linear, total strain based, (g) JSCE softening, (h) CEB-FIP 1990,(i) *fib* 2010, (j) Fiber reinforced, Total Strain based, (k) Fiber Reinforced, Crack Opening based and (l) Cervenka model.

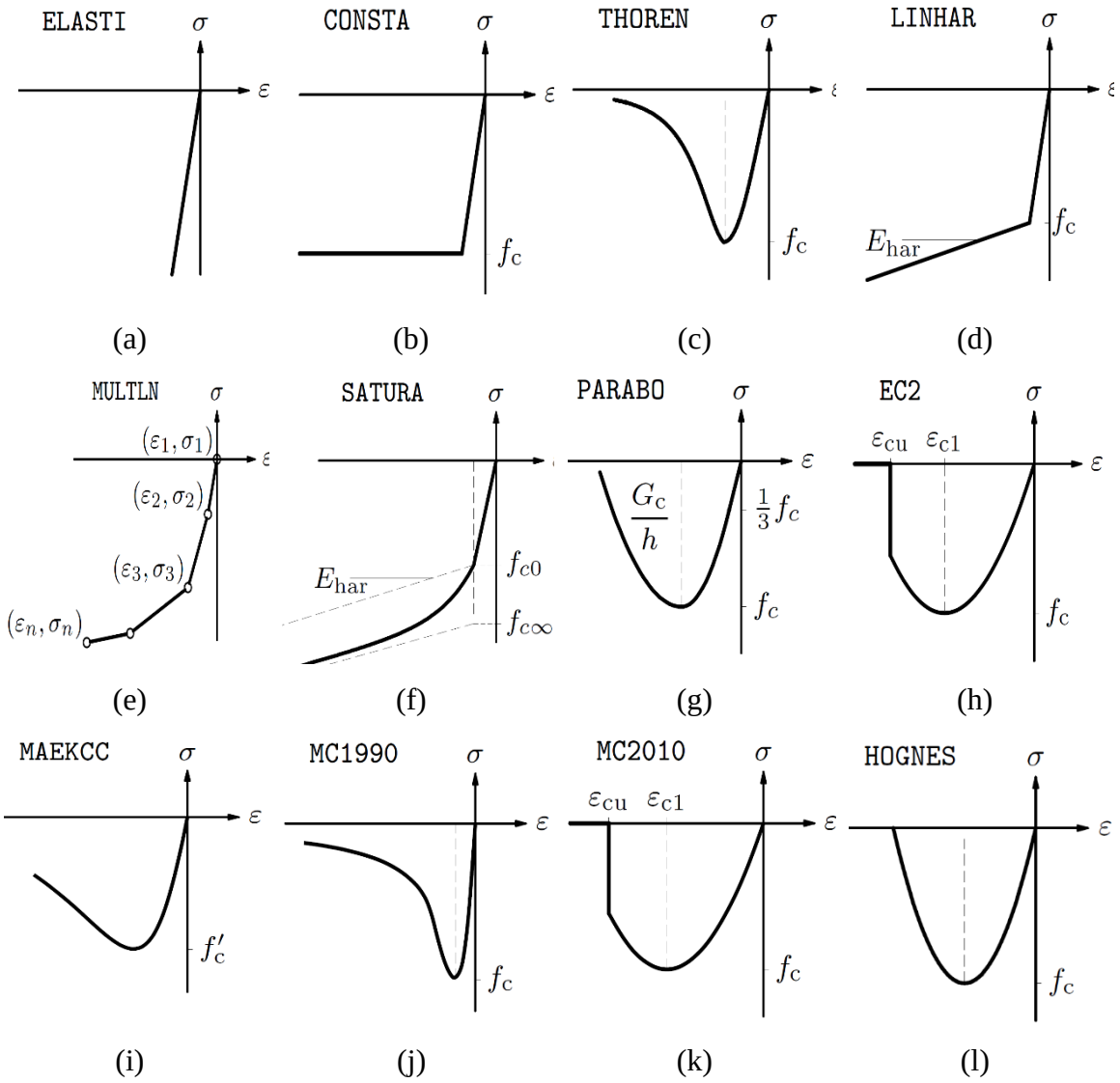

Figure 4.10: Compression softening curves for Total Strain Crack model (a)elastic, (b) ideal,(c) Thorenfeldt, (d)linear, (e) multi-linear, (f) saturation type, (g) parabolic, (h) EN 1992-1-1, (i) Maekawa, (j) CEB-FIP 1990, (k) *fib* 2010 and (l) Hognestad model.

In this study, the *fib* 2010 model is used for describing the tensile behavior of concrete as shown in Fig. 4.9 (i), while the Fiber Reinforced Concrete model that included in *fib* Model Code 2010 is used to simulate the tensile behavior of TRM composite material (Fig. 4.9 j). These tensile softening curves are selected to define the tensile behavior of these materials, since they follow the experimental values with good accuracy including

the materials' cyclic non-linear behavior (section 4.6.1.1 and 4.6.1.2). It is important to mention that the unloading branch of the stress-strain relationship of the Fiber Reinforced Concrete model directs towards zero without residual strain. Consequently, this model cannot capture adequately the cyclic non-linear behavior of TRM in which a residual relative displacement at zero stress during the unloading exists. For the purpose of this study the limitation of Fiber Reinforced Concrete model does not influence the behavior of masonry-infilled RC frame retrofitted with TRM under cyclic loading as will be discussed in section 4.6.1.2.

For describing the compressive behavior of concrete, the Maekawa Fukuura model (Fig. 4.10 i) is selected since this model can be combined with the *fib* 2010 model used for the tensile behavior of concrete. The combination of these two models is able to describe the non-linear cyclic behavior of concrete (more details regarding the required parameters of this material model and its validation will be discussed in section 4.6.1.1). For simulating the compressive behavior of the TRM composite material, the *fib* 2010 model (Fig. 4.10 k) is selected.

It is important to mention that several stress-strain relationships were proposed by Maekawa et al. (1993a, b, 2014, 2016) in order to define the Maekawa Fukuura compressive curve as presented in Fig. 4.11.

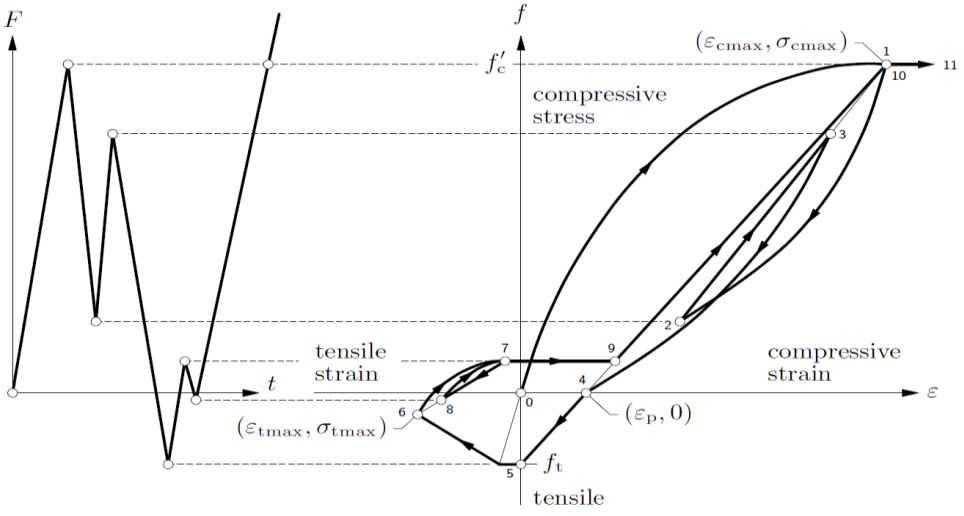

Figure 4.11: Maekawa Fukuura model (Maekawa et al. 1993a, b, 2014, 2016) .

The Maekawa Fukuura compressive curve is defined as follows:

- Compressive loading when $\varepsilon \leq \varepsilon_{cmax}$

$$\sigma = K * E(\varepsilon - \varepsilon_p) \tag{4.1}$$

$$K = \exp\left(-0.73\frac{\varepsilon}{\varepsilon_c}\left(1 - \exp\left(-1.25\frac{\varepsilon}{\varepsilon_c}\right)\right)\right) \tag{4.2}$$

$$\varepsilon_p = \left(\frac{\varepsilon}{\varepsilon_c} - \frac{20}{7}\left(1 - \exp\left(-0.35\frac{\varepsilon}{\varepsilon_c}\right)\right)\right)\varepsilon_c \tag{4.3}$$

- Compressive unloading when $(\varepsilon > \varepsilon_{cmax}, \varepsilon > \varepsilon_0, \varepsilon < 0)$

$$\sigma = K * E(\varepsilon - \varepsilon_p)*\alpha \tag{4.4}$$

where a is estimated as follows :

$$\alpha = K^2 + \left(\frac{\sigma_0}{KE(\varepsilon_0 - \varepsilon_p)} - K^2\right)\left(\frac{\varepsilon - \varepsilon_p}{\varepsilon_0 - \varepsilon_p}\right)^2 \tag{4.5}$$

- Compressive reloading when $(\varepsilon > \varepsilon_{cmax}, \varepsilon \leq \varepsilon_0, \varepsilon < 0)$

$$\sigma = \sigma_{cmax} - \left((\sigma_{cmax} - \sigma_0) * \left(\frac{\varepsilon_{cmax} - \varepsilon}{\varepsilon_{cmax} - \varepsilon_0}\right)\right) \tag{4.6}$$

where ε is the actual total strain, and σ is the corresponding stress, ε_p is the plastc strain, ε_0 is the total strain at the begin of increment, and σ_0 is the corresponding stress, ε_{cmax} is the maximum compressive strain at the corresponding stress σ_{cmax} and K the damaged parameter. The ε_c is the uniaxial strain and it is defined as follows:

$$\varepsilon_c = 2.0\ \frac{f_c'}{E} \tag{4.7}$$

where f_c is the compressive strength and E is the modulus of elasticity.

The Maekawa Fukuura model includes three options for taking into account the reduction in tensile strength. In this numerical study, the reduction factor for the tensile strength, R_f , is selected to be equal to the damage parameter K (Eq. 4.2). The other

options are $R_f = 1$ and $R_f = K^3$. Furthermore, the Maekawa Fukuura model defines the non-linear relation between the normalized shear strain, ω, and the crack shear stress, τ, for every crack in shear direction as shown in figure below (Fig. 4.12). In this study, the Maekawa Constant Density model is selected in which constant shear retention is assumed where the factor b, that defines the amount of shear stiffness remaining after crack occurs is required. In this study, this factor b, is selected to be equal to 0.1 as DIANA FEA recommended as a safe assumption.

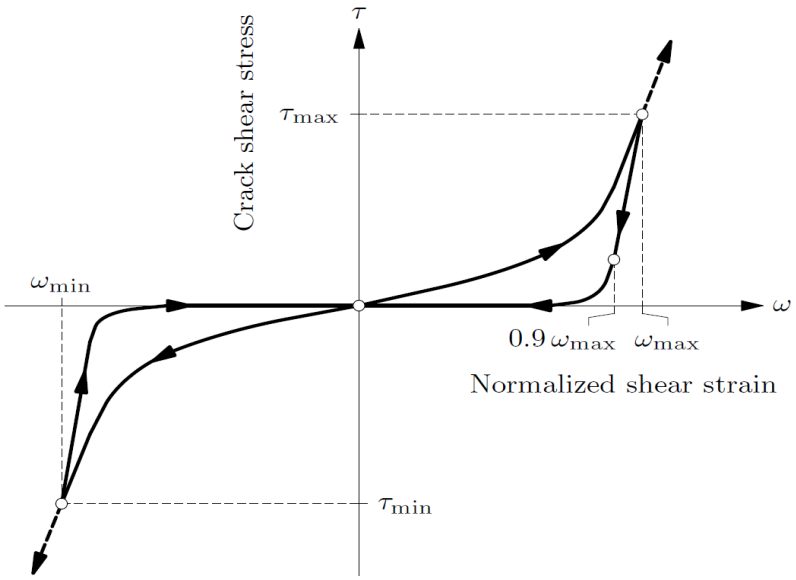

Figure 4.12: Constant Density Shear transfer model according to Maekawa Fukuura model.

Sub-sections 4.6.1.1 and 4.6.1.2 present the required parameters in order to adapt the selected models for concrete and TRM, particularly for the *fib* 2010 model and Maekawa Fukuura model which is a combination for capturing the cyclic non-linear behavior of concrete, and for the Fiber Reinforced Concrete model and *fib* 2010 model which is a combination for simulating the cyclic non-linear behavior of TRM composite material. The following sections include also the validation of these material models against the experimental data.

4.6.1.1 Concrete

The *fib* 2010 model combined with Maekawa Fukuura model are used in this study as a tension and compression softening function, respectively, for the Total Strain Crack model in order to represent the non-linear cyclic behavior of the concrete. The Maekawa Fukuura model requires the compressive strength f_{cm}, of concrete which is equal to 27.2 MPa according to the compression cylinder tests performed by Koutas et al. 2014 (section 4.2). The *fib* 2010 model requires the maximum tensile strength f_t, and the first mode fracture energy G_F, of the concrete. The tensile strength of the concrete is calculated according to *fib* Model Code 2010 as follows:

$$f_t = 0.3\, f_{ck}^{\frac{2}{3}} \tag{4.9}$$

where f_{ck} is the characteristic compressive strength equal to:

$$f_{ck} = f_{cm} - \Delta_f \tag{4.10}$$

where $\Delta_f = 8\text{MPa}$.

Based on the above equations, the tensile strength of the concrete is equal to 2.15 MPa and this value is verified by *table 5.1-5* that is included in *fib* Model Code 2010 which indicates the tensile strength for different concrete classes. The fracture energy is estimated according to *fib* Model Code 2010 which proposed an approximation for estimating the fracture energy G_f, expressed in N/m, of normal aggregated concrete as follows:

$$G_F = 73 * f_{cm}^{\ 0.18} \tag{4.11}$$

where f_{cm} is the compressive strength of the concrete in MPa. Following the Eq. (4.11) the fracture energy of the concrete in tension is equal to 130 N/m. Furthermore, the crack bandwidth, h, is also required in order to define the *fib* 2010 model in DIANA FEA. In this study, it is considered that the value of the crack band width is related to the area of the element as described by Rots 1991. As mentioned in previous section, in this study the cracking orientation is considered rotating (Rots 1991).

Amongst the basic mechanical properties of the concrete its modulus of elasticity is required in order to define the selected material model in DIANA FEA. The modulus of elasticity of the concrete is selected to be equal to 9.1 GPa. This value is two times smaller compared to that obtained from the experimental test performed by Koutas et al. (2014) (section 4.2). This reduction is necessary since the Total Strain Crack model does not take into account the reduction in stiffness due to early cracking of the concrete. Consequently, the modulus of elasticity of the concrete used in this study is derived following the Eurocode 2 which proposed a reduction factor for the Moment of inertia (I) of the concrete members in order to take into account the reduction in stiffness due to early cracking of the concrete (existing structure) as follows:

$$I_{elastic} \approx 2 * I_{cracked} \tag{4.12}$$

where $I_{elastic}$ and $I_{cracked}$ is the elastic and cracked moment of inertia of the concrete member, respectively. Based on the above equation (Eq. 4.12) and on the fact that the moment of inertia of the members cannot be changed in this study, the modulus of elasticity of the concrete is changed instead of the moment of inertia as follows:

$$E_C' \approx \frac{E_{c,elastic}}{2} \tag{4.13}$$

where $E_{c,elastic}$ is the modulus of elasticity obtained from the test performed by Koutas et al.(2014) as given in section 4.2, equal to 20-25 GPa, and E_C' is the corresponding cracked modulus of elasticity that is defined in the DIANA FEA for the purpose of this study. Furthermore, the modulus of elasticity is reduced because this value is the result of eigenvalue analysis, as will be presented in Chapter 5, section 5.3 that gives the periods of vibration measured experimentally, and the modulus of elasticity of the concrete which is about 50% of the elastic one.

The parameters adopted for the Total Strain crack model are given in Table 4.2. It is important to mention that the Total Strain based Crack model describes the tensile and compressive behavior of concrete without taking into account the stress confinement effects.

Table 4.2: Parameters of the concrete material model.

Maekawa Fukuura model combined with *fib* 2010 model for the Total Strain Crack model	
Elastic parameters	
Modulus of elasticity (E)*	9.1 GPa
Poison ratio (v)	0.2
Mass density (ρ)	2548 kg/m³
Crack orientation	Rotating
Tensile behavior CEB-FIP model code 2010	
Tensile strength (f_t)	2.15 MPa
Fracture energy (G_{ft})	130 N/m
Crack bandwidth specification	Rots
Compressive behavior: Maekawa concrete model	
Uniaxial compressive strength (f_c)	27.2 MPa
Damage based tensile strength reduction	Linear
Confinement model	No increase

After defining the required parameters of the concrete material model, the validation of this model is necessary. In order to achieve this, a 2D single block concrete model is developed in DIANA FEA which is comprised of a continuum plane-stress element with nominal size of 1000x1000x100 mm (Fig. 4.13 a). Numerical monotonic and cyclic tensile tests are performed on the single block concrete model through force control analysis by applying force loading (maximum force 10 kN by 5000 loading steps) as shown in Fig. 4.13 (b). Figure 4.13 (c) shows the results obtained from the non-linear cyclic analysis on the single block concrete model in terms of stress-strain. This figure (Fig. 4.13 c) indicates the maximum tensile and compressive strength of the concrete as given in Table 4.2. This stress-strain curve follows the Maekawa Fukuura model as presented in Fig. 4.11. The numerical results show good agreement with the experimental ones in terms of peak and ultimate stress and strain, and in terms of stiffness.

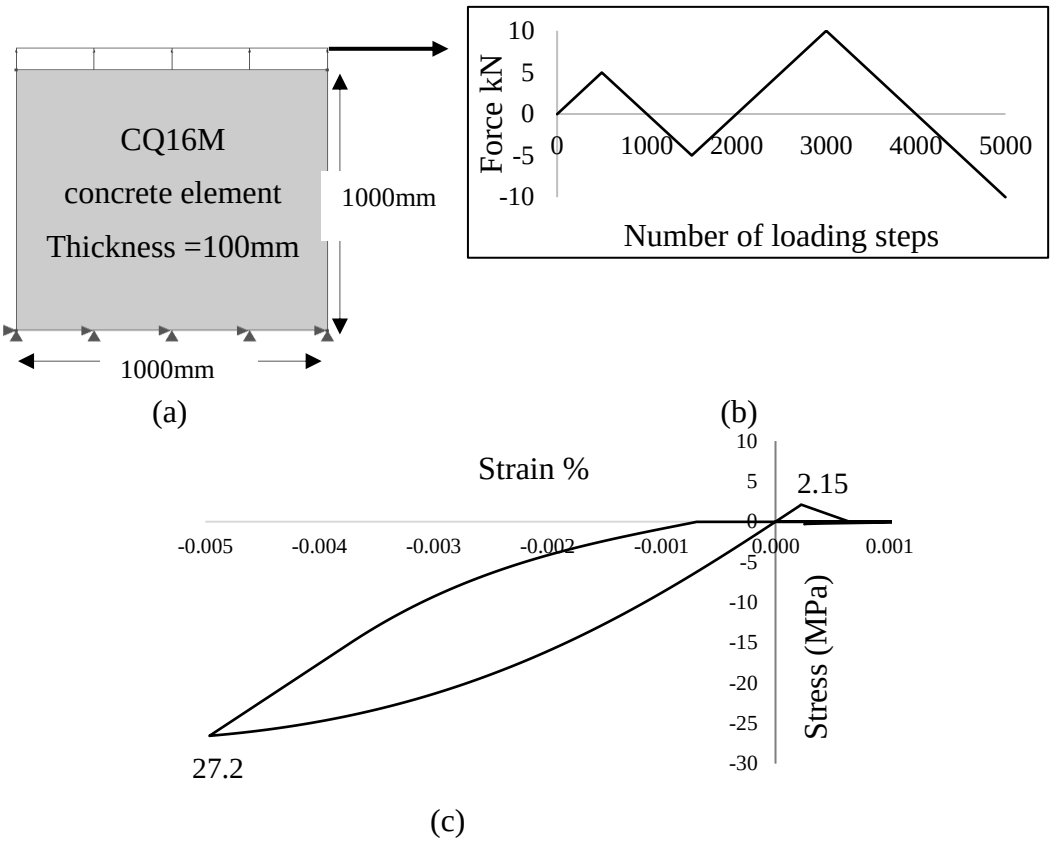

Figure 4.13: (a) 2D single continuum plane-stress concrete element, (b) cyclic force loading, and (c) results obtained from the cyclic analysis on a single block concrete model in terms of stress-strain.

Hence, the selected material models, specifically the Maekawa Fukuura model as a compression function and the *fib* 2010 model as a tension function of the Total Strain Crack model can be considered adequate for the purpose of this study, since these models can simulate adequately the non-linear cyclic response of concrete with a limited number of parameters.

4.6.1.2 TRM composite material

In this study the TRM composite is modeled by continuum elements (the textile reinforcement and mortar layer are lumped in a homogenized layer, section 4.5), and therefore, a material model must be adopted for these elements without defining the textile and mortar behavior separately. The Fiber Reinforced concrete model combined with *fib* 2010 model are used in this study as a tension and compression softening

function, respectively, for the Total Strain Crack model in order to represent the non-linear cyclic behavior of the TRM composite material. The required parameters for this model are obtained from the glass-TRM coupon tests conducted by Koutas et al. (2014), and by using the proposed analytical model of TRM as presented in Chapter 3. In this study, four material models are defined in DIANA FEA in order to represent separately the one and two layers of glass-TRM, and the two and three layers of carbon-TRM.

The Total Strain Crack model requires a number of parameters and amongst them is the modulus of elasticity of the composite material. The modulus of elasticity of this composite material obeys the law of mixture and it can be calculated by the Eq. (3.2) according to the proposed analytical model (Chapter 3, section 3.2.3.2). In order to use this equation the modulus of elasticity of the textile reinforcement and that of the inorganic-matrix are required. The modulus of elasticity of the textile is taken from the manufacturer (section 4.2) while that of the mortar is estimated according to the equation included in the *fib* Model Code 2010 for calculating the modulus of elasticity of the concrete, since the test performed by Koutas et al. (2014) regarding the mechanical characterization of the mortar used for binding the textile reinforcement gives only the tensile and the compressive strength of the mortar (section 4.2). The modulus of elasticity of the one and two layers of glass-TRM, and of the two and three layers of carbon-TRM as obtained from the Eq. (3.2) is presented in Table 4.3. It is important to mention, that the modulus of elasticity of the carbon- and glass-TRM composite material is almost the same with that of the mortar, since the contribution of the textile is negligible in the elastic behavior of TRM (State I), as mentioned in previous Chapter (sections 3.2.2 and 3.5.2).

The Fiber Reinforced Concrete model which is used for describing the tensile behavior of TRM requires several parameters as shown in Fig. 4.14 (a). The following parameters are necessary in order to define this model in DIANA FEA: the tensile strength f_t , the tensile stress at point i f_{RI}, the strain at reference point i ε_{RI}, the tensile stress at reference point j f_{Rj}, the strain at reference point i ε_{Rj}, the tensile stress at reference point k f_{Rk}, the strain at reference point k ε_{Rk} and the ultimate strain ε_u. In the case of

one and two layers of glass-TRM the above parameters are determined by the average values obtained from the tensile coupon tests performed by Koutas et al. (2014) as presented in Fig. 4.14 (b), while in the case of the two and three layers of carbon-TRM the above parameters are obtained by using the proposed analytical model of TRM as presented in Chapter 3. A detailed example for applying the proposed model is presented in Appendix I.

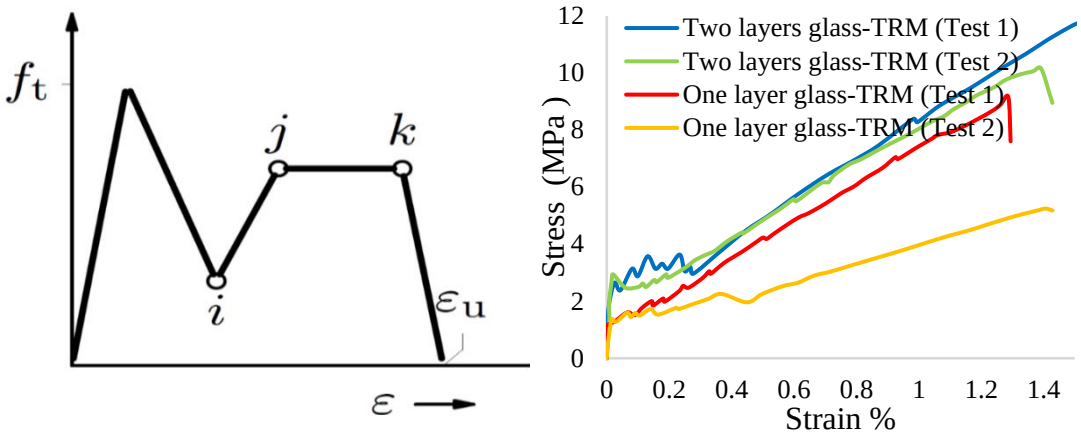

(a) (b)

Figure 4.14: (a) Fiber Reinforced Concrete model, and (b) stress-strain curves obtained from coupon tests on one and two layers of glass-TRM performed by Koutas et al. (2014).

The required parameters of the *fib* 2010 model which is used for capturing the compressive behavior of TRM must be also be specified. This model requires the compressive strength f_c, the strain at the peak strength ε_{cc} , and the ultimate strain ε_{cu} of the composite material. These parameters are almost the same with those of inorganic-matrix used for binding the textile reinforcement, since the textile reinforcement has no significant influence on the compressive behavior of the composite. Consequently, the compressive strength of TRM is equal to 18.9 MPa a value obtained from the compressive test on mortar conducted by Koutas et al. 2014. The strain at the peak stress and the failure strain is equal to 0.21% and 0.35%, respectively, according to *fib* Model Code 2010 (Table 5.1-8 in the *fib* Model Code 2010 which gives the strain values for different class of concrete), and according to past experimental studies aiming to examine the compressive behavior of fiber-reinforced inorganic-matrix

composite. For example, Li (1996), De Caso et al. (2012), Pereira et al. (2015) and Baloevic et al. (2018) investigated that the strain at the peak stress of fiber-reinforced mortar ranges from 0.2% to 0.32% and the failure strain ranges from 0.35% to 0.6%.

The parameters adopted in DIANA FEA for one and two layers of glass-TRM and for two and three layers of carbon-TRM are presented in Table 4.3. It is important to mention that, the Total Strain Crack model describes the tensile and compressive behavior of TRM without taking into account the stress confinement effects and without considering reduction due to lateral cracking.

Table 4.3: Parameters of the TRM material model.

Fiber reinforced concrete model combined with fib 2010 model for the Total Strain Crack model				
	One-layer Glass–TRM	Two-layers Glass-TRM	Two-layers Carbon-TRM	Three-layers Carbon-TRM
Elastic modulus (GPa)	30	30.5	34.00	34.8
Poison ratio	0.2	0.2	0.2	0.2
Mass density (Kg/m³)	2400	2400	2400	2400
Total crack strain model	**Crack orientation Rotating**			
Tensile behavior	**Fib Fiber Reinforced Concrete**			
Tensile strength (MPa)	1.9	2.6	4.7	5.5
Tensile stress point I (MPa)	1.9	2.6	4.7	5.5
Strain at point I (%)	0.000072	0.000082	0.000145	0.000164
Tensile stress point J (MPa)	1.9	2.6	4.7	5.5
Tensile strain point J (%)	0.0016	0.0021	0.0009	0.00095
Tensile stress point k (MPa)	10	10	17	17
Tensile strain point K (%)	0.015	0.015	0.007	0.007
Ultimate strain (%)	0.015	0.015	0.007	0.007
Crack band width	Rotating			
Compressive behavior	**Fib model code for concrete structure 2010**			
Compressive strength (MPa)	18.9	18.9	18.9	18.9
Strain at maximum stress (%)	0.021	0.021	0.021	0.021
Strain at ultimate stress (%)	0.035	0.035	0.035	0.035
Stress confinement:	**No increase**			

After defining the required parameters for the TRM material model, the assessment of the proposed analytical model of TRM which is used to define the stress-strain relationship of TRM composite (required parameters for the Fiber Reinforced Concrete model in case of two and three layers of carbon-TRM), and the validation of the material model adopted for the purpose of this numerical study is necessary. The assessment of the proposed analytical model of TRM is presented in Chapter 3, section 3.4. The validation of the Fiber Reinforced Concrete model is achieved by developing, a 2D single block TRM model in DIANA FEA. This model is comprised of a single continuum plane-stress element (with the assumption of having homogenized layer of mortar and textile) with nominal size of 1000x1000x100mm for representing the two-layers of glass-TRM. Monotonic and cyclic tensile tests are performed on the TRM model through force control analysis. The stress-strain curve obtained from the monotonic tensile numerical test on two layers of glass-TRM is presented and compared with that obtained from the experiment (Koutas et al. 2014) in Fig. 4.15 (a). Furthermore, Fig. 4.15 (b) shows the results obtained from the cyclic test on single block TRM model in terms of stress-strain.

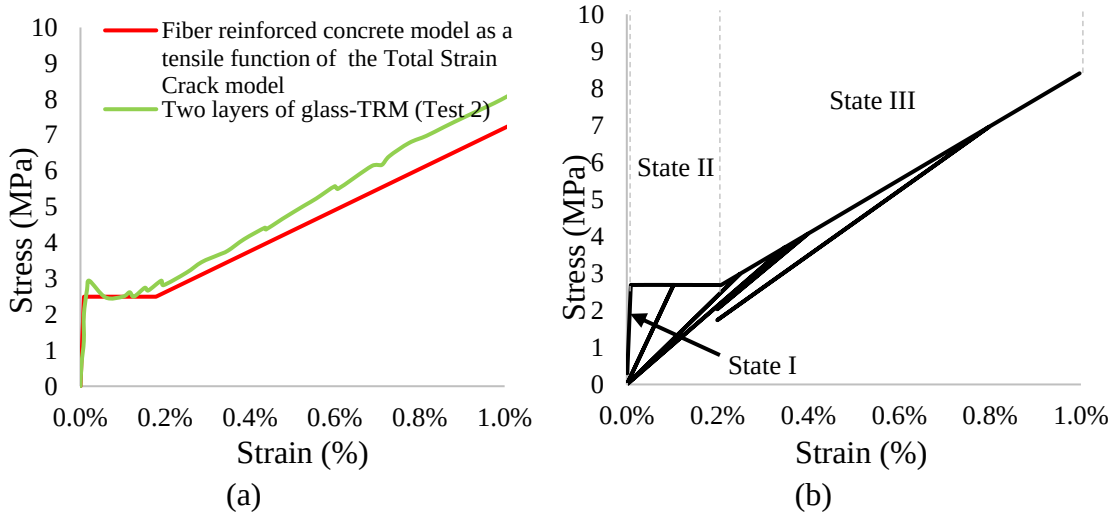

Figure 4.15: (a) Comparison between numerical and experimental results on two layers of glass-TRM, and (b) results obtained from the cyclic numerical test on two layers of glass-TRM in terms of stress-strain.

From Fig. 4.15 (a) it is observed that the numerical results show good agreement with the experimental ones since the discrepancy between them is less than 20%. Figure 4.15 (b) shows that the unloading branch of the stress-strain curve directs towards zero residual strain. Hence, this model cannot capture adequately the cyclic behavior of TRM, especially after the State II, since the studies conducted by Jesse 2004 and Keer (1981) showed that as the loading/unloading continues after the cracking on the composite is completed (State II) the modulus of elasticity of the composite material decreases and high residual strain is occurred at State III. The above limitation of the material model selected for the purpose of this study does not influence the accuracy of masonry-infilled RC frame model with TRM. This is attributed to the fact this type of structure cannot reach the high value of strains of the TRM (State III). Specifically, the behavior of infilled frames with TRM is limited to early stage of loading of TRM (State II) thus very limited residual strain is anticipated. The above is supported by Pohoryles and Bournas (2020) who investigated that the average effective strain of TRM on masonry infill walls under cyclic loading is equal to 0.24%, whereas its maximum and minimum value was equal to 0.66% (with glass-TRM) and 0.03% (with carbon-TRM), respectively.

Therefore, the Fiber Reinforced concrete model combined with *fib* 2010 model as a tension and compression softening function, respectively, for the Total Strain Crack model can be considered adequate for describing the monotonic and the cyclic non-linear behavior of the TRM composite material, for the purpose of this study. It is important to note that there is no suitable constitutive model for defining the non-linear cyclic response of TRM composite material leading the development of a relevant model a challenging issue.

4.6.2 Menegotto-Pinto plasticity model

In this study, the steel reinforcement is modeled with two-noded bar element while a material model must be adopted for this element for describing the non-linear behavior of steel reinforcement bar. The non-linear cyclic response of the reinforcing bar must be

defined in order to capture adequately the behavior of reinforced concrete member under lateral cyclic loading since during the unloading/reloading processes the reinforcing bar allows the cracks to close more easily leading to an increase in the tensile capacity of the RC member. It is important to mention that the Bauschinger effect, wherein the steel reinforcement bar exhibits premature yielding during load reversals, must be also taken into account in the reinforcement bar model in order to capture accurately the cyclic behavior of RC members (Abel and Muir 1972; Brown 1995; Prasad and Maekawa 2002).

Over the years several models have been proposed for describing the non-linear cyclic behavior of steel reinforcing bar. Amongst them, the Menegotto-Pinto model (Menegotto and Pinto 1973), the Monti-Nuti model (Monti and Nuti 1993) and the Dodd-Restreppo model (Dodd and Restrebo 1995) are the most commonly used. These models represent the hysteretic behavior of steel reinforcing bar by taking into account the buckling of the reinforcement bar considering the Bauschinger effect. For the purpose of this numerical study, the Menegotto-Pinto model is used. According to Menegotto-Pinto model, the cyclic behavior of the steel reinforcing bar is described with a hysteresis loop, loading unloading curve, as shown in Fig. 4.16 (a). This curve is expressed in terms of dimensionless stress, σ^*, and strain, ε^*, as follows:

$$\sigma^* = b * \varepsilon^* + \frac{(1-b)\varepsilon^*}{(1+\varepsilon^{*R})^{1/R}} \tag{4.14}$$

where b is the strain-hardening ratio (the ratio between the intended slope at the target point and the unloading/reloading stiffness at the origin), and R is the curvature parameters controlling the shape of the unloading-reloading cycles as follows:

$$R = R^0 - \frac{A_1 * \xi_{rp}^{max}}{A_2 * \xi_{rp}^{max}} \tag{4.15}$$

where, R^0 is the value of parameter R during the first loading, and the ξ_{rp}^{max} is the maximum plastic excursion during a previous half-cycle. The isotropic hardening behavior of the steel reinforcement bar is defined by Eq. 4.16:

$$\frac{\sigma_{sh}}{\sigma_{yo}} = A_3 \left(\frac{\varepsilon^t_{max}}{\varepsilon_{yo}} - A_4 \right) \quad (4.16)$$

where σ_{yo} and ε_{yo} is the initial yield stress and corresponding strain, ε^t_{max} is the maximum absolute total strain at the instant of strain reversal, σ_{sh}, is the stress shift in the linear yield asymptote for isotropic hardening, and the $A_1 - A_4$ are the material constants which are determined by experimental test.

Table 4.4 presents the required parameters to define the Menegotto-Pinto model in DIANA FEA. The mean yield stress of longitudinal ribbed reinforcement is equal to 550 MPa (class of B500C) and that of smooth steel stirrups is equal to 270 MPa (class of S220) (section 4.2). The curvature parameters R^0, $A_1$and A_2 and the parameters A_3 and A_4 were also defined as presented in Table 4.4.

Table 4.4: Parameters of the Menegotto-Pinto material model.

Menegotto-Pinto model	
Modulus of elasticity (E)	206 GPa
Initial yield stress ($\sigma_y{}^0$)	Longitudinal bar :550 MPa Stirrups: 270 MPa
Initial tangent slope (b^0)	0.05
Initial curvature parameter (R^0)	20
Constant parameter A_1	18.5
Constant parameter A_2	0.01
Constant parameter A_3	0.2
Constant parameter A_4	3

After defining the required parameters of the steel reinforcement material model, the validation of the Menegotto-Pinto model is necessary. In order to achieve this, a 2D reinforced concrete model is developed in DIANA FEA which is comprised of a single continuum plane-stress element for the concrete, with nominal size of 1000x1000x100mm (Fig. 4.13 a), and of a two-noded bar element embedded in plane-stress element with cross-sectional area equal to 200 mm². Monotonic and cyclic tensile

tests are performed on the single block reinforced concrete model through force control analysis by applying force loading (maximum force 10kN by 5000 loading steps) as shown in Fig. 4.13 (b). Figure 4.16 (b) shows the results obtained from the cyclic test in terms of stress-strain (S_{xx}-E_{xx}) of the reinforcement bar element. Figure 4.16 (b) indicates the maximum tensile strength of the steel longitudinal reinforcing bar as it is defined in Table 4.4 while the stress-strain curve follows the Menegotto-Pinto model as presented in Fig. 4.16 (a). The numerical results show good agreement with the experimental data in terms of peak and ultimate stress and strain, and stiffness.

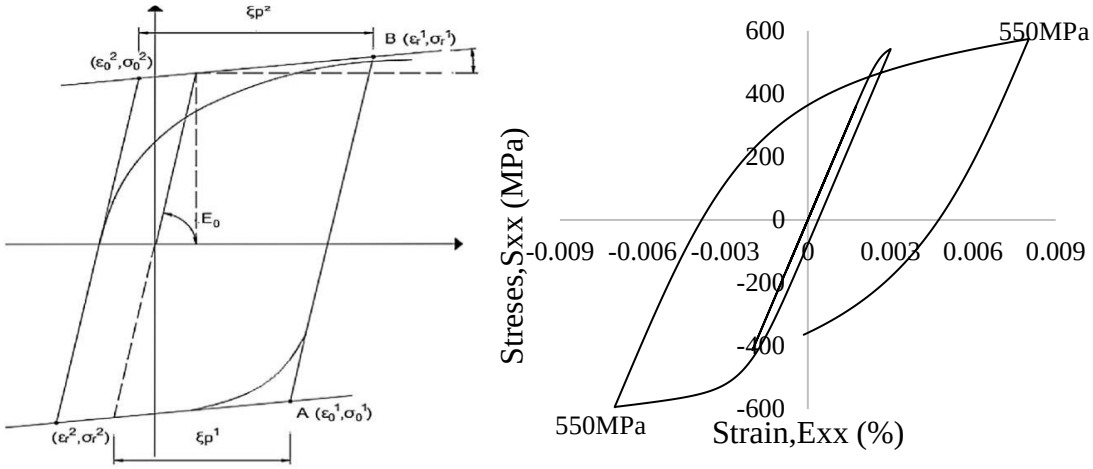

(a) (b)

Figure 4.16: (a) Menegotto-Pinto model, and (b) results obtained from the non-linear cyclic analysis on reinforcement bar in terms of stress-strain.

Therefore, the Menegotto-Pinto model can be considered adequate for describing the non-linear cyclic behavior of the steel reinforcement bar for the purpose of this study.

4.6.3 Engineering Masonry model

The masonry infill wall is modeled by continuum elements following the macro-level approach (the brick units, mortar and unit-mortar interfaces are modeled by continuum elements, Fig. 2.10), while a suitable material model representative of both the brick units and the mortar, and their interaction must be defined for these elements. In this numerical study, the Engineering Masonry model is adopted for continuum elements of

the masonry infill wall. For the purpose of this study, the Total Strain Crack model can be also adopted for the masonry infill wall, since this model is able to describe the behavior of a brittle material. However, according to Rots (2017) the Total Strain Crack model underestimates the ultimate stiffness and the dissipated energy of the masonry infill wall under cyclic loading compared to the Engineering Masonry model. Also, the Total Strain Crack model cannot simulate adequately the shear failure of masonry infill wall (Rots 2017). Furthermore, the Engineering Masonry model describes the non-linear cyclic behavior of a masonry infill wall more realistically compared to the Total Strain Crack model.

The Engineering Masonry model is a smeared crack model available in DIANA FEA, and it can be applied for the plane-stress elements, which are used in this study to model the masonry infill wall (section 4.5). This model covers the in-plane failure modes that may occur in a masonry infill wall as presented in Chapter 2, section 2.2 such as: the tensile cracking (either in the direction normal to the bed joints or to head joints), the compressive crushing (either in the direction normal to the bed joint and the head joint), the cracking in the direction normal to the diagonal stair-step cracks (when one of the diagonal cracks is active and the crack is opened, the tensile stress in the direction normal to the diagonal crack and the shear stress in the diagonal plane are reduced; when the crack is closing a linear stiffness equal to the initial elastic stiffness is applied), and the frictional shear sliding (the shear stresses are limited by a standard Coulomb friction failure criterion based on the stress normal to the bed joint). In addition, this model covers also the out-of-plane failure of the infill wall.

The Engineering Masonry model defines the tensile behavior of the infill wall considering the Young's modulus E, the tensile strength f_t, and the crack energy G_{ft}, of the infill wall for both x- and y-directions as shown in Fig. 4.17. The maximum tensile strain is called $a_{tensile}$ and the corresponding tensile stress is σ_{rf}. The tension softening curve according to this model is linear as shown in Fig. 4.17. The ultimate tensile strain ε_{ult}, is defined as the strain value at which the crack is fully opened (no stress can be transferred at this strain) as follows :

$$\varepsilon_{ult} = \frac{2\, G_{ft}}{h\, f_t} \qquad (4.17)$$

where h is the crack bandwidth of the element.

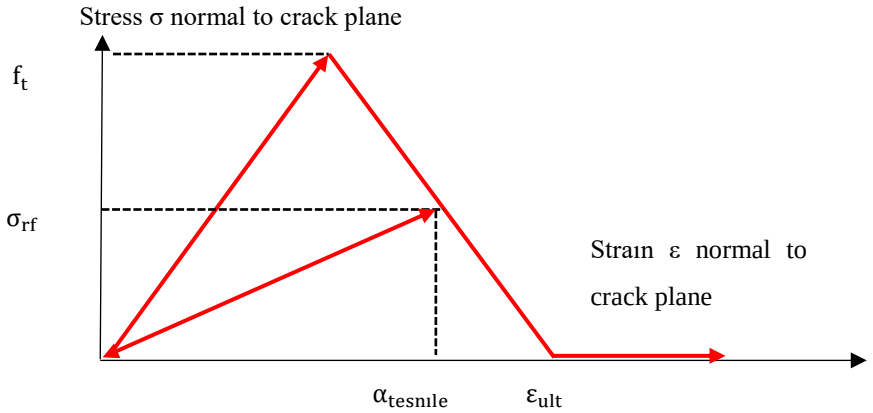

Figure 4.17: Tensile cracking function of Engineering Masonry model.

Furthermore, according to the Engineering Masonry model the compressive behavior of infill wall is defined by the Young modulus E, the compressive strength f_c, the crack energy G_{fc} and by the factor n (which is based ion compressive strain ε_{peak}) of the infill wall for both x- and y-directions as shown in Fig. 4.18. The factor n is defined as follows:

$$n = \frac{E\ \varepsilon_{peak}}{f_c} \qquad (4.17)$$

The minimum compressive strain ever reached is called a_{comp} and the corresponding stress is σ_{rf}. In addition, an unloading factor λ $(0 \leq \lambda \leq 1)$ must be defined, as presented in Fig. 4.18, where λ equal to zero corresponds to unloading with the initial stiffness E, and λ equal to one corresponds to secant unloading to the origin stiffness equal to $\frac{\sigma_{rf}}{a_{comp}}$. For the unloading, the initial stiffness E is considered until the

compressive stress level of $\lambda\ \sigma_{rf}$ is reached from which the secant stiffness equal to $\frac{\lambda\ \sigma_{rf}}{a_{comp-}\ \lambda\frac{\sigma_{rf}}{E}}$ is followed to the origin.

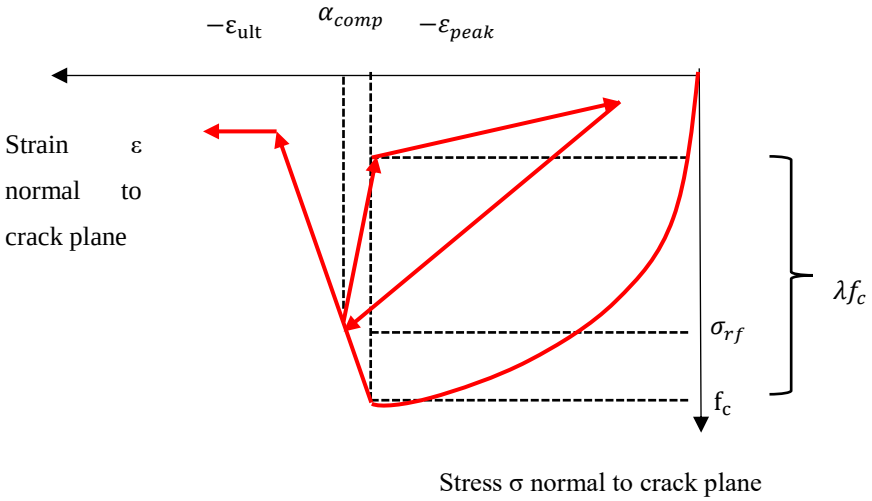

Figure 4.18: Compressive crushing function of the Engineering Masonry model.

The ultimate compressive strain ε_{ult} is defined as the strain value for which the linear softening curve would have reached to zero stress level as follows:

$$\varepsilon_{ult} = \max\left[\varepsilon_{peak}, \frac{2\ G_c}{h\ f_c} - \frac{f_c}{A^2\ E} - \frac{A+1}{A}\left(\varepsilon_{peak} - \frac{f_c}{E}\right) + \varepsilon_{peak}\right] \quad (4.18)$$

where h is the crack band width of the element and A is estimated as:

$$A = \left(\frac{E\ \varepsilon_{peak}}{f_c}\right)^{1/3} \quad (4.19)$$

Based on the Engineering Masonry model, the in-plane shear stress τ, of the infill wall is defined by the in-plane shear strain γ, and by the normal stress σ_{yy}, in the direction normal to horizontal joint, as shown in Fig. 4.19.

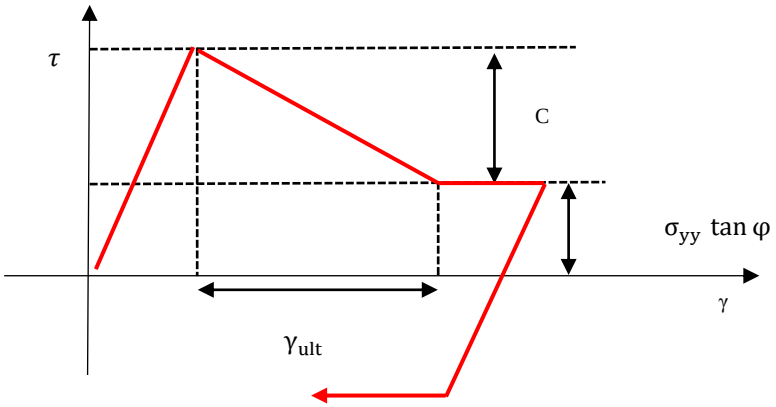

Figure 4.19: Shear function of Engineering Masonry model.

The shear stress is limited by the maximum friction stress τ_{max} which is defined by Coulomb friction as follows:

$$\tau_{max} = \max\left(0, c - \sigma_{yy} \tan(\varphi)\right) \tag{4.20}$$

where c is the cohesion and φ is the friction angle. The ultimate frictional shear strain γ_{ult} is defined by the shear fracture energy G_{fs}, as follows :

$$\gamma_{ult} = \frac{2\, G_{fs}}{ch} - \frac{c}{G} \tag{4.21}$$

where G is the initial shear stiffness.

Therefore, the Engineering Masonry model is a smeared crack model available in DIANA FEA that covers the tensile, shear and compression failure of the infill wall. This model can capture also the response of a masonry infill wall under cyclic loading with good accuracy in terms of shear strength, stiffness, and dissipated energy, and in terms of the crack patterns and the failures that occur in a masonry infill wall under cyclic loading. Nevertheless, the Engineering Masonry model requires a large number of parameters to be specified in DIANA FEA. Most of these parameters were not given by compression and diagonal tests on infill walls conducted by Koutas et al. (2014) (section 4.2). Therefore, it was decided to define some of the required parameters of the this model from the literature as described in the following paragraphs, and at the same

time by fitting the numerical results to the experimental ones. It is important to mention that the mechanical properties of the masonry infill wall are strongly dependent upon the properties of its constituents. In this numerical study, where the Engineering Masonry model is used for continuum elements of the masonry infill wall it is not sufficient to define separately the properties of the brick and the mortar joint but rather the whole composite needs to be considered together.

The following input set of parameters are necessary for the Engineering Masonry model: the Young's modulus of infill wall in the x-direction E_x, and in the y-direction E_y, the shear modulus $G_{x,y}$, the mass density ρ, the tensile strength normal to the bed joint f_{ty} and to the head joint f_{tx} , the residual tensile strength f_{tr}, the fracture energy in tension G_{ft} and in compression G_{fc} , the compressive strength f_c, the factor to the strain at maximum compressive stress n, the cohesion c, the friction angle φ and the shear fracture energy G_{fs}. This model offers four options for the head joint failure. In this numerical study, the Head joint failure not to be considered option is selected where with this option only the cracking and crushing in the direction normal to the bed joint is considered, and the Coulomb friction criterion for shear failure is evaluated. It is important to mention that in the case where another option for the head joint failure is selected, such as diagonal crack option, the results obtained from the analysis of the infill wall are less realistic with overestimation of the shear capacity and dissipated energy of the infill wall (Rots 2017).

The required parameters to specify the Engineering Masonry model in DIANA FEA are given in Table 4.5. The modulus of elasticity in the direction normal to bed joints E_y, is obtained from the compression test on masonry infill wall conducted by Koutas et al. (2014) equal to 3.37 GPa. Furthermore, the uniaxial diagonal compression test on masonry infill gives the shear modulus $G_{x,y}$, of the infill wall which is equal to 1.38 GPa and the mass density ρ, of the infill wall which is equal to 800 Kg/m³. Since the information for the Young's modulus in the direction parallel to the bed joints E_x was not available, it was estimated according to the ratio between the Young's modulus in

the y-direction with the one in the x-direction, which ranges from 1.5 to 2 for masonry infills (Lourenço and Rots 1997a, b). Therefore, the Young modulus in the x-direction E_x, is equal to 1.62 GPa.

Besides the Young modulus of the masonry infill wall, the Engineering Masonry model requires the parameters related to the tensile behavior of the infill wall. These parameters have been defined according to the information provided by the respective experimental tests and numerical studies or related reports available in the literature. Several experimental studies have been performed aiming to estimate the tensile strength of the masonry infill wall through bending tests or diagonal compression tests or shear sliding tests or tensile tests (Anthonie and Magonette 1994; Tomaževič 2009; Messali et al. 2017; Sandoval and Arnau 2017; Weissmann and Wonsiewicz 2018; Garcia-Ramonda et al. 2020). Furthermore, numerical studies have been conducted in order to capture the tensile behavior of masonry infill wall. Most of these studies proposed strategies regarding the choice of the material model for the infill wall and its corresponding parameters for a reliable non-linear analysis of masonry infill wall (Dhanasekar 1986; Lourenço 1996; Dehghani 2008; Eshghi and Pourazin 2009a; Grande et al. 2013; Lourenço and Pereira 2018). The researchers concluded that it is difficult to relate the tensile strength of a masonry infill wall to its compressive and shear strength due to different shapes and materials of the brick units, different materials of the mortar joint, different manufacture process that exist in a masonry infill wall. Reviewing the literature, it is found that the tensile strength normal to the bed joints ranges from 0.1MPa to 1MPa for different brick unit-mortar combinations (Dhanasekar 1986; Lourenço, 1998; Sandoval and Arnau 2017). For this study, the tensile strength normal to the bed joint f_{ty}, is selected to be equal to 0.5 MPa according to Lourenço and Rots (1997a,b) while the residual tensile strength is equal to 40% of the tensile strength f_{ty}.

Important parameters to define the Engineering Masonry model are also the fracture energy of the masonry infill wall in tension and compression. These parameters are

estimated according to the experimental data and formulas available in the literature (Pierto Bocca, Alberto Caprinteri 1989; Rob van der Pluij 1997; Zucchini and Lourenço 2007; Chaimoon and Attard 2009;Angelillo 2014; Drougkas et al. 2015) since in the experimental case-study conducted by Koutas et al. (2014) these parameters were not provided. According to the available literature, it is found that the compressive fracture energy ranges from 10 N/mm to 50 N/mm for similar types of masonry infill wall (Drougkas et al. 2015; Sandoval and Arnau 2017). Furthermore, Van der Pluijm (1997) reported that the value of the tensile fracture energy of the infill wall ranges from 0.05 N/mm to 0.13N/mm. In this numerical study, it is decided to determine the compressive fracture energy G_{fc}, and the tensile fracture energy G_{ft} , according to the following formulation, (Eq. 4.22 and Eq. 4.23, respectively) as Rots (2017) proposed:

$$G_{fc} = 15 + 0.43\, f_c - 0.0036 {f_c}^2 \tag{4.22}$$

$$G_{ft} = 0.025(2f_t)^{0.7} \tag{4.23}$$

where f_c is the compressive strength of the masonry infill wall in MPa, and f_t is the tensile strength of the wall normal to the bed joint in MPa. The value of the compressive strength is obtained from the average value provided by uniaxial compression test on masonry infill wall conducted by Koutas et al. (2014) and it is equal to 5.1 MPa. According to the Eq. (4.22) and Eq. (4.23) the value of the compressive fracture energy G_{fc} is equal to 17 N/mm and the tensile fracture energy G_{ft} is equal to 0.025N/mm. It was decided to change the value of these parameters (almost double), as given in Table 4.5, by fitting the numerical results with the experimental ones.

Furthermore, the parameters able to define the shear behavior of masonry infill wall are required for the Engineering Masonry model. The value of cohesion c, and friction angle φ, cannot be obtained from the diagonal compression test on the infill wall performed by Koutas et al. (2014) due to remarkable deviation that occurred in the testing (large coefficient of variation equal to 20%-40%). Several experiments have been performed so far to examine the shear behavior of a masonry infill wall. Reviewing the literature, it is observed that the cohesion ranges from 0.2 MPa to 1.2

MPa for different brick unit-mortar combinations (Dhanasekar 1986; Magenes and Calvi 1997; Corradi et al. 2003; Vasconcelos et al. 2008; Mosalam et al. 2009; Borri et al. 2012; Batikha and Alkam 2015). Several researchers proposed analytical equations based on their experimental tests to predict the cohesion of the masonry infill wall (Dusko et al. 2009; Kueh 2015; Sarhosis et al. 2015). In this numerical study, it was decided to set the cohesion equal to 1.2-1.5 times of the tensile strength of infill wall (f_{ty}) according to the relation proposed by Cur (1994). Following the Mohr-Coulomb failure criterion, and taking into account that the value of shear strength of the masonry infill wall as obtained from the experimental test performed by Koutas et al. (2014) ranges from 0.30 MPa to 0.80 MPa, the friction angle φ is equal to 20 degrees. Furthermore, according to the Engineering Masonry model the cohesion and the friction angle are used to calculate the shear fracture energy G_{fs}, (Eq. 4.21). The factor n was set equal to 1 following the Eq. (4.17). The unloading factor λ ranges from 0 to 1 as described before. An accurate definition of this parameter is not possible therefore it was decided to define the value of this parameter by fitting the numerical results with the experimental ones.

Table 4.5: Parameters of the Engineering Masonry material model.

Engineering masonry model	
Young modulus (E_y)	3.37 GPa
Young modulus (E_x)	1.62 GPa
Shear modulus ($G_{x,y}$)	1.38 GPa
Cracking behaviour: <u>Head joint failure</u>	
Tensile strength normal to the bed joint (f_{ty})	0.5 MPa
Tension fracture energy (G_{ft})	0.05 N/mm
Residual tensile strength (f_{tr})	0.2 MPa
Shear behavior	
Friction angle (φ)	20 °
Cohesion (c)	0.7 MPa
Compressive behavior	
Compressive strength (f_c)	5.1 MPa
Compression fracture energy (G_{fc})	40 N/mm
Factor to strain at compressive strength (n)	1
Unloading factor λ	0.2
Crack band width specification	Rots

The Engineering Masonry model is selected to represent the non-linear behavior of masonry infill wall although it requires a lot of parameters to be defined in DIANA FEA. Due to the large number of the required parameters of this model, the value of some parameters is selected according to the literature and at the same time by fitting the numerical results to the experimental ones but one of the parameters (unloading factor λ) is obtained by fitting the numerical results with experimental ones since an accurate definition of this parameter is not possible.

4.6.4 Interface model

In this numerical study, the discontinuity between masonry infill wall and RC frame is modeled using an interface element (three-point line interface element, section 4.5) and an appropriate model must be defined for this interface element. The infill-frame interface model is a key aspect for the modeling of masonry-infilled RC frames, since it controls the gap-opening and the sliding that occur at the infill-frame interface, and consequently the lateral response of this type of structure as will be presented in Chapter 5 section 5.5. For the purpose of this study an interface gap, plasticity-based model is used as Lourenço and Rots (1997c) proposed namely Coulomb Friction model.

The interface element which is used in this study (section 4.5) permits the discontinuities in the displacement field. The stress-strain relation of the interface element is defined in terms of traction t, and relative displacement Δu, across the interface element as follows:

$$\sigma = D\,\varepsilon \tag{4.24}$$

where D is the stiffness matrix:

$$D = \mathrm{diag}\,[k_n, k_s] \tag{4.25}$$

The components of the stiffness matrix (k_n, k_s) are depended on the elastic properties of the masonry infill wall and of the frame.

The Coulomb Friction model which is adopted for the infill-frame interface element in this numerical study is based on the plasticity theory including all the modern concepts used in computation plasticity (Lourenço and Rots 1997). This model is able to capture the gap-opening and the sliding at the infill-frame interface. The Coulomb Friction model is a convex composite yield criterion, which consists of a tension cut-off tensile failure criterion (mode I), a Coulomb friction shear failure criterion (mode II) and a gap mode compressive failure criterion as shown in Fig. 4.20. Further details regarding this model is presented in Lourenço (1994), Lourenco and Rots (1997), and Oliveira and Lourenço (2004).

The brittle failure at the infill-frame interface is taken into account in this model using the tension cut-off exponential softening function (vertical line in the positive region in Fig. 4.20). The shear failure at the infill-frame interface is considered in this model by the Coulomb Friction yield surface as follows:

$$f = |\tau| + \sigma \tan(\varphi) - c \tag{4.26}$$

where φ is the friction angle, c is the cohesion, τ is the shear stress and σ is the normal stress. In this model the friction angle is assumed to be proportional to the cohesion.

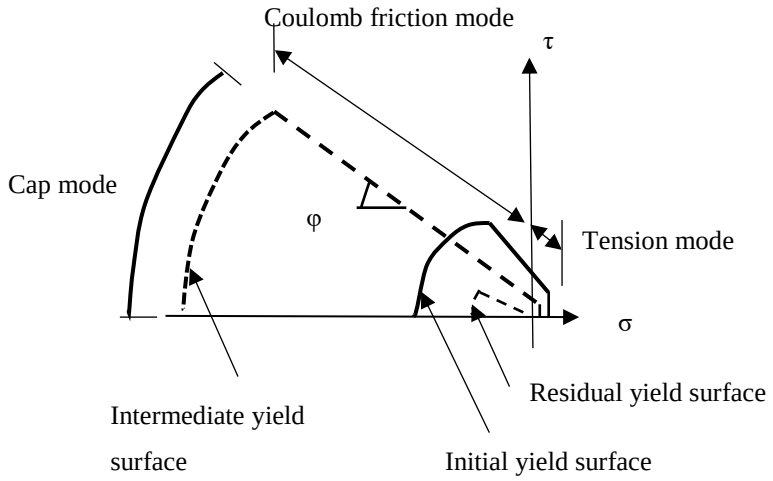

Figure 4.20: Coulomb friction interface model (Lourenço and Rots 1997).

The following input set of parameters are necessary to specify the Coulomb friction interface model in DIANA FEA: the normal and tangential stiffness K_n and K_s, respectively, the cohesion c, the friction angle φ, the dilatancy angle ψ, and the tensile strength f_t. These parameters should be determined experimentally. One drawback regarding the use of this model is the lack of experimental test regarding the direct measurement of the required parameters of this model. Consequently, in this study, it is decided to define the required parameters of the interface model according to the information provided by the experimental and numerical studies or related reports available in the literature, and at the same time by fitting the numerical results to the experimental ones (global and local results). Specifically, non-linear cyclic analyses on masonry-infilled RC frame are performed by varying some of the parameters of the interface model until the gap-opening at the infill-frame interface as derived from the selected experimental test (section 4.2) is almost the same with that obtained from the cyclic analysis of the masonry-infilled RC model.

Table 4.6 presents the required parameters of the infill-frame interface model in order to be specified DIANA FEA. These parameters depend on the relative infill wall-to-frame stiffness, and on the friction and bond strength at the infill-frame interface. It is difficult to define the value of these parameters, especially the values of normal K_n, and shear stiffness K_s, of the interface, since they do not represent actual masonry infill wall mechanical properties, but they are mathematical values which control the interpenetration of adjacent element in the model. Over the years, many researchers proposed equations to predict the stiffness parameters (K_n and K_s) of the infill-frame interface and of the brick-mortar interface (Kiarash M. Dolatshahi 2011; Asteris et al. 2013; Lin et al. 2014; Ehgri and King 2018). For example, Cur (1994) stated that the stiffness of the brick-mortar interface can be calculated according to the thickness of the brick units, and to the Young and shear modulus of the brick units and of the mortar joints. In this study, a recommendation proposed by DIANA FEA, which is based on the equations that already exist in the literature (Cur 1994, Lourenço 1996), is used for

calculating the value of the normal K_n (Eq. 4.27), and shear (tangential) stiffness K_s (Eq. 4.28) as follows :

$$K_n = (100 - 1000)\frac{E_x}{l_{element}} \tag{4.27}$$

$$K_s = \frac{K_{normal}}{(10 - 100)} \tag{4.28}$$

where the E_x is the Young modulus of a masonry infill wall parallel to the bed joint in GPa and $l_{element}$ is the length of the masonry infill wall plane-stress element in mm. The above equations show that the normal and shear stiffness of the infill-frame interface depend on the modulus of elasticity of the masonry infill wall in x-and y-direction (E_x and E_y). Based on the above equations, the normal and tangential stiffness are varied between 3-30 kN/mm³ and 0.03-3 kN/mm³, respectively, for the beam-infill wall interface, while for the interface between column and infill wall the normal and tangential stiffness are varied between 6-60 kN /mm³ and 0.06-6 kN /mm³, respectively. In order to specify the value of the normal and tangential stiffness several non-linear cyclic analyses on the infilled frame model are performed by varying the value of these parameters within the range obtained from these formulae until a good correlation between the numerical and experimental results is achieved, as will be presented in the next Chapter in section 5.5.

Besides the normal and tangential stiffness, the internal friction angle φ, and cohesion c of the infill-frame interface must be defined. It is difficult to estimate these parameters since there are no experimental tests. Reviewing the literature regarding the cohesion of the brick-mortar interface it is found that the value of the cohesion ranges from 0.2 MPa to 1.2 MPa (Liauw and Kwan 1983; Dhanasekar 1986; Eshghi and Pourazin 2009; Akhoundi et al. 2016). Several researchers proposed equations to predict the cohesion of the brick-mortar interface based on the friction angle and compressive strength of masonry infill wall (Ardiaca 2009; Siamak 2013; Sarhosis et al. 2016). In this study the cohesion c, at the infill-frame interface associated with the Coulomb friction interface

model has been determined according to the relation (Eq. 4.29) proposed by Sarhosis et al. (2016) as follows :

$$c = 0.1065\, f_c + 0.531 \qquad (4.29)$$

where f_c is the compressive strength of the masonry infill wall in MPa. The friction angle φ ranges from 20 to 50 degrees as reported in Cur (1994) and Lourenço (1996). In this numerical study the friction angle is assumed to be equal to 30 degree. Another required parameter of interface model is the dilatancy angle ψ, which depends on the level of confining stresses of masonry infill wall and on the roughness of the infill-frame interface surface (Mosalam et al. 1997; Institute 2001; Angelillo 2014). Lourenco (1996) recommended that the dilatancy angle must be equal to zero based on his numerical study of infilled frames. In this numerical study the dilatancy angle ψ is assumed to be equal to zero.

The last required parameter of the interface model is the tensile strength at the infill-frame interface. It is difficult to relate the tensile strength of the infill-frame interface with other parameters of the infill-frame interface, since the tensile strength of the brick-mortar interface, and as well as the tensile strength of the infill-frame interface is still a subject of research. Therefore, the tensile strength of the infill-frame interface is assumed according to the related studies or reports available in the literature (Liauw and Kwan 1983; Eshghi and Pourazin 2009; Koutromanos et al. 2011), and by fitting the numerical results to the experimental ones (local and global). The value suggested by literature is used in this study as the initial guess in this calibration process. In this numerical study, the tensile strength of infill-frame interface is assumed to be equal to 1^{-10} MPa. The value of the tensile strength is nearly zero in order capture the gap-opening at the infill-frame interface of the real case.

Table 4.6: Parameters of the Coulomb friction interface model.

Coulomb friction interface model.		
	Y-direction (column-infill interface)	X-direction (beam-infill interface)
Normal stiffness (Kn)	6 kN /mm³	3 kN /mm³
Shear stiffness (Ks)	0.06 kN /mm³	0.03 kN /mm³
Cohesion (C)	1N/mm²	1N/mm²
Friction angle (φ)	30 degree	30 degree
Dilatancy (ψ)	0	0
Model for gap appearance	Brittle	Brittle
Tensile strength	1^{-10}N /mm²	1^{-10}N /mm²

In this numerical study, the Coulomb Friction model for the infill-frame interface element is adopted and the required parameters for this model are determined according to the information provided by the respective numerical reports or related references available in the literature.

4.7 Constrains and loading scheme

The constrains and the loading scheme of the numerical models developed for the purpose of this numerical study is presented in this part of the thesis. It is important to mention that the RC frame model and the infilled frame model with and without TRM are imposed to constant axial load and to cyclic lateral displacement load similar as possible to experimental case-study (section 4.2) by taking into account the assumptions presented in section 4.3.

In this numerical study, 40kN axial load is applied in each column of the masonry-infilled RC frame model with and without TRM in order to represent the axial load which imposed in each story in the test specimens (through a set of four prestressing rods per story) equal to 120kN, 80 kN, and 40 kN at the first, second, and third story, respectively. In order to avoid the stress concertation in the numerical model, the 40kN

axial load is distributed along the length of the column (0.174 KN/mm) as shown in Fig. 4.21.

Furthermore, the weight of the concrete members which were not modeled due to the 2D simplification followed in this study, must be considered as a dead loads (axial loads) in the numerical models, since the weight of the numerical models must be equal to that of the real-case specimens. More specifically, the T-shaped beam used in the experimental case-study has width equal to 900 mm (web width of 170mm), and height equal to 330 mm (flange height equal to 120mm and web height of 210mm) as shown in Fig. 4.1, while in the numerical model the rectangular beam has dimensions equal to 330 x 170 mm as shown in Fig. 4.7. So, the volume of the T-shaped beam, which is not modeled, is equal to 0.239m^3 considering that the length of the beam is equal to 2.73 m (Fig. 4.1). Consequently, the corresponding weight of the T-shaped beam which is not modeled is equal to 609Kg considering that the mass density of reinforced concrete is equal to 2548Kg/m^3. Therefore, an axial load equal to 3 kN is applied along the length of each column in the infilled frame model with and without TRM (Fig. 4.21) assuming that the weight of the part of the T-shaped beam which is not modeled is restrained by the two columns of frame at each floor. Following the same procedure, the weight of beam-plates (365x210x230 mm in each site of the column) which were used to apply the history of imposed cycles of displacements in the experimental case-study (Fig. 4.2 a) is considered in the numerical models by applying axial dead load equal to 0.9 kN along the length at the top of each column (0.017 kN/mm as shown in Fig. 4.21). It is important to mention that the stiffness of concrete members which are not modeled is not taken into account to the stiffness of the numerical models and this does not influence the accuracy of the numerical models because the torsional effects are negligible in the experimental case-study.

Important parameter to capture adequately the real response of masonry-infilled frame with and without TRM is the cyclic loading scheme adopted for these models which must be similar as possible to that of the experimental case-study (Fig. 4.2 b and c). Based on the assumptions considered in this study (section 4.3), the cyclic loading

scheme of the real case, where displacement loading was applied at the top-floor and the force loading was applied at the second and first floor on the infilled frame with and without TRM, is simulated by applying only displacement loading at the three stories of the numerical models. Particularly, point prescribed deformation equal to 1mm is applied at each of the nodes at the end of each floor (Fig. 4.21), and then 10 and 14 factored load combinations (considering that the load factor of the displacement of the third floor is equal to 1) are created for the unretrofitted and retrofitted model, respectively, (Table 4.7) to represent the non-uniform height-wise distribution of the displacement. Then, the evolution of displacement loading is done through the analysis procedure. Specifically, 13 independent non-linear analyses are developed where each one represents each half cycle of the cyclic loading. For each of the analyses, the relevant specific load combination is selected, and the corresponding maximum displacement is defined. Adding to this, the displacement cyclic loading is discretized in loading steps using automatic incrementation procedure in which both the number of steps and the corresponding size of each step are automatically computed by DIANA FEA as it is going to be discussed in the next section. Consequently, the displacement cyclic loading applied on the unretrofitted and on the retrofitted model is discretized in load steps, approximately 110, and 160 steps, respectively, as shown in Fig. 4.21, instead of time steps used in the experiment (Fig. 4.2 b and c).

Besides the loading scheme, the boundary conditions of the numerical models must be also defined in order to complete the FE numerical models. Particularly, all the nodes at the bottom of the lower of masonry-infill RC frame model with and without TRM are restrained by preventing any translation in the x- and y-direction as shown in Fig. 4.21 in order to represent the fixed condition provided by the RC-beam plate and by 16 prestressing rods (full clamping between the foundation RC-beam) used in the experimental case-study (section 4.2). It is decided to prevent any translation in the x- and y-direction since in the experimental case-study no significant rotation and failures were observed at the base of the test specimens. It is important to mention that the gap-

opening and the sliding that occurred between the base-beam and masonry infill wall is considered in the numerical models as described in section 4.5.

Figure 4.21 presents the constrains (preventing any translation in the x- and y-direction) and the loading scheme (constant axial load and to cyclic lateral displacement load) considered in the RC frame model and in the infilled frame model with and without TRM. The constrains and loading scheme of the numerical models are similar as possible to experimental case-study.

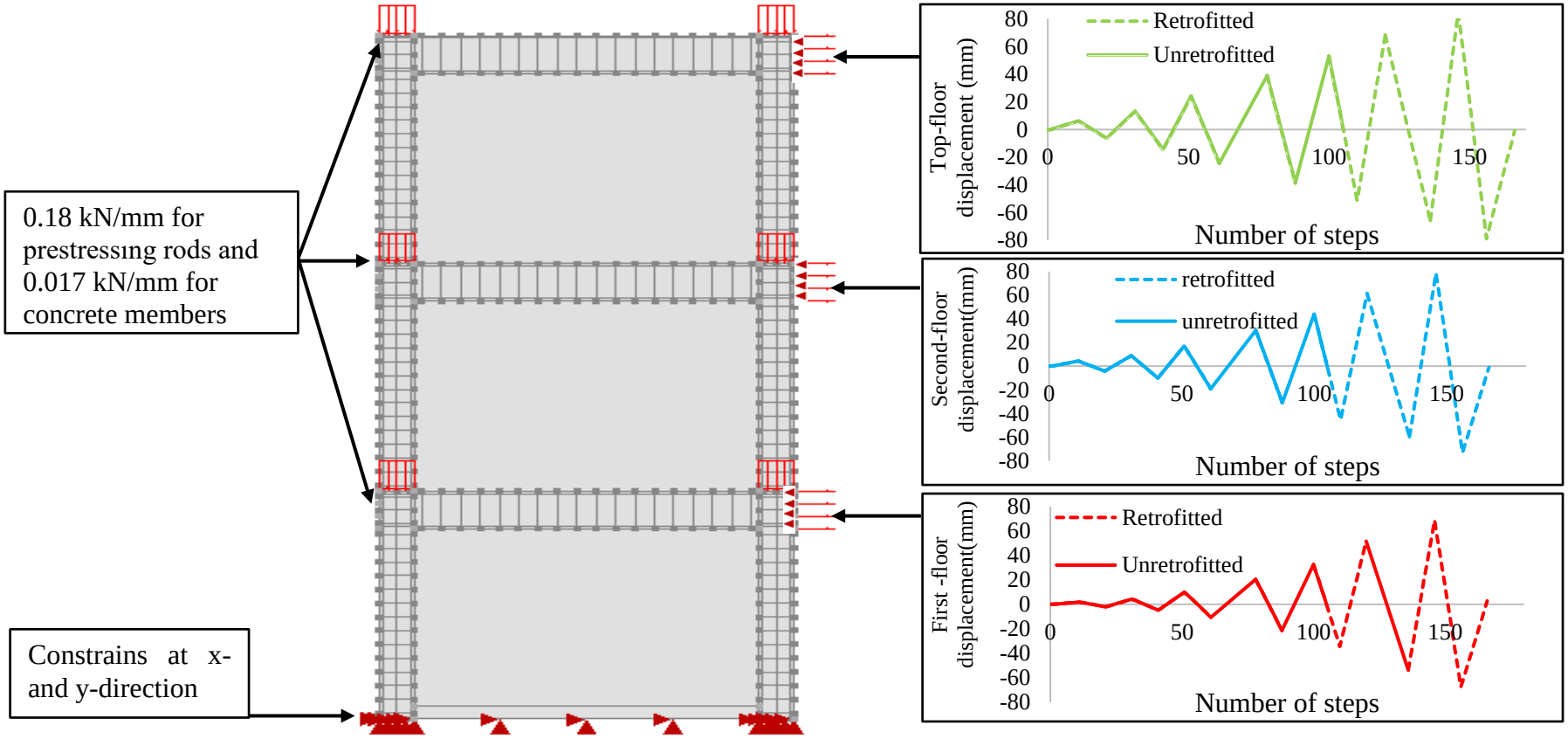

Figure 4.21: Constrains and loading scheme of the numerical models.

Table 4.7: Load combinations.

Load combination	Axial dead load (Prestressing rods)	Axial dead load (extra weight of the concrete members)	Dead weight of the structure as it is defined by DIANA FEA.	Point prescribed deformation at the third floor	Point prescribed deformation at the second floor	Point prescribed deformation at the first floor
0	1	1	1			
1				1	0.7	0.3
2				1	0.68	0.3
3				1	0.65	0.31
4				1	0.67	0.31
5				1	0.69	0.37
6				1	0.73	0.41
7				1	0.77	0.48
8				1	0.78	0.53
9				1	0.81	0.58
10				1	0.85	0.63
11				1	0.89	0.71
12				1	0.9	0.78
13				1	0.92	0.81
14				1	0.93	0.83

4.8 Types of analysis

As the input data for the geometry, the material models, the boundary conditions, and for the loading scheme are defined, the types of analysis used for the purpose of this study are presented in this part of the thesis. Linear static analysis, eigenvalue analysis, and non-linear cyclic analysis are performed on the bare frame model, and on the masonry-infilled RC frame model with and without TRM. The results obtained from these analyses will be presented and discussed in the next Chapter (Chapter 5).

Firstly, linear static analysis is performed in order to confirm that the behavior of the three numerical models is as expected under self-weight load (weight, deformation etc.). Then, eigenvalue analysis is performed to estimate the fundamental period and the mode shape of the three numerical models. In order to perform the above analyses, additional elements must be introduced to the FE models (besides CQ16M and CL12I the elements presented in section 4.5). Specifically, point elements (PT3T) are used to simulate the axial load of the numerical models without influencing their stiffness. A mass node (PT3T) equal to 395 Kg is applied at the top of each column in order to represent the concrete elements which were not modeled in this numerical study as previously described (section 4.7). It is important to mention that the axial load due to prestressing rods is not included in the mass nodes, and consequently this axial load is not considered in the linear static and eigenvalue analysis, because this axial load was not applied on the structure during the vibration test in the lab. The target of the linear static analysis is to calculate the displacement vector that equilibrates the internal and external forces. For this analysis, parallel direct sparse method is used with tolerance value equal to 10^{-8}. For the eigenvalue analysis the first six modes are calculated and the calculation is based on the Implicitly restarted Arnoldi solution method while a parallel direct solver type is selected.

In the non-linear cyclic analysis, the relation between a force vector and a displacement vector is no longer linear, which means that the calculated displacement depends on the displacement of the previous stage. To determine the state of equilibrium, the problem must be discretized in space and in time or in load step (increments). To achieve equilibrium at the end of an increment, an iterative solution algorithm must be used. In

this numerical study, to enable a numerical solution, load steps discretization is considered where the displacement load is divided into a finite number of increments. The number of loading steps (increments) and their corresponding size are automatically computed using the cutback-based automatic load stepping tool where the load increments are adapted for a given final loading. Therefore, the total increments according to the automatic step-control procedure depend on the maximum displacement of each of the half cycle of the cyclic loading (peak displacements in Fig. 4.21), since in this study several independent non-linear analyses are performed where each one represents each half cycle of the cyclic loading as explained in previous section. The automatic load-step controller tries to take as few load steps as possible and at the same time tries to limit the number of steps in the iterative procedure. First the full loading is applied in a single step. If the iterative procedure fails to converge, the load step is decreased by a factor (cutb) equal to 0.25 and the calculation is restarted. The maximum and minimum limit of the steps size are equal to 0.1 and 0.001, respectively.

After defining the discretization of the problem in load steps (increments), an iterative solution algorithm must be used in order to achieve equilibrium at the end of an increment. In this numerical study, the non-linear problem is solved using the local quadratic Quasi-Newton (Secant) procedure which linearizes the non-linear equilibrium equations at each iteration until the appropriate convergence criteria are satisfied. The Quasi-Newton method sets up a new tangential stiffness at the start of each step, while this method uses the information of the previous solution vectors, and of the out-of-balance force vectors during the increment to achieve a better approximation as shown in Fig. 4.22 (Martínez 1991, 2000; Taylor and Zhu 2000). Furthermore, the secant stiffness matrix is calculated using the Broyden method while the linear stiffness iteration method is selected where a linear stiffness matrix is used all the time, and the stiffness matrix needs to be set up only one time per iteration. In this numerical study, the criteria used to stop the iteration process is defined in terms of energy with tolerance value ranging from 10^{-4} to 10^{-6}. Besides the convergence criteria, the iteration process is also stopped if the specified maximum number of iterations is reached or if the iteration obviously leads to no convergence. In this numerical study, the maximum

number of iterations is equal to 1000. One of the drawbacks of the procedure described above has to do with the fact that the convergence is strongly dependent on the starting solution. This means that a good starting point can lead to convergence otherwise divergence would occur.

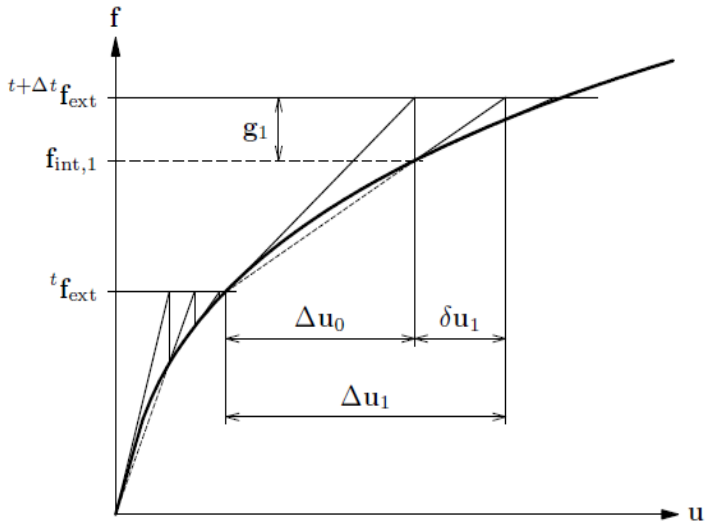

Figure 4.22: Quasi-Newton method.

To conclude, in this numerical study three types of analysis are performed: (1) linear static analysis, (2) eigenvalue analysis, and (3) non-linear cyclic analysis while special attention is given to the cyclic non-linear analysis.

4.9 Summary

In this part of the thesis, the development of the masonry-infilled RC frame model with and without TRM, which are both experimentally tested under cyclic loading in the study carried out by Koutas et al. (2014), is presented. Firstly, a brief review of the experimental case-study conducted by Koutas et al. (2014), which is used for calibration purposes in the current research, and the details regarding the software used, namely DIANA FEA, are presented. This is followed by the assumptions considered for the development of the numerical models. A detailed description of the type of elements, material models, boundary constrains, and the loading scheme considered in the infilled frame model with and without TRM is presented.

For the purpose of this study, a 2D simple FE micro-model of the bare frame, and of the masonry-infilled RC frame with and without TRM, is developed in the DIANA FEA software. The numerical models were developed following a simple micro-modeling approach. The concrete members, the masonry infill wall and the TRM are modeled separately by continuum elements (CQ16M quadrilateral isoperimetric plane stress element), and the infill-frame interface is modeled with three-point line interface element (CL12I). The steel reinforcement is modeled with two-noded bar element. Following the simple-micro modeling approach, the masonry infill wall is simulated by continuum elements, where the brick units, mortar and unit-mortar interfaces are modeled a homogenized layer (Chapter 2, section 2.4, Fig. 2.10), and the TRM composite material is modeled by continuum elements, where the textile reinforcement and mortar layer are lumped in a homogenized layer (Chapter 3, section 3.2, Fig. 3.4). In order to develop accurate numerical models, special attention is given for representing the bond conditions provided by the presence of textile anchors, and for representing the debonding and the rupture of TRM, since the above are not modeled. Furthermore, the interaction between the foundation beam with the infilled frame is included in the numerical model, although that the foundation beam that used to support the infilled frame in the experimental case-study is not modeled.

Following the smeared crack approach, appropriate models are used to represent the non-linear cyclic behavior of the components of the infilled frame with and without TRM-frame. The Maekawa Fukuura model as a compression function and the *fib* 2010 model as a tension function of the Total Strain Crack model are used for describing the non-linear cyclic behavior of the concrete. The Menegotto-Pinto plasticity model is adopted for the steel reinforcement two-noded bar elements. The Engineering Masonry model which is a smeared crack model available in DIANA FEA is adopted for the masonry infill wall elements. This model covers the tensile, shear and compression failure of the infill wall and it can capture also the behavior of a masonry infill wall under cyclic loading. The Engineering Masonry model requires a large number of parameters to be specified in DIANA FEA. The Fiber Reinforced concrete model combined with *fib* 2010 model is used in this study as a tension and compression softening function, respectively, for the Total Strain Crack model, in order to represent

the non-linear cyclic behavior of the TRM composite material. The required parameters for this model are obtained from the coupon tests conducted by Koutas et al. (2014), and by using the proposed analytical model of TRM as presented in Chapter 3. Furthermore, the Coulomb Friction model is adopted for the infill-frame interface elements in order to capture the gap-opening and the sliding between masonry infill wall and RC frame. In this study, most of the required parameters to define the selected models in DIANA FEA are taken from the experimental case-study selected for calibration purposes, and other parameters were taken from the literature. Particularly, special attention is given to the required parameters of the masonry infill wall model and to that of the interface model, such as compressive and tensile fracture energy, tensile strength, cohesion, friction angle, normal and shear stiffness of interface, etc. The value of some of these parameters is selected according to the literature and at the same time by fitting the numerical results to the experimental ones. It is important to mention that the concrete, steel reinforcement and TRM material models used in this study are validated against the available experimental data.

Finally, the numerical models are completed by applying the constrains and the loading scheme. Specifically, all nodes at the base of the first floor of the masonry-infilled RC frame model with and without TRM are restrained by preventing any translation in the x- and y-direction. Two types of loads, representing the vertical compression and horizontal cyclic load, have been applied on the numerical models. Specifically, axial compressive load equal to 45kN is applied along the length of each column of the numerical models in order to represent the axial load which imposed in each story in the test specimens through the prestressing rods, and to represent the weight of the members which were not modeled. Furthermore, the RC frame model and the infilled frame model with and without TRM are imposed to cyclic lateral displacement load similar, as possible, to the experimental case-study. More specifically, the cyclic loading scheme of the real case is simulated by applying displacement loading at the three stories of the numerical models. The evolution of displacement loading is done through the analysis procedure and it is discretized in loading steps using automatic incrementation procedure in which both the number of steps and the corresponding size of each step are automatically computed by DIANA FEA.

The numerical models presented in this Chapter of the thesis can be considered reliable when the results obtained from the linear static, eigenvalue and non-linear cyclic analysis on bare frame and infilled frame model with and without TRM will be close to the experimental ones as will be presented in the following Chapter. In such a case, the numerical models developed in this study may be used as a tool to generate a very large database taking into account all the possible ranges of the critical parameters affecting the behavior of the masonry-infilled RC frame with and without TRM and make a significant contribution to the knowledge in this subject.

CHAPTER 5

5. VALIDATION OF THE NUMERICAL MODELS AND ANALYSIS RESULTS

5.1 Introduction

The modeling methodology proposed in the previous Chapter for the RC frame model and for the masonry-infilled RC frame model with and without TRM is evaluated in this Chapter through a linear static, eigenvalue, and non-linear cyclic analysis. The validation of the numerical models is necessary in order to fulfill the aim of this research, which is to extend today's knowledge regarding the effectiveness of using the TRM composite material for seismic retrofitting masonry-infilled RC frames by performing numerical experiments.

For the validation of the three numerical models, the experimental case-study conducted by Koutas et al. (2014) is used (Chapter 4). Firstly, the eigenvalues of the three numerical models are compared to the corresponding experimental data. Secondly, the behavior of the numerical models under self-weight is compared to that observed in the real case. Then, the results obtained from the non-linear cyclic analysis of the unretrofitted and retrofitted masonry-infilled RC frame are compared to those obtained from the experimental case-study. The behavior of the bare frame model under cyclic loading is also assessed based on relevant past studies. It is important to mention that the calibration of the numerical models is achieved by performing several analyses by varying some parameters for the selected material models presented in the previous Chapter, which require adjustment in order to represent the experimental results accurately.

After the validation of the numerical models, sensitivity analyses are performed. In this context, numerical experiments are performed in order to investigate the in-plane

behavior of the three-story integral and non-integral masonry-infilled RC frame under cyclic loading. Numerical experiments are also carried out to examine the influence of the stiffness properties of the infill-frame interface (normal and tangential stiffness) on the in-plane response of the three-story retrofitted infilled frame under cyclic loading. The calibrated models are also used to perform a parametric study, through numerical experiments which is presented in Chapters 6 and 7 of the thesis.

In the first part of this Chapter, the linear static analysis (self-weight load) of the bare frame model and of the masonry-infilled RC frame model with and without TRM is presented (section 5.2). This is followed by the results of the eigenvalue analysis of the three numerical models (section 5.3). Then, the results obtained from the non-linear cyclic analysis of the masonry-infilled RC frame model with and without TRM are presented and compared with those obtained from the experiment at a global and local level (section 5.4). Adding to this, the results from the cyclic analysis of bare frame model are also discussed. Then, the sensitivity analyses are presented and discussed (section 5.5). This Chapter concludes with the summary and with the most important findings regarding the validation of the numerical models and regarding the numerical analysis results (section 5.6).

5.1 Linear static analysis

In this section, the results obtained from the linear static analysis of the three numerical models are presented and discussed. The linear static analysis is performed prior to the non-linear cyclic analysis in order to confirm that the behavior of the three numerical models is as expected under self-weight load (weight, deformation etc.). In this analysis, a mass node equal to 395 Kg is applied at the top of each column of the numerical models in order to represent the self-weight of the concrete elements of the test specimens which were not modeled (section 4.8). No other loads are considered for the purpose of this analysis.

Table 5.1 shows the weight of the three numerical models as obtained from the linear static analysis. The weight of the numerical models is estimated correctly based on the information provided by Koutas et al. (2014) regarding the weight of the components of the infilled frame with and without TRM.

Table 5.1: The weight of the bare frame model and of the masonry-infilled frame model with and without TRM.

Numerical model	Weight (Tones)
Bare frame	4.54
Masonry-infilled RC frame	5.53
Masonry-infilled RC frame retrofitted with TRM	6.25

Figures 5.1 and 5.2 show the principal strains (deformation) and principal stresses in the y-direction, respectively, of the three numerical models when subjected to self-weight load. From Fig. 5.1, it is observed that the deformation is symmetrical in the three numerical models, and their shape and intensity are as expected (Oinam et al. 2014). The deflection under self-weight load of the masonry-infilled RC frame with TRM is relatively small when compared to that of the bare frame, and to that of the infilled frame without TRM. Based on Fig. 5.2 it can be concluded that the high tensile (positive) and compressive (negative) stresses are as expected in terms of their position.

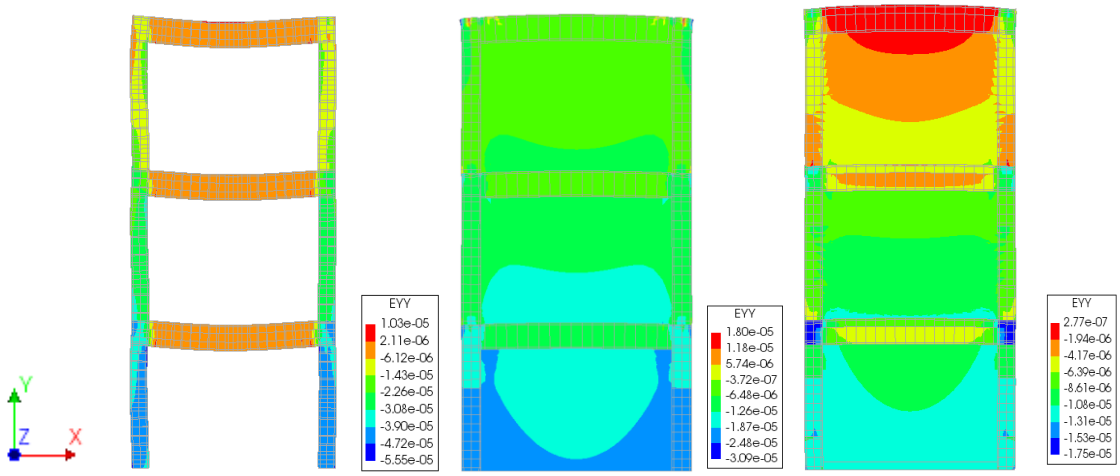

(a) (b) (c)

Figure 5.1: Principal strains in y-direction as obtained from the linear static analysis of the (a) bare frame model, (b) masonry-infilled RC frame model, and of the (c) masonry-infilled RC frame model with TRM.

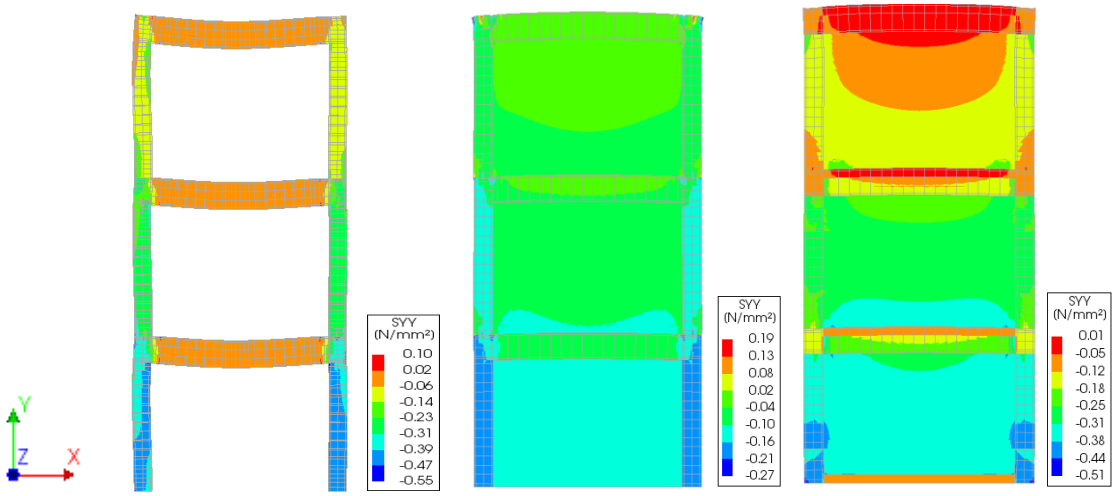

(a) (b) (c)

Figure 5.2: Principal stresses in y-direction as obtained from the linear static analysis of the (a) bare frame model, (b) masonry-infilled RC frame model, and of the (c) masonry-infilled RC frame model with TRM.

The results obtained from the linear static analysis of the bare frame and of the masonry-infilled RC frame with and without TRM confirm that the behavior of the numerical models is as expected under self-weight load, and ensure that the three numerical models are representative of what is tested in the experiment. After the validation of the numerical models developed in this study through the linear static analysis, an eigenvalue analysis was performed as presented in the following section.

5.2 Eigenvalue analysis

In this part of the thesis, the results obtained from eigenvalue analysis on the three numerical models are presented and compared with the experimental ones. It is necessary to perform the eigenvalue analysis before the non-linear cyclic one, since the eigenvalue analysis (vibration tests) provides necessary information (dynamic parameters) for the correct implementation of numerical models' characteristics. For the purpose of this analysis, the bare frame model and the masonry–infilled RC frame model with and without TRM were vibrated without damping, and the first six modes are calculated. Furthermore, a mass node equal to 395 Kg is applied at the top of each column of the numerical models in order to represent the self-weight of the concrete

elements of the test specimen which were not modeled (section 4.8). No other loads are considered for the purpose of this analysis.

The fundamental period of the bare frame and of the masonry-infilled RC frame with and without TRM is presented in Table 5.2. The results obtained from the eigenvalue analysis present good correlation to the experimental ones despite the small difference between idealization and reality.

Table 5.2: Comparison of numerical and experimental results regarding the fundamental period of the bare frame and of the masonry-infilled frame with and without TRM.

Fundamental period (Seconds)	**Bare frame**	**Masonry-infilled RC frame**	**Masonry-infilled RC frame with TRM**
Experiment	0.24	0.06	0.047
Numerical model	0.23	0.06	0.046

From Table 5.2 it is observed that the presence of the infill wall in RC frame influences its dynamic characteristic. More specifically, the fundamental period of the infilled frame decreases four times compared to that of the bare frame. The above observation is also supported by several studies conducted in the past (Bertero and Brokken 1983; Liauw1979; Chiou et al. 1999; Kappos and Ellul 2000).

It is important to mention that the eigenvalue analysis of the three numerical models is performed using the linear stiffness of each component of the structure (without considering the early cracking of the concrete members). Hence, in order to take into account in the analysis the initial cracking of the concrete elements and to obtain acceptable results in terms of accuracy, especially to represent the fundamental period as accurately as possible, the modulus of elasticity of the concrete is adjusted. Specifically, the modulus of elasticity of the concrete must be equal to 10-12.5 GPa according to Eurocode 2 (Eq. 4.13) instead of that measured in the experimental study, which is ranging from 20 GPa to 25 GPa (section 4.2). Based on the above, the numerical model updating consists of constantly tuning the modulus of elasticity of the concrete adopted in the Total Strain Crack model until the dynamic response of the

numerical models fits the experimental one. The results of the calibration process resulted in a modulus of elasticity of concrete of 9.1 GPa.

Figures 5.3 and 5.4 show the eigenvalue parameters, particularly, the effective mass participation factor and the mode shapes of the three numerical models. The effective mass participation factor (the amount of system mass participating in a particular mode) provides a measure of the energy contained within each resonant mode. From Fig. 5.3 it is observed that the 63%-82% of the system's mass is participating in the first mode shape in the x-direction for the three numerical models. For the rest of the modes (3, 4, 5, and 6), the mass participation factors are getting to zero for all the numerical models. The mode shape of each model as presented in Fig. 5.4 is associated with the corresponding fundamental period as given in Table 5.2. From Fig. 5.4 it can be concluded that the numerical models' deformed shape is as expected corresponding to the real ones observed in similar structures.

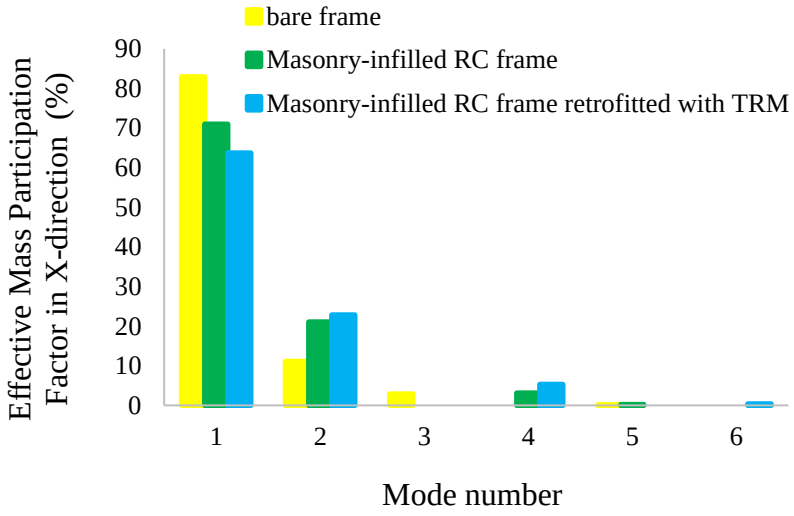

Figure 5.3: Effective mass participation factor for the three numerical models in the x-direction.

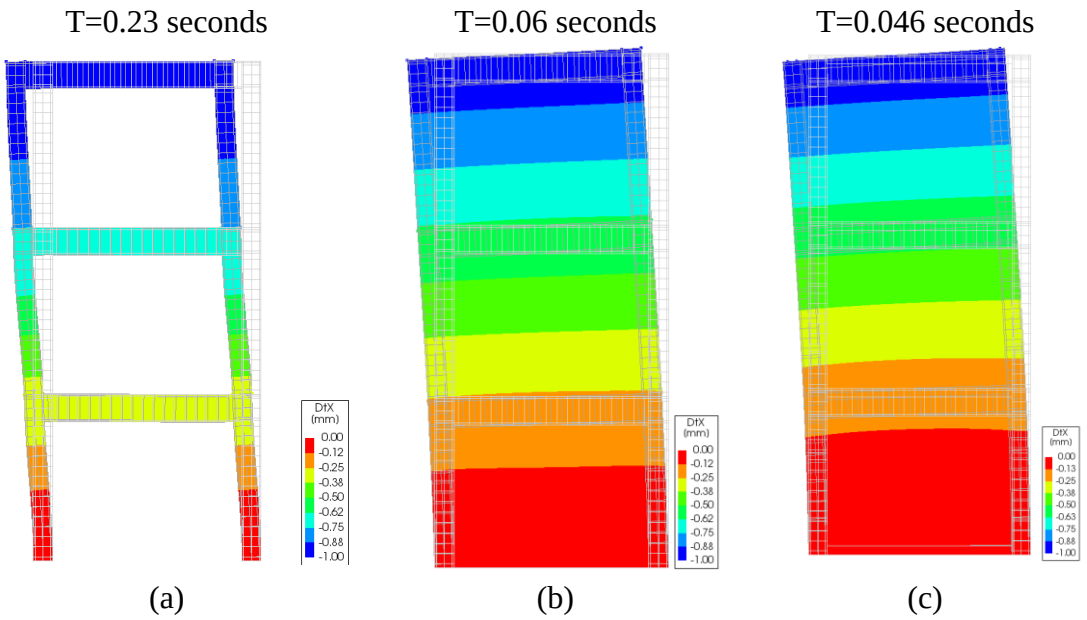

Figure 5.4: Mode shape of (a) bare frame model, and of the (b) masonry-infilled RC frame model without, and (c) with TRM in x-direction as derived from the eigenvalue analysis.

The eigenvalue parameters of the real cases are very well estimated by the proposed numerical models. Particularly, the fundamental period, the mode shape and the effective mass participation factor obtained from the eigenvalue analysis of the bare frame model and of the masonry-infilled RC frame model with and without TRM are very close to those obtained from the experimental study or to those observed in similar structures.

5.2 Non-linear cyclic analysis

In this part of the thesis, the frame model, and the masonry-infilled RC frame model with and without TRM are validated by performing non-linear cyclic analysis on these numerical models. Besides the validation of the proposed numerical models, in this part of the thesis the influence of the infill walls on the lateral behavior of RC frames, and the effectiveness of using the TRM composite material for retrofitting infilled frames are discussed, as well. To achieve the above-mentioned, the masonry-infilled RC frame model with and without TRM are subjected to five and seven cycles of prescribed displacement loading, respectively, through displacement control analysis (section 4.7). The bare-frame model is tested under vertical loading, and under cyclic displacement

loading similar to that applied to the infilled frame model. The required parameters for non-linear cyclic analysis were presented in the previous Chapter, in section 4.8 (number of steps, iteration process, type of solver, etc.).

In the following sections, the results obtained from the non-linear cyclic analysis on the masonry-infilled RC frame model with and without TRM are presented and compared with those obtained from the experiment in global level (section 5.4.1) and in local level (section 5.4.2). The results derived from the non-linear cyclic analysis of the bare frame model are also presented. It is important to mention that, the results presented in the following sections are obtained by performing a lot of non-linear cyclic analyses on the infilled frame model with and without TRM by varying some of the required parameters (when no experimental data is available) of the material models selected for describing the non-linear behavior of the components of the unretrofitted and retrofitted infilled frame (especially for the masonry infill wall model and for the interface model), and by varying also the required parameters for the non-linear cyclic analysis until reliable results were reached.

5.2.1 Global results

In this section, the global results obtained from the non-linear cyclic analysis of the unretrofitted and the retrofitted infilled frame model are presented, discussed and compared with the experimental ones in terms of base-shear, shear capacity of each floor, height-wise distribution of the shear force, global stiffness, and dissipated energy. The results derived from the non-linear cyclic analysis of the bare frame are also presented in this section.

Figure 5.5 (a) presents the base-shear in relation to the top-floor displacement (hysteresis curve) as obtained from cyclic analysis of the bare frame (red line). The hysteresis curves as obtained from the experiment (blue line) and from the numerical analysis (red line) for the infilled frame without and with TRM are given in Figs. 5.5 (b) and (c), respectively.

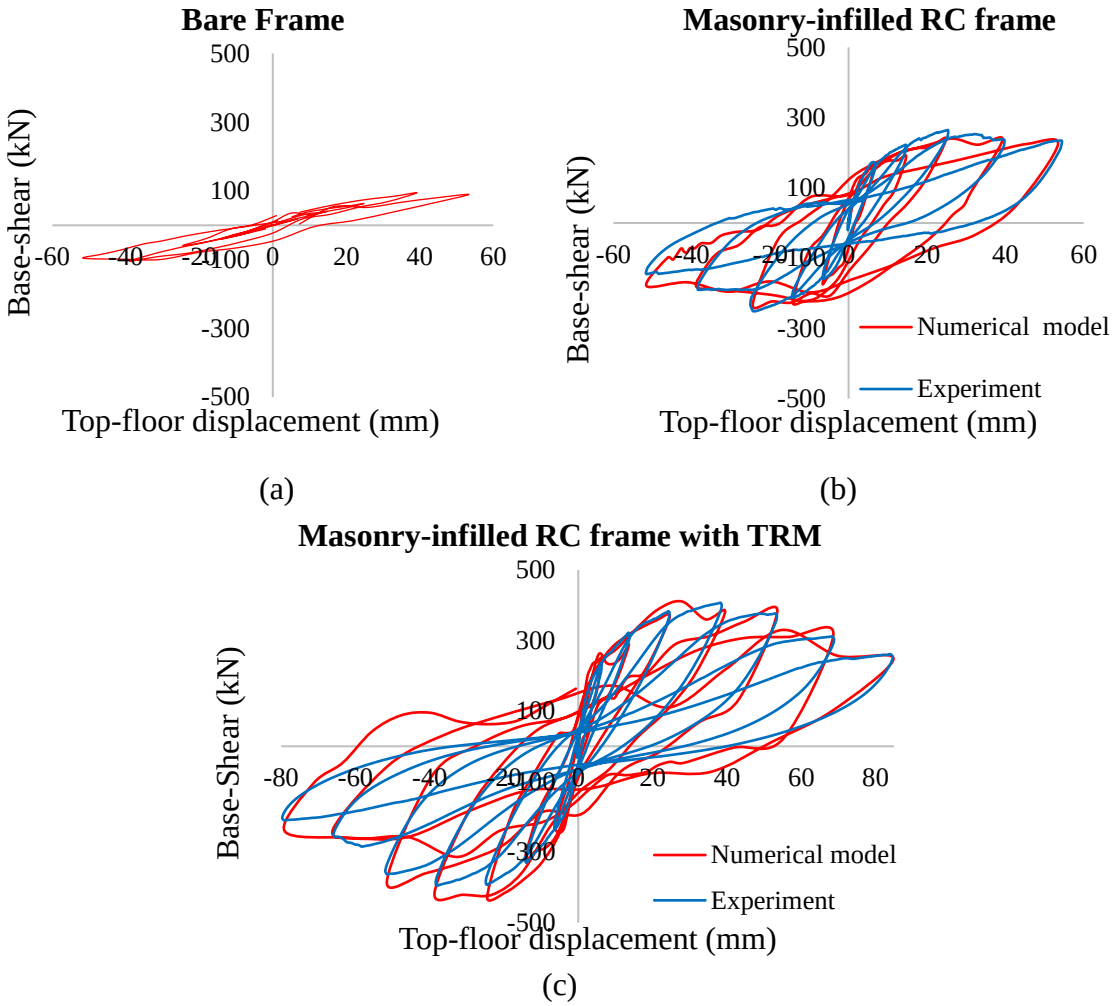

Figure 5.5: (a) Base-shear versus top-floor displacement for the bare frame model, and (b) the comparison of the experimental and numerical results in terms of base-shear versus top-floor displacement for the unretrofitted infilled frame, and (c) for the retrofitted infilled frame.

Based on Fig. 5.5 (a), it can be concluded that the bare frame model is accurate, since the hysteresis curve derived from this numerical study is almost similar to that obtained from the experimental and numerical studies conducted in the past (Chiou et al. 1999; Matsumiya et al. 2004; Kakaletsis and Favvata 2005; Altin 2007; Pujol and Fick 2010; Oinam et al. 2014; Basha and Kaushik 2016; Peng et al. 2018). Hence, the bare frame model is representative of what is tested in the experiment.

Comparing Fig. 5.5 (a) with Fig. 5.5 (b) it can be pointed out that the presence of the infill wall in the RC frame contributes to improve significantly the lateral response of the frame structure by increasing significantly the lateral capacity of the frame.

Specifically, the maximum base-shear of the infilled frame is about ±250MPa, and that of the bare frame is about ±95MPa. This observation is supported by several past studies as mentioned in Chapter 2, section 2.3 (Bertero and Brokken 1983; Liauw and Kwan 1992; Merhabi et al. 1996; Chiou et al. 1999; Kwan and Xia 1995; Lee and Woo 2002; Calvi and Bolognini 2001; Pujol and Fick 2010; Basha and Kaushik 2016).

From Fig. 5.5 (b) and (c) it is observed that the difference between experimental and numerical results is relatively small, except in the last cycle of loading where this difference is more pronounced. Furthermore, the comparison of Fig. 5.5 (b) with Fig. 5.5 (c) indicates that the TRM technique contributes to increase the maximum base-shear of the infilled frame and the area enclosed by the loop in the base-shear versus top-floor displacement diagram, and consequently the TRM increases the energy dissipation capacity of the system. Furthermore, the maximum base-shear during the fourth cycle of loading, for both directions of loading, of the retrofitted infilled frame is about ±400MPa, while that of the unretrofitted infilled frame is about ±250MPa.

The base-shear of the bare frame model in relation to the load step is presented in Fig. 5.6 (a). Figures 5.6 (b) and (c) show the comparison of the experimental (blue line) and the numerical results (red line) in terms of base-shear in relation to the load step for the unretrofitted and retrofitted infilled frame, respectively. For the benefit of the reader and for obvious comparison of the numerical and experimental data regarding the base-shear, Table 5.3 shows the peak base-shear in each cycle of loading; for the two directions of loading, $V_{max,i}$ (positive direction of i^{th}cycle) and $V_{max,j}$ (negative direction of j^{th} cycle), of the bare frame and of the infilled frame, while the corresponding ones of the retrofitted infilled frame are given in Table 5.4. Both tables include the difference (percentage) between the experimental and numerical values, as well.

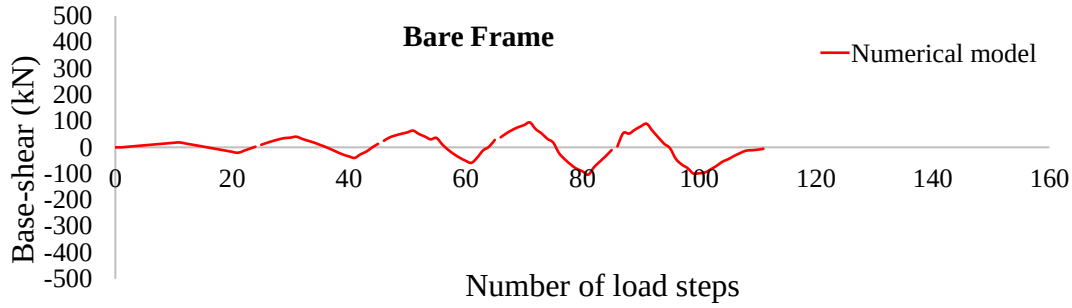

(a)

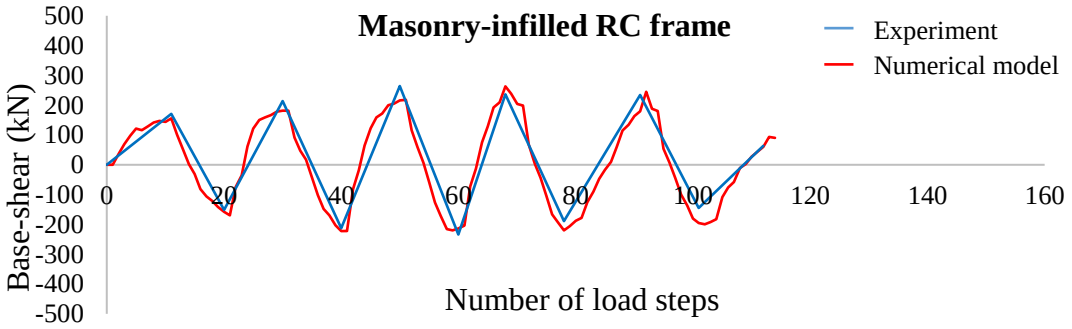

(b)

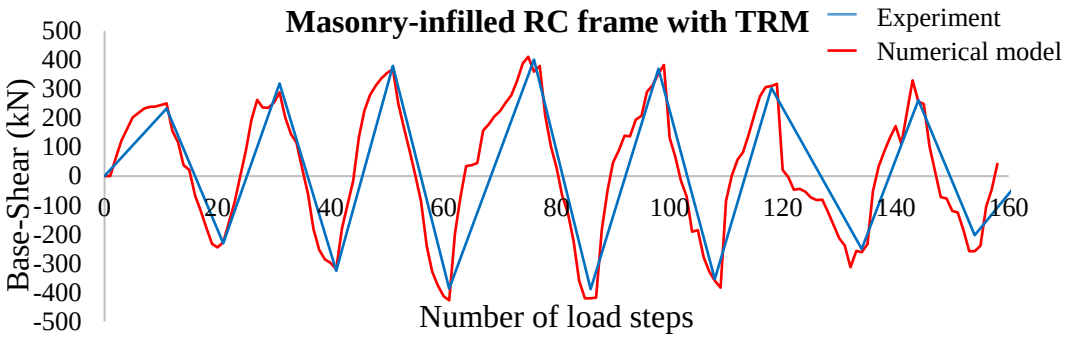

(c)

Figure 5.6: (a) Base-shear of the bare frame model in relation to the load steps, and (b) the comparison of the experimental and numerical results for unretrofitted infilled frame and (c) for retrofitted infilled frame in terms of base-shear versus number of load steps.

Table 5.3: Peak base-shear in each cycle of loading for both directions of the bare frame and of the masonry-infilled frame without TRM as obtained from experiment and numerical analysis.

	Bare frame		**Masonry-infilled RC frame**					
Cycle	**$V_{max,i}$ (kN)**	**$V_{max,j}$ (kN)**	**Experiment $V_{max,i}$ (kN)**	**Numerical $V_{max,i}$(kN)**	**Difference (%)**	**Experiment $V_{max,j}$ (Kn)**	**Numerical $V_{max,j}$ (kN)**	**Difference (%)**
1	18	-21	170.44	163.40	-4.13%	-150.90	-171.70	13.78%
2	40.	-40	214.32	188.43	-12.08%	-212.14	-225.35	6.23%
3	63	-59	264.25	239.06	-9.53%	-233.94	-231.91	-0.87%
4	95	-104.	236.51	236.94	0.18%	-189.27	-180.60	-4.58%
5	90	-96	233.88	224.08	-4.19%	-144.68	-179.34	23.96%

Table 5.4: Peak base-shear in each cycle of loading for both directions of the masonry-infilled RC frame with TRM as obtained from experiment and numerical analysis.

Masonry-infilled RC frame retrofitted with TRM						
Cycle	**Experiment $V_{max,i}$ (kN)**	**Numerical $V_{max,i}$ (kN)**	**Difference (%)**	**Experiment $V_{max,j}$ (kN)**	**Numerical $V_{max,j}$ (kN)**	**Difference (%)**
1	232	250.61	8.03%	-230.1	-227.947	-0.93%
2	318.17	287.68	-9.58%	-325.72	-320.45	-1.62%
3	378.81	368.34	-2.76%	-387.61	-427.14	10.20%
4	400.92	390.60	-5.32%	-388.97	-417.76	7.40%
5	369.241	382.65	3.63%	-354.4	-384.07	8.37%
6	302.97	317.77	4.89%	-250.42	-233.86	-6.61%
7	261.058	247.65	-5.13%	-203.32	-239.94	18.01%

From Figs. 5.6 (a) and (b), and from Table 5.3, it is observed that the presence of the infill wall in RC frame increases the maximum base-shear of the frame structure (which is attained in the fourth cycle of loading) by about 2.5-3 times. Furthermore, the peak base-shear of infilled frame during the first and second cycle of loading, in both directions, is increased by about 4-8 times compared to that of the bare frame. Therefore, the contribution of infill walls to increase the lateral capacity of RC frames is more pronounced during the first cycles of loading, which occur at small displacements. The same observations are also reported in Bertero and Brokken (1983), Liauw and

Kwan (1992), Mehrabi et al. (1994, 1996), Kwan and Xia (1995), Lee and Woo (2002), Hashemi and Mosalam (2006), and Pujol and Fick (2010).

Figure 5.6 (b) and Table 5.3 show that the peak base-shear of the infilled frame model is underestimated by about 4%-13% during the positive direction of loading, while during the negative one is overestimated by about 6%-23% in comparison with the corresponding ones obtained from the experiment. For the retrofitted infilled frame, the peak base-shear in each cycle of loading is either overestimated or underestimated, by a percentage of less than 10%, except at the last cycle of unloading where the numerical model overestimates the peak base-shear of the retrofitted infilled frame by 18% (Fig. 5.6 c and Table 5.4). This difference is considered acceptable for the purpose of this study.

Table 5.5 presents the comparison of peak base-shear in each cycle of loading of the retrofitted infilled frame with that of the unretrofitted one as resulted from the experiment and the numerical analysis. From Table 5.5, it is observed that the TRM technique increases the base-shear of the infilled frame in each cycle of loading by about 30%-100%. This increase is almost the same in the experimental and in the numerical study. The maximum base-shear force of the retrofitted infilled frame recorded during the fourth cycle of loading (positive direction) in the experiment and in the numerical study increases by about 69% and 60%, respectively, compared to that of the unretrofitted one.

Table 5.5: Comparison of retrofitted with unretrofitted infilled frame in terms of peak base-shear in each cycle of loading for both directions as obtained from the experiment and from the numerical analysis.

	$\frac{V_{max\,i_{retrofitted}} - V_{max\,i_{unretrofitted}}}{V_{max\,i_{unretrofitted}}}$		$\frac{V_{max\,j_{retrofitted}} - V_{max\,j_{unretrofitted}}}{V_{max\,j_{unretrofitted}}}$	
Cycle	**Experiment**	**Numerical model**	**Experiment**	**Numerical model**
1	36%	53%	52%	33%
2	48%	53%	54%	42%
3	43%	54%	66%	84%
4	69%	60%	106%	131%
5	58%	71%	145%	114%

Figure 5.7 shows the shear force at the second and third floor of the three-story masonry-infilled RC frame with and without TRM in relation to the load steps as resulted from the experiment (blue line) and from the numerical analysis (red line). From Figs. 5.7 (a) and (b) it is observed that the average difference between the experimental and numerical results regarding the shear force at the second floor is 12 % for the infilled frame, and 20% for the infilled frame with TRM. Furthermore, Fig. 5.7 (c) indicates that the discrepancy between the experimental and numerical results is relatively small (10%) in terms of shear force at the third floor of the infilled frame. From Fig. 5.7 (d), it can be pointed out that the infilled frame model with TRM can capture the shear force at the third floor until only the fifth cycle of loading (with a relative error equal to 25%). So, during the last two cycles of loading the retrofitted infilled frame model cannot predict the real shear force at the third floor. This might depend on the cyclic loading process followed in this numerical study, since it is different from that of the experimental case-study as mentioned in Chapter 4, sections 4.4 and 4.7. Adding to this, the discrepancy between the numerical and experimental results regarding the shear force at the third floor of the retrofitted infilled frame might depend on the complexity of the retrofitted infilled frame model, and on the nonlinearities that were introduced on the retrofitted infilled frame in the last two cycles of loading during the experiment (failure due to *soft-story mechanism* at the ground floor). Furthermore, it is important to mention that the calibration process followed in this study for both numerical models is done by comparing the experimental and numerical results in terms of base-shear force in relation to the top-floor displacement.

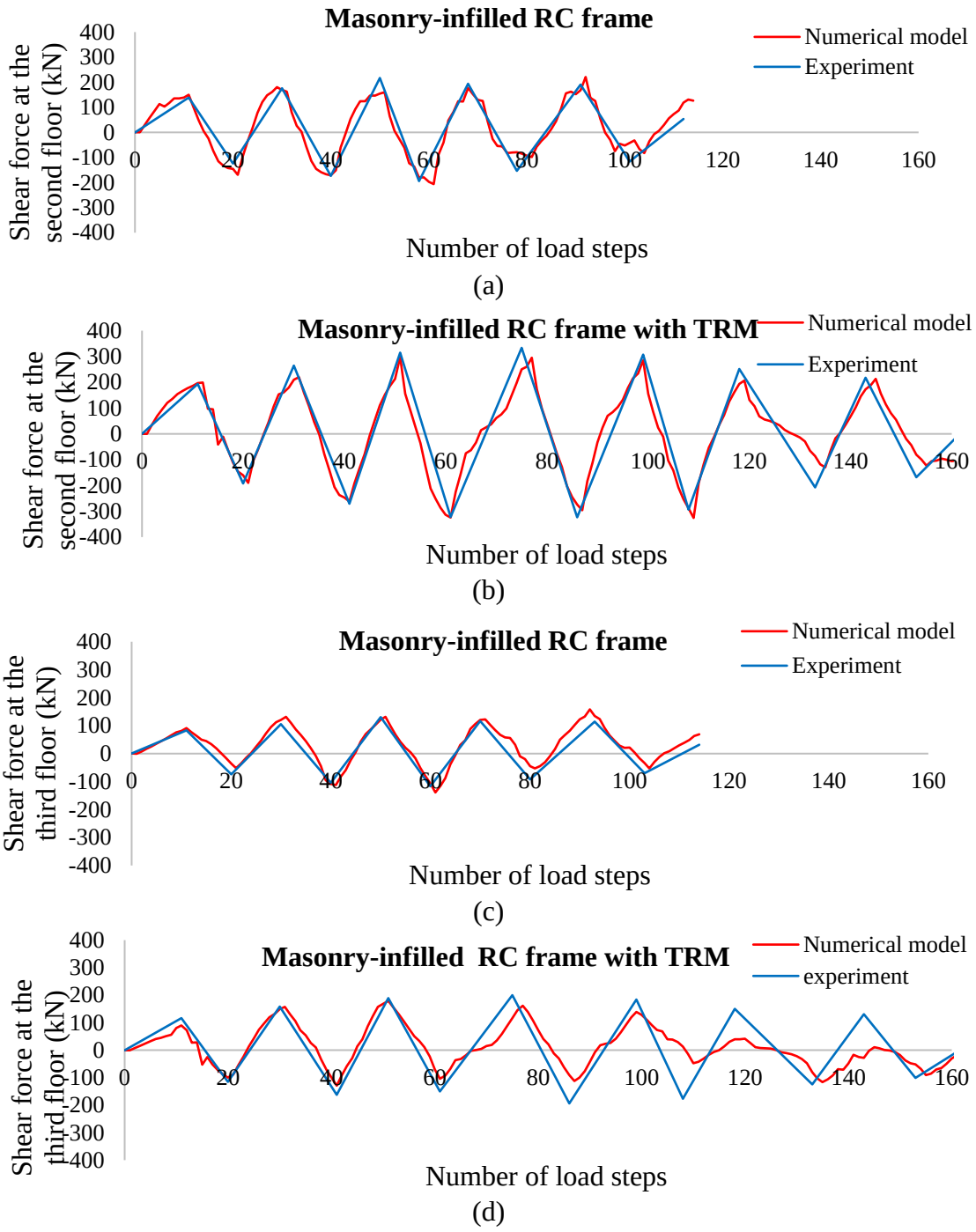

Figure 5.7: Comparison of the experimental and numerical results (a) in terms of shear force at the second floor versus number of load steps for the unretrofitted and (b) the retrofitted infilled frame, and (c) in terms of shear force at the third floor versus number of load steps for the unretrofitted and (d) for the retrofitted infilled frame.

Figure 5.8 shows the height-wise distribution of the shear force (peak shear force at each cycle of loading at each floor) of the unretrofitted infilled frame (dashed line) and of the retrofitted one (solid line) as obtained from the experiment (blue line) and from the numerical analysis (red line) during the first to fifth cycle of loading and unloading.

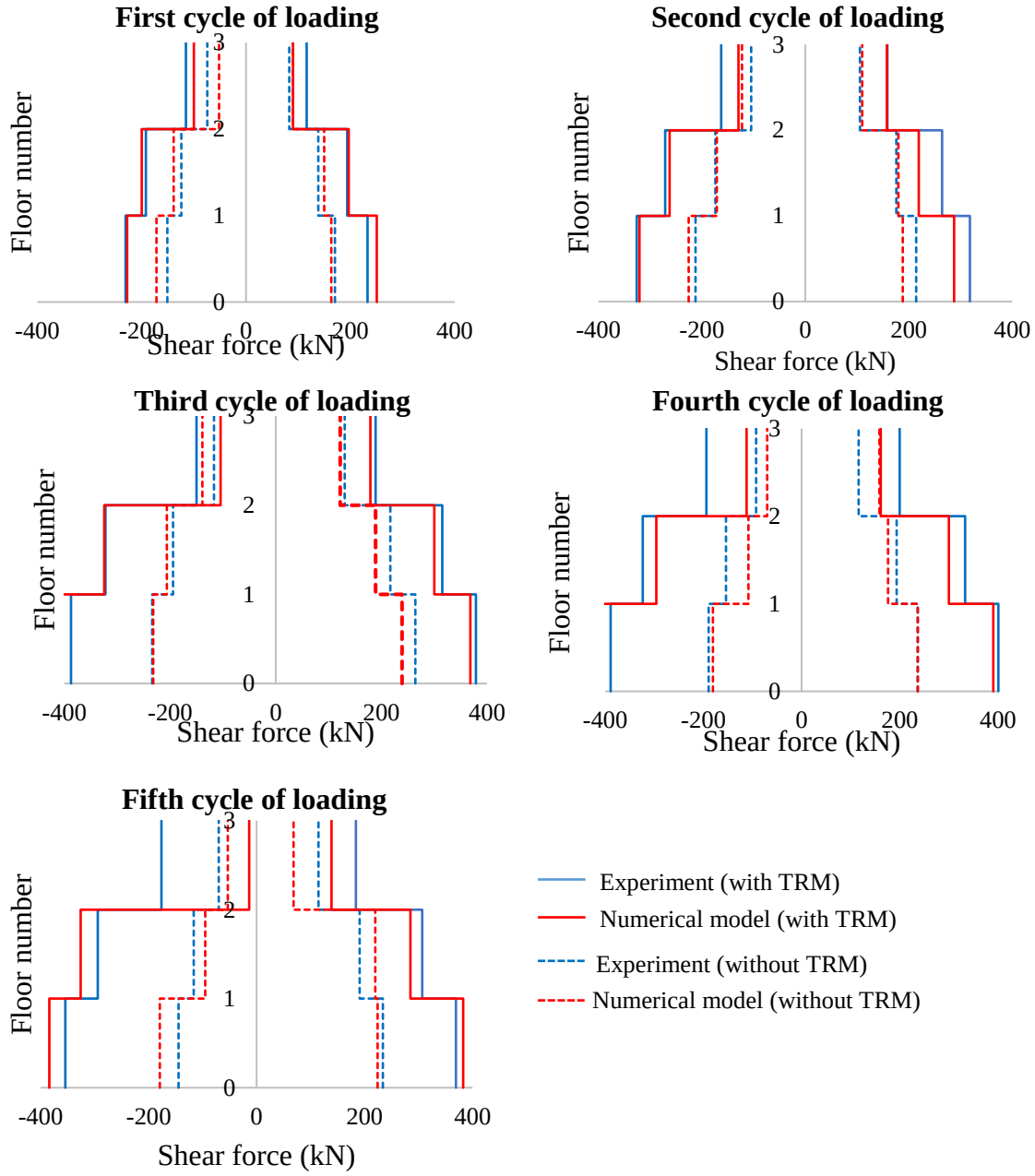

Figure 5.8: Comparison of height-wise distribution of the shear force of the unretrofitted (dashed line) and retrofitted (solid line) infilled frame as obtained from experiment (blue line) and from the numerical analysis (red line) during the first to fifth cycle of loading and unloading.

Figure 5.8 indicates that the proposed numerical models (infilled frame with and without TRM) accurately predict the height-wise distribution of the shear force of both infilled frames until the fifth cycle of loading since these models can also capture the peak-shear force in each cycle of loading at each floor of the structures with a relatively good accuracy as previously discussed (Figs. 5.6 and 5.7). Furthermore, from Fig. 5.8 it is observed that, as expected, the shear forces are not uniformly distributed (nonlinear variation) along the height of the three-story unretrofitted infilled frame (experiment and numerical model), and this leads to brittle failures at the first floor of the structure associated with the formation of a *soft–story mechanism,* as will be discussed in the next section. For the retrofitted infilled frame, while in general the shear forces do not vary linearly along the height of the three-story retrofitted infilled frame, they tend to a linear distribution along the height of the structure compared to the unretrofitted one, except for the fourth and fifth cycle of loading due to large lateral displacements. Therefore, the TRM retrofitting technique, for this case-study, is not adequate to prevent the damage on the first floor of the structure but it is effective for delaying some failures (such as the formation of a soft-story at the first floor in early lateral loading).

The global stiffness of the unretrofitted and retrofitted infilled frame is discussed in this paragraph. Figure 5.9 (a) illustrates the global stiffness in relation to the number of cycles of loading as obtained from non-linear cyclic analysis of the bare frame. Figures 5.9 (b) and (c) show the experimental (blue line) and numerical results (red line) in terms of global stiffness of the unretrofitted and retrofitted infilled frame, respectively, in relation to the number of cycles of loading. The secant stiffness degradation is calculated as follows (Eq. 5.1):

$$K_i = \frac{\left|+V_{max,i}\right| + \left|-V_{max,j}\right|}{\left|+x_{max,i}\right| + \left|-x_{max,j}\right|} \tag{5.1}$$

where $|+V_{max,i}|$ is the absolute value of the positive peak base-shear value of i^{th} cycle (as presented in Tables 5.3 and 5.4), and $|+x_{max,i}|$ is the absolute value of displacement corresponding to the positive peak base-shear of the of i^{th} cycle and $|-V_{maxj}|$ is the absolute value of the negative peak base-shear value of j^{th} cycle (as presented in Tables

5.3 and 5.4), and $|-x_{max,j}|$ is the absolute value of displacement corresponding to the negative peak base-shear of the of j^{th} cycle.

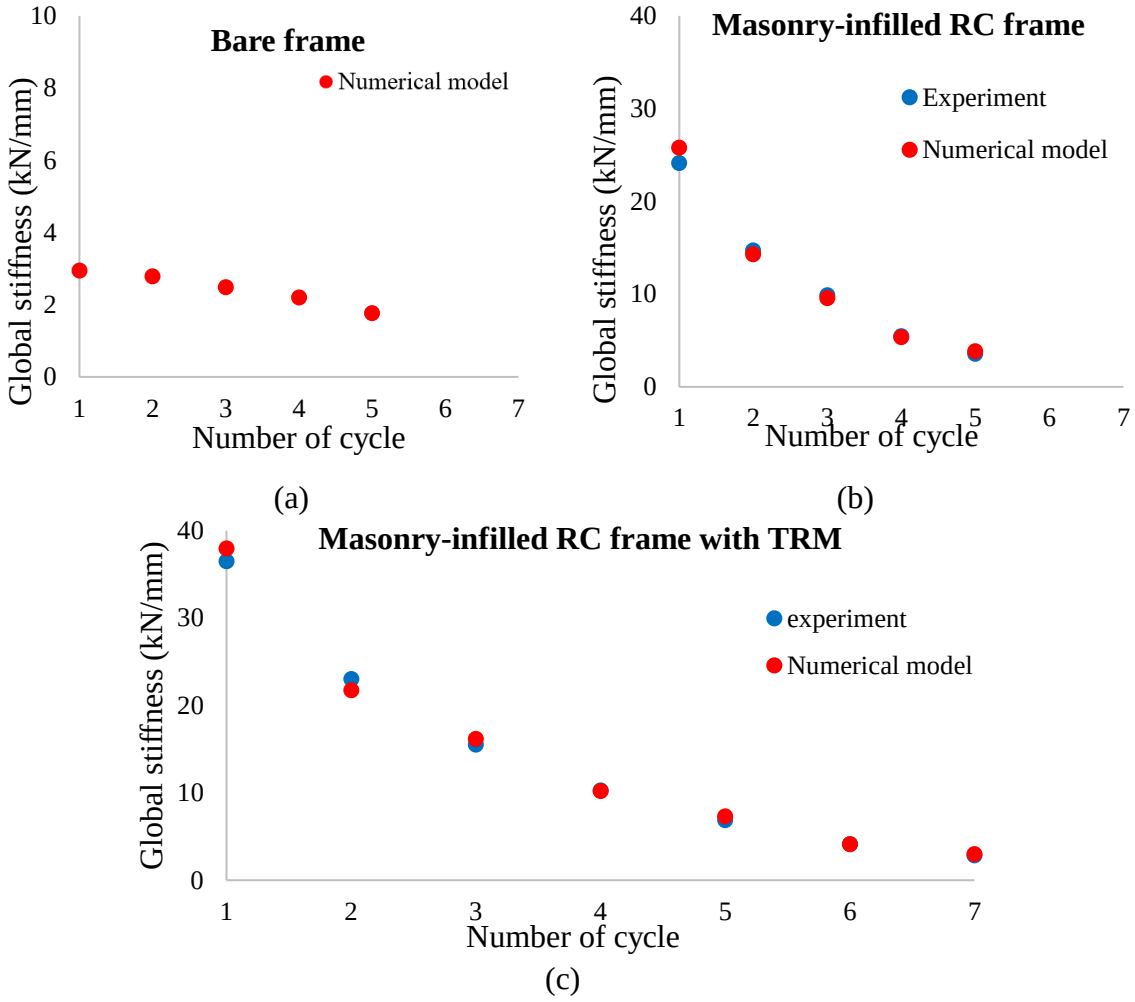

Figure 5.9: (a) Global stiffness of the bare frame model during the cyclic loading, and (b) comparison of the experimental and numerical results in terms of global stiffness of the unretrofitted infilled frame and (c) of the retrofitted infilled frame.

Comparing Fig. 5.9 (a) with Fig.5.9 (b) it is observed that the initial stiffness of the infilled frame is increased ten times compared to that of the bare frame, while from the second to fifth cycle of loading the stiffness of the infilled frame is increased by about 2-5 times compared to that of the bare frame. The significant contribution of the infill walls in the stiffness of frame structures is also reported in Murty and Jain (2000), Manos et al. (2000), Kappos and Ellul (2000), Hashemi and Mosalam (2006), Kaushik (2016) and in Basha and Kaushik (2016) as discussed in Chapter 2, section 2.3. Based on Figs. 5.9 (a) and (b) it can be pointed out that the existence of masonry infills in RC

frames can significantly increase the stiffness and the lateral capacity of RC frames when subjected to small lateral loading, while as the lateral load is increased the infill wall does not provide substantial gain to the stiffness of the structure due to the brittle nature of the infill wall, and the stiffness degradation of the infill wall. This observation is also supported by Zarnic and Tomazevic (1988).

From Figs. 5.9 (b) and (c) it is observed that the global stiffness of the unretrofitted and of retrofitted infilled frame model is either overestimated or underestimated by a percentage smaller than 12 % compared to that obtained from the experiment. It should be noted that the inaccuracy between the experimental and numerical results in terms of the stiffness is almost the same with that observed in the peak base-shear in each cycle of loading (Tables 5.3 and 5.4), since the stiffness is estimated according to the peak base-shear and to the peak top-floor displacement in each cycle of loading (Eq. 5.1). Furthermore, by comparing the experimental results with the numerical ones in terms of global stiffness of the unretrofitted and retrofitted infilled frame in each step of the displacement loading (the slope of base-shear versus top-floor displacement diagram), Figs. 5.5 (b) and (c), it is observed that after the fourth cycle of loading (the maximum base-shear) the numerical models' hysteresis curve starts to deviate giving a larger stiffness compared to the experimental one for both cases. This is probably caused by the progression of compression failure of the masonry infill wall on the first floor that was observed in the experiment, and this failure cannot be adequately reproduced by the numerical models, since the experimental results show extra loss of stiffness after this point. This will be discussed in the next section.

Besides the assessment of the global stiffness of the three structures, their dissipated energy is estimated, as well. The dissipated energy of the infilled frames with and without TRM is mainly associated with the propagation of damage through the masonry infill wall (crack opening), which leads to a higher area inside the hysteric loop, and consequently, to an increase of the energy dissipation capacity of the structure. The area enclosed by each hysteresis loop in the base-shear versus top-floor displacement diagram is the energy dissipated at each cycle of loading. For a simple calculation, the evolution of the dissipated energy is expressed by Eq. (5.2):

$$S_i = S_{i-1} + 0.5 * (V_{b,i} + V_{b,i-1}) * (X_{b,i} - X_{b,i-1}) \quad (5.2)$$

where $(V_{b,i}, V_{b,i-1})$ is the base-shear in two consecutive points of the loading and the $(X_{b,i}, X_{b,i-1})$ is the corresponding displacement. Figure 5.10 (a) illustrates the dissipated energy of the bare frame model in relation to the number of half cycles of loading. Figures 5.10 (b) and (c) show the comparison of experimental results (blue lines) with the numerical ones (red line) in terms of dissipated energy of the unretrofitted and retrofitted infilled frame, respectively, in relation to the number of half cycles of loading.

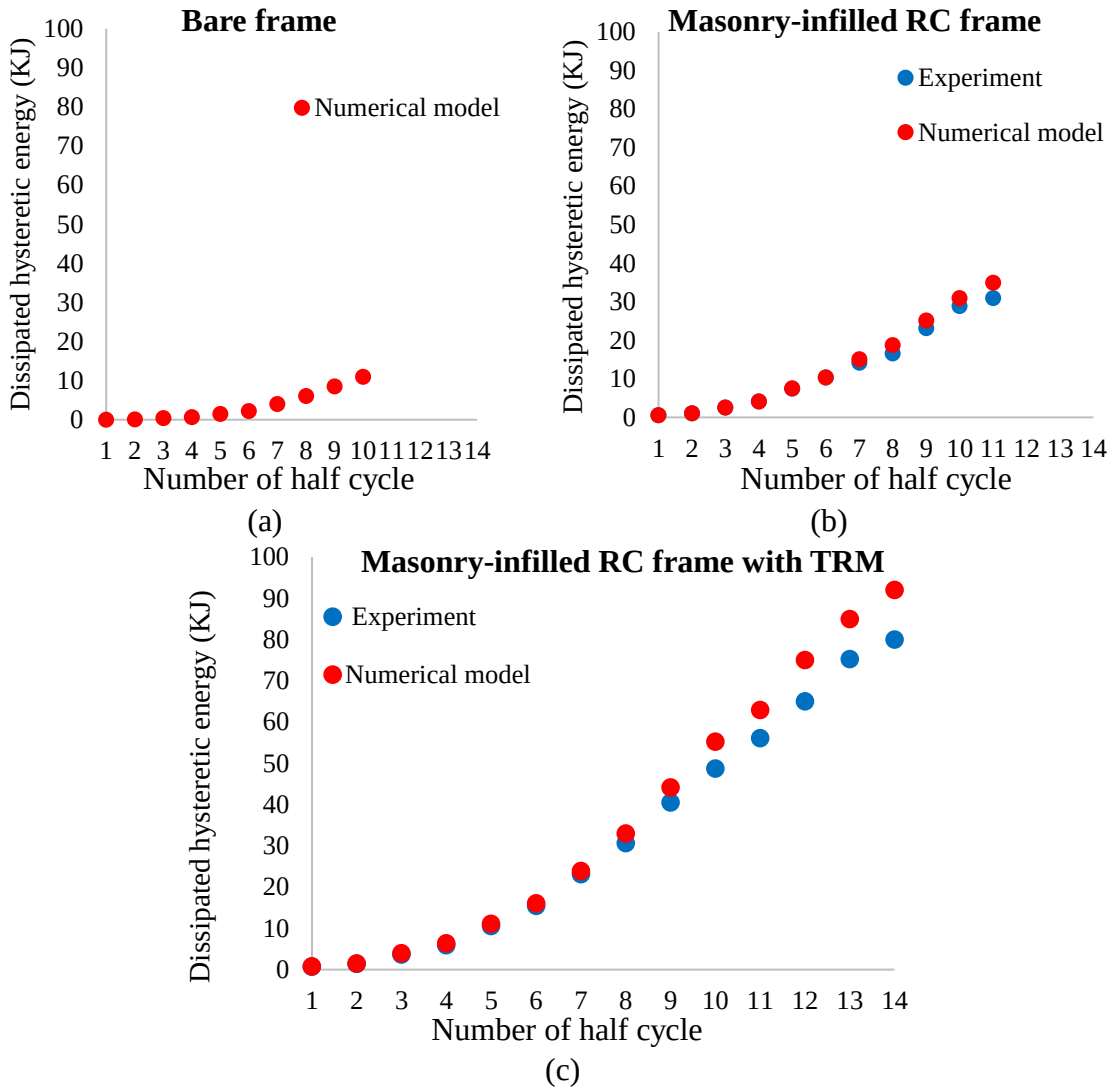

Figure 5.10: (a) Dissipated energy of the bare frame model, and (b) comparison of the experimental and numerical results in terms of dissipated energy of the unretrofitted infilled frame and (c) of the retrofitted infilled frame.

Comparing Fig. 5.10 (a) with Fig. 5.10 (b) it is observed that the presence of a masonry infill in a RC frame can increase the dissipated energy of the RC frame. Particularly, the total dissipated energy of the infilled frame is increased three times compared to that of the bare frame. Furthermore, the masonry infill provides a substantial gain in the dissipated energy of the frame, where this increase is more pronounced during the first cycles of loading which occur in small lateral displacements. The same observation is also reported in past studies (Manos et al. 2000; Kappos and Ellul 2000; Calvi and Bolognini 2001;Basha and Kaushik 2016).

From Figs. 5.10 (b) and (c) it is observed that the dissipated energy of both infilled frame models is overestimated by about 8%-12% compared to the real one during the first cycles of loading (one to fourth). For the rest cycles of loading (last two) the dissipated energy is overestimated by about 15%-22%. This might depend on the analysis convergence and on the nonlinearities that were introduced in the last cycle of loading during the experiment (failure due to *soft-story mechanism* at the ground floor). Besides the discrepancy between the experimental and numerical results it can be pointed out that both models can capture adequately the dissipated energy of the unretrofitted and retrofitted infilled frame during the cyclic loading.

The effectiveness of using the TRM composite material for retrofitting infilled frames is presented in Tables 5.6 and 5.7. These tables give the comparison of the unretrofitted infilled frame with the retrofitted one in terms of global stiffness and dissipated energy as obtained from the experiment and numerical analysis. From both tables it is observed that the TRM increases significantly the global stiffness and dissipated energy of the infilled frame by about 50%-90% and 30%-70%, respectively. This increase is almost the same in the experimental and in the numerical study. During the first cycle of loading, the stiffness of the retrofitted infilled frame is increased by about 50% compared to that of the unretrofitted infilled frame. Furthermore, the retrofitted infilled frame displayed higher stiffness compared to the unretrofitted one, especially, during the fourth and fifth cycle of loading (90%). The dissipated energy of the retrofitted specimen during the fifth cycle of loading is increased by about 61%-72% compared to that of the unretrofitted infilled frame. The increase in this cycle of loading in the numerical model is equal to 72%-78%.

Table 5.6: Comparison of the retrofitted and unretrofitted infilled frame in terms of global stiffness for both direction of loading as obtained from the experiment and numerical analysis.

	$\frac{K_{i,retrofitted} - K_{i,unretrofitted}}{K_{i,unretrofitted}}$	$\frac{K_{i,retrofitted} - K_{i,unretrofitted}}{K_{i,unretrofitted}}$
Cycle	**Experiment (%)**	**Numerical model (%)**
1	51%	47%
2	56%	52%
3	57%	70%
4	89%	91%
5	93%	90%

Table 5.7: Comparison of the retrofitted and unretrofitted infilled frame in terms of dissipated energy for both direction of loading as obtained from the experiment and numerical analysis.

	$\frac{S_{i,retrofitted} - S_{i,unretrofitted}}{S_{i,unretrofitted}}$	$\frac{S_{i,retrofitted} - S_{i,unretrofitted}}{S_{i,unretrofitted}}$
Half Cycle	**Experiment (%)**	**Numerical model (%)**
1	25%	34%
2	37%	31%
3	38%	37%
4	43%	39%
5	41%	45%
6	48%	56%
7	53%	58%
8	63%	72%
9	61%	72%
10	72%	78%

Based on the aforementioned observations, it should be pointed out that the TRM increases significantly the stiffness and the dissipated energy of infilled frame, and consequently the lateral capacity of the infilled frame, especially during the last cycles of loading. This is attributed to the fact that, the TRM is fully activated at the last stage of lateral loading, since it takes the high shear stresses and deformations that occur in the infilled frame during these cycles of loading. Specifically, the shear stresses on the

infill wall are transferred to the TRM in local level during the last cycles of loading, and the composite material sustains high tensile and shear stresses (without losing the structural integrity of the textile reinforcement), since it consists of high strength mortar and high strength textile.

The comparison of the experimental and numerical results regarding the global response of both infilled frames subjected to cyclic loading shows that the proposed numerical models (infilled frame with and without TRM) proved capable of simulating the in-plane behavior of the unretrofitted and retrofitted masonry-infilled RC frame under cyclic loading with good accuracy in terms of base-shear, shear capacity of each floor, height-wise distribution of the shear force, global stiffness, and dissipated energy.

5.2.2 Local results

In this section, the shear stresses, the deformed shape, the infill wall-frame separation and the crack pattern resulted from the non-linear cyclic analysis of the three-story masonry-infilled RC frame model with and without TRM are presented and compared with the corresponding ones obtained from the experiment. The results from the non-linear cyclic analysis of the bare frame are also presented in this section.

Figure 5.11 shows the shear stress distribution and the deformed shape of the bare frame model during the first, third and fifth cycle of loading for both directions. Also, Fig. 5.12 shows the propagation of the cracks in the bare frame model during the third and fifth cycle of loading, for both directions.

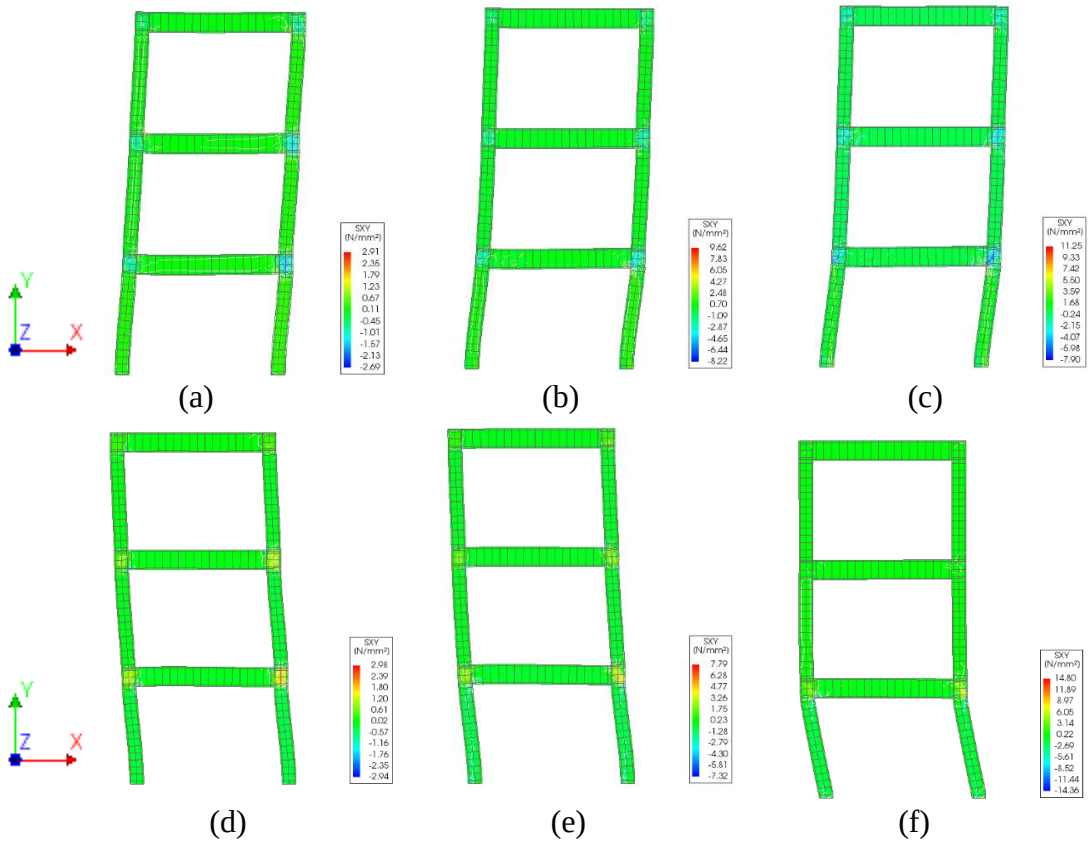

Figure 5.11: Shear-stress distribution in the bare frame model during the (a) first, (b) third and (c) fifth cycle of loading in the positive direction, and during the (d) first, (e) third and (f) fifth cycle of loading in the negative direction.

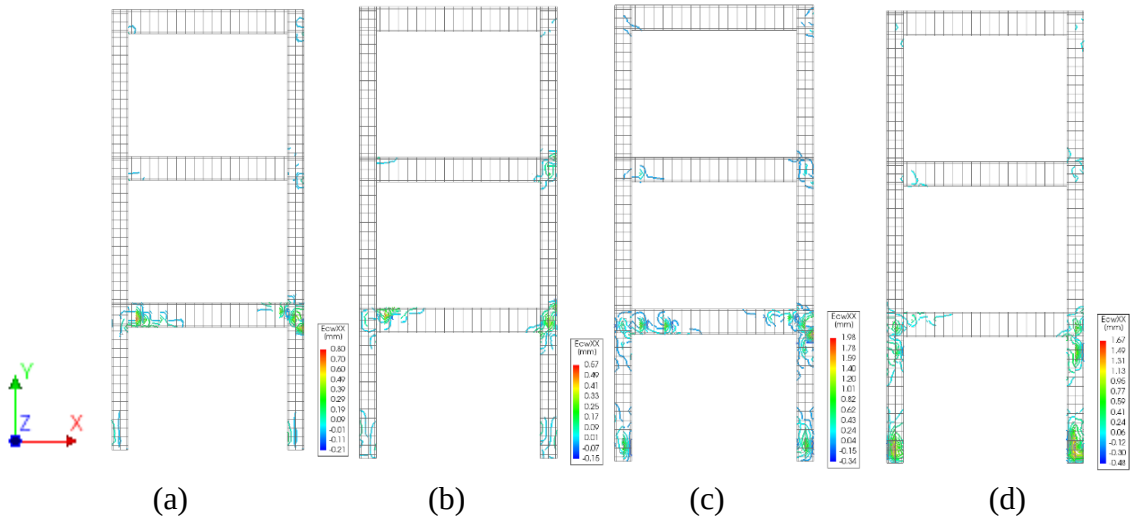

Figure 5.12: Crack propagation in the bare frame model during the (a) third and (b) fifth cycle of loading in the positive direction, and during the (c) third and (d) fifth cycle of loading in the negative direction.

From Figs. 5.11 and 5.12, it is observed that high shear stresses and large crack widths are developed at the first floor of the three-story RC frame. All the high stresses and the major cracks are mainly concentrated at the ends of the columns, and at the column-beam joint region at the first floor of the RC frame (development of plastic hinges at the ends of the columns). In addition, some minor shear cracks are developed on the beam of the bare frame at the first floor. Nevertheless, no major cracks were observed on the bare frame at the second and third floor. Therefore, the main failures occur at the first floor of the three-story RC frame. Especially, Fig. 5.11 indicates the formation of the *column-mechanism* (Comité Euro-International du Béton ,CEB, 1996) at the first floor of the frame. The same failure mechanism is also observed in the experimental studies conducted by Kakaletsis and Favvata (2005), Matsumiya et al.(2004), Altin (2007), Oinam et al. (2014) and by Peng et al. (2018). The above observations confirm that the RC frame was constructed with non-seismic design and detailing as mentioned in Koutas et al. (2014). So, the presence of the infill wall in this weak RC frame may introduced brittle shear failures on the frame as will be discussed in the following paragraphs. Although there is no data from Koutas et al. (2014) experiment's concerning the response of bare frame under cyclic loading, this bare frame model is considered to be accurate, since the type of failures and the crack pattern (location and crack width) that occur on the bare frame model are almost similar to those observed in the experimental and numerical studies conducted in the past (Chapter 2 in section 2.3) (Bertero and Brokken 1983; Zarnic and Tomazevic 1988; Liauw and Kwan 1992; Merhabi et al. 1996; Buonopane and White 1999; Calvi and Bolognini 2001; Stavridis 2012; Basha and Kaushik 2016; Morandi et al. 2018).

After the assessment of the bare frame model, the shear stresses, deformed shape, infill wall-frame separation and the crack pattern of the unretrofitted infilled frame during cyclic loading are discussed in the following paragraphs. Figure 5.13 presents the shear stress distribution and the deformed shape of the infilled frame during the first, third and fifth cycle of loading for both directions.

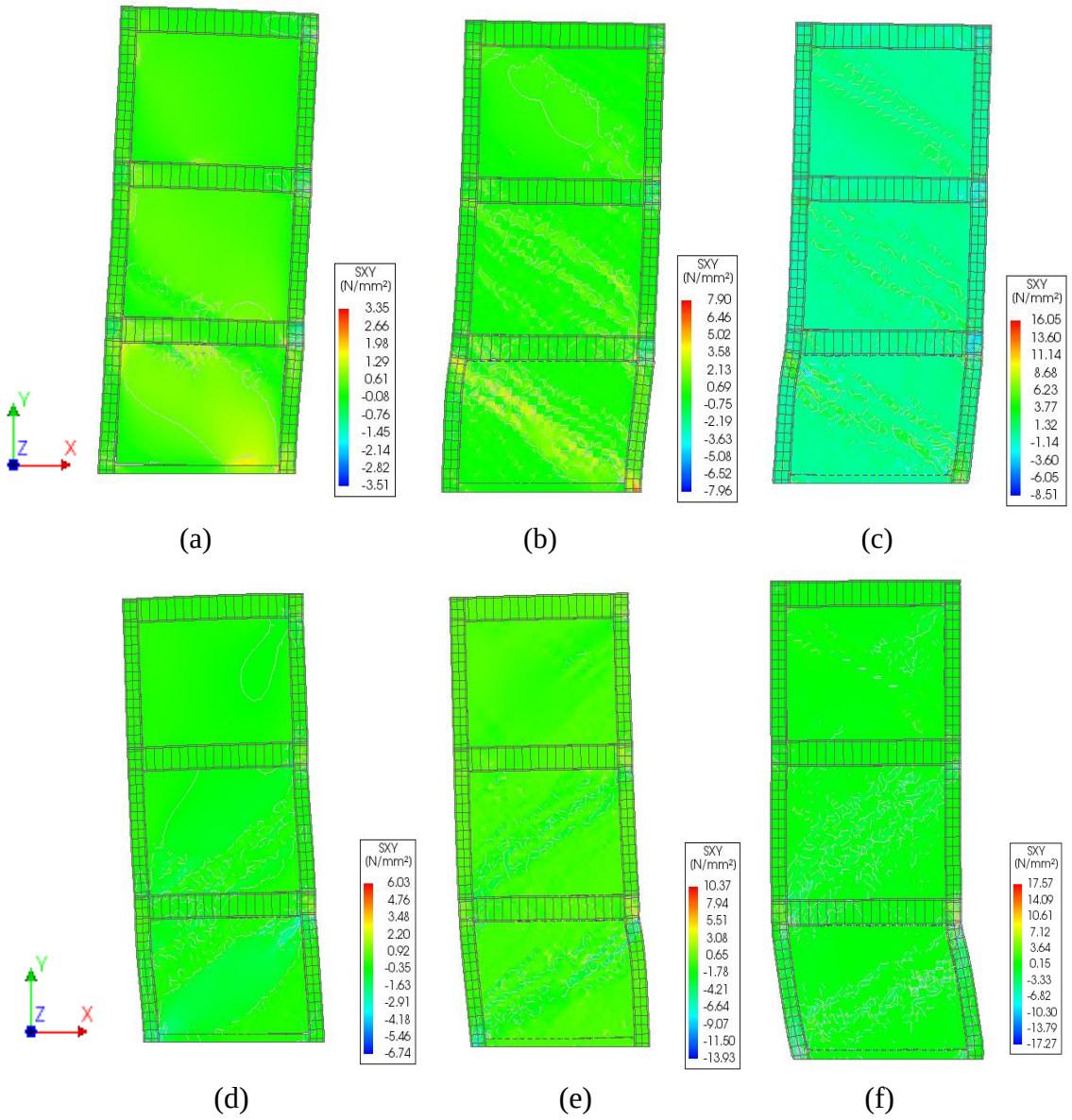

Figure 5.13: Shear stress distribution in the infilled frame model during the (a) first, (b) third and (c) fifth cycle of loading in the positive direction, and during the (d) first, (e) third and (f) fifth cycle of loading in the negative direction.

Figure 5.13 shows that high shear stresses are concentrated in the first floor, somewhat less in the second floor and almost no shear stresses in the third floor. From Figs. 5.13 (a) and (d), it is observed that during the first cycle of loading, high shear stresses are concentrated near the loaded corners of the infill wall where the diagonal compression path is developed. As the lateral loading is increased (Figs. 5.13 b, c, e, and f), high shear stresses are concentrated along the diagonal of the infill wall. Adding to this, high

concentration of shear stresses is observed at the beam-column joints and at the ends columns in the area which contacted the diagonal of the infill wall at the first floor. Furthermore, Fig. 5.13 indicates that the deformation along the height of the structure is not linearly varying, especially, during the last cycles of loading (Figs. 5.13 c and f). Specifically, the inter-story deformation along the height of the second and third floor of structure is almost the same and completely different from that of the first floor, especially during the fifth cycle of loading (*soft-story mechanism*). This is also supported by Fig. 5.8 which shows that the height-wise distribution of the shear forces of the three-story unretrofitted infilled frame is not linearly varying (high shear forces at the first floor). The above observations are associated with the brittle failures that occurred at the first floor of the structure as it will be discussed in the following paragraphs.

Figure 5.13 clearly indicates that the infill wall acts as a diagonal strut (as mentioned in sections 2.3 and 2.4). During the first cycle of loading, the diagonal strut is observed only at the first floor, and during the third and fifth cycle of loading the diagonal strut is observed at all floor levels. Adding to this, as the imposed displacement loading increases the width of the compression diagonal strut also increases. The width of the compression diagonal strut is depended on several parameters, as it is reported by several researchers (Chapter 2, section 2.4), such as: the wall's aspect ratio, the relative infill wall-to-frame stiffness, the contact length between infill panel and frame (Polyakov 1960; Liauw and Kwan 1984; Klinger and Bertero 1978; Bazãn and Meli 1980; Bertero and Brokken 1983, Dawe 1985; Paulay and Priestley 1992; Durrani and Luo 1994). Figure 5.13 also shows that the masonry infill wall could be better represented by multi-diagonal no-tension strut elements instead of a single-diagonal strut element. This observation is also supported by several researchers such as Thiruvengadam (1985), Chrysostomou (1991), Crisafulli (1997), Chrysostomou et al. (2002), El-Dakhakhni et.al (2001, 2002, 2004), and in Crisafulli and Carr (2007).

Figures 5.14, 5.15 and 5.16 show the crack propagation in the infilled frame at the first floor, as observed in the test specimen and in the numerical model during the first, third and fifth cycle of loading, respectively, for both directions. The crack propagation in the

infilled frame as formed in the test specimen and in the numerical model upon test completion is presented in Fig. 5.17.

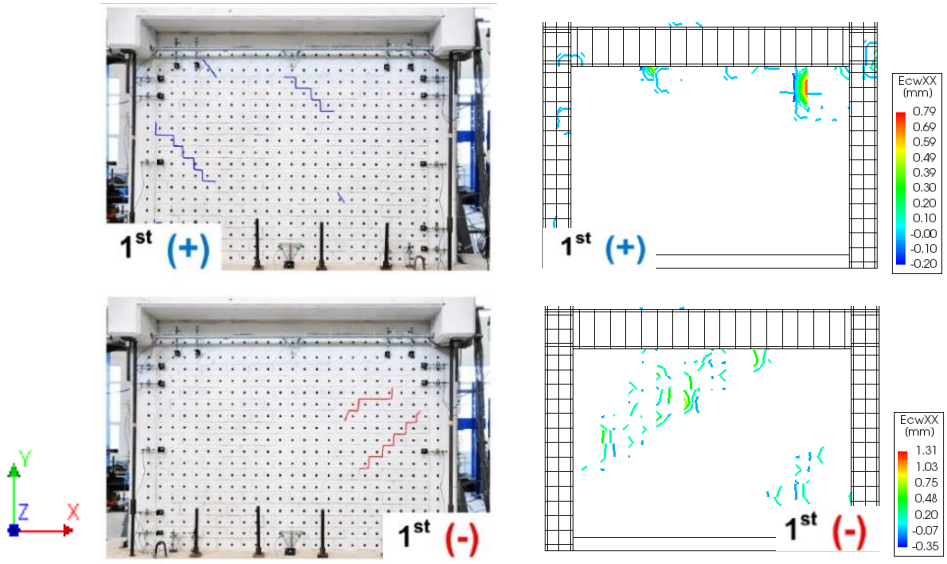

(a) (b)

Figure 5.14: Crack propagation in the infilled frame at the first floor during the first cycle of loading in the positive and negative direction of loading as occurred in the (a) experiment, and (b) in the numerical model.

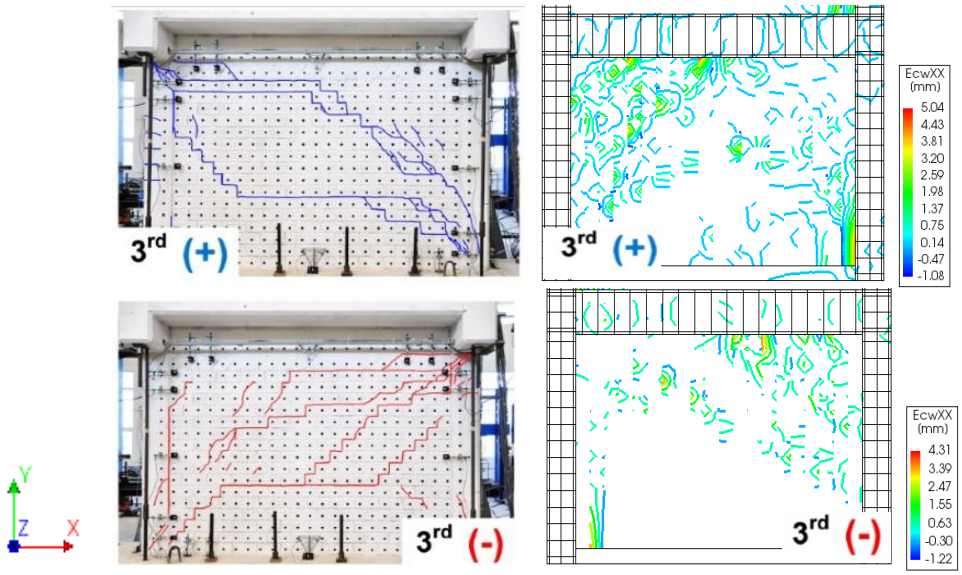

(a) (b)

Figure 5.15: Crack propagation in the infilled frame at the first floor during the third cycle of loading in the positive and negative direction of loading as occurred in the (a) experiment and (b) in the numerical model.

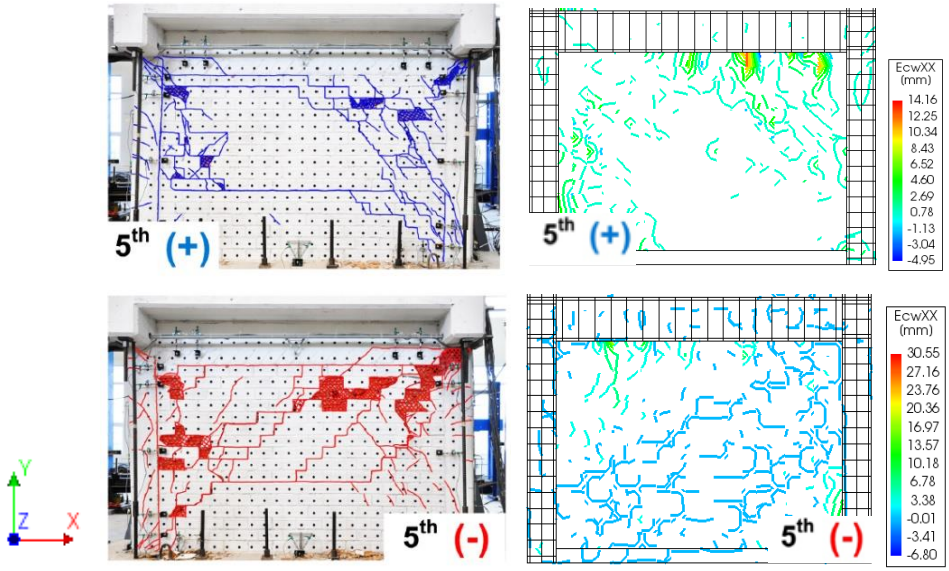

(a) (b)

Figure 5.16: Crack propagation in the infilled frame at the first floor during the fifth cycle of loading in the positive and negative direction as occurred in the (a) experiment and (b) in the numerical model.

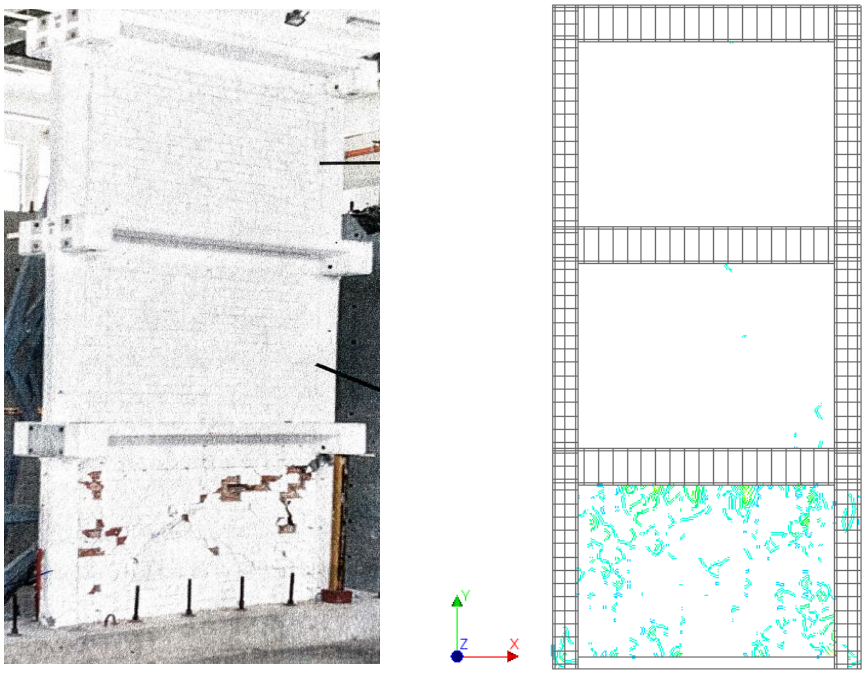

(a) (b)

Figure 5.17: Crack propagation in the three-story masonry-infilled RC frame as occurred in the (a) experiment and (b) in the numerical model upon test completion.

Figure 5.14 (a) shows that two parallel stair-step-type cracks were formed running along the diagonal of the infill wall but not progressing much lower than the mid-height of the infill wall. In the numerical model (Fig. 5.14 b), during the first cycle of loading, vertical and horizontal cracks are formed at the top and bottom of the infill wall, and at the top ends of the columns at the first floor, with maximum crack width equal to 1.3 mm. Comparing Fig. 5.14 (a) with Fig. 5.14 (b), it is observed that the crack pattern of the infilled frame is not well reproduced by the proposed numerical model during the first cycle of loading, since the shear cracks along the diagonal of the infill wall are not observed in the numerical model. It should be noted that the inaccuracy of the numerical model to capture adequately the real crack propagation in the infilled frame will be explained at the end of this Chapter.

Comparing Fig. 5.15 (a) with Fig. 5.15 (b), it is observed that the crack pattern developed in the test specimen at the first floor during the third cycle of loading is accurately reproduced by the numerical model. From Fig. 5.15 (b) it is observed that stair-step-type and sliding cracks are developed at the diagonal of the infill wall, followed by distinct diagonal shear cracks at the top of the columns (near the area which contacted the diagonal of the infill wall) in the same location as in the real case (Fig. 5.15 a). Furthermore, Fig. 5.15 (b) shows that upon increasing the horizontal loading, the cracks tend to concentrate from the one loaded corner of the infill wall to the other, with the maximum crack width equal to 5mm. Also, as the displacement loading increases in the test specimen and in the numerical model the previously opened cracks reopened, became wider and propagated in the body of the infill wall, resulting in a marked decrease of the overall lateral stiffness of the infilled frame as indicated in Fig. 5.15 (b).

Figure 5.16 shows that the crack pattern developed in the infilled fame during the fifth cycle of loading is accurately reproduced by the numerical model. From Fig. 5.16 (b) it is observed that during the fifth cycle of loading, the crack pattern was completed in the infilled frame model with the formation of horizontal sliding cracks (caused by a too high compression load) and stair-step-type cracks in the infill wall, which is the same crack pattern developed in the real case (Fig. 5.16 b). Furthermore, the shear cracks at the top of both columns at the first floor became wider, especially at the top of the east-

bound column as will be discussed later. Figure 5.16 (b) shows that the maximum crack width in the top of the east-bound column is equal to 6.1 mm, while the maximum crack width near the loaded corners of the infill wall (right-bottom corner) is equal to 14 mm.

Upon cyclic analysis completion, diagonal cracks and horizontal sliding cracks are observed in the infill wall at the first floor of the infilled frame model as shown in Fig. 5.17 (b) which is the same crack pattern as observed in the experiment (Fig 5.17 a). From Figs. 5.15, 5.16 and 5.17 it is observed that the compression failure of the infill wall is more spread over the infill wall in the experiment compared to the numerical model. So, the compression failure of masonry infill wall at the first floor of the structure during the last cycles of loading is not very well capture by the numerical model. The above observation is also supported by Fig. 5.5 (b) in which the numerical models' hysteresis curve starts to deviate giving a larger stiffness compared to the experimental one during the last cycles of loading. As previously mentioned, the inaccuracy of the numerical model to capture adequately the real crack propagation in the infilled frame will be discussed at the end of this Chapter.

As shown in Fig. 5.13, the maximum shear stresses are concentrated near the loaded corners of the infill wall (where the compression diagonal path is developed along two opposite corners of the infill wall), while near the non-loaded corners, the infill wall separates from the RC frame (zero shear stresses). In this numerical study, in order to capture the infill-frame separation, an interface element between the infill wall and the frame is used and an appropriate model is adopted for this element as presented in the previous Chapter (sections 4.5 and 4.6.4). It is important to mention, that special attention is given for the required parameters of this interface model, since these parameters could significantly influences the overall behavior of the infilled frame under lateral loading as will be presented in the next section of this Chapter. Figure 5.18 shows the gap-opening along the infill-frame interface at the first story and at the bottom of the second story of the three-story masonry-infilled RC frame model during the first, third and fifth cycle of loading in the two directions of loading.

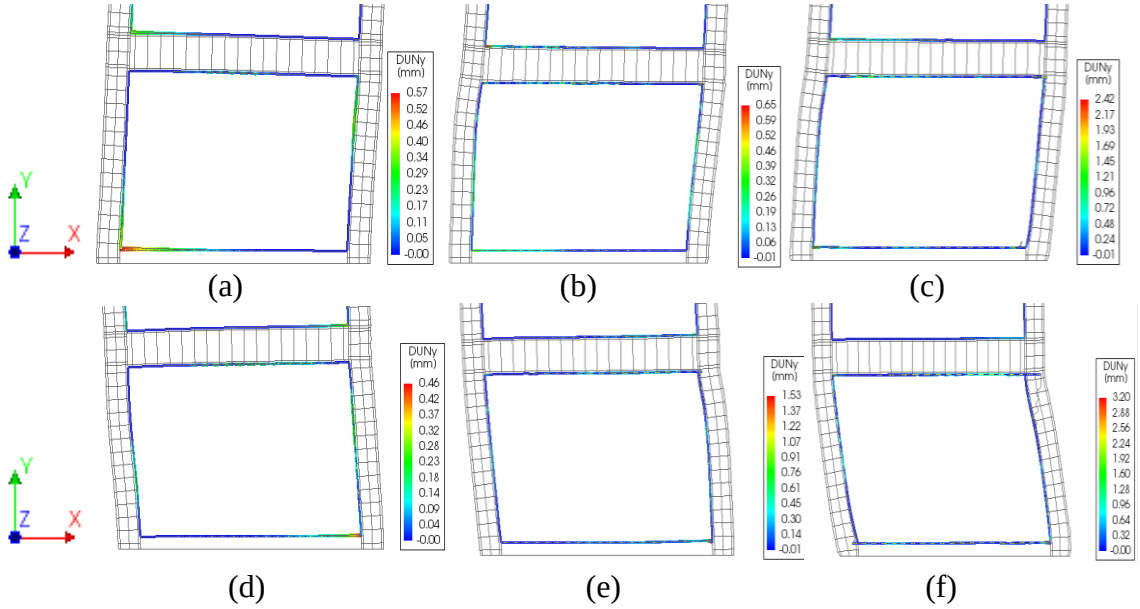

Figure 5.18: Gap-opening along the infill-frame interface at the first story and at bottom of the second story of the infilled frame model during the (a) first, (b) third and (c) fifth cycle of loading in the positive direction of loading, and during the (d) first, (e) third and (f) fifth cycle of loading in the negative direction of loading.

During the experimental and the numerical test, the infill-frame separation occurred at the very early stages of loading. From Figs. 5.18 (a) and (d) it is observed that the average gap-opening at infill-frame interface in the numerical model is almost the same with that in the test specimen as Kouta's reported (average gap-opening at column-infill interface equal to 0.1 mm and at beam-infill interface equal to 0.3 mm), except for the gap-opening at the bottom beam-infill interface at the first floor which is equal to 0.56 mm in the numerical model instead of 0.3 mm in the test specimen. For the benefit of the reader, Table 5.8 shows the opening of the gap between the infill wall and frame of the three-story infilled frame, at specific locations, as measured in the experimental test, and as obtained from the cyclic analysis of the infilled frame model during the third and fifth cycle of loading.

Table 5.8: Gap-opening at the infill-frame interface of the unretrofitted infilled frame as obtained from the experimental test and from the numerical analysis.

	Gap-opening (mm)					
Number of cycle	**Top beam-infill interface first floor**		**Bottom beam-infill interface second floor**		**Column-infill interface first floor**	
	Experiment	**Numerical model**	**Experiment**	**Numerical model**	**Experiment**	**Numerical model**
3	0.8-1.0	0.4-1.1	0.8-1.0	0.4-0.9	1-1.5	0.8-1.6
5	1-1.5	1.1-1.8	1-1.5	0.9-1.45	1.5-2.0	2.0-3.20

Table 5.8 shows that there is no significant discrepancy between the experimental and numerical data in terms of gap-opening along the infill-frame interface (maximum difference equal to 1.2 mm). The difference between the experimental and numerical results concerning the infill-frame separation is in terms of the location that the maximum gap-opening between the infill wall and frame has occurred. So, in the numerical model, the maximum gap-opening appeared at the corners of the infilled frame at the first floor, while in the experiment, the maximum gap-opening occurred along the column-infill interface at the first floor. This difference is due to the fact that in the experimental case-study, the separation of the infill wall from the surrounding frame was not measured at the corners of the infilled frame, since no potentiometers were installed at these locations.

Furthermore, from Figs. 5.13 (c) and (f) and from Fig. 5.16 it is observed that high shear stresses and large crack widths are concentrated along the diagonal and near the loaded corners of the infill wall during the last cycles of loading. This indicates the *corner crushing* of the infill wall at the first floor. After that, high shear stress and large crack widths are observed at the beam-column joints and at the ends columns in the area which contacted the diagonal of the infill wall. This is associated to the shear failure of the upper ends of the column (*short-column mechanism*). More details regarding the force mechanism causing the shear failure of the columns will be discussed in the following paragraphs. Figure 5.19 shows the shear failure at the top of the east-bound column at the first floor in the experiment and in the numerical model at the end of cyclic test. This figure indicates that the same damage (shear failure) at the top of the

east-bound column of the first floor is observed in the experiment and in the numerical model upon test completion.

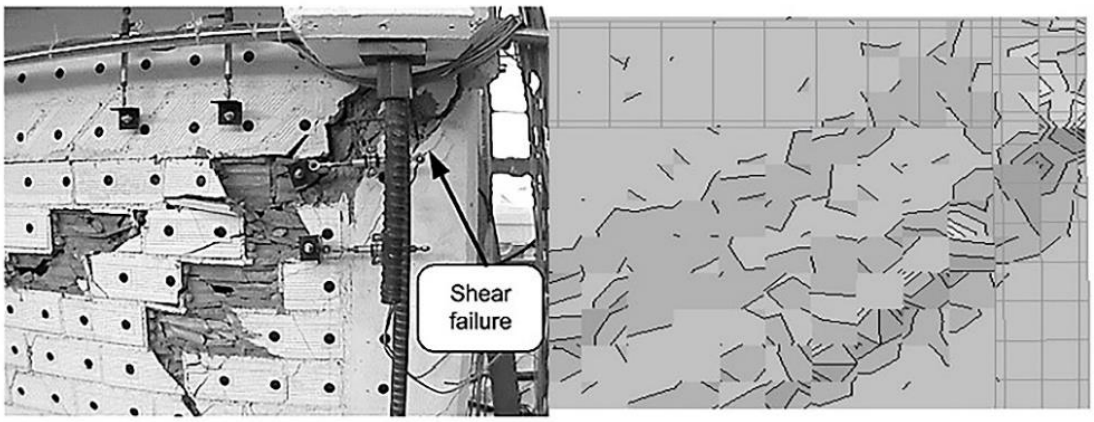

(a) (b)

Figure 5.19: Shear failure at the top of the east-bound column at the first floor in the (a) test specimen and in the (b) numerical model upon test completion.

By examining the shear stress distribution, the developed crack pattern, and the infill-frame separation during the experimental and the numerical test, it can be concluded that as the lateral loading increases the failures occur in the masonry infill wall and propagate to the RC frame. The following combination of failure modes is observed in the infilled frame during the experimental and the numerical test due to the interaction of infill wall with the RC frame: *corner crushing, diagonal cracking,* and *sliding shear* (Chapter 2, section 2.2). Eventually, the *frame failure* mode occurs which consists of the failure of column-beam joints and of the shear failure of the columns at the first floor of the structure. The *frame failure* mode is associated with a weak frame and with weak joints in the frame (non-seismic design and detailing of RC frame), as well as with the formation of a short column after the *corner crushing* of the infill, as previously mentioned. Furthermore, a *soft-story mechanism* (Chapter 2 section 2.2) is developed in the infilled frame model (Figs. 15.3 c and f), which is the same mechanism observed in the experimental specimen. The development of the *soft-story mechanism* is due to the large concentration of damage in a few members of the infilled frame at the first floor.

Comparing the failures on the bare frame (shear stress distribution, deformed shape, and propagation of the cracks Fig.5.11-5.12) with that on masonry-infilled frame (Figs. 5.13-5.17) it is observed that the presence of an infill wall in a RC frame introduces

brittle shear failures on the frame. The shear failure of the columns (*short-column mechanism*) is caused by the infill wall strut action due to the relatively high resistance of the strong infill with respect to the RC frame (weak RC frame since it was constructed with non-seismic design and detailing as previously mentioned). More specifically, high shear forces are transferred from the masonry infill wall, especially from the loaded corners of the infill wall (corner crushing) to finite portions of RC columns of the frame in the area which contacted the diagonal of the infill wall (increases in contact length of wall and RC columns as the lateral loading increases). Therefore, after the failure of the infill wall (*corner crushing*), the contribution of the infill wall to the lateral resistance of the infilled frame reduces significantly resulting to shear failure of the columns (Fig. 5.9 b). The above observation is also supported by several studies conducted so far as mentioned in Chapter 2, section 2.3 and 2.4 (Zarnic and Tomazevic 1988; Merhabi et al. 1996; Buonopane and White 1999;Stavridis 2012; Basha and Kaushik 2016 and Morandi et al. 2018).

In the following paragraphs, the failures that occurred on the retrofitted infilled frame subjected to cyclic loading are presented and discussed. It is important to mention that the shear stresses and the cracks patterns on the retrofitted infilled frame model as it will be presented in this section are those observed on the external face of TRM since the TRM plane-stress elements overlay the masonry plane-stress elements (section 4.5). Nevertheless, this leads to sufficient indication about the failures that occurred in the infilled frame (without the TRM). Figure 5.20 shows the distribution of the shear stress on the infilled frame model with TRM and its deformed shape, during the first, third, fifth and seventh cycle of loading for both directions of loading.

From Fig. 5.20, it is observed that high shear stresses are concentrated in the first floor, somewhat less in the second floor and almost no shear stresses at the third floor. Figures 5.20 (a) and (e) show that at the early stage of loading the shear stresses are concentrated on the external face of the TRM at the location corresponding to the diagonal of the infill wall and to the loaded corners of the infill wall at the first floor. As the lateral loading increases, the shear stresses are spread all over the external face of the TRM at the infill wall (shear stress along the diagonal, and along the opposite of the diagonal), and at the ends of the columns at the first floor of the structure (Figs. 5.20 b-

h). Furthermore, Fig. 5.20 indicates that the inter-story deformation along the height of the second and third floor of structure is almost the same and completely different from that of the first floor, especially during the last cycle of loading (*soft-story mechanism*). This is also supported by Fig. 5.8 which shows that the height-wise distribution of the shear forces of the three-story retrofitted infilled frame is not linearly varying (high shear forces at the first floor). The above observations are associated with the brittle failures that occurred at the first floor of the retrofitted structure as will be discussed in the following paragraphs.

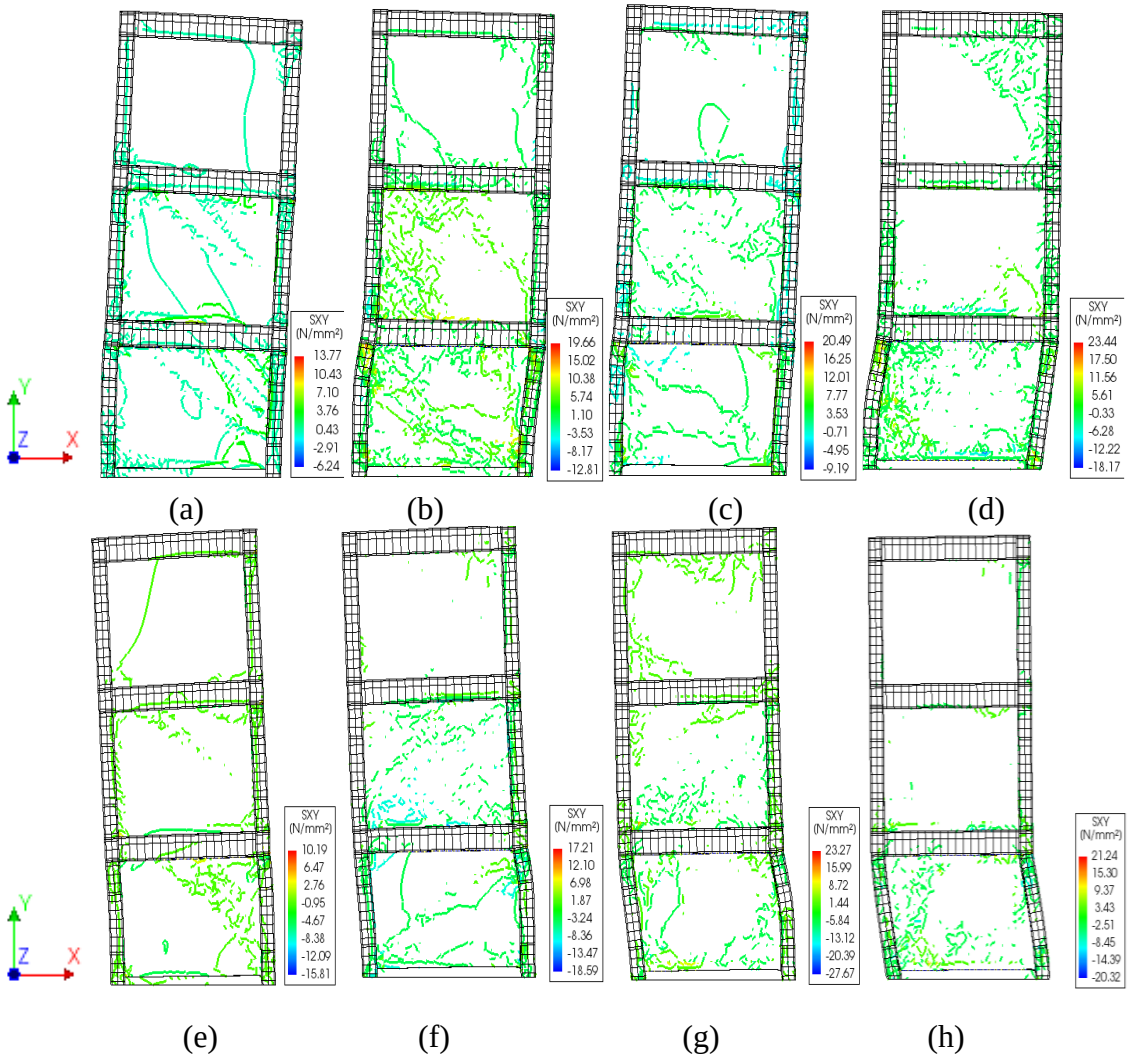

Figure 5.20: Shear stress distribution in the retrofitted infilled frame model during the (a) first, (b) third, (c) fifth and (d) seventh cycle of loading in the positive direction, and during the (e) first, (f) third, (g) fifth and (h) seventh cycle of loading in the negative direction.

Figures 5.20 (a) and (e) clearly indicate that the retrofitted infill wall acts as a diagonal compression strut during the first cycle of loading. As the imposed displacement loading increases, shear stresses are also observed along the opposite of the diagonal, especially at the external face of TRM near the un-loaded corners of the infill wall (Figs. b and f). This indicates that the retrofitted infill wall acts as a pair of alternatively activated compression strut and tension tie (tension diagonal). This is also reported in the studies conducted by Koutas et al. (2014) and Pohoryles et al. (2020).

Figures 5.21 and 5.23 present the crack propagation on the external face of TRM at first floor of the retrofitted infilled frame model, during the first, third, fifth and sixth cycle of loading for both directions. Figure 5.22 shows the propagation of the cracks at the second floor of the retrofitted infilled frame as observed in the test specimen and in the numerical model during the fourth cycle of loading. Furthermore, the crack pattern in the three-story retrofitted infilled frame as formed in the experimental specimen and in the numerical model upon test completion is given in Fig. 5.24. It is important to note that, the crack propagation that occurred on the external face of TRM apply also to the infill .

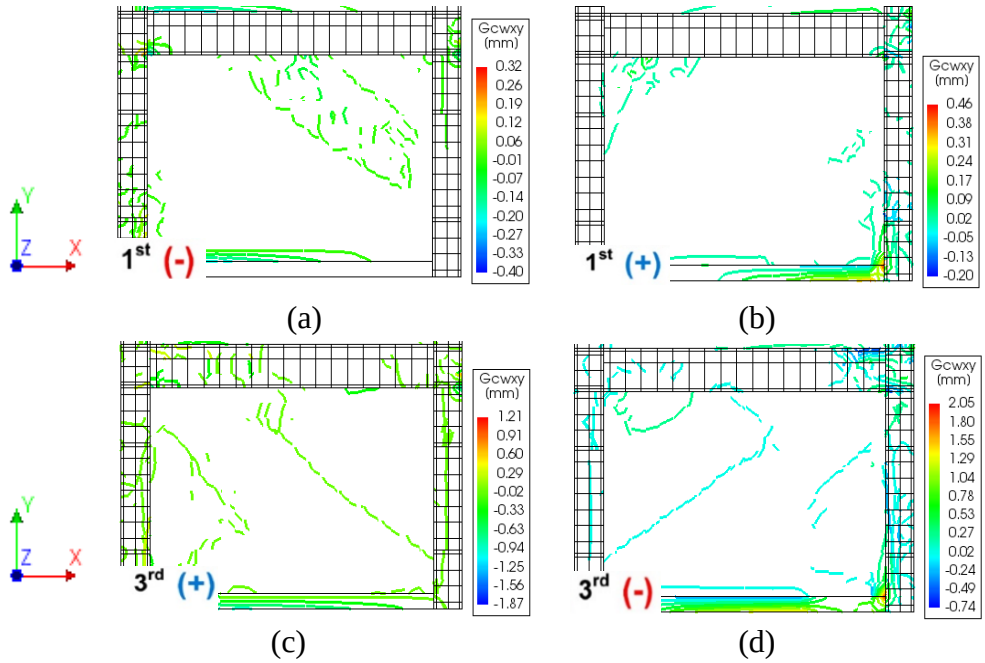

Figure 5.21: Crack propagation in the retrofitted infilled frame model at the first floor (a) during the first cycle of loading in the positive and (b) negative direction of loading, and (c) during the third cycle of loading in the positive and (d) negative direction of loading.

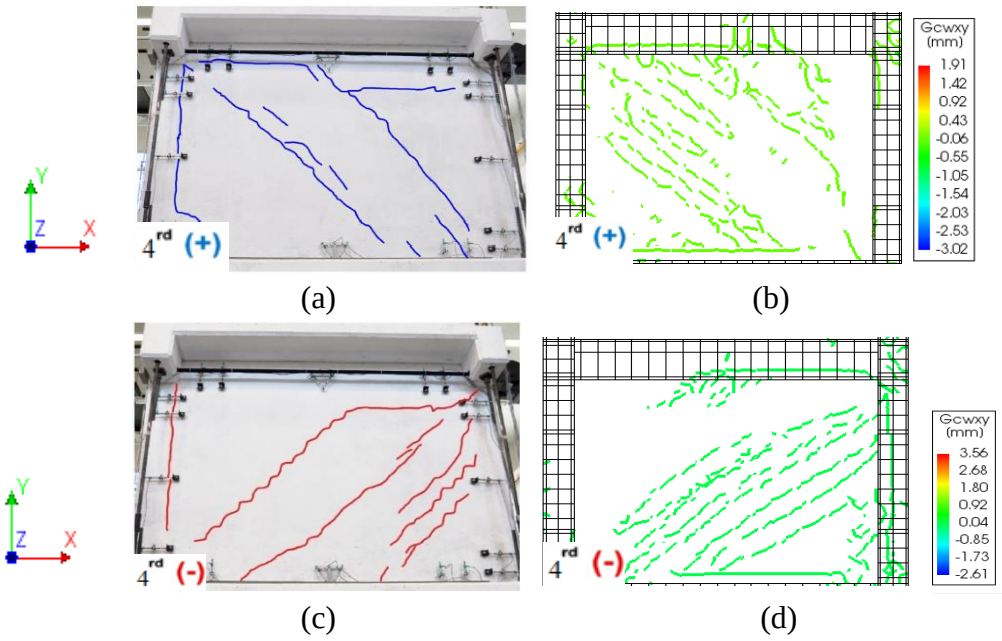

Figure 5.22: Crack propagation in the retrofitted infilled frame at the second floor during the fourth cycle of loading in the positive and negative direction of loading as occurred in the (a) experiment and (b) in the numerical model.

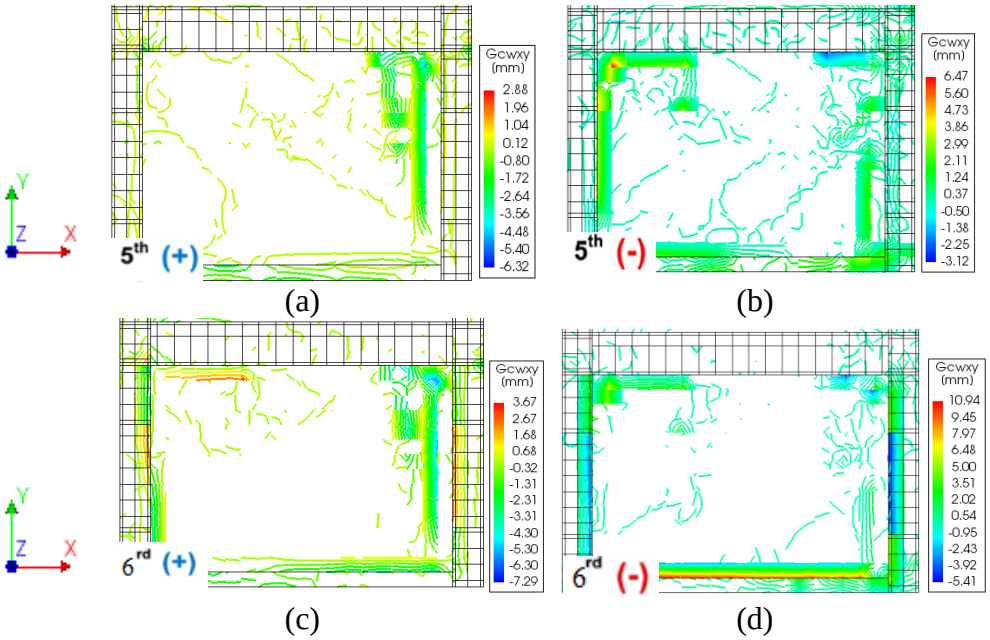

Figure 5.23: Crack propagation in the retrofitted infilled frame model at the first floor (a) during the fifth cycle of loading in the positive and (b) negative direction of loading, and (c) during the sixth cycle of loading in the positive and (d) negative direction of loading.

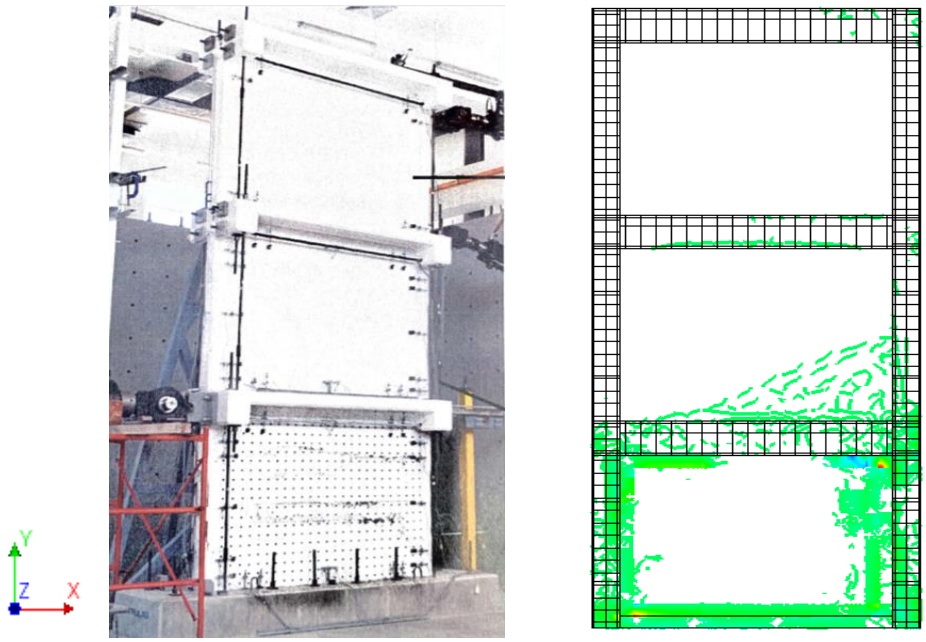

(a) (b)

Figure 5.24: Crack propagation in the three-story masonry-infilled RC frame retrofitted with TRM as occurred in the (a) experiment and (b) in the numerical model upon test completion.

From Figs. 5.21 (a) and (b), it is observed that shear cracks are developed on the external face of the TRM at the diagonal of the infill wall and at the loaded corners of the infill wall at the first story, with maximum crack width equal to 0.46 mm. Almost the same crack pattern was observed in the test specimen (maximum crack width was less than 1 mm). Upon increase of the horizontal loading (third cycle of loading), in the numerical model, the previously opened cracks reopened (along the diagonal and near the loaded corners), became wider with maximum crack width at the external face of TRM ranging from 1.20 mm to 2.1 mm (Figs. 5.21 c and d). The same crack pattern was observed in the experimental case-study during the third cycle of loading.

Comparing Fig. 5.22 (a) with Fig. 5.22 (b) it is observed that the crack pattern developed at the second floor in the retrofitted infilled frame is accurately reproduced by the numerical model during the fourth cycle of loading. More specifically, in the numerical model shear cracks are formed on the TRM at the diagonal of infill wall and close to the loaded corner of the infill wall in the same location as in the real case.

Figures 5.23 (a) and (b) show that shear cracks are developed on the external face of TRM at the diagonal of the infill wall and close to the loaded and un-loaded corners of

the infill wall with the maximum crack width ranging from 3 mm to 6.5 mm. In addition, sliding cracks on the external face of the TRM near the top of the infill-frame interface at the first floor (6.5 mm crack width) are developed accompanied by shear cracks at the ends of the columns at the first floor. During the sixth cycle of loading, the previously open cracks reopened, became wider and propagated to the frame (Figs. 5.23 c and d), where the crack width ranges from 7 mm to 10 mm near the loaded corners of the infill wall. From Fig. 5.23 it can be concluded that the maximum crack width on the external face of TRM is occurred in the area where the TRM anchors failed and in the location where the debonding of the TRM occurred in the experiment (debonding of TRM from the beam surface on the front side of the first story during the sixth cycle of loading due to fracture of the anchors at the top of the first floor). Therefore, the proposed numerical model is able to indicate the location of the main failures that occurred on the retrofitted infilled frame, such as, the debonding and rupture of TRM, and the rupture of anchors, although that in this numerical study the anchors are not modeled and the slippage and the debonding between the TRM jacket and masonry infill wall is not taken into account directly in the numerical model of the retrofitted infilled frame (there is no interface element between infill wall and TRM, sections 4.4 and 4.5).

Figure 5.25 shows the crack pattern at the first floor of the retrofitted infilled frame at the end of the experimental and numerical test. Comparing Figs. 5.25 (a) and (b) with Fig. 5.25 (c), it is observed that the crack propagation in the retrofitted infilled frame at the end of the cyclic loading is accurately reproduced by the numerical model except from the cracks formed on the external face of the TRM at the central region of the infill wall (Fig. 5.25 b) which are not so well captured by the numerical model. As shown in Fig. 5.25 (c), during the last cycle of loading, the cracks are formed on the external face of TRM close to the loaded and un-loaded corners of the infill wall, while cracks appeared and extended on the face of TRM at the bounding RC frame. This indicates the failure of the infill wall (*corner crushing*) and of the columns at the first floor, and consequently the debonding and the rupture of the TRM.

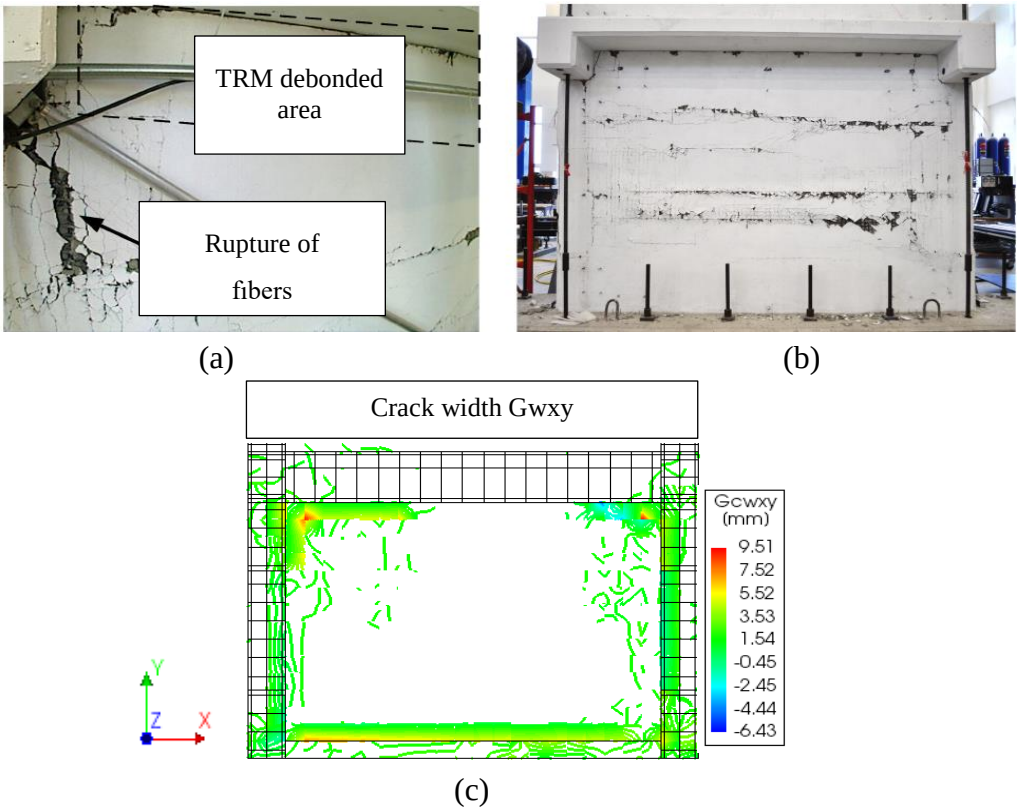

Figure 5.25: (a) Damage at the first story east-column, and (b) damage at first story of retrofitted infill wall after the end of the experimental test, and (c) crack pattern at the first floor in the retrofitted infilled frame model at the end of the test.

It is important to mention that the shear stresses and crack patterns that occurred on the external face of TRM apply also to infill wall. From Figs. 5.21-5.25 it can be concluded that the crack pattern observed in the real case as reported in Koutas et al. (2014) is well predicted by the numerical model, except for the compression failure of the infill wall at the first floor. In particular, during the last cycles of loading (Figs. 5.23 c, d, g and h–5.25), the crack pattern and the shear stress distribution on the retrofitted infilled frame model are not so speared over the external face of TRM at the central region of the infill wall at the first floor as observed in the real case. The above observation is also supported by Fig. 5.5 (c) in which the numerical models' hysteresis curve starts to deviate giving a larger stiffness compared to the experimental one during the last cycles of loading. This is due to high nonlinearities introduced in these cycles of loading. It should be noted that the inaccuracy of the numerical model to capture adequately the

real crack propagation in the retrofitted infilled frame will be explained at the end of this Chapter.

Figure 5.26 shows the gap-opening along the infill-frame interface at the first story and at bottom of the second story of the three-story masonry-infilled RC frame model with TRM during the first, third, fifth and seventh cycle of loading in the two directions of loading.

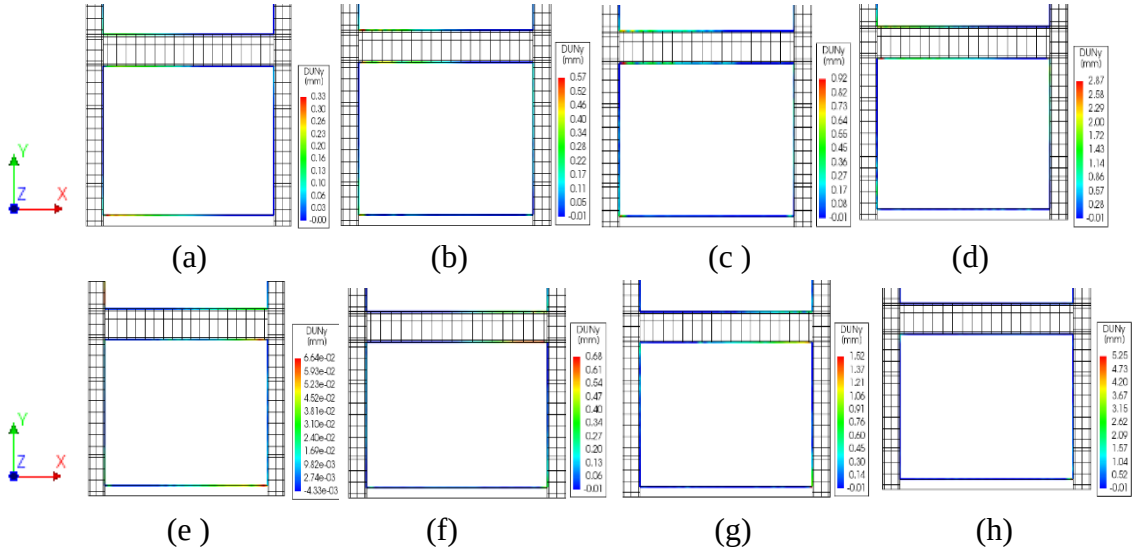

Figure 5.26: Gap-opening at the infill-frame interface at the first story and at bottom of the second story of the retrofitted model during the (a) first, (b) third (c) fifth and (d) seventh cycle of loading in the positive direction, and during the (d) first, (e) third (f) fifth and (g) seventh cycle of loading in the negative direction of loading.

During the experimental and numerical test, the infill-frame separation occurred at the very early stages of loading. Specifically, in the experiment during the first cycle of loading the average gap-opening at column-infill interface, and at top beam-infill interface at the first floor, and at the bottom beam-infill interface at the second floor was less than 0.3 mm which is the same as observed in the numerical model (Fig. 5.26 a and e). As Kouta's reported, the gap-opening between the bottom-beam and the infill wall at the first floor ranges from 0.3mm to 0.5mm during the experimental test. Almost the same gap-opening is observed in the numerical model as shown in Fig. 5.26. For the benefit of the reader, Table 5.9 shows the opening of the gap between infill wall and frame of the three-story retrofitted infilled frame, at specific locations, as measured in

the experiment and as obtained from the cyclic analysis of the retrofitted infilled frame during the third, fifth and seventh cycle of loading.

Table 5.9: Gap-opening at the infill-frame interface of the retrofitted infilled frame as obtained from the experimental test and from the numerical analysis.

	Gap-opening (mm)					
Number of Cycle	**Top beam-infill interface first floor**		**Bottom beam-infill interface second floor**		**Column-infill interface first floor**	
	Experiment	**Numerical model**	**Experiment**	**Numerical model**	**Experiment**	**Numerical model**
3	0.3-0.5	0.12.-0.3	0.3-0.5	0.12.-0.3	0.3-0.6	0.4-0.6
5	0.35-0.7	0.4-0.7	0.35-0.7	0.4-0.7	1-1.5	0.8-1.7
7	1-1.5	1 -2	1-1.5	1 -2	1.2-2	1.5-5

From Fig. 5.26 and from Table 5.9 it is observed that as the lateral displacement loading increases, the gap-opening at the infill-frame interface also increases during the experimental and numerical test, while no significant discrepancy appears between the experimental and numerical data (maximum difference equal to 1.5 mm). The difference between the experimental and the numerical results is in terms of the location that the maximum gap-opening at the infill-frame interface occurred as previously explained.

By examining the shear stress distribution, the developed crack pattern, and the infill-frame separation of the retrofitted infilled frame during the experimental and the numerical test, it is observed that the failures occur on the retrofitted infilled frame are the same with those on the unretrofitted infilled frame, but at different cycles of loading. More specifically, for both infilled frames as the lateral loading increases the failures occur in the masonry infill wall and propagate to the RC frame, while the TRM retrofitting technique contributes to delay the *corner crushing* and the *diagonal cracking* of the infill wall, and the shear failure of the column (*short-column* mechanism) at the first floor, and consequently the formation of the *soft-story mechanism.* Specifically, *diagonal cracking* and *corner crushing* failure mode are observed in the unretrofitted infilled frame during the third cycle of loading (Figs. 5.13

b and e and Fig. 5.15) while in the retrofitted infilled frame these failure modes are completed during the fifth cycle of loading (Figs. 5.20 c and g and in Figs. 5.23 a and b). Therefore, this composite material is able to sustain high compressive and tensile stresses which are transferred from infill wall to the TRM (without losing the structural integrity of the textile reinforcement), since it consists of high compressive strength mortar and high tensile strength textile. So, this retrofitting technique contributes to prevent the large shear deformation of the infilled frame when subjected to large lateral loading by transferring the shear stresses of the infill wall to the TRM layer in the local level as indicted by multi-crack pattern observed on the external face of TRM at the diagonal of the infill wall and at the opposite of the diagonal of the infill wall in Figs. 5.21-5.25. It is important to mention that the contribution of the compressive and tensile strength of the TRM to sustain the shear stresses of the infill wall, and consequently to improve the lateral response of the infilled frame will be discussed in the next Chapter. Furthermore, the TRM confinement applied at the columns cannot avoid the shear failure of the columns, but it is effective to delay this shear failure, since in the retrofitted specimen the shear failure of the columns (east-bound column at the first floor) occurs when the top-floor displacement is equal to ±70-85 mm (Fig. 5.20 d and h, Fig. 5.23 c and d and Fig. 5.25), while in the unretrofitted infilled frame during the fourth and fifth cycle of loading when the top-floor displacement is equal to ±40-55 mm (Figs. 5.13 c and f and Fig. 5.16). This indicates that the columns should be strengthened in shear along their full height. In addition, the deformed shape of the retrofitted infilled frame model (Figs. 5.20 d and h), indicates that a *soft-story mechanism* (Chapter 2 section 2.2) is developed during the seventh cycle of loading, while in the unretrofitted infilled frame this mechanism is observed during the fifth cycle of loading (Figs. 5.13 c and f). Finally, comparing Fig. 5.18 with Fig. 5.26 and comparing also Table 5.8 with Table 5.9 it can be concluded that the TRM retrofitting technique contributes to delay the infill-frame separation (the same gap-opening in the retrofitted and unretrofitted infilled frame but at different cycles of loading), but it is not able to prevent the infill-frame separation, especially during the last cycles of loading. This is attributed to the fact that during the last cycles of loading the tensile strain of the TRM composite is increased while the stress remains constant (State II).

The comparison of the experimental and numerical results indicates that the proposed numerical models proved capable of simulating the main failures that occurred on both infilled frames subjected to cyclic loading with good accuracy in terms of shear stresses, deformed shape, infill-frame separation and in terms of crack pattern. Therefore, after the validation of the numerical models developed in this study, by comparing the global and local results obtained from the numerical analysis with those obtained from the experiment, these numerical models can be used to perform numerical experiments as will be presented in the following section and in Chapters 6 and 7.

5.3 Sensitivity analyses

In this part of the thesis, numerical experiments are performed aiming to expand today's knowledge regarding the influence of the infill-frame interface on the response of masonry-infilled RC frames subjected to cyclic loading. Relevant experiments and numerical studies have been conducted so far, but they are still regarded as very limited, and consequently more research must be carried out. Towards this direction, in this section, sensitivity analyses are performed aiming to investigate the in-plane behavior of the integral and non-integral masonry-infilled RC frame under cyclic loading, and to examine the influence of the stiffness properties of the infill-frame interface (normal and tangential) on the in-plane response of the retrofitted infilled frame subjected to cyclic loading.

Over the years, significant research has been conducted aiming to examine the behavior of infilled frames under lateral loading in global sense (shear capacity, stiffness, dissipated energy, failure modes, etc.) as presented in Chapter 2 (sections 2.2 and 2.3), however, much less has been focused on the effect of the infill-frame interface (gap-opening and sliding) on the lateral response of infilled frames (Sachanski 1960; Kadir 1974; Yong 1984, Flanagan and Bennett 1999; Stylianidis 2012; Nazief 2014). Most of the studies concluded that infill wall separates from the surrounding frame at relatively low lateral displacement loading, and the failures occur and propagate eventually in either the frame or in the masonry infill wall. Recently, Teguh (2017) and Gao et al. (2018) performed cyclic test on a masonry-infilled RC frame in order to investigate the effect of the gap-opening and sliding at the infill-frame interface on the lateral behavior

of infilled frames. He concluded that the cohesion of the sliding surfaces determines the lateral load capacity of an infilled frame, since this parameter influences the activation of the sliding at the infill-frame interface. Furthermore, several researchers reported that when the infill wall is integrated into the RC frame along the structural interface (by means of bonding or by using connectors at the infill-frame interface) this leads to the elimination of the separation of the infill wall from the RC frame, and consequently, to even the prevention of the brittle failures that occur on infilled frames subjected to large lateral loads (Liauw 1979; Liauw and Kwan 1983; 1984). In the case when the infill wall and the frame are bonded together the system is called integral infilled frame, where the lateral strength and stiffness of integral infilled frames are significantly increased compared to the corresponding ones of non-integral infilled frames (Mallick and Garg 1971; Liauw 1972; Valiasis and Stylianidis 1989; Kwan and Xia 1995; Verzeletti 1996; Negro and Verzeletti 1996; Fardis and Panagiotakos 1997; Benetti et al. 1998; Lee and Woo 2002). Jiang et al. (2015) investigated experimentally the response of masonry-infilled RC frame under cyclic loading using rigid and weak connection between infill wall and RC frame. The results showed that the lateral strength, stiffness and dissipated energy of the infilled frame with rigid connection are increased significantly compared to those of the infilled frame with weak connection, while the infilled frame with flexible (weak) connection failed in between the bare frame and the infilled with rigid connection. Furthermore, researchers concluded that the lateral capacity of non-integral infilled frames is decreased significantly compared to that of integral infilled frames, especially in the case of the presence of openings on infill walls (Mallick and Garg 1971 and Benetti et al. 1998).

Reviewing the literature, it can be concluded that more experimental and numerical studies must be carried out aiming to examine the influence of the infill-frame interface on the behavior of the masonry-infilled RC frames subjected to cyclic loading. Towards this direction, the validated three-story masonry-infilled RC frame model without TRM is used to perform numerical experiments considering firstly that the infill wall is separated from the RC frame using interface elements between the infill wall and RC frame (non-integral infilled frame), which is the numerical model presented in Chapter 4, and considering secondly that the infill wall is fully bonded to RC frame, without

using any interface element between the infill wall and RC frame (integral infilled frame). The two numerical models, the non-integral infilled frame model (validated infilled frame model) and the integral infilled frame model, are subjected to five cycles of prescribed displacement loading (Chapter 4, section 4.7). The results of these numerical experiments include the base-shear versus top-floor displacement, the stiffness, and the dissipated energy of the integral and non-integral infilled frame.

Figure 5.27 shows the results obtained from non-linear cyclic analysis on the three-story integral and non-integral infilled frame in terms of base-shear versus top-floor displacement, and in terms of base-shear versus number of steps.

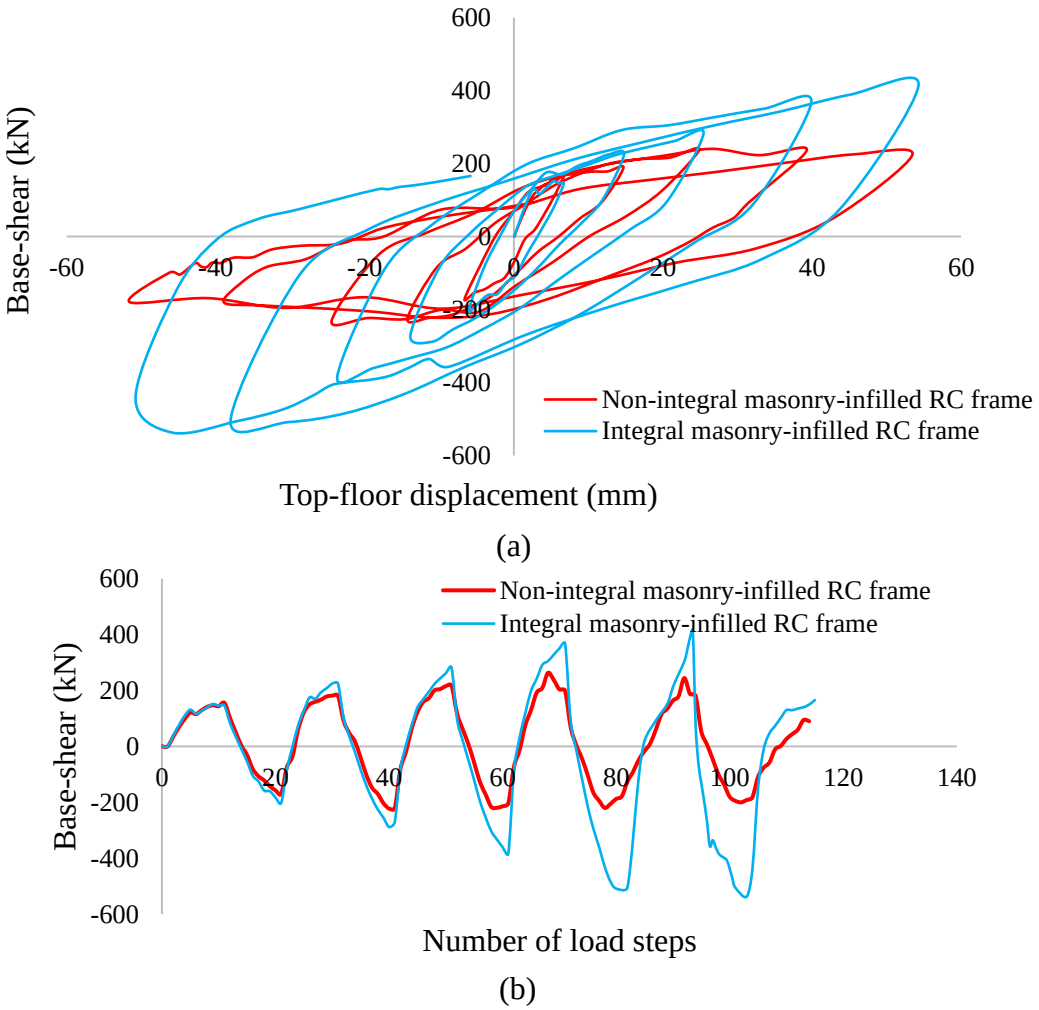

Figure 5.27: Comparison of the integral and non-integral masonry-infilled RC frame subjected to cyclic loading in terms of (a) base-shear versus top-floor displacement, and in terms of (b) base-shear versus number of load steps.

From Fig. 5.27 it is observed that the base-shear and the area enclosed by the loop in the base-shear versus the top-floor displacement diagram of the integral infilled frame are almost two times greater than the non-integral infilled frame ones. Therefore, the lateral capacity of the integral infilled frame is increased by about two times compared to that of the non-integral one.

Table 5.10 presents the comparison of integral and non-integral infilled frame in terms of the peak base-shear in each cycle of loading; for the two directions of loading, $V_{max,i}$ (positive direction of i^{th}cycle), and $V_{max,j}$ (negative direction of j^{th} cycle). Table 5.10 shows that during the first two cycles of loading the base-shear of the integral infilled frame is 20% greater compared to that of the non-integral infilled frame. As the lateral loading increases, the base-shear of the integral infilled frame is significantly increased compared to that of the non-integral infilled frame, by about 85% in the positive direction of loading and by about 145% in the negative one (fifth cycle of loading). Therefore, in the case where the infill wall is integrated to the RC frame, the base-shear of the infilled frame is significantly increased, especially during the last cycles of loading, where large lateral displacements occur.

Table 5.10: Comparison of the integral and non-integral masonry-infilled RC frame subjected to cyclic loading in terms of peak base-shear for both directions of loading.

Cycle	$\frac{\mathbf{V_{max\,i,integral}} - \mathbf{V_{max\,i,non-integral}}}{\mathbf{V_{max\,i,non-integral}}}$	$\frac{\mathbf{V_{max\,j,integral}} - \mathbf{V_{max\,j,non-integral}}}{\mathbf{V_{max\,j,non-integral}}}$
	Positive direction of loading (%)	**Negative direction of loading (%)**
1	15%	18%
2	19%	20%
3	18%	66%
4	56%	129%
5	85%	145%

Figure 5.28 shows the comparison of the integral and non-integral infilled frame subjected to cyclic loading in terms of global stiffness (Eq. 5.1) versus the number of cycle of loading, and in terms of dissipated energy (Eq. 5.2) in relation to the number of half cycle of loading. From Fig. 5.28 it is observed that the stiffness and the dissipated energy in the case of considering full bond condition at the infill-frame interface (integral) is about 20% and 25% higher, respectively, than the corresponding ones for the case where the infill wall is not fully bonded to the RC frame (non-integral) during the first two cycles of loading. As the lateral loading increases, the global stiffness and the dissipated energy of the integral infilled frame are about two times greater than the corresponding ones of the non-integral infilled frame.

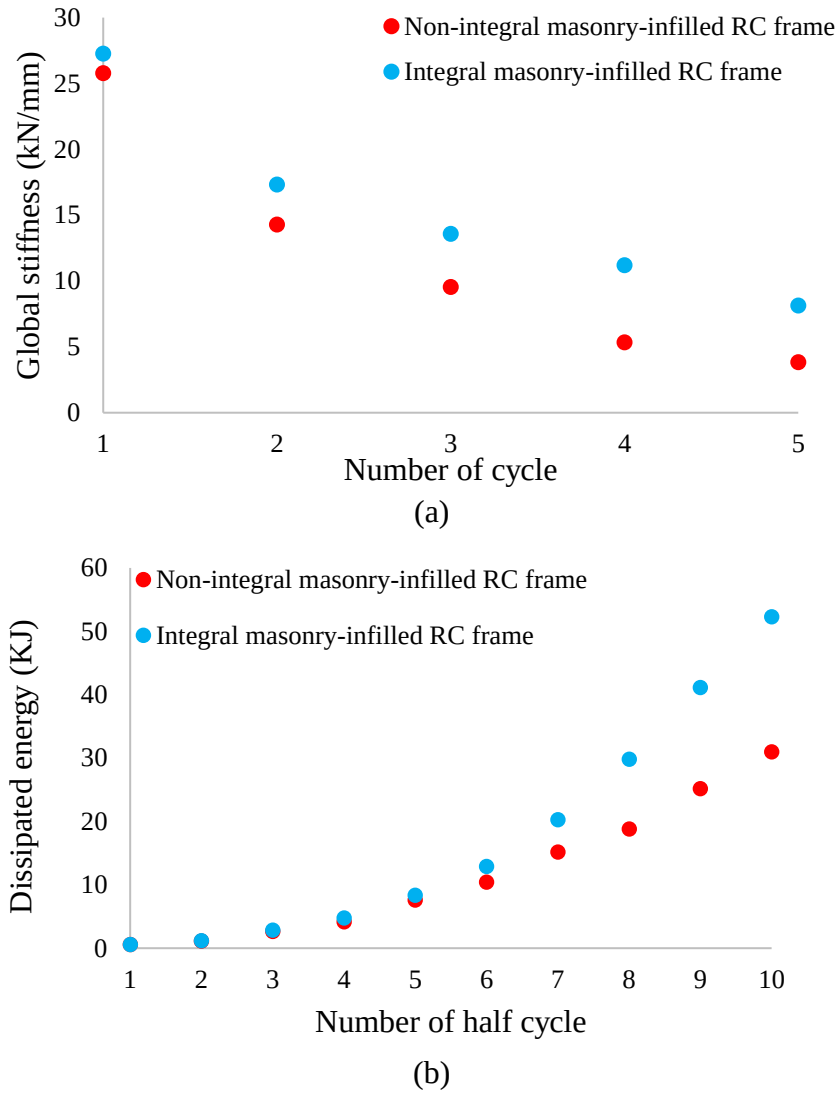

Figure 5.28: Comparison of the integral and non-integral masonry-infilled RC frame subjected to cyclic loading in terms of (a) global stiffness and in terms of (b) dissipated energy.

Based on the results obtained from the non-linear cyclic analysis of the integral and non-integral infilled frame it can be concluded that the lateral response of the masonry-infilled RC frames is improved significantly in terms of lateral strength, global stiffness and dissipated energy when the infill wall is integrated to the RC frame. Therefore, the bond conditions at the infill-frame interface, and consequently the gap-opening and the sliding at the infill-frame interface influence significantly the lateral response of infilled frames. Based on the above, in the numerical modeling of non-integral masonry-infilled RC frames, the gap-opening and the sliding that occur between the infill wall and the bounding frame must be taken into account through an interface element. Otherwise, in the case of considering full bond between the infill wall and RC frame the results obtained from the numerical analysis will overestimate the results of the real case by about two times.

After investigating the importance of the infill-frame interface element in the numerical modeling of non-integral infilled frames, sensitivity analysis through numerical experiments is then performed to examine the influence of the stiffness properties of the infill-frame interface element on the lateral response of retrofitted infilled frame model. In particular, the numerical experiments are performed using the validated infilled frame model with TRM by varying the normal and shear (tangential) stiffness of the infill-frame interface element. As mentioned in Chapter 4 (section 4.6.4), an interface gap plasticity-based model is adopted for the infill-frame interface element in this numerical study, where the normal stiffness K_n, and shear (tangential) stiffness K_t, of the infill-frame interface which are required parameters for this interface model are estimated using the Eq. 4.27 and Eq. 4.28, respectively. Following these approximations for estimating the stiffness of the infill-frame interface (required parameter for Coulomb friction model which is adopted for the infill-frame interface element), the retrofitted infilled frame model is subjected to seven cycles of prescribed displacement loading (section 4.7) considering three different sets of values for the normal stiffness K_n, and shear (tangential) stiffness K_s, of the beam-infill interface and of column-infill interface as shown in Table 5.11. The results of these numerical experiments include the base-shear versus top-floor displacement, the stiffness, the dissipated energy and the opening of the gap between the infill wall and RC frame.

Table 5.11: Summary of the infilled frame models with TRM considering different values of the normal and tangential (shear) stiffness of the infill-frame interface in x-and y-direction (beam-infill and column-infill).

Name of analysis	$\mathbf{K_n \frac{KN}{mm^3}}$	$\mathbf{K_t \frac{KN}{mm^3}}$	$\mathbf{K_n \frac{KN}{mm^3}}$	$\mathbf{K_t \frac{KN}{mm^3}}$
	Column-infill interface (y-direction)		**Beam-infill interface (x-direction)**	
Case 0(validated model)	3	0.030	6	0.06
Case 1	3	0.30	6	0.6
Case 2	30	0.30	60	0.6
Case 3	30	3	60	6

Table 5.12 shows the peak base-shear in each cycle of loading; for the two directions of loading, $V_{max,i}$ (positive direction of i^{th}cycle), and $V_{max,j}$ (negative direction of j^{th} cycle), as obtained from the non-linear cyclic analysis on masonry-infilled RC frame model with TRM by varying the normal and shear stiffness of the infill-frame interface as presented in Table 5.11.

Table 5.12: Peak base-shear for both direction of loading of the TRM-retrofitted masonry-infilled RC frame model by varying the normal and shear stiffness of the infill-frame interface.

	$V_{max,i}$ **(kN) positive direction of loading**				$V_{max,j}$ **(kN) negative direction of loading**			
Cycle	**case 0**	**case 1**	**case 2**	**case 3**	**case 0**	**case 1**	**case 2**	**case 3**
1	250.6	253.3	281.2	243.8	-227.9	-283.6	-226.4	-327.4
2	287.7	296.5	316.4	350.6	-320.5	-333.5	-372.9	-406.1
3	368.3	421.8	394.4	447.4	-427.1	-519.7	-504.8	-756.5
4	379.6	457.2	490.0	526.5	-417.8	-420.8	-509.4	-543.2
5	382.7	607.9	498.8	541.2	-384.1	-399.8	-459.5	-596.4
6	317.8	402.3	526.6	582.8	-233.9	-440.1	-466.6	-723.3
7	247.7	524.7	523.9	528.3	-239.9	-387.1	-372.5	-522.3

From Table 5.12 it is observed that the peak base-shear of the retrofitted infilled frame in Case 1 increases by about 20% until the fourth cycle of loading, while during the last cycles of loading by about 80%-100% compared to the corresponding ones of the retrofitted infilled frame in Case 0, where the tangential stiffness (K_s) of the infill-frame interface is ten times smaller than the corresponding one used in the Case 1. Furthermore, comparing the Case 2 with Case 1 (where the normal stiffness of the infill-frame interface in Case 1 is ten times higher than in Case 2) it is observed that the peak-base shear of retrofitted infilled frame increases by 10%-30% during the fifth and sixth cycle of loading (positive direction of loading). Comparing Case 3 with Case 0 (where the normal and shear stiffness of the infill-frame interface is ten and hundred times higher, respectively, than the corresponding ones used in Case 0) it can be noted that the peak base-shear of the retrofitted infilled frame during the fifth cycle of loading in the positive and negative direction of loading increases by 40% and 55%, respectively. Therefore, it can be concluded that as the normal and shear stiffness of the infill-frame interface increases (Case 2 and Case 3), the peak base-shear of the retrofitted infilled frame in each cycle of loading, for the two directions of loading, increases.

Figures 5.29 and 5.30 show the results obtained from the non-linear cyclic analyses performed on masonry-infilled RC frame model with TRM by varying the normal and shear stiffness of the infill-frame interface (Table 5.11) in terms of global stiffness, dissipated energy, and in terms of gap-opening at the infill-frame interface.

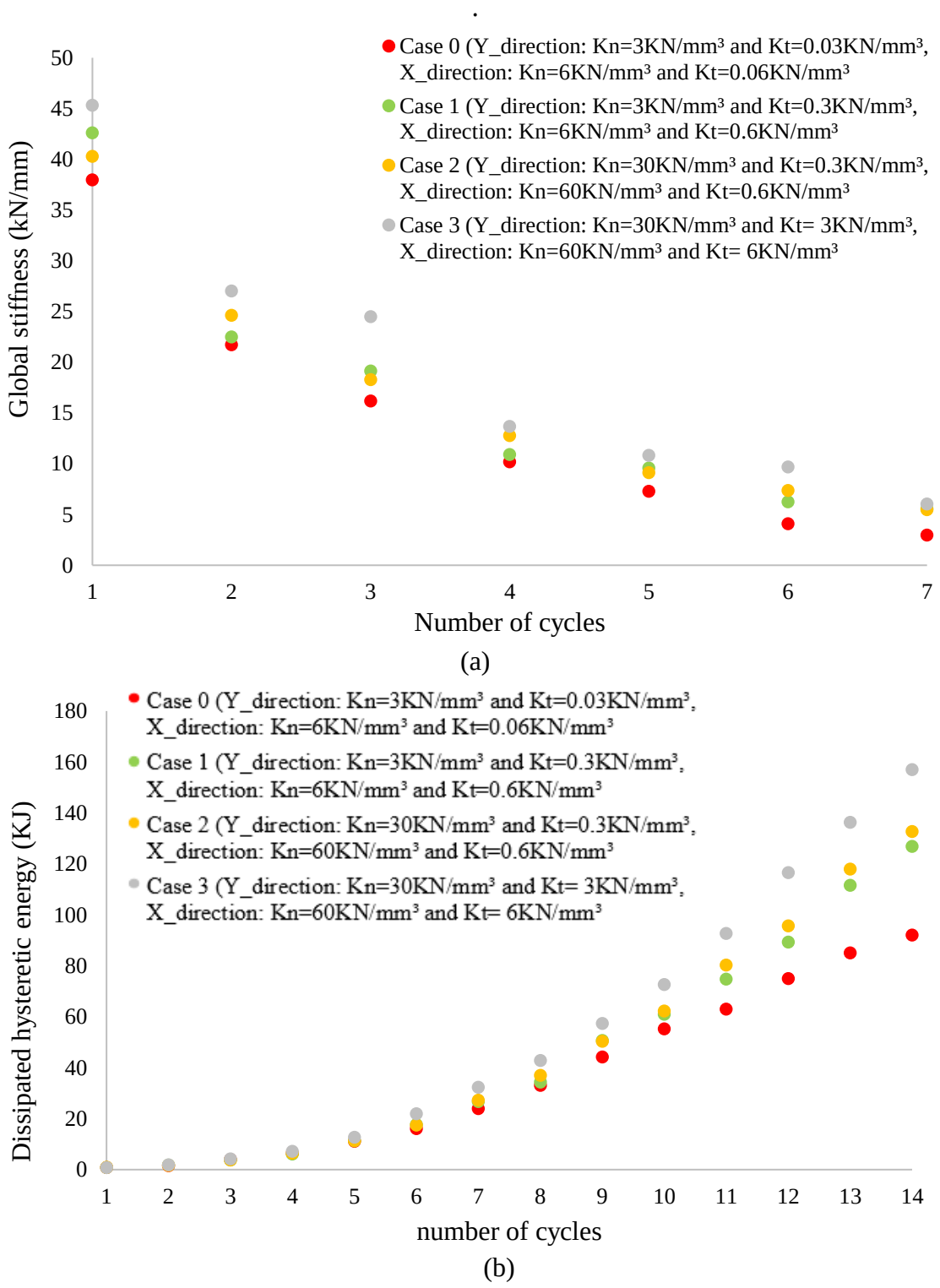

Figure 5.29: Comparison of the results obtained from the non-linear cyclic analyses on masonry-infilled RC frame model with TRM by varying the normal and shear stiffness of the beam-infill and column-infill interface in terms of (a) global stiffness per cycle and in terms of (b) dissipated hysteretic energy per half cycle.

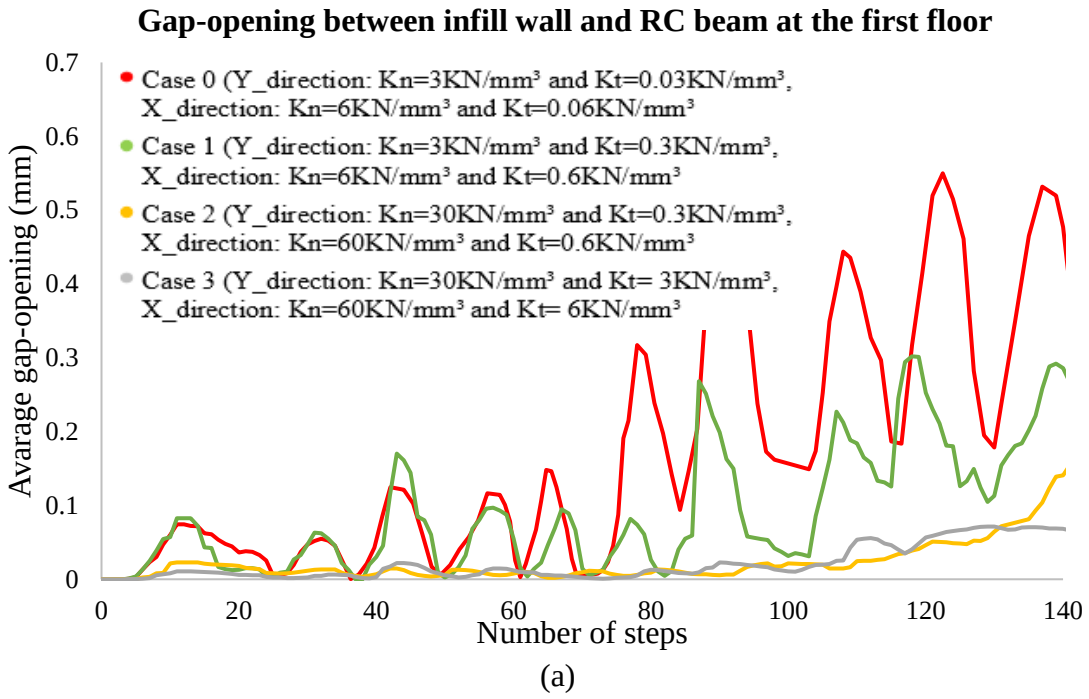

(a)

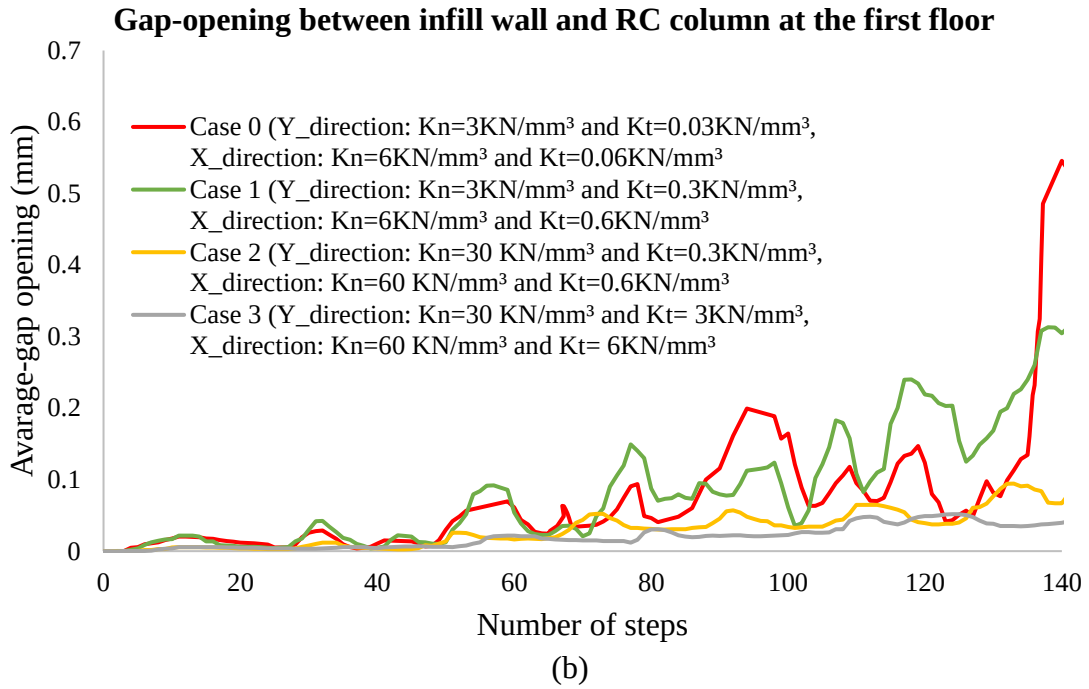

(b)

Figure 5.30: Comparison of the results obtained from the non-linear cyclic analyses on masonry-infilled RC frame model with TRM by varying the normal and shear stiffness of the beam-infill and column-infill interface in terms of gap-opening at the (a) infill-beam and (b) at infill-column interface at the first floor.

From Figs. 5.29 and 5.30, it is observed that by increasing the normal and shear (tangential) stiffness of the infill-frame interface, the average gap-opening at the infill-frame interface decreases, while the dissipated energy and the global stiffness of the retrofitted infilled frame increase. Comparing Case 1 with Case 0 (where the tangential stiffness of the infill-frame interface in Case 1 is ten times higher than in Case 0), it is observed that the gap-opening at the infill-beam interface decreases by about two times, while the stiffness and the dissipated energy of the retrofitted infilled frame increase by about 50%–87%, and 20%–40%, respectively. Furthermore, comparing Case 2 with Case 1 (where the normal stiffness of the infill-frame interface in Case 2 is ten times higher than in Case 1), the average gap-opening at the beam-infill and column-infill interface decreases by about 7–9 times, while the stiffness and the dissipated energy of the retrofitted infilled frame increase by about 5% and 10%, respectively. Comparing Case 2 and Case3 with Case 0 (where the normal and shear stiffness are ten and hundred times higher than the normal and shear stiffness used in Case 0, respectively) it is observed that the stiffness and the dissipated energy of the retrofitted infilled frame are increased by 70%–100%, and 45%–75%, respectively, in the last cycles of loading. Furthermore, as the normal and shear stiffness of the infill-frame interface increases (Case 2 and Case 3), the gap-opening tends to zero, causing almost a monolithic behavior of the masonry-infilled RC frame subjected to cyclic loading. Comparing the Case 2 with Case 3, it seems that the average gap-opening between the masonry infill and the RC frame (beam and column) is almost the same for the two cases, while the dissipated energy in Case 3 is 35% higher than in Case 2.

Based on Figs. 5.29 and 5.30 and on Table 5.12 it can be pointed out that the non-linear cyclic response of the masonry-infilled RC frame model with TRM is sensitive to the normal and shear stiffness of the infill-frame interface. These parameters are able to control the gap-opening and the sliding of adjacent elements, although they do not represent actual mechanical properties of the masonry infill wall. More specifically, if the stiffness of the infill-frame interface is too high then a small gap-opening will occur causing almost a monolithic behavior of the masonry-infilled RC frame, leading to an increase in the shear strength, global stiffness and the dissipated energy of the retrofitted infilled frame. This is supported by several past studies as mentioned in Chapter 2,

which reported that the infill-to-frame interaction depends on infill-frame relative stiffness since this relative stiffness (normal and tangential stiffness of the interface model) describes the stress deformation characteristics of the infill-frame interface (Dawe 1989, Yong 1984, Mohammed 2014, Flanagan 1999, Teguh, 2017, Stavridis et al. 2018, Dautaj et al. 2018).

5.4 Summary and conclusions

This Chapter presents the validation of the FE numerical models developed in Chapter 4 through linear static, eigenvalue, and non-linear cyclic analysis. For the validation of the three numerical models, the experimental-case study conducted by Koutas et al. (2014) is used (Chapter 4). Firstly, the eigenvalue properties of the three numerical models are compared to the corresponding experimental data. Secondly, the behavior of the numerical models under self-weight is compared to that observed in the real case. Then, the results obtained from the non-linear cyclic analysis of the unretrofitted and retrofitted masonry-infilled RC frame are compared to those obtained from the experimental case-study in global and local level. The behavior of the bare frame model under cyclic loading is also assessed based on relevant past studies. The following paragraphs summarize the main observations regarding the validation of the three numerical models. Besides the validation of the proposed numerical models, the influence of the infill walls on the lateral behavior of RC frames, and the effectiveness of using the TRM composite material for retrofitting infilled frames are discussed in the following paragraphs, as well.

It is important to mention that the results presented in this Chapter are derived by performing a lot of analyses (eigenvalue and cyclic non-linear analysis) on the bare frame model, and on the infilled frame model with and without TRM by varying some parameters for the selected material models (representing the non-linear behavior of the components of these infilled frames as presented in section 4.6) which require adjustment in order to represent the experimental results accurately, and by varying also the required parameters for the non-linear cyclic analysis until reliable results are reached.

The results obtained from the linear static analysis on the three numerical models confirm that the numerical models' behavior under self-weight load is as expected corresponding to the real observed behavior in similar structures. Furthermore, the fundamental period of the bare frame model and of the masonry-infilled RC frame model with and with TRM is compared and represented an agreed correlation to the experimental ones while the deformed shape of the three numerical models is similar to that observed in past studies.

Following the validation procedure, the results obtained from the non-linear cyclic analysis of the bare frame model in global and local level are presented and compared well with those observed in the experimental and numerical studies conducted in the past, so the bare frame model is representative of what is tested in the experiment.

The results obtained from the non-linear cyclic analysis on the unretrofitted and the retrofitted infilled frame are compared to those obtained from the experimental case-study, and they show acceptable degree of accuracy in terms of base-shear in relation to the top-floor displacement (hysteresis curves), shear capacity in each floor in relation to the load steps, height-wise distribution of the shear force, initial stiffness, stiffness degradation, and dissipated energy. The discrepancy between the experimental and numerical results for both infilled frames (unretrofitted and retrofitted) in terms of peak base-shear in each cycle of loading, and in terms of the base-shear in relation to top-floor displacement (hysteresis curve) ranges from 5% to 15%, where this difference is more pronounced during the last two cycles of loading (20%). Furthermore, after the maximum base-shear is reached in the unretrofitted and retrofitted infilled frame, the numerical models' hysteresis curve starts to deviate giving a larger stiffness compared to the experimental ones. Nevertheless, the numerical results of both infilled frames produce an acceptable envelope with the experimental ones. Also, the infilled frame model with and without TRM accurately predict the shear force at the second floor of the structure, since the discrepancy of the experimental and numerical results varies from 12% to 20%. Although the infilled frame model accurately predicts the shear force at the third floor of the structure, the retrofitted one gives comparable results with the real ones until only the fifth cycle of loading. This may depend on the cyclic loading process followed in this numerical study, since it is different from that of the

experimental case-study (section 4.8). The proposed numerical models accurately predict the height-wise distribution of the shear force until the fifth cycle of loading, which is not linearly varying for both infilled frames. Furthermore, the global stiffness of both models in each cycle of loading either is overestimated or underestimated by 12% compared to the real one, while the dissipated energy is overestimated by about 8%-12% for the first cycles of loading and for the rest of the cycles (last two) it is overestimated by about 15%-22%. This may depend on the analysis convergence and on the nonlinearities that were introduced in the last cycle of loading during the experiment (failure due to *soft-story mechanism* at the ground floor).

Furthermore, the proposed numerical models proved capable of capturing the main failures occurred on the unretrofitted and retrofitted masonry-infilled RC frame subjected to cyclic loading with good accuracy in terms of shear stresses, deformed shape, infill-frame separation and in terms of crack pattern. Firstly, the shear stress distribution on the infilled frames confirm that the infilled frame acts as a diagonal strut while the retrofitted one acts as a pair of diagonal compression and tensile tie. The crack pattern observed in the experimental specimen is accurately reproduced by the infilled frame model, where at the early stage of loading diagonal cracks develop along the diagonal of the infill wall, and as the lateral loading increases these cracks became wider, especially near the loaded corners of the infill wall, and they are propagated towards the bounding frame. Furthermore, almost the same crack patterns are observed in the experimental specimen and in the retrofitted infilled frame model, where during the early stage of the lateral loading, diagonal cracks are developed on the external face of TRM along the diagonal of the infill wall and near the loaded corners, and as the lateral loading increases shear cracks are developed at the diagonal, and close to the loaded and un-loaded corners of the infill wall (cracks are speared over the external face of TRM), and they are propagated to the bounding frame. Adding to this, sliding cracks on the external face of the TRM near the top of the infill-frame interface at the first floor are also developed, which indicates the location of the debonding and the rupture of TRM that occurred in the experiment. Furthermore, the gap-opening at the infill-frame interface of the unretrofitted and retrofitted infilled frame is well predicted by the numerical models since the difference between experimental and numerical results in

terms of gap-opening is relatively small. Considering the above, the proposed models proved capable of capturing the main failures that have occurred on the unretrofitted and retrofitted masonry-infilled RC frame which include the *corner crushing, diagonal cracking, and* the *sliding shear* of the infill wall, and the shear failure of the column (*short-column* mechanism) at the first floor, and consequently the formation of the *soft-story mechanism.* These failures occurred at different cycles of loading for the two infilled frames since the TRM contributes to delaying these failures because this composite material is able to sustain high compressive and tensile stresses which are transferred from infill wall to TRM.

Although the proposed numerical models under cyclic loading give acceptable results when compared with the experimental ones in global and local level, some deficiencies exist regarding the compression failure of the masonry infill wall at the first floor and regarding the failures that occurred in the retrofitted infilled frame, the debonding and the rupture of the TRM. These deficiencies are mainly due to the modeling procedure and assumptions followed in this study (sections 4.4 and 4.5) such as: (a) meso-modeling is used (Fig. 2.9) to simulate the masonry infill wall, and macro-level approach is used for TRM composite where the TRM is modeled as homogenized layer by continuum elements (Fig. 3.4); (b) full bond between the TRM layer with the masonry infill wall is considered; (c) the TRM anchors were not modeled; and (d) a considerable number of parameters are needed for the material models selected for simulating the non-linear behavior of the components of the infilled frames as input for a meaningful analysis. Adding to the above reasons, any finite element method always includes some degree of approximation while the simulation of this type of structure is a complex task due to the large number of parameters affecting the lateral behavior of masonry-infilled RC frames (section 2.3 and 2.4).

For the purpose of this study, the degree of accuracy of the proposed numerical models is considered acceptable, and therefore important findings can be drawn from the current study regarding the influence of the existence of infill walls in RC frames as follows:

- The fundamental period of the infilled frame decreases four times compared to that of the bare frame.

- The lateral capacity of the infilled frame is significantly higher than that of the bare frame one since the base-shear and the total dissipated energy of the infilled frame are increased by about 4-8 times compared to the corresponding ones of the bare frame. Adding to the above, the initial stiffness of the infilled frame is increased by about ten times compared to that of the bare frame, while the stiffness of the infilled frame is 2-5 times higher than that of the bare frame one during the last cycles of loading, which occurs at large lateral displacements.
- The existence of infill walls in RC frames leads to the shear failure of columns, *short-column mechanism*, especially in the case of weak RC frames and strong infills. The shear failure of the column is caused by the infill wall strut action where the high shear forces near the loaded corners of the infill wall (failure of the infill wall) are transferred to finite portions of RC columns of the frame (contact length of wall and RC columns forming a short column).

Furthermore, the following important conclusions can be also obtained from the current numerical study regarding the effectiveness of using the TRM for retrofitting three-story masonry-infilled RC frames subjected to in-plane cyclic loading as experimentally investigated by Koutas et al. (2014):

- The TRM increases the maximum base-shear, the stiffness, and the dissipated energy of the three-story infilled frame by about 60%-70%.
- The selected TRM retrofitting scheme applied on the three-story masonry-infilled RC frame (two layer of TRM at the first floor and one-layer TRM at the second and third floor) slightly improves the height-wise distribution of shear force, while in general the shear forces are not linearly varying along the height of the structure.
- The TRM strengthening technique delays the main failures that occurred in the three-story infilled frame such as the *corner crushing, diagonal cracking,* and the shear failure of the column (*short-column* mechanism) at the first floor, and consequently, the formation of the *soft-story mechanism*. This is attributed to the fact that this composite material is able to sustain the high compressive and tensile stresses which are transferred from infill wall to the TRM (without losing the structural integrity of the textile reinforcement), due to its high compressive

and tensile capacity (consists of high compressive and tensile strength mortar and high tensile strength textile).

- The TRM delays the infill-frame separation, but it is not able to avoid or eliminate it, since under large displacements the tensile strain of the TRM composite is increased while its stress remains constant (State II).
- The TRM confinement used at the ends of the first and second story columns successfully prevents the shear failure at the top of the east-bound column at the first story which occurred in the unretrofitted infilled frame at an early stage of lateral loading, but it cannot prevent it under large lateral loading. Therefore, the columns should be strengthened in shear along their full height.

After the assessment of the numerical models developed in this study, the validated three-story masonry infilled frame with and without TRM are then used to perform sensitivity analyses in order to investigate the influence of the infill-frame interface on the lateral response of infilled frames. The numerical results showed that the lateral capacity of the three-story integral infilled frame is higher, about two times, than the corresponding one of the non-integral infilled frame. Furthermore, it is pointed out that the infilled frames retrofitted with TRM are sensitive to the normal and shear (tangential) stiffness of the infill-frame interface. More specifically, if the stiffness of the infill-frame interface is too high then a small gap-opening will occur causing almost a monolithic behavior of the three-story masonry-infilled RC frame with TRM subjected to cyclic loading leading to an increase in the shear capacity, global stiffness and the dissipated energy of the structure. Although these parameters do not represent actual mechanical properties of the masonry infill wall, they are required parameters for simulating the interface between masonry infill and RC frame because they control the gap-opening and the sliding of adjacent elements in the model.

Findings of this part of the thesis sufficiently demonstrate that the adopted modeling procedure including the element types, the material models selected for simulating the non-linear behavior of the components of the infilled frames, the type of constrains, and the loading scheme as presented in Chapter 4 can adequately represent the behavior of the masonry-infilled frame with and without TRM under cyclic loading at global and local level. For the purpose of this study, the degree of approximation of the proposed

modeling approach is considered acceptable, since the discrepancy between the experimental and numerical results is relatively small without any large computational cost. Hence, the validated numerical models can be used to perform parametric studies, through numerical experiments, in order to investigate numerically: (a) the critical parameters that influence the effectiveness of using the TRM composite material for retrofitting infilled frames, (b) the effect of a central opening on the lateral response of masonry-infilled RC frames, and (c) the effectiveness of using the TRM for retrofitting masonry-infilled RC frames with central openings. These will be presented in Chapters 6 and 7.

CHAPTER 6

6. EFFECT OF THE TRM REINFORCEMENT RATIO AND OF THE TYPE OF MORTAR USED FOR BINDING THE TEXTILE ON THE LATERAL RESPONSE OF MASONRY-INFILLED RC FRAMES RETROFITTED WITH TRM SUBJECTED TO CYCLIC LOADING

6.1 Introduction

In this part of the thesis an effort has been made to expand today's knowledge regarding the use of TRM as a method for retrofitting masonry-infilled RC frames since it is a relatively new concept (proved by the reduced number of relevant studies as reported in Chapter 2, Fig. 2.17), and therefore, a deeper investigation is required. To achieve this, numerical experiments are performed, using the validated model, aiming to examine the parameters that can influence the response of masonry-infilled RC frames retrofitted with TRM under cyclic loading such as: the TRM reinforcement ratio and the type of mortar used for binding the textile reinforcement.

Reviewing the literature as presented in Chapter 2 (section 2.5), it can be concluded that the TRM contributes to increase significantly the lateral capacity of infilled frames subjected to large lateral loading by preventing its large shear deformation since the high shear stresses of the infill wall are transferred to the TRM layer in the local level, where this composite material is able to sustain these shear stresses due to its high compressive and tensile capacity. It is worth mentioning that the tensile capacity of TRM is influenced by several parameters, and amongst them, is the type of inorganic-matrix used for binding the textile reinforcement and the textile reinforcement ratio, as presented in detail in Chapter 3 (sections 3.2, and 3.5). This is attributed to the fact that these parameters can control the bond strength (adhesion properties) between textile

reinforcement and matrix, and consequently they are able to determine whether the failure of the TRM will occur (rupture of TRM, debonding and slippage of the textile from the matrix). By increasing the reinforcement ratio of the composite material, the tensile capacity of the TRM at State I and II increases but not proportionally, while the distance between the cracks decreases. Furthermore, by increasing the tensile strength of the matrix used for binding the textile reinforcement (using sand with small grain size, adding polymers, resins, and adding short fibers of steel, glass, or carbon), the tensile capacity of the TRM at State I and II increases, while by increasing the modulus of elasticity of the matrix, the strain of the composite at State I and II decreases.

Furthermore, reviewing the literature, it can be pointed out that the effectiveness of using the TRM composite material for retrofitting masonry walls and masonry-infilled RC frames depends on several factors, as described extensively in Chapter 2 (section 2.5), and amongst them is the TRM reinforcement ratio, and the type of matrix used for binding the textile reinforcement. The following conclusions are summarized below regarding the influence of these parameters on the lateral response of masonry walls and infilled frames: (1) the load-carrying capacity, the lateral strength and stiffness, and the dissipated energy of TRM-retrofitted masonry walls or masonry-infilled frames are increased by increasing the reinforcement ratio, but not proportionally, due to different failure mechanisms that may develop when the number of layers increases, (2) the type of mortar used for binding the textile reinforcement influences the lateral capacity of the retrofitted masonry walls, since the type of the mortar is able to control the rupture of TRM, the slippage of textile from the mortar and the debonding (delamination) of TRM from the masonry wall surface, (3) the lateral capacity of the retrofitted masonry walls is usually higher if the spacing between the yarns in the textile is small but such that it allows the mortar to pass and correctly bonded to the wall surface.

The above findings are obtained from the past experimental and numerical studies aiming to investigate the effectiveness of using the TRM for retrofitting masonry walls and one-story masonry-infilled RC frames subjected to monotonic lateral loading (sections 2.5.2 and 2.5.3). None of either experimental or numerical studies were geared towards the influence of the TRM reinforcement ratio and type of the mortar used for binding the textile reinforcement on the response of multi-story masonry-infilled RC

frames retrofitted with TRM subjected to cyclic loading. One way of closing this gap of knowledge is to investigate numerically the influence of these parameters on the behavior of three-story infilled frames retrofitted with TRM under cyclic loading.

Towards this direction, in this part of the thesis, the validated three-story masonry-infilled RC frame model with TRM is used to perform a parametric study through numerical experiments to quantify the influence of TRM reinforcement ratio on the response of the retrofitted three-story masonry-infilled RC frame subjected to cyclic loading, by means of using a different number of TRM layers and different geometry of textile reinforcement on each floor of the TRM-retrofitted three-story masonry-infilled RC frame, (section 6.2), and to investigate the effect of using different types of cement-based mortars for binding the textile reinforcement (section 6.3) on the response of the TRM-retrofitted three-story masonry-infilled RC frame subjected to cyclic loading. The main conclusions obtained from these numerical experiments are summarized at the end this Chapter (section 6.3).

6.2 Effect of the TRM reinforcement ratio on the lateral response of the three-story masonry-infilled RC frame retrofitted with TRM.

In this section, the influence of the TRM reinforcement ratio, by means of using different number of TRM layers and different geometry of textile (spacing between the yarns in the textile) on each floor of the TRM-retrofitted three-story masonry-infilled RC frame, on the response of the three-story masonry-infilled RC frame retrofitted with TRM under cyclic loading is investigated through numerical experiments as shown in Table 6.1. The numerical specimens were developed following the same modeling scheme with the validated numerical model (Chapter 4) and using the proposed analytical model of TRM for predicting the tensile behavior of TRM (Chapter 3) as will be described later.

The notation of the model specimen is L or (D) F_ number S_ number, where: the L and D denotes the mesh opening (spacing between the yarns) equal to 21mm and 11mm, respectively; the second letter denotes the floor of the three-story infilled frame: F (first floor) and S (second floor); and the number represents the number of layers of the TRM

(1, 2 and 3 TRM-layers). The thickness and reinforcement ratio of one, two and three layers of TRM with 21mm spacing between the yarns in the textile (mesh opening), and that of three-layers of TRM with 11 mm mesh opening are given in Table 6.2. The validated infilled frame model with TRM is considered as a reference case for this study as shown in Table 6.1. Furthermore, for all the numerical specimens in this parametric study (including the reference case), carbon-TRM is used at the ends of columns on the first (three layers) and second (two layers) stories as described in Chapter 4 (section 4.5).

Table 6.1: Summary of the numerical specimens of three-story masonry-infilled RC frame with TRM by varying the TRM reinforcement ratio in each floor of the structure.

Specimen name	First floor	Second floor	Third floor
Reference	Two layers of glass-TRM	One layer of glass-TRM	One layer of glass-TRM
LF1S1	One layer of glass-TRM	One layer of glass-TRM	No strengthening
LF2S1	Two layers of glass-TRM	One layer of glass-TRM	No strengthening
LF2S2	Two layers of glass-TRM	Two layers of glass-TRM	No strengthening
LF3S1	Three layers of glass-TRM	One layer of glass-TRM	No strengthening
DF3S1	Three layers of glass-TRM TRM (11mm spacing between the yarns of the textile mesh)	One layer of glass-TRM	No strengthening

Table 6.2: Thickness and reinforcement ratio of one, two and three layers of glass-TRM.

	Thickness (mm)	Reinforcement ratio (%)
One layer of glass-TRM	7.5	0.86
Two layers of glass-TRM	12.5	1.3
Three layers of glass-TRM	17.5	1.6
Three layers of glass-TRM (11mm mesh opening)	17.5	3.2

Although that the numerical specimens for this parametric study are developed following the same modeling scheme with the validated numerical model, in order to take into

account in these numerical specimens the different reinforcement ratio and the different geometry of the textile on the TRM considered in this parametric study, the required parameters for the TRM material model (Total Strain Crack material model) used for describing the non-linear cyclic behavior of TRM composite material need to be defined. More specifically, the required parameters of this material model are defined from the glass-TRM coupon tests conducted by Koutas et al. (2014) for the case of one and two layers of glass-TRM (Table 4.3), and from the proposed analytical model of TRM as presented in Chapter 3, able to predict the tensile behavior of TRM in terms of stress-strain for the case of the three layers of glass-TRM with 11 mm and 21mm mesh opening (a detailed example for applying the proposed model is presented in Appendix I). So, the required parameters in order to specify the TRM material model in DIANA FEA for simulating the tensile behavior of the three layers of glass-TRM with 21 mm and 11 mm mesh opening are defined from the salient points of the stress-strain curves as presented in Fig. 6.1, while the required parameters for the compressive behavior are obtained from Table 4.3 (section 4.6.1.2).

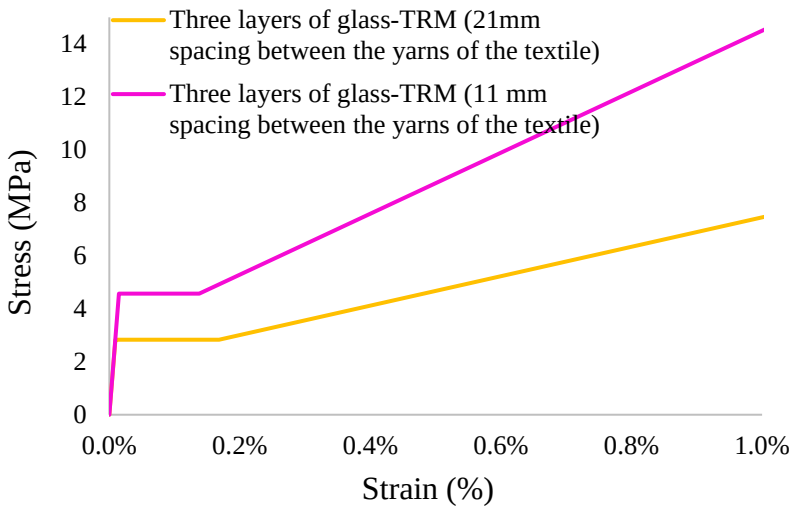

Figure 6.1: Tensile behavior of three-layers of glass-TRM with 21mm and 11mm mesh opening in terms of stress-strain as obtained from the proposed analytical model of TRM.

After defining the required parameters of the TRM material model in DIANA FEA, the developed numerical models for the purpose of this parametric study are subjected to seven cycles of displacement loading (Fig. 4.21). The results obtained from the numerical experiments performed in this part of the thesis are presented in the following

paragraphs in terms of base-shear versus top-floor displacement, shear capacity at each floor, stiffness, dissipated energy, and in terms of height-wise distribution of the shear force of the retrofitted infilled frames during the cyclic loading.

The results obtained from the non-linear cyclic analysis of the reference specimen, and of the LF2S1 specimen are presented in Fig. 6.2 in terms of base-shear versus top-floor displacement and in terms of base-shear versus the number of load steps, and in Fig. 6.3 in terms of height-wise distribution of the shear force (peak shear force at each cycle of loading at each floor) during the second and third cycle of loading.

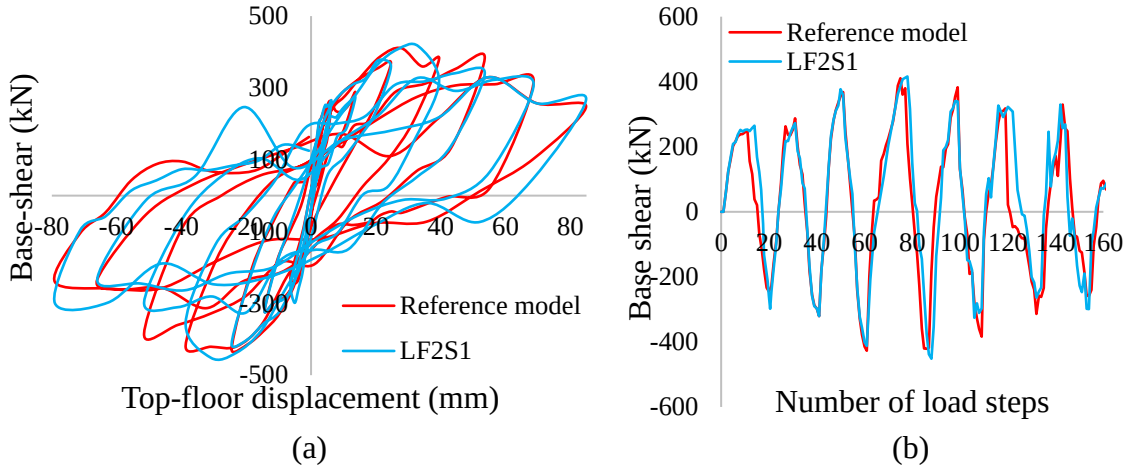

Figure 6.2: Comparison of the reference specimen and of the LF2S1 specimen in terms of (a) base-shear versus top-floor displacement and (b) base-shear in relation to the load steps.

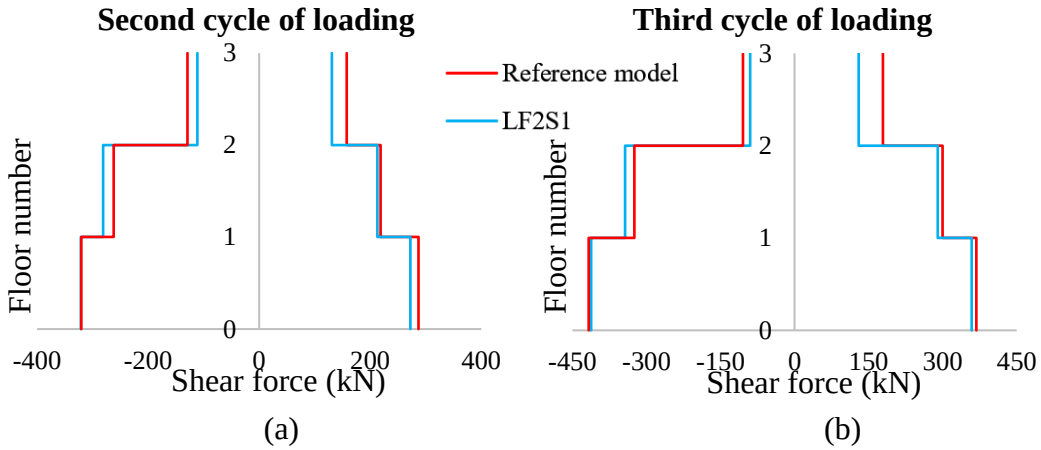

Figure 6.3: Comparison of the reference specimen and of the LF2S1 specimen in terms of the height-wise distribution of the shear force during the (a) second and (b) third cycle of loading.

The results of the two cases, reference specimen and LF2S1specimen, as illustrated in Fig. 6.2, show that there is no significant difference between them during each cycle of loading, while a small decrease (with an average percentage equal to 5%) in the base-shear of the LF2S1 specimen in each load step (Fig. 6.2 b) is observed compared to that of the reference specimen. From Fig. 6.3 it is observed that the shear force at the third floor of the LF2S1 specimen is quite smaller than the corresponding one of the reference specimen, but this does not affect considerably the distribution of the shear force along the height of the structure. Therefore, the use of TRM at the third floor of the three-story infilled frame retrofitted with two layers of TRM at the first floor and one layer of TRM at the second floor, does not provide any gain to the lateral capacity of the retrofitted structure. Based on this, in the following numerical specimens, LF1S1, LF2S1, LF2S2, LF3S1, and DF2S1, their third floor is not retrofitted.

Figure 6.4 presents the comparison of the results obtained from the non-linear cyclic analysis of the LF2S1 specimen and of the LF1S1 specimen in terms of base-shear versus top-floor displacement. For the benefit of the reader, Table 6.3 shows the peak base-shear in each cycle of loading; for the two directions of loading, $V_{max,i}$ (positive direction of i^{th}cycle) and $V_{max,j}$ (negative direction of j^{th} cycle), of the LF2S1 and LF1S1 specimen, and the difference between them, as well.

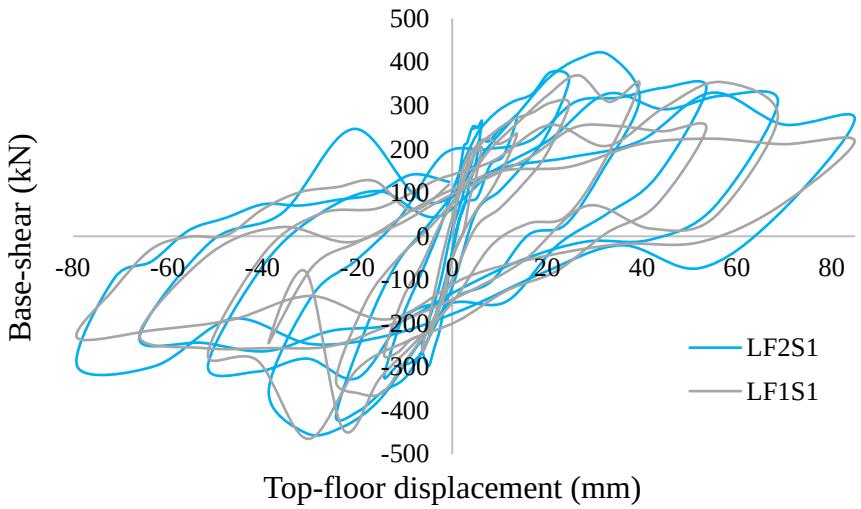

Figure 6.4: Comparison of the LF1S1 specimen and of the LF2S1 specimen in terms of base-shear versus top-floor displacement.

Table 6.3: Peak base-shear for both directions of loading of the LF2S1 and LF1S1 specimen and the difference between them.

	$V_{max,i}$ **Positive direction of loading**			$V_{max,j}$ **Negative direction of loading**		
Cycle	$V_{max,i}$ **(kN) LF2S1**	$V_{max,i}$ **(kN) LF1S1**	$\frac{V_{max\,i_{LF2S1}} - V_{max\,i_{LF1S1}}}{V_{max\,i_{LF1S1}}}$	$V_{max,j}$ **(kN) LF2S1**	$V_{max,j}$ **(kN) LF1S1**	$\frac{V_{max\,j_{LF2S1}} - V_{max\,j_{LF1S1}}}{V_{max\,j_{LF1S1}}}$
1	264.9	204.0	30%	-245.2	-241.9	1%
2	272.4	233.2	17%	-321.0	-271.2	18%
3	358.9	302.4	19%	-412.5	-328.4	26%
4	416.1	350.2	19%	-410.5	-245.6	67%
5	339.8	248.8	37%	-310	-270.6	15%
6	308.4	274.4	12%	-233.1	-225.6	3%
7	268.8	217.6	24%	-299.2	-233.4	28%

Comparing the results of the two specimens, it is observed that the lateral capacity of LF2S1 specimen is increased by about 30% compared to that of LF1S1 specimen. Figure 6.4 clearly indicates that the area enclosed by the loop in the base-shear versus top-floor displacement diagram in each cycle of loading of the LF2S1 specimen is increased compared to that of LF1S1 specimen. Adding to this, the peak base-shear of LF2S1 specimen is increased by about 12%-37% during the positive direction of cyclic loading compared to that of the LF1S1 specimen. Therefore, it is important to apply more than one layer of TRM at the first floor and one layer of TRM at the second floor in a three-story masonry-infilled RC frame, in order to increase its lateral capacity and to delay or even prevent the brittle failures at the first floor which lead to the development of a *soft-story mechanism.*

Furthermore, the lateral response of the three-story masonry-infilled frame retrofitted with two layers of TRM at the first and second floor subjected to cyclic loading is investigated (LF2S2), as well (Figs. 6.5 and 6.6). From Figs. 6.5 and 6.6 it is observed that there is no significant difference between the lateral capacity of the LF2S2 specimen with that of the LF2S1 one, despite the fact that in the LF2S2 specimen a double layer of TRM is used at the second floor. From Fig. 6.5 (b) it is observed that the

base-shear in each load step of the LF2S2 specimen is slightly greater compared to that of the LF2S1 one (with an average percentage equal to 10%). Additionally, Fig. 6.6 shows that the shear force at the second floor of the LF2S2 specimen is increased by about 10%-12% compared to that of the LF2S1 specimen. Therefore, the lateral capacity of the three-story infilled frame retrofitted with two layers of TRM at the first and second floor increases by about 12% compared to the case of using one layer of TRM at the second floor, while the distribution of the shear force along the height of the structure is not changed significantly.

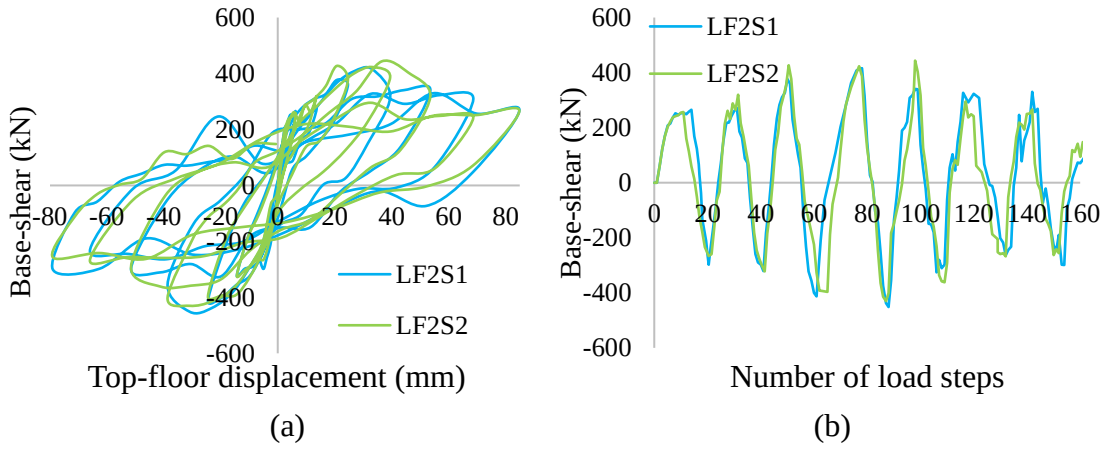

Figure 6.5: Comparison of the LF2S1 specimen and of the LF2S2 specimen in terms of (a) base-shear versus top-floor displacement, and in terms of (b) base-shear in relation to the load steps.

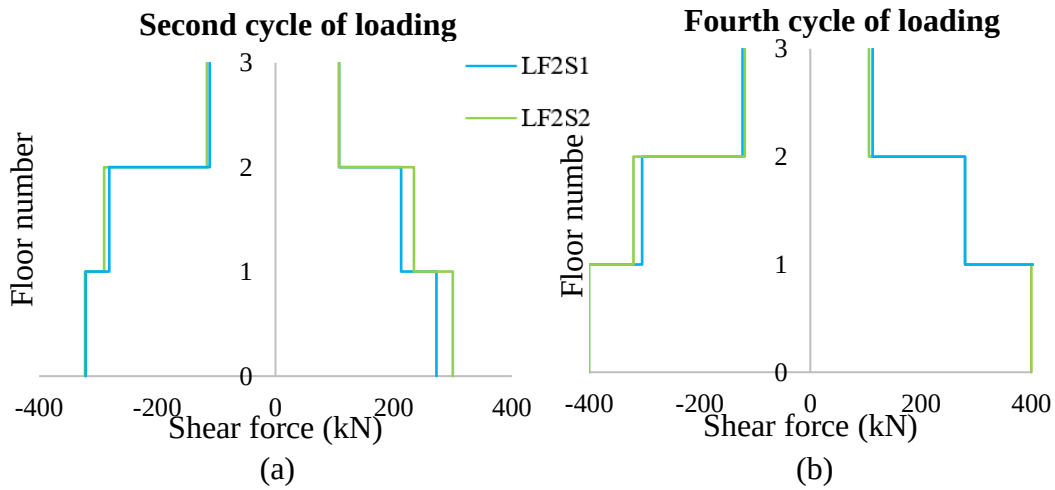

Figure 6.6: Comparison of the LF2S1 specimen and of the LF2S2 specimen in terms height-wise distribution of the shear force during the (a) second and (b) fourth cycle of loading.

Figure 6.7 presents the base-shear versus top-floor displacement of the three-story masonry-infilled frame specimen considering one layer of TRM at the second floor, and two and three layers of TRM at the first floor with 21mm and 11 mm spacing between the yarns of the textile (LF2S1, LF3S1 and DF3S1). Furthermore, Table 6.4 shows the peak base-shear in each cycle of loading; for the two directions of loading, $V_{max,i}$ (positive direction of i^{th}cycle) and $V_{max,j}$ (negative direction of j^{th} cycle), of the three above-mentioned specimens (LF2S1, LF3S1 and DF3S1).

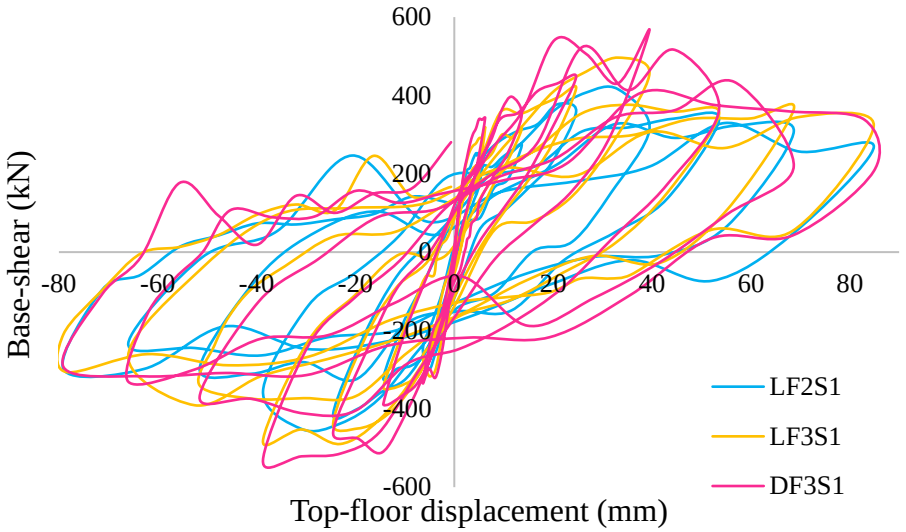

Figure 6.7: Comparison of the LF2S1, LF3S2 and DF3S1 specimen in terms of base-shear versus top-floor displacement.

Table 6.4: Peak base-shear force for both directions of loading of the LF2S1, LF3S1, and DF3S1 specimens.

	$V_{max,i}$ (kN) Positive direction of loading			**$V_{max,j}$ (kN) Negative direction of loading**		
Cycle	**LF2S1**	**LF3S1**	**DF3S1**	**LF2S1**	**LF3S1**	**DF3S1**
1	264.9	316.6	342.8	-245.2	-265.1	-332.5
2	272.4	314.2	350.2	-321.0	-344.3	-387.4
3	358.9	417.7	446.9	-412.5	-437.4	-459.4
4	416.1	455.7	505.3	-410.5	-481.5	-531.0
5	339.8	353.9	367.5	-310.2	-340.3	-369.6
6	308.4	364.6	434.5	-233.1	-264.0	-330.5
7	268.8	322.7	338.0	-299.2	-306.0	-317.2

From Fig. 6.7 and Table 6.4 it is observed that the base-shear in each cycle of loading and the area enclosed by the loop in the base-shear versus top-floor displacement diagram of the LF3S1 and DF3S1 specimen are significantly increased compared to the corresponding ones of the LF2S1 specimen. Especially, for the LF3S1 and DF3S1 specimen the maximum base-shear is about ±450MPa and ±500MPa, respectively, while for the LF2S1 specimen is about ±400MPa during the fourth cycle of loading for both directions of loading. Tables 6.5 and 6.6 show the increase on the peak base-shear in each cycle of loading and unloading of the three-story infilled frame retrofitted with one layer of TRM at the second floor, and three-layers of TRM at the first floor (LF3S1 and DF3S1) compared to the case of using two layers of TRM at the first floor and one layer of TRM at the second floor (LF2S1). The average increase in the peak base-shear during the cyclic loading is equal to 15% for the LF3S1 specimen and 25% for the DF3S1 specimen. This increase is not proportional to that of the TRM reinforcement ratio, since using double amount of TRM reinforcement ratio, for example comparing the LF2S1 specimen with DF3S1 specimen (reinforcement ratio for three layer of TRM with 11mm mesh opening is equal to 3.2% and for two layers is equal to 1.3%), does not provide double shear capacity of the retrofitted infilled frame.

Table 6.5: Comparison of the LF3S1 and DF3S1 specimen with the LF2S1 specimen, and the comparison of the DF3S1 specimen with the LF3S1specimen in terms of peak base-shear in each cycle of loading for the positive direction of loading.

Cycle	$\frac{V_{max\,i_{LF3S1}} - V_{max\,i_{LF2S1}}}{V_{max\,i_{LF2S1}}}$	$\frac{V_{max\,i_{DF3S1}} - V_{max\,i_{LF2S1}}}{V_{max\,i_{LF2S1}}}$	$\frac{V_{max\,i_{DF3S1}} - V_{max\,i_{LF3S1}}}{V_{max\,i_{LF3S1}}}$
1	20%	29%	8%
2	15%	29%	11%
3	16%	25%	7%
4	9%	21%	10%
5	4%	8%	4%
6	18%	41%	19%
7	20%	26%	5%

Table 6.6: Comparison of the LF3S1 and DF3S1 specimen with the LF2S1 specimen, and the comparison of the DF3S1 specimen with the LF3S1specimen in terms of peak base-shear in each cycle of loading for the negative direction of loading.

Cycle	$\frac{V_{max}J_{LF3S1} - V_{max}J_{LF2S1}}{V_{max}J_{LF2S1}}$	$\frac{V_{max}J_{DF3S1} - V_{max}J_{LF2S1}}{V_{max}J_{LF2S1}}$	$\frac{V_{max}J_{DF3S1} - V_{max}J_{LF3S1}}{V_{max}J_{LF3S1}}$
1	8%	36%	25%
2	7%	21%	13%
3	6%	11%	5%
4	17%	29%	10%
5	9%	19%	9%
6	13%	42%	25%
7	2%	6%	4%

Figures 6.7 and 6.8 show the comparison of the height-wise distribution of the shear force of the LF3S1 and DF3S1 specimen with that of LF2S1 specimen. From these figures it is observed that the height-wise distribution of the shear force of the three-story infilled frames retrofitted with three layers of TRM at the first floor and one layer of TRM at the second floor (LF3S1 and DF3S1) is almost linearly varying until the fourth cycle of loading (maximum base-shear). After the fourth cycle of loading, the shear forces are not linearly varying along the height of the LF3S1 and DF3S1 specimen, but they are slightly better distributed than the LF2S1 specimen. Therefore, using three layers of TRM at the first floor of the three-story masonry-infilled RC frame instead of two is not adequate to avoid the damages on the first floor during the last cycles of loading, but it is effective for delaying or even preventing some failures (such as the formation of a soft-story at the first floor in early lateral loading).

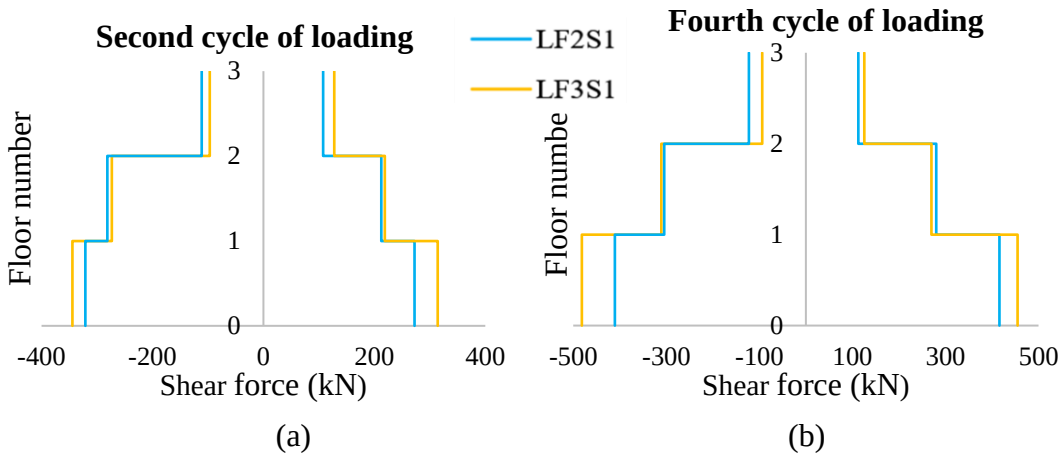

Figure 6.8: Comparison of the LF2S1 specimen and of LF3S1 specimen in terms height-wise distribution of the shear force during the (a) second and (b) fourth cycle of loading.

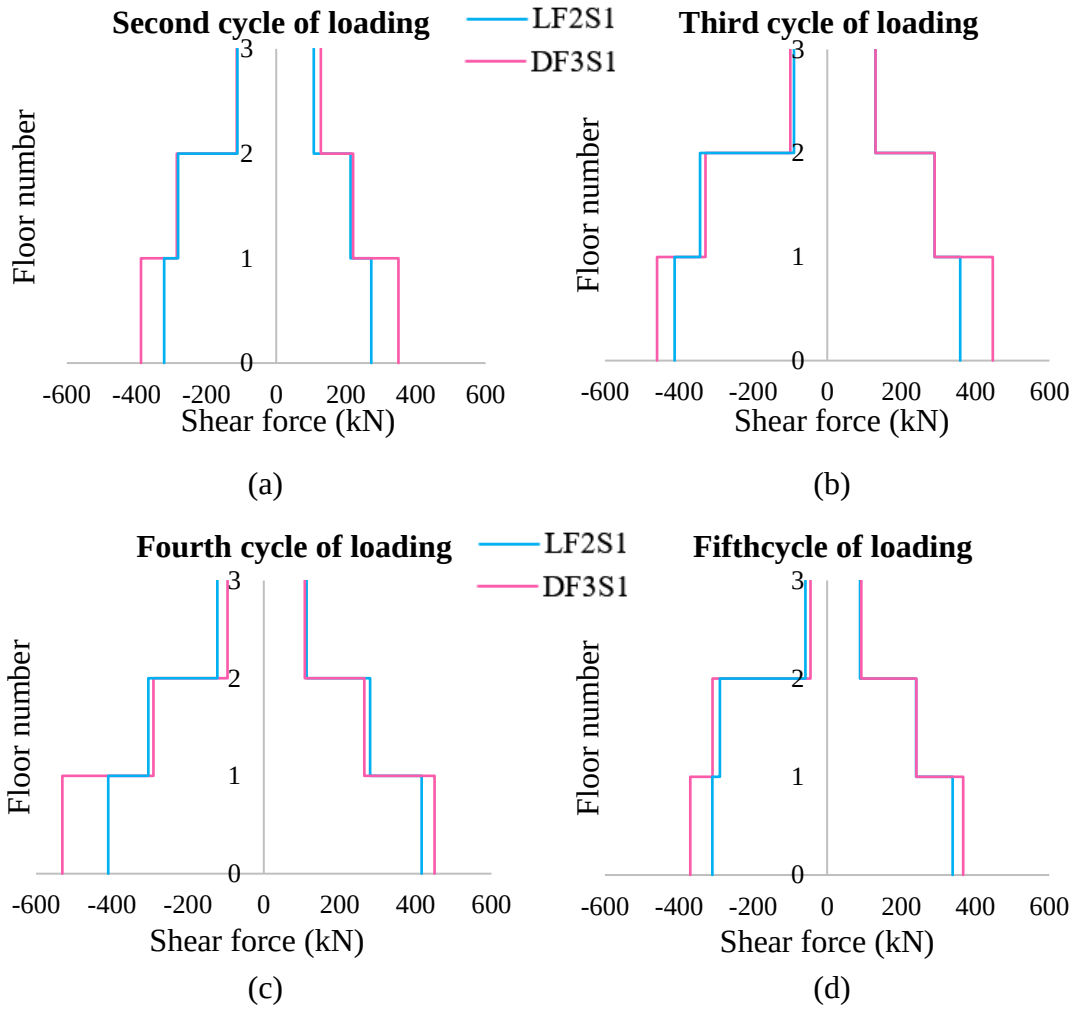

Figure 6.9: Comparison of the LF2S1 specimen and of DF3S1 specimen in terms height-wise distribution of the shear force during the (a) second, (b) third, (c) fourth and (d) fifth cycle of loading.

Figures 6.10 and 6.11 present the influence of the TRM reinforcement ratio on the response of the three-story masonry-infilled RC frame retrofitted with TRM under cyclic loading in terms of global stiffness (Eq. 5.1) versus the number of cycles of loading and in terms of dissipated energy (Eq. 5.2) in relation to the number of half cycles of loading. From these figures it is obvious that as the TRM reinforcement ratio varies (increases or decreases) at each floor of the three-story retrofitted infilled frame its global stiffness and its dissipated energy fluctuate. The difference between the results obtained from the non-linear cyclic analysis of the six specimens considered in this study is more pronounced in the case of using three layers or one layer of TRM at the first floor of the structure compared to the other cases. From Figs. 6.10 and 6.11 it is observed that the global stiffness and the dissipated energy of the reference specimen, and those of the LF2S1 and LF2S2 specimen are almost the same (difference less than 10%-12%). The above observation is also supported by Figs. 6.2 and 6.3 and by Figs. 6.5 and 6.6. Furthermore, Figs. 6.10 and 6.11 show that the global stiffness and the dissipated energy of LF2S1 are increased by about 23% compared to the corresponding ones of the LF1S1 specimen.

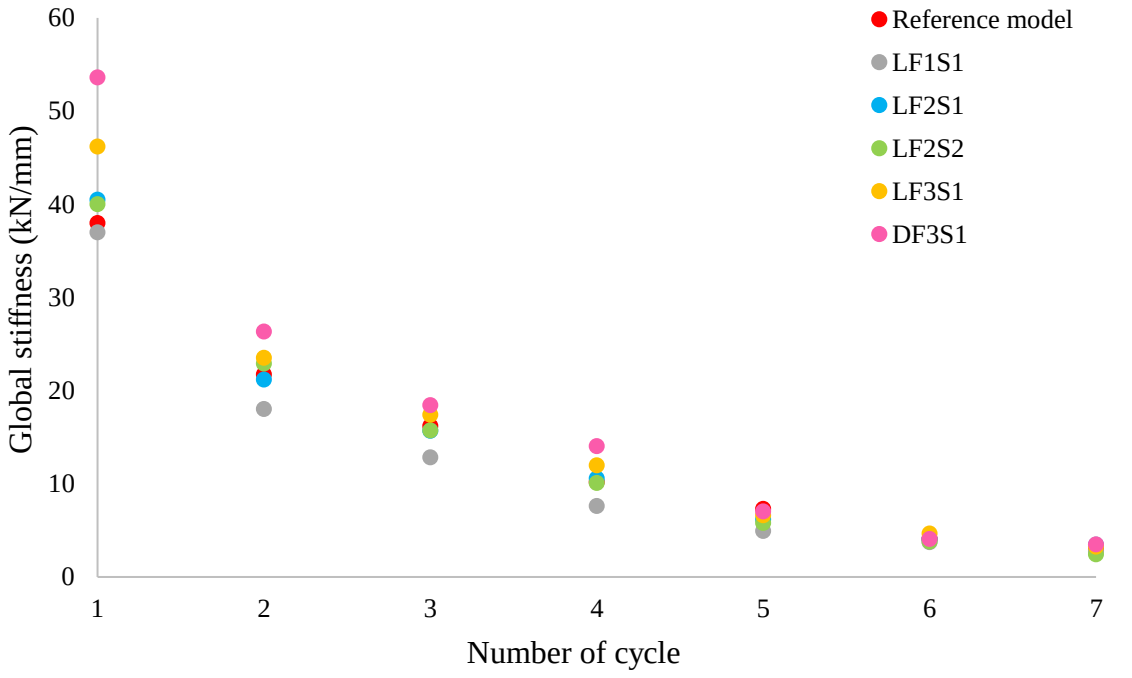

Figure 6.10: Comparison of results obtained from non-linear cyclic analysis of the masonry-infilled RC frame with different TRM reinforcement ratio in terms of global stiffness.

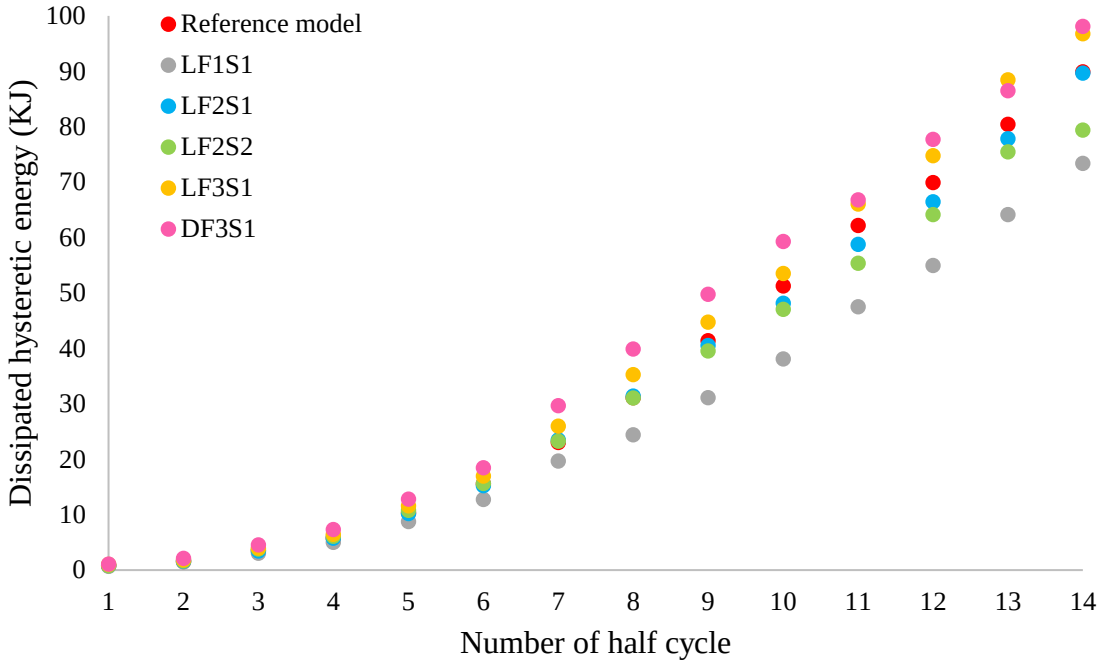

Figure 6.11: Comparison of results obtained from non-linear cyclic analysis of the masonry-infilled RC frame with different TRM reinforcement ratio in terms of dissipated energy.

Figure 6.12 shows that the global stiffness and the dissipated energy of the three-story infilled frame retrofitted with TRM subjected to cyclic loading is highly depended on the TRM reinforcement ratio at the first floor of the structure. From Fig. 6.12 it is observed that the global stiffness and the dissipated energy of the specimens with two or three layers of TRM at the first floor and one layer of TRM at the second floor (LF2S1, LF3S2 and DF3S1) are increased by about 10%-60% compared to the corresponding ones of the specimen with one layer of TRM at the first floor (LF1S1) during the first cycles of loading. After the maximum base-shear is reached (fourth cycle of loading), the use of more than one layers of TRM at the first floor results in smaller gains in the global stiffness and the dissipated energy of the retrofitted structure compared to that observed during the first cycles of lading. More specifically, the global stiffness and the dissipated energy of the LF3S1 specimen (reinforcement ratio equal to 1.6%) is increased by 15% and 20% respectively, compared to the corresponding ones of the LF2S1 specimen (with reinforcement ratio equal to 1.3%) during the last cycles of loading, which occur at large lateral displacement. This might depend on the failures that occur in the last two cycles of loading at the first floor of the retrofitted structure.

Finally, the global stiffness and the dissipated energy of the three-story masonry-infilled frame with TRM are increased (average value of 25%-45% and 32%-50%, respectively) in the case of using three layers of TRM with small spacing between the yarns of the textile at the first floor (DF3S1) compared to the case of using three layers of TRM with large spacing between the yarns of the textile (LF3S1). Therefore, the geometry of textile reinforcement influences the effectiveness of using TRM composite material for retrofitting masonry-infilled frames. It should be noted that, the size of mesh opening must be such that it allows the mortar to pass and correctly bond to the masonry wall surface, as it is reported by several researchers (Peled et al. 2008 a, b; Colombo et al. 2013; Portal 2013).

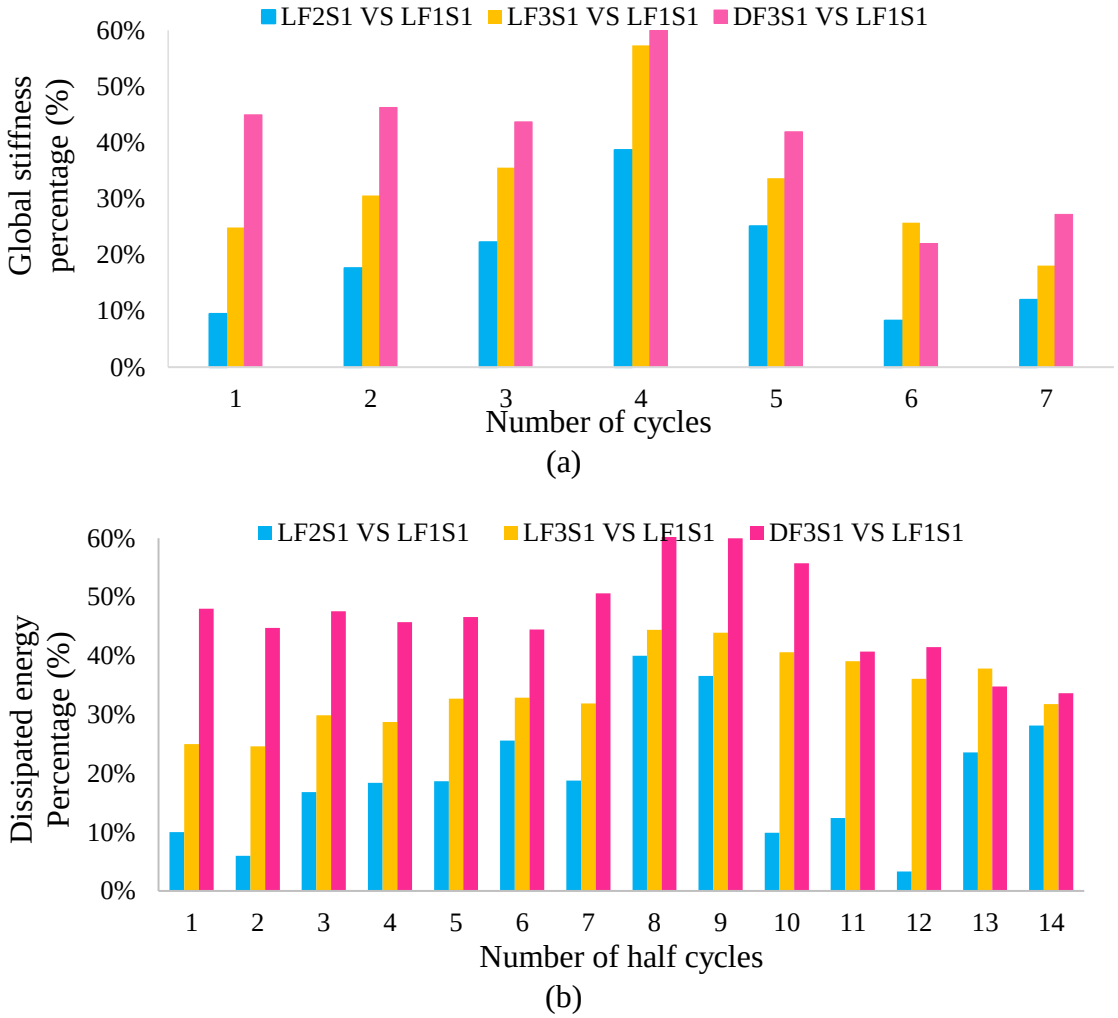

Figure 6.12: Comparison of the LF2S1, LF3S1 and DF3S1 specimen with that of LF1S1 specimen in terms of (a) global stiffness versus a number of cycles of loading and in terms of (b) the dissipated energy versus a number of half-cycles of loading.

Based on the numerical experiments performed in this part of the thesis it can be pointed out that the number of TRM layers and the geometry of textile reinforcement used in each floor of a multi-story masonry infilled RC frame are important factors influencing the effectiveness of using the TRM composite material for retrofitting multi-story infilled frames, since they affect the lateral capacity, stiffness, dissipated energy of the structure and they can modify the distribution of the shear force along the height of the structure.

6.3 Effect of the type of mortar used for TRM on the lateral response of the three-story masonry-infilled RC frame retrofitted with TRM.

In this section, the influence of the type of mortar used for binding the textile reinforcement on the effectiveness of using the TRM composite material for retrofitting masonry-infilled frames is investigated. Towards this direction, the validated three-story masonry-infilled RC frame model with TRM is used to perform numerical experiments considering different types of mortars for TRM. For the purpose of this study, four different commercial mortars for the TRM (manufactured by SIKA and TSIRCON company) are selected to be examined as shown in Table 6.7, where each mortar represents a different class of mortar according to European Standard UNI EN 1504-3 (defines four classes of repair mortars as follows: R1 and R2 for non-structural mortar, and R3 and R4 for structural mortar). The same modeling scheme was used for the numerical specimens as for the validated numerical model (Chapter 4), while the proposed analytical model of TRM (Chapter 3) is used, as will be discussed later.

Table 6.7: Summary of the numerical specimens of three-story masonry-infilled RC frame with TRM using different types of mortars for binding the textile reinforcement.

Name of the model	Name of the mortar used on TRM
Reference (R2C18)	Commercial fiber-reinforced mortar (R2)
R2C22	Sika MonoTop-722 Mur (R2)
R3C33	Sika MonoTop-615 (R3)
R4C45	Sika MonoTop-627 HP (R4)
R4C50	TSIRCON PER122 (R4)

The notation of the model specimen is R _ number C _ number, where the letters R and C represent the repair mortar and its compressive strength, respectively, while the first number denotes the class of the mortar (2, 3 and 4) and the second number denotes the value of the compressive strength of mortar. The validated masonry-infilled RC frame model with TRM (Chapter 4) is considered as a reference case for this study as shown in Table 6.8. For the reference case, a commercial fiber-reinforced cement-based mortar mixed with re-dispersible polymers is used, while the results (mechanical properties) obtained from the flexural and compressive tests conducted by Koutas et al. (2014) led to categorizing this mortar in the R2 class according to European Standard UNI EN 1504-3. Furthermore, for all the numerical specimens in this parametric study (including the reference case), carbon-TRM with commercial fiber-reinforced cement-based mortar is used at the ends of columns on the first (three layers) and second (two layers) stories as described in Chapter 4 in section 4.5.

Although the same modeling scheme was used for the numerical specimens as for the validated numerical model, in order to take into account in these numerical specimens the different types of mortars used for TRM, the required parameters for the TRM material model (Total Strain Crack material model) used for describing the non-linear cyclic behavior of TRM composite material need to be defined. In particular, the required parameters of this material model are defined from the proposed analytical model of the TRM as presented in Chapter 3, able to predict the tensile behavior of TRM in terms of stress-strain. In order to use the proposed analytical model of TRM, the mechanical properties and the geometric characteristics of the cement-based matrix and that of glass textile reinforcement are required (section 3.3.4). Most of the above required parameters are given in Table 3.3 in section 3.4, while the compressive strength and the tensile strength (obtained from bending test) of the mortars used for the purpose of this study are taken from the data sheets of the manufacturer (Sika and TSIRCON) as shown in Table 6.8. In this table, the modulus of elasticity of the mortar (E_m) and the tensile strength of the mortar (σ_{mu}) as estimated for the predictive equations proposed by *fib* Model Code 2010 are also presented. Using these values in the proposed analytical model, the tensile behavior of the one and two layers of glass-TRM considering four different types of mortars is estimated in terms of stress-strain as

presented in Fig. 6.13 (detailed example for applying the proposed model is presented in Appendix I). So, the required parameters in order to specify the TRM material model in DIANA FEA for simulating the tensile behavior of one and two layers of Glass-TRM considering four different types of mortars are defined from the salient points of the stress-strain curves as presented in Fig. 6.13, while the required parameters for their compressive behavior are obtained from Table 6.8. Based on Fig. 6.13 it can be pointed out that the type of mortar influences significantly the tensile behavior of TRM mainly at the first cracking state (State I) and at the multi-cracking state (State II), and not so in State III. More details regarding the effect of the type of inorganic matrix used for binding the textile reinforcement on the tensile behavior of TRM are presented in Chapter 3 (section 3.5.4).

Table 6.8: Mechanical properties of mortar as given by manufacturer and as obtained from *fib* Model Code 2010.

Name of the mortar used for TRM	**Mechanical properties of mortar given by manufacturer**		**Mechanical properties of mortar using *fib* Model code (2010)**	
	Compressive strength (MPa)	Tensile strength (from bending test) (MPa)	Tensile strength (σ_{mu}) (MPa)	Modulus of elasticity E_m (GPa)
Commercial fiber-reinforced cement-based mortar (R2)	18.9	4.3	2.2	27.2
Sika MonoTop-722 Mur (R2)	22	6	2.9	27.9
Sika MonoTop-615 (R3)	33	7	3.6	32.1
Sika MonoTop-627 HP (R4)	45	8	4.2	35.4
TSIRCON PER122 (R4)	50	10	4.5	36.8

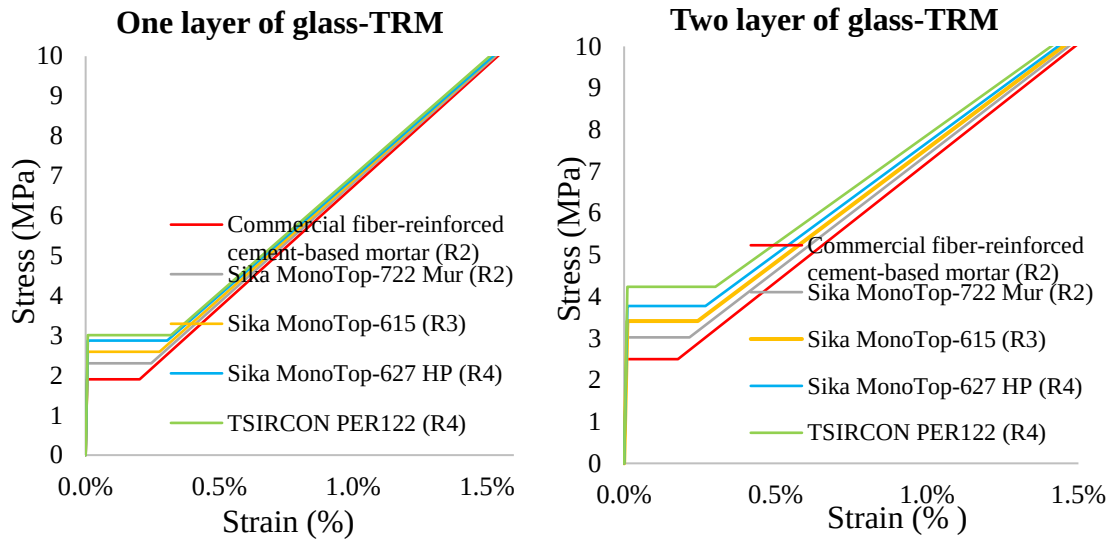

Figure 6.13: Tensile behavior of (a) one-layer and (b) two-layers of glass-TRM considering four different types of mortars in terms of stress-strain as obtained from the proposed analytical model of TRM.

After the defining the required parameters of the TRM material model in DIANA FEA, the developed numerical models for the purpose of this parametric study are subjected to seven cycles of displacement loading (Fig. 4.21). The results obtained from the numerical experiments performed in this part of the thesis are presented in the following paragraphs in terms of base-shear versus top-floor displacement, global stiffness, and dissipated energy of the retrofitted infilled frames during the cyclic loading.

The results obtained from the non-linear cyclic analysis of the reference specimen R2C18, and of the R2C22 specimen are presented in Fig. 6.14 in terms of base-shear versus top-floor displacement and in terms of base-shear versus the number of load steps. From Fig. 6.14 it is observed that the results of the two cases (reference specimen and R2C22 specimen), where a similar type of mortar is used (R2 class of mortar), are almost the same in terms of the base-shear versus top-floor displacement (Fig. 6.14 a). Furthermore, from Fig. 6.14 (b) it is observed that the base-shear of the R2C22 specimen in each load step is increased by about 5% compared to that of the reference specimen. Therefore, a slight increase in the compressive and tensile strength of the mortar (R2 class of mortar) used for binding the textile reinforcement of 22% and 11%

respectively, does not contribute to increase the lateral capacity of the infilled frame retrofitted with TRM in which the compressive and tensile strength of mortar is equal to is equal to 18.9 MPa and 2.2 MPa, respectively.

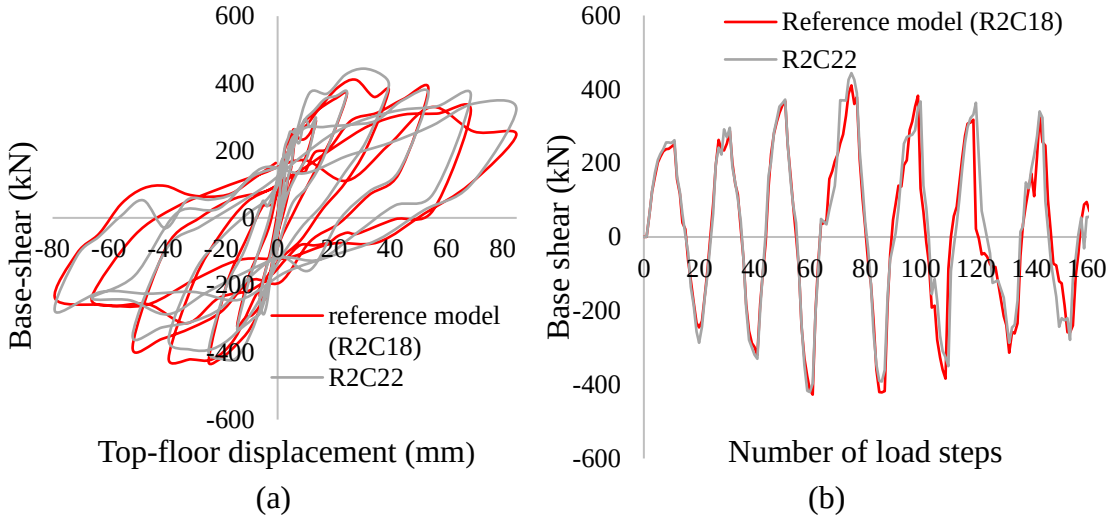

Figure 6.14: Comparison of the reference specimen (R2C18) and of the R2C22 specimen in terms of (a) base-shear versus top-floor displacement, and in terms of (b) base-shear in relation to the load steps.

Figure 6.15 indicates the effect of using TRM with R3 class of mortar (R3C33 specimen) instead of using TRM with R2 class of mortar (R2C18 and R2C22) on the lateral capacity of the retrofitted infilled frame subjected to cyclic loading.

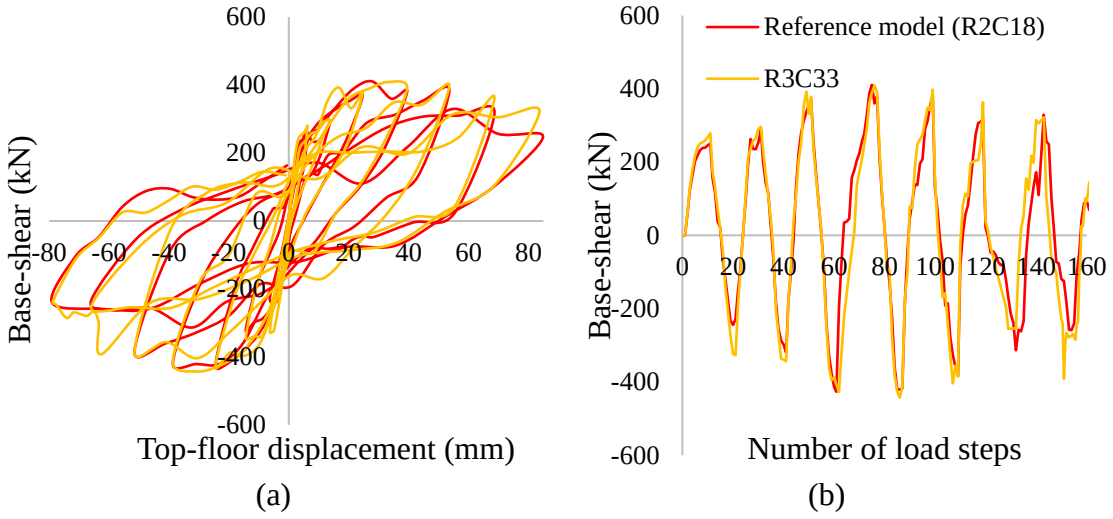

Figure 6.15: Comparison of the reference specimen (R2C18) and of the R3C33 specimen in terms of (a) base-shear top-floor displacement, and in terms of (b) base-shear in relation to the load steps.

Comparing the results of the reference specimen with those of the R3C33 specimen it is observed that there is no significant difference between them (Fig. 6.15), despite the fact that in the R3C33 specimen almost a double compressive and tensile strength of the mortar is used for TRM (Table 6.8). Furthermore, Fig. 6.15 shows that the area enclosed by the loop in the base-shear versus top-floor displacement diagram of the R3C33 specimen is slightly increased compared to that of the reference specimen, while the peak base-shear in each cycle of loading is increased by about 10% (Table 6.9). Therefore, the lateral capacity of the infilled frame retrofitted with TRM is increased by about 10% of using mortars for TRM which belong to the R3 class, instead of low-strength mortars, R2 class (where the compressive and tensile strength of the R3 mortar is 20%-80% and 10%-65% higher than the corresponding ones of the R2 mortar).

The results obtained from the non-linear cyclic analysis of the R4C45, R4C50 and of reference specimen R2C18 are presented in Fig. 6.16 in terms of base-shear versus top-floor displacement. For the benefit of the reader, Tables 6.9 and 6.10 show the increase in peak base-shear in each cycle of loading; for the two directions of loading, $V_{max,i}$ (positive direction of i^{th}cycle) and $V_{max,j}$ (negative direction of j^{th} cycle), of the specimens with high-strength mortars (R3 and R4) for TRM compared to that of the specimens with low-strength mortar (R2) for TRM.

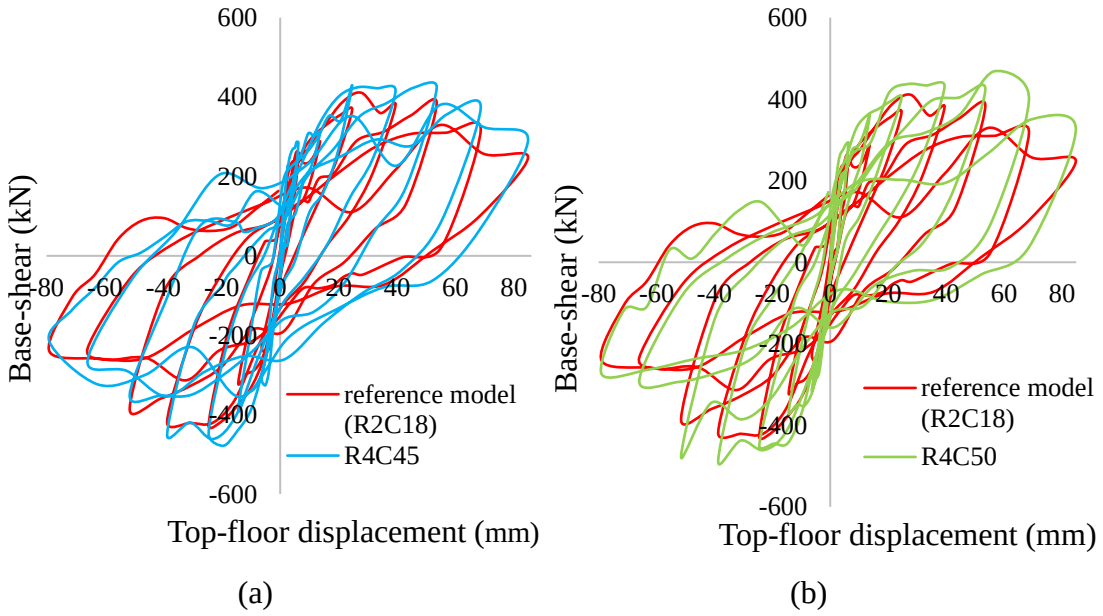

Figure 6.16: Comparison of the reference specimen (R2C18) with the (a) R4C45 specimen, and with the (b) R4C50 specimen in terms of base-shear top-floor displacement.

Table 6.9: Comparison of the R3C33, R4C45 and R4C50 specimens with the reference specimen (R2C18) in terms of peak base-shear in each cycle of loading for the positive direction of loading.

	$V_{max,i}$ **Positive direction of loading**		
cycle	$\frac{V_{maxi_{R3C33}} - V_{maxi_{R2C18}}}{V_{maxi_{R2C18}}}$	$\frac{V_{maxi_{R4C45}} - V_{maxi_{R2C18}}}{V_{maxi_{R2C18}}}$	$\frac{V_{maxi_{R4C50}} - V_{maxi_{R2C18}}}{V_{maxi_{R2C18}}}$
1	11%	14%	17%
2	3%	8%	25%
3	3%	16%	10%
4	0%	9%	10%
5	4%	11%	11%
6	14%	17%	26%
7	30%	18%	31%

Table 6.10: Comparison of the R3C33, R4C45 and R4C50 specimens with the reference specimen (R2C18) in terms of peak base-shear in each cycle of loading for the negative direction of loading.

	$V_{max,j}$ **Negative direction of loading**		
cycle	$\frac{V_{maxJ_{R3C33}} - V_{maxJ_{R2C18}}}{V_{maxJ_{R2C18}}}$	$\frac{V_{maxJ_{R4C45}} - V_{maxi_{R2C18}}}{V_{maxJ_{R2C18}}}$	$\frac{V_{maxJ_{R4C50}} - V_{maxJ_{R2C18}}}{V_{maxJ_{R2C18}}}$
1	14%	36%	37%
2	7%	21%	15%
3	1%	5%	39%
4	1%	8%	16%
5	0%	9%	24%
6	9%	14%	24%
7	0%	15%	14%

From Fig. 6.16 it is observed that the energy dissipation capacity of the R4C45 and R4C50 specimen is higher than the R2C18 specimen, since the area enclosed by the

loop in the base-shear versus top-floor displacement diagram is increased. Furthermore, the peak base-shear of the R4C45 and R4C50 specimen in each cycle of loading is increased by about 10%-30% compared to the corresponding ones of the R2C18 specimen (Tables 6.9 and 6.10). The lateral capacity of the retrofitted infilled frame is increased by using TRM with high-strength mortars (R4C45 and R4C50) instead of using low-strength mortars (R2C18). This is attributed to the fact that by increasing tensile and compressive capacity of the TRM, by using high-strength mortars for TRM (compressive strength > 45MPa and tensile strength > 4MPa), the large shear deformation of the infilled frame decreases. Therefore, this composite material is able to prevent the large shear deformation of the infilled frame since the high shear stresses of the infill wall are transferred to the TRM layer in the local level, where this composite material is able to sustain these shear stresses due to its high compressive and tensile capacity (consists of high compressive and tensile strength mortar, and of high tensile strength textile).

Table 6.11 shows the increase in peak base-shear in each cycle of loading; for the two directions of loading, $V_{max,i}$ (positive direction of i^{th}cycle) and $V_{max,j}$ (negative direction of j^{th} cycle), of the R4C45 and R4C50 specimen compared to that of specimen R3C33 specimen.

Table 6.11: Comparison of the R4C45 and R4C50 specimens with the R3C33 specimen in terms of peak base-shear in each cycle of loading for both directions of loading.

	$V_{max,i}$ Positive direction of loading		**$V_{max,j}$Negative direction of loading**	
cycle	$\frac{V_{max\,i_{R4C45}} - V_{max\,i_{R3C33}}}{V_{max\,i_{R3C33}}}$	$\frac{V_{max\,i_{R4C50}} - V_{max\,i_{R3C33}}}{V_{max\,i_{R3C33}}}$	$\frac{V_{max\,J_{R4C45}} - V_{max\,j_{R3C333}}}{V_{max\,j_{R3C33}}}$	$\frac{V_{max\,J_{R4C50}} - V_{max\,j_{R3C333}}}{V_{max\,j_{R3C33}}}$
1	3%	5%	19%	20%
2	5%	21%	13%	7%
3	13%	7%	4%	38%
4	8%	9%	7%	15%
5	7%	7%	9%	24%
6	3%	11%	5%	14%
7	2%	9%	15%	14%

From Table 6.11 it is observed that the peak base-shear of R4C45 specimen and of R4C50 specimen is increased by about 7%-20% until the fourth cycle of loading and by 5%-15% in the last two cycles of loading compared to the corresponding ones of the R3C33 specimen. More specifically, with a substantial increase of the compressive strength of mortar by about 36%-52%, and with an increase of lower magnitude in the tensile strength, 10%-12%, the lateral capacity of the retrofitted infilled frame is increased by about 15% (average increase). Therefore, the contribution of the compressive strength of the mortar used for TRM to increase the lateral capacity of infilled frame subjected to cyclic loading is more pronounced compared to the tensile strength of mortar used for TRM, especially during the first cycles of loading. This is attributed to the fact that, at early stage of lateral loading, high compressive stresses along the diagonal of the infill are transferred to the TRM at local level, so using high-compressive strength mortars for TRM prevent the large shear deformation of the infilled frame by enhancing the capacity of the compression strut of the infill wall (compression path along the diagonal of the infill wall is developed due to the high concentration of the shear stresses near the loaded corners of the infill wall and along the diagonal of the infill wall). As the lateral loading increases, the compressive failure of the infill wall occurs (fourth cycles of loading), and therefore during these cycles of loading, high tensile stresses are mainly transferred from infill wall to the TRM at local level. So at this stage, where large lateral displacement loads are imposed to the infilled frame, the contribution of the tensile capacity TRM to increase the lateral capacity of retrofitted infilled frame becomes more pronounced than the compressive capacity of the TRM. It is important to mention that the average effective tensile strain of the glass-TRM ranges from 0.24% to 0.64% when used on infilled frames as reported in Koutas et al. (2014) and Pohoryles and Bournas (2020). Based on the above, it can be concluded that the lateral response of retrofitted infilled frames is influenced by the tensile capacity of TRM only at State I and II. The tensile capacity of TRM at State I and State II is mainly controlled by the mortar used for binding the textile reinforcement as mentioned in Chapter 3. Therefore, by increasing the tensile strength of the mortar contributes to delay the first cracking of TRM, State I, and to extend the multi-cracking region of TRM, State II, (as mentioned in section 3.5.4), causing the full activation of

the TRM composite material (increasing the effective strain of TRM beyond the State II) in infilled frames subjected to large lateral displacement loads, leading to the increase of the lateral capacity of infilled frames retrofitted with TRM.

The effect of the type of mortar used for binding the textile reinforcement on the lateral capacity of the three-story masonry-infilled RC frame retrofitted with TRM subjected to cyclic loading is given in Figs. 6.15 and 6.15 in terms of global stiffness (Eq. 5.1) versus the number of cycles of loading and in terms of dissipated energy (Eq. 5.2) in relation to the number of half cycles of loading, respectively.

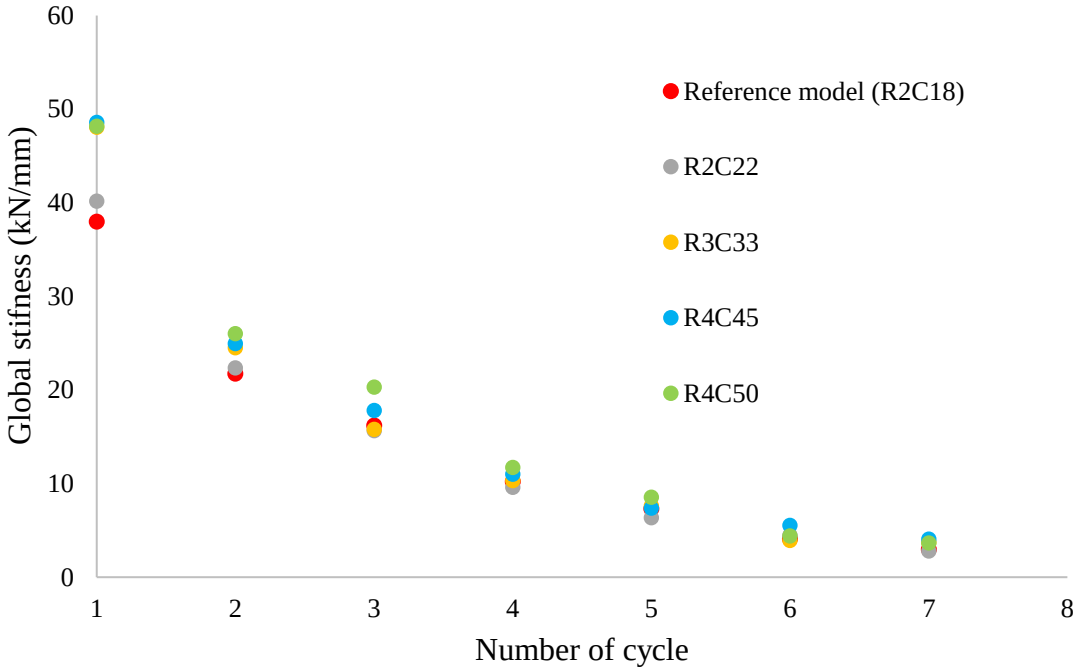

Figure 6.17: Comparison of the results obtained from non-linear cyclic of the masonry-infilled RC frame retrofitted with TRM using different types of mortar for TRM in terms of global stiffness.

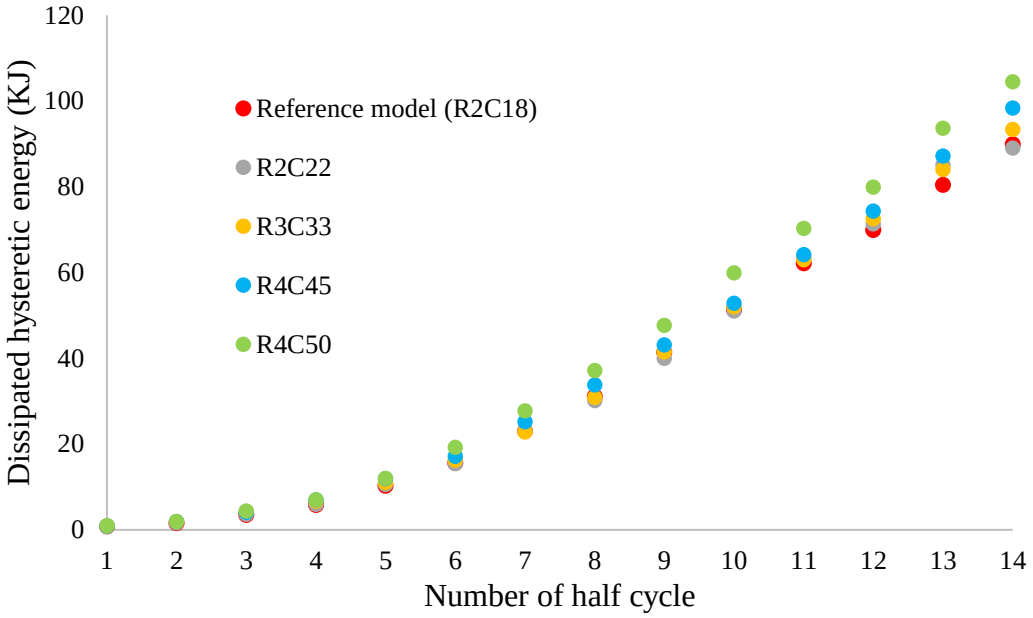

Figure 6.18: Comparison of results obtained from non-linear cyclic analysis of the masonry-infilled RC frame retrofitted with TRM using different types of mortar for TRM in terms of dissipated energy.

From Figs. 6.17 and 6.18 it is obvious that the global stiffness and dissipated energy of the retrofitted infilled frame is sensitive to the type of the mortar used for binding the textile reinforcement. It is also observed that the global stiffness and the dissipated energy of the infilled frame retrofitted with TRM are not increased proportionally with the increase of the mechanical properties of the mortar used for TRM. Furthermore, Figs. 6.17 and 6.18 show that the global stiffness and the dissipated energy of the reference specimen, and those of the R2C22 and R3C35 specimen are almost the same (difference less than 10%-12%). The above observation is also supported by the base-shear versus top-floor displacement diagrams and by the base-shear in each load step as previously discussed (Figs. 6.14 and 6.15). Therefore, the global stiffness and dissipated energy of infilled frame retrofitted with TRM subjected to cyclic loading is not increased significantly in the case of using TRM with mortars belonging to the R3 class instead of the R2 class of mortar. On the other hand, the global stiffness and dissipated energy of the infilled frame retrofitted with TRM are increased significantly of using high-strength mortars for TRM, which belong to the R4 class, instead of low-strength mortars, as shown in Figs. 6.19.and 6.20.

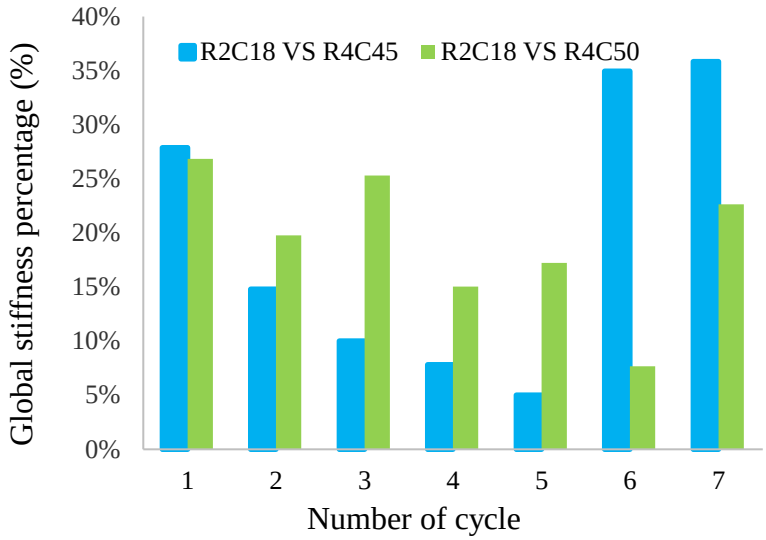

Figure 6.19: Comparison of the R4C45 and R4C50 specimen with the reference model (R2C18) in terms of global stiffness versus a number of cycles of loading .

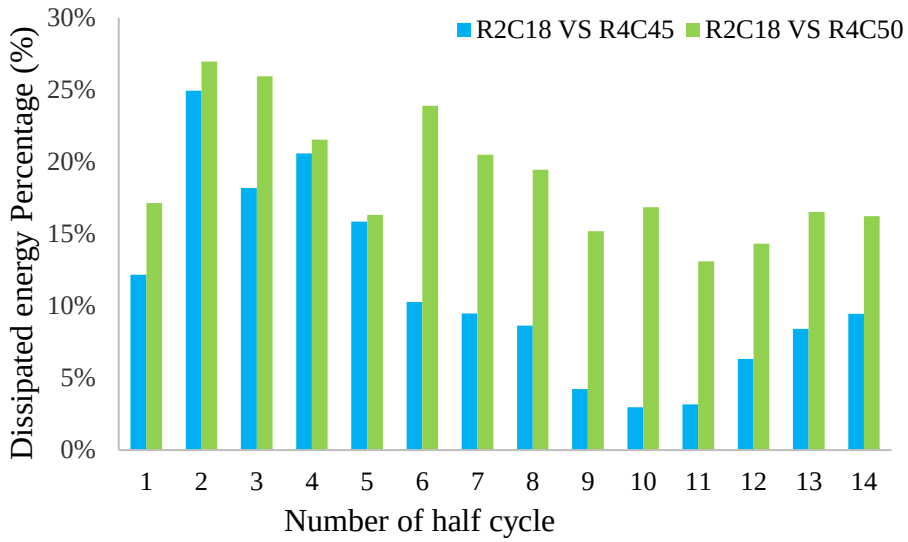

Figure 6.20: Comparison of the R4C45 and R4C50 specimen with the reference model (R2C18) in terms of dissipated energy versus a number of half cycles of loading .

From Figs. 6.19 and 6.20 it is observed that the global stiffness and dissipated energy of the infilled frame retrofitted with TRM in which the compressive and tensile strength of the mortar used for TRM is equal to 18.9 MPa and 2.2 MPa (R2C18), respectively, is increased by about 12%-25% during the first cycles of loading and by about 10%-15% during the last cycles of loading, with a substantial increase of the compressive strength of mortar by about 150%-180%, and with an increase of lower magnitude in the tensile

strength of the mortar, 60%-75% (R4C45 and R4C50). This occurs because the influence of the compressive strength of the mortar used for TRM on the lateral capacity of the retrofitted infilled frame is more pronounced compared to the tensile strength of the mortar used for TRM during the first cycles of loading, since the compressive capacity of TRM contributes to enhance the compression strut of the infill wall, as previously explained. Adding to this, as the lateral loading increases, the contribution of the tensile capacity TRM to increase the lateral capacity of retrofitted infilled frame becomes more pronounced than the compressive capacity of TRM since at this stage this composite material sustains the high tensile stresses which are transferred from infill wall to the TRM at local level.

Based on the above numerical experiments, it can be pointed out that the type of the mortar used for binding the textile reinforcement, especially its compressive and tensile strength, influences significantly the lateral capacity of the retrofitted infilled frames subjected to cyclic loading, where the influence of the compressive strength of the mortar is more pronounced than the tensile strength of the mortar during the first cycles of loading, while the influence of the tensile capacity of TRM becomes more pronounced than the compressive capacity of TRM during the last cycles of loading which occurs at large lateral displacement loads. Therefore, special type of mortar with high mechanical properties must be used in order to improve the lateral response of masonry-infilled RC frames retrofitted with TRM.

6.4 Summary and conclusions

In this part of the thesis, numerical experiments are performed to investigate, firstly, the influence of the amount of the TRM reinforcement ratio, by means of using different number of textile layers and different textile geometry (varying the TRM retrofitting scheme on the three-story masonry-infilled RC frame), and secondly, the effect of using different types of mortars (different mechanical properties of the mortar) for binding the textile reinforcement, on the in-plane response of the three-story masonry-infilled RC frame retrofitted with TRM under cyclic loading. The same modeling scheme was used for the numerical specimens as for the validated numerical model (Chapter 4), while the proposed analytical model of TRM (Chapter 3) is used for predicting the tensile

behavior of TRM (by varying the reinforcement ratio, the textile geometry and the type of mortar) in terms of stress-strain in order to define the required parameters for the TRM material model in DIANA FEA.

From the parametric study regarding the TRM reinforcement ratio, by means of using different number of TRM layers and different geometry of textile, the following conclusions are obtained:

- The use of TRM at the third floor of the three-story masonry-infilled RC frame retrofitted with TRM is pointless, since strengthening the third floor does not provide any gain to the lateral capacity of the retrofitted structure.
- By applying more than one layer of TRM at the second floor of a three-story infilled frame retrofitted with TRM is meaningless considering the cost of TRM and considering that the lateral capacity of retrofitted structure is increased by about 12%, while the distribution of the shear force along the height of the structure is not changed significantly.
- It is important to apply more than one layer of TRM at the first floor and one layer of TRM at the second floor in a three-story masonry-infilled RC frame subjected to cyclic loading, in order to increase its lateral capacity (30%) and to delay or even prevent the brittle failures at the first floor (*soft-story mechanism*).
- The lateral strength, the global stiffness and the dissipated energy of the three-story masonry-infilled RC frame retrofitted with TRM is increased by about 15%-25% as the TRM reinforcement ratio at the first floor increases from 1.3% (two layers of TRM) to 3.2% (adding more than two layers of TRM or using denser textile), while after the maximum base-shear is reached, by increasing the reinforcement ratio results in smaller gains in lateral capacity of the retrofitted structure compared to that observed during the first cycles of lading. This might depend on the failures that occur in the last two cycles of loading at the first floor of the retrofitted structure.
- The lateral capacity of the three-story masonry-infilled RC frame retrofitted with TRM is increased as the TRM reinforcement ratio at the first floor increases but not proportionally, since using double amount of TRM reinforcement ratio does not provide double lateral capacity of the retrofitted structure.

- By increasing the reinforcement ratio from 1.3% to 3.2% at the first floor of the three-story masonry infilled frame retrofitted with TRM, contributes to delay or even prevent some failures (such as the formation of a soft-story at the first floor in early lateral loading), since the height-wise distribution of the shear force is almost linearly varying until the fourth cycle of loading while as the lateral loading increases (top-floor displacement equal to 50mm) the shear forces are not linearly varying along the height of the retrofitted structure, but they are slightly better distributed.
- The geometry of textile reinforcement can be considered an important factor influencing the effectiveness of using the TRM composite material for retrofitting masonry-infilled RC frame, since the lateral capacity of the three-story infilled frame retrofitted with TRM is increased if the mesh spacing of the textile is small (TRM reinforcement ratio increases).

From the parametric study regarding the type of the mortar used for binding the textile reinforcement (each mortar represents a different class of mortar according to European Standard UNI EN 1504) the following conclusions are derived:

- The lateral capacity of the infilled frame retrofitted with TRM is increased by about 10% in the case of using mortars for TRM which belong to the R3 class, instead of low-strength mortars, R2 class.
- The use of high-strength mortars for the TRM, especially R4 class of mortar, results in higher lateral strength, global stiffness and dissipated energy of the three-story masonry-infilled RC frame retrofitted with TRM by about 10%-30% instead of using TRM with relatively low strengths (R2 and R3 class of mortar). This increase is not proportional to that of the mortar mechanical properties, since using mortar with double tensile or compressive strength does not provide double lateral capacity of the retrofitted infilled frame.
- The lateral capacity of the retrofitted infilled frame is increased by about 12%-25% during the first cycles of loading and by about 10%-15% during the last cycles of loading, with a substantial increase of the compressive strength of mortar by about 150%-180%, and with an increase of lower magnitude in the tensile strength of the mortar, 60%-75%. Therefore, the

contribution of the compressive strength of the mortar used for TRM to increase the lateral capacity of infilled frame subjected to cyclic loading is more pronounced compared to that of the tensile strength of mortar used for TRM during the first cycles of loading, since the compressive capacity of TRM contributes to enhance the compression strut of the infill wall, while as the lateral loading increases, the contribution of the tensile capacity TRM to increase the lateral capacity of retrofitted infilled frame becomes more pronounced than the compressive capacity of the TRM since at this stage this composite material sustains the high tensile stresses which are transferred from infill wall to the TRM at local level.

- The increase in the lateral capacity of the retrofitted infilled frame by using TRM with high-strength mortars (compressive strength > 45MPa and tensile strength > 4MPa) instead of using low-strength mortars is due to the fact that by increasing the tensile and compressive capacity of the TRM, the large shear deformation of the infilled frame decreases since this composite material is able to sustain higher shear stresses, which are transferred from the infilled frame to the TRM.

It is important to mention that the results obtained from this parametric study can be considered as indicative since the bond conditions (shear strength and adhesion properties) between the textile and the mortar is not taken into account in this study, either in the numerical model (homogenized layer of textile and mortar) or in the proposed analytical model used for predicting the tensile behavior of TRM. Adding to this, full bond between TRM layer with the infill wall is considered in this study. Considering the above, special attention should be given to the size of the mesh opening of the textile reinforcement, which must be such that to allow the mortar to pass and correctly bonded to the wall surface, and special attention in the mortar composition which must be such that to achieve full penetration of the textile to the matrix in order to enhance the bond strength between matrix and textile. In order to achieve appropriate mortar for retrofitting infilled frames, sand with small grain size, high binder contents (by adding different pozzolanic additives), high performance plasticizers, short fibers

(steel, glass, carbon and synthetics), polymers and resins must be used in the mortar composition as mentioned in Chapter 3 (section 3.2.2).

Finally, reviewing the literature concerning the use of TRM technique for retrofitting masonry infill walls and masonry-infilled frames (Chapter 2, section 2.5), and based on the numerical experiments performed in this part of the thesis it can be concluded that the TRM reinforcement ratio and the type of mortar used for binding the textile reinforcement influences significantly the effectiveness of using the TRM composite material for retrofitting masonry-infilled RC frames.

CHAPTER 7

7. SEISMIC RETROFITTING OF MASONRY-INFILLED RC FRAMES WITH OPENINGS USING TRM

7.1 Introduction

In this part of the thesis, the use of TRM as a retrofitting technique for masonry-infilled RC frames with openings is, to my knowledge, investigated for the first time ever. This is achieved by performing numerical experiments to examine the in-plane response of the three-story masonry-infilled RC frame with openings retrofitted with TRM subjected to cyclic loading. Prior to the above tests, numerical experiments should be performed to examine the effect of openings on the lateral response of the three-story masonry-infilled RC frame without TRM, and validate this numerical model using relevant past studies.

Reviewing the literature concerning the different retrofitting techniques developed over the years, it seems that significant research has been conducted for retrofitting solid masonry-infilled RC frames, however, much less for masonry-infilled frame RC frames with openings (Ghobarah and Mandooh 2004; Motamedi et al. 2012; Koutromanos et al. 2013; Nayak and Dutta 2015). For example, Benedetti et al. (1998) conducted shake table tests on two-story masonry-infilled RC frames with window and door openings in different positions to evaluate the lateral response of existing buildings, and to study the effect of using different retrofitting methods (using cement mixtures for cracks, and steel grids covered with cement layers) on this type of structure. The lateral resistance of the retrofitted structure is significantly increased by 75% compared to that of the original one. Later, tests on large-scale masonry-infilled frames with window and door openings retrofitted with high-density polymeric-grids embedded in a mortar layer were conducted by Colombo et al. (2000), and they concluded that the maximum strength of

the retrofitted specimen is increased by about 65% compared to that of the unretrofitted one. Furthermore, several authors pointed out that the FRP retrofitting technique provides a substantial gain in the lateral strength, deformation capacity, and in the dissipated energy (50%-80%) of infilled frames with openings (Kalali and Kabir 2012; Triller et al. 2016, 2017; Gu et al. 2018). Mohan and Jacob (2016) developed a masonry-infilled RC frame model with two openings retrofitted with CFRP (using ANSYS software). The results showed that the load-bearing capacity of the retrofitted infilled frame with openings is two times greater compared to that of the unretrofitted one. Recently, Proença et al. (2019) evaluated experimentally and numerically the lateral response of masonry-infilled RC frames with openings under cyclic loading by installing a steel window frame inside the opening. The results showed that using this strengthening solution the lateral capacity of the infilled frame with opening is increased by about 150% compared to that of the unretrofitted specimen.

None of either past experimental or numerical studies were geared towards the use of TRM for retrofitting masonry-infilled RC frames with openings, despite that significant research has been conducted for solid masonry-infilled RC frames retrofitted with TRM in the last decade (Fig. 2.17, section 2.5). One way of closing this gap of knowledge is to investigate numerically the effectiveness of using the TRM composite material for retrofitting masonry-infilled RC frames with openings as will be achieved in this part of the thesis.

It is important to mention that several experimental and numerical studies have been conducted so far aiming to examine the influence of the openings and their position on the in-plane response of infilled frames under lateral loading, as mentioned in Chapter 2 (section 2.3). Reviewing the relevant literature, it can be concluded that the presence of an opening in infilled frames, results in a more flexible structural system with lower lateral capacity compared to infilled frames without opening, while this decrease is not in proportion to the reduction of the cross-sectional area of the infilled frame due to opening. Mallick and Garg (1971) concluded that the loss of strength and stiffness of infilled frames due to a centrally square opening having dimension one-fifth of the infill wall is about 25%-50%. Later, Kakaletsis and Karayannis (2008, 2009) pointed out that in the cases where the opening percentage is equal to 12.5% and 25% the lateral

strength of the structure decreases by about 19% and 32%, respectively. Furthermore, previous studies showed that the interaction between the infill wall and frame is adversely affected as the opening position is moved towards the compression diagonal of the infill wall (Mallick and Garg 1971; Liauw 1979; Utku 1980), while if the opening interrupts the compression diagonal this gives an opportunity for two diagonal struts to develop in the infill wall (Dawe 1985). Asteris et al. (2011, 2012) concluded that the higher value of stiffness reduction of the infilled frame with opening occurs when the opening is upon the diagonal of the infill wall. The authors, among others, proposed a stiffness reduction factor to modify the equivalent strut stiffness. Moreover, previous studies showed that the failure mechanisms and crack patterns of masonry-infilled RC frames with openings are affected by the location and by the size of the opening, where the cracks are usually developed at the corner of the openings, and as the lateral load increases these cracks are propagated towards the loaded corners of the infilled frame (Buonopane and White 1999; Chiou et al. 1999; Kakaletsis and Karayannis 2009). Decanini et al. (2012) found that if the opening is located in the corner of the infill wall it may create unfavorable effects like a *short-column mechanism*. Recently, numerical models were developed using the DIANA FEA software in order to examine the lateral response of masonry-infilled RC frame with openings (Akhoundi et al. 2016; Scheen 2016; Allen et al. 2017; Proença et al. 2019).

Therefore, it is important to fulfill the need for examining the effectiveness of using the TRM composite material for retrofitting masonry-infilled RC frames with openings, which is one of the main scopes of the current thesis. Towards this direction, the validated three-story masonry-infilled RC frame model with and without TRM (Chapter 4) is used to perform numerical experiments through a parametric study, to investigate firstly, the influence of a central window opening on the response of infilled frames subjected to cyclic loading, and then to examine the use of TRM for seismic retrofitting infilled frames with openings. In order to enhance the current numerical study, the influence of opening on the lateral response of infilled frames as obtained from these numerical experiments is compared with that obtained from relevant past studies. To achieve a reasonable comparison, the location, the size and the geometry of the opening were selected in such a way to match those used in previous experimental studies.

Specifically, it was selected to have an opening that ranges from 5% to 27% (square and rectangular shape) in the central part of the infill upon its diagonal and slightly closer to the top side of the infilled frame (Fig. 7.1 a), as it has been also previously studied by other researchers (Dawe 1985; Mosalam 1997; Rathi and Pajgade 2002; Nwofor et al. 2002; Voon and Ingham 2008; Kakaletsis 2009; Asteris et al. 2003, 2011; Díaz and Fukuyama 2008; Surendran et al.2012; Decanini et al. 2012; Surendran et al.2012; Cetisli et al. 2015; Akhoundi et al. 2016; Griffith et al. 2016). Consequently, in this study, numerical experiments are performed through non-linear cyclic analysis on the three-story masonry-infilled RC frame model with and without TRM considering different central opening area as shown in Table 7.1. In this parametric study, the maximum height of the opening is set at 780 mm in order to be realistic.

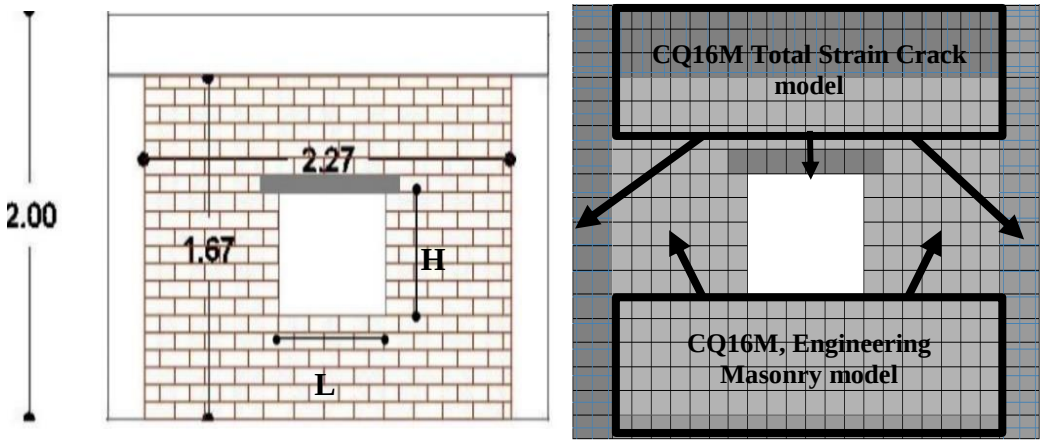

(a) (b)

Figure 7.1: (a) Geometry of the masonry infill wall with central opening and (b) details of FE masonry-infilled frame model with central opening.

The notation of the model specimen (Table 7.1) is SO (%) or O (%) where the O and SO denote the unretrofitted and retrofitted specimen, respectively, and the percentage denotes the ratio of the opening area to the infill wall area. The percentage ratio of the opening area is defined as: the area of the opening divided by the area of the infill wall multiplied by 100. Three reference cases were considered in this study as follows: the masonry-infilled RC frame without openings, O (0%), the masonry-infilled RC frame without openings retrofitted with TRM, SO (0%) and the bare RC frame, O (100%). It is important to note that, the numerical specimens were developed following the same

modeling scheme with the validated numerical model (material models, type of elements, mesh, loading scheme, boundary conditions and the type of analysis as presented in Chapter 4), while the convergence criteria of the non-linear cyclic analysis changes where is needed. Furthermore, in these numerical models, a lintel-beam in the upper part of the window of the infilled frame model is considered as shown in the Fig. 7.1 (b) which is modeled by plane-stress elements and the concrete material model is adopted for these elements as presented in Chapter 4 (Section 4.6.1).

Table 7.1: Geometric characteristics of the masonry-infilled RC frame model with openings, with and without TRM.

Model name without TRM	**Model name with TRM**	**Length of opening (L) (mm)**	**Height of opening (H) (mm)**	**Length of infill (mm)**	**Height of infill (mm)**	**Percentage ratio of opening area to infill area (%)**
O (0%)	SO (0%)	0	0	2270	1670	0
O (5%)	SO (5%)	454	445	2270	1670	5
O (8%)	SO (8%)	681	445	2270	1670	8
O (12%)	SO (12%)	681	668	2270	1670	12
O (16%)	SO (16%)	908	668	2270	1670	16
O (20%)	SO (20%)	1135	668	2270	1670	20
O (27%)	SO (27%)	1362	780	2270	1670	27
O (100%)	SO (100%)	2270	1670	2270	1670	100

Therefore, in this part of the thesis, the influence of a central window opening on the response of infilled frames subjected to cyclic loading (section 7.2), and the use of TRM for seismic retrofitting infilled frames with openings (section 7.3) are investigated by performing numerical experiments using the validated numerical models. The most important conclusions derived from these numerical experiments are presented at the end of this Chapter (section 7.4).

7.1 Effect of central openings on the lateral response of the three-story masonry-infilled RC frame

In the first part of this Chapter, the influence of the variation of the area of a centrally located window opening on the lateral response of the three-story masonry-infilled RC frame subjected to cyclic loading is investigated through numerical experiments as shown in Table 7.1. The numerical specimens were developed following the same modeling scheme with the validated numerical model (Chapter 4) and they are subjected to five cycles of prescribed displacement loading (section 4.7).

The results obtained from the non-linear cyclic analyses on the three-story masonry-infilled RC frame model with different size of central opening is given in Fig. 7.2 in terms of envelope curves derived from the base-shear versus top-floor displacement diagrams (hysteresis curves, positive direction of loading) as will be presented in the next section.

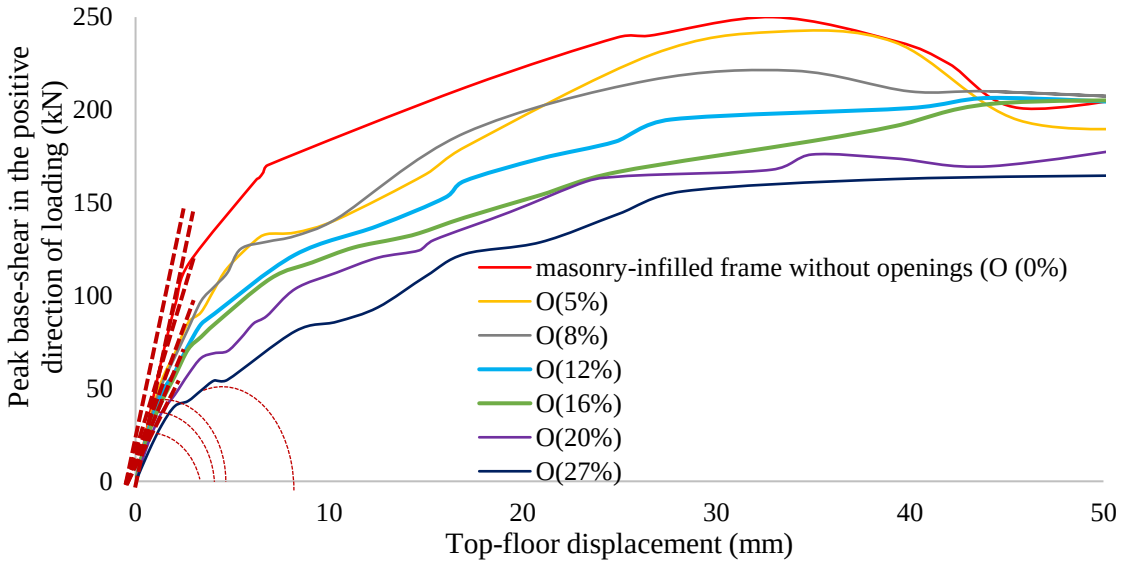

Figure 7.2: Envelope curves obtained from the base-shear versus top-floor displacement, hysteric curves, in the positive direction of loading of the infilled frame model with 5% to 27% central opening.

From Fig. 7.2 it is observed that the presence of the central opening influences the lateral capacity of the three-story masonry-infilled RC frame under in-plane cyclic loading, since as the area of the central opening increases the lateral strength and stiffness of the infilled frame decreases. More specifically, in the cases where the area

of the central opening is equal to 8%, 12%, 16% and 27% leads to a decrease in the lateral strength of the infilled frame equal to 10%, 14%, 20%, and 30%, respectively. Furthermore, for all the numerical specimens the maximum base-shear is attained when the top-floor displacement is equal to 40 mm (fourth cycle of loading). The decrease of the maximum base-shear of the infilled frame in relation to the increase of the opening area is given in Fig. 7.3 (ratio of the maximum base-shear of infilled frame with a central opening to the maximum base-shear of a solid infilled frame).

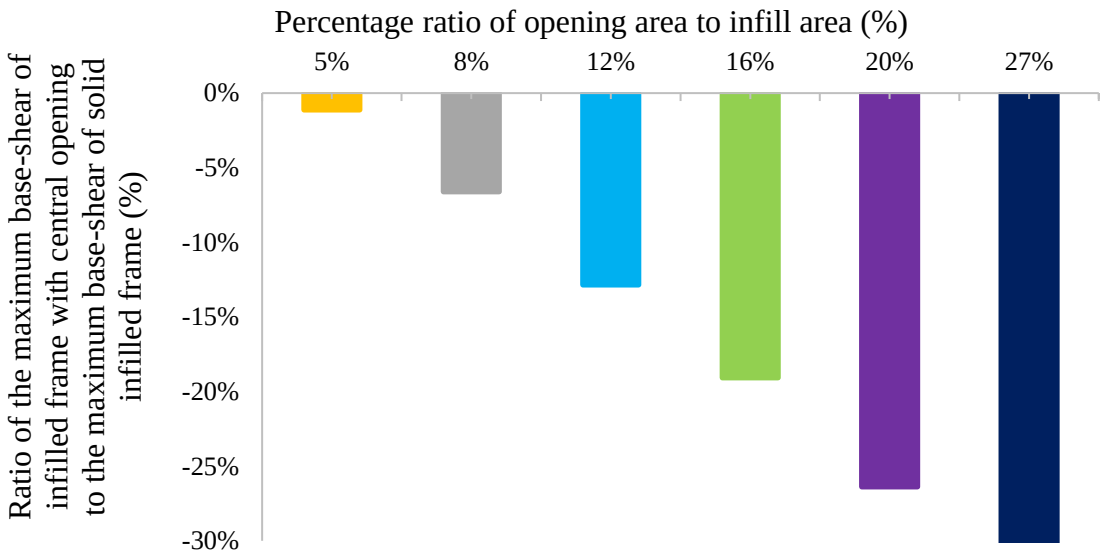

Figure 7.3: Effect of central opening area percentage on the maximum base-shear of the infilled frame during the fourth cycle of loading.

From Fig. 7.3 it is observed that the maximum base-shear of the infilled frame with 20% and 27% opening percentage decreases by 26% and 31%, respectively, compared to that of infilled frame without opening. Furthermore, the maximum base-shear of the infilled frame with 12% opening percentage decreases by about 15% compared to that of the infilled frame without opening. These observations are almost the same with those reported by Mallick and Garg (1971) and Kakaletsis and Karayannis (2009), where Kakaletsis and Karayannis (2009) found the maximum base-shear of the infilled frame with opening percentage equal to 12.5 % and 25% decreases by 19 % and 32 %, respectively, compared to the infilled frame without openings. This leads to the

validation of the three-story masonry-infilled RC frame model with central opening equal to 12%, 20% and 27%.

Furthermore, the numerical specimens developed in this study are validated using past experimental studies conducted by Kakaletsis and Karayannis (2007, 2008, 2009), Akhoundi et al. (2016), Tekeli and Aydin (2017), and Ahani et al. (2019). All the above-mentioned studies mainly differ in the scale of the tested specimens (full or reduced), in the loading scheme, in the boundary conditions, in the geometry of the infilled frame, in the material used for assembling the masonry infill wall (mortar and bricks), and provide large amount of information about the in-plane response of infilled frames with central openings (failure modes, lateral capacity, crack patterns, etc.). From the available data of each of the above study, it is decided to use the envelope curve obtained from the base-shear versus displacement diagram (hysteresis curve) or from push-over curve for each case-study. Consequently, the ratio of the base-shear (failure envelope) in each load step of solid infilled frame to the base-shear of infilled frame with different opening area percentage is calculated for each case-study, in order to be able to compare the results obtained from these studies with those of the current study. The comparison of the results of the above-mentioned studies with the ones of the current study is given in Fig. 7.4 in terms of base-shear ratio in each displacement loading (envelope curve), which indicates the decrease in the shear capacity of infilled frame caused by the presence of a central opening.

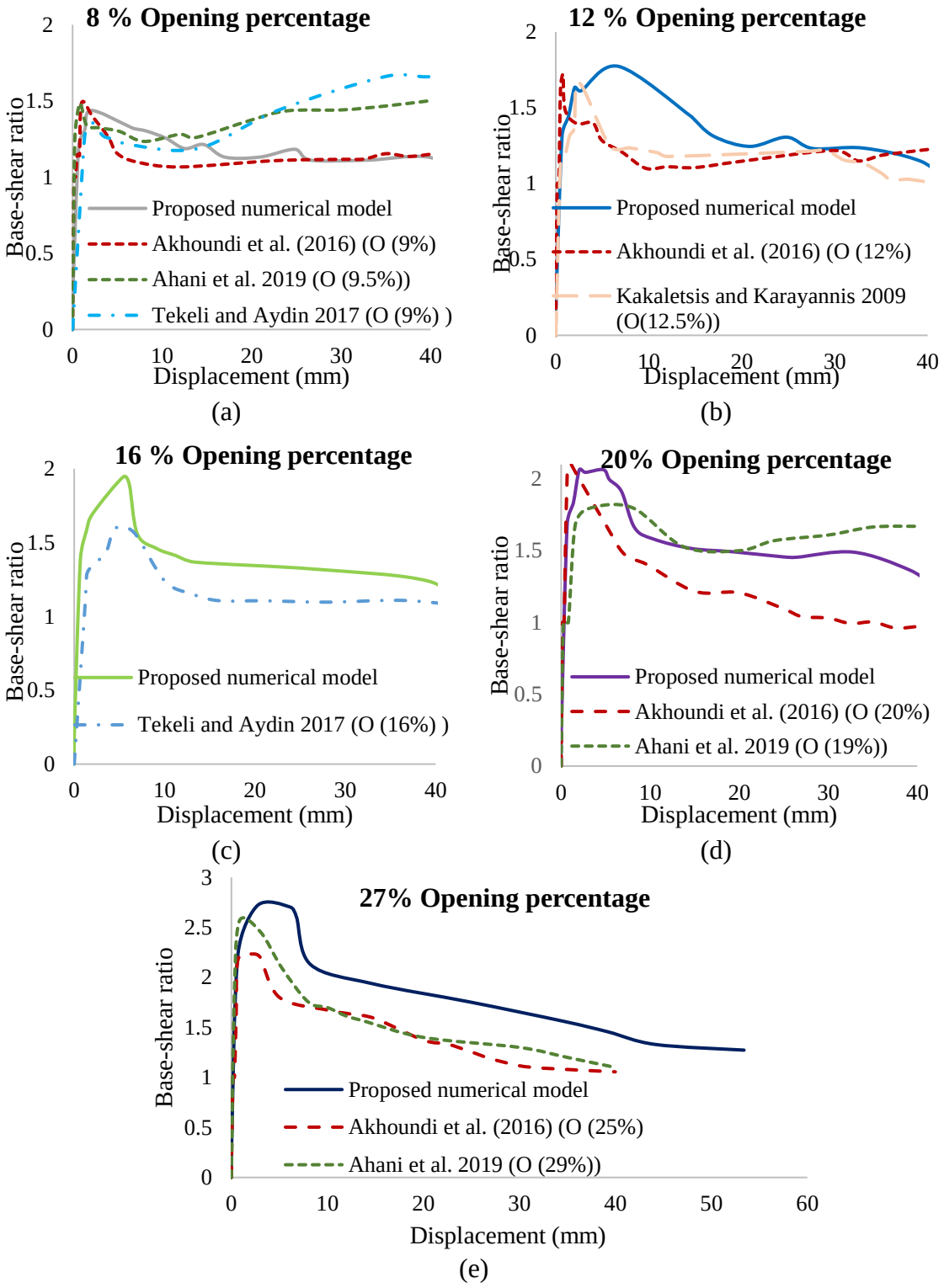

Figure 7.4: The decrease in the shear capacity of infilled frame under lateral loading caused by the presence of (a) 8%, (b) 12%, (c) 16%, (d) 20% and (e) 27% central opening as obtained from the studies conducted in the past and from the current study.

From Fig. 7.4 it is observed that the results obtained from the current study present good correlation to those obtained from the past experimental and numerical studies. Specifically, the base-shear of the infilled frame with 8% central opening as obtained from the current study decreases by about 1.4 times compared to that of the solid infilled frame at a corresponding lateral displacement less than 10mm where is the same decrease resulted from studies conducted by Akhoundi et al. (2016), Tekeli and Aydin (2017) and Ahani et al. (2019) as shown in Fig. 7.4 (a). Furthermore, the base-shear of the infilled frame with a 27% central opening is decreased by about 23%-62% compared to that of solid infilled frame according to the current study, while Akhoundi et al. (2016) and Ahani et al. (2019) found that this decrease is equal to 10%-60% in the case of 29% central opening (Fig. 7.4 e). From Fig. 7.4, it is also observed that the discrepancy between the results obtained from the current study with those obtained from the selected case-studies is more pronounced as the lateral displacement increases, with an average difference equal to 25%. This difference is the same with that obtained by comparing the base-shear ratio of the Akhoundi et al. (2016) case-study with that of Ahani et al. (2019) case-study, as shown Figs. 7.4 (a) and (d). Therefore, taking into account all the above, it can be considered that the three-story masonry-infilled RC frame model with different areas of central opening used in this parametric study is accurate, and consequently it can predict the real response of such type of structure subjected to in-plane cyclic loading.

Furthermore, the influence of the central opening ranging from 5% to 27% on the lateral capacity of masonry-infilled RC frame is given in Fig. 7.5 in terms of global stiffness (Eq. 5.1) versus the number of cycles of loading, and in terms of dissipated energy (Eq. 5.2) in relation to the number of half cycles of loading. Figure 7.6 shows the comparison of the dissipated energy of the infilled frame with that of the infilled frame with opening ranging from 5% to 27%.

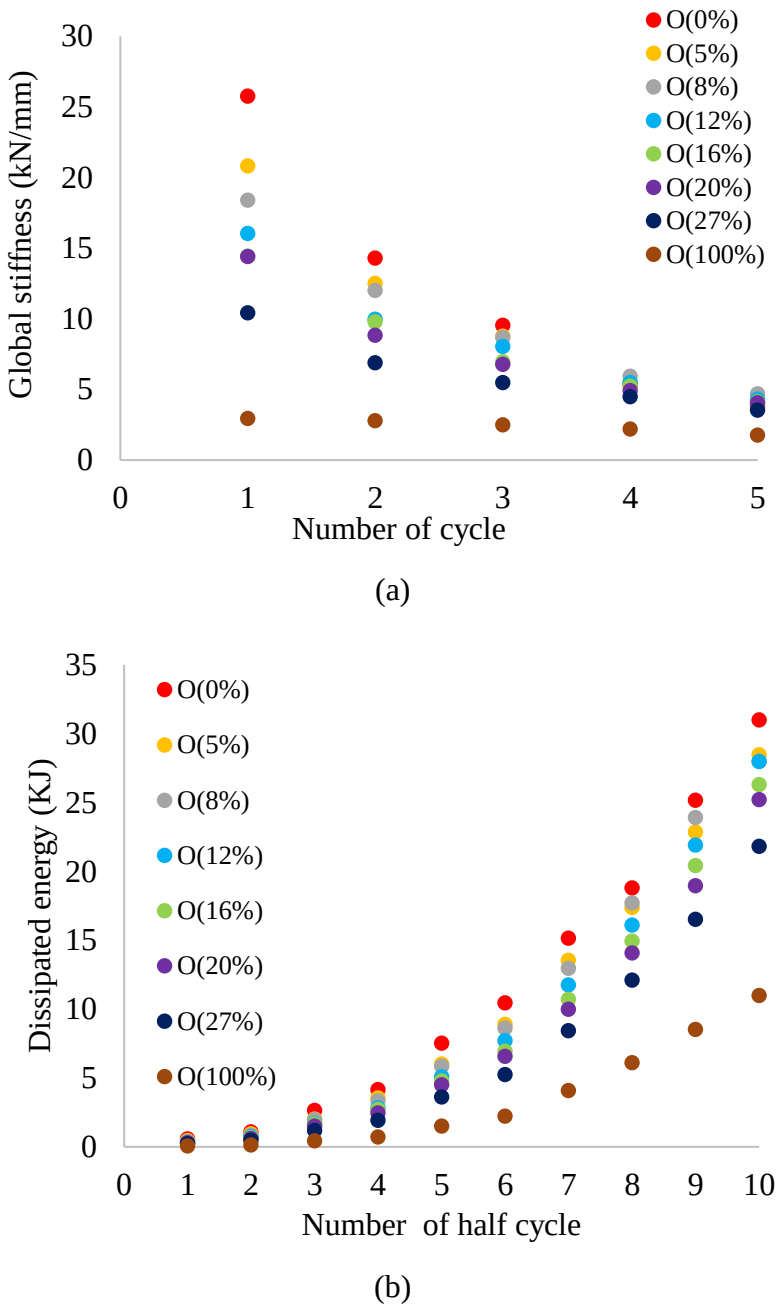

Figure 7.5: Effect of central opening area percentage on the lateral capacity of the masonry-infilled RC frame subjected to cyclic loading in terms of (a) global stiffness and (b) dissipated energy.

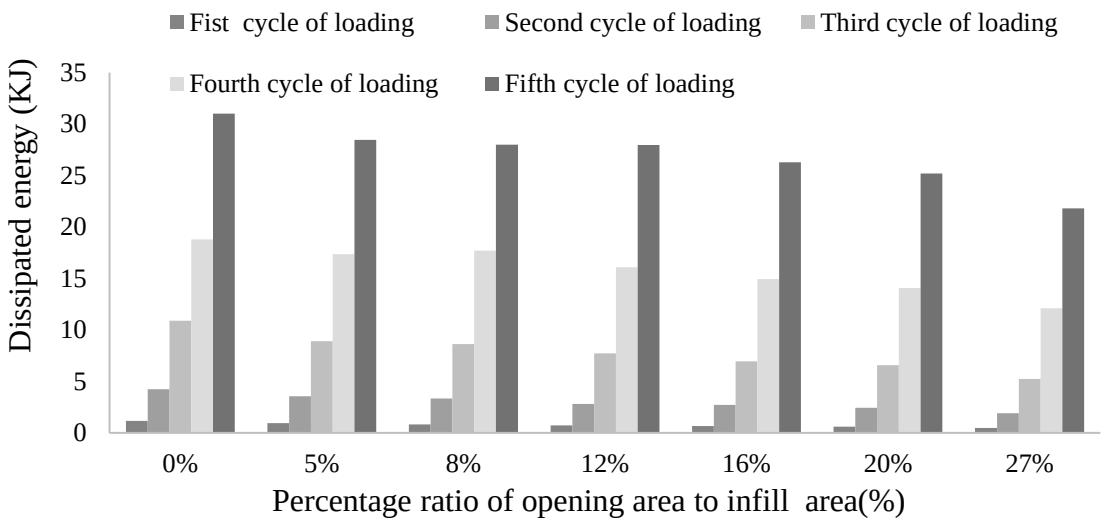

Figure 7.6: Dissipated energy of the infilled frame in relation to the opening area percentage in each cycle of loading.

Figure 7.5 indicates that the global stiffness and the dissipated energy of infilled frame with 100% opening (bare frame) are decreased by about 3-8 times compared to the corresponding ones of the infilled frame with central opening areas ranging from 5% to 27 % during the first cycles of loading, while as the lateral loading increases, the global stiffness and the dissipated energy is decreased by about 60%-75% and 100%-300%, respectively. The above observation is also supported by Asteris et al. (2011) and Kakaletsis and Karayannis (2008). Furthermore, from Figs. 7.5 and 7.6 it is observed that the global stiffness and the dissipated energy of the infilled frame with 27% opening percentage, during the first cycle of loading, decreases by about 40% and 56%, respectively, compared to the corresponding ones of the infilled frame without openings, where almost the same decrease is reported in Kakaletsis and Karayannis (2009) study (for a 25% opening, the stiffness and the dissipated energy decreases by 35% and 50%, respectively). In the same study, the authors found that for a 12.5% opening the dissipated energy of infilled frame decreases by 20%, which is the same decrease observed in this study as shown in Figs. 7.5 (b) and 7.6. Finally, according to the current study, the global stiffness and dissipated energy of the infilled frame with central opening areas ranging from 5% to 8% decrease by about 7%-15 % compared to the corresponding ones of the infilled frame without opening for all cycles of loading,

except of the stiffness at the first cycle of loading, which decreases by about 15%-20 %. Similar results regarding the global stiffness and dissipated energy of infilled frames with central openings are obtained from the experimental studies carried out by Mallick and Garg (1971), Liauw (1972), Fiorato (1970), Mosalam et al. (1997), Kakaletsis and Karayannis (2009), and by Morandi et al. (2018) as mentioned in Chapter 2 (section 2.3).

From previous observations, it can be concluded that the stiffness of the masonry-infilled RC frame decreases with the increase of the opening area while this decrease is more pronounced during early lateral loading. The trend of the variation of the initial stiffness of the infilled frame due to presence of the opening as obtained from the present study is given in Fig. 7.7 (a), and it is compared to the experimentally obtained one by Syrmakezis and Asteris (2001), Asteris et al. (2003, 2011), Surendran (2012), Cetisli (2015), and by Akhoundi et al. (2016). From this figure, it is observed that the variation of the initial stiffness as obtained from the current study is almost similar to that obtained from the studies conducted by Akhoundi et al. (2016) and Cetisli (2015). The results of the present parametric study are used to perform multiple regression analysis in order to obtain the best-fit data. Based on this fitting, the following relationship for the infill wall stiffness reduction factor is proposed:

$$\lambda_{\text{opening}} = 1 - 2.16\, {a_w}^{0.32} + {a_w}^{0.16} \tag{7.1}$$

where a_w is the percentage of the opening area expressed as a decimal number.

The proposed stiffness reduction factor is compared with the relevant ones provided by Cetisli (2015) and Asteris et al. (2011) as shown in Fig. 7.7 (b), and it is almost similar to the corresponding one obtained from Cetisli (2015) study. The proposed reduction factor is applicable for infilled frames with central openings along the diagonal, since the effect of the location opening on the lateral response of infilled frames is not considered in this study. In addition, extreme cases where the openings are extended to full height or full width of the infilled frame cannot be covered by the proposed equation.

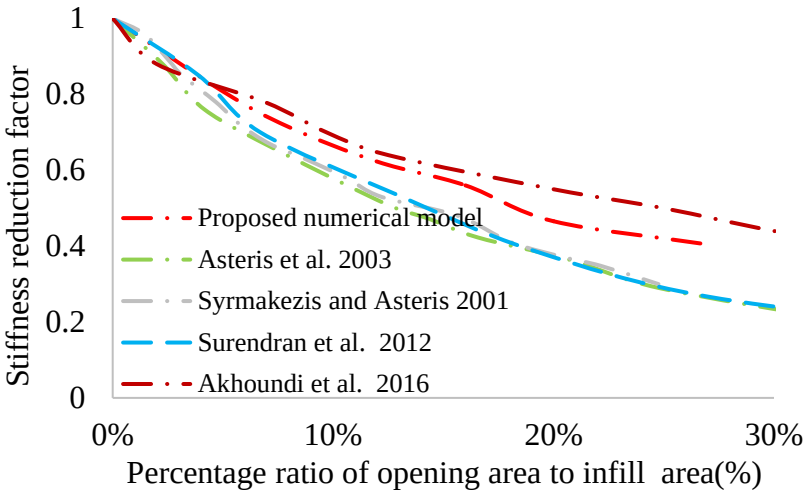

(a)

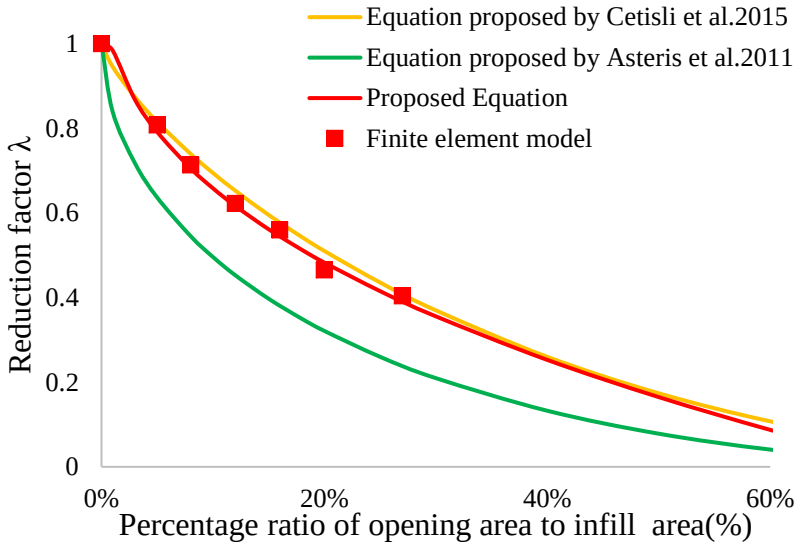

(b)

Figure 7.7: Stiffness reduction factor in relation to the opening area percentage as obtained from (a) the numerical model, and from (b) the proposed equation (Eq. 7.1) in comparison with the corresponding ones of previous studies.

The proposed reduction factor can be used with an equivalent strut model, which is a macro-model for everyday practice as mentioned in Chapter 2 (Stafford-Smith 1967; Mainstone 1974; Bazãn et al. 1980; Crisafulli et al. 2007; Asteris et al. 2011), for simulating masonry-infilled frames with openings. Hence, the proposed stiffness reduction factor (Eq. 7.1) can be used to modify the equivalent strut stiffness in case of the presence of openings. The initial stiffness of the infilled frame is determined as follows:

$$K_{elastic} = \frac{E_w(W_{infill} * t_w)}{d} \tag{7.2}$$

where E_w elastic modulus of the masonry infill, d is the clear length of diagonal of the infill, t_w is the actual thickness of the wall (thickness of the strut), and the W_{infill} is the width of equivalent strut. The equivalent strut width is calculated using the empirical equation proposed by Mainstone (1974), which is widely used approach, and it is also recommended by FEMA 306 guidelines (Eq. 2.2, section 2.4.2). For the benefit of the reader this equation is repeated below:

$$W_{infill} = 0.175\ (\lambda\, h)^{-0.4} d \tag{7.3}$$

where h is the height of the infill wall (column height between centerlines of beams), and λ represents the relative panel-to-frame stiffness and it can be calculated according to Mainstone (1974) by Eq. (2.1). For the benefit of the reader this equation is repeated below:

$$\lambda h = h * \sqrt[4]{\frac{E_w t_w \sin\theta_{str}}{4 E_c I_c H_{cl}}} \tag{7.4}$$

where H_{cl} is the clear height of the infill, E_c is the modulus of elasticity of concrete, θ_{str} is the inclination of the diagonal strut to the horizontal, arctan (H_{cl}/L_{cl}), and I_c is the moment of inertia of the column section with respect to the axis perpendicular to the plane of the infill wall.

Therefore, the equivalent strut width in case of central opening ($W_{infill\_opening}$) can be calculated as follows using the proposed stiffness reduction factor (Eq. 7.1):

$$W_{infill\_opening} = \lambda_{opening} * W_{infill} \tag{7.5}$$

The required parameters for estimating the initial stiffness of the infilled frame with central opening according to Eqs. (7.1)-(7.5) are summarized in Table 7.2.

Table 7.2: Required parameters for calculating the initial stiffness of the infilled frame according to Mainstone (1974).

Property	Value
E_w	3.37GPa
t_w	0.110m
H_{cl}	1.67m
H	2.0m
d_m	2.82m
θ_{str}	36
E_c	9.1 GPa*
I_c	$1.72*10^{-4}$ m^4

**The modulus of elasticity of the concrete is taken equal to the cracked modulus of elasticity as defined in the numerical model (Chapter 4 section 4.6.1.1).*

The initial stiffness of the infilled frame with central opening ranging from 5% to 27% as obtained from the above simplified-approach, and as obtained from the current numerical model (the initial slope of the curves in Fig. 7.2) are presented in Table 7.3.

Table 7.3: Initial stiffness of the infilled frame with 5%-27% central opening as obtained from Mainstone model using the proposed reduction faction, and as obtained from the numerical analysis.

Opening percentage	0%	5%	8%	12%	16%	20%	27%
$K_{elastic}$ (Eq. 7.2 Mainstone 1974)	36.25	29.29	25.87	22.58	20.318	16.88	14.66
$K_{elastic}$ numerical model	34.52	26.88	25.77	22.05	20.76	19.12	15.3

Based on Table 7.3 it is observed that the results obtained from Mainstone's (1974) empirical equation (Eq. 7.3 and Eq. 7.4) using the proposed stiffness reduction factor to modify the equivalent strut stiffness in case of the presence of the openings are compared and presented an agreed correlation with those obtained by the cyclic analysis of the three-story masonry-infilled RC frame model considering different central opening area percentage, ranging from 5% to 27%.

In the following paragraphs, the shear stresses, the deformed shape, the infill wall-frame separation, and the crack pattern resulted from the non-linear cyclic analysis of the three-story masonry-infilled RC frame model with central opening are presented and discussed, as well. The shear stress distribution and the deformed shape of the three-story masonry-infilled RC frame with central opening ranging from 5% to 27%, during the fourth cycle of loading (maximum base-shear) in the positive and negative direction of loading are presented in Fig. 7.8 and Fig. 7.9, respectively.

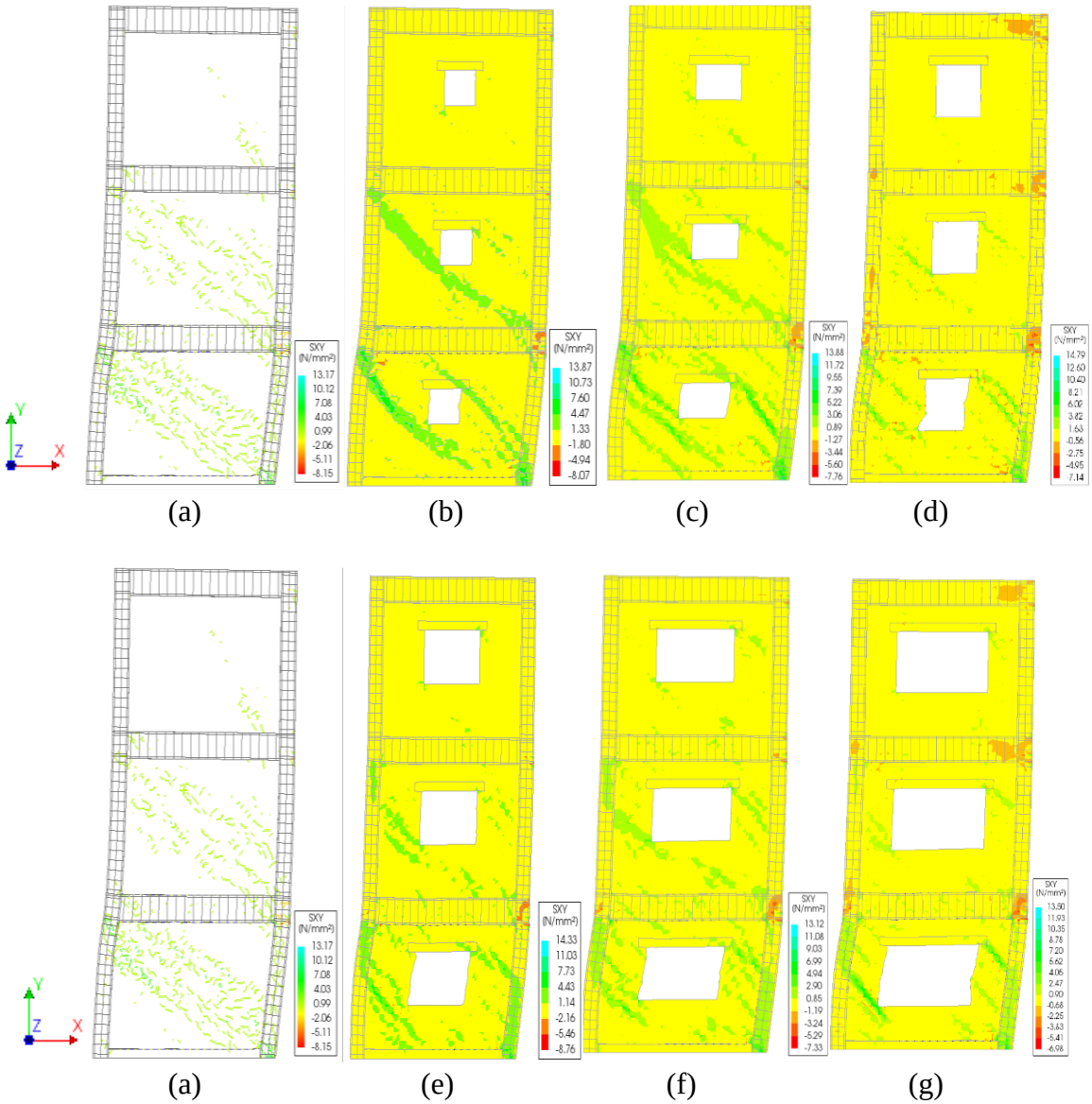

Figure 7.8: Shear stress distribution in the masonry-infilled RC frame with central opening area equal to (a) 0%, (b) 5%, (c) 8%, (d) 12%, (e) 16%, (f) 20%, and (g) 27% during the fourth cycle of loading in the positive direction.

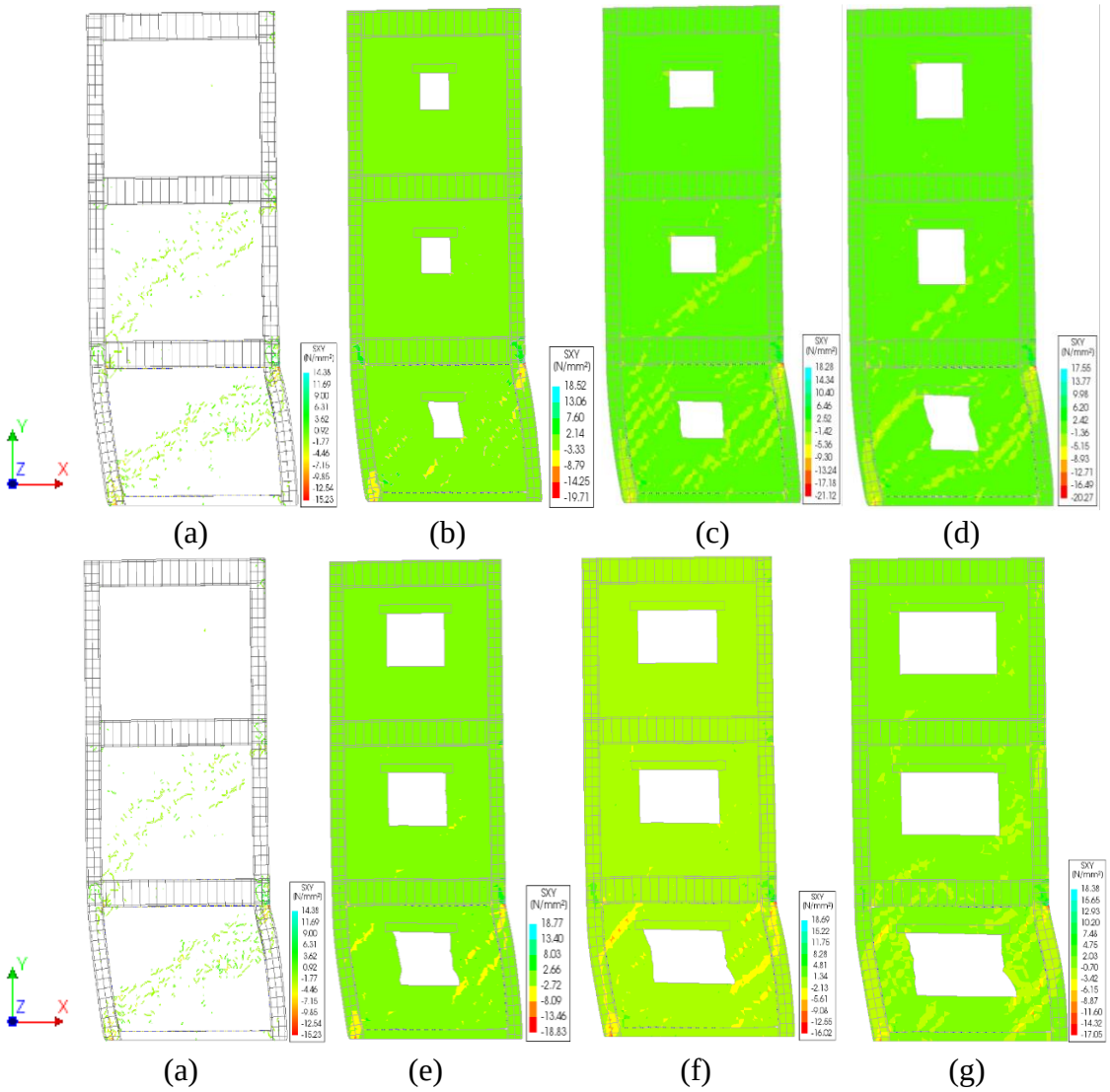

Figure 7.9: Shear stress distribution in the masonry-infilled RC frame with central opening area equal to (a) 0%, (b) 5%, (c) 8%, (d) 12%, (e) 16%, (f) 20%, and (g) 27% during the fourth cycle of loading in the negative direction.

Figures 7.8 and 7.9 show that high shear stresses are concentrated in the first floor, somewhat less in the second floor and almost no shear stresses in the third floor. From these figures it is observed that high shear stresses are concentrated at the corners of the opening (above and below the opening), and they are propagated near the loaded corners of the infill wall where the diagonal compression path is developed. Adding to this, high concentration of shear stresses is observed at the beam-column joints, and at the ends columns in the area which contacted the diagonal of the infill wall at the first

floor. This occurs mainly at the first floor in all three-story masonry-infilled RC frames with any opening percentage. Furthermore, as the central opening area increases, the shear stresses are increased and are more speared over the surface of the infill wall, since they are transmitted from the upper and lower parts of the opening to the sides of it, and then they are propagated to the bounding frame (Figs. 7.8 c, d, f, g and Figs. 7.9 c, d, f, g). Therefore, as the opening area increases it leads to a brittle shear failure of the columns (deformed shape of the column in Figs. 7.8 e, f, g and 7.9 e, f, g), due to the increases in the concentration of the shear stresses at the ends columns in the area which contacted the diagonal of the infill wall. The same observations to the above were reported in the experimental studies conducted by Asteris (2011), Kakaletsis and Karayannis (2008), Akhoundi et al. (2016), Tekeli and Aydin (2017), Morandi, Hak, and Magenes (2018) and Ahani et al. (2019). Furthermore, Figs. 7.8 and 7.9 indicate that the deformation along the height of the structure is not linearly distributed, especially in the case of large openings (Figs. 7.8 c, d, f, and g and Figs. 7.9 c, d, f, and g). More specifically, the inter-story deformation along the height of the second and third floor of structure is almost the same and completely different from that of the first floor. This indicates that the height-wise distribution of the shear forces of the three-story infilled frame with openings is not linearly varying leading to *soft-story mechanism* at the first floor.

Figures 7.8 and 7.9 clearly indicate that the infill wall with opening acts as a multi-diagonal no-tension struts (as mentioned in sections 2.3 and 2.4). Specifically, the distribution of the shear stresses over the infilled frame with different percentage of central opening shows that two diagonal struts develop within the infill at the first and second floor passing through the upper-left and lower-right of the infill wall during the positive direction of loading (Fig. 7.8). The increase of the opening area results in the restriction of these struts in a much small area of the infill at the top and lower parts of it as it is clearly indicated in Figs. 7.8 (e), (f), (g) and 7.9 (e), (f), (g). Based on Figs. 7.8 and 7.9 it can be concluded that the masonry infill wall with openings could be better represented by multi-diagonal no-tension strut elements instead of a single-diagonal strut element. This observation is also supported by several researchers such as

Thiruvengadam (1985), Chrysostomou (1991), Crisafulli (1997), Chrysostomou et al. (2002), El-Dakhakhni et.al (2001, 2002, 2004), and in Crisafulli and Carr (2007).

Figure 7.10 shows the crack propagation on the infilled frame with 16% central opening area at the first floor during the first, third, fourth and fifth cycle of loading for both directions. It is important to note that, the crack propagation that occurred on the infilled frame with 16% central opening area is almost the same with that which has occurred on the infilled frame with any opening percentage.

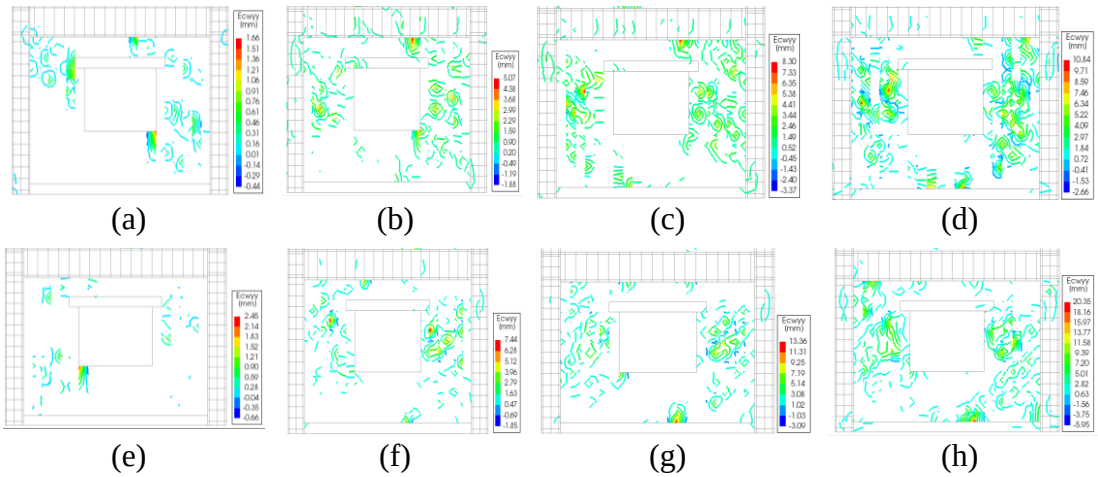

Figure 7.10: Crack propagation in the infilled frame with central opening area equal to 16% at the first floor during the (a) first, (b) third, (c) fourth and (d) fifth cycle of loading in the positive direction, and during the (e) first, (f) third, (g) fourth and (h) fifth cycle of loading in the negative direction of loading.

From Fig. 7.10 (a) it is observed that diagonal cracks appear at the upper left and bottom-right corners of the opening with maximum crack width equal to 1.7 mm, and these cracks are propagated to the loaded corners of the infill wall (where the diagonal compression path is developed). During the third cycle of loading, the diagonal cracks extend to the other corners of the opening with maximum crack width equal to 5 mm (Figs. 7.10 b and f), while distinct diagonal shear cracks appear near the loaded corners of the infill wall. During the subsequent cycles of loading, the previously opened cracks reopened, became wider and propagated in the body of the infill wall (Figs.7.10 c, d, g and h). More specifically, upon increasing the horizontal loading the shear cracks are transmitted from the upper and lower parts of the opening to the sides of it, and they tend to concentrate from one loaded corner to the other of the infill wall. This indicates the *corner crushing* of the infill wall at the first floor. After that, high diagonal shear

cracks are observed at the beam-column joints, and at the ends columns in the area which contacted the diagonal of the infill wall, with maximum crack width equal to 10 mm, especially during the last cycle of loading (Figs.7.10 d and h). This is associated to the shear failure in the upper ends of the column (*short-column mechanism*) resulting in a marked decrease of the overall lateral stiffness of the infilled frame as shown in Fig.7.5 (a). The shear failure of the columns (*short-column mechanism*) is caused by the infill wall strut action as described in Chapter 5 (section 5.4.2).

As previously mentioned, the crack propagation that occurred on the infilled frame with 16% central opening area is almost the same with that occurred on the infilled frame with any opening percentage. In this paragraph, the crack pattern that may occur in the infilled frame with central opening equal to 5%, 20% and 27% subjected to cyclic loading is discussed according to the distribution of the shear stresses presented in Figs. 7.8 and 7.9, which is able to indicate the location where the cracks arise. From Figs. 7.8 and 7.9 is it observed that the shear stress distribution, and consequently the crack pattern in the case where the opening percentage was equal to 5% (Figs. 7.8 b and 7.9 b) is quite similar to that observed in solid infilled frame model (Figs. 7.8 and 7.9 a). Probable reason for this is the size of the opening in the infill wall which is quite small. More details regarding the shear stress distribution and crack pattern on the solid masonry-infilled RC frame presented in Chapter 5 (section 5.4.2). Furthermore, in cases where the opening percentage is equal to 20% and 27% shear cracks are observed at the corners of the opening and continue horizontally and diagonally towards the columns leading to a brittle shear failure of the columns.

As shown in Figs. 7.8 and 7.9, the maximum shear stresses are concentrated near the loaded corners of the infill wall (compression diagonal path developed along two opposite corners of the infill wall), while near the non-loaded corners, the infill wall separates from the RC frame (zero shear stresses). Figure 7.11 shows the gap-opening along the infill-frame interface at the first story, and at the bottom of the second story of the three-story masonry-infilled RC frame model with central opening ranging from 5% to 27%, during the first cycle of loading.

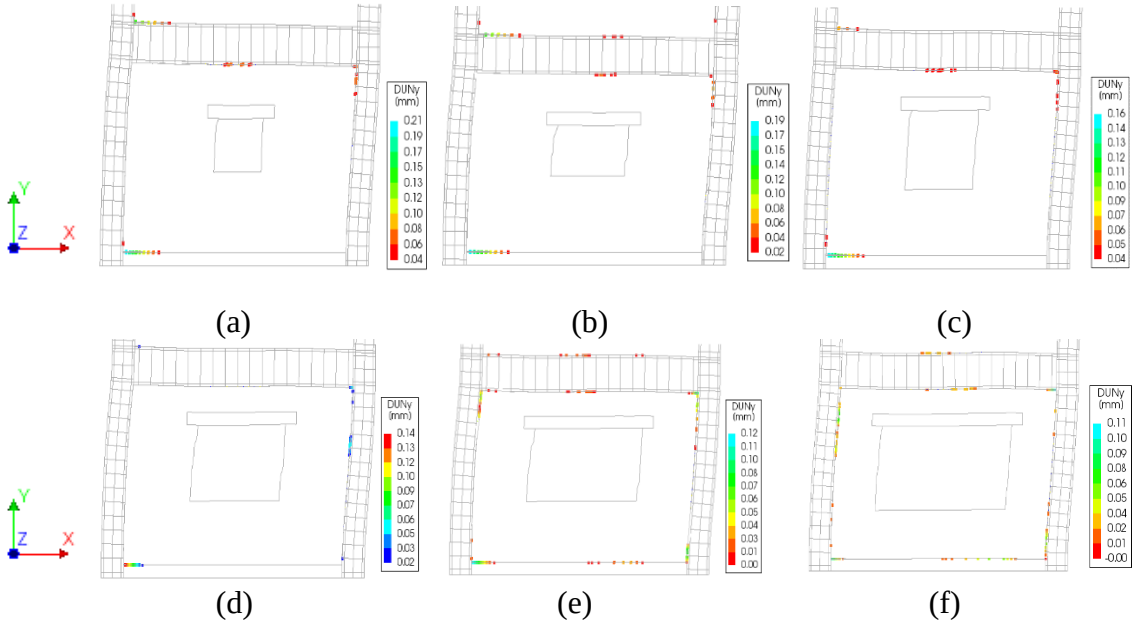

Figure 7.11: Gap-opening between masonry infill wall and RC frame at the first story and at bottom of the second story during the first cycle of loading in the positive direction of loading in the cases where the opening area is equal to : (a) 5%, (b) 8%, (c) 12%, (d) 16%, (e) 20%, and (f) 27%.

From Fig. 7.11 it is observed that the infill-frame separation occurs at a very early stage of loading in the infilled frame with any opening percentage. Specifically, during the first cycle of loading the average gap-opening at the columns-infill interface in the first floor is less than 0.1mm, while at the top beam-infill interface at the first floor and at the bottom beam-infill interface at the second floor ranges from 0.1mm to 0.2mm. In Fig. 7.11 the dots depict the area of infill-frame that separation occurs in each case of opening. From this figure it is observed that the infill-frame separation depends on the area of the opening, since as the opening percentage increases leads to an increase in the area where the infill-frame separation occurs.

By examining the shear stress distribution, the developed crack pattern, and the infill-frame separation on the infilled frame with central opening ranging from 5% to 27% subjected to cyclic loading, it can be concluded that as the lateral loading increases the failures occur in the masonry infill wall and propagate to the RC frame. The following combination of failure modes in the infilled frame with central opening ranging from 5% to 27% during the cyclic test is observed due to the interaction of infill wall with the RC frame: *corner crushing*, *diagonal cracking*, and *sliding shear* (Chapter 2, section

2.2). Eventually, the *frame failure* mode occurs which consists of the failure of column-beam joints, and of the shear failure of the columns at the first floor of the structure. The *frame failure* mode is associated with a weak frame and with weak joints in the frame (non-seismic design and detailing of RC frame), as well as the formation of a short column after the *corner crushing* of the infill wall with opening. The *short-column mechanism* is more pronounced in the cases where the opening area ranges from 20% to 27%, since the shear cracks and stresses at the top of both columns at the first floor became wider as shown in Figs. 7.8 (f), (g) and 7.9 (f) (g). Therefore, as the opening area increases, brittle failures may occur in infilled frames with opening such as a *short-column mechanism*, which is very typical for some types of windows, since the infill walls are not continuous through all the height of the frame. Furthermore, a *soft-story mechanism* (Chapter 2, section 2.2) is developed in the infilled frame with any opening percentage, due to the large concentration of damage in a few members of the infilled frame at the first floor, where this mechanism is more pronounced in the cases of large openings.

Therefore, the presence of the central window opening influences significantly the lateral response of infilled frames subjected to cyclic loading as obtained from non-linear cyclic analysis on the validated three-story masonry-infilled RC frame model with opening ranging from 5% to 27. More specifically, as the area of the central opening increases the lateral strength, stiffness and the dissipated energy of the infilled frame decreases. Furthermore, the three-story masonry-infilled RC frame model with different areas of central opening used in this parametric study can predict the real response of such type of structure subjected to in-plane cyclic loading, since the results obtained from the current study are almost similar with that obtained from relevant experimental and numerical studies conducted in the past in terms of lateral capacity of infilled frames with different central opening percentages, while this numerical model can capture the most important failures that may occur on infilled frames with different central opening percentages, since the failure modes and crack pattern observed in the current study are almost the same with that observed in the experimental studies conducted by Buonopane and White (1999), Chiou et al. (1999b), Kakaletsis and Karayannis (2009).

7.2 Effect of the TRM retrofitting technique on the lateral response of the three-story masonry-infilled RC frame with central openings

In this part of the thesis, the effectiveness of using the TRM composite material for retrofitting masonry-infilled RC frames with central openings is investigated. This is achieved by performing numerical experiments through a non-linear cyclic analysis on the validated three-story masonry-infilled RC frame model with TRM considering different central opening area as shown in Table 7.1. The numerical specimens were developed following the same modeling scheme with the validated numerical model (Chapter 4), and they are subjected to five cycles of prescribed displacement loading (section 4.7). The TRM strengthening scheme considered on the numerical models in this parametric study is the same with that of the validated numerical model as follows: carbon-TRM fully wrapped at the ends of columns at the first (three layers) and second floor (two layers), glass-TRM externally bonded on the face of the infill walls, two layers of glass-TRM at the first floor, and one layer of glass-TRM on the second and third floor.

The results obtained from the non-linear cyclic analysis on the three-story masonry-infilled RC frame model with different size of central opening without (dashed-line) and with TRM (solid-line) are presented in Fig. 7.12 in terms of base-shear versus top-floor displacement (hysteresis curves). From Fig. 7.12 it is observed that the TRM contributes to increase significantly the lateral capacity of the three-story masonry-infilled RC frame with any central opening percentage. More specifically, the area enclosed by the loop in the base-shear versus top-floor displacement diagram in each cycle of loading of the retrofitted infilled frame with openings is almost two times larger compared to that of the unretrofitted one. Furthermore, the maximum base-shear of the retrofitted infilled frame with openings is about 1.5 times larger than the corresponding one of the unretrofitted infilled frame with openings. This occurs for all infilled frames with any opening percentage. It is important to mention that the results of the retrofitted specimen with small opening area (5%) as shown in Fig. 7.12 (a), and the results of the retrofitted specimen without opening (Fig. 5.5 c, in section 5.4.1) are almost similar in terms of maximum base-shear, and in terms of base-shear versus top-floor displacement.

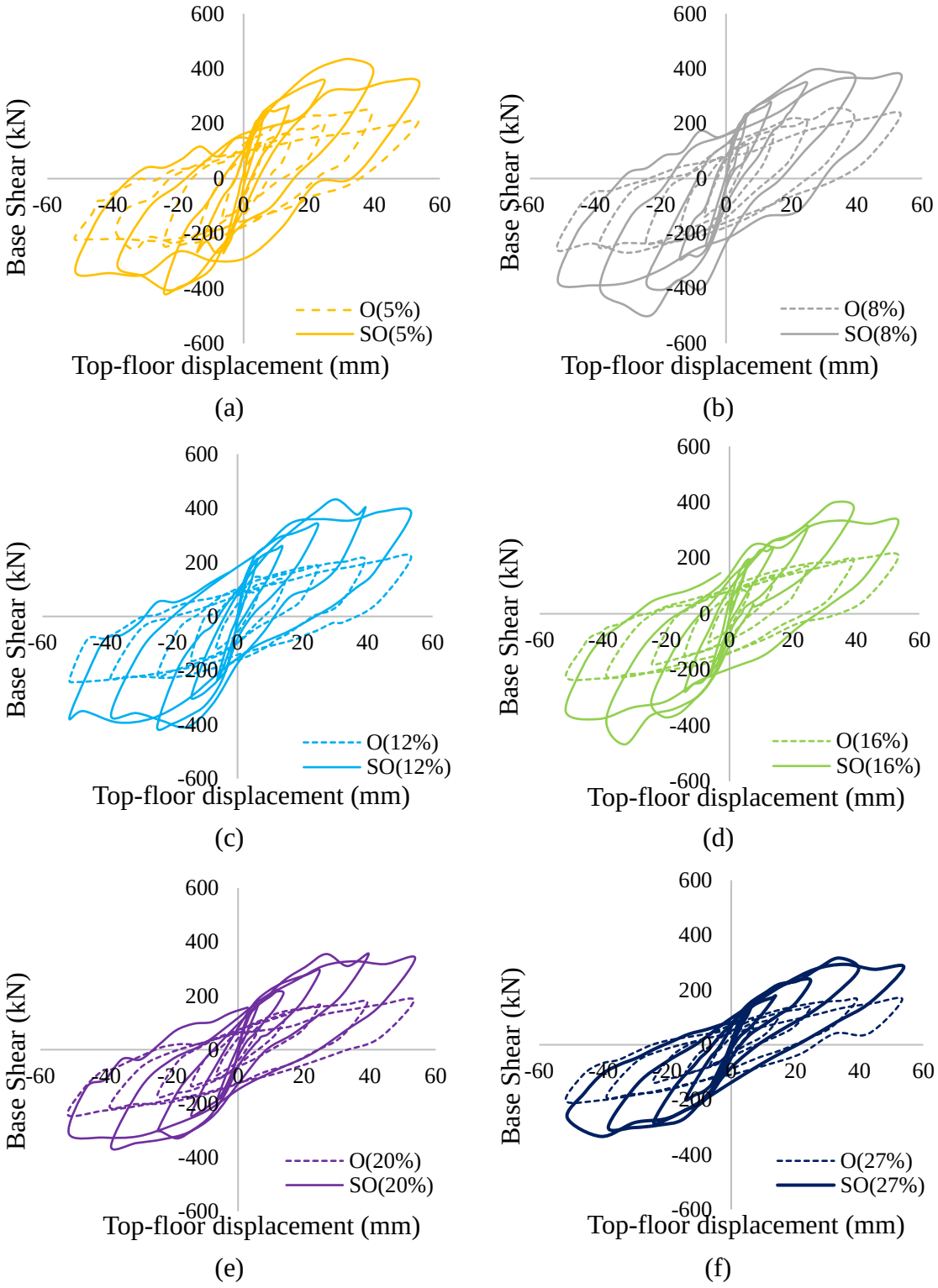

Figure 7.12: Base-shear versus top-floor displacement of three-story masonry-infilled RC frame with different central opening area percentage without (dashed line) and with TRM (solid line).

For the benefit of the reader, Tables 7.4 and 7.5 show the increase in peak base-shear in each cycle of loading of the retrofitted infilled frame with openings compared to that of unretrofitted infilled frame with openings; for the positive ($V_{max,i}$), and negative ($V_{max,j}$) direction of loading, respectively.

Table 7.4: Comparison of the retrofitted and unretrofitted infilled frame with different central opening percentage in terms of peak base-shear in each cycle of loading for the positive direction of loading.

		$\frac{V_{max\,i_{retrofitted}} - V_{max\,i_{unretrofitted}}}{V_{max\,i_{unretrofitted}}}$ (%)					
Percentage ratio of opening area to infill area (%)	**0%**	**5%**	**8%**	**12%**	**16%**	**20%**	**27%**
Cycle							
1	53%	76%	80.0%	97.8%	90.0%	89.9%	88.0%
2	53%	80%	77.6%	96.5%	75.7%	68.0%	77.7%
3	54%	79%	71.5%	84.7%	87.7%	78.3%	70.6%
4	60%	64%	63.9%	93.9%	97.3%	78.5%	69.0%
5	71%	67%	58.8%	74.3%	60.1%	70.5%	71.2%

Table 7.5: Comparison of the retrofitted and unretrofitted infilled frame with different central opening percentage in terms of peak base-shear in each cycle of loading for the negative direction of loading.

		$\frac{V_{max\,j_{retrofitted}} - V_{max\,j_{unretrofitted}}}{V_{max\,j_{unretrofitted}}}$ (%)					
Percentage ratio of opening area to infill area (%)	**0%**	**5%**	**8%**	**12%**	**16%**	**20%**	**27%**
Cycles							
1	33%	83%	78%	92%	90%	85%	98%
2	42%	50%	51.1%	88.8%	83.6%	84.4%	95.2%
3	84%	74%	66.2%	90.3%	75.1%	75.6%	96.2%
4	131%	58%	60.5%	63.0%	71.6%	69.8%	59.0%
5	114%	57%	45.6%	60.4%	54.7%	28.4%	29.7%

From Tables 7.4 and 7.5 it is observed that the base-shear of the retrofitted infilled frame with 8% and 27% opening percentage increases by about 76%-83% and 70%-

98%, respectively, compared to that of the unretrofitted one during the first three cycles of loading, while during the fourth and fifth cycle of loading this increase is equal to 57%-64%, and to 30%-60% for 8% and 27% opening percentage, respectively. Furthermore, it is observed that the increase in the peak base-shear during the first three cycles of loading for both directions of loading of the retrofitted infilled frame with opening area ranging from 8% to 27% is more significant compared to the corresponding one of the retrofitted infilled frames without openings (comparing the unretrofitted solid masonry-infilled frame with the retrofitted one), especially in the cases where the opening area ranges from 16% to 27%. On the other hand, during the last cycles of loading, the TRM contributes to increase the base-shear of the infilled frame with central opening ranging from 8% to 27% by about 60%-80%, while the base-shear of the infilled frame without openings is increased by about 60%-120%.

Therefore, from Tables 7.4 and 7.5 it is observed that the lateral capacity of the retrofitted infilled frame with central openings is significantly increased compared to that of the unretrofitted one, while this increase is more pronounced at the first to third cycles of loading compared to that at the fourth and fifth cycles, which occur at large displacements. This is attributed to the fact that at early stage of lateral loading the TRM is fully activated, since it takes the high shear stresses and deformations that occur in the infilled frame due to the presence of the opening (the shear stresses and the cracks of the infilled frame became larger due to the presence of the opening, especially in the case of large openings). Specifically, the high shear stresses on the infill wall with openings are transferred to the TRM in local level during the first cycles of loading, and the composite material sustains these high tensile and shear stresses (without losing the structural integrity of the textile reinforcement), due to its high tensile and compressive capacity (consists of high strength mortar and high strength textile). Therefore, from the early loading stage the TRM prevents the large shear deformation of the infill wall due to the presence of the opening leading to significant increase in the lateral capacity of the structure. Furthermore, from the above tables it is also observed that as the lateral loading is increased, the TRM provides a smaller increase to the lateral capacity of the infilled frame with central openings compared to that observed during the early lateral loading, while the increase on the lateral capacity of the infilled frame with central

openings became smaller as the opening area increases. This is due to the brittle failures that occur in the infilled frame in the last cycles of loading, especially when the opening percentages ranging from 20% to 27% (the *short-column mechanism* is more pronounced in the cases where the opening area ranges from 20-27% as shown in Figs. 7.8 f, g and 7.9 f, g).

Figure 7.13 presents the global stiffness (Eq. 5.1) versus the number of cycles of loading (Fig. 7.13 a), and the dissipated energy (Eq. 5.2) in relation to the number of half cycles of loading (Fig. 7.13 b) as obtained from the non-linear cyclic analysis on three-story masonry-infilled RC frame with different central opening area percentage without (dashed-line) and with TRM (solid-line). From Figs. 7.13 (a) and (b) it is observed that the global stiffness and dissipated energy of retrofitted infilled frame with any opening percentage are increased by about two times during the first three cycles of loading, and by 1.2-1.8 times during the rest of cycles of loading, compared to the corresponding ones of the unretrofitted specimen. The increase in the global stiffness and dissipated energy is more pronounced at the first to third cycles of loading compared to that at the fourth and fifth cycles, due to the full activation of TRM from the early stage of loading, and due to brittle failures that occur during the last cycles of loading as previously explained. Furthermore, Fig. 7.13 (a) shows that the global stiffness of the retrofitted infilled frame with opening percentage equal to 27% is almost the same with that of the infilled frame without openings during the cyclic loading. Adding to this, the retrofitted infilled frame with opening percentage equal to 20% and 27 % has almost the same dissipated energy with that of the infilled frame without openings until the fourth cycle of loading as shown in Fig. 7.13 (b). Therefore, the TRM contributes to increase the global stiffness and the dissipated energy of the infilled frame with openings by restoring the load-bearing capacity to that of the infilled frame without opening, and by delaying the strength degradation of the infilled frame due to presence of the opening.

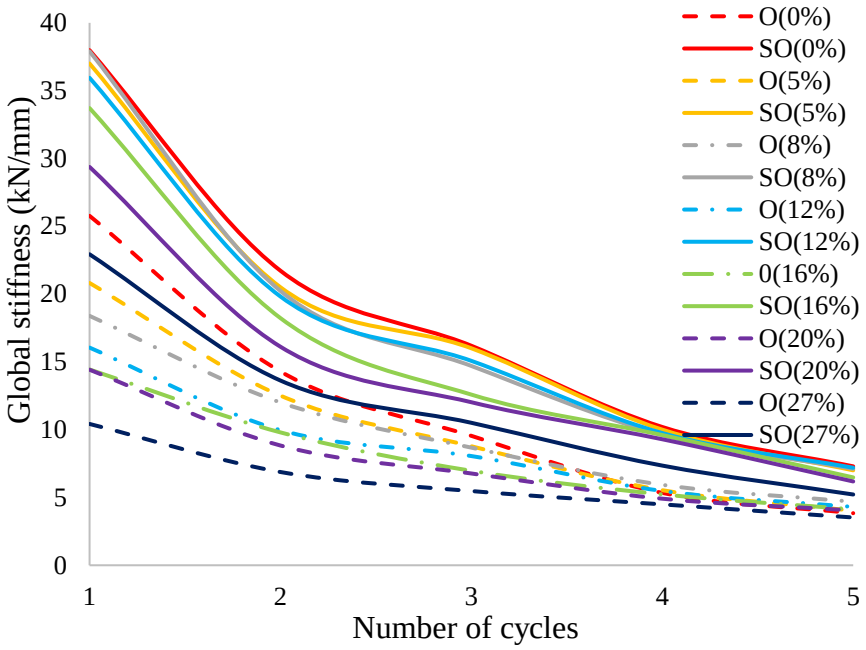

(a)

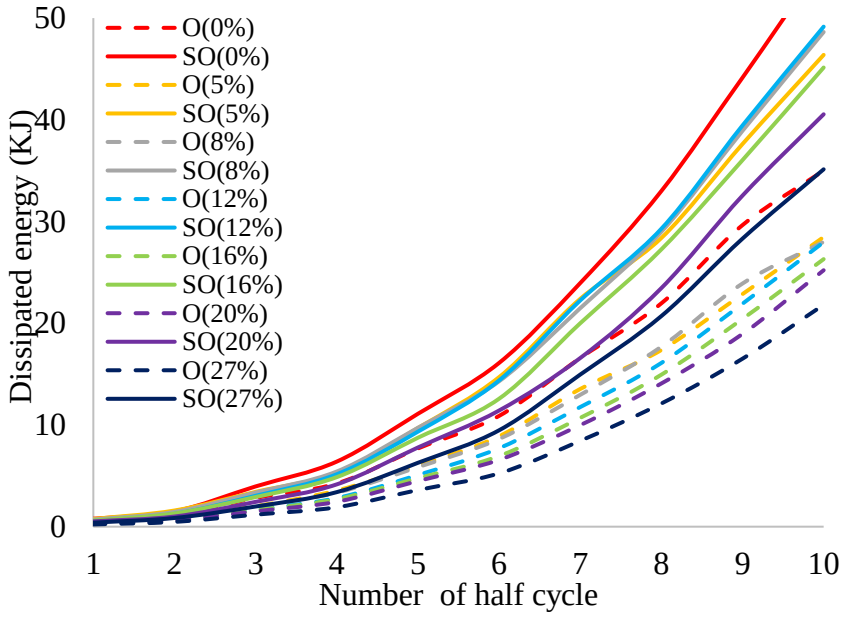

(b)

Figure 7.13: Comparison of the results for different size of central opening in masonry-infilled RC frame with and without TRM in terms of (a) global stiffness and (b) dissipated energy.

The effectiveness of using the TRM for retrofitting infilled frames with openings is given in Fig. 7.14, which shows the global stiffness and the dissipated energy of the retrofitted and unretrofitted specimen with any opening percentage during the fourth

cycle of loading. From Fig. 7.14 it is observed that the global stiffness of the retrofitted specimen with any opening percentage at the maximum base-shear (fourth cycle of loading) increases by almost two times compared to that of the unretrofitted one. The same increase is observed by comparing the solid infilled frame with and without TRM. Furthermore, the dissipated energy of the retrofitted specimen with any opening percentage during the fourth cycle of loading increases by about 1.5-1.8 times compared to that of the unretrofitted specimen.

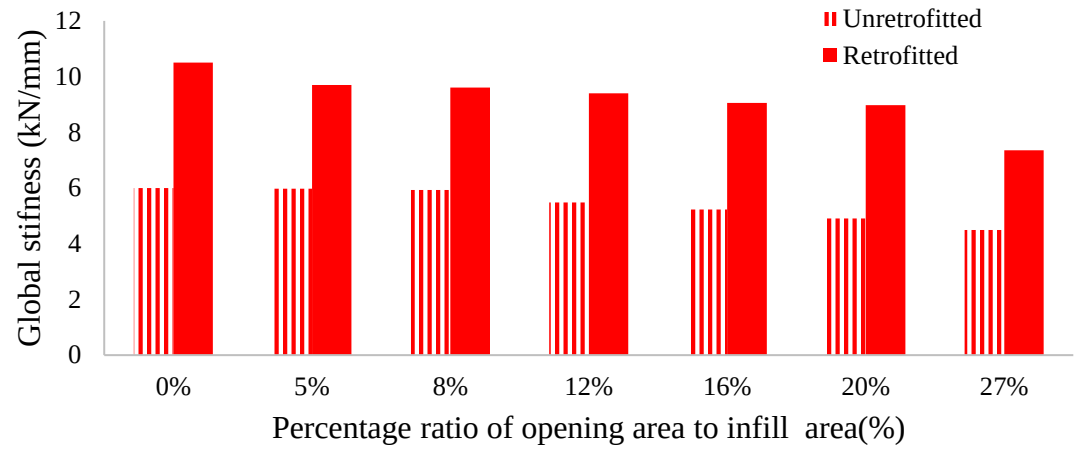

(a)

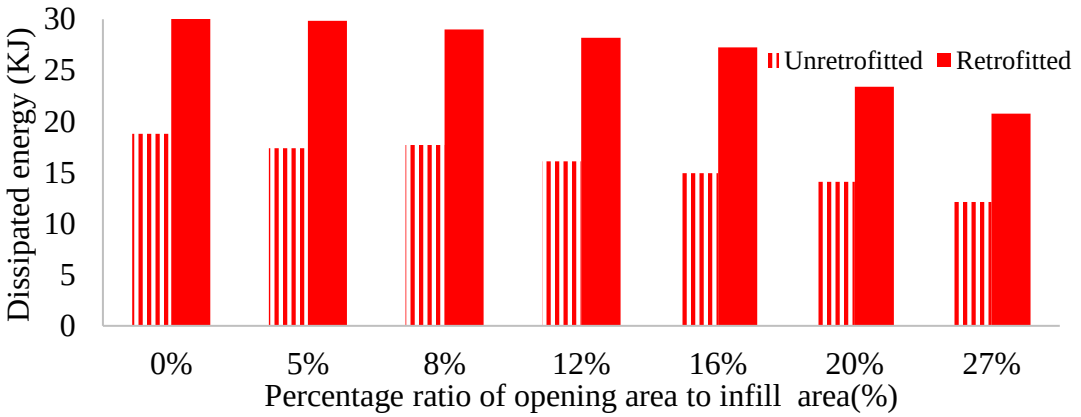

(b)

Figure 7.14: Comparison of the retrofitted and unretrofitted specimen with different central opening percentage in terms of (a) global stiffness, and (b) dissipated energy at the fourth cycle of loading.

The results of the present parametric study concerning the stiffness of the retrofitted infilled frame with different opening area percentage are used to perform a regression

analysis, leading to the following initial stiffness reduction factor for the retrofitted infilled frame with central opening:

$$\lambda_{TRM\_opening} = 1 - 2.0\ {a_w}^{0.38} + {a_w}^{0.15} \quad (7.6)$$

where a_w is the percentage of the opening area expressed as a decimal number.

The proposed reduction factor is applicable for infilled frames retrofitted with TRM with central openings along the diagonal of the infill wall with a percentage of opening over 5%. This reduction factor can be used for simulating retrofitted masonry-infilled frames with openings following the macro-modeling approach, where the contribution of externally bonded layers of TRM are considered by introducing an additional term in the equations usually employed for unstrengthened infilled frames. More specifically, this proposed reduction factor can be used in the TRM equivalent tie-element model proposed by Koutas et al. (2014b) and Pohoryles et al. (2020a) as mentioned in Chapter 2 (section 2.5.3) in order to predict the lateral strength and stiffness of retrofitted masonry infilled frames with central openings subjected to lateral loading.

Figure 7.15 presents the comparison of the proposed initial stiffness reduction factor for the retrofitted (Eq. 7.6) and unretrofitted (Eq. 7.1) infilled frame in relation to the central opening percentage. Comparing the two curves, a sharper decrease in the reduction factor is observed in the unretrofitted infilled frame than the retrofitted one. This is attributed to the full activation of TRM due to the presence of the opening in the infilled frame from an early stage of loading as previously discussed. Furthermore, from Fig. 7.15 it is observed that in the cases where the opening percentage ranging from 20% to 30%, the initial stiffness of retrofitted infilled frame is reduced by about 30%-55%, while the initial stiffness of unretrofitted infilled frame is reduced by about 50%-65%. Therefore, this retrofitting method is able to delay the stiffness degradation of infilled frames due to presence of the opening.

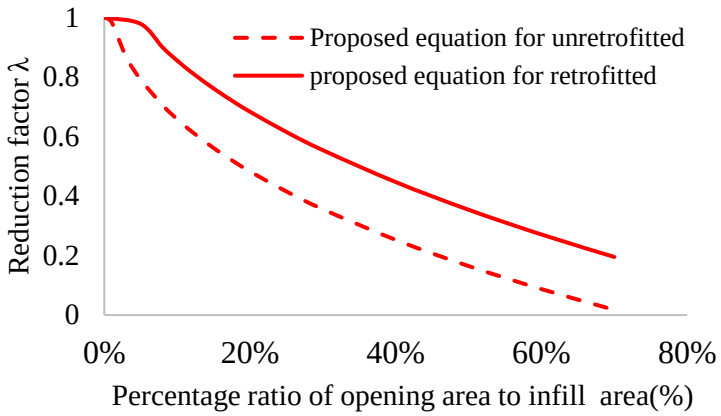

Figure 7.15: Comparison of the proposed initial stiffness reduction factor for the retrofitted and unretrofitted infilled frame with different central opening percentage.

In the following paragraphs, the shear stresses, the deformed shape, the infill wall-frame separation and the crack pattern resulted from the non-linear cyclic analysis of the three-story retrofitted masonry-infilled RC frame model with central opening are presented and discussed, as well. It is important to mention that the shear stresses and cracks patterns of the retrofitted infilled frame model with different central openings as will presented in this section are those observed on the external face of TRM since the TRM plane-stress elements overlay the masonry plane-stress elements (section 4.5). Nevertheless, this leads to sufficient indication about the failures occurred in the infilled frame with openings (without the TRM).

The shear stress distribution and the deformed shape of the three-story retrofitted masonry-infilled RC frame with central opening ranging from 5% to 27%, during the fourth cycle of loading in the positive and negative direction of loading are presented in Fig. 7.16 and Fig. 7.17, respectively.

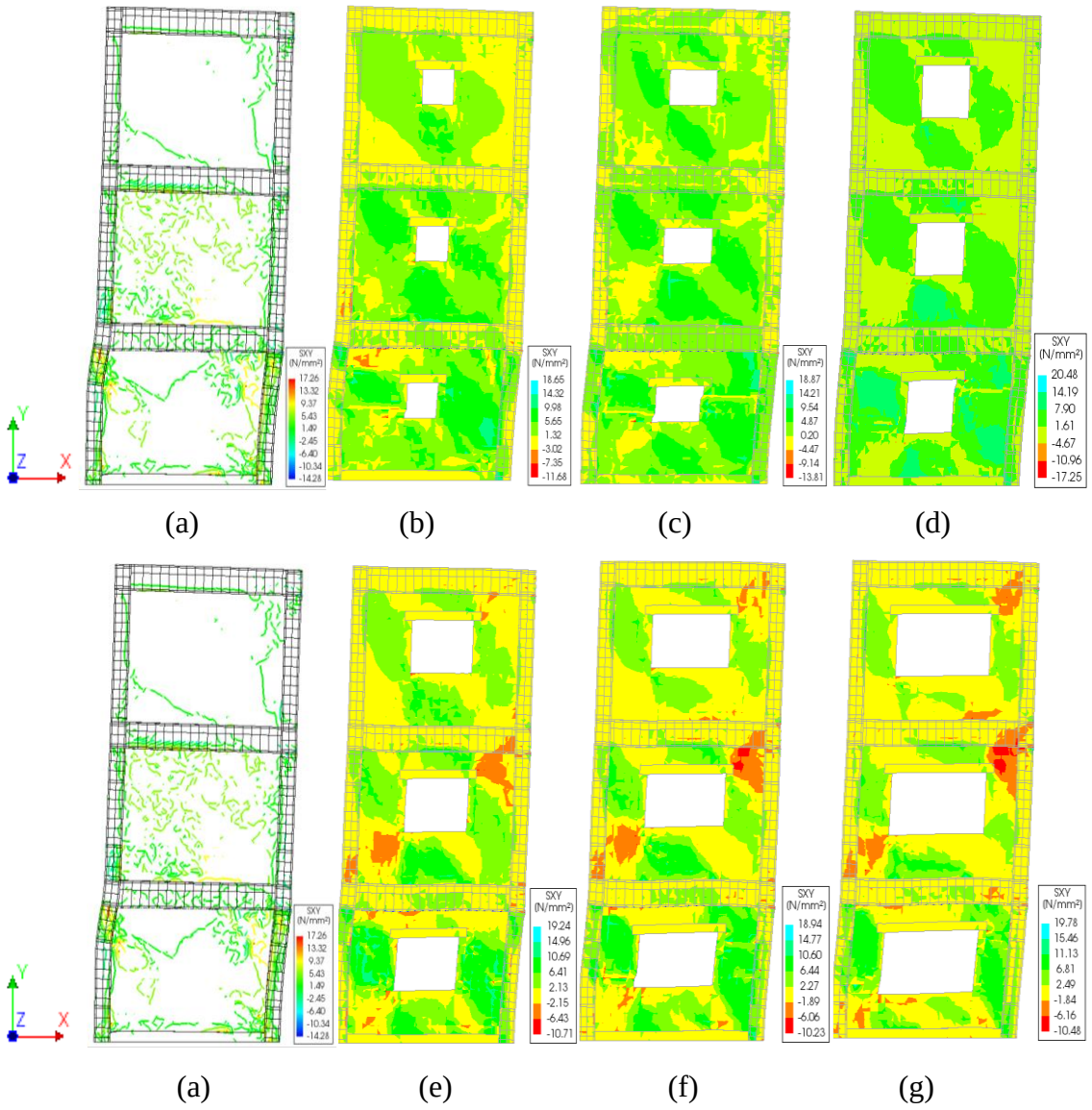

Figure 7.16: Shear stress distribution in the retrofitted infilled frame with central opening area equal to (a) 0%, (b) 5%, (c) 8%, (d) 12%, (e) 16%, (f) 20%, and (g) 27% during the fourth cycle of loading in the positive direction of loading.

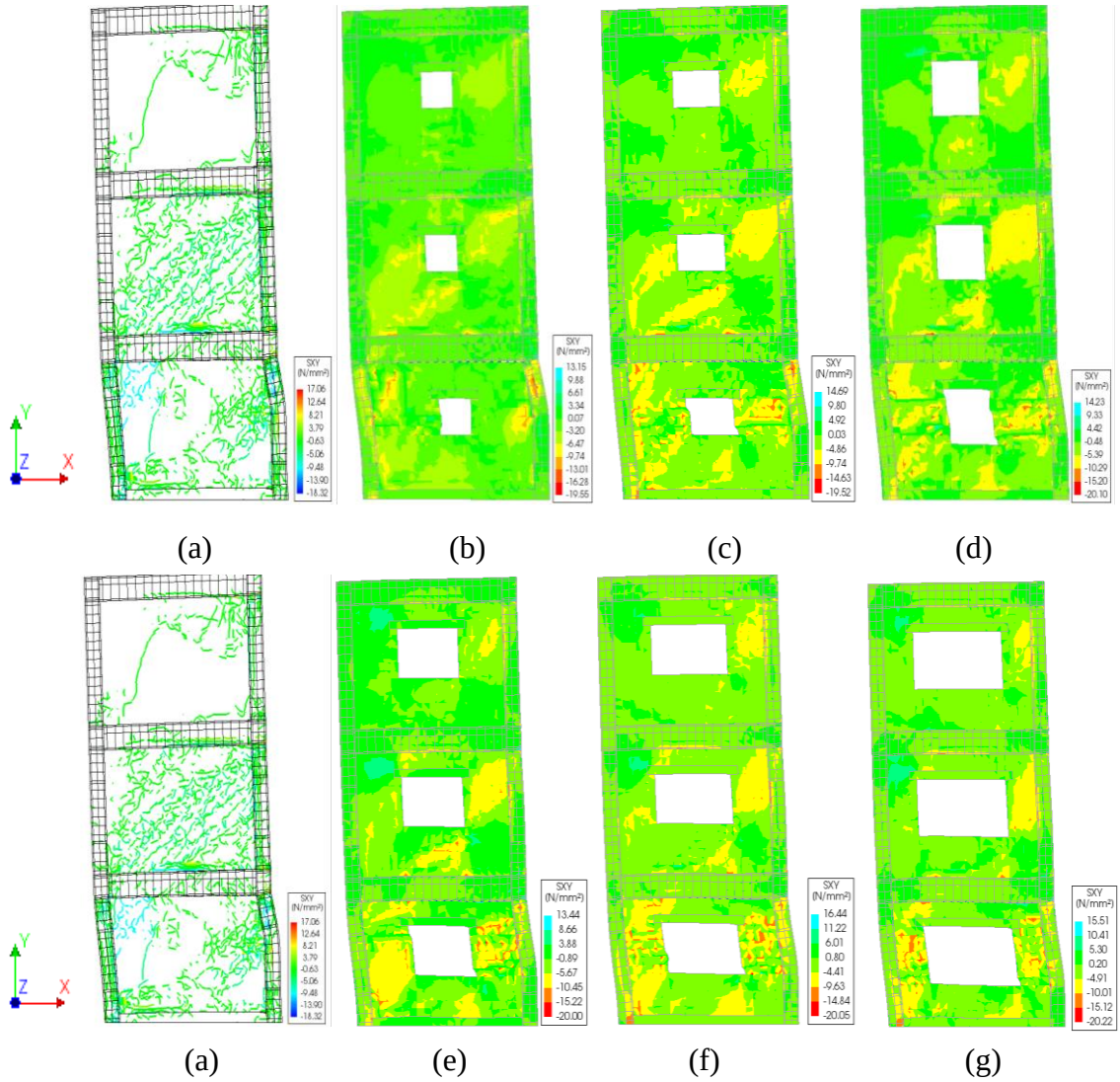

Figure 7.17: Shear stress distribution in the retrofitted infilled frame with central opening area equal to (a) 0%, (b) 5%, (c) 8%, (d) 12%, (e) 16%, (f) 20%, and (g) 27% during the fourth cycle of loading in the negative direction of loading.

From Figs. 7.16 and 7.17, it is observed that high shear stresses are concentrated in the first floor, somewhat less in the second floor and almost no shear stresses at the third floor. Specifically, high shear stresses are concentrated on the external face of the TRM at the location corresponding to the corners of the opening (above and below of the opening), to the loaded corners of the infill wall (where the diagonal path is developed), and to the ends of the columns in the area which contacted the diagonal of the infill wall. This occurs mainly at the first floor in all three-story masonry-infilled RC frames with any opening percentage retrofitted with TRM. Furthermore, as the central opening

area increases the shear stresses are more widely spread over the external face of TRM at the infill wall, since they are transmitted from the upper and lower parts of the opening to the sides of it, and then they propagate to the bounding frame. From these figures it is also observed that the deformation along the height of the second and third floor of structure is almost uniformly and completely different from that of the first floor (*soft-story mechanism)*, especially in the case of large openings (Figs. 7.17 c, d, f, and g and Figs. 7.18 c, d, f, and g). This indicates that the shear forces are not linearly varying along the height of the three-story retrofitted infilled frame with openings, but they are slightly better distributed compared to the unretrofitted one (Figs. 7.8 c, d, f, and g and Figs. 7.9 c, d, f, and g).

Figure 7.18 shows the crack propagation on the external face of TRM of the three-story retrofitted infilled frame with central opening area equal to16% during the first, third, fourth and fifth cycle of loading for both direction of loading. It is important to note that, the crack propagation that occurred on the retrofitted infilled frame with 16% central opening area is almost the same with that which has occurred on the retrofitted infilled frame with any opening percentage.

From Figs. 7.18 (a) and (e) it is observed that during the first cycle of loading (positive and negative direction of loading), diagonal cracks are formed on the external face of the TRM at the corners of the openings, especially at the first and second floor. The maximum crack width of these diagonal cracks is equal to 0.23 mm and 0.35 mm for the positive and negative direction of loading, respectively. It is important to note that the maximum diagonal crack width in the retrofitted infilled frame without openings was equal to 0.12 mm, and 0.17 mm for the positive and negative direction, respectively, during the first cycle of loading (Fig. 5.21 a and b). Therefore, the crack width on the external face of TRM in the case of infilled frame with openings is wider than the retrofitted infilled frame one without openings. This is attributed to the fact that at early stage of lateral loading the TRM is fully activated since it takes the high shear stresses and deformations that occur in the infilled frame due to the presence of the opening. Therefore, from the early loading stage the TRM prevents the large shear deformation of the infill wall due to the presence of the opening.

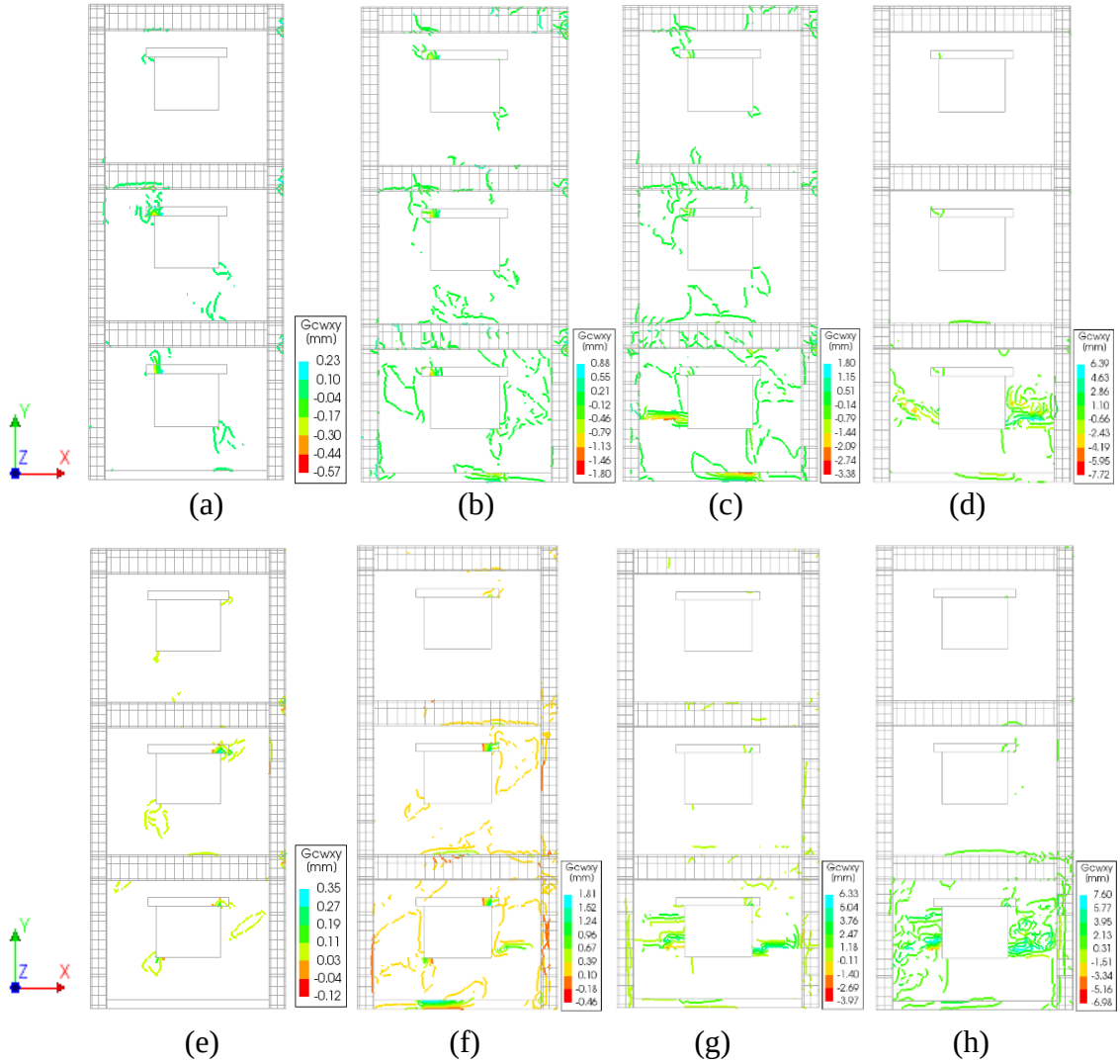

Figure 7.18: Crack propagation on the external face of TRM in the three-story retrofitted masonry-infilled RC frame with central opening area equal to 16% during the (a) first, (b) third, (c) fourth and (d) fifth cycle of loading in the positive direction, and during the (e) first, (f) third ,(g) fourth and (h) fifth cycle of loading in the negative direction of loading.

Upon increase of the horizontal loading (third cycle of loading), it is observed that diagonal cracks appear on the external face of TRM at the corners of the opening with maximum crack width ranges from 0.8 mm to 1.8 mm, and these cracks propagate to the loaded corners of the infill wall (where the diagonal compression path is developed) (Figs. 7.18 b and f). During the fourth cycle of loading, the previously open cracks reopened, became wider and propagate to the frame. More specifically, horizontal sliding cracks are developed on the external face of TRM at the corners of the opening,

and they are extended to the other corners of the opening with maximum crack width ranges from 2 mm to 6 mm (Figs. 7.18 c and g).

During the last cycle of loading, the shear cracks are transmitted from the external face of TRM at the upper and lower parts of the opening to the sides of it and to the other corners of the opening, and they are propagated horizontally to the upper ends of the columns leading to the shear failure of the column (*short-column mechanism*) (Figs. 7.18 d and h). The maximum crack width is equal to 5.50 mm and 7.2 mm near the corners of the opening in the positive and negative direction of loading during the fifth cycle of loading, respectively (Figs. 7.18 d and h). This indicates the failure of the infill wall (*corner crushing*), and consequently the possible rupture and debonding of the TRM at the corners of the opening. Therefore, special attention must be paid for anchoring the TRM along the perimeter of the opening. Furthermore, during the last cycle of loading (fifth cycle), sliding cracks on the external face of the TRM near the top of the infill-frame interface at the first floor (4.5 mm crack width) are developed which indicates the possible debonding of the TRM. It is important to mention that the debonding of TRM from the infilled frame with openings cannot be represented in this study since full bond between infill wall and TRM is considered in the numerical models (sections 4.4 and 4.5).

Comparing the crack propagation on the external face of TRM of the three-story retrofitted infilled frame without and with central opening during the last cycles of loading (comparing Fig. 5.23 with Fig. 7.18) it is observed that the crack width on the external face of TRM in the case of infilled frame with openings is much wider than the retrofitted specimen one without openings since the TRM takes the high shear stresses and deformations (brittle failures on the structure) that occur in the infilled frame due to the presence of the opening. Furthermore, it is also observed that the possible rupture or debonding of the TRM in retrofitted infilled frame without openings occurred during the sixth cycle of loading near the corners of the infill wall (section 5.4.2), while in the retrofitted infilled frame with openings the possible rupture or debonding of the TRM occurred during the fifth cycle of loading along the perimeter of the opening of the infill wall.

As previously mentioned, the crack propagation that occurred on the retrofitted infilled frame with 16% central opening area is almost the same with that occurred on the retrofitted infilled frame with any opening percentage. In this paragraph, the crack pattern that may occur in the retrofitted infilled frame with central opening ranging from 5% to 27% under cyclic loading is discussed according to the distribution of the shear stresses (Figs. 7.16 and 7.17), which is able to indicate the location where the cracks arise. From Figs.7.16 and 7.17 it is observed that as the opening area increases, the shear stresses, and henceforth the cracks became wider and propagated in the body of the infill wall. More specifically, as the opening area increases shear cracks are concentrated on the external face of TRM at the corners of the opening, and they are extended to the other corners of the opening and to the sides of it, and they propagate to the loaded corners of the infill wall indicating the failure of the infill wall with opening and the possible rupture of the TRM along the perimeter of the opening, especially in the case of large openings. Furthermore, these shear cracks are propagated horizontally towards the external face of TRM at the top of the columns at the first floor (in the area which contacted the diagonal of the infill wall) leading to the shear failure of the columns which is more pronounced in the case of large openings (Figs. 7.16 c, d, f and g and Figs. 7.17 c, d, f and g). Therefore, the TRM confinement applied at the columns cannot avoid the shear failure of the columns at the first floor during the last cycles of loading, especially in the case of large openings.

As shown in Figs. 7.16 and 7.17, the maximum shear stresses are concentrated near the loaded corners of the infill wall (compression diagonal path developed along two opposite corners of the infill wall), while near the non-loaded corners the infill wall separates from the RC frame (zero shear stresses). The figure below (Fig. 7.19) shows the gap-opening along the infill-frame interface at the first story, and at the bottom of the second story of the three-story retrofitted masonry-infilled RC frame model with central opening ranging from 5% to 27%, during the first cycle of loading.

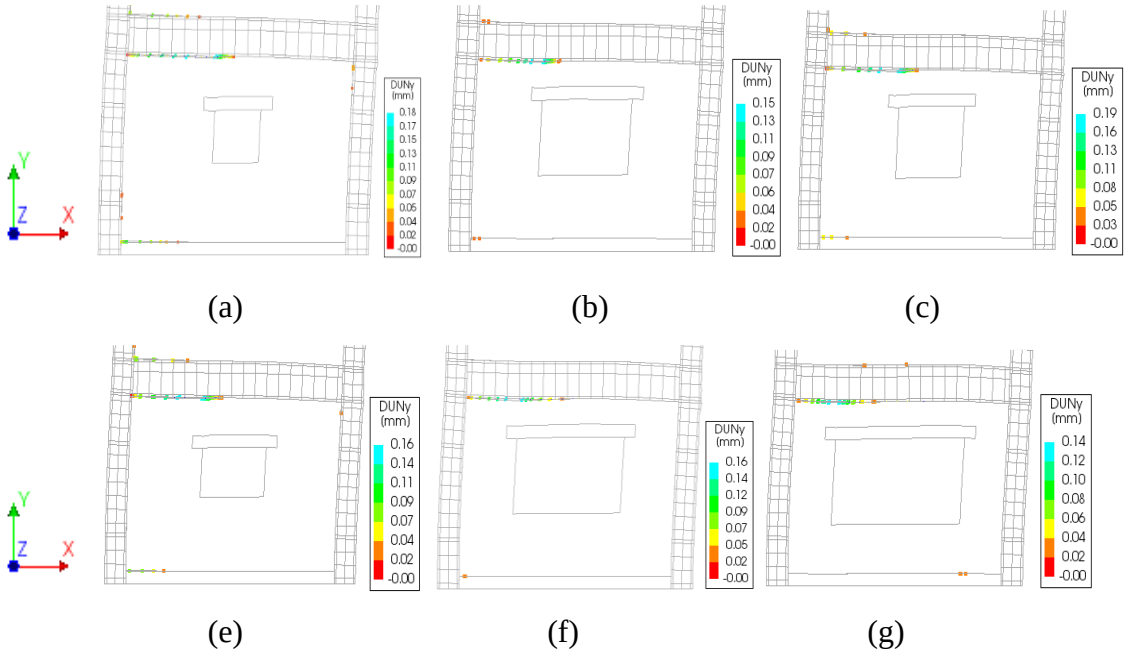

Figure 7.19: Gap-opening between infill wall and RC frame at the first story and at bottom of the second story during the first cycle of loading in the cases where the opening area is equal to : (a) 5%, (b) 8%, (c) 12%, (d) 16%, (e) 20%, and (f) 27%.

From Fig.7.19 it is observed that the infill-frame separation occurs at the very early stage of loading in the retrofitted infilled frame with any opening percentage. Based on Fig. 7.19, it can be concluded that the infill-frame separation depends on the area of the opening, since as the opening percentage increases leads to an increase in the area where the infill-frame separation occurs. Furthermore, comparing the gap-opening at the infill-frame interface in the retrofitted and unretrofitted specimens (Fig. 7.19 with Fig. 7.11), it is observed that the gap-opening is slightly decreased in the retrofitted specimens compared to that of the unretrofitted one.

By examining the shear stress distribution, the developed crack pattern, and the infill-frame separation of the retrofitted infilled frame it is observed that the failures that occur on the retrofitted infilled frame with any central opening percentage are the same with those observed on the unretrofitted one but at different cycles of loading. More specifically, for both infilled frames as the lateral loading increases the failures occur in the masonry infill wall and propagate to the RC frame, while the TRM retrofitting technique contributes to delay the *corner crushing* and the *diagonal cracking* of the

infill wall, and the shear failure of the column (*short-column* mechanism) at the first floor, and consequently the formation of the *soft-story mechanism.* This observation is supported by the distribution of the shear stresses of both infilled frames where the maximum shear stress of the unretrofitted and the retrofitted infilled frame with any opening percentage is equal to ±13-20 MPa and ±8-14MPa, respectively (Figs. 7.8-7.9 and Figs.7.16-7.17). Furthermore, the cracks of unretrofitted infilled frame with any opening percentage are more widely spread at the corners of the opening than the retrofitted ones (Fig. 7.10 and Fig. 7.18). Therefore, this retrofitting technique prevents large shear deformation of the infilled frame due to the presence of the opening by transferring the shear stresses of the infill wall to TRM layer as indicated by the multi-crack pattern on the external face of TRM at the corners of the opening and at the sides of it (Fig. 7.18). Furthermore, the TRM confinement applied at the columns cannot avoid the shear failure of the columns, especially in the case where the opening area ranges from 16% to 27%, but it is effective to delay the shear failure of the columns (comparing Figs. 7.16 and 7.17 with Figs. 7.8 and 7.9). This indicates that the columns should be strengthened in shear along their full height. Also, by comparing the deformed shape of the retrofitted infilled frame with any opening percentage with that of unretrofitted one it is observed that the formation of a *soft-story mechanism* is more pronounced in the unretrofitted specimen than the retrofitted one (comparing Figs. 7.8 and 7.9 with Figs. 7.16 and 7.17). Adding to this, from Figs. 7.16 and 7.17 it is observed that the width of the compression path developed along the diagonal of the infill wall with openings in the retrofitted specimen is decreased compared to that of the unretrofitted specimen with any opening percentage (Figs. 7.8 and 7.9). Finally, comparing Fig. 7.11 with Fig. 7.19, it is observed that the TRM retrofitting technique contributes to delay the infill-frame separation (the same gap-opening in the retrofitted and unretrofitted infilled frame but at different cycles of loading), but it is not able to avoid the infill-frame separation, especially in the case of large openings during the last cycles of loading. This is attributed to the fact that during the last cycles of loading the tensile strain of the TRM composite is increased while the stress remains constant (State II).

Therefore, the TRM retrofitting technique improves the lateral response of the three-story masonry-infilled RC frame with any opening percentage subjected to cyclic loading since the lateral capacity of the retrofitted infilled frame with openings is almost two times larger than the unretrofitted one. This increase is more pronounced at the first to third cycles of loading compared to the one at the fourth and fifth cycles, due to the full activation of TRM from the early stage of loading, and due to brittle failures that occurred during the last cycles of loading. Furthermore, the TRM retrofitting technique reduces the negative effect of openings by delaying the failures that occurred on the infilled frame with any opening percentage. Nevertheless, special attention must be paid for anchoring the TRM along the perimeter of the opening since a lot of failures occurred at this location (rupture and debonding of TRM).

7.3 Summary and conclusions

In this part of the thesis, numerical experiments are performed aiming to investigate firstly, the influence of a central window opening on the lateral response of a masonry-infilled RC frames, and then to examine the use of TRM for seismic retrofitting infilled frames with openings. This is achieved by performing non-linear cyclic analysis on the validated three-story masonry-infilled RC frame model without and with TRM considering central opening ranging from 5% to 27% upon the diagonal of the infill wall. The location, the size and the geometry of the opening were selected in such a way to match those used in previous experimental studies in order to compare results of the current study with those of past studies.

The three-story masonry-infilled RC frame model with different areas of central opening used in this parametric study can predict the real response of such type of structure subjected to in-plane cyclic loading since the results obtained from the current study presented good correlation to those obtained from the past experimental and numerical studies in terms of base-shear, global stiffness, initial stiffness, stiffness degradation, and dissipated energy. Furthermore, the failure modes and the crack pattern observed on the infilled frame model with different central openings in this study are almost the same with that observed in the experimental studies conducted in the past.

From the parametric study regarding the influence of a central opening by varying its area on the in-plane behavior of the three-story masonry-infilled RC frame subjected to cyclic loading the following conclusions are derived:

- The presence of a central window opening on the infilled frame influences the lateral response of the structure since in the cases where the area of the central opening is equal to 8%, 12%, 16% and 27% it leads to a decrease in the lateral strength of the infilled frame equal to 10%, 14%, 20%, and 30%, respectively. Furthermore, the dissipated energy and the global stiffness of the infilled frame decrease by about 16%-50% and 7%-40%, respectively, when the central opening ranges from 5% to 27%, while this decrease is more pronounced in the cases where the central opening percentage is ranging from 16%-27% (decreases by 30%-50%).
- The decrease on the lateral capacity of the infilled frame due to the presence of the opening is more pronounced during the early stages of lateral loading compared to that during the last cycles of loading, which occur at large displacements, due to the brittle nature of the infill wall with opening and its stiffness degradation.
- The masonry infill wall with openings could be better represented by multi-diagonal no-tension strut elements instead of a single-diagonal strut element.
- The new stiffness reduction factor which is proposed in this study can be used with an equivalent strut model, which is a macro-model for everyday practice, to model infilled frames with central openings along the diagonal, since the initial stiffness of the infilled frame with different central opening area percentage as obtained from the macro-model approach using this reduction factor presented an agreed correlation with that obtained from the current numerical study.
- The failure modes of the infilled frame with a central opening ranging from 5% to 27% during the cyclic loading include firstly, the *corner crushing, diagonal cracking,* and *sliding shear* of the infill wall, and then the *frame failure* mode which consists of the failure of column-beam joints, and of the shear failure of the columns (*short-column mechanism*), since the shear cracks are concentrated at the corners of the opening (above and below the opening), and they propagate

towards the loaded corners of the infill wall where the diagonal compression path is developed. As the lateral loading increases these shear cracks propagate to the beam-column joints, and to the ends of the columns in the area which is in contact with the diagonal of the infill wall at the first floor leading to significant decrease in the lateral capacity of the structure.

- The deformation and the shear forces along the height of the three-story infilled frame with openings is not linearly varying leading to a *soft-story mechanism* at the first floor.
- The *corner crushing* failure mode and the *short-column mechanism, and* consequently the soft-*story mechanism* at the first floor of the three-story masonry-infilled frame is more pronounced in the cases where the opening is large (20%-27%) since the shear cracks are more widely spread over the surface of the infill wall (they are transmitted from the upper and lower parts of the opening to the sides of it) and become wider.
- The infill-frame separation on the infilled frame with opening depends on the area of the opening, since as the opening percentage increases leads to an increase in the area where the infill-frame separation occurs.

From the parametric study regarding the effect of TRM retrofitting technique on the in-plane response of the three-story masonry-infilled RC frame with central opening subjected to cyclic loading the following conclusions are obtained:

- The TRM retrofitting technique increases the lateral strength, global stiffness, and dissipated energy of the three-story masonry-infilled RC frame with central opening by about two times, while this increase becomes smaller as the opening area increases (1.2-1.5 times).
- The increase in the lateral capacity of the infilled frame with any opening percentage due to TRM is more pronounced at the first to third cycles of loading compared to the one at the fourth and fifth cycles. This is due to the full activation of TRM from the early stage of loading, and due to brittle failures that occur in the infilled frame in the last cycles of loading (failures in the infill wall and *short-column mechanism).* More specifically, the shear stresses and deformations that occur in the infilled frame become larger due

to the presence of the opening, especially in the case of large openings, and these shear stresses are transferred to the TRM in local level, and therefore, this composite material sustains these shear stresses from early stage of loading.

- The TRM contributes to increase the lateral capacity of the infilled frame with openings by restoring the load-bearing capacity to that of the infilled frame without opening, and by delaying the strength degradation of the infilled frame due to presence of the opening.
- The new stiffness reduction factor which is proposed in this study can be used for simulating masonry-infilled frames with central openings along the diagonal of the infill wall retrofitted with TRM following the macro-modeling approach where the contribution of externally bonded layers of TRM are considered by introducing an additional term in the equations usually employed for unretrofitted infilled frames.
- The TRM retrofitting technique contributes to delay the failures that occur on the infilled frame with any central opening percentage since the failures that occur in the retrofitted specimen are the same with those observed on the unretrofitted one but at different cycles of loading. More specifically, for both infilled frames as the lateral loading increases the failures occur in the masonry infill wall and propagate to the RC frame, while the TRM retrofitting technique contributes to delaying the *corner crushing* and the *diagonal cracking* of the infill wall, and the shear failure of the column (*short-column* mechanism) at the first floor.
- The TRM confinement applied to the columns cannot avoid the shear failure of the columns. This suggests that the columns should be strengthened in shear along their full height.
- The deformation and the shear forces along the height of the retrofitted three-story infilled frame with openings are not linearly varying leading to *soft-story mechanism* at the first floor, but they are slightly better distributed than the unretrofitted ones.

- The TRM retrofitting technique contributes to delay the infill-frame separation but it is not able to avoid the infill-frame separation because during the last cycles of loading the tensile strain of the TRM composite is increased while the stress remains constant (State II).
- The possible rupture and debonding of TRM of the retrofitted infilled frame with openings may occur at the corners of the openings, since high shear stresses are concentrated at the external face of the TRM at the location corresponding to the corners of the opening (above and below of the opening).

Therefore, there is no doubt that the TRM retrofitting technique improves the lateral response of masonry-infilled RC frames with openings subjected to lateral loading while special attention should be given for anchoring the TRM along the perimeter of opening. Due to the lack of experimental data for infilled frames with openings retrofitted with TRM to be used to validate the numerical models, the results presented here are considered a good approximation for the case when infilled frame structures with openings are retrofitted with TRM, taking into account the sophistication of the masonry-infilled RC frame model and its validation with openings (unretrofitted masonry-infilled RC frame with openings as presented in this part of the thesis) and without openings (unretrofitted and retrofitted solid masonry-infilled RC frame as presented in Chapter 5).

CHAPTER 8

8. CONCLUSIONS

8.1 Summary

During the last decade, the TRM composite material, encompassing a combination of inorganic matrix (lime- or cement-based) and non-corrosive multi-axial textile fabrics, has emerged as a promising novel alternative for the seismic retrofitting of masonry-infilled RC frame buildings. Nevertheless, the studies performed, so far, on infill walls within RC frames retrofitted with TRM are very limited, and for this reason, there are no specific guidelines for infilled frames retrofitted with TRM, leading to the inapplicability of this method for the retrofitting of real structures. In order to bridge the gap of knowledge and to enhance the implementation of this composite material as a regular method for retrofitting existing buildings, the current study focuses on investigating numerically the effectiveness of using the TRM composite material for the seismic retrofitting masonry-infilled RC frames, with and without openings, and on the parameters that influence the TRM's efficiency. An essential step towards this direction is the development of a simplified analytical model able to predict the tensile behavior of the TRM.

In the first part of this study, a simple and easy to-implement analytical model is developed, able to predict the tensile behavior of TRM in terms of stress-strain, which is divided into three States: State I (the uncracked matrix), State II (the crack formation), and State III (the crack stabilization and failure). The proposed analytical model extends the Aveston-Cooper-Kelly (ACK) theory, which applies for fiber-brittle matrix, to TRM. To do so, recommendations proposed by Eurocode 2 and by *fib* Model Code 2010 for estimating the crack spacing and the fracture energy of the composite material, respectively, are used to facilitate the use of the ACK theory without requiring testing.

Particularly, the simple mathematical expression proposed by *fib* Model Code 2010, which correlates the fracture energy of concrete with the tensile strength of concrete, to describe the resistance of concrete subjected to tensile loading, is used for estimating the fracture energy of the TRM, since this composite material has similar tensile behavior of concrete before multi-cracking occurs. Furthermore, in order to apply the ACK model for TRM, the easy mathematical expression proposed by Eurocode 2 for calculating the crack spacing of steel reinforced concrete is used for estimating the crack spacing of TRM composite material, since the tensile behavior of steel reinforced concrete is very similar to that of fiber or textile reinforced composite (TRM). This expression is transferred to TRM without any modification, since the assumptions considered in the ACK theory and in Eurocode 2 are almost the same, where for both cases the bond strength between the reinforcement (fiber/textile or steel bars) and the matrix (mortar or concrete) is considered constant before cracking occurs. The proposed tri-linear analytical model of TRM, which predicts the tensile behavior of TRM in terms of a stress-strain curve, following the ACK theory, is a simple and easy to-implement model, since only the mechanical properties and the geometric characteristic of the cement-based matrix and those of the textile reinforcement are necessary, without any required information from experimental tests. This model provides the strength envelope of the tensile behavior of TRM, while its cyclic behavior, which is described with the hysteresis loops, or loading unloading curves, is not considered in this model. The proposed model is verified by comparing its results with those obtained by experimental and analytical studies conducted in the past, and then a parametric study is performed, aiming to examine the sensitivity of the proposed model to a range of parameters, including the fiber's material used for assembling the textile, the reinforcement ratio, the cross-sectional area of the yarn and the mechanical properties of the cement-based matrix. Although the proposed model proved accurate for predicting the tensile behavior of TRM in terms of stress-strain curve, some deficiencies exist between experimental and analytical data (less than 30%), due to the fact that the proposed model does not take into account (a) the real distribution of the cracking in the composite, since the crack spacing in the proposed model has a unique value, (b) the substantial strain hardening behavior of the composite when multiple cracking occurs,

since this model assumes a constant composite stress, and (c) the stiffness degradation of the textile after the multi-cracking is completed, since in the proposed model a linearity hypothesis is assumed for evaluating the effective amount of textile reinforcement, by multiplying the volume fraction of the textile with the stiffness of the textile. Adding to the above, the proposed model does not take into account in detail the bond condition existing between the textile and matrix in the real case (bond between the fibers, how the layout and the geometry of the textile affects the bond strength at the textile-matrix interface etc.).

After the development and the validation of the proposed analytical model of the TRM, a 2D simple FE micro-model of the three-story bare frame, and of the three-story masonry-infilled RC frame, with and without TRM, which were experimentally tested under cyclic loading in the study carried out by Koutas et al. (2014), were developed in the DIANA FEA software. The numerical models were developed following a simple micro-modeling approach. The concrete members, the masonry infill wall and the TRM are modeled separately by continuum elements (CQ16M quadrilateral isoperimetric plane-stress element). The infill-frame interface was modeled with three-point line interface elements (CL12I). The steel reinforcement was modeled with a two-noded bar element and it was connected to the eight-noded concrete element (CQ16M) at the two external nodes. Although the textile-based anchors were not explicitly modeled, the bond condition provided by the existence of anchors was taken into account in the numerical models. Following the smeared crack approach, four material models were used for describing the non-linear cyclic behavior of the components of this type of structure. Specifically, the Maekawa Fukuura model, as a compression function, and the *fib* 2010 model, as a tension function of the Total Strain Crack model, adopted for the concrete elements. For the steel reinforcement two-noded bar elements the Menegotto-Pinto plasticity model was used. Furthermore, the Engineering Masonry model was used for the masonry infill wall elements which is a smeared crack model available in DIANA FEA that covers the tensile, shear and compression failure of the infill wall. This model requires a large number of parameters to be specified in DIANA FEA. The Fiber Reinforced concrete model, combined with *fib* 2010 model were used in this study as a tension and compression softening function, respectively, for the Total Strain Crack

model, in order to represent the non-linear behavior of the TRM composite material. The required parameters of this model were obtained from the coupon tests conducted by Koutas et al. (2014), and by using the proposed analytical model of TRM. Furthermore, the Coulomb Friction model was adopted for the infill-frame interface elements in order to capture the gap-opening and the sliding between the masonry infill wall and the RC frame. The required parameters to define the above-mentioned models in DIANA FEA were taken from the experimental case-study selected for the calibration purposes in this numerical study, and other parameters were taken from the literature and at the same time by fitting the numerical results to the experimental ones (especially the parameters for the masonry infill wall model and for the interface model). To complete the numerical model, all nodes at the base of the first floor were restrained by preventing any translation in the x- and y-direction. The RC frame model, and the infilled frame model, with and without TRM, were imposed to constant axial load and to cyclic lateral displacement loading, as similar as possible to the experimental case-study. The cyclic loading scheme of the real case was simulated by applying displacement loading at the three stories of the numerical models (five cycles of displacement loading in the bare frame and in the unretrofitted infilled frame, and seven cycles of displacement loading in the retrofitted infilled frame). The evolution of displacement loading was done through the analysis procedure and it was discretized in loading steps, using an automatic incrementation procedure in which both the number of steps and the corresponding size of each step were automatically computed by DIANA FEA. The development of the three-story bare frame model and of the three-story masonry-infilled RC frame model, with and without TRM, is based on the assumptions considered for the purpose of this study. These numerical models are validated by comparing the results obtained from the linear static, eigenvalue, and non-linear cyclic analysis of the bare frame model and of the infilled frame model with and without TRM with those obtained from the experimental study conducted by Koutas et al. (2014) and from relevant experimental studies conducted in the past. Although the numerical models proved accurate for predicting the real response of the infilled frame with and without TRM under cyclic loading in global level (base-shear, shear capacity of each floor, height-wise distribution of the shear force, global stiffness, and dissipated energy)

and in local level (shear stresses, deformed shape, infill wall-frame separation and crack pattern), some deficiencies existed. Specifically, the discrepancy between the experimental and numerical results for both infilled frames at global level is more pronounced during the last two cycles of loading (20%), due to the cyclic loading process followed in this numerical study, since it is different from that of the experimental case-study, and due to the analysis convergence and to the nonlinearities that were introduced in the last cycle of loading during the experiment (failure due to *soft-story mechanism* at the ground floor). In addition to the above, the deficiencies that exist between the experimental and numerical results at local level regarding the compression failure of the masonry infill wall at the first floor, and regarding failures that occur in the retrofitted infilled frame, such as, debonding and rupture of the TRM, are mainly due to the modeling procedure and the assumptions followed in this study. Therefore, the small differences that were observed between the experimental and numerical results shed light to some errors in assumptions and in the modeling procedure followed in this numerical study. In order to achieve more accurate results, (a) the bond conditions between the infill wall and the TRM must be considered through an interface element (surface element) to capture the possible debonding of the TRM from the masonry infill wall surface, (b) the textile and the mortar must be modeled, separately and an interface element must be considered between the mortar and the textile to simulate the possible slippage of the textile from the mortar (micro-modeling approach), (c) the anchors must be modeled to capture the possible rupture of the anchors, and finally (d) the masonry infill wall must be modeled following a more detailed approach where the brick units and mortar joints are modeled separately by continuum elements and the mortar–brick interface is modeled by an interface element with zero thickness (detailed micro-modeling approach). To consider all the above, the development of a three-dimensional (3D) model of this type of structure is required. However, by taking into account all the above-mentioned suggestions in a FE modeling of a masonry-infilled RC frame with and without TRM, it will lead to a high computational cost and a very large number of parameters that need to be defined.

For the purpose of this study, the degree of accuracy of the proposed numerical models is considered acceptable, and, therefore, important findings can be drawn from the

current study regarding the influence of the existence of infill walls in RC frames and regarding the effectiveness of using the TRM for retrofitting three-story masonry-infilled RC frames subjected to in-plane cyclic loading, as experimentally investigated by Koutas et al. (2014). These conclusions will be discussed in section 8.2.

After the validation of the proposed numerical models, sensitivity analyses are performed to investigate the in-plane behavior of the three-story integral and non-integral masonry-infilled RC frame under cyclic loading, and to examine the influence of the infill-frame interface stiffness properties (normal and tangential) on the in-plane response of the three-story retrofitted infilled frame under cyclic loading. The numerical results showed that the lateral capacity of the three-story integral infilled frame is higher than the corresponding one of the non-integral infilled frame, while the non-linear cyclic response of masonry-infilled RC frames with TRM is sensitive to the normal and shear stiffness of the infill-frame interface.

In the third part of this study, numerical experiments were performed, using the validated numerical model, to examine the effect of the TRM reinforcement ratio on the behavior of the three-story masonry-infilled RC frame retrofitted with TRM under cyclic loading, by means of using a different number of TRM layers and different geometry of textile reinforcement on each floor of the three-story masonry-infilled RC frame retrofitted with TRM. Numerical experiments were also performed aiming to investigate the effect of the type of inorganic-matrix (mortar) used for binding the textile reinforcement (each mortar represents a different class of mortar according to EN 1504) on the behavior of the three-story masonry-infilled RC frame retrofitted with TRM under cyclic loading. In order to perform this parametric study, the same modeling scheme was used for the numerical specimens as for the validated numerical model, while the tensile behavior of the TRM composite considering different reinforcement ratio, different geometry of the textile, and different types of mortar for binding the textile reinforcement is estimated using the proposed analytical model of TRM in order to define the required parameters for the TRM material model in DIANA FEA for the purpose of these numerical experiments.

In the last part of this study, the effectiveness of using the TRM composite material for retrofitting masonry-infilled RC frame buildings with openings is investigated. Towards this direction, the validated three-story masonry-infilled RC frame model with and without TRM was used to perform numerical experiments considering different size of central opening ranging from 5% to 27%, to investigate, firstly, the influence of a central window opening, on the response of infilled frames subjected to cyclic loading, and then to examine the use of TRM for the seismic retrofitting of infilled frames with openings. In order to enhance the current numerical study, the influence of openings on the lateral response of infilled frames without TRM, as obtained from these numerical experiments is validated using relevant past studies. Specifically, the three-story masonry-infilled RC frame model with central opening ranging from 5% to 27%, used in this parametric study could predict the real response of such type of structure subjected to in-plane cyclic loading, since the results obtained from the current study presented good correlation to those obtained from the past experimental and numerical studies in terms of base-shear, global stiffness, initial stiffness, stiffness degradation, and dissipated energy. Furthermore, the failure modes and the crack pattern observed on the infilled frame model with central opening ranging from 5% to 27% in this study are almost the same with those observed in the experimental studies conducted in the past.

The above paragraphs summarize the content of the current study, as presented in the previous Chapters, for the benefit of the reader, while the conclusions that resulted from the above will be presented at section 8.2.

8.2 Conclusions

The objectives of this research have been achieved, particularly, a simplified model able to predict the tensile behavior of TRM was developed, the in-plane cyclic response of masonry-infilled RC frames with and without TRM was numerically investigated, and the numerical experiments aiming to examine the critical parameters that influence the effectiveness of TRM for retrofitting masonry-infilled RC frames, and to investigate the effectiveness of using the TRM for retrofitting masonry-infilled RC frames with openings were performed. This study met these objectives, and a number of interesting

conclusions can be drawn from each of the different tasks of the present research, as follows:

- The proposed analytical model of TRM has shown good accuracy at predicting the tensile behavior of TRM in terms of stress-strain in a macroscopic level, considering that the limitations of the proposed model occur at a microscopic level, and considering that the degree of approximation of the proposed model is acceptable, since remarkable deviation occurred also in each testing of this composite in other studies (coefficient of variation equal to 20%-50%). The proposed analytical model of TRM may therefore be used to represent the TRM constitutive equation in non-linear analysis of reinforced concrete and masonry structures retrofitted with TRM due to its simplicity and accuracy.
- The detailed FE numerical model of the bare frame and of the masonry-infilled RC frame, with and without TRM, developed in this study, showed an acceptable degree of accuracy for predicting the real response of such types of structures when subjected to cyclic loading, and therefore these models can be used as a tool to generate a very large database (treated parametrically), by taking into account all the possible ranges of the critical parameters affecting the complex behavior of masonry-infilled RC frames with and without TRM, leading to a significant contribution to the knowledge in this subject, without performing experimental tests which are costly ineffective.
- The existence of masonry infill walls, even with openings, in RC frames contributes to increase significantly the lateral capacity of the building, and, at the same time introduces brittle shear failure mechanisms associated with the infill-frame interaction, such as the shear failure of the columns (*short-column mechanism*), especially in the case of weak RC frames and strong infills, or in the case of large openings (16%-27%). Specifically, the lateral capacity of infilled frames is about four-six times higher than the bare frame one, while this increase becomes smaller as the lateral loading increases due to the brittle nature and the stiffness degradation of the infill wall, leading to brittle shear failures on RC frames. Furthermore, the lateral capacity of masonry-infilled RC frames is increased by about two times when the infill wall is integrated to the RC frame.

On the other hand, the presence of a central opening in infilled frames causes a reduction in the lateral capacity of the structure, while this reduction is more pronounced in the cases where the central opening percentage is large. For example, in the cases where the area of the central opening is equal to 8%, 12%, 16% and 27%, leads to a decrease in the lateral strength of the infilled frame by about 10%, 14%, 20%, and 30%, respectively, while this decrease is more pronounced during the early stages of lateral loading, compared to that during the last cycles of loading, which occur at large displacements, due to the brittle nature of the infill wall with opening and its stiffness degradation leading to brittle shear failures on RC frames from early stage of lateral loading. Adding to the above, as the opening percentage increases, it leads to an increase in the area where the infill-frame separation occurs. In the case of the three-story masonry infilled frame with a central opening ranging from 5% to 27% examined in this study, the failure modes include, firstly, the *corner crushing*, *diagonal cracking*, and *sliding shear* of the infill wall, and then the *frame failure* mode which consists of the failure of column-beam joints, and of the shear failure of the columns (*short-column mechanism*), leading to the development of the *soft-story mechanism* at the first floor (shear forces along the height of the three-story infilled frame with openings are not linearly varying). These failures are more pronounced in the cases where the opening is large (20%-27%). The new stiffness reduction factor, which is proposed in this study, can be used with an equivalent strut model, which is a macro-model for everyday practice, to model infilled frames with central openings along the diagonal. In that case, the masonry infill wall, even with openings, could be better represented by multi-diagonal no-tension strut elements, instead of a single-diagonal strut element.

- The TRM retrofitting technique contributes to improving the lateral response of infilled frames subjected to cyclic loading, since it provides an increase to the lateral strength and deformation capacity of infilled frames by about 60%, and 50%, respectively, by delaying the failures that occur on infilled frames, leading to a more ductile behavior. In the case of the three-story masonry infilled frame examined in this study, the TRM strengthening technique delays the infill-frame

separation, but it is not able to avoid or eliminate it, since under large displacements the tensile strain of the TRM composite is increased, while its stress remains constant (State II). Also, the TRM delays the main failures that occurred in the three-story infilled frame, such as the *corner crushing, diagonal cracking,* and the shear failure of the column (*short-column* mechanism) at the first floor, and, consequently, the formation of the *soft-story mechanism*. This is because the shear stresses of the infill wall are transfered to the TRM layer and this composite material can sustain these shear stresses due to its high tensile and compressive capacity. A potential way to increase the compressive and tensile capacity of TRM, and further to increase the lateral capacity of infilled frames retrofitted with TRM, considering that full bond is achieved between the TRM and the wall surface, is to increase the tensile and compressive strength of the matrix used for binding the textile reinforcement, at the same time keeping the modulus of elasticity low, and to increase the textile reinforcement ratio, using a relatively small distance between the yarns in the textile, and using a textile with a relatively high density yarns. Furthermore, the lateral response of a TRM-retrofitted infilled frame is between that of an integral and a non-integral infilled frame, hence making the anchorage of the TRM to the bounding RC frame elements the most important parameter regarding the TRM strengthening method when used on masonry infilled RC frame.

- The TRM reinforcement ratio influences the effectiveness of using the TRM composite for retrofitting infilled frames, since by increasing the reinforcement ratio, the lateral capacity of infilled frames is increased, leading to a more ductile performance, while this increase is not proportional to the increase of the reinforcement ratio. For example, the lateral strength, stiffness and dissipated energy of the infilled frame receiving TRM with 3.2% textile reinforcement ratio are increased by about 15%-25%, compared to the corresponding ones of the infilled frame receiving TRM with 1.3% textile reinforcement ratio, at early stage of the lateral loading, by delaying or even preventing the brittle failures, while after the maximum base-shear is reached, which occurs at large lateral displacement, this increase becomes smaller due to brittle failures that occur on

the infilled frame. Adding to the above, the lateral capacity of the infilled frame is increased by using TRM with a relatively small distance between the yarns (TRM reinforcement ratio increases), but such that it allows the mortar to pass and be correctly bonded to the wall surface. In the case of a multi-story infilled frame building, it is important to apply more layers of TRM at its first floor, compared to that applied to the upper stories of the building in order to increase its lateral capacity by delaying or even preventing the brittle failures that usually occur at the first floor (*soft-story mechanism*), since the height-wise distribution of the shear force is almost linearly varying as the TRM reinforcement ratio increases. For example, in the case of the three-story masonry infilled frames examined in this study, three-layers of TRM must be applied at the first floor (more than 3.2% reinforcement ratio), one layer of TRM at the second floor and no TRM-layer at the third floor. Furthermore, in this case, the use of TRM at the third floor, or the use of more than one layer of TRM at the second floor of the three-story masonry-infilled RC frame retrofitted with TRM, is pointless, since this retrofitting scheme does not provide any significant gain to the lateral capacity of the retrofitted structure, and considering the cost of TRM, as well.

- The type of inorganic-matrix used for binding the textile reinforcement influences the effectiveness of using the TRM composite material for retrofitting infilled frames. More specifically, the use of high-strength mortars for binding the textile reinforcement, especially R4 class mortar according to EN-1504 (compressive strength > 45MPa and tensile strength > 4MPa) results in higher lateral strength, global stiffness, and dissipated energy of the infilled frames by about 10%-30%, instead of using TRM with relatively low-strength mortar (R2 and R3 class mortar), hence delaying or even preventing the large shear deformation of infilled frames. This increase is not proportional to that of the mortar mechanical properties, since using mortar with double tensile or compressive strength does not provide double lateral capacity of the retrofitted infilled frame. It is important to mention that the contribution of the compressive strength of the mortar used for TRM to increase the lateral capacity of infilled frame subjected to cyclic loading is more pronounced, compared to that of the

tensile strength of mortar used for TRM, when the infilled frame is subjected to small lateral loads, since the compressive capacity of TRM contributes to enhance the compression strut of the infill wall, while as the lateral loading increases, the contribution of the tensile capacity TRM, to increase the lateral capacity of retrofitted infilled frame becomes more pronounced than the compressive capacity of the TRM, since at this stage this composite material sustains the high tensile stresses which are transferred from infill wall to the TRM at local level. Furthermore, special attention should be given to the mortar composition, which must be such to achieve full penetration of the textile to the matrix and to achieve also full bond between the masonry infill wall and TRM.

- The TRM retrofitting technique contributes to improve significantly the lateral response of infilled frames with openings, leading to a more ductile behavior, since it increases the lateral capacity of infilled frames with openings by about 80%-100%, by delaying the strength degradation, the failures, and the infill-frame separation of infilled frames, due to the presence of the opening. In the case of infilled frames with openings retrofitted with TRM, there is a tendency that the efficiency of TRM is higher than in the case of solid infilled frames, due to the high shear deformation of infilled frames caused by the openings, where these shear stresses are transferred to the TRM at local level, and therefore, this composite material sustains these shear stresses from early stage of loading, making the TRM a suitable retrofitting technique for in-plane enhancement of masonry-infilled RC frame buildings with openings. The possible rupture and debonding of TRM of the retrofitted infilled frames with openings may occur at the corners of the openings (above and below of the opening). Therefore, special attention should be given for anchoring the TRM along the perimeter of the opening. The new stiffness reduction factor which is proposed in this study can be used for simulating retrofitted masonry-infilled frames with central openings along the diagonal of the infill wall, following the macro-modeling approach. In this case the retrofitted infill wall, even with openings, could be better represented as a pair of alternatively activated multi-diagonal compression-only

strut elements and tension ties elements (tension diagonal), instead of a single-diagonal strut and tie elements.

The conclusions derived from this study are valuable, as they contribute to the expansion of existing knowledge related to TRM, while promoting the prospective use of this novel material for retrofitting existing structures. Particularly, this research work contributes to facilitate the implementation of numerical models of retrofitted structures using TRM, to gather and clarify the complex behavior of infilled frames with and without openings, to expand today's knowledge regarding the parameters able to influence the TRM's efficiency for retrofitting infilled frames, and to expand the use of this composite material as a regular method for retrofitting existing buildings, since the effectiveness of using TRM composite material for the seismic retrofitting of masonry-infilled RC frames with openings was assessed for the first time in the current study.

8.3 Future research

Although the objectives of this study have been accomplished, the present research has allowed the identification of some knowledge gaps in need for additional investigation. Additional research is needed on this promising new retrofit approach, considering the variability found in the performance of existing infilled frame buildings. Future work in this field should be directed at establishing design guidelines in the context of current design formulations, in order to facilitate the implementation of this composite material as a regular method for retrofitting existing buildings. A proposal of the main topics to be included in further research is presented in the following paragraphs.

Firstly, it would be interesting to validate further the analytical model of TRM proposed here to increase the level of confidence in this model as a prediction tool. More experimental tests on this composite material are required, considering various inorganic-matrix and textile systems, in order to assess the predictive capacity of this analytical model or to modify this model by introducing proper coefficients for quantifying some important issues, such as the bond at the textile-matrix interface, the strength degradation of the textile reinforcement, in order to eliminate the discrepancy between the analytical and experimental data observed in the present study.

Furthermore, more cyclic tests on TRM composite materials are necessary to extend the model proposed in this study for capturing the cyclic behavior of this composite. It would be suitable to develop a standardized uniform testing procedure in order to homogenize the information provided for TRM composites and to reduce the coefficient of variation in such tests, as well.

Further research would be essential to characterize the seismic behavior of infilled frames retrofitted with TRM by performing experimental or numerical tests. The expansion of the experimental database is required to study in more depth this method, by taking into account all the possible critical parameters able to affect its efficiency. Towards this direction, more experimental tests must be carried out in order to investigate (a) the effect of using different types of connectors for anchoring the TRM to the bounding RC frame, since it is one of the most important details of the TRM based solution, (b) the influence of extending the retrofitting layers applied to infill walls to the faces of the columns and the beams, by using different lengths of overlapping of the mesh along the infill-frame transition, and (c) the influence of using different TRM composites, including the textile orientations, the TRM layout by means of using diagonal bands of TRM, by varying its width, the reinforcement ratio, the number of TRM layers, and the type of inorganic-matrix used for binding the textile reinforcement.

Furthermore, the assessment of using the TRM composite material for retrofitting infilled frames with openings, as derived from the current study, is far from complete, due to the lack of experimental data, and therefore, experimental research is required to assess the TRM effectiveness of retrofitting masonry-infilled RC frames containing different opening configurations, such as for windows and unsymmetrical door openings. Relevant experimental tests must be performed by taking into account all the above-mentioned critical parameters able to affect the TRM's efficiency for retrofitting solid infilled frames, while special attention should be given for anchoring the TRM along the perimeter of the openings.

The numerical tests on masonry-infilled RC frames, with and without openings, retrofitted with TRM, following either a macro- or a micro- modeling approach, are also essentiall, in order to study in more depth this method without performing experimental

tests, which are economically prohibitive. Therefore, the development of a reliable numerical model for describing the complex behavior of the TRM-retrofitted infilled frames by considering interface elements to model the contact phenomena and by using an established material model for the TRM composite material is required.

Finally, the future use of TRM for retrofitting existing structures will also be greatly dependent on the development of design guidelines, in which the design and detailing of using this strengthening solution is described, since as of now it is not specified. Therefore, in order to attract attention and considerably expand the application of the new composite material by the engineering community, it is important to develop simplified methodologies (analytical models) for predicting the structural behavior of infilled frames retrofitted with TRM, by taking into account important issues, such as; the bond between the TRM and masonry infilled frames, the effective stress-strain of TRM, and the parameters able to affect the TRM's efficiency, as previously presented. It would be important to formulate simplified methodologies by which a designer may assess the benefits of using TRM to reduce the seismic vulnerability of masonry infill walls (local level) and of the entire building (global level).

REFERENCES

Abel A, Muir H (1972) The bauschinger effect and discontinuous yielding. Philos Mag 26:489–504. doi: 10.1080/14786437208227444

Achyutha H, Jagadish R, Rao PS, Rahman SS (1986) Finite element simulation of the elastic behaviour of infilled frames with openings. Comput Struct 23:685–696. doi: 10.1016/0045-7949(86)90077-5

ACI-549-13 (2013) American Concrete Institute (ACI). Committee 549. Design and construction guide of externally bonded FRCM systems for concrete and masonry repair and strengthening.

Ahani E, Mousavi MN, Ahani A, Kheirollahi M (2019a) The Effects of Amount and Location of Openings on Lateral Behavior of Masonry Infilled RC Frames. KSCE J Civ Eng 23:2175–2187. doi: 10.1007/s12205-019-0714-x

Ahani E, Mousavi MN, Rafezy B, Osmanzadeh F (2019b) Effects of Central Opening in Masonry Infill on Lateral Behavior of Intermediate RC Frames. Adv Civ Eng Mater 8:20180040. doi: 10.1520/acem20180040

Ahmed A, Afreen A, Moin PK (2017) State of Art Review: Behaviour of Masonry Structures under Gravity and Seismic Loads. 7:14

Ahn LK, Curtin W. (1997) Strain and hysteresis by stochastic matrix cracking in ceramic matrix composites. Mech Compos Mater 45:177–209

Akhoundi F, Lourenco PB, Palha C (2015) In-Plane and Out-of Plane Experimental Characterization of Rc in-Plane and Out-of Plane Experimental. 26–30

Akhoundi F, Lourenço PB, Vasconcelos G (2016) Numerically based proposals for the stiffness and strength of masonry in fi lls with openings in reinforced concrete frames. Earthq Eng Struct Dyn 45:869–891. doi: org/10.1002/eqe.2688

Akhoundi F, Vasconcelos G, Lourenço P, et al (2018) In-plane behavior of cavity masonry infills and strengthening with textile reinforced mortar. Eng Struct 156:145–160. doi: 10.1016/j.engstruct.2017.11.002

Al-chaar G (2002a) Evaluating Strength and Stiffness of Unreinforced Masonry Infill Structures ERDC / CERL TR-02-1

Al-Chaar G, Issa M, Sweeney S (2002) Behavior of masonry-infilled nonductile reinforced concrete frames. J Struct Eng 128:1055–1063. doi: 10.1061/(ASCE)0733-9445(2002)128:12(1544)

Al-Chaar G, Lamb GE, Abrams DP (2003) Effect of openings on structural performance of unreinforced masonry infilled frames. ACI Spec Publ 211:247–262

Al-chaar GK, Mehrabi A (2008) Constitutive Models for Nonlinear Finite Element Analysis of Masonry Prisms Infill Walls.

Allen C, Mark M, Page A, et al (2017) Nonlinear finite element modelling of unreinforced masonry walls with openings subjected to in-plane shear. 13Th Can Mason Symp

Allen C, Page A, Griffith M, et al (2016) Experimental testing of unreinforced masonry

walls with openings subject to cyclic in-plane shear. Brick Block Mason 1401–1408. doi: 10.1201/b21889-187

Altin S (2007) An experimental study on reinforced concrete partially infilled frames. 29:449–460. doi: 10.1016/j.engstruct.2006.05.011

Amato G, Cavaleri L, Fossetti M, Papia M (2008) Infilled frames: influence of vertical loads on the equivalent diagonal strut model. Proc 14th WCEE

Andreas Stavridis I, Shing PB (2010) Finite-Element Modeling of Nonlinear Behavior of Masonry-Infilled RC Frames. J Struct Eng 136:285–296. doi: 10.1061/(ASCE)ST.1943-541X.116

Andreas Stavridis IK and PBS (2012) Shake-table tests of a three-story reinforced concrete frame with masonry infill walls. Earthq Eng Struct Dyn 44:657–675. doi: 10.1002/eqe

Andreaus U (1988) A 3-D Finite Element Model for the Analysis of Masonry Structures. Proc Eighth Int Brick Block Mason Conf Repub Irel 1405–1416

Angel R (1994) Behavior of Reinforced Concrete Frames With Masonry Infills. University of illinois

Angelillo M (2014) Mechanics of Masonry Structures

Anil Ö, Altin S (2007) An experimental study on reinforced concrete partially infilled frames. Eng Struct 29:449–460. doi: 10.1016/j.engstruct.2006.05.011

Anthonie A, Magonette G (1994) Shear-compression testing and analysis of brick masonry walls. In: 10th European Conference on Earthquake Engineering. pp 1–10

Antino TD, Papanicolaou C (2017) Mechanical characterization of textile reinforced inorganic-matrix composites. 127:78–91. doi: 10.1016/j.compositesb.2017.02.034

Ardiaca DH (2009) Mohr-Coulomb parameters for modelling of concrete structures. Plaxis Bull 12–15

ASCE 41-17 (2017) Seismic Evaluation and Retrofit of Existing Buildings; American Society of Civil Engineers: Reston, VA, USA.

Asteris PG (2003) Lateral Stiffness of Brick Masonry Infilled Plane Frames. J Struct Eng 129:1071. doi: DOI: 10.1061/~ASCE!0733-9445~2003!129:8~1071!

Asteris PG, Antoniou ST, Sophianopoulos DS, Chrysostomou CZ (2011a) Mathematical Macromodeling of Infilled Frames: State of the Art. J Struct Eng 137:1508–1517. doi: 10.1061/(ASCE)ST.1943-541X.0000384

Asteris PG, Cavaleri L, Di Trapani F, Sarhosis V (2016) A macro-modelling approach for the analysis of infilled frame structures considering the effects of openings and vertical loads. Struct Infrastruct Eng 12:551–566. doi: 10.1080/15732479.2015.1030761

Asteris PG, Chrysostomou CZ, Giannopoulos IP, Smyrou E (2011c) Masonry Infilled Reinforced Concrete Frames With. III ECCOMAS Themat Conf Comput Methods Struct Dyn Earthq Eng

Asteris PG, Giannopoulos IP, Chrysostomou CZ (2012) Modeling of Infilled Frames With Openings. Open Constr Build Technol J 6:81–91

Asteris PG, Kakaletsis DJ, Chrysostomou CZ, Smyrou EE (2011d) Failure modes of in-filled frames. Electron J Struct Eng 11:11–20

Asteris PG, Tzamtzis AD (2003) On the Use of a Regular Yield Surface for the Analysis of Unreinforced Masonry Walls. Struct Eng 3:23–42

Augenti N, Parisi F, Prota A, Manfredi G (2010) In-Plane Lateral Response of a Full-Scale Masonry Subassemblage with and without an Inorganic Matrix-Grid Strengthening System. J Compos Constr 15:578–590. doi: 10.1061/(asce)cc.1943-5614.0000193

Aveston J, Kelly a. (1973) Theory of multiple fracture of fibrous composites. J Mater Sci 8:352–362. doi: 10.1007/BF00550155

Aveston J, Kelly A (1980) Tensile first cracking strain and strength of hybrid composites and laminates. doi: 10.1098/rsta.1979.0079

Babaeidarabad S, Arboleda D, Loreto G, Nanni A (2014) Shear strengthening of un-reinforced concrete masonry walls with fabric-reinforced-cementitious-matrix. Constr Build Mater 65:243–253. doi: 10.1016/j.conbuildmat.2014.04.116

Baloevic G, Radnic J, Matesan D, Grgic N (2018) Behavior of fiber reinforced mortar composites under impact load. Lat Am J Solids Struct 15:. doi: 10.1590/1679-78254168

Banholzer B, Brameshuber W, Jung W (2006) Analytical evaluation of pull-out tests—The inverse problem. Cem Concr Compos 28:564–571. doi: 10.1016/j.cemconcomp.2006.02.015

Barhum R, Mechtcherine V (2012) Effect of short, dispersed glass and carbon fibres on the behaviour of textile-reinforced concrete under tensile loading. Eng Fract Mech 92:56–71. doi: 10.1016/j.engfracmech.2012.06.001

Bartos P (1981) Review paper: Bond in fibre reinforced cements and concretes. Int J Cem Compos Light Concr 3:159–177. doi: 10.1016/0262-5075(81)90049-X

Basha SH, Kaushik HB (2016a) Behavior and failure mechanisms of masonry-infilled RC frames (in low-rise buildings) subject to lateral loading. Eng Struct 111:233–245. doi: 10.1016/j.engstruct.2015.12.034

Basili M, Marcari G, Vestroni F (2016) Nonlinear analysis of masonry panels strengthened with textile reinforced mortar. Eng Struct 113:245–258. doi: 10.1016/j.engstruct.2015.12.021

Batikha M, Alkam F (2015) The effect of mechanical properties of masonry on the behavior of FRP-strengthened masonry-infilled RC frame under cyclic load. Compos Struct 134:513–522. doi: 10.1016/j.compstruct.2015.08.105

Bazãn E, Meli R (1980) Seismic Analysis of Structures Hth Masonry Walls. Iitk.Ac.in

Bazant Z, Oh B (1983) Crack band theory of concrete. Mater Struct 16:155. doi: 10.1007/BF02486267

Bazant ZP (1984) Size Effect in Blunt Fracture: Concrete, Rock, Metal. J Eng Mech 110:518–535. doi: 10.1061/(ASCE)0733-9399(1984)110:4(518)

Bažant ZP (2001) Concrete fracture models: Testing and practice. Eng Fract Mech

69:165–205. doi: 10.1016/S0013-7944(01)00084-4
Bažant ZP, Belytschko TB, Chang T (1984) Continuum Theory for Strain-Softening. J Eng Mech 110:1666–1692. doi: 10.1061/(ASCE)0733-9399(1984)110:12(1666)
Bažant ZP, Kazemi MT (1990) Determination of fracture energy, process zone length and brittleness number from size effect, with application to rock and concrete. Int J Fract 44:111–131
Bažant ZP, Yu Q (2011) Size-Effect Testing of Cohesive Fracture Parameters and Nonuniqueness of Work-of-Fracture Method. J Eng Mech 137:580–588. doi: 10.1061/(ASCE)EM.1943-7889.0000254
Benedetti A, Pelà L, Aprile A (2008) Masonry properties determination via splitting tests on cores with a rotated mortar layer. 8th Int Semin Struct Mason Proc 05-07 Novemb 2008 1–8
Benetti D, Carydis P, Pezzoli P (1998) Shaking-table test on 24 simple masonry buildings. Earthq Eng Struct Dyn 27:67–90
Bentur A, Mindess S (1990) Fibre reinforced Cementitious Composites. Appl Sci 2:1–10
Bernat E, Gil L, Roca P, Escrig C (2013) Experimental and analytical study of TRM strengthened brickwork walls under eccentric compressive loading. Constr Build Mater 44:35–47. doi: 10.1016/j.conbuildmat.2013.03.006
Bertero.V and Brokken. S (1983) Infills in seismic resistant building 3. ASCE J Struct Eng 109:1337–1361
Bertero V, Brokken S (1983) Infills in seismic resistant building. ASCE J Struct Eng 109:1337–1361
Berto L, Saetta A, Scotta R, Vitaliani R (2002) An orthotropic damage model for masonry structures. Int J Numer Methods Eng 55:127–157. doi: 10.1002/nme.495
Bertolesi E, Carozzi FG, Milani G, Poggi C (2014) Numerical modeling of Fabric Reinforce Cementitious Matrix composites (FRCM) in tension. Constr Build Mater 70:531–548. doi: 10.1016/j.conbuildmat.2014.08.006
Bertolesi E, Milani G, Poggi C (2016) Simple holonomic homogenization model for the non-linear static analysis of in-plane loaded masonry walls strengthened with FRCM composites. Compos Struct 158:291–307. doi: 10.1016/j.compstruct.2016.09.027
Blom J, Cuypers H, Itterbeeck P Van, Wastiels J (2008) DETERMINATION OF MATERIAL PARAMETERS OF A TEXTILE REINFORCED COMPOSITE USING AN INVERSE METHOD. 1–11
Bocca P, Caprinteri A, Valente S (1989) Fracture mechanics of brick masonry : size effects and snap-back analysis. Mater Struct 22:364–373
Borri A, Castori G, Corradi M (2012) Evaluation of shear strength of masonry panels through different experimental analyses. In: 14th Structural Faults and Repair. pp 1–13
Brameshuber W (2006) Textile Reinforced Concrete - State-of-the-Art Report of

RILEM TC 201-TRC
Brameshuber W (2014) Influence of short fibres on strength, ductility and crack development of textile reinforced concrete. pp 105–112
Brencich A, Gambarotta L, Lagomarsino S (1998) A macroelement approach to the three-dimensional seismic analysis of masonry buildings. 11th Eur an Conf ce Ear thqua ke Eng 90:1–10. doi: 10.1063/1.4932540
Brockmann T (2007) Mechanical and Fracture Mechanical Properties of Fine Grained Concrete for TRC Structures
Brown P (1995) The Bauschinger Effect In High Strength Steels Thesis
Bruckner A, Ortlepp R, Curbach M (2006) Textile reinforced concrete for strengthening in bending and shear. Mater Struct 39:741–748. doi: 10.1617/s11527-005-9027-2
Bruneau M (1994) State-of-the-art report on seismic performance of unreinforced masonry buildings. J Struct Eng 120:230–251
Buonopane SG, White RN (1999b) Pseudodynamic Testing of Masonry Infilled Reinforced. J Struct Eng 578–589. doi: 10.1061/(ASCE)0733-9445(1999)125:6(578)
Burton H DG (2013) Simulation of seismic collapse in non-ductile reinforced concrete frame buildings with masonry infills. Struct Eng 148:
Butler M, Hempel R, Schiekel M (2006) The Influence of short glass fibres on the working capacity of textile reinforced concrete. p 10
Butler M, Mechtcherine V, Hempel S (2010) Durability of textile reinforced concrete made with AR glass fibre: effect of the matrix composition. Mater Struct 43:1351–1368. doi: 10.1617/s11527-010-9586-8
CA Syrmakezis VV (1986) Influence of infill walls to RC frames response. In: 8th European Conference on Earthquake Engineering
Çağatay IH (2005) Failure of an industrial building during a recent earthquake in Turkey. Eng Fail Anal 12:497–507. doi: 10.1016/j.engfailanal.2004.09.004
Caggegi C, Lanoye E, Djama K, et al (2017) Tensile behaviour of a basalt TRM strengthening system : In fl uence of mortar and reinforcing textile ratios. Compos Part B 130:90–102. doi: 10.1016/j.compositesb.2017.07.027
Calvi GM, Bolognini D (2001) Seismic response of reinforced concrete frames infilled with weakly reinforced masonry panels. J Earthq Eng 5:153–185. doi: 10.1080/13632460109350390
Carozzi FG, Poggi C (2015) Mechanical properties and debonding strength of Fabric Reinforced Cementitious Matrix (FRCM) systems for masonry strengthening. Compos Part B Eng 70:215–230. doi: 10.1016/j.compositesb.2014.10.056
Carpinteri A, Spagnoli A, Vantadori S (2006) An elastic-plastic crack bridging model for brittle-matrix fibrous composite beams under cyclic loading. Int J Solids Struct 43:4917–4936. doi: http://dx.doi.org/10.1016/j.ijsolstr.2005.06.059
Cavaleri L (2002) Infilled frames: developments in the evaluation of cyclic behaviour under lateral loads. ASCE J Struct Eng

Cavaleri L, Di Trapani F (2014a) Cyclic response of masonry infilled RC frames: Experimental results and simplified modeling. Soil Dyn Earthq Eng 65:224–242. doi: 10.1016/j.soildyn.2014.06.016

Červenka V, Gerstle K Inelastic Analysis of Reinforced Concrete Panels: Part I. Theory, Part II: Experimental Verification, Part I: Vo. IABSE, Zurich,

Cetisli F (2015) Effect of openings on infilled frame stiffness. Gradjevinar 67:787–797. doi: 10.14256/JCE.1155.2014

Chaimoon K, Attard MM (2009) Experimental and numerical investigation of masonry under three-point bending (in-plane). Eng Struct 31:103–112. doi: 10.1016/j.engstruct.2008.07.018

Chen SY, Moon FL, Yi T (2008) A macroelement for the nonlinear analysis of in-plane unreinforced masonry piers. Eng Struct 30:2242–2252. doi: 10.1016/j.engstruct.2007.12.001

Chiou Y-J, Tzeng J-C, Liou Y-W (1999c) Experimental and Analytical Study of Masonry Infilled Frames. ASCE J Struct Eng 125:

Chiou YJ, Tzeng JC HS (1998) Discontinuous deformation analysis for reinforced concrete frames infilled with masonry walls. Struct Eng Mech 6:201–215

Chrysostomou, C. Z., Gergely, P., & Abel JF (2002) A six-strut model for nonlinear dynamic analysis of steel infilled frames. Int J Struct Stab Dyn 02:335–353. doi: 10.1142/s0219455402000567

Chrysostomou CZ (1991) Effects of degrading infill walls on the nonlinear seismic response of two-dimensional steel frames. Diss Abstr Int 51:348

Chrysostomou CZ, Asteris PG (2012) On the in-plane properties and capacities of infilled frames. Eng Struct 41:385–402. doi: 10.1016/j.engstruct.2012.03.057

Chudoba R, Moller B, Meskouris K (2006) Numerical modeling of Textile-reinforced concrete

Colajanni P, Fossetti M, Macaluso G (2014) Effects of confinement level, cross-section shape and corner radius on the cyclic behavior of CFRCM confined concrete columns. Constr Build Mater 55:379–389. doi: 10.1016/j.conbuildmat.2014.01.035

Colombo A, Negro P, Verzeletti G (2000) Improving Ductility and Energy-Dissipation Capacity of Infills By Means of Polymeric Nets. Proc 12th World Conf Earthq Eng Auckland, New Zeal Paper No.:1–7

Colombo IG, Magri A, Zani G, et al (2013a) Textile Reinforced Concrete: experimental investigation on design parameters. Mater Struct 46:1933–1951. doi: 10.1617/s11527-013-0017-5

Combescure D, Pegon P (2000) Application of the local to global approach to the study of inifllled frame structure under seismic loading. In: 12wcee. pp 1–8

Comité Euro-International du Béton (CEB) TTS (1996) RC frames under earthquake loading." State of the Art Report

Contamine R, Si Larbi a., Hamelin P (2011) Contribution to direct tensile testing of textile reinforced concrete (TRC) composites. Mater Sci Eng A 528:8589–8598.

doi: 10.1016/j.msea.2011.08.009
Corradi M, Borri A, Vignoli A (2003) Experimental study on the determination of strength of masonry walls. Constr Build Mater 17:325–337. doi: 10.1016/S0950-0618(03)00007-2
Crisafulli FJ (1997) Seismic behaviour of reinforced concrete structures with masonry infills. university of Canterbure New Zeland
Crisafulli FJ (2000a) Analytical modeling of infilles frame structure- a general review. Earthq Eng Struct … 33:30–74
Crisafulli FJ, Carr AJ (2007) Proposed macro-model for the analysis of infilled frame structures. Bull New Zeal Soc Earthq Eng 40:69–77
Crowley H, Pinho R (2006) Simplified Equations for Estimating the Period of Vibration of. First Eur Conf Earthq Eng Seismol 3–8. doi: 1122
Cur C (1994) Structural masonry: an experimental/numerical basis for practical design rules. Gouda, Netherlands.
Curbach, M., Ortlepp, R., & Triantafillou TC (2006) TRC for rehabilitation. In W. Brameshuber (Ed.), Textile Reinforced Concrete. RILEM Rep 36 221–236
Curtin,WA, BK A, N T (1998) Modeling Brittle and Tough Stress-Strain Behaviour in Unidirectional Ceramic Composites. Acta Metall Mater 3409– 3420
Curtin W (1999) Stochastic Damage Evolution and Failure in Fibre-Reinforced Composites. Adv Mater Sci Eng 163–253
Cuypers H, Wastiels J (2006) Stochastic matrix-cracking model for textile reinforced cementitious composites under tensile loading. Mater Struct 39:777–786. doi: 10.1617/s11527-005-9053-0
D'Altri, A, Sarhosis, v, Rots J (2019) A review of numerical. In: Numerical modelling of masonry and historical structures
D'Ambrisi A, Focacci F (2011) Flexural Strengthening of RC Beams with Cement-Based Composites. J Compos Constr 15:707–720. doi: 10.1061/(ASCE)CC.1943-5614.0000218
Da Porto F, Guidi G, Dalla Benetta M, Verlato N (2013) Combined In-Plane/Out-of-Plane Experimental Behaviour of Reinforced and Strengthened Infill Masonry Walls. In: 12th Canadian Masonry Symposium. pp 1–11
Da Porto F, Guidi G, Verlato N, Modena C (2015) Effectiveness of plasters and textile reinforced mortars for strengthening clay masonry infill walls subjected to combined in-plane/out-of-plane actions / Wirksamkeit von Putz und textilbewehrtem Mörtel bei der Verstärkung von Ausfachungswänden aus Ziegel. Eur J Mason 19:334–354. doi: 10.1002/dama.201500673
Dautaj AD, Kadiri Q, Kabashi N (2018) Experimental study on the contribution of masonry infill in the behavior of RC frame under seismic loading. Eng Struct 165:27–37. doi: 10.1016/j.engstruct.2018.03.013
Dawe J, Seah C (1989a) Out-of-plane resistance of concrete masonry infilled panels.pdf. Civ Eng 16:854–864

Dawe JL, Seah CK (1989b) Behaviour of masonry infilled steel frames. Can J Civ Eng 16:865–876

Dawe JL, Seah CK (1989c) Out-of-plane resistance of concrete masonry infilled panels.pdf. Civ Eng 16:854–864

Dawe JL, Seah CK, Liu Y (2001) A computer model for predicting infilled frame behaviour. Can J Civ Eng 28:133–148. doi: 10.1139/l00-083

Dawe JL YT (1985) An Investigation of Factors Influencing the Behaviour of Masonry Infill. In: Proc, of the seventh international brick masonry conference, vol. 2, Melbourne, Australia. pp 803–814

De Caso Y Basalo FJ, Matta F, Nanni A (2012) Fiber reinforced cement-based composite system for concrete confinement. Constr Build Mater 32:55–65. doi: 10.1016/j.conbuildmat.2010.12.063

De Santis S, Ceroni F, de Felice G, et al (2017) Round Robin Test on tensile and bond behaviour of Steel Reinforced Grout systems. Compos Part B Eng 127:100–120. doi: 10.1016/j.compositesb.2017.03.052

Decanini, L.D., Gavarini, C. and Mollaioli F (2004) Seismic Performance of Masonry Infilled R/C Frames. 13th World Conf. Earthq. Eng. 165

Decanini L, Liberatore L, Mollaioli F (2012) The influence of openings on the seismic behaviour of infilled framed structures. Conf 15th World Conf Earthq Eng

Decanini LD, Liberatore L, Mollaioli F (2014) Strength and stiffness reduction factors for infilled frames with openings. Earthq Eng Eng Vib 13:437–454. doi: 10.1007/s11803-014-0254-9

Dehghani FN-E and A (2008) Analytical and numerical study of rc frames with urm infilled retrofitted by CFRP. In: 14 World Conference on Earthquake Engineering. Beijing, China

Dhanasekar M (1986) The influence of brick masonry fill properties on the behavior of infilled frames. J Civ Eng 81:593–605

Di Domenico M, Ricci P, Verderame GM (2019) Experimental assessment of the out-of-plane strength of URM infill walls with different slenderness and boundary conditions. Springer Netherlands

Di Ludovico M, Prota A, Manfredi G (2010a) Structural Upgrade Using Basalt Fibers for Concrete Confinement. J Compos Constr 14:541–552. doi: 10.1061/(ASCE)CC.1943-5614.0000114

Di Ludovico M, Prota A, Manfredi G, et al (2010b) Confinement of medium strength concrete cylinders with basalt Textile Reinforced Mortar. J Compos Constr 14:541–552. doi: 10.1061/(ASCE)CC.1943-5614.0000114

Díaz EMV, Fukuyama H (2008) Effect of the openings in the strength and stiffness of reinforced concrete structural walls. Bull Int Inst Seismol Earthq Eng 42:73–78

Dodd LL, Restrebo JI (1995) Model for Predicting Cyclic Behavior of Reinforcing Steel. Struct Eng 121:433–445

Dolatshahi KM, Aref AJ (2011) Two-dimensional computational framework of meso-

scale rigid and line interface elements for masonry structures. Eng Struct 33:3657–3667. doi: 10.1016/j.engstruct.2011.07.030

Dolšek M, Fajfar P (2008) The effect of masonry infills on the seismic response of a four-storey reinforced concrete frame - a deterministic assessment. Eng Struct 30:1991–2001. doi: 10.1016/j.engstruct.2008.01.001

Donà M, Minotto M, Saler E, et al (2017) Combined in-plane and out-of-plane seismic effects on masonry infills in RC frames. Ing Sismica 34:157–173

Doudoumis.N,Mistopoullou N (1994) A macroelement for the simulation of the infill panels in multistorey frames under horizontal seismic actions A macroelement for the simulation of the infill panels in multistorey frames under horizontal seismic actions. In: 10th European Conference on Earthquake Engineering

Drougkas A, Roca P, Molins C (2015) Numerical prediction of the behavior , strength and elasticity of masonry in compression. Eng Struct 90:15–28. doi: 10.1016/j.engstruct.2015.02.011

Durrani, A.J. and Luo YH (1994) Seismic Retrofit of Flat-Slab Buildings with Masonry Infills. In: Workshop on Seismic Response of Masonry Infills. pp 1–8

Dusko A, Ardiaca H, Enginyers M (2009) Mohr-Coulomb parameters for modelling of concrete structures. 12–15

EC8-1 (2004) Eurocode 8: Design of structures for earthquake resistance – Part 1: General rules, seismic actions and rules for buildings. EN 1998-1

EC8-3 (2005) EN 1998-3 Eurocode 8: Design of structures for earthquake resistance, part 3: assessment and retrofitting of buildings

Ehgri C, King GJN (2018) The analysis of infilled frames using finite eletnents. 38:749–760

El-Dakhakhni (2002) Experimental and Analytical Seismic Evaluation of Concrete Masonry-Infilled Steel Frames Retrofitted using GFRP Laminates

El-Dakhakhni WW, Elgaaly M, Hamid AA (2003) Three-strut model for concrete masonry-infilled steel frames. J Struct Eng 129:177–185. doi: 10.1061/(ASCE)0733-9445(2003)129:2(177)

El-Dakhakhni WW, Elgaaly M, Hamid AA (2001) Finite Element Modeling of Concrete Masonry-Infilled Steel Frame. 9th Can Mason Symp

El-Dakhakhni WW, Hamid AA, Elgaaly M (2004) Strength and Stiffness Prediction of Masonry Infill Panels. 13th World Conf Earthq Eng

El Messiry M, Mito A-B, Al-Oufy A, El-Tahan E (2014) Effect of fabric material and tightness on the mechanical properties of fabric–cement composites. Alexandria Eng J 53:795–801. doi: 10.1016/j.aej.2014.09.002

EN 1504-3 (2006) Products and systems for the protection and repair of concrete structures. Definitions, requirements, quality control and evaluation of conformity. Part 3: Structural and non-structural repair

Eshghi S, Pourazin K (2009) In-Plane Behavior of Confined Masonry Walls – With and Without Opening. 7:49–60

Eurocode 2 British Standard (2008) Eurocode 2 : Design of concrete structures. London

F. Jesse GC (2003) Strength of continuous AR-glass fibre reinforcement of cementitious composites. In: International Workshop High Performance Fiber Reinforced Cement Composites. pp 337–348

Fantilli AP, Mihashi H, Vallini P (2009) Multiple cracking and strain hardening in fiber-reinforced concrete under uniaxial tension. Cem Concr Res 39:1217–1229. doi: 10.1016/j.cemconres.2009.08.020

Fardis MN (2000) Design Provisions for Masonry-Infilled Rc Frames. 12th World Conf. Earthq. Eng. 1–8

Fardis MN, Panagiotakos TB (1997) Seismic design and response of bare and masonry-infilled reinforced concrete buildings . part i : bare structures response of bare and masonry-infilled reinforced concrete buildings . J Earthq Eng 24:219–256. doi: 10.1080/13632469708962367

Felice G De, Santis S De, Garmendia L (2014) Mortar-based systems for externally bonded strengthening of masonry. Mater … 1–22

FEMA-308 (1998) Repair of Earthquake Damaged Concrete and Masonry Wall Buildings. FEMA, Washington, D.C.

FEMA 273 (1997) NEHRP guidelines for the seismic rehabilitation of buildings. FEMA Washington, DC

FEMA 306 (1998) Evaluation of earthquake damaged concrete and masonry wall buildings. FEMA, Washington, DC

FEMA 368 (2000) NEHRP Recommended Provisions for Seismic Regulations for New Buildings and other Structures. FEMA, MD

Fenu L, Forni D, Cadoni E (2015) Energy absorption at high strain rate of glass fiber reinforced mortars. EPJ Web Conf 94:01030. doi: 10.1051/epjconf/20159401030

Fib Model Code (2010) Fédération Internationale du Béton (fib), MC2010, Model Code for Concrete Structures 2010. Lausanne, Switzerland

Fiorato A, Sozen MA, Gamble W (1970) An investigation of the interaction of reinforced concrete frames with masonry filler walls. UNIVERSITY OF ILLINOIS

Firdous M, Gupta S (2017) A Critical Evaluation of the Effect of Soft Storey and Column Orientation on RC Buildings. IJSTE -International J Sci Technol Eng 3:44–47

Flanagan DR, Bennett RM (1999a) In-plane behavior of structural clay tile infilled frames. ASCE J Struct Eng 125:590–599

Flanagan R., Bennett RM (1999b) Bidirectional behaviour of structural clay tile infilled Frames. J Struct Eng 123:236–244

Flores and Alcocer (1996) Calculated response of confined masonry structures

Furtado A, Rodrigues H, Arêde A (2015) Modelling of masonry infill walls participation in the seismic behaviour of RC buildings using OpenSees. Int J Adv Struct Eng 117–127. doi: 10.1007/s40091-015-0086-5

Furtado A, Rodrigues H, Arêde A, Varum H (2016) Experimental evaluation of out-of-plane capacity of masonry infill walls. Eng Struct 111:48–63. doi: 10.1016/j.engstruct.2015.12.013

Furtado A, Rodrigues H, Arêde A, Varum H (2018) Out-of-plane behavior of masonry infilled RC frames based on the experimental tests available: A systematic review. Constr Build Mater 168:831–848. doi: 10.1016/j.conbuildmat.2018.02.129

Furtado A, Teresa De Risi M (2020) Recent Findings and Open Issues concerning the Seismic Behaviour of Masonry Infill Walls in RC Buildings. Adv Civ Eng 2020:. doi: 10.1155/2020/9261716

G Magenes AF (1998) Simplified non-linear seismic analysis of masonry buildings. In: 12th World Conference on Earthquake Engineering, Auckland, New Zealand

Gao X, Stavridis A, Bolis V, Preti M (2018) Experimental study on the seismic performance of non-ductile rc frames infilled with sliding Frames Infilled with Sliding Subpanels. In: 11th U.S. National Conference on Earthquake Engineering

Garcia-Ramonda L, Pelá L, Roca P, Camata G (2020) In-plane shear behaviour by diagonal compression testing of brick masonry walls strengthened with basalt and steel textile reinforced mortars. Constr Build Mater 240:. doi: 10.1016/j.conbuildmat.2019.117905

García D, Alonso P, San-José J-T, et al (2010) Confinement of medium strength concrete cylinders with basalt Textile Reinforced Mortar. 13th Int Congr Polym Concr [ICPIC 2010] 0–7

Garmendia L, San-José JT, García D, Larrinaga P (2011) Rehabilitation of masonry arches with compatible advanced composite material. Constr Build Mater 25:4374–4385. doi: 10.1016/j.conbuildmat.2011.03.065

Gettu R, Bazant Z., Karr ME (1990) Fracture Properties and Brittleness of High Strength Concrete. ACI J Mater

Ghassan Al-Chaar, Armin B. Mehrabi and TM (2008) Finite Element Interface Modeling and Experimental Verificaion of Masonry-Infilled R/C Frames. 30:

Ghobarah A, El Mandooh Galal K (2004) Out-of-Plane Strengthening of Unreinforced Masonry Walls with Openings. J Compos Constr 8:298–305. doi: 10.1061/(asce)1090-0268(2004)8:4(298)

Gil L, Escrig C, Bernat E (2014) Bending Performance of Concrete Beams Strengthened with Textile Reinforced Mortar TRM. Key Eng Mater 601:203–206. doi: 10.4028/www.scientific.net/KEM.601.203

Graf W, Hoffmann A, Möller B, et al (2007) Analysis of textile-reinforced concrete structures under consideration of non-traditional uncertainty models. Eng Struct 29:3420–3431. doi: 10.1016/j.engstruct.2007.08.013

Grande E, Imbimbo M, Sacco E (2013) Finite element analysis of masonry panels strengthened with FRPs. Compos Part B 45:1296–1309. doi: 10.1016/j.compositesb.2012.09.002

Gu J Ben, Tao Y, Xin R, et al (2018) Seismic Performance of Multistorey Masonry

Structure with Openings Repaired with CFRP Grid. Adv Civ Eng 2018:9–13. doi: 10.1155/2018/4374876

H.P Backes (1985) Tesnile strength of masonry. In: roceedings of the 7th International Brick Masonry. pp 779–790

Haddad EL (1991) Finite element analysis of infilled frames considering cracking and separation phenomena. Comput Struct 41:439–441

Hamilton (2005) Flexural capacity of glass FRP strengthened concrete masonry walls. J Compos Constr 4:1–20

Hannant DJ, Zonsveld JJ, Hughes DC (1978) Polypropylene film in cement based materials. Composites 9:83–88. doi: 10.1016/0010-4361(78)90584-0

Hartig J, Häußler-Combe U (2010) A model for the uniaxial tensile behaviour of textile reinforced concrete (trc) covering effects at the micro and meso scales. In: Proceedings of ECF18, Dresden,. pp 1–8

Hartig J, Häußler-Combe U, Schicktanz K (2008) Influence of bond properties on the tensile behaviour of Textile Reinforced Concrete. Cem Concr Compos 30:898–906. doi: 10.1016/j.cemconcomp.2008.08.004

Hashemi A, Mosalam KM (2006) Shake-table experiment on reinforced concrete structure containing masonry infill wall. 1827–1852. doi: 10.1002/eqe

Hatrig J, Haubler-combe H, Schichtanz K (2004) A lattice model approach t o the uniaxial behaviour of Textile Reinforced Concrete. Compos Mater

Häußler-Combe U, Hartig J (2007) Bond and failure mechanisms of textile reinforced concrete (TRC) under uniaxial tensile loading. Cem Concr Compos 29:279–289. doi: 10.1016/j.cemconcomp.2006.12.012

Häußler-Combe U, Jesse F, Curbach M (2004) Textile reinforced concrete-overview, experimental and theoretical investigations. Fract Mech Concr Struct Proc fifth Int Conf Fract Mech Concr Concr Struct Ia-FraMCos, Vail, CO, USA 204:12–16

Hegger J, Voss S (2008) Investigations on the bearing behaviour and application potential of textile reinforced concrete. Eng Struct 30:2050–2056. doi: 10.1016/j.engstruct.2008.01.006

Hegger J, Will N, Bruckermann O, Voss S (2006) Load–bearing behaviour and simulation of textile reinforced concrete. Mater Struct 39:765–776. doi: 10.1617/s11527-005-9039-y

Hinzen M, Brameshuber W (2006) Hybrid short fibres in fine grained concrete. p 10

Holler S, Butenweg C, Noh S, Meskouris K (2004) Computational model of textile-reinforced concrete structures. Comput Struct 82:1971–1979. doi: 10.1016/j.compstruc.2004.03.076

Holmes M (1961) Steel frames with brickwork and conrete infilling. Proc Inst Civ Eng 25:473–478

Hugo F, Anto R (2015) Modelling of masonry infill walls participation in the seismic behaviour of RC buildings using OpenSees. 117–127. doi: 10.1007/s40091-015-0086-5

ICC-Evaluation Service. (2013) AC434 Acceptance criteria for masonry and concrete strengthening using fiber-reinforced cementitious matrix (FRCM) composite systems

Institute SSZM (2001) Modelling of Friction and Dilatancy Effects. Mech Compos Mater 3:707–739

International Building Code (2018) International Code Council, Inc

Ismail N, El-maaddawy T, Khattak N (2018) Quasi-static in-plane testing of FRCM strengthened non-ductile reinforced concrete frames with masonry infills. Constr Build Mater 186:1286–1298. doi: 10.1016/j.conbuildmat.2018.07.230

J Aveston, GA Cooper AK (1971a) Single and multiple fracture: the properties of fibre composites. In: The properties of fibre composites

J Aveston, GA Cooper AK (1971b) The properties of fiber composites. In: Conference proceedings National Physical Laboratory (IPC Science and Technology Press Ltd). p 15

Jesse F (2006) Load-bearing behavior of Textile-reinforced concrete

Jesse F (2004) Load Bearing Behaviour of Filament Yarns in cementitous matrix

Jesse F, Ortlepp R, Curbach M (2005) Tensile Stress-Strain Behaviour of Textile Reinforced Concrete. 15:

Jesse F, Will N, Curbach M, Hegger J (2008) Load-Bearing Behavior of Textile-Reinforced Concrete. 250:59–68

Jiang H, Liu X, Mao J (2015) Full-scale experimental study on masonry infilled RC moment-resisting frames under cyclic loads. Eng Struct 91:70–84. doi: 10.1016/j.engstruct.2015.02.008

Johnson, Sanya I university (2006) Comparison of Nonlinear Finite Element Modeling Tools for Structural Concrete. 1–56

Kadir MRA (1974) The structural behavior of masonry-iniflled panels in framed structures. Edinburgh

Kadysiewski S, Mosalam KM (2009) Modeling of unreinforced masonry infill walls considering in-plane and out-of-plane interaction. PEER Rep 2008/102 144

Kakaletsis D, Karayannis C (2007) Experimental investigation of infilled r/c frames with eccentric openings. Struct Eng Mech 26:231–250. doi: 10.12989/sem.2007.26.3.231

Kakaletsis DJ (2009) Masonry infills with window openings and influence on reinforced concrete frame constructions. Earthq Eng Struct Dyn 104:445–455. doi: 10.2495/ERES090401

Kakaletsis DJ, Karayannis CG (2008) Influence of masonry strength and openings on infilled R/C frames under cycling loading. J Earthq Eng 12:197–221. doi: 10.1080/13632460701299138

Kakaletsis DJ, Karayannis CG (2009) Experimental investigation of infilled reinforced concrete frames with openings. ACI Struct J 106:132–141

Kalali A, Kabir MZ (2012) Cyclic behavior of perforated masonry walls strengthened

with glass fiber reinforced polymers. Sci Iran 19:151–165. doi: 10.1016/j.scient.2012.02.011

Kamal A, Kunieda M, Ueda N, Nakamura H (2008) Evaluation of crack opening performance of a repair material with strain hardening behavior. Cem Concr Compos 30:863–871. doi: 10.1016/j.cemconcomp.2008.08.003

Kappos AJ, Ellul F (2000) Seismic design and performance assessment of masonry infilled r/c frames. 12th World Conf. Earthq. Eng. Auckland, New Zeal. 1–8

Karayannis CG, Kakaletsis DJ, Favvata MJ (2005) Behavior of bare and masonry infilled R/C frames under cyclic loading: Experiments and analysis. WIT Trans Built Environ 81:429–438

Kareem KM, Güneyisi EM (2019) Effect of Masonry Infill Wall Configuration and Modelling Approach on the Behaviour of RC Frame Structures. Arab J Sci Eng 44:4309–4324. doi: 10.1007/s13369-018-3389-6

Kiarash M. Dolatshahi AJA (2011) Two dimensional computational framework of meso scale rigid and line.pdf. Eng Struct 33:3657–3667

Konrad M, Chudoba R, Kang B (2006) Numerical and experimental evaluation of damage parameters for textile reinforced concrete under cyclic loading. Building 2006

Kouris LAS, Ph D, Triantafillou TC, Asce M (2019) Design Methods for Strengthening Masonry Buildings Using Textile-Reinforced Design Methods for Strengthening Masonry Buildings Using Textile-Reinforced Mortar. ASCE J Struct Eng. doi: 10.1061/(ASCE)CC.1943-5614.0000906

Koutas L, Triantafillou T, Bousias S (2014a) Seismic Strengthening of Masonry-Infilled RC Frames with TRM: Experimental Study. J Compos Constr 19:04014048. doi: 10.1061/(ASCE)CC.1943-5614.0000507

Koutas L, Triantafillou T, Bousias S (2014b) Analytical Modeling of Masonry-Infilled RC Frames Retrofitted with Textile-Reinforced Mortar. J Compos Constr 19:1–14. doi: 10.1061/(ASCE)CC.1943-5614.0000553.

Koutromanos I, Asce a M, Kyriakides M, et al (2013) Shake-Table Tests of a 3-Story Masonry-In fi lled RC Frame Retro fi tted with Composite Materials. J Struct Engineering 139:1340–1351. doi: 10.1061/(ASCE)ST.1943-541X.0000689.

Koutromanos I, Stavridis A, Shing PB, Willam K (2011) Numerical modeling of masonry-infilled RC frames subjected to seismic loads. Comput Struct 89:1026–1037. doi: 10.1016/j.compstruc.2011.01.006

Krenchel H (1975) Fibre spacing and specific fibre surface. In: RILEM Symposium 1975 on fibre reinforced eemen t and concrete. pp 69-79 and vol 2 pp 511-513

Krüger M, Ožbolt J, Hans-W. Reinhardt (2002) a Discrete Bond Model for 3D Analysis of Textile Rein-Forced and Prestressed Concrete Elements. Otto-Graf-Journal 13:111–128

Kueh A (2015) concrete-to-concrete bond A numerical and analytical study on optimization and efficiency of structural forms. Cem Concr Compos 56:1–14. doi:

10.1016/j.cemconcomp.2014.10.003
Kwan A, Xia J (1995) Shake-table tests of large-scale shear. Proc Twelfth Eur Conf Earthq Eng 110:66–77
Kyriakides MA (2011) Seismic Retrofit of Unreinforced Masonry Infills in Non-Ductile Reinforced Concrete Frames Using Engineered Cementitious Composites. STANFORD UNIVERSITY
Larrinaga P, Chastre C, Biscaia HC, San-José JT (2014) Experimental and numerical modeling of basalt textile reinforced mortar behavior under uniaxial tensile stress. Mater Des 55:66–74. doi: 10.1016/j.matdes.2013.09.050
Larrinaga P, Chastre C, San-José JT, Garmendia L (2013) Non-linear analytical model of composites based on basalt textile reinforced mortar under uniaxial tension. Compos Part B Eng 55:518–527. doi: 10.1016/j.compositesb.2013.06.043
Laurent Pasticier, Claudio Amadio and MF (2007) Measuring bias in structural response caused by ground motion scaling. Earthq Eng Struct Dyn 37:467–485. doi: 10.1002/eqe
Lee HS, Woo S (2002) Effect of masonry infills on seismic performance of a 3-storey R/C frame with non-seismic detailing. Earthq Eng Struct Dyn 31:353–378. doi: 10.1002/eqe.112
Lee J, Lopez MM (2014) An Experimental Study on Fracture Energy of Plain Concrete. Int J Concr Struct Mater 8:129–139. doi: 10.1007/s40069-014-0068-1
Li S, Shan S, Zhai C, Xie L (2016) Experimental and numerical study on progressive collapse process of RC frames with full-height infill walls. Eng Fail Anal 59:57–68. doi: 10.1016/j.engfailanal.2015.11.020
Li VC (1996) Tensile Behavior of Cement Based Composites With Random Distributed Fibers. 74–78
Li VC, Stang H, Krenchel H (1993) Micromechanics of crack bridging in fibre-reinforced concrete. Mater Struct 26:486–494. doi: 10.1007/BF02472808
Liauw and Kwan (1983) Nonlinear behaviour of non-integral infilled frames. Proc Inst Civ Eng 18:551–560
Liauw T, Kwan K (1984) Nonlinear behaviour of non-integral infilled frames. Compos Struct 18:551–560
Liauw T, Kwan K (1984) Plastic theory of infilled frames with finite interface shear strength. Proc Inst Civ Eng 75:707–723
Liauw TC (1972) An approximate method of analysis for infilled frames with or without opening. Build Sci 7:233–238. doi: 10.1016/0007-3628(72)90004-7
Liauw TC (1979) Tests on Multistory Infilled Frames Subject to Dynamic Lateral Loading. Proc Inst Civ Eng 76:551–564
Liauw TC, Kwan KH (1992) Experimental study of shear wall and infilled frame on shake-table.pdf. Earthq. Eng. Tenth world Conf. 2659–2663
Lin K, Totoev YZ, Liu HJ, Page AW (2014) Modeling of dry-stacked masonry panel con fi ned by reinforced concrete frame. Arch Civ Mech Eng 14:497–509. doi:

10.1016/j.acme.2013.12.006
Lingeshwaran N, Poluraju P (2019) Experimental analysis of seismic performance on bed joint reinforced solid brick masonry walls – A state of the art. Int J Recent Technol Eng 7:536–540
Löfgren I (2007) Calculation of crack width and crack spacing. Nord Mini-seminar "Fibre Reinf Concr 1:1–12
Lorenz E, Ortlepp R (2012) Bond Behavior of Textile Reinforcements - Development of a Pull-Out Test and Modeling of the Respective Bond versus Slip Relation. Hpfrcc 6 479–486. doi: 10.1007/978-94-007-2436-5_58
Lotfi, H. and Shing P (1994) Interface model applied to fracture of masonry structures. J Struct Eng 120:
Lotfi HR, Shing PB (1991) An appraisal of smeared crack models for masonry shear wall analysis. Comput Struct 41:413–425. doi: 10.1016/0045-7949(91)90134-8
Lourenco B, Rots G (1997) Multisurface interface model for anallysis of maosnry structures. ASCE J Struct Eng 123:660–668
Lourenço P, Rots J (1997a) A plane stress softening plasticity model for orthotropic materials. Int J Numer Anal Methods Eng 40:4033–4057
Lourenço P, Rots J (1997b) Multisurface Interface Model for Analysis of Masonry Structures. ASCE J Struct Eng 9:660–688
Lourenco PB (1996) Computational Strategies for Masonry Structures. Delft University of Technology.
Lourenço PB (1996) A user/programmer guide for the micro-modelling of masonry structures. TNO Build Constr Res - Comput Mech
Lourenço PB (1994) Analysis of masonry structures with interface elements tno Building and Construction Research
Lourenço PB (2002) Computations on historic masonry structures. Prog Struct Engng Mater 4:301–319. doi: 10.1002/pse.120
Lourenço PB, De Borst R, Rots JG (1997) A plane stress softening plasticity model for orthotropic materials. Int J Numer Methods Eng 40:4033–4057. doi: 10.1002/(SICI)1097-0207(19971115)40:21<4033::AID-NME248>3.0.CO;2-0
Lourenço PB, Jan.G R, Johan B (1998) Continuum model for masonry:parameter estimation and validation. J Struct Eng June:642–652
Lourenço PB, Pereira JM (2018) Recommendations for Advanced Modeling
Lourenço PB, Rots J, Blaauwendraad J (1995) Two approaches for the analysis of masonry structures. Heron 40:313–340
M. N. Fardis and T. B. Panagiotakos (1997) Seismic Design and Response of Bare and Masonry-Infilled Reinforced Concrete Buildings Part II: Infilled Structures. J Earthq Eng 1:475–503
M.Holmes (1961) Steel frames with brickwork and concrete infilling. Proc. Inst. Civ. Eng. 19:473–478
M.M. Scheen (2016) Experimental and numerical simulations of various unreinforced

masonry walls with openings under in-plane static cyclic loading conditions
M.N. Fardis TBP (1996) Hysteretic Damping of Reinforced Concrete Elements. 11th World Conf. Earthq. Eng.
Madan et al. (1997) Modelling of masonry inifll panels for structural analysis. ASCE J Struct Eng 1:
Martin J, Darwin D, Terry RE (1991) Cement Paste, Mortar and Concrete Under Monotonic, Sustained and Cyclic Loading. university of kansas
Maekawa K, Fukuura N (2014) Nonlinear Modeling of 3D Structural Reinforced Concrete and Seismic Performance Assessment. Infrastruct Syst Nucl Energy 153–184
Maekawa K, Okamura H, Junichi izumo (2016) Reinforced concrete plate element subjected to cyclic loading. ASCE J Compos Constr 575–590
Maekawa K, Takemura J, Irawan P, Irie M (1993a) Plasticity in concrete nonlinearity under triaxial confinement. Proc. of JSCE 18, 460 (February 1993), 123–130. In: Proc. of JSCE 18, 460 (February). pp 123–130
Maekawa K, Takemura J, Irawan P, Irie M (1993b) Continuum fracture in concrete nonlinearity under triaxial confinement. Proc. of JSCE 18, 460 (February 1993), 113–122. In: Proc. of JSCE 18, 460. pp 113–122
Magenes G, Calvi GM (1997) In-plane seismic response of brick masonry walls. Earthq Eng Struct Dyn 26:1091–1112. doi: 10.1002/(SICI)1096-9845(199711)26:11<1091::AID-EQE693>3.0.CO;2-6
Mainstone, R.J., Weeks G. (1970) The influence of Bounding Frame on the Racking Stiffness and Strength of Brick Walls. Proc 2nd Int Brick Mason Conf 165–171
Mainstone, R.J. (1971) On the stiffness and strengths of infilled frames. In: ICE Proceedings. p 230
Mainstone RJ (1974) Supplementary note on the stiffness and strength of infilled frames. Build Res
Mallick, D. V., and Garg RP (1971) Effect of openings on the lateral stiffness of infilled frames. Proc Inst Civ Eng 49:
Mallick, D.V and Severn R. (1967) The behaviour of infilled frames under static loading. Proc Inst Civ Eng 38:639–656
Mallick DV GR (1971) Effect of openings on the lateral stiffness of infilled frames. Civ Eng 49:193–201
Manos G, Thaumpta J, Yasin B (2000) Influence of Masonry Infills on the Earthquake Response of Multi-story Reinforced Concrete Structures. Impulse (Sydney) 1–8
Marcari G, Manfredi G, Prota A, Pecce M (2007) In-plane shear performance of masonry panels strengthened with FRP. Compos Part B Eng 38:887–901. doi: 10.1016/j.compositesb.2006.11.004
Martínez J (1991) Quasi-Newton methods for solving underdetermined nonlinear simultaneous equations. J Comput Appl Math 34:171–190. doi: 10.1016/0377-0427(91)90040-Q

Martínez JM (2000) Practical quasi-Newton methods for solving nonlinear systems. J Comput Appl Math 124:97–121. doi: 10.1016/S0377-0427(00)00434-9

Matsumiya.T,Nakashima.M, Suita.K D. (2004) Scale Test of Three-Story Steel Moment Frames for Examination of Extremely Large Deformation and. 13th World Conf Earthq Eng

Mechtcherine V (2013) Novel cement-based composites for the strengthening and repair of concrete structures. Constr Build Mater 41:365–373. doi: 10.1016/j.conbuildmat.2012.11.117

Mehrabi,Armin, Shing P (1997) Finite Element Modeling of Masonry-Infilled RC Frames. J Struct Eng 123:604–613

Mehrabi A, Shing PB, Schuller M, Noland J (1994) Performance of masonry-infilled R/C frames under in-plane lateral loads

Menegotto M, Pinto PE (1973) Method of Analysis for Cyclically Loaded Reinforced Concrete Plane Frames Including Changes in Geometry and Nonelastic Behavior of Elements Under Combined Normal Force and bending. In: In Proc. IABSE Symposium on Resistance and ultimate Deformability of Structures

Merhabi A, Shing B, Sculler P, Noland J (1996) Experimental evaluation of masonry-infilled RC frame. ASCE 122:228–237

Messali F, Ravenshorst G, Esposito R, Rots JG (2017) Large-scale testing program for the seismic characterization of Dutch masonry walls. 16th World Conf Earthq Paper N° 4753

Mesticou Z, Bui L, Junes A, Larbi AS (2017) Experimental investigation of tensile fatigue behaviour of Textile- Reinforced Concrete (TRC): Effect of fatigue load and strain rate. Compos Struct 160:1136–1146. doi: 10.1016/j.compstruct.2016.11.009

Mininno G, Ghiassi B, Oliveira D V. (2017) Modelling of the in-plane and out-of-plane performance of TRM-strengthened masonry walls. Key Eng Mater 747 KEM:60–68. doi: 10.4028/www.scientific.net/KEM.747.60

Mobasher B (2005) Distributed cracking and stiffness degradation in fabric-cement composites. Mater Struct 0–0. doi: 10.1617/14163

Mobasher B (2011) Mechanics of Fiber and Textile Reinforced Cement Composites

Mobasher B, Pahilajani J, Peled A (2006) Analytical simulation of tensile response of fabric reinforced cement based composites. Cem Concr Compos 28:77–89. doi: 10.1016/j.cemconcomp.2005.06.007

Mobasher B, Peled A, Pahilajani J (2004) Pultrusion of fabric reinforced high flyash blended cement composites. RILEM Tech Meet BEFIB 1473–1482

Mohammad Noh N, Liberatore L, Mollaioli F, Tesfamariam S (2017) Modelling of masonry infilled RC frames subjected to cyclic loads: State of the art review and modelling with OpenSees. Eng Struct 150:599–621. doi: 10.1016/j.engstruct.2017.07.002

Mohammadi M, Nikfar F (2013) Strength and stiffness of masonry-infilled frames with

central openings based on experimental results. J Struct Eng (United States) 139:974–984. doi: 10.1061/(ASCE)ST.1943-541X.0000717

Mohan A, Jacob B (2016) Strength and Ductility in unreinforced masonry walls with two openings retrofitted by Carbon Fiber Reinforced Polymers. 346–352

Mojsilovic N (2013) Modelling of the behaviour of seismically strengthened masonry walls subjected to cyclic in-plane shear. Eng Struct 56:1117–1129. doi: 10.1016/j.engstruct.2013.06.033

Mojsilović N (2011) Strength of masonry subjected to in-plane loading: A contribution. Int J Solids Struct 48:865–873. doi: 10.1016/j.ijsolstr.2010.11.019

Moller M (2001) Load bearing capacity and servisability of textile reinforced beams. In: First colloqiuium on special research Areas, Aachen University. pp 435–446

Molter M (2005) Zum Tragverhalten von textilbewehrtem Beton

Mondal G, Jain SK (2008) Lateral stiffness of masonry infilled reinforced concrete (RC) frames with central opening. Earthq Spectra 24:701–723. doi: 10.1193/1.2942376

Monti B, Nuti C (1993) Nonlinear cyclic behavior of reinforcing bars including buckling. Struct Eng 118:3268–3284

Morandi P, Hak S, Magenes G (2018) Performance-based interpretation of in-plane cyclic tests on RC frames with strong masonry infills. Eng Struct 156:503–521. doi: 10.1016/j.engstruct.2017.11.058

Moroni M, Astroza M, Mesias P (1996) Displacement Capacity and Required Story Drift in Confined Masonry Buildings. 11th World Conf. Earthq. Eng. 7

Mosalam K, Glascoe L, Bernier J (2009) Mechanical Properties of Unreinforced Brick Masonry ,

Mosalam KM (1997) Static Response of Infilled Frames Using Quasi-Static Experimentatio. J Struct Eng 123:1462–1469. doi: 10.1061/(ASCE)0733-9445(1997)123

Mosalam KM, White RN, Gergely P (1997b) Seismic Evaluation of Frames with Infill Walls Using Pseudo-dynamic Experiments

Mosalam KM, White RN, Gergely P (1997c) Computational Strategies for Frames with Infill Walls : Discrete and Smeared Crack Analyses and Seismic Fragility by

Motamedi M, Kakolvand H, Yekrangnia M (2012) Evaluation of A Retrofit Solution Used for Concrete Masonry Walls with Large Openings Using FEM Nonlinear Analysis. 15 Wcee

Murthy A, Palani G, Iyer N (2009) State-of-the-art review on fracture analysis of concrete structural components. Sadhana 34:345–367

Murty CVR, Jain SK (2000) Beneficial Influence of Masonry Infill Walls on Seismic Performance of Rc Frame Buildings. Twelfth World Conf Earthq Eng 1–6

N.Klingner BB (1978) Earthquake Resistance of Infilled Frames. J Struct Div ASCE 104:973–989

Nayak S, Dutta SC (2015) Improving Seismic Performance of Masonry Structures with

Openings by Polypropylene Bands and L-Shaped Reinforcing Bars. J Perform Constr Facil 30:04015003. doi: 10.1061/(asce)cf.1943-5509.0000733

Nazief MA (2014) Finite Element Characterization of the Behaviour of Masonry Infill Shear Walls With and Without Openings

Negro P, Verzeletti G (1996) Effect of infills on the global behaviour of R/C frames: Energy considerations from pseudodynamic tests. Earthq Eng Struct Dyn 25:753–773. doi: 10.1002/(SICI)1096-9845(199608)25:8<753::AID-EQE578>3.0.CO;2-Q

Nicola T, Leandro C, Guido C, Enrico S (2015) Masonry infilled frame structures : state - of - the - art review of numerical modelling. Earthquakes Struct 3:733–759. doi: http://dx.doi.org/10.12989/eas.2015.8.1.225

Nila ND, Sivan PP, Ramya KM (2018) Study on Effect of Openings in Seismic Behavior of Masonry Structures. Int Assoc Earthq Eng 5:4712–4717

Nwofor TC (2002) Shear Resistance of Reinforced Concrete infilled Frames. Int J Appl Sci Technol 2:148–163

Ohno J, Hannat D (1994) Modeling the stress-strain response of continuous fiber reinforced cement composites. J Mater Sci 31:306–312

Oinam RM, Sahoo DR, Sindhu R (2014) Cyclic response of Non-ductile rc frame with steel fibers at Beam-Column joints and plastic hinge regions. J Earthq Eng 18:908–928. doi: 10.1080/13632469.2014.916239

Oliveira D V., Lourenço PB (2004) Implementation and validation of a constitutive model for the cyclic behaviour of interface elements. Comput Struct 82:1451–1461. doi: 10.1016/j.compstruc.2004.03.041

Ombres L (2011) Flexural analysis of reinforced concrete beams strengthened with a cement based high strength composite material. Compos Struct 94:143–155. doi: 10.1016/j.compstruct.2011.07.008

Ombres L (2014) Concrete confinement with a cement based high strength composite material. Compos Struct 109:294–304. doi: 10.1016/j.compstruct.2013.10.037

Ortlepp R (2007) Development Length for Textile Reinforced Concrete Determination of development lengths of textile reinforcement in fine concrete

Ortlepp R (2011) Textilbetonverstärkte Stahlbetonstützen. 106:640–648. doi: 10.1002/best.201100017

Ortlepp R, Lorenz A, Curbach M (2009) Column strengthening with TRC: Influences of the column geometry onto the confinement effect. Adv Mater Sci Eng 2009:1–6. doi: 10.1155/2009/493097

Palieraki V, Zeris C, Vintzileou E, Adami CE (2018) In-plane and out-of plane response of currently constructed masonry infills. Eng Struct 177:103–116. doi: 10.1016/j.engstruct.2018.09.047

Panagiotakos M, Fardis MN (1996) Seismic Response of Infilled RC Frame Structures. 11th World Conf. Earthq. Eng. 225

Papa E (1996) Unilateral damage model for masonry based on a homogenisation procedure. Mech Cohesive-Frictional Mater 1:349–366. doi: 10.1002/(sici)1099-

1484(199610)1:4<349::aid-cfm18>3.3.co;2-d

Papanicolaou C, Triantafillou T, Papantoniou I, Balioukos C (2009) Strengthening of two-way reinforced concrete slabs with Textile Reinforced Mortars (TRM). In: 4th Colloquium on Textile Reinforced Structures (CTRS4). pp 409–420

Papanicolaou C, Triantafillou TC, Lekka M (2011) Externally bonded grids as strengthening and seismic retrofitting materials of masonry panels. Constr Build Mater 25:504–514. doi: 10.1016/j.conbuildmat.2010.07.018

Papanicolaou CG, Triantafillou TC, Papathanasiou M, Karlos K (2007) Textile reinforced mortar (TRM) versus FRP as strengthening material of URM walls: out-of-plane cyclic loading. Mater Struct 41:143–157. doi: 10.1617/s11527-007-9226-0

Papanicolaou CG, Triantafillou TC, Papathanasiou M, Karlos K (2006) Textile reinforced mortar (TRM) versus FRP as strengthening material of URM walls: in-plane cyclic loading. Mater Struct 41:143–157. doi: 10.1617/s11527-007-9226-0

Papia M, Cavaleri L, Fossetti M (2003) Infilled frames : developments in the evaluation of the stiffening effect of infills. 16:675–693

Parisi F, Iovinella I, Balsamo A, et al (2013) In-plane behaviour of tuff masonry strengthened with inorganic matrix-grid composites. Compos Part B Eng 45:1657–1666. doi: 10.1016/j.compositesb.2012.09.068

Parisi F, Lignola GP, Augenti N, et al (2011) Nonlinear Behavior of a Masonry Subassemblage Before and After Strengthening with Inorganic Matrix-Grid Composites. J Compos Constr 15:821–832. doi: 10.1061/(asce)cc.1943-5614.0000203

Paulay, T and Priestley MJ. (1992) Seismic design of reinforced concrete and masonry buildings

Peled a., Bentur a. (2003) Fabric structure and its reinforcing efficiency in textile reinforced cement composites. Compos Part A Appl Sci Manuf 34:107–118. doi: 10.1016/S1359-835X(03)00003-4

Peled A (2007) Confinement of damaged and nondamaged structural concrete with FRP and TRC sleeves. J Compos Constr 11:514–522. doi: Doi 10.1061/(Asce)1090-0268(2007)11:5(514)

Peled A, Bentur D, Yankelevsky D (1999) Flexural p erformance of c ementitious c omposites. J Mater Civ Eng 325–330

Peled A, Cohen Z, Pasder Y, et al (2008a) Influences of textile characteristics on the tensile properties of warp knitted cement based composites. Cem Concr Compos 30:174–183. doi: 10.1016/j.cemconcomp.2007.09.001

Peled A, Sueki S, Mobasher B (2006) Bonding in fabric– cement systems : Effects of fabrication methods. 36:1661–1671. doi: 10.1016/j.cemconres.2006.05.009

Peled A, Zaguri E, Marom G (2008b) Bonding characteristics of multifilament polymer yarns and cement matrices. Compos Part A Appl Sci Manuf 39:930–939. doi: 10.1016/j.compositesa.2008.03.012

Peng Q, Zhou X, Yang C (2018) Influence of connection and constructional details on masonry-infilled RC frames under cyclic loading. Soil Dyn Earthq Eng 108:96–110. doi: 10.1016/j.soildyn.2018.02.009

Pereira-de-Oliveira L a., Castro-Gomes JP, Nepomuceno MCS (2012) Effect of acrylic fibres geometry on physical, mechanical and durability properties of cement mortars. Constr Build Mater 27:189–196. doi: 10.1016/j.conbuildmat.2011.07.061

Pereira MV, Fujiyama R, Darwish F, et al (2015) On the Strengthening of Cement Mortar by Natural Fibers. Mater Res 18:177–183

Perera ricardo (2005) Performance evaluation ofmasonry-infilled RC frames under cyclic loading based on damage mechanics. Eng Struct 27:1278–1288

Petracca M, Pelà L, Rossi R, et al (2017) Micro-scale continuous and discrete numerical models for nonlinear analysis of masonry shear walls. Constr Build Mater 149:296–314. doi: 10.1016/j.conbuildmat.2017.05.130

Pinto A, Varum H, Molina J (2002) Experimental Assessment and Retrofit of Full-Scale Models of Existing RC Frames. In: Proceedings of the Twelfth European Conference on Earthquake Engineering. pp 855–865

Planas J, Elices M, G J (2002) The cohesive zone model: advantages, limitations and challenges. Eng Fract Mech 69:137–163. doi: 10.1016/S0013-7944(01)00083-2

Pohoryles DA, Bournas DA (2020) Seismic retrofit of infilled RC frames with textile reinforced mortars: State-of-the-art review and analytical modelling. Compos Part B Eng 183:107702. doi: 10.1016/j.compositesb.2019.107702

Pohoryles DA, Bournas DA (2020) A unified macro-modelling approach for masonry-infilled RC frames strengthened with composite materials. Eng Struct 223:111161. doi: 10.1016/j.engstruct.2020.111161

Polyakov S (1956) Masonry in framed buildings (An investigation into the strength and stiffness of masonry infill). National, Moscow

Polyakov S (1960) On the interaction between masonry filler walls and enclosing frame when loaded in the plane of the wall. Earthq Eng Res Inst 36–42

Portal NW (2013) Sustainability and Flexural Behaviour of Textile Reinforced Concrete

Pradhan P, Pradhan P, Maskey R (2012) A Review On Partial Infilled Frames Under Lateral Loads. J Sci Eng Technol 8:142–152. doi: 10.3126/kuset.v8i1.6054

Prasad R, Maekawa K (2002) Path-dependent cyclic stress – strain relationship of reinforcing bar including buckling. Eng Fract Mech 24:1383–1396

Proença JM, Gago AS, Vilas Boas A (2019) Structural window frame for in-plane seismic strengthening of masonry wall buildings. Int J Archit Herit 13:98–113. doi: 10.1080/15583058.2018.1497234

Prota a., Marcari G, Fabbrocino G, et al (2006) Experimental In-Plane Behavior of Tuff Masonry Strengthened with Cementitious Matrix–Grid Composites. J Compos Constr 10:223–233. doi: 10.1061/(ASCE)1090-0268(2006)10:3(223)

Pryce A, Smith P (1992) Behaviour of unidirectional and crossply ceramic matrix composites under quasi-static tensile loading. J Mater Sci 27:2695–2704. doi:

10.1007/BF00540692
Pryce AW (1993) MATRIX CRACKING IN UNIDIRECTIONAL CERAMIC MATRIX COMPOSITES U N D E R QUASI-STATIC A N D CYCLIC LOADING. Acta Metall Mater 41:1269–1281
Pujol S, Fick D (2010) για να ξέρει . Επιβάλλει αναυκλιζομεμη φόρτιση στο κτήριο με τοίχους Contents των The test of a full-scale three-story RC structure with masonry infill walls. Eng Struct 32:3112–3121. doi: 10.1016/j.engstruct.2010.05.030
Ramachandra Murthy a., Karihaloo BL, Iyer NR, Raghu Prasad BK (2013) Bilinear tension softening diagrams of concrete mixes corresponding to their size-independent specific fracture energy. Constr Build Mater 47:1160–1166. doi: 10.1016/j.conbuildmat.2013.06.004
Rambo DAS, de Andrade Silva F, Toledo Filho RD, da Fonseca Martins Gomes O (2015) Effect of elevated temperatures on the mechanical behavior of basalt textile reinforced refractory concrete. Mater Des 65:24–33. doi: 10.1016/j.matdes.2014.08.060
Rampini MC, Zani G, Colombo M, di Prisco M (2019) Mechanical Behaviour of TRC Composites: Experimental and Analytical Approaches. Appl Sci 9:1492. doi: 10.3390/app9071492
Raoof SM, Koutas LN, Bournas DA (2016) Bond between textile-reinforced mortar (TRM) and concrete substrates : Experimental investigation. 98:350–361. doi: 10.1016/j.compositesb.2016.05.041
Rashid Y. (1968) Ultimate Srength Analysis of Pre-stressed Concrete Pressure Vessels. Nucl Eng Des 7:334–344
Rathi R, Pajgade P (2002) Study of Masonary Infilled RC Frame With & Without Opening. Int J Sci Eng Res 3:1–7
RE Klingner VB (1978) Earthquake resistance of infilled frames
Ricci P, Di Domenico M, Verderame GM (2018) Experimental assessment of the in-plane/out-of-plane interaction in unreinforced masonry infill walls. Eng Struct 173:960–978. doi: 10.1016/j.engstruct.2018.07.033
Richter M, Zastrau BW (2006) On the nonlinear elastic properties of textile reinforced concrete under tensile loading including damage and cracking. Mater Sci Eng A 422:278–284. doi: 10.1016/j.msea.2006.02.007
Roca P, Cervera M, Gariup G, Pela' L (2010) Structural analysis of masonry historical constructions. Classical and advanced approaches. Arch Comput Methods Eng 17:299–325. doi: 10.1007/s11831-010-9046-1
Rodrigues H, Varum H, Costa A (2010) Simplified macro-model for infill masonry panels. J Earthq Eng 14:390–416. doi: 10.1080/13632460903086044
Romão X, Costa AA, Paupério E, et al (2013) Field observations and interpretation of the structural performance of constructions after the 11 May 2011 Lorca earthquake. Eng Fail Anal 34:670–692. doi: 10.1016/j.engfailanal.2013.01.040
Rots G (2017) DIANA Validation report for Masonry modelling. netherlands

Rots JANG (1991) Smeared and discrete representations of localized fracture. Int J Fract 51:45–59

S.Surendran BK (2012) Masonry Infill RC Frames with Openings: Review of In-plane Lateral Load Behaviour and Modeling Approaches. Open Constr Build Technol J 6:126–154. doi: 10.2174/1874836801206010126

Sachanski S (1960) Analysis of the earthquake resistance of frame buildings taking into consideration the carrying capacity of the filling masonry. In: second wrold conference on earthquake engineering Tokyo. pp 2127–2141

Sagar S, Singhal V, Durgesh C, Rai M (2019) In-Plane and Out-of-Plane Behavior of Masonry-Infilled RC Frames Strengthened with Fabric-Reinforced Cementitious Matrix. ASCE J Struct Eng 23:

Sanaz R, Armen DK (2012) A stochastic ground motion model with separable temporal and spectral nonstationarities. Earthq Eng Struct Dyn 41:1549–1568. doi: 10.1002/eqe

Sandoval C, Arnau O (2017) Experimental characterization and detailed micro-modeling of multi-perforated clay brick masonry structural response. Mater Struct. doi: 10.1617/s11527-016-0888-3

Saneinejad BA, Hobbs B (1995) Inleastic design of iniflled frame. ASCE J Struct Eng 121:634–650

Saouma V., Ingraffea AR (1981) Fracture Mechanics Analysis of Discrete Cracking. In: Proc. IABSE Coll. in Advanced Mechanics of Reinforced Concrete,Delft. pp 393–416

Sarhosis, Vasilis, Bagi, Katalin, Lemos, José V., Milani G (2016) Computational Modeling of Masonry Structures Using the Discrete Element Method. Advances in Civil and Industrial Engineering

Sarhosis V, Garrity SW, Sheng Y (2015) Influence of brick-mortar interface on the mechanical behaviour of low bond strength masonry brickwork lintels. Eng Struct 88:1–11. doi: 10.1016/j.engstruct.2014.12.014

Sarhosis V, Lemos J V. (2018) A detailed micro-modelling approach for the structural analysis of masonry assemblages. Comput Struct 206:66–81. doi: 10.1016/j.compstruc.2018.06.003

Sarhosis V, Lemos J V, Milani G (2016) Computational Modeling of Masonry Structures Using the Discrete Element Method

Sattar S, Liel AB (2016) Seismic performance of nonductile reinforced concrete frames with masonry infill walls - I: Development of a strut model enhanced by finite element models. Earthq Spectra 32:795–818. doi: 10.1193/90914EQS139M

Shadlou M, Kashani MM (2019) A review on the current trends on computational modelling of masonry-infilled reinforced concrete frames. J Phys Conf Ser 1264:. doi: 10.1088/1742-6596/1264/1/012044

Shah SP (1990) Experimental methods for determining fracture process zone and fracture parameters. Eng Fract Mech 35:3–14. doi: 10.1016/0013-7944(90)90178-J

Shams A, Hegger J, Horstmann M (2014) An analytical model for sandwich panels made of textile-reinforced concrete. Constr Build Mater 64:451–459. doi: 10.1016/j.conbuildmat.2014.04.025

Shing PB, Mehrabi AB (2002) Behaviour and analysis of masonry-infilled frames. Prog Struct Eng Mater 4:320–331. doi: 10.1002/pse.122

Siamak S (2013a) Influence of masonry infill walls and other building charactristics on seismic collapse of concrete frame building

Siamak S (2013b) Influence of masonry infill walls and other building charactristics on seismic collapse of concrete frame building. PhD Propos 1:. doi: 10.1017/CBO9781107415324.004

Siamak Sattar and Abbie B. Liel (2010) Seimic performance of reinforced concrete frames with and without masonry infill walls

Silva F de A, Mobasher B, Filho RDT (2009) Cracking mechanisms in durable sisal fiber reinforced cement composites. Cem Concr Compos 31:721–730. doi: 10.1016/j.cemconcomp.2009.07.004

Silva FDA, Butler M, Mechtcherine V, et al (2011) Strain rate effect on the tensile behaviour of textile-reinforced concrete under static and dynamic loading. Mater Sci Eng A 528:1727–1734. doi: 10.1016/j.msea.2010.11.014

Singh H (1998) Inelastic dynamic response of reinforced concrete infilled frames. Comput Concr 69:685–693

Sonpal A, Kumar M, Sarma H (2019) Effect of gap between column and masonry infill on the response of masonry-infilled reinforced concrete frames. 623–635

Soranakom C, Mobasher B (2009) Flexural Analysis and Design of Textile Reinforced Concrete. 4th Colloq Text Reinf Struct 273–288

Soranakom C, Mobasher B (2010) Modeling of tension stiffening in reinforced cement composites: Part I. Theoretical modeling. Mater Struct 43:1217–1230. doi: 10.1617/s11527-010-9594-8

Stafford-Smith B (1967) Methods for predicting the lateral stiffness and strength of multi-storey infilled frames. Build Sci 2:247–257. doi: 10.1016/0007-3628(67)90027-8

Stafford-Smith B (1966) Behavior of square infilled frames. J Struct Div ASCE 92:381–403

Stafford-Smith B (1962) Lateral stiffness of infilled frames. J Struct Div ASCE 5:183–199

Stafford SB (1962) Lateral Stiffness of Infilled Frames. J Struct Div ASCE 88:183–226

Stavridis A (2009) Analytical and Experimental Study of Seismic Performance of Reinforced Concrete Frames Infilled with Masonry Walls

Stylianidis K (2012) Experimental Investigation of Masonry Infilled R/C Frames. Open Constr Build Technol J 6:194–212. doi: 10.1201/b21889-152

Su Q, Cai G, Cai H (2017) Seismic behaviour of full-scale hollow bricks-infilled RC frames under cyclic loads. Bull Earthq Eng 15:2981–3012. doi: 10.1007/s10518-

016-0074-6
Surendran S (2012) Masonry Infill RC Frames with Openings: Review of In-plane Lateral Load Behaviour and Modeling Approaches. Open Constr Build Technol J 6:126–154. doi: 10.2174/1874836801206010126
Suzuki T, Choi H, Sanada Y, et al (2017) Experimental evaluation of the in-plane behaviour of masonry wall infilled RC frames. Bull Earthq Eng 15:4245–4267. doi: 10.1007/s10518-017-0139-1
SV Polyakov (1960) On the interaction between masonry filler walls and enclosing frame when loaded in the plane of the wall. Transl Earthq Eng EERI, Oakl 3:36–42
Syed Humayun Basha; Sachin Surendran; and Hemant B. Kaushik (2020) Empirical Models for Lateral Stiffness and Strength of Masonry-Infilled RC Frames Considering the Influence of Openings. ASCE J Struct Eng 146:
Syrmakezis C, Asteris P (2001) Influence of infilled walls with openings to the seismic response of plane frames. In: Proc. 9th Can. Masonry Symp
Tasnimi AA, Mohebkhah A (2011) Investigation on the behavior of brick-infilled steel frames with openings, experimental and analytical approaches. Eng Struct 33:968–980. doi: 10.1016/j.engstruct.2010.12.018
Taylor R, Zhu J (2000) Method : Its Basis and Fundamentals UNESCO Professor of Numerical Methods in Engineering
Teguh M (2017) Experimental Evaluation of Masonry Infill Walls of RC Frame Buildings Subjected to Cyclic Loads. Procedia Eng 171:191–200. doi: 10.1016/j.proeng.2017.01.326
Tekeli H, Aydin A (2017) An experimental study of the seismic behavior of Infilled RC frames with opening. Sci Iran 24:2271–2282. doi: 10.24200/sci.2017.4150
Tetta ZC, Triantafillou TC, Bournas DA (2018) On the design of shear-strengthened RC members through the use of textile reinforced mortar overlays. Compos Part B Eng 147:178–196. doi: 10.1016/j.compositesb.2018.04.008
Thomas FG (1953) The strength of brickwork. Struct Eng 36:35–41
Tomaževič M (2009) Shear resistance of masonry walls and Eurocode 6: Shear versus tensile strength of masonry. Mater Struct Constr 42:889–907. doi: 10.1617/s11527-008-9430-6
Trapani F Di, Macaluso G, Cavaleri L, et al (2016) Masonry infills and RC frames interaction : literature overview and state of the art of macromodeling approach. J Civ Eng 8189:. doi: 10.1080/19648189.2014.996671
Triantafillou T (2011) Innovative textile-based composites for strengthening and seismic retrofitting of concrete and masonry structures. Adv FRP Compos Civ Eng
Triller P, Tomaževič M, Gams M (2016) Seismic behaviour of multistorey plain masonry shear walls with openings: An experimental study. Brick Block Mason 1949–1954. doi: 10.1201/b21889-256
Triller P, Tomaževič M, Lutman M, Gams M (2017) Seismic Behavior of Strengthened URM Masonry - An Overview of Research at ZAG. Procedia Eng 193:66–73. doi:

10.1016/j.proeng.2017.06.187
Tzmatzis A, Asteris P (2003) Finite element analysis of masonry structures: Part I-Review of previous work. 9th North Am Mason Conf 101–111
Utku B (1980) Stress magification in walls with opoenigs. In: 7th World Conf. on Earthquake Engineering. Istanbul, Turkey, p Vol. 4 pages 217–224
V. Thiruvengadam (1985) On the natural frequencies of infilled frames. Earthq Struct 13:401–419
Valiasis T, Stylianidis K (1989) Masonry infilled RC frames undr horizontal loading . experimental results. Earthq Struct 3:10–20
Van der Pluijm R (1997) Non-linear behavior of masonry under tension. Heron 42:24–54
Vasconcelos G, Lourenço PB, Oliveira D (2008) Experimental shear behavior of stone masonry joints. Struct Eng 1:771–779
Vecchio FJ, Collins MP (1986) The modified compression field theory for reinforced concrete elements subjected to shear. ACI Mater J 83:219–231
Voon,k and Ingham M (2008) Experimental in-plane strength investigation of reinforced concrete masonry walls with openings. ASCE J Struct Eng 1:1–7. doi: 10.1061/(ASCE)0733-9445(2008)134
Wang X, Ghiassi B, Oliveira D V., Lam CC (2017) Modelling the nonlinear behaviour of masonry walls strengthened with textile reinforced mortars. Eng Struct 134:11–24. doi: 10.1016/j.engstruct.2016.12.029
Weibull W (1952) A Statistical Distribution Function of Wide Applicability. 293–297
Weissmann GF, Wonsiewicz BC (2018) Characterization of the Mechanical Properties of Spring Materials. In: 11th National Congress on Experimental Mechanics. pp 797–802
Wiberg A (2003) Strengthening of Concrete Beams Using Cementitious Carbon Fibre Composites
Williams N, Lundgren K, Walter M, et al (2013) Numerical modelling of textile reinforced concrete. In: VIII International Conference on Fracture Mechanics of Concrete and Concrete Structures
Wood R. (1958) The stability of tall buildings. Proc Inst Civ Eng 11:69–102
Xu S, Krüger M, Reinhardt H-W, Ožbolt J (2004) Bond Characteristics of Carbon, Alkali Resistant Glass, and Aramid Textiles in Mortar. J Mater Civ Eng 16:356–364. doi: 10.1061/(ASCE)0899-1561(2004)16:4(356)
Yao Y, Bonakdar A, Faber J, et al (2016) Distributed cracking mechanisms in textile-reinforced concrete under high speed tensile tests. Mater Struct 49:2781–2798. doi: 10.1617/s11527-015-0685-4
Yong TC (1984) Shear strength of masonry panels in steel frames. New Brunswick Canada
Zarnic R, Tomazevic M (1988) An experimentally obtained mehtod for evaluation of the behavior of masonry infilled R/C frames. In: Ninth world conference of

eartquake engineering. Tokyo,Japan
Zok FW, Barbara S (1992) Matrix crack spacing in brittle matrix composites. 40:2033–2043
Zuccaro G, Dato F, Cacace F, et al (2017) Seismic collapse mechanisms analyses and masonry structures typologies: A possible correlation. Ing Sismica 34:121–149
Zucchini A, Lourenço PB (2007) Mechanics of masonry in compression: Results from a homogenisation approach. Comput Struct 85:193–204. doi: 10.1016/j.compstruc.2006.08.054

APPENDIX I

Example of the Analytical Model for Textile Reinforced Mortar under Monotonic Loading

A detailed example is presented to clarify the process, step by step, of the proposed model of TRM for convenience and better understanding. The required data in order to implement the proposed model for a specific experimental case-study (Case 1) are given below (Table A1). The data refer to Larrinaga et al. (2013) as also presented in detail in the main text (Chapter 3, section 3.4, Table 3.3).

Table A1. Data given in experimental study conducted by Larrinaga et al. (2013).

Case study	$\mathbf{E_f}$ **(GPa)**	$\mathbf{e_{fu}}$ **(%)**	$\mathbf{V_f}$ **(%)**	$\mathbf{A_{yarn}}$ **(mm²)**	$\mathbf{E_m}$ **(GPa)**	$\boldsymbol{\sigma_{mu}}$ **(MPa)**	$\mathbf{V_m}$ **(%)**	$\boldsymbol{\rho_m}$ **(Kg/m³)**
Case 1 (Larrinaga et al. 2013)	67	1.82	0.70	0.89	8.25	2.8	99.3	1950

First, the linear-elastic strain at State I (e_{mu}) is calculated according to the proposed model as follows (see Eq.3.17 in the main text section 3.3.3):

$$e_{mu} = \left(\frac{1.41\ 10^{-4}\ n_1\ {\sigma_{mu}}^2\ E_f\ {V_f}^2}{E_c\ r_{yarn}\ {E_m}^2}\right)^{\frac{1}{3}} \tag{A1}$$

where the values of $\sigma_{mu}, E_f, E_m, V_f$ are given above (Table A1), and r_{yarn}, n_1, and E_c are calculated as follows :

$$r_{yarn} = \sqrt{\frac{A_{yarn}}{\pi}} = \sqrt{\frac{0.89}{\pi}} = 0.53\text{mm} = 5.39\ 10^{-4}\text{m} \tag{A2}$$

$$n_1 = \left(0.4 + 0.6\ \frac{\rho_m}{2200}\right) = \left(0.4 + 0.6\ \frac{1950}{2200}\right) = 0.89 \tag{A3}$$

$$E_c = E_f\ V_f + E_m\ V_m = 67000\ 0.7\% + 99.3\%\ 8250 = 8661.25\ (\text{MPa}) \tag{A4}$$

By substituting the above to Eq. (A1), the linear-elastic strain of the composite (e_{mu}) is equal to : $e_{mu}\left(\frac{1.41\ 10^{-4}\ 0.89\ 2.8^2\ 67000\ 0.7\%^2}{8661.25\ 5.39\ 10^{-4}\ 8250^2}\right)^{\frac{1}{3}}$=0.026%

Then, the equivalent composite multi-cracking stress (σ_{mc}) at the corresponding strain capacity estimated above (e_{mu}) is directly given (Eq.3.4) as:

$$\sigma_{mc} = E_c \; e_{mu} = 8661.25 \; 0.026\% = 2.25 \text{MPa} \quad \text{(A5)}$$

The composite strain when the multi-cracking is completed at State II (e_{mc}), is calculated by Eq. (3.5) as presented in Chapter 3 as follows:

$$e_{mc} = \left(1 + 0.667 \frac{E_m \; V_m}{E_f \; V_f}\right) = \left(1 + 0.667 \frac{8250 \; 99.3\%}{67000 \; 0.7\%}\right) 0.026\% = 0.34\% \quad \text{(A6)}$$

Finally, the composite strain at the end of State III (e_{fc}) is determined by Eq. (3.6) as given in Chapter 3 (section 3.2.3.3), using the value of e_{fu} given above (Table A1), as follows:

$$e_{fc} = \left(e_{fu} - 0.341 \frac{E_m \; V_m}{E_f \; V_f} e_{mu}\right) = \left(1.82 - 0.341 \frac{8250 \; 99.3\%}{67000 \; 0.7\%} \; 0.026\%\right) = 1.65\% \quad \text{(A7)}$$

The equivalent composite stress at State III (σ_{fc}) corresponding to the above strain capacity (e_{fc}) is directly provided by Eq.(3.18) in Chapter 3 (section 3.3.3):

$$\sigma_{fc} = Ec.\,III \; e_{fc} \quad \text{(A8)}$$

where, $Ec.\,III$ of the composite at State III is calculated as follows (Eq. (3.7) :

$$Ec.\,III = E_f \; V_f = 67000 \; 0.7\% = 469 \text{ MPa} \quad \text{(A9)}$$

By substituting the $Ec.\,III$ to Eq. (A8), the stress of the TRM at State III (σ_{fc}) is equal to:

$\sigma_{fc} = 469 \; 1.65\% = 7.8$MPa.

The results obtained by applying the proposed model are presented in Figs.3.8-3.13 in Chapter 3 (section 3.4) where the comparison between the proposed model results with experimental ones is given.